



Sorbonne Université

École Doctorale Physique en Ile-de-France

Institut d'Astrophysique de Paris

Unveiling Early Universe Physics Through Cosmological Correlators

This dissertation is submitted for the degree of

Doctor of Philosophy

Author:
Denis Werth

Supervisor:
Prof. Dr. S. Renaux-Petel

Presented and publicly defended on June, 4th 2025
in front of the following jury

Prof. Dr. A. Achúcarro	Leiden University	Examiner
Prof. Dr. M. Cirelli	Sorbonne Université	President
Prof. Dr. X. Chen	Harvard University	Referee
Prof. Dr. P. Creminelli	ICTP Trieste	Examiner
Dr. D. Stefanyszyn	University of Nottingham	Referee
Prof. Dr. F. Vernizzi	Université Paris-Saclay	Invited

This work has been accomplished at the Institut d'Astrophysique de Paris (IAP) at Sorbonne University. This research is funded by a Contrat Doctoral Spécifique Normalien (CDSN), awarded by the French Ministry of Higher Education and Research, and by the European Research Council (ERC) under the European Union's Horizon 2020 research and innovation programme (grant agreement No 758792, Starting Grant project GEODESI).

Copyright © 2025 by Denis Werth.
"*The copyright of this thesis rests with the author. No quotation from it should be published without the author's prior written consent and information derived from it should be acknowledged*".

À celles et ceux qui rêvent

Abstract

Primordial fluctuations retain imprints of the high-energy physics that shaped the earliest moments of our Universe, which is ultimately recorded in spatial correlation functions observed at later times. On the phenomenological side, potential new physics leaves distinct signatures in these cosmological correlators. However, a complete dictionary mapping the landscape of inflationary theories and the corresponding observable signatures is not yet available. From a theoretical perspective, the conventional procedure to compute these cosmological correlators is technically challenging, and a fundamental understanding of their mathematical structure is still at its infancy. This thesis is devoted to both developing new techniques to compute and study cosmological correlators, and to use these methods to explore the rich physics of the early Universe.

In the first part, we develop off-shell perturbative methods to cosmological correlators. We show that such approach not only makes the origin of the correlator singularity structure and factorisation manifest, but also renders practical analytical computations more tractable, as complex correlators are shown to be constructed by gluing lower-point off-shell correlators. We establish cosmological largest-time equations that relate different channels on in-in branches via analytic continuation. These universal relations hold promise for developing cosmological recursion relations, further connecting techniques from modern scattering amplitudes to cosmology. We also develop a novel saddle point technique to generate approximate solutions for non-analytic signals concealed in cosmological correlators. This provides an in-depth new physical insight into the hidden bulk dynamics during inflation.

The second part deals with boost-breaking physics. When the Goldstone boson of broken time translations during inflation acquires a reduced speed of sound, we introduce a novel discovery channel to detect new physics. This signal is characterised by a distinctive resonance lying in mildly-soft kinematic configurations of cosmological correlators, indicating the presence of a heavy particle, whose position enables us to reconstruct its mass. We show that this resonance can be understood in terms of a non-local single-field effective field theory. We also show that the presence of massive spinning particles coupled to a helical chemical potential lead to a large parity-violating cosmological correlators, that arise due to emergent non-locality.

The last part presents a framework to compute cosmological correlators based on following their time evolution: the cosmological flow. From first principles, the structure of the bulk time evolution imposes a set of universal differential equations

in time satisfied by cosmological correlators. We automatise the process of systematically solving these equations. This allows us to accurately capture all physical effects and obtain exact results in theories formulated at the level of inflationary fluctuations that include any number of degrees of freedom with arbitrary dispersion relations and masses, coupled through any time-dependent interactions. We then illustrate the power of this formalism by exploring the phenomenology of inflationary physics.

Keywords: Primordial cosmology, Inflation, Cosmological correlators, Quantum field theory in de Sitter spacetime, Cosmological collider phenomenology.

Résumé

Les fluctuations primordiales contiennent de précieuses informations sur la physique qui a façonné les premiers instants de notre Univers. Ces informations sont encodées dans les fonctions de corrélation spatiales que nous mesurons aujourd'hui. Du point de vue de la phénoménologie, toute nouvelle physique laisse des traces bien particulières dans ces corrélateurs cosmologiques. Pourtant, nous ne disposons pas encore d'une cartographie complète qui relie les différentes théories de l'inflation aux signaux qu'elles prédisent. De plus, sur le plan théorique, les méthodes traditionnelles pour calculer ces corrélateurs cosmologiques sont très complexes, et leur structure mathématique reste encore mal comprise. Cette thèse vise à développer de nouvelles méthodes pour calculer et analyser les corrélateurs cosmologiques et à utiliser ces outils pour explorer la riche physique de l'Univers primordial.

Dans la première partie, nous proposons une nouvelle approche pour les corrélateurs qui permet de mieux comprendre les singularités et la structure de ces derniers, tout en simplifiant les calculs analytiques. Nous montrons qu'on peut construire des corrélateurs complexes à partir de blocs plus simples. Nous introduisons également des relations universelles qui relient différents processus in-in par continuation analytique. Ces résultats ouvrent la voie au développement de nouvelles méthodes inspirées des amplitudes de diffusion en physique des particules. Enfin, nous développons une technique innovante basée sur le point col pour extraire la partie non-analytique des signaux cachés dans les corrélateurs, apportant un nouvel éclairage sur la dynamique des particules pendant l'inflation.

La deuxième partie explore ce qui se passe lorsque certaines symétries sont brisées pendant l'inflation. Lorsque le boson de Goldstone associé à la brisure des translations temporelles se propage plus lentement que la vitesse de la lumière, un nouveau signal caractéristique apparaît. Ce signal prend la forme d'une résonance particulière dans certaines configurations cinématiques des corrélateurs cosmologiques, révélant la présence d'une particule massive et permettant de reconstruire sa masse. Nous montrons que cette résonance peut être interprétée à l'aide d'une théorie effective non locale. De plus, nous examinons l'effet des particules massives de spin-1 couplées à un potentiel chimique hélicoïdal, générant des corrélateurs cosmologiques violant la parité, due à une non-localité émergente.

Dans la dernière partie, nous présentons une nouvelle méthode pour calculer les corrélateurs cosmologiques en suivant leur évolution dans le temps : le flot cosmologique. Partant de principes fondamentaux, nous montrons que l'évolution tem-

porelle impose un ensemble d'équations différentielles universelles sur les corrélateurs. Nous développons un cadre permettant de résoudre ces équations de manière systématique, qui permet d'obtenir des résultats exacts et de capturer tous les effets physiques pertinents. Nous illustrons ensuite l'efficacité de cette méthode en explorant la riche physique inflationnaire.

Mots-clés : Cosmologie primordiale, Inflation, Corrélateurs cosmologiques, Théorie quantique des champs en espace-temps de de Sitter, Phénoménologie du collisionneur cosmologique.

Publications

This thesis is based on the following publications (in anti-chronological order):

The Exact and Approximate Tales of Boost-Breaking Cosmological Correlators [2506.01555]
Accepted to JCAP
Z. Qin, S. Renaux-Petel, X. Tong, D. Werth, Y. Zhu

Spectral Representation of Cosmological Correlators [2409.02072]
JHEP **12** (2024) 017
D. Werth

CosmoFlow: Python Package for Cosmological Correlators [2402.03693]
Class. Quant. Grav. **41** (2024) 17
D. Werth, L. Pinol, S. Renaux-Petel

The Cosmological Flow: A Systematic Approach to Primordial Correlators [2312.06559]
JCAP **02** (2025) 019
L. Pinol, S. Renaux-Petel, D. Werth

Parity Violation from Emergent Nonlocality during Inflation [2308.11315]
Phys. Rev. D **108** (2023) 12
S. Jazayeri, S. Renaux-Petel, X. Tong, D. Werth, Y. Zhu

Shapes of the Cosmological Low-Speed Collider [2307.01751]
JCAP **12** (2023) 035
S. Jazayeri, S. Renaux-Petel, D. Werth

Cosmological Flow of Primordial Correlators [2302.00655]
Phys. Rev. Lett. **133** (2024) 14
D. Werth, L. Pinol, S. Renaux-Petel

During the course of the PhD, the author also worked on the following projects:

Primordial Sharp Features through the Nonlinear Regime of Structure Formation [2502.02571]
Phys. Rev. D **111** (2025) 16
C. Stahl, D. Werth, V. Poulin

Reconstructing Primordial Curvature Perturbations via Scalar-Induced Gravitational Waves with LISA [2501.11320]
JCAP **05** (2025) 062
LISA Cosmology Working Group

Review: Multi-Field Inflationary Cosmology [25XX.XXXX]
Invited Review for Physics Reports
S. Garcia-Saenz, L. Pinol, S. Renaux-Petel, D. Werth

No-go Theorem for Scalar-Trispectrum-Induced Gravitational Waves [2207.14267]
JCAP **03** (2023) 057
S. Garcia-Saenz, L. Pinol, S. Renaux-Petel, D. Werth

Acknowledgements

> *"Once again I repeat: the aim of physics at its most fundamental level is not just to describe the world but to explain why it is the way it is."*
>
> — Steven Weinberg, *Dreams of a Final Theory (1992)*

As my PhD journey in Paris comes to an end, I feel deeply grateful, knowing I would never have come this far without the unwavering support of so many wonderful people.

First and foremost, I would like to express my deepest gratitude to Sébastien Renaux-Petel. Thank you for your extraordinary guidance and for placing your trust in me throughout these years of research. Your inspiration, both scientifically and personally, has been invaluable. All the blackboard sessions and countless hours on Zoom truly fuelled my motivation and curiosity. I am especially grateful for your meticulous attention to detail in writing papers, your rigour has been priceless. Thank you, too, for steering me back on track whenever I was messing things up. In many ways, you have taught me not just how to do research, but how to become a researcher. You are truly the best advisor I could have hoped for. I will always remember your boundless passion for physics and your unwavering enthusiasm, and I will forever consider you my mentor.

Second, I would like to sincerely thank the chair of my PhD defence, Marco Cirelli, as well as the members of the jury: Ana Achúcarro, Xingang Chen, Paolo Creminelli, David Stefanyszyn, and Filippo Vernizzi. It is an incredible privilege to have people I deeply admire, and who have essentially shaped the field I work in, on my jury. Having you all as part of this important moment in my career is a true honour, and it means a lot to me.

Thanks are also due to my collaborators: Sebastian Garcia-Saenz, Sadra Jazayeri, Lucas Pinol, Vivian Poulin, Zhehan Qin, Clément Stahl, Xi Tong, and Yuhang Zhu, for their brilliant ideas and inspiring discussions. I will always remember your remarkable physical intuition, the clever mathematical tricks I learned from you, and some of your fearless enthusiasm in tackling the most intense Mathematica computations. Most of you have become more than collaborators, you have become my friends. It has been an absolute joy and privilege to work alongside you! This is one of the aspects of being a researcher that I cherish most: the opportunity to collaborate with brilliant minds from all around the world.

I would also like to thank everyone else at IAP who shared my daily life. You have made this place so vibrant, constantly buzzing with energy and inspiration. This is what a laboratory is made for! I would like to thank all the members of the GReCo group, whom I consider true titans of physics. Your knowledge, curiosity, and expertise continue to amaze and inspire me. I would like to give special thanks to Chantal, who has always done her utmost to ensure that I could work in perfect conditions. Without her, there would have been no trips, no seminars. Thank you! And of course, many thanks to all brilliant young minds and friends: Pierre, Clément, Louise, Aline, Émilie, Emma, Amaury, Mathieu, David, Axel, Hugo, Louis, Iryna, Marie, Chi An, Nai, Angelo, Julien, Joe, Virginia, Étienne, Alix, Léonard, Simon, Arthur, Nathan, Rosa, Marko, Lukas, Grégoire, Céline, Eduardo, Mike, Neda, Lisa, Lennart, Ali. I will remember YMCAs, enjoyable lunches, coffee breaks, and of course all the drinks!

To my family. I would like to thank my sisters, Nina and Nastia, who nonetheless took an interest in what I do, even when it is completely incomprehensible. Most importantly, I want to thank my parents. I would not be where I am now without them. Thank you for your unwavering support, both moral and, yes, financial! You have always let me follow my own path, never checking whether I had done my schoolwork. You watched me go through phases of wanting to be an actor, a chef, an economist, an engineer, a mathematician, and finally a physicist. You have passed on to me your love, your passion, your music, your cooking, your sense of adventure, and your love for travel, including 8-hour car rides to go camping in the mountains. I am so proud to have grown up in such an international and inspiring family.

Finally, I'll end with the most important person, the sunshine of my life, Chou! Thank you for being there every day. We've already shared so many incredible experiences together, travels, road trips, movie nights, more festive nights, walks around Paris, concerts, work stress, running, climbing, browsing book stores, tidying up the apartment together, eating, etc. I want to continue sharing all of life's adventures with you. As they say in Finnish: Minä rakastan sinua.

Denis Werth
Paris, June 2025

Contents

Abstract v

Résumé vii

Publications ix

Acknowledgements xi

1 Introduction 1
Outline of the Thesis . . . 5

2 Basics of Inflationary Cosmology 6
2.1 Standard Big-Bang Cosmology . . . 7
2.1.1 FLRW Background . . . 7
2.1.2 Parametrising the Universe: ΛCDM Model . . . 8
2.1.3 Cosmological Observables . . . 10
2.2 Inflationary Background . . . 14
2.2.1 Standard Model Problems . . . 14
2.2.2 Slow-Roll Inflation . . . 16
2.2.3 High-Energy Aspects of Inflation . . . 17
2.3 Primordial Fluctuations . . . 19
2.3.1 Density Perturbations . . . 19
2.3.2 Gravitational Waves . . . 22

I Physics of Cosmological Correlators 24

3 Shape of non-Gaussianities 25
3.1 Three-Point Correlators . . . 25
3.1.1 Standard Bispectrum Shapes . . . 27
3.1.2 Scalar Product of Shapes . . . 30
3.1.3 Importance of Product-Separable Templates . . . 31
3.2 Higher-Order, Mixed & Graviton Correlators . . . 32
3.2.1 Standard Trispectrum Shapes . . . 32
3.2.2 Parity-Violating Trispectra . . . 34
3.2.3 Mixed Scalar-Tensor & Graviton Correlators . . . 35

3.3 Observational Constraints & Prospects . . . 37

4 Cosmological Collider Physics 39
4.1 Spontaneous Particle Production . . . 40
4.1.1 Massive Field in de Sitter . . . 40
4.1.2 Production of Particles . . . 42
4.1.3 Stokes-Line Method . . . 44
4.1.4 Enhanced Particle Production . . . 46
4.2 Soft Limits of Cosmological Correlators . . . 48
4.2.1 Late-Time Non-Analytic Scaling . . . 49
4.2.2 Cosmological Collider Signal . . . 50
4.2.3 Particle Collider Analogy & Observational Prospects . . . 52
4.3 Phenomenology of Cosmological Colliders . . . 54
4.3.1 Spinning Particles . . . 55
4.3.2 Charting Cosmological Colliders . . . 58

II Fundamental Aspects of Cosmological Correlators 62

5 Schwinger-Keldysh Formalism 63
5.1 Preliminaries . . . 64
5.1.1 Constructing Path Integrals . . . 64
5.1.2 Generating Correlation Functions . . . 67
5.2 Schwinger-Keldysh Path Integral . . . 69
5.2.1 Forward & Backward Evolution . . . 69
5.2.2 $i\epsilon$ Prescription . . . 71
5.3 Diagrammatic Rules . . . 73
5.3.1 Generating Functional . . . 73
5.3.2 Propagators . . . 75
5.3.3 List of Standard Free Propagators . . . 76
5.3.4 Vertices . . . 80
5.3.5 Worked Out Examples . . . 85

6 Spectral Representation 88
6.1 From Time Ordering to Contour Integrals . . . 90
6.1.1 Multiple Propagators: a Matter of Contour . . . 90
6.1.2 Spectral Representation of Massive Propagators . . . 91
6.1.3 Derivation . . . 95
6.2 Cosmological Largest-Time Equation . . . 96
6.2.1 Propagator Identity from an Off-Shell Perspective . . . 96
6.2.2 Largest-Time Equation . . . 98
6.2.3 Application to Simple Diagrams . . . 103

7 Bootstrapping Cosmological Correlators 110
7.1 Via Spectral Representation . . . 111
7.1.1 Off-Shell Three-Point Function . . . 112
7.1.2 Dispersive Integral in the Energy Domain . . . 114

7.1.3 Bootstrapping via the Spectral Representation . . . 116
7.1.4 Singularities & Analytic Structure . . . 120
7.2 Via Boundary Kinematic Differential Equation . . . 123
7.2.1 Cosmological Bootstrap: Light Review . . . 123
7.2.2 Helical Seed Correlator & Boundary Equation . . . 129
7.2.3 Boost-Breaking Helical Massive Exchange Solution . . . 130
7.2.4 Discussion . . . 133

8 Classifying Non-Analyticities 137
8.1 Extracting & Approximating Cosmological Collider Signals . . . 138
8.2 Application to Tree-Level Exchange Correlators . . . 141
8.2.1 Unit Sound Speed & No Chemical Potential . . . 141
8.2.2 Turning on a Non-Trivial Sound Speed . . . 146
8.2.3 Further Turning on the Chemical Potential . . . 150

III Physics at Low Speed & Non-Locality 157

9 EFT of Inflationary Fluctuations 158
9.1 Adopting the EFT Philosophy . . . 159
9.2 Constructing the Action for Adiabatic Perturbations . . . 160
9.2.1 Geometric Construction . . . 160
9.2.2 Tadpole Cancellation . . . 162
9.2.3 Derivative Expansion . . . 163
9.2.4 Stückelberg Procedure . . . 164
9.2.5 Decoupling Limit . . . 167
9.3 From Fluctuations to Observables . . . 170
9.3.1 Scalar Power Spectrum: from π to ζ . . . 170
9.3.2 Graviton Power Spectrum . . . 171
9.3.3 Scales of Inflation . . . 173
9.4 Additional Hidden Sectors . . . 175
9.4.1 Massive Scalar Field . . . 175
9.4.2 Spin-1 Helical Field . . . 177
9.5 Strong Coupling Scales & Naturalness . . . 180
9.5.1 Weak Mixing . . . 180
9.5.2 Strong Mixing . . . 184
9.5.3 Radiative Corrections . . . 186

10 Going Non-Local 188
10.1 Low-Speed Yukawa Limit . . . 189
10.2 Integrating out Heavy Fields . . . 190
10.2.1 Time-Independent Backgrounds . . . 190
10.2.2 Integrating out via the Path Integral . . . 192
10.2.3 Non-Local Effective Action . . . 194
10.3 Dispersion Relation . . . 196
10.3.1 Reduced Effective Sound Speed . . . 197
10.3.2 Modified Dispersion Relation . . . 198

10.4 Regimes of Validity . . . 199
10.4.1 Flat-space Intuition . . . 200
10.4.2 Soft Limits of Cosmological Correlators . . . 200
10.5 Non-locally Integrating out the Chemical Potential . . . 202

11 Boost-Breaking Cosmological Correlators 206
11.1 Cosmological Correlators at Low Speed . . . 208
11.1.1 Weight-Shifting Operators . . . 208
11.1.2 Non-local EFT Seed Integrals . . . 210
11.1.3 Bispectrum . . . 212
11.2 Low-Speed Collider Phenomenology . . . 214
11.2.1 Physics of the Low-Speed Collider . . . 214
11.2.2 Shapes of the Low-Speed Collider . . . 218
11.2.3 Shape Correlation . . . 220
11.2.4 Low-Speed Collider Template . . . 221
11.2.5 Self-Interaction Contamination . . . 223
11.3 Parity Violation from Emergent Non-Locality . . . 225
11.3.1 Size of Parity-odd Signals . . . 225
11.3.2 Parity Violation as a Residue . . . 226
11.3.3 Singularity at Higher Orders . . . 229
11.3.4 Shape Characteristics . . . 230

IV Cosmological Flow 234

12 In-in Operator Formalism 235
12.1 Preliminaries: a Matter of Picture . . . 236
12.2 From Heisenberg to Interaction Picture . . . 238
12.2.1 $i\epsilon$ Prescription . . . 239
12.2.2 In-in Master Formula . . . 240
12.3 Perturbative Expansion . . . 240
12.3.1 Factorised Forms . . . 241
12.3.2 Commutator Forms . . . 242
12.4 In-in Formalism in Action . . . 243
12.4.1 Wick Contractions . . . 243
12.4.2 Worked out Examples . . . 244

13 Following the Time Evolution 248
13.1 Equal-Time Correlators . . . 249
13.1.1 Equations of Motion . . . 249
13.1.2 Tree-Level Cosmological Correlators . . . 251
13.2 Two- & Three-point Correlators . . . 251
13.2.1 Two-Point Correlators . . . 251
13.2.2 Three-Point Correlators . . . 252
13.2.3 Resumming Quadratic Mixings . . . 254
13.3 Higher-Order Correlators . . . 255
13.3.1 Four-Point Correlators . . . 255

13.3.2 Diagrammatic Rules for n-Point Correlators . . . 258

14 Implementing the Cosmological Flow 260
14.1 Inspiration from Particle Physics . . . 260
14.2 Landscape of Theories . . . 262
14.2.1 Action . . . 262
14.2.2 Conjugate Momenta . . . 263
14.3 Flow Equations . . . 264
14.3.1 Differential Equations in Time . . . 265
14.3.2 Derivative Interactions . . . 267
14.3.3 Boundary Terms . . . 267
14.4 Initial Conditions . . . 268
14.4.1 Two-Point Correlators . . . 269
14.4.2 Three-Point Correlators . . . 270
14.5 CosmoFlow: Python Package for Cosmological Correlators . . . 273

15 Exploring the Phenomenology of Cosmological Correlators 275
15.1 Quadratic Theory . . . 277
15.1.1 Effective Mass & Resonance at Strong Mixing . . . 277
15.1.2 Phase Diagram . . . 280
15.2 Size of non-Gaussianities Beyond Weak Mixing . . . 281
15.3 Cosmological Collider Phenomenology . . . 287
15.3.1 Strongly Mixed Colliders . . . 287
15.3.2 Sound-Speed Colliders . . . 290
15.3.3 Cosmological Collider Flow . . . 292
15.4 Primordial Features . . . 293
15.4.1 Effective Description of Features . . . 293
15.4.2 Correlated Sharp Features . . . 295
15.4.3 Probing the Inflationary Landscape . . . 297

16 Conclusions & Perspectives 305

Appendices 310

A Details on Massive Fields in de Sitter 311
A.1 Glossary of Hankel and Legendre Functions . . . 312
A.2 Non-Analytic Signal from Bulk Cutting Rules . . . 314
A.3 Mellin-Barnes Techniques . . . 316

B Mathematical Interlude 320
B.1 Riemann Surfaces from Multi-Valued Functions . . . 320
B.2 Saddle Point Approximation of Complex Integrals . . . 324

C Details on Physics at Low Speed 329
C.1 Weight-Shifting Operator Derivation . . . 329
C.2 Higher-Order Non-Local EFT Corrections . . . 331
C.3 Non-Local EFT Resummation in Flat Space . . . 332

D Details on the Cosmological Flow **335**
D.1 Extended Fourier Summation 335
D.2 Two-point Correlator Initial Conditions 336
D.3 Three-point Correlator Initial Conditions 337

E Notation and Conventions **343**

Summary **355**

Résumé Long en Français **360**

Bibliography **361**

1

Introduction

Cosmology is a fascinating science. Everything we know so far from our Universe's origin, evolution, and ultimate fate relies on observations. At its core, understanding the cosmos relies on fundamental pillars of modern physics: the quantum principles governing elementary particles at the smallest scales, the theory of gravity on the largest scales, and the nature of time itself. Together, these principles help us trace the Universe's history, from the beginnings of the hot Big Bang to the formation of cosmic structures and their gravitational collapse that gave birth to the galaxies we see today.

Although we can only observe the Universe in its later stages, our challenge is to reconstruct its history and explain the correlations we detect. Cosmology, in this sense, is like tracing time backward, from the Large-Scale Structure (LSS) we see today to the Cosmic Microwave Background (CMB), and further back to the primordial fluctuations at the end of reheating, see Fig. 1.1. However, these structures exhibit correlations over vast distances that, in a traditional hot Big Bang scenario, could never have been in causal contact. To resolve this paradox, the leading paradigm suggests that the early Universe underwent a phase of rapid expansion known as *inflation*. Remarkably, inflation not only accounts for these large-scale correlations but also provides the very mechanism for the formation of cosmic structures. The structures we see today actually originate from tiny quantum fluctuations during inflation, which were stretched to cosmological scales and eventually imprinted as spatial correlations on the future boundary of the inflationary spacetime—marking the starting point of the hot Big Bang evolution.

Since cosmological fluctuations can only be described statistically, the fundamental observables are spatial correlation functions of cosmological structures. These *cosmological correlators* of density fluctuations and tensor modes hold valuable information about the laws that govern the cosmos, and—for connected n-point correlators with $n \geq 3$—are conventionally called non-Gaussianities. More importantly,

they preserve traces of the physics that shaped the very early Universe. Recent years have shown increasing interests in studying these higher-point correlators as they ultimately hold the key to fundamental physics. However, they have not been detected so far.

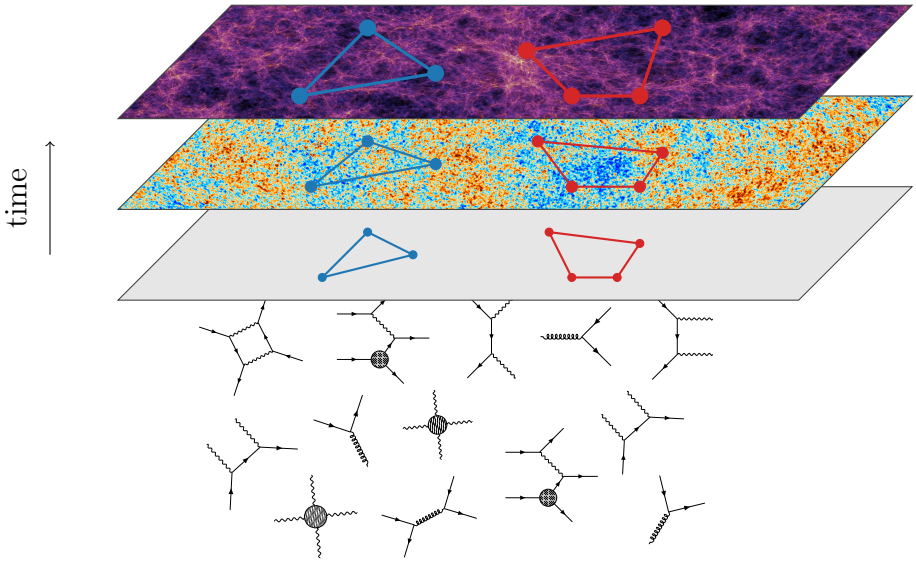


Figure 1.1: Cosmological correlators capture the statistical properties of key observables, such as the Large-Scale Structure (LSS) of the Universe and the Cosmic Microwave Background (CMB). These correlations can be traced back in time to the reheating surface and originate from quantum fluctuations generated during inflation. They provide a unique window into the fundamental laws of nature at the highest energy scales.

On observational grounds, it is expected that substantial progress is to be made in the coming years. Compared to future CMB experiments that would lead to interesting yet modest improvements on bounds for non-Gaussianities, the qualitative leap ahead of us lies in the constraining power of three-dimensional LSS surveys. Indeed, a host of galaxy surveys ambition to improve current constraints by one order of magnitude in the near future and reach an important threshold marking the border between a weakly or strongly coupled description of the inflationary background dynamics. In the longer term, 21cm surveys will have the raw statistical power to improve limits by several orders of magnitude, reaching the gravitational floor.

The phenomenological interest in cosmological correlators lies in the fact that the energy scale of inflation can be as high as $10^{14}\,\mathrm{GeV}$. This energy makes the study of cosmological correlators a unique opportunity to learn about potential new physics at the highest reachable energies, much higher than those achievable in ground-based experiments such as the Large Hadron Collider. This one-of-a-kind window to fundamental physics has opened a "cosmological collider physics" programme. Essentially, even very heavy particles have been spontaneously produced during inflation, whose subsequent decays lead to imprints in cosmological correlators. These specific signatures—whose prospects for detection are bright although

the experimental challenge to observe them is enormous—could inform us about the inflationary field content, including the mass spectra of particles, their spins and dispersion relations.

On the theory side, the early Universe is a remarkable laboratory to study quantum field theory (QFT) in curved spacetime, see Fig. 1.2. The study of cosmological correlators has triggered recent developments both in deriving analytical closed-form solutions for correlators, and in revealing formal aspects such as their analytic structure. These advancements mirror our understanding of flat-space scattering amplitudes or that of boundary correlators in anti-de Sitter (AdS) space. The motivations for such progress lie in the fact that, on cosmological scales probed in the CMB and LSS, inflation is reliably described by a (weakly-coupled) QFT on top of a fixed quasi-de Sitter (dS) space. New techniques, such as solving differential equations on the dS infinite future boundary, AdS-inspired methods, and (partial) Mellin-Barnes representations have led to new analytical results for cosmological correlators. These advances have also provided a better understanding of their mathematical structure, and have triggered fruitful developments in understanding QFT in dS, as well as how fundamental principles like unitarity, locality, and causality are encoded in cosmological correlators.

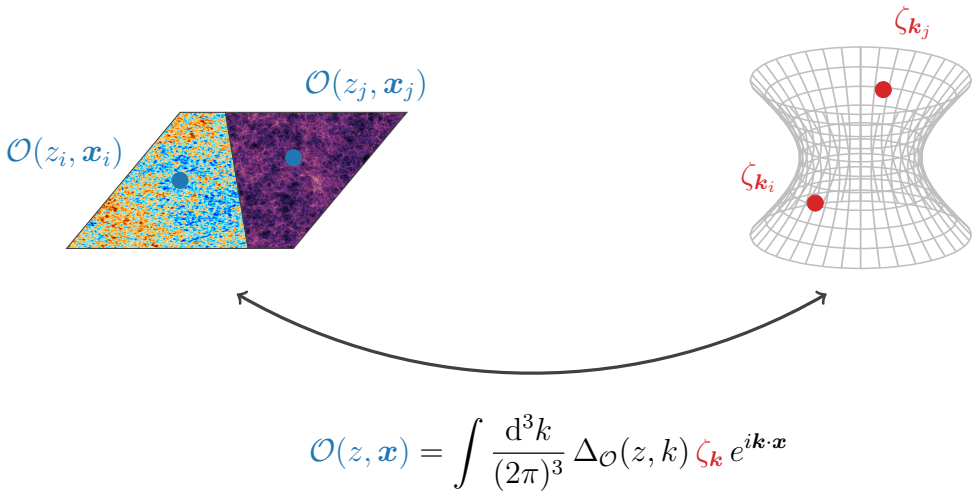


Figure 1.2: The early Universe serves as a remarkable natural laboratory for exploring high-energy physics. Cosmological observables $\mathcal{O}(z, \boldsymbol{x})$—such as those extracted from the CMB or LSS—are directly linked to the evolution of quantum fields $\zeta_{\boldsymbol{k}}$ in a curved spacetime. This connection is encoded in transfer functions $\Delta_{\mathcal{O}}(z, k)$, which describe how primordial quantum fluctuations generated during inflation propagate and imprint themselves onto late-time cosmic structures.

This thesis aims to develop new techniques to study and compute cosmological correlators, and to use them to unveil the physics of the early Universe.

Outline of the thesis

The outline of the thesis is as follows. Chap. 2 contains a brief summary of modern cosmology, presenting both essential elements of cosmological backgrounds and per-

turbations, and reviewing the relevant observables underlying the rest of the thesis. Of most importance, this chapter introduces the basics of inflation. The rest of the thesis is made of four main parts.

Part. I is devoted to an in-depth review of the physics of cosmological correlators, and contains the essential aspects that are used throughout the remaining of the thesis. Chap. 3 discusses the bispectrum standard shapes, their connection to the physics of inflation, as well as observational constraints and prospects. We also present higher-order, mixed and graviton correlators with an emphasize on reviewing modern literature on the subject. Chap. 4 contains a detailed exposition of cosmological collider physics, discussing the spontaneous production of massive particles and notably the Stokes line method, as well as their imprint in soft limits of cosmological correlators. The chapter concludes with a comprehensive review of the phenomenological landscape of studied signals and theories in the literature.

Part. II presents fundamental aspects of cosmological correlators. We begin in Chap. 5 with a detailed review of the Schwinger-Keldysh formalism. In Chap. 6, we present a new off-shell approach to cosmological correlators. We also derive cosmological largest-time equations that relate different in-in branches through analytic continuation of external energies. Chap. 7 is dedicated to using two novel approaches to compute cosmological correlators. The first one relies on performing a spectral integral, and offers an intuitive understanding of the underlying physics. There, we present the new simplest partially resummed representation so far of the four-point correlator of conformally coupled scalars mediated by the tree-level exchange of massive scalars. The second method consists in solving boundary differential equation in external kinematics, with which we have bootstrapped the most general boost-breaking tree-level four-point correlator up to second-order in derivatives. This includes a reduced sound speed and a helical chemical potential. In passing, we discuss analytic properties of these correlators. In Chap. 8, we develop a novel method to find approximate simple solutions for non-analytic signals hidden in cosmological correlators. This technique is based on the saddle point approximation, and naturally yields theoretically well-motivated templates that can be searched for in current and future experiments.

Part. III aims to study boost-breaking theories and the corresponding signals concealed in cosmological correlators. Chap. 9 reviews the construction of the effective field theory (EFT) of inflationary fluctuations, and couples the visible sector to a massive and helical hidden one. Notably, we classify the interactions of these particles and provide a complete dictionary of strong coupling scales, and perturbativity bounds, and discuss naturalness. In Chap. 10, we introduce a novel class of non-local EFTs that describes the physics at reduced sound speed. In particular, we chart the complete phase diagram of the quadratic theory, including the strong mixing regime. Chap. 11 is dedicated to imprints of boost-breaking physics in cosmological correlators. We introduce new cosmological low-speed collider signals, and discuss in detail their physics and characteristics. In passing, we also explore the physics of parity violation.

Part. IV introduces the cosmological flow. Starting from reviewing the in-in operator formalism for cosmological correlators in Chap. 12, we derive universal differ-

ential equations in time satisfied by correlators in phase space in Chap. 13. Chap. 14 discusses how these flow equations can be systematically solved, which leads to the design of an automatic numerical tool to generate theoretical data, CosmoFlow. Chap. 15 aims to explore the rich inflationary physics using the cosmological flow. In particular, we provide a complete and non-perturbative (in quadratic mixings) dictionary of the shape and amplitude of three-point cosmological correlators in the most generic inflationary theory. We also present novel signatures from non-scale invariant theories, which can lead to striking features in the scale-dependent bias.

Conclusions are given in Chap. 16, together with comments on future directions. Apps. A, B, C, and D contain details that were left out of the main text. We summarise the structure of the thesis in the following roadmap.

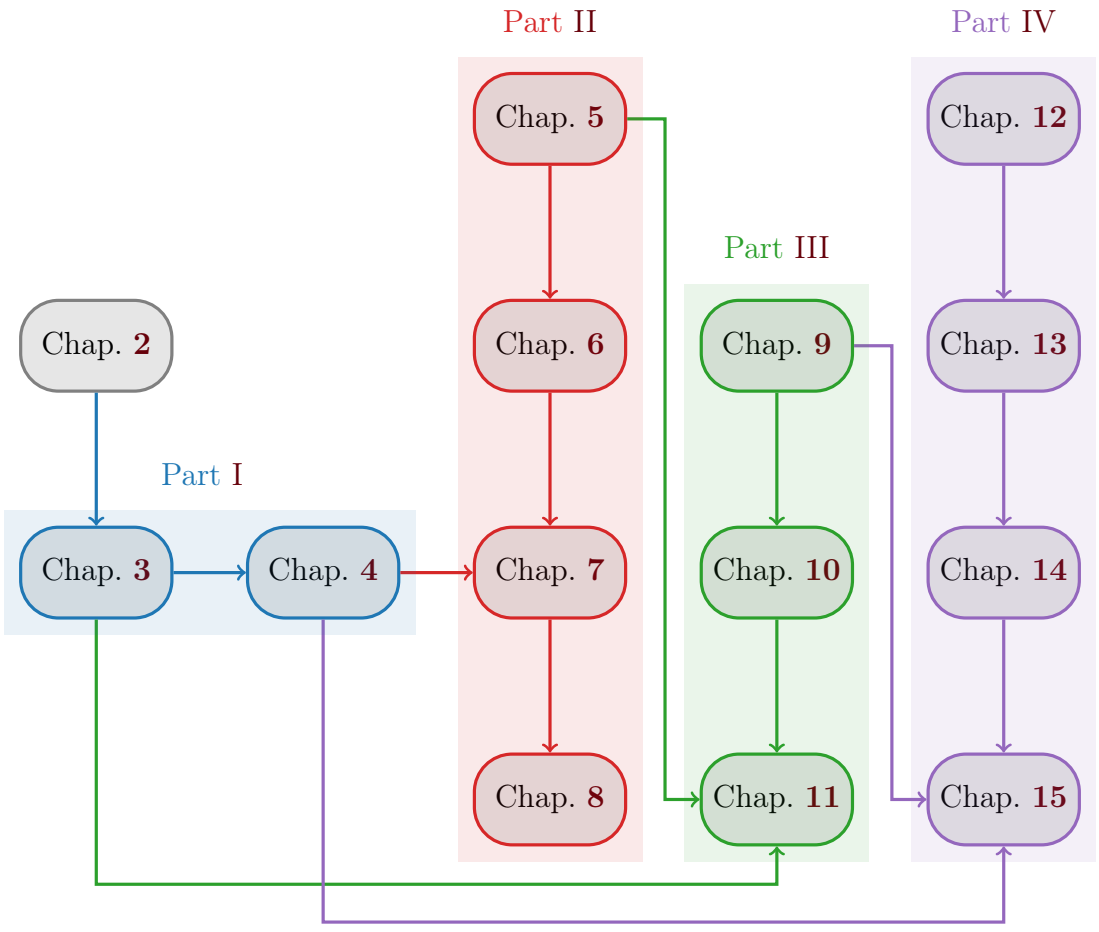


Figure 1.3: Roadmap illustrating the structure of the thesis, which highlights the interconnections between its chapters. For instance, Chap. 14 builds upon the concepts, notations, and results introduced in Chap. 13, which itself draws from Chap. 12. The diagram also emphasizes the relationships between various parts of this manuscript, represented as coloured shaded regions. Notably, Chaps. 5, 9 and 12 can serve as starting points to read the thesis as they are independent of any other chapter.

2

Basics of Inflationary Cosmology

One of the most remarkable aspects of cosmology is that our entire understanding of the Universe—its structure and evolution—stems from observing the sky. This is exemplified by some of the field's greatest achievements, from the precise measurements of temperature anisotropies in the Cosmic Microwave Background (CMB) to cataloguing vast maps of the Large-Scale Structure (LSS). Yet, deciphering the fundamental laws that govern the cosmos also requires *theoretical input*. By bridging fundamental physics with cosmological data, current cosmological analyses have achieved percent-level precision in constraining key parameters that describe both the early and late Universe.

Quite beautifully, as we look further back in time, modern cosmology becomes increasingly theory-driven rather than observational-based. This is especially true when tracing the origins of cosmic structures to the very onset of the hot Big Bang. There, it is believed that these structures have emerged from quantum zero-point fluctuations, amplified during a primordial period of accelerated expansion known as *inflation*. Having passed rigorous observational tests, inflation stands as the leading paradigm for describing the early Universe and the genesis of cosmic structure. Despite its apparent simplicity, this profound idea offers a unique window into the most fundamental laws of Nature at the highest energy scales.

In this chapter, we begin with a brief introduction to modern cosmology, discussing the Universe's dynamics, key parameters describing its content, and cosmological observables to measure them. Then, we introduce the inflationary paradigm both at the background and fluctuation level. The material presented here follows standard treatments found in any cosmology textbooks. Excellent reviews on inflation include [1, 2, 3]. See this goldmine of Cosmology Resource Materials for additional resources. Historical papers on the background mechanism of inflation are [4, 5, 6, 7, 8, 9, 10], and fluctuations were first discussed in [11, 12, 13, 14, 15, 16, 17, 18].

2.1 Standard Big-Bang Cosmology

Our understanding of the Universe is grounded in the well-established hot Big Bang model, which provides the foundation for the inflationary paradigm. In this section, we review essential aspects of this remarkably successful framework.

2.1.1 FLRW Background

Cosmological observations suggest that the Universe is both spatially homogeneous and isotropic on large scales. Assuming general relativity is a valid description of spacetime and gravity at these scales, this cosmological principle constrains the possible forms of the spacetime metric $g_{\mu\nu}$ to be that of Friedmann-Lemaître-Robertson-Walker (FLRW):

$$\mathrm{d}s^2 = g_{\mu\nu}\mathrm{d}x^\mu \mathrm{d}x^\nu = -\mathrm{d}t^2 + a^2(t)\left[\frac{\mathrm{d}r^2}{1-kr^2} + r^2\mathrm{d}\Omega_2^2\right], \quad (c \equiv 1)\,, \tag{2.1}$$

where $\mathrm{d}\Omega_2^2 \equiv \mathrm{d}\theta^2 + \sin^2\theta \mathrm{d}\varphi^2$ is the line element of a two-dimensional sphere, and k is the curvature that can only take the discrete values $+1, -1$ or 0 corresponding to closed, open, or spatially flat spatial geometries, respectively. This metric is described by a single function of (cosmic) time: the scale factor $a(t)$. It is convenient to define conformal time, τ, by $\mathrm{d}\tau \equiv \mathrm{d}t/a(t)$, to describe the propagation of photons and the causal structure of spacetime. This way, the metric is conformal to the one of Minkowski space. According to general relativity, the dynamics of the Universe is dictated by the Einstein equations

$$R_{\mu\nu} - \tfrac{1}{2}Rg_{\mu\nu} = 8\pi G T_{\mu\nu}\,, \tag{2.2}$$

where $R_{\mu\nu}$ is the Ricci tensor, and R is the Ricci scalar. The energy-momentum tensor $T_{\mu\nu}$ describes the content of the Universe, and, assuming a homogeneous and isotropic background, takes the form of that of a relativistic perfect fluid

$$T_{\mu\nu} = (\rho + P)u_\mu u_\nu + P g_{\mu\nu}\,, \tag{2.3}$$

where P is the pressure, ρ the energy density, and $u_\mu = (1,0,0,0)$ is the four-velocity for the isotropic fluid in comoving coordinates (in its local rest frame). With the perfect fluid source, the 00 and ij components of the Einstein's equations lead to the Friedmann equations

$$H^2 = \frac{8\pi G}{3}\rho - \frac{k}{a^2}\,, \quad \frac{\ddot{a}}{a} = -\frac{4\pi G}{3}(\rho + 3P)\,, \tag{2.4}$$

where $H \equiv \frac{\dot{a}}{a}$ is the Hubble parameter, and $\dot{} \equiv \frac{\mathrm{d}}{\mathrm{d}t}$. Conservation of the energy-momentum tensor, $\nabla_\mu T^{\mu\nu} = 0$, leads to the continuity equation (which also follows from the Friedmann equations or directly ensured by the Bianchi identities)

$$\dot{\rho} + 3H(\rho + P) = 0\,, \tag{2.5}$$

from which we obtain the evolution $\rho \propto a^{-3(1+w)}$ if we assume a given constant equation of state $w \equiv P/\rho$. The main components of our Universe are radiation,

	w	$\rho(a)$	$a(t)$
radiation	$1/3$	a^{-4}	$t^{1/2}$
matter	0	a^{-3}	$t^{2/3}$
Λ	-1	a^{0}	e^{Ht}

Table 2.1: Summary of the evolution of single-component Universe.

pressurless matter, and dark energy described by a cosmological constant Λ. For $w \neq 1$, we obtain $a(t) \propto t^{2/[3(1+w)]}$ if one neglects curvature. We give a summary of the evolution of various components in Tab. 2.1. It is useful to define several measurable cosmological parameters in addition to the Hubble parameter. We define the critical density

$$\rho_c \equiv \frac{3H^2}{8\pi G} = 1.05 \times 10^{-5}\, h^2\, \mathrm{GeV\,cm^{-3}}\,, \tag{2.6}$$

where the scaled Hubble parameter h is defined by $H \equiv 100\, h\, \mathrm{km\,s^{-1}\,Mpc^{-1}}$. The fractional cosmological density parameter Ω_i for a component i is defined as the energy density relative to the critical density, $\Omega_i \equiv \rho_i/\rho_c$. In terms of individual components, one defines

$$\Omega_r \equiv \frac{\rho_r}{\rho_c}\,, \quad \Omega_m \equiv \frac{\rho_m}{\rho_c}\,, \quad \Omega_\Lambda \equiv \frac{\Lambda}{3H^2}\,. \tag{2.7}$$

The Friedmann equation can be rewritten as

$$H^2 + \frac{k}{a^2} = H_0^2 \left[\Omega_{\Lambda,0} + \Omega_{m,0} \left(\frac{a}{a_0}\right)^{-3} + \Omega_{r,0} \left(\frac{a}{a_0}\right)^{-4} \right], \tag{2.8}$$

where the subscript 0 indicates present-day values. The sum of the densities in matter, relativistic particles and dark energy determines the overall sign of the curvature $\Omega_{k,0} \equiv -k/(a_0^2 H_0^2)$.

2.1.2 Parametrising the Universe: ΛCDM Model

Advances in observational cosmology have led to the establishment of a precise cosmological model based on six independent parameters, whose values are given in Tab. 2.2. The matter content is assumed to be composed only of baryons—i.e. visible matter comprised of the known Standard Model particles—, cold dark matter, and a cosmological constant describing dark energy. Relevant for the remaining of the thesis are two parameters characterising the initial conditions of the Universe, namely the primordial fluctuation amplitude A_s and the spectral tilt n_s. They parametrise an almost scale-invariant primordial power spectrum

$$\mathcal{P}_\zeta(k) \equiv A_s \left(\frac{k}{k_\star}\right)^{n_s - 1}\,, \tag{2.9}$$

where the pivot scale $k_\star$ is set to $k_\star = 0.05\,\mathrm{Mpc^{-1}}$, and the curvature perturbation is properly defined in Sec. 2.3. We will see in what follows that such a power spectrum

is predicted by inflation. The history of the Universe is divided into three large epochs: the radiation-dominated, matter-dominated and dark energy-dominated eras. Although two main ingredients (dark energy and dark matter) have not yet been verified by laboratory experiments, this ΛCDM (Λ Cold Dark Matter) model is universally accepted by cosmologists as the best description of the present data.

	Planck TT, TE, EE+lowE+lensing
$\Omega_b h^2$	0.02237 ± 0.00015
$\Omega_c h^2$	0.1200 ± 0.0012
h	0.674 ± 0.005
n_s	0.965 ± 0.004
τ	0.054 ± 0.007
$\ln(10^{10} A_s)$	3.044 ± 0.014
$100\,\theta_{\rm MC}$	1.0409 ± 0.0003
σ_8	0.811 ± 0.006
Ω_m	0.315 ± 0.007
Ω_Λ	0.685 ± 0.007

Table 2.2: Constraints on the ΛCDM parameters, reproduced from [19]. These values assume the ΛCDM model with power-law primordial power spectrum initial conditions, no tensor modes, spatial flatness, a cosmological constant as dark energy, and the sum of neutrino masses fixed to 0.06 eV, and use *Planck* primary CMB data plus the *Planck* measurement of CMB lensing. The six independent parameters fit to the data are above the line: baryon density today $\Omega_{b,0}h^2$, cold dark matter density today $\Omega_{c,0}h^2$, reduced Hubble parameter h, spectral tilt of the scalar primordial power spectrum n_s, reionisation optical depth τ, and primordial power spectrum amplitude $\mathcal{P}_\zeta$. Below the line are some of the derived parameters: measure of the sound horizon at last scattering $\theta_{\rm MC}$, fractional root-mean-square in density when a spherical filter of radius $8h^{-1}$ Mpc is applied in linear theory σ_8, total matter density today including massive neutrinos $\Omega_{m,0}$, and dark energy density parameter $\Omega_{\Lambda,0}$. The primordial amplitude A_s is specified at the scale $0.05\,\mathrm{Mpc}^{-1}$. Uncertainties are shown at 68% confidence level. We have coloured primordial parameters, related to inflation, in red.

Cosmic tensions. Despite the ΛCDM success, "cosmic tensions" have appeared over the last decade. Most notably, there exists a 5σ 'Hubble tension' between direct measurement of the Hubble parameter in the late-Universe using cepheid-calibrated supernovae [20] and the ΛCDM prediction when calibrated on *Planck* data [19]. There is in addition, a milder (2-3σ) 'S_8 tension' between galaxy weak-lensing [21, 22, 23] and CMB [19] determinations of the amplitude of matter fluctuations, parametrised as $S_8 = \sigma_8\sqrt{\Omega_{m,0}/0.3}$. There is also a less known (yet potentially related) tension between determinations of the tilt of the matter power spectrum at redshift $z = 3$ and around $k \sim 1\,h\,\mathrm{Mpc}^{-1}$ using Lyman-α (Ly-α) data from eBOSS [24] and the CMB under ΛCDM, which has reached a statistical level of 5σ [25, 26, 27]. While the possibility of unknown systematic effects explaining

these discrepancies remains extensively studied, they may also indicate the existence of physics beyond ΛCDM, see e.g. [28, 29, 30] for reviews. More recently, the latest data release from DESI has called into question the very nature of dark energy itself [31, 32]. Indeed, based on observations of tens of millions of extragalactic objects, including galaxies and Ly-α forest tracers, these results suggest a time-evolving dark energy component, deviating from the standard cosmological constant ($w = -1$). This potential departure poses a significant challenge to our current theoretical understanding of the Universe.

2.1.3 Cosmological Observables

We now relate the photons travelling through the cosmos to quantities that we actually observe. This includes temperature anisotropies of the CMB, location of galaxies in the LSS, and scale-dependent galaxy bias. Given that all these structures were generated during inflation and provided we understand well the subhorizon evolution of fluctuations, one can trace these observables back in time to learn about the initial conditions. We refer the reader to [33, 34] for a discussion of other observables such as weak lensing, Ly-α forest and 21cm tomography.

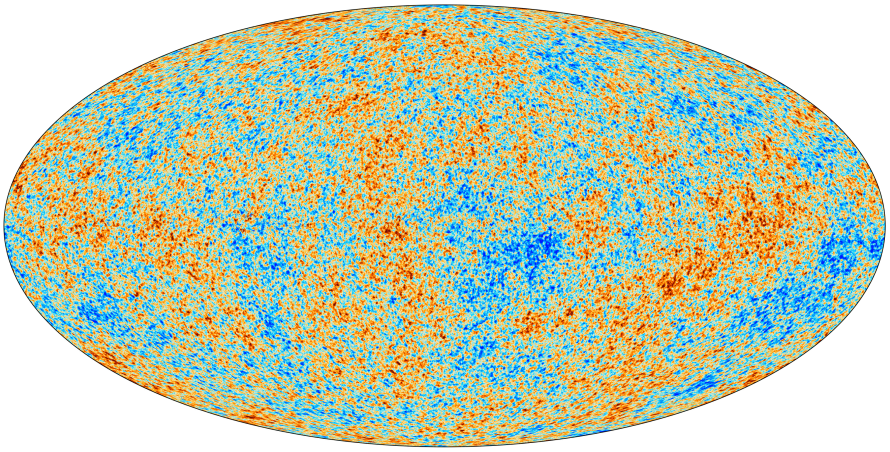


Figure 2.1: CMB temperature anisotropies as observed by the Planck satellite.

CMB temperature anisotropies. In the early Universe, the primordial plasma composed of protons and electrons was effectively opaque to electromagnetic radiation due to Thomson scattering $e + \gamma \leftrightarrow e + \gamma$ as the mean free path of photons was very short. Eventually, at a temperature of about 0.3 eV, the formation of neutral hydrogen $e + p \leftrightarrow H + \gamma$, termed *recombination* ($z \approx 1100$), became energetically favoured, and the photons *decouple*. Since the moment of last scattering around 380,000 years after the Big Bang, these primordial photons have travelled freely through the Universe and constitute the CMB observed today, around 13.7 billion years later. CMB experiments mapping the sky at microwave frequencies have measured an almost perfect black body spectrum with a mean temperature

of $\bar{T} = 2.7255\,\mathrm{K}$. Subtracting the mean temperature and the induced Doppler effect coming from the motion of our solar system with respect to the CMB rest frame which results in an overall dipole, we are left with temperature anisotropies $\delta T(\hat{\boldsymbol{n}}) \equiv T(\hat{\boldsymbol{n}}) - \bar{T}$, where $\hat{\boldsymbol{n}}$ indicates the line-of-sight direction in the sky. Fig. 2.1 shows temperature anisotropies of the order of $\delta T/T \sim 10^{-5}$. Since this two-dimensional CMB map lies on a sphere, it is convenient to describe temperature anisotropies in harmonic space by expanding $\delta T(\hat{\boldsymbol{n}})$ in spherical harmonics

$$\frac{\delta T}{\bar{T}}(\hat{\boldsymbol{n}}) = \sum_{\ell=0}^{\infty} \sum_{m=-\ell}^{+\ell} a_{\ell m} Y_\ell^m(\hat{\boldsymbol{n}})\,, \tag{2.10}$$

where ℓ is the multipole number while m is the azimuthal number. The coefficients $a_{\ell m}$ measure the amplitude of the angular oscillation along the multipole $Y_\ell^m(\hat{\boldsymbol{n}})$. The most important statistical object for studying such maps is the two-point correlation function, i.e. correlation between the temperature at distinct points $\hat{\boldsymbol{n}}$ and $\hat{\boldsymbol{n}}'$. If fluctuations are drawn from a perfectly Gaussian distribution function, this object contains all statistical information. The two-point function of the multipole moments $a_{\ell m}$ is defined to be

$$\langle a_{\ell m} a_{\ell' m'} \rangle = C_\ell^{TT}\, \delta_{\ell\ell'}\, \delta_{mm'}\,. \tag{2.11}$$

The angular power spectrum, C_ℓ^{TT}, is the Legendre transform of the two-point function of temperature anisotropies

$$C_\ell^{TT} \equiv 2\pi \int_{-1}^{+1} \mathrm{d}\cos\theta \left\langle \frac{\delta T}{\bar{T}}(\hat{\boldsymbol{n}})\, \frac{\delta T}{\bar{T}}(\hat{\boldsymbol{n}}') \right\rangle P_\ell(\cos\theta)\,, \tag{2.12}$$

where P_ℓ are Legendre polynomials, and $\cos\theta \equiv \hat{\boldsymbol{n}} \cdot \hat{\boldsymbol{n}}'$. Fig. 2.2 shows the CMB angular power spectrum as measured by the Planck satellite. The shape of this spectrum is well understood theoretically. Large scales (low multipoles) are dominated by the Sachs-Wolfe effect, namely the gravitational redshift of photons. Overdense regions with a negative gravitational potential lead to cold spots in the CMB map because photons loose more energy climbing up this potential. At intermediate scales ($\ell \sim 200$), the spectrum features acoustic oscillations of the photon-baryon fluid coming from a competition between radiation pressure and gravity. The smallest scales are exponentially damped (Silk damping). There is also an integrated Sachs-Wolfe effect due to the propagation of photons through the Universe. For adiabatic initial conditions, we have

$$C_\ell^{TT} = \frac{4\pi}{(2\ell+1)^2} \int \frac{\mathrm{d}k}{k} \left(\Delta_\ell^T(k)\right)^2 \mathcal{P}_\zeta(k)\,, \tag{2.13}$$

where the transfer function $\Delta_\ell^T(k)$ describes the evolution of primordial fluctuations from the moment of horizon entry to the time of recombination. This function is usually computed numerically by solving a coupled Einstein-Boltzmann system [35, 36]. This way, the angular power spectrum C_ℓ^{TT} is directly related to the primordial power spectrum $\mathcal{P}_\zeta$. Notably, on very large scales, the observed modes appear

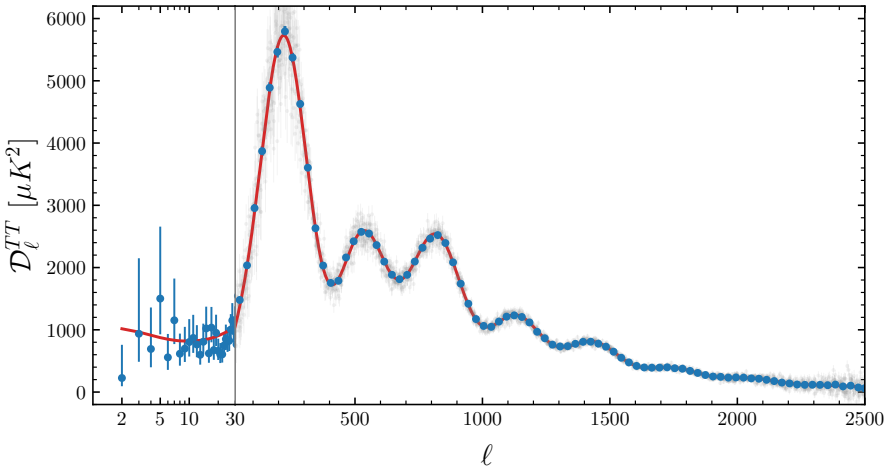


Figure 2.2: Angular power spectrum of CMB temperature anisotropies $\mathcal{D}_\ell^{TT} \equiv \ell(\ell+1)/(2\pi)C_\ell^{TT}$ as measured by Planck (2018 data). Both the data for individual multipoles and the binned averages are shown. The red line shows the best-fit theoretical spectrum based on the six-parameter ΛCDM model.

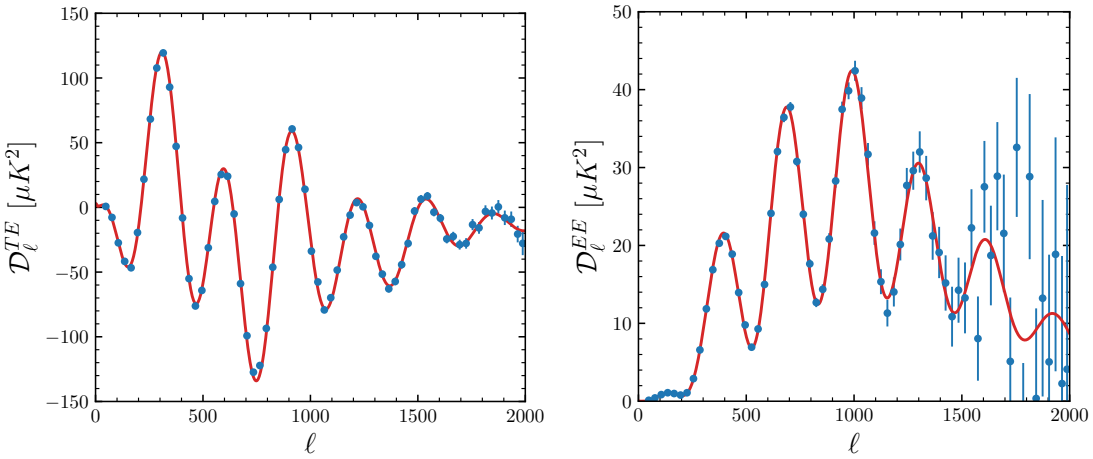


Figure 2.3: Planck TE and EE power spectra, $\mathcal{D}_\ell^{TE}$ and $\mathcal{D}_\ell^{EE}$. The red line shows the theoretical prediction with ΛCDM parameters inferred from the TT power spectrum. The impressive agreement with the data provides a non-trivial confirmation of the standard cosmological model.

acausal and the constant plateau reflects the near scale-invariance of the primordial power spectrum. We will come back to this point in Sec. 2.2.1.

Due to Thomson scattering, we also expect that the CMB radiation is linearly polarised at the level of a few μK at the time of decoupling. Fig. 2.3 shows the temperature-polarisation cross- and polarisation auto-spectra. Importantly, the theoretical curves are *not* a fit but a prediction based on calibrating the ΛCDM parameters on the temperature anisotropies power spectrum, showing impressive agreement with the data. We refer to [37] for more details.

LSS. After recombination, matter fluctuations grew under the influence of gravity. Eventually, these fluctuations formed galaxies that we observe today. At linear order, the power spectrum of dark matter density contrast $\delta_m = \delta\rho/\bar{\rho}$ at redshift z is directly related to the primordial power spectrum

$$P_m(z,k) = \Delta_m^2(z,k) P_\zeta(k)\,, \tag{2.14}$$

where $\Delta_m(z,k)$ is a transfer function that can be easily computed in perturbation theory on large scales ($k \lesssim 0.1\,\mathrm{Mpc}^{-1}$). However on small scales, one usually resorts to emulators calibrated on N-body simulations for fast evaluation. A major difficulty arises from the fact that we don't measure dark matter density directly. Instead, we observe biased tracers such as galaxies or Ly-α fluctuations whose density contrast δ_g is only related to dark matter via a bias expansion with unknown parameters, that is linear on large scales. On small scales, this relation can become non-linear, non-local and stochastic. Modelling the bias is the principal challenge to extract primordial physics from LSS. We show the (linear) matter power spectrum in Fig. 2.4 reconstructed from various observables, together with the best-fit ΛCDM model.

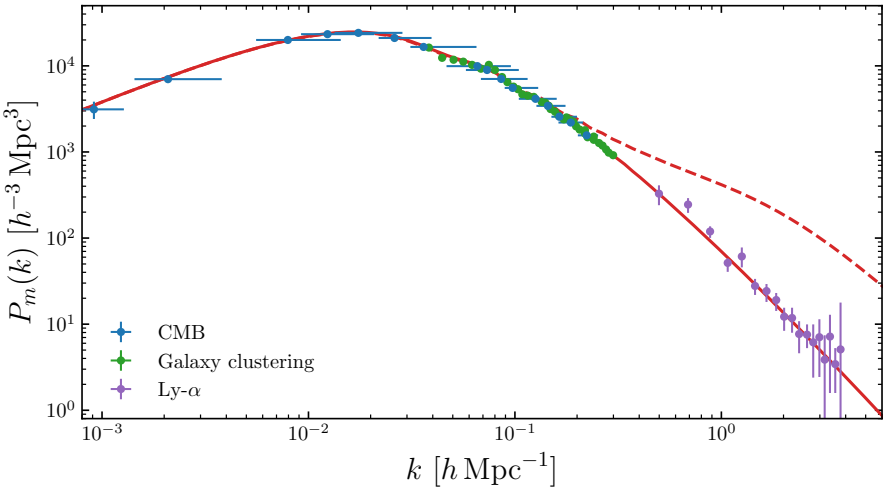


Figure 2.4: Linear matter power spectrum at $z = 0$ reconstructed from observables at various scales together with the best-fit ΛCDM in red. The dashed red line corresponds to the non-linear power spectrum generated with the Halofit emulator implemented in CLASS [36]. Galaxy clustering and Ly-α data are taken from SDSS [38, 39].

Scale-dependent bias. Real-space local non-linearities of the Newtonian potential Φ of the form

$$\Phi(\boldsymbol{x}) = \Phi_g(\boldsymbol{x}) + f_{\mathrm{NL}}^{\mathrm{loc}}(\Phi_g^2(\boldsymbol{x}) - \langle\Phi_g^2(\boldsymbol{x})\rangle)\,, \tag{2.15}$$

where Φ_g is a Gaussian field, impact structure formation in a local way, meaning that the gravitational collapse happens on small distance scale. Yet, we are interested in measuring correlations of galaxies separated by large cosmological distances. For

the Gaussian field $\Phi_g \equiv \Phi_s + \Phi_\ell$, the short ($k_s$) and long ($k_\ell$) wavelength modes are uncorrelated. However, the non-Gaussian nature of the full Newtonian field Φ induces a mixing between these two modes. At the level of the local matter density contrast which is linearly related to Φ by a transfer function

$$\delta_m(\boldsymbol{k}, z) = \frac{2k^2\Delta(k)D(z)}{3\Omega_m H_0^2}\Phi(\boldsymbol{k}) \equiv \mathcal{T}(k, z)\Phi(\boldsymbol{k})\,, \tag{2.16}$$

where $D(z)$ is the growth function, small-scale matter fluctuations are modulated by the long wavelength Newtonian potential according to

$$\langle\delta_m(\boldsymbol{k}_s)\delta_m(\boldsymbol{k}'_s)\rangle = \mathcal{T}^2(k, z)\,\langle\Phi_g(\boldsymbol{k}_s)\Phi_g(\boldsymbol{k}'_s)\rangle\,(1 + 2f_{\rm NL}^{\rm loc}\Phi_\ell)\,. \tag{2.17}$$

This means that long Newtonian potential wavelength modes affect the number of galaxies in the bias expansion

$$\begin{aligned}\delta_g(\boldsymbol{x}) &= b_1\delta_m(\boldsymbol{x}) + b_2\delta_m^2(\boldsymbol{x}) + 2b_\Phi f_{\rm NL}^{\rm loc}\Phi_\ell(\boldsymbol{x}) + \dots \\ &= \left(b_1 + b_\Phi f_{\rm NL}^{\rm loc}\frac{3\Omega_m H_0^2}{k^2\Delta(k)D(z)}\right)\delta_m(\boldsymbol{k}) + \dots\,.\end{aligned} \tag{2.18}$$

This phenomenon is called scale-dependent bias because the bias parameter relating the tracer δ_g to dark matter δ_m becomes a function of the scale k whose dependence is partly given by the amplitude of (primordial) non-linearities. At large distances, since $\Delta(k \to 0) \to 1$, we have $\delta_g \propto b_\Phi f_{\rm NL}^{\rm loc}\delta_m/k^2$ which tells us that this signal peaks at the largest possible scale away from the non-linear regime. The scale-dependent bias is used to constrain primordial local non-Gaussianities and the presence of light fields during inflation, see Chap. 3. The primary limitation for characterising this signal is cosmic variance, i.e. that the errors are fundamentally limited by the number of available modes, especially on large scales. We refer the reader to the complete review [40] for more details.

2.2 Inflationary Background

The standard hot Big Bang model provides a successful framework to understand the evolution of the Universe and the growth of structures. However, it is incomplete. Notably, it fails to provide an explanation for the apparent fine-tuned initial conditions, i.e. an initial almost scale-invariant distribution of primordial density fluctuations described by the power spectrum $\mathcal{P}_\zeta(k)$ (2.9). In the following, we describe the inflationary mechanism as a natural solution to some of the most notable problems.

2.2.1 Standard Model Problems

The following three fundamental problems have led many cosmologists to reconsider the early expansion history of the Universe, providing strong motivation for proposing an initial phase of accelerated expansion: inflation.

Flatness problem. Observations are consistent with a Universe that is highly spatially flat, $|\Omega_{k,0}| < 0.005$ [19], where $\Omega_{k,0} = 1 - \Omega_{\mathrm{tot},0}$ is the relative effective density of curvature today defined in Sec. 2.1. However, Ω_k is increasing with time $\Omega_k \approx \Omega_{k,0}(a/a_0)^{1+3w}$. This means that the curvature density was even smaller at earlier times, $|\Omega_k| < 10^{-5}$ at the last scattering of the CMB, and even $|\Omega_k| < 10^{-16}$ at the time of nucleosynthesis. This apparent fine-tuning of the initial geometry of the Universe is called the flatness problem.

Horizon problem. The second problem is that of causality. In simple words, the causality structure of the cosmological spacetime is such that two points on the CMB sphere separated by more than 2^o ($\ell \sim 200$) could not have been in causal contact in the past: their past light cones do not overlap. However, CMB photons coming from all directions are correlated as they share the same overall temperature to one part in 10^4, as we measure a non-vanishing power on large (superhorizon) scales, see Fig. 2.2. This is the horizon problem. To see this more quantitatively, we define the comoving distance travelled by light between the cosmic times t_1 and t_2

$$D(t_1, t_2) = \int_{t_1}^{t_2} \frac{\mathrm{d}t}{a(t)} = \int_{\log(a_1)}^{\log(a_2)} \frac{\mathrm{d}\log(a)}{aH} \,. \tag{2.19}$$

From this definition, we derive the *comoving particle horizon* $D(t,0) \propto a^{(1+3w)/2}$ as the maximal distance over which two spatial points at the time t are causally connected in the past. In a radiation- or matter-dominated Universe, light can only propagate a finite distance from the initial time of decoupling. However, if $w < -1/3$, violating the "strong energy condition", then the integral $D(t,0)$ diverges at the lower bound and any two points seem to be causally connected in the past. Solving this problem therefore requires a Universe filled with a fluid that violates the strong energy condition.

Coherent phase problem. The very fact that we observe acoustic peaks in the CMB power spectrum, see Fig. 2.2, implies that all Fourier modes have the *same coherent phase*. This is a problem because on super-horizon scales the phases could not have been "synchronised" by any causal mechanism and their coherence would be a very fine-tuned coincidence. When a density fluctuation mode with physical wavelength λ enters the horizon $\lambda \sim H^{-1}$, it starts oscillating. In general, each Fourier mode could be a linear combination of sine and cosine modes. However, it appears that the observed modes are only excited in the pure cosine mode. At cartoonish level, temperature fluctuations in the CMB reflect density perturbations $\delta T/\bar{T} \sim \delta$ whereas the polarisation measures the divergence of the primordial plasma velocity $E \sim \partial_i v^i$, so that the temperature-polarisation TE cross power spectrum is a measure of $\mathcal{D}_\ell^{TE} \sim \langle \delta \partial_i v^i \rangle$. Let us now specify to the simplest possible model: a single monochromatic (sound) wave

$$\delta(t) = \delta_0 \cos(\omega t + \varphi) \,, \tag{2.20}$$

with a fixed frequency ω, where we have factored out the space dependence. Using the linearised continuity equation $\dot{\delta} + \partial_i \left[(1+\delta)v^i\right] \approx \dot{\delta} + \partial_i v^i = 0$, we obtain the

divergence of the velocity field

$$\partial_i v^i = -\dot{\delta} = \delta_0 \omega \sin(\omega t + \varphi)\,. \tag{2.21}$$

Assuming a uniform distribution for the phase $\varphi \in [0, 2\pi)$, we obtain that the TE cross-correlation vanishes

$$\langle TE \rangle \propto \int_0^{2\pi} \mathrm{d}\varphi \cos(\omega t + \varphi) \sin(\omega t + \varphi) = 0\,. \tag{2.22}$$

This is in contradiction with the observed non-zero power in the TE power spectrum in Fig. 2.3 on large scales $\ell \leq 200$. We conclude that initial super-horizon phases were not random but coherent just before horizon entry. This coherent phase problem strongly suggests the existence of a primordial phase of the Universe, prior to the hot Big Bang, during which perturbations were produced and synchronised.

2.2.2 Slow-Roll Inflation

Postulating a period of inflation solves the aforementioned problems. We now discuss the basics elements of inflationary backgrounds.

Defining inflation. Let us start by defining inflation. In its simplest form, inflation is a period of accelerating expansion $\ddot{a} > 0$. From the second Friedmann equation (2.4), this can be achieved if the Universe is dominated by a form of matter/fluid that violates the strong energy condition $w < -1/3$ (note that if $w \approx -1$, space expands quasi-exponentially). During such a phase, the comoving Hubble radius $(aH)^{-1}$ decreases since

$$\frac{\mathrm{d}}{\mathrm{d}t}(aH)^{-1} = -\frac{\ddot{a}}{\dot{a}^2} < 0\,. \tag{2.23}$$

Therefore, the observable Universe becomes smaller during inflation. This can be taken as a defining property of inflation. An accelerating expansion also implies

$$\epsilon \equiv -\frac{\dot{H}}{H^2} < 1\,. \tag{2.24}$$

The exponential expansion limit is reached for $\epsilon \to 0$, with the critical case $\epsilon = 0$ describing a de Sitter background.

Scalar field cosmology. Inflation would never end if the background was driven by a cosmological constant that would lead to a perfect de Sitter space. Instead, the simplest realistic inflationary scenario involves a scalar field, called the inflaton, that mimics an almost exponential background expansion if its potential is sufficiently flat, as we now review. Consider the inflaton field ϕ minimally coupled to gravity whose action reads

$$S = \int \mathrm{d}^4x\sqrt{-g}\left[\tfrac{1}{2}M_{\rm Pl}^2 R - \tfrac{1}{2}(\partial_\mu\phi)^2 - V(\phi)\right]\,, \tag{2.25}$$

where V is the inflaton potential. In a purely homogeneous background, $\phi = \phi(t)$ is a function of time only. This corresponds to a perfect fluid with energy density and pressure given by

$$\rho = \tfrac{1}{2}\dot{\phi}^2 + V(\phi)\,, \quad P = \tfrac{1}{2}\dot{\phi}^2 - V(\phi)\,. \tag{2.26}$$

Neglecting curvature $k = 0$, the Friedmann equation (2.4) gives

$$H^2 = \frac{1}{3M_{\rm Pl}^2}\left[\tfrac{1}{2}\dot{\phi}^2 + V(\phi)\right]\,. \tag{2.27}$$

Varying the action (2.25) yields the equation of motion

$$\ddot{\phi} + 3H\dot{\phi} + V'(\phi) = 0\,, \tag{2.28}$$

where the prime denotes derivative with respect to ϕ. Differentiating (2.27) with respect to time and using (2.28), we obtain the *slow roll condition* on the inflaton velocity to obtain an almost exponential background expansion

$$\epsilon = \frac{\dot{\phi}^2}{2H^2M_{\rm Pl}^2} \ll 1\,. \tag{2.29}$$

Moreover, in order for inflation to last long enough to solve the Standard Model problems (typically more than 60 e-folds), we also require

$$\eta \equiv \frac{\dot{\epsilon}}{\epsilon H} = 2(\epsilon - \delta) \ll 1\,, \tag{2.30}$$

with $\delta \equiv -\ddot{\phi}/(H\dot{\phi})$.

Slow-roll dynamics. The two conditions (2.29) and (2.30) imply that the potential energy dominates the kinetic energy, $\frac{1}{2}\dot{\phi}^2 \ll V(\phi)$ for a sufficiently long period, so that $w = P/\rho \approx -1$. This results in the inflaton slowly rolling down its potential. In this case, the field acceleration $\ddot{\phi}$ in (2.28) can be neglected and one can give an approximate solution for the inflationary attractor: the potential gradient is approximately balanced by Hubble friction $3H\dot{\phi} \approx -V'(\phi)$. The slow-roll conditions therefore translate into flatness conditions on the inflaton potential $\epsilon_V, |\eta_V| \ll 1$ with

$$\epsilon_V \equiv \frac{M_{\rm Pl}^2}{2}\left(\frac{V'}{V}\right)^2 \approx \epsilon\,, \quad \eta_V \equiv M_{\rm Pl}^2\frac{V''}{V} \approx \epsilon + \delta = 2\epsilon - \eta/2\,. \tag{2.31}$$

In words, both the slope and the curvature of the inflaton potential must be small in Planck units to feature a slow-roll dynamics.

2.2.3 High-Energy Aspects of Inflation

Inflation is a very successful framework to model the dynamics of the early Universe. However, we currently lack a physical origin of the inflationary expansion. Realising a prolonged phase of slow-roll inflation in a fundamental theory (e.g. string theory) presents significant challenges. A key difficulty arises from the condition $|\eta_V| \ll$

1, which implies that the inflaton mass should be much smaller than the Hubble parameter as $V'' \sim m^2 \ll V/M_{\rm Pl}^2 \approx 3H^2 \ll M_{\rm Pl}^2$. This hierarchy raises concerns about the *naturalness* of (single-field) slow-roll inflation. In particular, it questions whether such a small inflaton mass can emerge naturally within a fundamental UV completion.

η problem. In conventional quantum field theory, high-dimensional operators introduce only minor corrections to the leading-order dynamics. These corrections become almost completely negligible if one pushes the UV cutoff all the way to the Planck scale, i.e. IR physics *decouples* from the UV. However, inflation inherently involves dynamical gravity, resulting in an unusual property: the low-energy leading-order inflationary dynamics is highly sensitive to Planck-suppressed physics. In this sense, inflation is *UV sensitive*. We illustrate this with the renormalisation of the slow-roll η_V parameter. Let us consider quite conservatively that the UV physics is encoded in the dimension-6 operator

$$\mathcal{O}_6 = \alpha V_0(\phi)\frac{\phi^2}{\Lambda^2}\,, \tag{2.32}$$

where $\alpha \sim \mathcal{O}(1)$ is an order-one dimensionless constant, V_0 denotes the renormalisable part of the slow-roll inflaton potential, and Λ is a UV cutoff. If the inflaton vacuum expectation value is much smaller than the cutoff, $\langle\phi\rangle \ll \Lambda$, then this operator only gives a small correction to the potential. However, it engenders a significant correction to the inflaton mass as it renormalises the η_V parameter, $\eta_{V,\rm eff} = \eta_V + \Delta\eta_V$ with

$$\Delta\eta_V = 2\alpha\left(\frac{M_{\rm Pl}}{\Lambda}\right)^2 . \tag{2.33}$$

For $\Lambda < M_{\rm Pl}$, $\Delta\eta_V > 1$ and the flatness condition $\eta_V \ll 1$ to maintain a long phase of slow-roll inflation is violated. Note that this holds even if one pushes the UV cutoff to the highest possible scale where physics becomes sensitive to quantum gravity, $\Lambda \to M_{\rm Pl}$, as $\Delta\eta_V \sim 1$.[1] This is also reflected in the inflaton mass, as radiative corrections will tend to drive the inflaton mass towards the cutoff $\Delta m^2 \approx \Lambda^2$. Unless protected by some symmetry (e.g. shift symmetry) or properly embedded in a well-motivated UV completion, slow-roll inflation is fine-tuned, highlighting our limited understanding of the underlying fundamental theory of inflation. Addressing this η *problem* requires studying string theory concrete realisations of inflation, see [2] for a review.

Lyth bound. Another fundamental problem of single-field slow-roll inflation is the large (super-Planckian) excursion of the inflaton in field space $\Delta\phi \gtrsim M_{\rm Pl}$. Indeed, when a field undergoes a displacement larger than the Planck scale, the assumption that the infinite tower of higher-dimensional operators, e.g. (2.32), remains small becomes questionable. Large-field inflationary models introduces uncontrolled quantum gravity corrections, and can lead to strong coupling. Assuming single-field

[1] Although rendering it less severe, supersymmetry is not able to completely solve the η problem.

slow-roll inflation, a lower bound on the inflaton field excursion is given by the *Lyth bound* [41]

$$\frac{\Delta\phi}{M_{\rm Pl}} \gtrsim \sqrt{\frac{r}{0.01}}\,, \tag{2.34}$$

where r is the tensor-to-scalar ratio (see Sec. 2.3 and Sec. 9.3.2), and $\Delta\phi$ is the inflaton displacement in field space from the time when modes that are observable in the CMB exited the horizon to the end of inflation. As such, the level of potentially observable tensor modes is fundamentally tied to the scale of quantum gravity, $M_{\rm Pl}$. This super-Planckian field range to have relatively large tensor modes is challenging to arrange for in specific classes of inflationary models.

To summarise, the UV sensitivity of inflation is both a blessing and a curse. On one hand, it is a formidable challenge as a truly UV-complete theory of inflation requires going beyond single-field slow-roll models and embedding inflation within a consistent framework of quantum gravity, such as string theory. On the other hand, this UV sensitivity makes cosmological observables fundamentally tied to Planck-scale physics. Few areas in physics bring us as close to probing the fundamental nature of quantum gravity in a tangible way.

2.3 Primordial Fluctuations

One of the most remarkable features of inflation is that it naturally provides a mechanism for generating the primordial density fluctuations necessary for cosmic structure formation. The origin of these fluctuations is both profound and disturbing: they arise from *quantum* zero-point fluctuations of the inflaton field which drives the accelerated expansion. In this section, we review how single-field slow-roll inflation produces primordial density perturbations that align perfectly with observations, exhibiting adiabaticity, near scale invariance, and approximate Gaussianity—features reconstructed from the CMB temperature anisotropies. As inflation intrinsically involves dynamical gravity, we will also see that it predicts gravitational waves.

2.3.1 Density Perturbations

Defining perturbations. In a homogeneous classical inflationary background, the inflaton field is space-independent $\phi = \phi(t)$. However, quantum fluctuations inevitably generates inhomogeneities. The inflaton field can then be expressed as

$$\phi(t, \boldsymbol{x}) = \bar{\phi}(t) + \delta\phi(t, \boldsymbol{x})\,, \tag{2.35}$$

where $\bar{\phi}$ is the homogeneous background solution that drives inflation, and $\delta\phi$ is a space-dependent perturbation. Small fluctuations on top of a stable inflationary background imposes $\delta\phi \ll \bar{\phi}$. At the same time, the FLRW spacetime metric acquires as well inhomogeneous perturbations that we parametrise at linear order by $g_{\mu\nu}(t, \boldsymbol{x}) = \bar{g}_{\mu\nu}(t) + \delta g_{\mu\nu}(t, \boldsymbol{x})$ with

$$\delta g_{\mu\nu}(t, \boldsymbol{x}) = -2A\mathrm{d}t^2 + 2aB_i\mathrm{d}x^i\mathrm{d}t + 2a^2E_{ij}\mathrm{d}x^i\mathrm{d}x^j\,, \tag{2.36}$$

where A, B_i and E_{ij} are functions of space and time, and encode 1+3+6 = 10 degrees of freedom. We can use the SVT decomposition to write $E_{ij} = C\delta_{ij}+\partial_i\partial_j E+\partial_{(i}E_{j)}+\gamma_{ij}$ with $\partial_i E_i = 0$ and $\partial_i\gamma_{ij} = \gamma_{ii} = 0$. Since vector perturbations can be eliminated using Einstein constraint equations in a scalar field-dominated Universe, we discard B_i and E_i. The transverse and traceless object γ_{ij} remains invariant under a gauge transformation $x^\mu \to x^\mu + \xi^\mu(t, \boldsymbol{x})$, and describes tensor modes, i.e. gravitational waves. However, both the scalar field and the scalar metric perturbations transform. For example, under a temporal gauge transformation $t \to t + \delta t(t, \boldsymbol{x})$, we have

$$\delta\phi \to \delta\phi - \dot{\bar{\phi}}\,\delta t\,, \quad C \to C - H\delta t\,. \tag{2.37}$$

One can then construct the following scalar gauge invariant combination

$$Q = \delta\phi - \frac{\dot{\bar{\phi}}}{H}C\,, \tag{2.38}$$

which describes the scalar field perturbations in the *spatially-flat gauge* ($C = 0$). In this gauge, this is simply related to the curvature perturbation[2]

$$\zeta \equiv -\frac{H}{\dot{\bar{\phi}}}\delta\phi\,. \tag{2.39}$$

The curvature perturbation ζ fully describes scalar fluctuations in the so-called *comoving* gauge where

$$\delta\phi = 0\,, \quad g_{ij} = a^2 e^{2\zeta}[e^\gamma]_{ij}\,, \quad \partial_i\gamma_{ij} = \gamma_{ii} = 0\,. \tag{2.40}$$

In this gauge, the field ζ can be interpreted as the longitudinal mode of the metric. A very important property of the curvature perturbation ζ is that it is conserved on superhorizon scales $\dot{\zeta}_{\boldsymbol{k}} = 0$ for $k \ll aH$ if the matter perturbations are adiabatic. We therefore describe primordial density perturbations in terms of the field $\zeta(t, \boldsymbol{x})$.

Canonical quantisation. Expanding the action (2.25) to second order, which requires using the ADM formalism and solving for the constraints before explicitly writing the result in terms of gauge-invariant quantities, one obtains the following exact result [42]

$$S = M_{\rm Pl}^2 \int \mathrm{d}t\mathrm{d}^3x a^3\epsilon\left[\dot{\zeta}^2 - \frac{(\partial_i\zeta)^2}{a^2}\right]\,. \tag{2.41}$$

In particular, no slow-roll approximation is required to derive this action. Note that in the pure de Sitter limit $\epsilon = 0$, the action vanishes, meaning that ζ becomes a pure gauge mode and does not correspond to a real physical degree of freedom. Let us now quantise the theory. To this end, we define $z \equiv \sqrt{2\epsilon a^2 M_{\rm Pl}^2}$, and the canonically

[2] There is an unfortunate confusion in the literature. The curvature perturbation on uniform-field hypersurfaces ($\delta\phi = 0$) is defined as $\mathcal{R} \equiv C - \frac{H}{\dot{\bar{\phi}}}\delta\phi$, and the curvature perturbation on uniform density hypersurface ($\rho(\phi) = \rho$) is defined by $\zeta \equiv C - \frac{H}{\dot{\bar{\rho}}}\delta\rho$. In single-field inflation, both quantities become equal on superhorizon scales and we can treat ζ and $\mathcal{R}$ interchangeably.

normalised Mukhanov-Sasaki variable $v \equiv z\zeta$ (in conformal time). The quadratic equation (2.41) then takes the following simple form

$$S = \frac{1}{2}\int \mathrm{d}\tau \mathrm{d}^3x \left[(v')^2 - (\partial_i v)^2 + \frac{z''}{z}v^2\right] , \tag{2.42}$$

from which we obtain the celebrated Mukhanov-Sasaki equation

$$v_{\boldsymbol{k}}'' + \left(k^2 - \frac{z''}{z}\right) v_{\boldsymbol{k}} = 0 , \tag{2.43}$$

which is nothing but a harmonic oscillator with a time-dependent frequency. Note that in a pure de Sitter space, $a(\tau) = -1/(H\tau)$ and $z''/z = a''/a = 2/\tau^2$. The conjugate momentum field is $p_v \equiv \delta S/\delta v' = v'$. We now promote the fields to Heisenberg-picture quantum operators $v(\tau, \boldsymbol{x}) \to \hat{v}(\tau, \boldsymbol{x})$ and $p_v(\tau, \boldsymbol{x}) \to \hat{p}_v(\tau, \boldsymbol{x})$ with[3]

$$\hat{v}(\tau, \boldsymbol{x}) = \int \frac{\mathrm{d}^3k}{(2\pi)^3}\left[v_k(\tau)\hat{a}_{\boldsymbol{k}} + v_k^*(\tau)\hat{a}_{-\boldsymbol{k}}^\dagger\right] e^{i\boldsymbol{k}\cdot\boldsymbol{x}} , \tag{2.44}$$

and similarly for the conjugate momentum, where $v_k(\tau)$ is the mode function that satisfies the classical equation of motion (2.43), and $\hat{a}_{\boldsymbol{k}}$ and $\hat{a}_{\boldsymbol{k}}^\dagger$ are the annihilation and creation operators that satisfy the usual commutation relation

$$[\hat{a}_{\boldsymbol{k}}, \hat{a}_{\boldsymbol{k}'}^\dagger] = (2\pi)^3\delta^{(3)}(\boldsymbol{k} - \boldsymbol{k}') . \tag{2.45}$$

This implies the commutation relation among the field and conjugate momentum operators

$$[\hat{v}(\tau, \boldsymbol{x}), \hat{p}_v(\tau, \boldsymbol{x}')] = i\delta^{(3)}(\boldsymbol{x} - \boldsymbol{x}') , \quad (\hbar \equiv 1) , \tag{2.46}$$

if the mode functions satisfy the Wronskian normalisation condition

$$v_k v_k^{*\prime} - v_k' v_k^* = i . \tag{2.47}$$

Importantly, this condition is valid *at all time* and fixes the amplitude of primordial fluctuations.

Bunch-Davies vacuum. We now need to specify a vacuum state, which is defined as usual by the condition

$$\hat{a}_{\boldsymbol{k}}\,|0\rangle = 0 . \tag{2.48}$$

However, the Hamiltonian is time dependent and in general there is no preferred choice of vacuum, as it depends on the time at which it is defined. In our case, it is natural to define the vacuum state in the infinite past such that all modes of interests are inside the horizon $|k\tau| \gg 1$ where they do not experience the effect of curvature, i.e. Eq. (2.43) becomes that of a simple massless harmonic oscillator with a time-independent frequency. Selecting the positive-frequency mode, we enforce the solution to behave as

$$\lim_{\tau\to-\infty} v_k(\tau) = \frac{e^{-ik\tau}}{\sqrt{2k}} , \tag{2.49}$$

up to an arbitrary phase. This choice of vacuum is known as the Bunch-Davies vacuum.

[3]Note that written in this form the field operator is manifestly Hermitian.

Classical dynamics. In slow-roll inflation, the classical dynamics (2.43) can be solved exactly. To first order in the slow-roll parameters $\epsilon, |\eta| \ll 1$, we have $\frac{z''}{z} \approx \frac{1}{\tau^2}(2 + 3\epsilon + \frac{3}{2}\eta)$. The Mukhanov-Sasaki equation (2.43) becomes

$$v_k'' + \left(k^2 + \frac{\nu^2 - \frac{1}{4}}{\tau^2}\right) v_k = 0\,, \tag{2.50}$$

with $\nu^2 \equiv \frac{9}{4} - 3\epsilon + \frac{3}{2}\eta$. Imposing the Bunch-Davies initial condition, the properly normalised solution is given by (up to an unimportant phase)

$$v_k(\tau) = \frac{\sqrt{\pi}}{2}(-\tau)^{1/2} H_\nu^{(1)}(-k\tau)\,, \tag{2.51}$$

where $H_\nu^{(1)}$ is the Hankel function of the first kind.

Power spectrum. The power spectrum of the Mukhanov-Sasaki variable at time τ reads

$$\langle 0|\hat{v}_{\boldsymbol{k}}\hat{v}_{\boldsymbol{k}'}|0\rangle = (2\pi)^3\delta^{(3)}(\boldsymbol{k} + \boldsymbol{k}')|v_k(\tau)|^2\,. \tag{2.52}$$

Integrating $\epsilon = 1 - \mathcal{H}'/H^2 \approx$ cst, we obtain $\mathcal{H} = -(1+\epsilon)/\tau$, from which we obtain $z(\tau) = z_\star(-k_\star\tau)^{1/2-\nu}$, where $\star$ means evaluated at horizon crossing of the mode of wavenumber $k_\star$, i.e. $\tau_\star = -k_\star^{-1}$. Using the late-time expansion of the Hankel function (dropping the most decaying mode)

$$\lim_{k\tau\to 0} |H_\nu^{(1)}(-k\tau)|^2 = \frac{4^\nu\Gamma(\nu)^2}{\pi^2}(-k\tau)^{-2\nu} \approx \frac{2}{\pi}(-k\tau)^{-2\nu}\,, \tag{2.53}$$

we obtain the dimensionless power spectrum of curvature perturbation

$$\mathcal{P}_\zeta \equiv \frac{k^3}{2\pi^2}P_\zeta = \frac{1}{8\pi^2\epsilon_\star}\left(\frac{H^2}{M_{\rm Pl}^2}\right)_\star\left(\frac{k}{k_\star}\right)^{3-2\nu}\,. \tag{2.54}$$

where we have in passing recovered the conservation of ζ on super-horizon scales as the time dependence has cancelled. The (dimensionless) primordial scalar power spectrum takes a power law form $\mathcal{P}_\zeta = A_s(k/k_\star)^{n_s-1}$ with

$$A_s \equiv \frac{1}{8\pi^2\epsilon_\star}\left(\frac{H^2}{M_{\rm Pl}^2}\right)_\star\,, \quad n_s - 1 \equiv \frac{\mathrm{d}\log\mathcal{P}_\zeta}{\mathrm{d}\log k} = -2\epsilon_\star - \eta_\star\,. \tag{2.55}$$

These two parameters are the ones constrained by observations, see Sec. 2.1.2. The detection of a non-zero red tilt $n_s - 1 \neq 0$, i.e. deviation from perfect scale invariance, is a major hint for slow-roll inflation. Due to the $\epsilon_\star$ factor in the power spectrum amplitude, one cannot fully fix the energy scale of inflation $H_\star$ during inflation with respect to the Planck scale.

2.3.2 Gravitational Waves

Another robust (and model-independent) prediction of inflation is a background of primordial gravitational waves. After the computation of the primordial scalar

power spectrum in the previous section, the one for tensor modes is essentially the same after replacing $z \to z \equiv \frac{1}{2} a M_{\rm Pl}$. This results in the (dimensionless) primordial tensor power spectrum $\mathcal{P}_t = A_t (k/k_\star)^{n_t}$ with

$$A_t \equiv \frac{2}{\pi^2} \left(\frac{H^2}{M_{\rm Pl}^2} \right)_\star , \quad n_t \equiv \frac{\mathrm{d} \log \mathcal{P}_t}{\mathrm{d} \log k} = -2\epsilon_\star , \tag{2.56}$$

where a factor 2 comes from the sum over polarisations. Note that the tensor tilt must still be negative if $\dot{H} \leq 0$, $n_t = 2\dot{H}/H^2 \leq 0$. Contrary to scalar perturbations, the amplitude of tensor modes is a direct measure of the energy scale of inflation. More details can be found in Sec. 9.3.2. In particular, observational constraints are usually phrased in terms of the tensor-to-scalar ratio

$$r \equiv \frac{\mathcal{P}_t}{\mathcal{P}_\zeta} = 16\epsilon_\star . \tag{2.57}$$

Note also that single-field slow-roll inflation implies the following consistency relation between the tensor amplitude and its tilt

$$r = -8 n_t . \tag{2.58}$$

In the presence of a sound speed for scalar perturbations or in multi-field inflationary scenarios, we instead have $r \leq -8 n_t$.

Part I

Physics of Cosmological Correlators

3

Shape of non-Gaussianities

During inflation, as primordial quantum fluctuations were generated and stretched to cosmological scales, they are ultimately imprinted as spatial correlations on the future boundary of inflationary spacetime, marking the beginning of the subsequent hot Big Bang evolution, as represented in Fig. 3.1. These cosmological correlators provide an exciting probe of the physics governing the earliest moments of our Universe, and—for connected n-point correlators with $n \geq 3$—are conventionally called *non-Gaussianities*. Recent years have shown increasing interests in computing these correlators as they ultimately hold the key to high-energy physics.

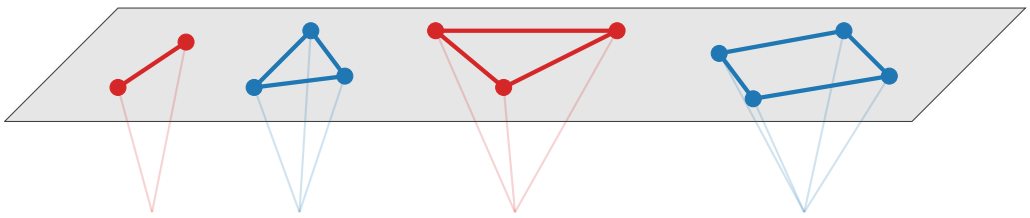


Figure 3.1: Schematic representation of cosmological correlators as spatial correlations of primordial fluctuations at the end of inflation.

In this chapter, we review the basics of phenomenological aspects of cosmological correlators, setting up all the relevant definitions. We primarily focus on the standard shapes of non-Gaussianities and the physical processes they conceal.

3.1 Three-Point Correlators

Fluctuations are defined around a homogeneous background, i.e. they have zero mean. If they follow Gaussian statistics, they must have vanishing (connected) n-point correlation functions for $n \geq 3$. This is the very reason why the first non-trivial

information about deviations from Gaussianity, so-called *non-Gaussianities*, is encoded in the thee-point correlation function, which is also known as the *bispectrum* in Fourier space. The (equal-time) three-point function defines the bispectrum B_ζ as

$$\langle \zeta_{\boldsymbol{k}_1} \zeta_{\boldsymbol{k}_2} \zeta_{\boldsymbol{k}_3} \rangle = (2\pi)^3 \delta^{(3)}(\boldsymbol{k}_1 + \boldsymbol{k}_2 + \boldsymbol{k}_3) B_\zeta(k_1, k_2, k_3)\,, \tag{3.1}$$

where the momentum conserving delta function is a consequence of global homogeneity of space: the wavevectors $\boldsymbol{k}_i$ ($i = 1, 2, 3$) are enforced to close and form a triangle in Fourier space. Global isotropy implies that the only momentum dependency is through rotational invariant contractions involving δ_{ij} and ϵ_{ijk} (and various combinations of their tensor products), which in the case of the bispectrum can be fully expressed in terms of the three magnitudes $k_i = |\boldsymbol{k}_i|$. Note that for a n-point correlator, imposing homogeneity and isotropy implies that correlation functions—after stripping off the momentum conserving delta function—depend on $3n - 6$ variables (with only one variable for $n = 2$).

Shape dependence. Scale dependence is encoded in the size of the triangle, for example in the total perimeter $k_t \equiv k_1 + k_2 + k_3$, or the size of the largest side in Fourier space. For a fixed scale, the triangle can also be deformed: for different *shapes* of triangles, the amplitude of the bispectrum may be very different. In order to investigate these dependencies, it is customary to define the so-called dimensionless bispectrum shape function S as

$$S(k_1, k_2, k_3) \equiv \frac{(k_1 k_2 k_3)^2}{(2\pi)^4 \mathcal{P}_\zeta^2} B_\zeta(k_1, k_2, k_3)\,, \tag{3.2}$$

where $\mathcal{P}_\zeta$ is the dimensionless power spectrum evaluated at a fiducial momentum scale. Without loss of generality, we order the momenta such that $k_3 \leq k_2 \leq k_1$ and fix the largest Fourier mode k_1 by virtue of scale invariance. Therefore, the shape information only depends on the two dimensionless ratios k_2/k_1 and k_3/k_1 that satisfy $0 \leq k_3/k_1 \leq k_2/k_1 \leq 1$ and $k_1 \leq k_2 + k_3$. The second condition follows from the triangle inequality. Before going to the definition of some often-encountered shapes and discuss their physical origins, let us discuss scale dependence.

Scale dependence. Information about the scale dependence of the bispectrum is found by fixing the ratios k_2/k_1 and k_3/k_1 and varying the overall scale k_1 (or equivalently k_t). Although it may be relevant to explore it for arbitrary fixed momentum ratios, it is customary to parameterise the scale-dependence in equilateral triangle configurations via $f_{\rm NL}(k) \equiv S(k, k, k)$.[1] In scenarios of inflation with a slow-varying background, the scale dependence (running) is proportional to logarithmic time derivatives of the background functions, and therefore remains negligible within any small range of k. It is therefore usual to discard the study of the bispectrum scale dependence at the largest cosmological scales and to focus on its shape dependence. Naturally, we will encounter counter-examples to this rule, precisely when

[1] Note that sometimes the definition of $f_{\rm NL}$ comes with an additional factor $\frac{5}{18}$, which is a historical accident. Non-Gaussianities were first defined in terms of the Newtonian potential which is related to ζ by a factor 3/5 during the matter-dominated era.

the inflationary dynamics is disturbed by a feature along the trajectory, introducing a stronger time dependence of the background.

For scale-invariant bispectra, the shape function S is invariant under rescaling of all momenta, and the $f_{\rm NL}$ parameter is constant. It is therefore convenient to extract this parameter from the shape function and define

$$B_\zeta(k_1,k_2,k_3) = f_{\rm NL}\,\frac{S(x_2,x_3)}{(k_1k_2k_3)^2}\,(2\pi)^4\mathcal{P}_\zeta^2\,, \tag{3.3}$$

with $x_{2,3} \equiv k_{2,3}/k_1$ and where the newly defined shape function is normalised to unity in the equilateral configuration $S(1,1) = 1$. In this sense, the $f_{\rm NL}$ parameter measures the amplitude of non-Gaussianity as the overall size of the bispectrum.

3.1.1 Standard Bispectrum Shapes

The bispectrum shape function encodes a lot of information about the physics of inflation. Let us now review the standard shapes, each one corresponding to a specific type of physical processes.

Local shape. The local shape is the one that results from a local definition of non-Gaussianity (in real space), where the primordial curvature perturbation $\zeta(t,\boldsymbol{x})$ can be expressed in terms of a set of Gaussian fluctuations at the exact same location in spacetime. In single-field inflation where the adiabatic perturbation is the unique fluctuating degree of freedom, the local ansatz at first non-trivial order amounts to parametrise non-Gaussianity phenomenologically with a non-linear correction to a Gaussian perturbation ζ_g

$$\zeta(\boldsymbol{x}) = \zeta_g(\boldsymbol{x}) + \frac{3}{5}f_{\rm NL}\left(\zeta_g^2(\boldsymbol{x}) - \left\langle\zeta_g^2(\boldsymbol{x})\right\rangle\right)\,, \tag{3.4}$$

with $f_{\rm NL}$ a dimensionless coefficient parameterising non-linearity. Going to Fourier space, the corresponding bispectrum is found to be

$$B_\zeta(k_1,k_2,k_3) = \frac{6}{5}f_{\rm NL}\left[P_\zeta(k_1)P_\zeta(k_2) + 2\,\text{perms.}\right]\,, \tag{3.5}$$

where we identified at this order $P_\zeta = P_{\zeta_g}$. Neglecting the scale-dependence of the dimensionless power spectra, i.e. assuming $P_\zeta(k) = (2\pi^2/k^3)\mathcal{P}_\zeta$, the shape function normalised to unity in the equilateral configuration is given by [43, 44, 45, 46]

$$S^{\rm loc}(k_1,k_2,k_3) = \frac{1}{3}\left(\frac{k_3^2}{k_1k_2} + 2\,\text{perm.}\right)\,, \tag{3.6}$$

and the corresponding amplitude is given by $f_{\rm NL}^{\rm loc} = \frac{9}{10}f_{\rm NL}$. The dimensionless number $f_{\rm NL}^{\rm loc}$ gives a quantitative measure of how much $\zeta(\boldsymbol{x})$ deviates from the Gaussian variable $\zeta_g(\boldsymbol{x})$. This naturally generalises to any number of Gaussian random fields.

The local shape $S^{\rm loc}$ is typically found in models of inflation with very light scalar fields interacting on super-horizon scales as gradients are suppressed and interactions must happen locally. The local shape also arises as the result of purely gravitational

interactions in single-field slow-roll inflation [42]. However, not only is the overall amplitude small in this case, but it has also been shown that the so-called squeezed limit $k_3/k_1 \to 0$ corresponds to a gauge artifact and should be removed from the predictions for realistic observations, see Sec. 15.4 for further details. Note that the local shape is divergent in the squeezed limit as k_1/k_3. This property makes the local shape an interesting probe of interactions in the primordial universe, through e.g. the scale-dependent bias measured via galaxy surveys [47], see Sec. 3.3. This exciting prospect explains why primordial non-Gaussianities are sometimes oversimplified to the information about a single number, $f_{\rm NL}^{\rm loc}$, although many different shapes may be encountered.

Equilateral shape. The equilateral shape differs sensibly from the local one: it is the largest at configurations of the triangle in Fourier space that are equilateral. The equilateral shape is typically encountered in models that feature derivative interactions, e.g. $\dot\varphi(\partial_i\varphi)^2$ or $\dot\varphi^3$ (see Chap. 9 for more details), which are non-negligible only around horizon crossing of the three modes. Since the field φ self-interacts locally in the bulk of spacetime during inflation, the amplitudes of their wavevectors must be similar $k_1 \sim k_2 \sim k_3$. Specifically, the equilateral shape template that is used in e.g. CMB analysis is [48, 49]

$$S^{\rm eq}(k_1,k_2,k_3) = \left(\frac{k_1}{k_2} + 5\,\text{perm.}\right) - \left(\frac{k_3^2}{k_1k_2} + 2\,\text{perm.}\right) - 2\,. \tag{3.7}$$

Note that it has been defined such that it is always positive. The corresponding dimensionless number $f_{\rm NL}^{\rm eq}$ measures the strength of the equilateral bispectrum.

Flattened shape. The flattened shape corresponds to a signal that is the largest in configurations of the triangle where the three vertices are aligned. It can be found in models of inflation with excited initial quantum states [50], different from the usual Bunch-Davies vacuum. It also arises is scenarios where the speed of sound of the fluctuations effectively takes imaginary values, $c_s^2 < 0$ [51]. The flattened shape (also called folded shape) is defined by

$$S^{\rm flat}(k_1,k_2,k_3) = -S^{\rm eq}(k_1,k_2,k_3) + 1\,. \tag{3.8}$$

The flattened shape $S^{\rm flat}$ therefore vanishes for equilateral configurations, but is of value unity along the flattened ones with $x_3 = 1 - x_2$ (i.e. in folded triangles $k_1 = k_2 + k_3$ where two of the wavevectors become colinear) that saturate the triangle inequality, and always remains positive. Signals of non-Gaussianity in flattened configurations are a way to test the quantum origin of primordial fluctuations (more precisely the initial vacuum state), analogous to a "cosmological Bell-type measurement" [52], as discussed in [53] although already known previously for general initial excited states, see e.g. [50, 54, 55, 56, 57]. Essentially, classical fluctuations, that can be associated to initial excited states with a large occupation number, are a superposition of positive and negative frequency modes. Correlating such states would generate interferences between positive and negative frequency modes that ultimately create poles in the folded limit $k_1 + k_2 \to k_3$. On the contrary, quantum

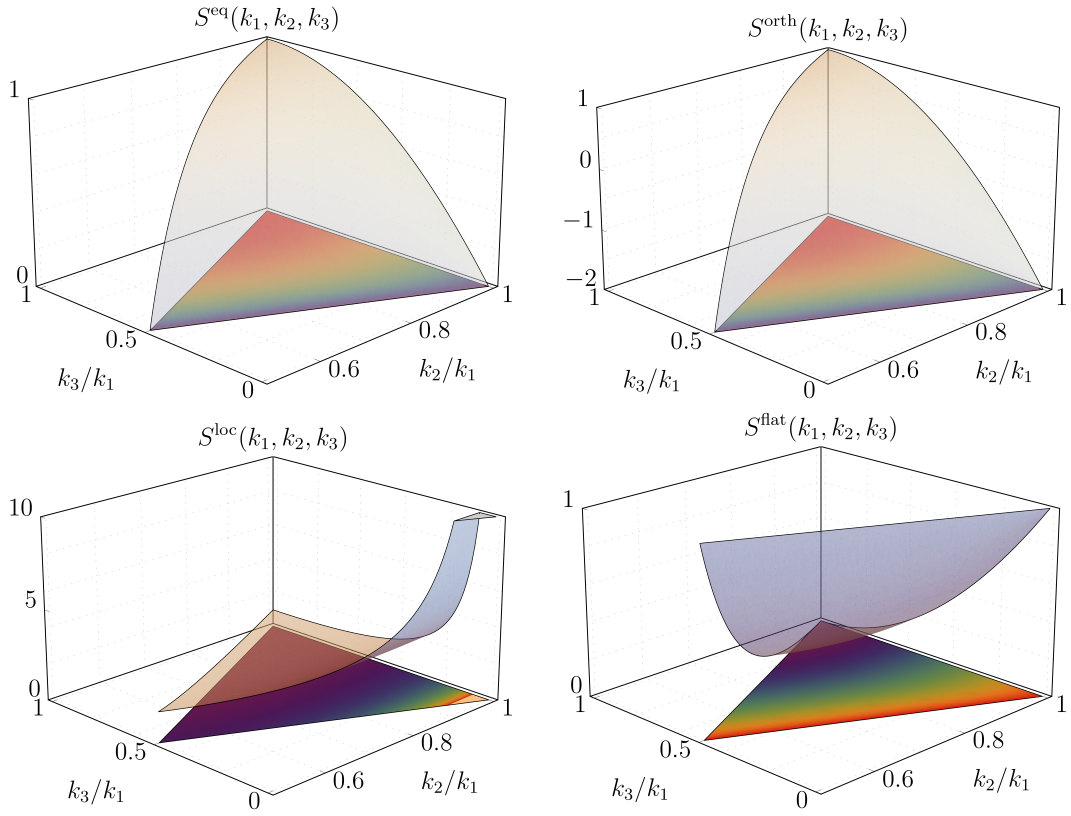


Figure 3.2: The dimensionless shape functions $S(k_1, k_2, k_3)$ for the four standard templates. The equilateral shape (3.7) is normalised to unity in the equilateral configuration ($k_1 = k_2 = k_3$) where it peaks. The orthogonal shape (3.12) also peaks and is normalised to unity in the equilateral configuration, but drops to negative values in flattened kinematic configurations ($k_1 = k_2 + k_3$). The flattened shape (3.8) is a linear combination of the two previous ones and gets most of its amplitude along flattened triangles where it is normalised to unity. The local shape (3.6) diverges as $\propto k_1/k_3$ in the squeezed limit $k_3/k_1 \to 0$ (and $k_2 \to k_1$).

fluctuations set in the Bunch-Davies vacuum do not exhibit such a signal, and the absence of non-Gaussianities in flattened configurations would be a strong hint for initial vacuum fluctuations seeding the later structures in the Universe.

Other shapes. Although the templates that we have defined are often sufficient to describe the bulk of the primordial bispectrum shape, a plethora of different functional dependencies have been found and described, and in particular in the squeezed limit $k_3/k_1 \to 0$. Behaviours in the squeezed limit that are *intermediate* between the ones of the local shape $\propto (k_3/k_1)^{-1}$, and the equilateral shape $\propto k_3/k_1$, have been found in the context of quasi-single-field inflation [58, 59]. The scaling is $\propto (k_3/k_1)^{1/2-\nu}$ where $0 < \nu \equiv \sqrt{9/4 - m^2/H^2} < 3/2$ is a dimensionless measure of the mass of a light ($m < 3H/2$) scalar fluctuation coupled to the adiabatic curvature fluctuation. This result has been later generalised to heavy ($m > 3H/2$) fields which feature oscillations in the squeezed limit $\propto (k_3/k_1)^{1/2\pm i\mu}$ with $\mu \equiv -i\nu > 0$ in this case [60, 61], giving rise to *cosmological collider signals* to which Chap. 4 is dedicated.

3.1.2 Scalar Product of Shapes

Given a theory for the physics in the bulk of spacetime, the bispectrum shape can be computed using the in-in formalism, see Chaps. 5 and 12. In general, computations do not exactly give the standard shapes defined above (or a linear combination of them). This means that the space of all shapes is of infinite dimension and the basis $(S^{\rm loc}, S^{\rm eq}, S^{\rm flat})$ is not complete. Moreover, if the bispectrum is computed numerically, one may not have at hand analytical functions of the momenta to compare with these shapes. Therefore, it is useful to define a measure of how much a bispectrum shape resembles the standard templates. This can be done by defining a scalar product in the space of shapes by [48, 62]

$$\langle S^a, S^b\rangle = \int_0^1 {\rm d}x_2 \int_{1-x_2}^1 {\rm d}x_3\, S^a(1,x_2,x_3)S^b(1,x_2,x_3)\,. \tag{3.9}$$

In order to access how shapes are similar, independently of their amplitude, it is customary to define the cosine (or correlation) between two different shape functions as the normalised scalar product

$$\mathcal{C}(S^a, S^b) = \frac{\langle S^a, S^b\rangle}{\sqrt{\langle S^a, S^a\rangle \langle S^b, S^b\rangle}} \in [-1,1]\,. \tag{3.10}$$

This correlation provides a quantitative measure of how distinguishable two shapes are, i.e. two shapes are highly correlated if $|\mathcal{C}|$ is close to unity. The cosine (3.10) is very simple to compute and allows one to quickly categorise new models of inflation and their degree of independence. This way, a common procedure after computing bispectrum shapes is to compute their correlations with the standard templates to see whether the latter give a relatively accurate description of the physical process. If the newly derived shape is poorly correlated with all the standard templates, this would mean that probing the bispectrum using only the shapes $(S^{\rm loc}, S^{\rm eq}, S^{\rm flat})$ could lead to a biased interpretation of data about the physics active during inflation, i.e. conventional templates would be blind to any new signal. In this case, it is essential to provide an new accurate template.

Orthogonal shape. We will see in Chap. 9 that cubic self-interactions of inflationary fluctuations can be described by the cubic part of the action for the Goldstone boson of broken time diffeomorphims π (to first order in derivatives)

$$S_\pi^{(3)} = \int {\rm d}t{\rm d}^3x a^3\, \frac{\epsilon M_{\rm Pl}^2 H^2}{c_s^2}\,(1-c_s^2)\left[-\dot\pi\frac{(\partial_i\pi)^2}{a^2} + \frac{A}{c_s^2}\dot\pi^3\right]. \tag{3.11}$$

Although there are two cubic operators, only the parameter A is free. This is a consequence of the non-linearly realised time diffeomorphisms, i.e. field operators are related at different orders in perturbation theory. These two operators generate two shapes that are not identical but both close to the equilateral one $S^{\rm eq}$ (they were first computed in [63]). In fact, using the inner product (3.10), it is possible to find a linear combination of the shapes generated by the two operators $\dot\pi(\partial_i\pi)^2$

and $\dot{\pi}^3$ that is orthogonal to $S^{\rm eq}$ (and to the local shape $S^{\rm loc}$). It has been chosen in order to minimise $|\mathcal{C}(S^{\rm eq}, S^{\rm orth})|$. The orthogonal template is [64]

$$S^{\rm orth}(k_1,k_2,k_3) = 3S^{\rm eq}(k_1,k_2,k_3) - 2 = S^{\rm eq}(k_1,k_2,k_3) - 2S^{\rm flat}(k_1,k_2,k_3)\,, \quad (3.12)$$

where $S^{\rm eq}$ is defined in Eq. (3.7), and $S^{\rm flat}$ in Eq. (3.8). Because it is simply a linear combination of the equilateral and flattened shapes, it inherits both of their properties: it is normalised to unity in the equilateral configuration and reaches -2 along flattened ones. In Table 3.1, we list the values of the cosines between the different standard shape templates that we have defined. In Fig. 3.2, we represent them in all physical kinematic configurations.

	$S^{\rm eq}$	$S^{\rm orth}$	$S^{\rm flat}$
$S^{\rm eq}$	1	0.02	0.51
$S^{\rm orth}$		1	−0.85
$S^{\rm flat}$			1

Table 3.1: Cosines $\mathcal{C}(S^a, S^b)$ as defined in Eq. (3.10) between the most commonly used shape templates in data analysis. Note that because $S^{\rm loc}$ formally diverges as (k_1/k_3) in the squeezed limit $k_3/k_1 \to 0$, its modulus in the sense of the inner product (3.9) is log-divergent, and it is not possible to unambiguously define its cosine with other shapes. For this reason, we have excluded it from the table.

3.1.3 Importance of Product-Separable Templates

Let us briefly digress from our main discussion to quickly highlight how non-Gaussianity in the CMB is related to primordial non-Gaussianities. This will illuminate some complications in extracting primordial signals when it comes to actual data analysis. We refer the reader to Sec. 2.1, and to excellent reviews e.g. [65, 66, 67, 68] and standard textbooks e.g. [69, 70] for more details on CMB physics.

The CMB map is a two-dimensional projection of the three-dimensional Universe. Because only modes $\boldsymbol{k}$ that are parallel to the plane of the sky are measured, a specific triangular configuration effectively receives contributions from various other configurations (these are projection effects). Technical details can be found in [71, 72].[2] Since we observe the CMB on the celestial sphere, temperature fluctuations are expanded in spherical harmonics (2.10). The CMB angular bispectrum is the three-point correlation function of the multipole moments $a_{\ell m}$. Assuming rotational invariance, one can define the reduced (angular averaged) bispectrum $B_{\ell_1\ell_2\ell_3}$ as

$$B_{\ell_1\ell_2\ell_3} = \sum_{m_1m_2m_3} \mathcal{G}^{\ell_1\ell_2\ell_3}_{m_1m_2m_3} \left\langle a_{\ell_1m_1} a_{\ell_2m_2} a_{\ell_3m_3} \right\rangle\,, \quad (3.13)$$

where $\mathcal{G}^{\ell_1\ell_2\ell_3}_{m_1m_2m_3}$ is a geometrical factor defined as the integral of three spherical harmonics $Y^{m_i}_{\ell_i}(\hat{\boldsymbol{n}})$ for $i = 1,2,3$ which can be expressed in terms of Wigner-3j

[2] Also see the review [73] for a discussion about gravitational and hydrodynamical non-linearities as an additional source of complexity when trying to extract primordial non-Gaussian signals from temperature anisotropies in the CMB.

symbols. Since fluctuations in the CMB are small, computing the transfer function (encoding the cosmological evolution) using linear theory is accurate. This way, temperature anisotropies are linearly related to curvature perturbations, and one obtains [48, 62]

$$\begin{aligned}\langle a_{\ell_1 m_1} a_{\ell_2 m_2} a_{\ell_3 m_3}\rangle = (4\pi)^3 i^{\ell_1\ell_2\ell_3} \int \frac{\mathrm{d}^3k_1}{(2\pi)^3}\frac{\mathrm{d}^3k_2}{(2\pi)^3}\frac{\mathrm{d}^3k_3}{(2\pi)^3}\,\langle \zeta_{\boldsymbol{k}_1}\zeta_{\boldsymbol{k}_2}\zeta_{\boldsymbol{k}_3}\rangle \\ \times \Delta^T_{\ell_1}(k_1)\Delta^T_{\ell_1}(k_2)\Delta^T_{\ell_1}(k_3)\, Y^{m_1}_{\ell_1}(\hat{\boldsymbol{k}}_1) Y^{m_2}_{\ell_2}(\hat{\boldsymbol{k}}_2) Y^{m_3}_{\ell_3}(\hat{\boldsymbol{k}}_3)\,,\end{aligned} \tag{3.14}$$

where $\Delta^T_\ell(k)$ is the transfer function. It is a standard procedure to rewrite the delta function enforcing momentum conservation in its integral form. After performing a plane-wave expansion on the introduced exponentials, the integral over the angular part factorises and can be computed independently. Still, the numerical evaluation of Eq. (3.14) is very challenging as both the spherical Bessel functions (from the plane-wave expansion) and the transfer functions are rapidly oscillating.

Separable templates. Inspecting Eq. (3.14), one sees that, except an additional integral that has been introduced to deal with the momentum conserving delta function, the CMB bispectrum requires performing three integrals on k_i (recall that the angular part has been factorised out). However, except the generic primordial bispectrum $B_\zeta(k_1, k_2, k_3)$ (or equivalently its shape), the three integrals on k_i are separable. Therefore, the computational complexity is drastically reduced if the shape templates are product separable, in the sense of a (sum of) product of functions of momentum variables. Usually, the derived shapes from actual computations lack this property, compromising factorisation. To address this issue, it is customary to introduce an additional integral layer to make the shapes product separable. In [74], shapes that exhibit poles in $k_1 + k_2 + k_3$ are made product separable by introducing a Schwinger parameter

$$\frac{1}{(k_1+k_2+k_3)^n} = \frac{1}{\Gamma(n)}\int_0^\infty \mathrm{d}x\, x^{n-1} e^{-(k_1+k_2+k_3)x}\,. \tag{3.15}$$

This generalises to arbitrary number of external momenta. In Sec. 11.2, we will present a novel trick involving introducing a Mellin parameter to factorise a non-trivial pole structure.

3.2 Higher-Order, Mixed & Graviton Correlators

In this section, we extend our previous discussion to higher-order correlation functions, mixed ones between scalar and tensor perturbations, and tensor non-Gaussianities. In particular, we will discuss potential parity violation in the sky, which will be further explored in detail in Chap. 11.

3.2.1 Standard Trispectrum Shapes

Although the bispectrum is the most straightforward indication of primordial non-Gaussianity, it sometimes proves interesting to also look at higher-order connected

correlation functions of ζ. The first of these is the connected four-point function, i.e. the trispectrum T_ζ in Fourier space

$$\langle \zeta_{\boldsymbol{k}_1} \zeta_{\boldsymbol{k}_2} \zeta_{\boldsymbol{k}_3} \zeta_{\boldsymbol{k}_4} \rangle = (2\pi)^3 \delta^{(3)}(\boldsymbol{k}_1 + \boldsymbol{k}_2 + \boldsymbol{k}_3 + \boldsymbol{k}_4) T_\zeta(\boldsymbol{k}_1, \boldsymbol{k}_2, \boldsymbol{k}_3, \boldsymbol{k}_4) \,. \tag{3.16}$$

The functional dependence of the trispectrum on the momenta is richer than for the bispectrum, because there are many ways to form a quadrangle in the three-dimensional Fourier space (for example it can be non-planar). The kinematic configuration of this object can be parameterised with the lengths of the four sides, $k_i \equiv |\boldsymbol{k}_i|$, as well as the lengths of the two diagonals, $k_{12} = |\boldsymbol{k}_1 + \boldsymbol{k}_2|$ and $k_{23} = |\boldsymbol{k}_2 + \boldsymbol{k}_3|$. For this reason, it is complex to visualise and represent the trispectrum in all configuration with a single figure, and one needs to resort to particular cases, e.g. fixing some momentum lengths or angles.

Local trispectrum. Single-field local non-Gaussianities at next-to-leading order can be parameterised as[3]

$$\zeta(\boldsymbol{x}) = \zeta_g(\boldsymbol{x}) + \frac{3}{5} f_{\rm NL} \left(\zeta_g^2(\boldsymbol{x}) - \langle \zeta_g^2(\boldsymbol{x}) \rangle \right) + \frac{9}{25} g_{\rm NL} \zeta_g^3(\boldsymbol{x}) \,, \tag{3.17}$$

from which one finds the local trispectrum

$$\begin{aligned} T_\zeta^{\rm loc} &= \tau_{\rm NL}^{\rm loc} \left[P_\zeta(k_{12}) P_\zeta(k_2) P_\zeta(k_3) + 11 \,\text{perms.} \right] \\ &\quad + \frac{54}{25} g_{\rm NL}^{\rm loc} \left[P_\zeta(k_1) P_\zeta(k_3) P_\zeta(k_3) + 3 \,\text{perms} \right] \,, \end{aligned} \tag{3.18}$$

with $\tau_{\rm NL}^{\rm loc} = \left(\frac{6}{5} f_{\rm NL}\right)^2$ and $g_{\rm NL}^{\rm loc} = g_{\rm NL}$. The $g_{\rm NL}^{\rm loc}$ parameter intuitively corresponds to "contact" interactions and is related to intrinsic cubic non-linearities, i.e. the third term in Eq. (3.17), while $\tau_{\rm NL}^{\rm loc}$ intuitively corresponds to "exchange" interactions and is related to second-order non-linearities. This generalises to any number of fields where $\tau_{\rm NL}^{\rm loc}$ is bounded from below by the amplitude of the local bispectrum via the Suyama-Yamaguchi inequality [75]

$$\tau_{\rm NL}^{\rm loc} \geq \left(\frac{6}{5} f_{\rm NL} \right)^2 \,. \tag{3.19}$$

Physically, this inequality puts a bound on the four-point function in terms of the squeezed limit of the three-point function. A geometric proof (which is nothing but the Cauchy-Schwarz inequality) is presented in [76] after the observation that individual loop diagrams can violate the inequality in [77] (see also [78] for a separate Universe approach derivation). The inequality (3.19) appears to be a specific case of more general consistency relations, as shown in [79].

Other standard trispectra. Similar to equilateral bispectra, in models of inflation featuring derivative contact interactions, we again expect most of the signal to be produced around horizon crossing, and therefore the trispectrum to peak in

[3] Note that we do not need to subtract $\langle \zeta_g^3(\boldsymbol{x}) \rangle$ in the last contribution simply because this quantity vanishes for the field ζ_g following Gaussian statistics.

"equilateralish" configurations for which all k_i are equal. The explicit (although lengthy) trispectrum in single-field inflation at leading-order in derivatives can be found in [80]. This calculation has been previously performed in [81] for the contact trispectrum coming from the interaction $\dot{\varphi}^4$, and lately in [82]. The trispectrum from generic slow-roll inflation was computed in [83], and that from a graviton exchange was computed in [84] where the authors have shown that its amplitude is of order the tensor-to-scalar ratio. A detailed analysis of the trispectrum shapes can be found in [85] for single-field DBI inflation, in [86, 87] for multi-field DBI inflation, and in [88, 89] for ghost inflation. We also refer to [90, 91, 92, 93, 94] for related works. Finding generic templates is challenging, often leading to trispectrum shape analyses being conducted on a case-by-case approach basis.

Higher-order correlation functions. Non-Gaussianities may also exist in the form of non-vanishing higher-order connected correlation functions. Then, it is very rare to explore the many-dimensional space of possible shapes, and it is most often customary to quote a single number $f_{\rm NL}^{(n)}$ measuring the typical size of such connected n-point function. Mostly for technical reasons and because they are even more suppressed than the trispectrum (and in practice unobservable), higher-order correlators have received limited attention in the literature. A notable exception is in the context of resonant non-Gaussianities where all n-point correlators have been computed in [95]. Such calculations were made possible because gravitational interactions among the perturbations can in this case be neglected, and because interactions are contact-like and weak.

3.2.2 Parity-Violating Trispectra

Parity involves a transformation that changes the algebraic sign of spatial coordinates $\boldsymbol{x} \to -\boldsymbol{x}$. In the cosmological context, it is natural to ask the question of which observables are sensitive to a violation of parity, i.e. which observables might be different when looking at their mirrored image. Though parity violation can be revealed in the tensor sector already at the level of the power spectrum (if each graviton helicity exhibits different power), the lowest-order correlator in the scalar sector that is sensitive to parity is the trispectrum. The reason is the following. Real fields are Hermitian operators in position space, i.e. $\varphi^\dagger(\boldsymbol{x}) = \varphi(\boldsymbol{x})$. In Fourier space, this implies that the Hermitian conjugation operation amounts to flipping the momentum sign, $\varphi^\dagger_{\boldsymbol{k}} = \varphi_{-\boldsymbol{k}}$. Naturally, the two-point function is unchanged after a parity transformation as it only depends on the momentum magnitude. For the bispectrum, one would notice that physical configurations are always planar so that its mirrored image is related to itself via a rotation. Therefore, the lowest-order scalar correlation function sensitive to chirality is the trispectrum, at least in *non-planar configurations*. Parity violation in the trispectrum manifests itself as a parity-odd imaginary component.

Signal of new exotic physics. It is known that parity is not a symmetry in particle physics (e.g. in the weak interactions [96, 97]). Because the observed cosmological structures were seeded by microscopic quantum fluctuations during inflation, it is

natural to ask whether parity is a symmetry on cosmological scales, see [98] where this question was initially pointed out. In fact, recent observations of the CMB birefringence [99, 100] and indications of parity-violation in the LSS [101, 102] (although not clear yet whether such signals are of primordial origin, see e.g. [103, 104, 105]) seem to suggest that parity violation is indeed possible on cosmological scales. On the theory side, parity violation is forbidden in tree-level correlation functions for vanilla single-field inflation assuming scale-invariance, linear dispersion relation for the fluctuations, Bunch-Davies initial conditions and local interactions [106, 107]. Therefore, detecting a parity-violating primordial trispectrum would signal non-standard physics active during inflation.

Parity violation during inflation. Let us now guide the reader through some of the theories leading to a parity-violating trispectrum that have been considered in the literature. First, such a trispectrum is generated in models where the inflaton field couples to a $U(1)$ gauge field via an $f(\phi)(F^2 + F\tilde{F})$ interaction [108, 109], see [110] for the corresponding CMB data analysis. Second, parity violation is generated when Chern-Simons gravity is considered, i.e. when $\phi R\tilde{R}$ is added to the standard action for the inflaton minimally coupled to gravity [111]. Thirdly, a parity-violating trispectrum can in principle arise from the exchange of massive spinning particles coupled to scalar fluctuations through parity-odd cubic interactions (e.g. $\epsilon_{ijk}\partial_i\partial_l\varphi\partial_j\partial_l\dot{\varphi}\sigma^k$ cubic interactions with ϵ_{ijk} the antisymetric Levi-Civita tensor), although the overall amplitude is expected to be small [107]. Contrarily, a large parity-odd trispectrum can be generated from the exchange of massive spinning fields with chemical potential but parity-preserving cubic interactions. In this case, the source of parity violation is entirely in the additional sector and only transferred to the scalar sector through less-suppressed interactions, and the drastic enhancement of such signals is observed when the curvature perturbation has reduced speed of sound. This will be presented in detail in Chap. 11. More generally, it has been pointed out in [112] that the parity-odd part of exchange trispectra can always be written in a factorised form, therefore simplifying practical calculations. Lastly, of course, relaxing any of the assumptions of the previously mentioned no-go theorem for vanilla single-field inflation can lead to parity violation, as discussed in [107].

3.2.3 Mixed Scalar-Tensor & Graviton Correlators

Although the main focus of this chapter is on non-Gaussianities in the scalar sector, correlations between scalar and tensor modes (the transverse dynamical part of the metric γ_{ij}) as well as among purely tensor modes are also generically expected to be produced, which constitute an additional source of primordial non-Gaussianities.

Mixed correlators. Bispectra mixing ζ and γ are defined by (see Sec. 9.3 for more details on tensor mode decomposition)

$$\begin{aligned}\sum_{\lambda}\langle\zeta_{\boldsymbol{k}_1}\zeta_{\boldsymbol{k}_2}\gamma^{\lambda}_{\boldsymbol{k}_3}\rangle &= (2\pi)^3\delta^{(3)}(\boldsymbol{k}_1+\boldsymbol{k}_2+\boldsymbol{k}_3)B_{\zeta\zeta\gamma}(k_1,k_2,k_3)\,,\\ \sum_{\lambda\lambda'}\langle\zeta_{\boldsymbol{k}_1}\gamma^{\lambda}_{\boldsymbol{k}_2}\gamma^{\lambda'}_{\boldsymbol{k}_3}\rangle &= (2\pi)^3\delta^{(3)}(\boldsymbol{k}_1+\boldsymbol{k}_2+\boldsymbol{k}_3)B_{\zeta\gamma\gamma}(k_1,k_2,k_3)\,.\end{aligned} \tag{3.20}$$

The minimal amount of mixed non-Gaussianities has been first reported in [42] where it was shown that they are slow-roll suppressed, e.g. $f_{\rm NL}^{\gamma\zeta\zeta} \sim \sqrt{r}$. The full bispectra mixing scalar and tensor fluctuations in the general single-field inflation model (equivalent to including higher-derivative interactions for perturbations) have been then computed [113, 114] (also see [115]). The shape of tensor-scalar-scalar mixed correlator (in particular its soft limit) resulting from an exchange process was studied in [116] where the authors have shown that its overall amplitude can be significantly larger than mixed bispectrum expected in slow-roll inflation. Constraints on $f_{\rm NL}^{\gamma\zeta\zeta}$ from B and T modes of the CMB are discussed in [117]. Large mixed bispectra have also been reported when the inflaton is coupled to a vector field [118], for general initial conditions for perturbations [119], in the context of axion monodromy models [120], and solid inflation [121]. We also refer to [122, 123, 124, 125, 126] for parity-violating mixed correlators.

Graviton non-Gaussianities. The graviton bispectrum is defined as

$$\sum_{\lambda\lambda'\lambda''} \langle \gamma^{\lambda}_{\boldsymbol{k}_1} \gamma^{\lambda'}_{\boldsymbol{k}_2} \gamma^{\lambda''}_{\boldsymbol{k}_3} \rangle = (2\pi)^3 \delta^{(3)}(\boldsymbol{k}_1 + \boldsymbol{k}_2 + \boldsymbol{k}_3) B_{\gamma\gamma\gamma}(k_1, k_2, k_3)\,. \tag{3.21}$$

This bispectrum was first computed in [42] in single-field slow-roll inflation. In [127], the use of de Sitter isometries (and notably conformal invariance on the infinite future boundary) has enabled the authors to restrict the graviton bispectrum to only three possible shapes, for standard Einstein gravity, the interactions W^3 and $W^2\tilde{W}$ where W is the Weyl tensor. There, a spinor helicity formalism was introduced to deal with the algebra involving polarisation tensors. See [128] for the CMB analysis using temperature and polarisation modes of these tensor bispectra (also see [129, 130, 131]). Tensor primordial non-Gaussianities are also typically found in multi-field scenarios with additional spinning degrees of freedom, like in axion-gauge fields models [132, 133, 134, 135]. In particular, when considering bispectra of individual helicity modes $B^{\lambda\lambda'\lambda''}_{\gamma\gamma\gamma}$ of the three graviton modes, one has $B^{+++}_{\gamma\gamma\gamma} \gg B^{++-}_{\gamma\gamma\gamma}, B^{+--}_{\zeta\zeta\zeta}, B^{---}_{\gamma\gamma\gamma}$. This is a consequence of the + graviton helicity mode being enhanced in this model. Its shape, e.g. used in Planck analysis [72], is of equilateral form

$$B^{+++}_{\gamma\gamma\gamma}(\boldsymbol{k}_1, \boldsymbol{k}_2, \boldsymbol{k}_3) = f_{\rm NL}^{\rm tens}\, \epsilon^{+*}_{ij}(\hat{\boldsymbol{k}}_1)\epsilon^{+*}_{jk}(\hat{\boldsymbol{k}}_2)\epsilon^{+*}_{ki}(\hat{\boldsymbol{k}}_3)\, \frac{(2\pi)^4 \mathcal{P}_\zeta}{(k_1k_2k_3)^2}\, S^{\rm eq}(k_1, k_2, k_3)\,, \tag{3.22}$$

where $S^{\rm eq}$ is defined in Eq. (3.7). See Sec. 9.3 for the definition of polarisation tensors. Such bispectrum being parity-violating (see [136]), the induced CMB bispectra have non-vanishing signal for not only the even but also the odd $\ell_1+\ell_2+\ell_3$ triplets. The best constraint is $f_{\rm NL}^{\rm tens} = (0\pm13)\times10^2$ (68% CL) [72] and no parity violation has been detected through this channel [137]. On the theory side, constraining the form of three-point correlators (and in particular the tensor bispectrum) using holographic methods or using conformal Ward identities can be found in [138, 139, 140, 141]. More recently, graviton non-Gaussianities have been reconsidered in [142, 143]. The inflationary graviton trispectrum was computed in [144, 145, 146].

3.3 Observational Constraints & Prospects

Primordial non-Gaussianities have not yet been detected for the simple reason that they are small. Their reliable detection would imply carefully removing sources of noise and an accurate description of late-time non-linear physics (e.g. weak gravitational lensing and galactic foregrounds). Another intrinsic limitation for detecting primordial non-Gaussianities is cosmic variance, i.e. the limited number of observed modes in the sky. In what follows, we briefly review observational constraints from CMB measurements, LSS surveys, and the galaxy scale-dependent bias, as well as give prospects. More details can be found in the review [73] and the references therein. This section will find its counter-part in Chap. 4.

From CMB. The most refined and robust constraints on the maximal amount of primordial non-Gaussianities come from the study of CMB temperature and polarisation anisotropies, as surveyed by the latest Planck satellite [137]. In Table 3.2, we list the central values and uncertainties at 1σ of the dimensionless parameters $f_{\rm NL}$ and $g_{\rm NL}$.

$f_{\rm NL}^{\rm loc}$	$f_{\rm NL}^{\rm eq}$	$f_{\rm NL}^{\rm orth}$	$g_{\rm NL}^{\rm loc}$
-0.9 ± 5.1	-26 ± 47	-38 ± 24	$(-5.8 \pm 6.5)\, 10^4$

Table 3.2: Observational constraints (68% CL, statistical) on scalar and tensor primordial non-Gaussianities from Planck [137].

However, little room is left for further improvements with the CMB because of its two-dimensional nature, as the number of available modes cannot be significantly increased. The search for primordial non-Gaussianities through bispectrum shape templates (having the parameters $f_{\rm NL}$ parameters to be constrained for a given shape) is made with several independent estimators, e.g. KSW, modal and binned bispectrum estimators, see [72, 147] for technical details. Current constraints are expected to be improved to reach $f_{\rm NL}^{\rm loc} \sim \mathcal{O}(1)$ whereas such level of precision is out of reach for equilateral-type non-Gaussianities. We refer the reader to [148] for recent CMB-S4 forecasts. First constraints on non-Gaussianities mixing scalar and tensor sectors can be found in [149] using WMAP data. Recent progress has been made using CMB B modes [150]. Despite the fact that constraining the primordial trispectrum is computationally much more involved than the bispectrum, recent progress in this direction are reported in [151, 152].

From LSS. A promising probe for primordial non-Gaussianities lies in the late-time structure formation. A considerable advantage that gives bright prospects is that LSS surveys explore a three-dimensional volume, as opposed to the CMB two-dimensional map, which in practice allows us to observe more modes. This increase in the number of available modes would lead to tighter constraints on primordial non-Gaussianities. However, several challenges are still on the way. First, gravity leading to structure formation is intrinsically non-linear, rendering complex the task to extract the statistics of primordial fluctuations. Second, luminous objects like

galaxies are biased and therefore non-linear tracers of the dark matter distribution. In addition to mapping statistical distribution of galaxies through spectroscopic and photometric surveys, line intensity mapping methods [153, 154, 155] (in particular for 21cm surveys, see e.g. [156]) would allow to chart LSS over a wider range of scales and redshifts. Recent progress in modeling gravitational non-linearities have been reported in [157, 158, 159], which enabled to put the constrains $f_{\rm NL}^{\rm eq,\ orth} \sim \mathcal{O}(100)$ from the measurement of the galaxy bispectrum of BOSS DR12 data [160]. Searching for primordial non-Gaussianities directly at the map-level (and not in Fourier space) would enable one to disentangle effects that are non-local in space (precisely primordial non-Gaussianities) from local processes (late-time non-Gaussianities) [161]. Upcoming spectroscopic surveys like DESI [162] and Euclid [163] are expected to provide an order-one constraint on $f_{\rm NL}^{\rm loc}$, with the SPHEREx [164] survey helping pushing down the constraints. In the long run, 21cm or mm-wavelengths surveys are expected to improve constraints from galaxy surveys [165, 166, 167, 168].

From scale-dependent bias. Local-type primordial non-Gaussianities have the unique feature that they can be probed directly at the level of the two-point statistics of galaxies, through the scale-dependent bias, see [40, 169] for reviews, and Chap. 2 for a short summary. In short, primordial non-Gaussianities that feature enhanced short/long mode correlations result in an enhancement of the galaxy power spectrum on large scales [47, 170, 171], see also e.g. [172, 173, 174, 175, 176, 177] (note that this enhancement can all the same be a suppression, depending on the sign of $f_{\rm NL}^{\rm loc}$). This signature allowed to put constraints on primordial features that are stronger than CMB ones [178] using BOSS data [179]. Results from the eBOSS collaboration [180, 181] have given the strongest constraints on local non-Gaussianities so far, but still less competitive than those from Planck data. Intermediate shapes interpolating between local and equilateral, encoding the exchange of massive (but still light compared to the Hubble scale) during inflation, have been recently considered in [182], also see [183].

4

Cosmological Collider Physics

Massive particles produced during inflation leave specific signatures in soft limits of correlation functions of primordial fluctuations. This novel discovery channel to fundamental physics has been dubbed "cosmological collider physics". In a nutshell, due to the time-dependent inflationary background, massive particles of order the Hubble scale during inflation could have been produced. The breaking of time translation invariance implies that the energy of a quantum field is not conserved, allowing for particles to be created in pairs, analogous to a "gravitational Schwinger effect". The subsequent decay of these particles into inflaton fluctuations leads to potentially observable imprints on cosmological correlators. Cosmological collider physics is about how the propagation of additional particles from their production to their decay (and therefore their presence) is encoded in correlators. As modes of different wavelength freeze or decay at different times, the corresponding time scales are translated into kinematic configurations of late-time correlators, as represented in Fig. 9.1. Thus, a long-enough on-shell propagation of massive particles to leave distinctive signatures requires probing a large hierarchy of scales.

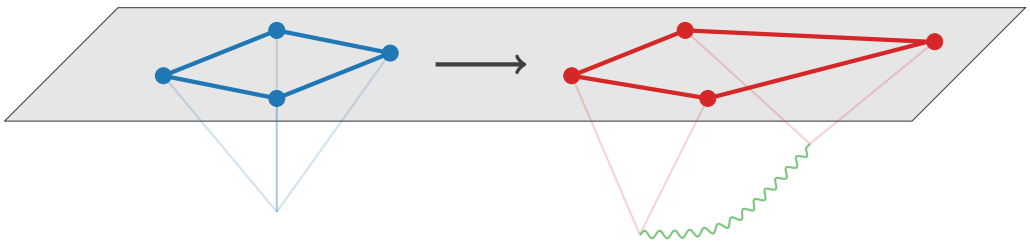


Figure 4.1: Schematic representation of physical processes giving rise to cosmological collider signals. These lie in soft kinematic configurations of cosmological correlators and indicate the presence and the propagation of an additional particle during inflation.

In this chapter, we begin by reviewing the phenomenon of spontaneous particle creation during inflation, with the massive scalar field in de Sitter as a primary illustrative example. Notably, we introduce the Stokes-line method that allows one to retrieve the entire particle production history without fully solving the particle on-shell propagation. This method will be thoroughly used in Chap. 8. Then, we explicitly show how the propagation of produced particles is encoded in soft limits of cosmological correlators and discuss observational prospects for these cosmological collider signals. Finally, we provide the reader with a review of works studying the phenomenology of cosmological collider signals.

4.1 Spontaneous Particle Production

We begin with a general discussion on the dynamics of free massive scalar fields during inflation, emphasising their spontaneous particle production due to the accelerated expansion. We will see that many features, such as their momentum scalings and Boltzmann suppression in the simplest case, are ultimately imprinted in late-time correlations of inflationary fluctuations.

4.1.1 Massive Field in de Sitter

Consider a free massive scalar field $\sigma(t,\boldsymbol{x})$ in a fixed de Sitter background. Using conformal time τ defined by $\mathrm{d}\tau = \mathrm{d}t/a$, setting $a(\tau) = -(H\tau)^{-1}$ and introducing the auxiliary Mukhanov-Sasaki field $\chi(\tau,\boldsymbol{x}) = a(\tau)\,\sigma(\tau,\boldsymbol{x})$, each Fourier mode $\chi_{\boldsymbol{k}}$ satisfies the following equation

$$\chi_{\boldsymbol{k}}'' + \omega_k^2(\tau)\chi_{\boldsymbol{k}} = 0\,, \quad \text{with} \quad \omega_k^2(\tau) = k^2 + \frac{m^2/H^2 - 2}{\tau^2}\,, \tag{4.1}$$

where a prime denotes derivative with respect to conformal time. Before explicitly solving this equation, we briefly comment on some limiting behaviours of the solutions.

- In the deep past, when the modes of interest have wavelengths smaller than the comoving mass-shell horizon $|k\tau| \gg m/H$,[1] we can drop the mass term and the equation boils down to a simple harmonic oscillator. Note that for the specific case of a conformally coupled field $m^2 = 2H^2$, one recovers the same equation satisfied by a massless scalar field in flat space. Therefore, the solutions are well described by plane-waves $\chi_{\boldsymbol{k}} \sim e^{\pm ik\tau}$.

- At late times, we can drop the gradient term and the time dependence of the massive field $\sigma = \chi/a$ is given by two power-law solutions $\sigma_{\boldsymbol{k}} \sim \tau^{\Delta_+}\mathcal{O}_{\boldsymbol{k}}^+ + \tau^{\Delta_-}\mathcal{O}_{\boldsymbol{k}}^-$ with

$$\Delta_\pm = \frac{3}{2} \pm \nu\,, \quad \text{with} \quad \nu = \sqrt{\frac{9}{4} - \frac{m^2}{H^2}}\,. \tag{4.2}$$

[1] For a heavy field $m/H \gg 1$, a mode first crosses its mass-shell horizon before crossing the Hubble horizon.

In the context of a holographic description of cosmology [184, 185, 186, 187, 188, 189, 127, 190, 191, 192, 139, 193, 194, 140, 195, 196, 197, 198], where the role de Sitter isometries prevail, the parameters $\Delta_\pm$ are referred to as the scaling dimensions of the field σ and $\mathcal{O}^\pm$ are three-dimensional boundary operators on the space-like hypersurface $\tau = 0$. For a light field $m/H < 3/2$, the solution decays following a power-law behaviour. When the field is heavy $m/H > 3/2$, the parameter ν becomes imaginary and it is customary to define $\nu = i\mu$. The field therefore decays as $\sim \tau^{3/2}$ while oscillating at a frequency set by the mass.[2]

After canonically quantising the field and imposing Bunch-Davies initial conditions, the exact solution to the equation of motion (4.1) is known and is famously given by a Hankel function, see App. A for more details. Note that for a heavy field, the *a priori* unimportant phase $e^{i\pi(1/4+\nu/2)}$ gives a mass-dependent amplitude $e^{-\pi\mu/2}$. We will discuss its interpretation in the following development and see that this exponential suppression plays an important role in cosmological collider physics.

Quasi-normal modes. Let us focus on the case $\mu > 0$. With the exact solution at hand, it is instructive to expand the massive field mode function in powers of $\tau^{\Delta_\pm}$ at late times that correspond to quasi-normal modes in the static patch of de Sitter spacetime [200, 201]

$$u_k(\tau) = \frac{H}{\sqrt{k^3}} \sum_{n=0}^{\infty} \sum_{\pm} c_n^\pm(\mu) \left(\frac{-k\tau}{2}\right)^{\frac{3}{2}+2n\pm i\mu} , \tag{4.3}$$

with

$$c_n^\pm(\mu) \equiv \pm \frac{(-1)^n}{n!} \frac{\sqrt{2\pi}}{\Gamma(n+1\pm i\mu)} \frac{e^{\pm\pi\mu/2}}{\sinh \pi\mu} . \tag{4.4}$$

The quasi-normal modes correspond to $e^{-\omega_n^\pm t}$ with frequencies $\omega_n^\pm/H = \frac{3}{2} + 2n \pm i\mu$. The factor 3/2 in the real part of $\omega_n^\pm$ reflects the dilution of the mode due to the expansion of the Universe. The imaginary part of $\omega_n^\pm$ represents the positive and negative frequency oscillation of massive states. For a light field, the frequency $\omega_n^\pm$ is real, and the negative frequency is the dominant contribution, i.e. that decays less quickly. As we will see in what follows, starting from an initial Bunch-Davies vacuum, the field develops a positive/negative-frequency mixing. This phenomenon is attributed to spontaneous particle production [202, 203, 204]. For the case of massless curvature perturbations, it is important to stress that there is no particle production during inflation. Essentially, these fluctuations, initialised in the Bunch-Davies vacuum, are only transported to the end of inflation. Therefore, there is a clear distinction between spontaneous production of massive particles, that decay on super-horizon scales for large enough masses, and fluctuations generated from vacuum fluctuations, that leave their imprints in the late-time cosmological structures.

[2] In de Sitter space, particles transform under irreducible unitary representations of the de Sitter isometry group $SO(1,4)$. The denoted light and heavy cases correspond to the *complementary* and *principal* series, respectively. There is a particular case when $m/H = 3/2$ for which the scalar representation falls into the *discrete* series, see e.g. [199] for more details.

4.1.2 Production of Particles

We now consider the gravitational particle production of these massive fields. Intuitively, a quantum field in a time-dependent gravitational background—as it is the case during inflation—gives rise to an interaction allowing energy to be transferred from the background to the field, which in turn can manifest as the phenomenon of spontaneous particle creation from an initial vacuum. To describe and measure this production, the main observable is the average particle number seen by an observer at later times, usually formalised in terms of Bogolyubov transformations. We refer to the reference textbooks [205, 206] for more details on the topic. More generally, starting from an initial positive-frequency solution, systems described by the equation of a harmonic oscillator with a *time-dependent frequency* experience the emergence of negative-frequency solutions over time. This mixing between positive and negative-frequency solutions is attributed to spontaneous particle production as we now review.

Bogolyubov transformation and mean particle number. Working with cosmic time t for concreteness, let us place ourselves in an idealised situation where we can properly define an *in* particle state in the infinite past $t \to -\infty$ and an *out* particle state in the infinite future $t \to +\infty$. Of course in cosmology, the notion of particle is not well-defined in a strict sense, since the background does not become static at the infinite future. A quantum scalar field $\hat{\sigma}$ is quantised in the usual following manner

$$\hat{\sigma}(t, \boldsymbol{x}) = \int \frac{\mathrm{d}^3 k}{(2\pi)^3} e^{i\boldsymbol{k}\cdot\boldsymbol{x}} \left[u_k(t)\, \hat{a}_{\boldsymbol{k}} + u_k^*(t)\, \hat{a}^\dagger_{-\boldsymbol{k}} \right] , \tag{4.5}$$

where the mode function $u_k(t)$ is the solution to a harmonic oscillator equation with a time-dependent frequency $\omega_k(t)$, whose precise form is unimportant for the following development. For the sake of presentation, we assume that $\omega_k^2(t)$ is positive at all times and that is satisfies the adiabatic conditions $|\dot{\omega}_k|/\omega_k^2 \to 0$ and $|\ddot{\omega}_k|/\omega_k^3 \to 0$ both in the infinite past and future $t \to \pm\infty$. The general asymptotic solution for the mode function $u_k(t)$ can be written as a linear combination of $u_k^{(0)}(t)$ and $u_k^{(0)*}(t)$ with

$$u_k^{(0)}(t) = \frac{e^{-i\int_{t_0}^t \mathrm{d}t' \omega_k(t')}}{\sqrt{2\omega_k(t)}} , \tag{4.6}$$

where the value of t_0 is irrelevant. This corresponds to the leading-order Wentzel–Kramers–Brillouin (WKB) approximation. Despite the significant surge in algebraic complexity, higher-order corrections in the WKB expansion can be computed iteratively, see e.g. [207] for more details. In our case of interest, we choose the positive-frequency solution only in the infinite past $u_k(t) = u_k^{(0)}(t)$, corresponding to having no particle as an initial condition. This implies that the operator $\hat{a}^\dagger_{\boldsymbol{k}}$ (resp. $\hat{a}_{\boldsymbol{k}}$) creates (resp. annihilates) quanta of the field $\hat{\sigma}$ at $t \to -\infty$, as seen by an *observer at the infinite past*. The vacuum state $|0\rangle_a$ is therefore defined as the eigenstate of all annihilation operators with eigenvalue 0, i.e. $\hat{a}_{\boldsymbol{k}} |0\rangle_a = 0$ for all $\boldsymbol{k}$. An excited state $|m_{\boldsymbol{k}_1}, n_{\boldsymbol{k}_2}, \ldots\rangle$ with the occupation numbers $m, n, \ldots$ can be constructed by acting

with creation operators $|m_{\boldsymbol{k}_1}, n_{\boldsymbol{k}_2}, \ldots\rangle = \frac{1}{\sqrt{m!n!\ldots}}(\hat{a}^\dagger_{\boldsymbol{k}_1})^m(\hat{a}^\dagger_{\boldsymbol{k}_2})^n \ldots |0\rangle_a$. Since the adiabatic condition is assumed to be satisfied at later times, the general solution for the mode function $u_k(t)$ in the infinite future $t \to +\infty$ must take the asymptotic form

$$u_k(t) = \alpha_k u_k^{(0)}(t) + \beta_k u_k^{(0)*}(t)\,, \tag{4.7}$$

where the constants α_k and β_k are usually referred to as Bogolyubov coefficients. The field $\hat{\sigma}$ therefore asymptotically reads

$$\hat{\sigma}(\boldsymbol{x}, t) = \int \frac{\mathrm{d}^3k}{(2\pi)^3}\, e^{i\boldsymbol{k}\cdot\boldsymbol{x}} \left[u_k^{(0)}(t)\, \hat{b}_{\boldsymbol{k}} + u_k^{(0)*}(t)\, \hat{b}^\dagger_{-\boldsymbol{k}}\right]. \tag{4.8}$$

After injecting Eq. (4.7) into Eq. (4.5), the newly defined operators $\hat{b}_{\boldsymbol{k}}$ and $\hat{b}^\dagger_{\boldsymbol{k}}$ are related to the creation and annihilation operators in the far past by

$$\hat{b}_{\boldsymbol{k}} = \alpha_k \hat{a}_{\boldsymbol{k}} + \beta_k^* \hat{a}^\dagger_{-\boldsymbol{k}}\,, \quad \text{and} \quad \hat{b}^\dagger_{\boldsymbol{k}} = \alpha_k^* \hat{a}^\dagger_{\boldsymbol{k}} + \beta_k \hat{a}_{-\boldsymbol{k}}\,. \tag{4.9}$$

By virtue of Eq. (4.8), the operator $\hat{b}_{\boldsymbol{k}}$ (resp. $\hat{b}^\dagger_{\boldsymbol{k}}$) is interpreted as the annihilation (resp. creation) operator as seen by an *observer at the infinite future* [208, 209], which annihilates (resp. creates quanta out of) the vacuum state $|0\rangle_b$. In particular, note that the vacuum state $|0\rangle_a$ is *not* annihilated by the operator $\hat{b}_{\boldsymbol{k}}$.[3] Particle production over time manifests itself as the presence of b-particles with wavenumber $\boldsymbol{k}$ in the vacuum state $|0\rangle_a$. Explicitly, using Eq. (4.9), the b-particle number operator evaluated in the state $|0\rangle_a$ is

$${}_a\langle 0|\hat{b}^\dagger_{\boldsymbol{k}}\hat{b}_{\boldsymbol{k}}|0\rangle_a = |\beta_k|^2 \delta^{(3)}(\boldsymbol{0})\,, \tag{4.10}$$

where the divergent factor $\delta^{(3)}(\boldsymbol{0}) = [\hat{a}_{-\boldsymbol{k}}, \hat{a}^\dagger_{-\boldsymbol{k}}]$ is a consequence of considering an infinite volume. The *mean density* of b-particles, defined after dividing by this divergent factor, is $n_k = |\beta_k|^2$.[4] It is interpreted as the occupation number of created particles at late times.

Mean particle density from exact mode function. The mean particle density can be computed analytically without approximation when the equation of motion is exactly solvable, as it is the case for a massive scalar field in de Sitter (4.1). Working with conformal time τ and for a heavy field, let us explicitly derive the mean density of produced particles for this case. To do so, one needs to define a proper *in* mode function that matches the positive-frequency only Bunch-Davies initial condition in the far past $|k\tau| \gg 1$, i.e. such that its asymptotic past form matches the leading-order adiabatic expansion $e^{-i\int^\tau \omega_k(\tau')\mathrm{d}\tau'}/\sqrt{2\omega_k(\tau)}$ in the limit $\omega_k(\tau) \approx k$. It is precisely given by (A.2). In the infinite future $|k\tau| \ll 1$, the notion of an *out* mode function is ill-defined as the time-dependent frequency does not evolve adiabatically. However, even if the field invariably continues decaying, it

[3] As usual in quantum field theory, we work in the Heisenberg picture where all the time dependence is in the operators. Accordingly, the states $|0\rangle_a$ and $|0\rangle_b$ are independent of time.

[4] Note that to have a finite mean density of particles in all modes $\int \mathrm{d}^3k|\beta_k|^2$, one needs that $|\beta_k|^2 \to 0$ faster than k^{-3} at large k.

asymptotically reaches a state that can be approximated by a leading-order adiabatic expansion. Indeed, one can show that the later-time mode function, solution to Eq. (4.1), is given by [210, 211, 212]

$$u_k(\tau) = \frac{\Gamma(1+i\mu)}{\sqrt{2\mu}} \left(\frac{k}{2}\right)^{-i\mu} J_{i\mu}(-k\tau) \xrightarrow[\tau\to 0]{} \frac{e^{-i\mu t}}{\sqrt{2\mu}}\,, \tag{4.11}$$

where $J_{i\mu}$ is the Bessel function of the first kind. After using its asymptotic behaviour, the Mukhanov-Sasaki variable to this mode function is chosen to agree with the adiabatic form $e^{-i\int^\tau \omega_k(\tau')\mathrm{d}\tau'}/\sqrt{2\omega_k(\tau)} \approx e^{-i\mu t}/\sqrt{2\mu}$ in the limit $\omega_k(\tau) \approx \mu/\tau$. The solution asymptotes the properly normalised positive-frequency plane-wave solution oscillating in cosmic time t at a frequency set by the mass of the field. Using the property of the Hankel function given in App. A, it is possible to write the *out* mode function as a linear combination of the *in* mode function and its complex conjugate, and extract the Bogolyubov coefficients (4.7). They read

$$\alpha_k = \frac{\Gamma(1+i\mu)}{\sqrt{2\pi\mu}} \left(\frac{k}{2}\right)^{-i\mu} e^{+\frac{\pi\mu}{2}-\frac{i\pi}{2}}\,, \quad \beta_k = \frac{\Gamma(1+i\mu)}{\sqrt{2\pi\mu}} \left(\frac{k}{2}\right)^{-i\mu} e^{-\frac{\pi\mu}{2}+\frac{i\pi}{2}}\,. \tag{4.12}$$

Using the identity $|\Gamma(1+i\mu)|^2 = \pi\mu/\sinh(\pi\mu)$, the mean particle density can be evaluated as

$$|\beta_k|^2 = \frac{1}{e^{2\pi\mu}-1}\,. \tag{4.13}$$

A notable feature of the mean particle density $|\beta_k|^2$ is that it takes the form of a Bose-Einstein distribution with zero chemical potential, when identifying the energy of the system with the rest-mass energy of the field together with the de Sitter temperature $T = T_{\mathrm{dS}} = \frac{H}{2\pi}$ [213, 214]. A geodesic observer in de Sitter would perceive the particle state as a bath of particles at a temperature T_{dS}. In the large-mass limit $\mu \gg 1$, or equivalently in the low particle density limit, it boils down to $e^{-2\pi\mu}$, which is the result from Maxwell–Boltzmann statistics. Note that this thermal factor cannot be captured by an expansion in powers of $1/\mu$, signalling the non-perturbative nature of spontaneous particle production.[5] In most cases, the dynamics is not analytically solvable and one needs to resort to approximate methods, such as the Stokes-line method.

4.1.3 Stokes-Line Method

The Stokes-line method enables one to compute the mean density of created particles without explicitly solving the full dynamics, eventually making the underlying physical processes more intuitive. Using WKB expansions, one can find asymptotic solutions with arbitrary accuracy, for example truncating the series at some optimal order. However, both WKB series in the infinite past and future are defined only locally, while spontaneous production production requires global information. In practice, the mode function at some initial time typically cannot be analytically

[5] The thermal transition amplitude corresponding to the creation of a pair of particles—with opposite wavenumber to conserve momentum—is $e^{-\pi\mu}$. One should take the square of it to get the probability of this event.

continued in the entire complex plane, due to the analytic structure of $\omega_k(t)$. This is the manifestation of violation of the adiabaticity conditions at some time in between both regions where the WKB series are well-defined.[6] The boundaries of these regions of validity of such local approximations are called *Stokes lines*.[7]

Stokes phenomenon. The complex points where the time-dependent frequency vanishes, i.e. $\omega_k(t_c) = 0$, are called *turning points*. In general, turning points come in conjugate pairs t_c and t_c^*. These points are surrounded by regions where the adiabatic conditions are violated, signalling a break-down of the WKB approximation. If the number of turning points are finite—which is the case for most of the applications—, then we can find a path in the complex plane that allows to go from $t \to -\infty$ to $t \to +\infty$ while staying arbitrarily far from these turning points. This implies that an initial positive-frequency solution would not acquire any negative-frequency component along this path, and no particles would have been spontaneously created, i.e. $|\beta_k|^2 = 0$. However, this reasoning misses the presence of Stokes lines along this path. In fact, crossing a Stokes line precisely generates a negative-frequency component allowing for particle production. This is known as the *Stokes phenomenon* [215, 216, 217, 218, 219, 220, 221], see also [222, 223, 224, 225, 226, 227, 228, 229, 230, 231, 232, 233] for some recent applications in physics.

Non-perturbative process. The Stokes phenomenon originates from the fact that the WKB expansion cannot be fully resummed to the exact result in the entire complex plane, i.e. some parts of the full solution do not appear at any order in the WKB series. In this sense, spontaneous particle production due to a time-dependent frequency is *non-perturbative*.[8] The Stokes-line method [215] provides a connection formula that links both WKB approximations and allows us to reconstruct the mode function on one side of a Stokes line—typically at later times—knowing it on the other side, which in the end gives a practical formula to compute the mean particle density $|\beta_k|^2$.

Stokes-line method. We define the so-called *singulant* by

$$F_k(t) \equiv -2i \int_{t_c}^{t} \omega_k(t')\mathrm{d}t' \,, \tag{4.14}$$

where t_c denotes a turning point such that $\omega_k(t_c) = 0$ and t is some time on the real (physical) axis. In the integration, one first performs the integration from t_c to

[6] Naturally, if the WKB series can be fully resummed, equivalently if adiabaticity is never violated, there is no particle creation. This is the case for massless fields in de Sitter which if initialised in the Bunch-Davies vacuum do not acquire a negative-frequency component, i.e. $\beta_k = 0$, see [207] for details.

[7] To give a trivial example, the function $\sinh(z)$ has the asymptotic expansion $e^z/2$ for $\mathrm{Re}(z) > 0$ and $-e^{-z}/2$ for $\mathrm{Re}(z) < 0$. The Stokes line can be taken to be the imaginary axis.

[8] Similarly, the Schwinger effect [234, 235] and the Hawing radiation [236] are non-perturbative in the coupling constants of the theory as these effects cannot be described by a finite sum of perturbative processes.

t_* where the Stokes line intersects the real time axis, then from t_* to t along the real axis, see Fig. 4.2. It represents the difference between the positive and negative phases accumulated from the turning point t_c. The Stokes lines are determined by the condition $\mathrm{Im}(F_k(t)) = 0$. Near the Stokes line, linking t_c and t_c^*, the negative-frequency component starts to be produced. The exact production history, including the time, the amount and the width, can be computed from the singulant $F_k(t)$.

- *Production time*: Particle production is maximally enhanced when the Stokes line crosses the real axis. The production time t_* satisfies the real-valued equation $\mathrm{Im}(F_k(t_*)) = 0$.
- *Production width*: The thickness of the Stokes line governs the particle production width $\Gamma_k(t)$. It is given by

$$\Gamma_k(t) = \frac{-\mathrm{Im}(F_k(t))}{\sqrt{2\mathrm{Re}(F_k(t))}}\,. \tag{4.15}$$

- *Production amount*: The Bogolyubov coefficient $\beta_k(t)$ associated to particle production when crossing the Stokes lines reads

$$\beta_k(t) \approx \frac{i}{2}\left[1 + \mathrm{erf}(\Gamma_k(t))\right] e^{i\int_{t_c}^{t_c^*}\omega_k(t')\mathrm{d}t'}\,, \tag{4.16}$$

  where erf denotes the error function and the integral is along the Stokes line joining the two complex conjugate turning points.

We concretely apply this method to a variety of examples in Chap. 8 with details in App. B.

4.1.4 Enhanced Particle Production

For heavy fields, the spontaneous particle production is Boltzmann suppressed. This typically leads to small imprints of massive fields in observable correlators, as this signal is proportional to $|\beta_k|^2 \propto e^{-\mathrm{Re}(F(z_c^*))}$. As we will see, the cosmological collider signal is a direct consequence of the inflationary background and this on-shell particle production, and is relatively independent of the inflationary models, e.g. specific couplings between the inflaton and the additional matter sectors. However, the size of this signal is very sensitive to the details of the inflationary physics, and they are many known mechanisms to enhance particle production. We now review some of them.

Chemical potential. Under relatively mild assumptions, many couplings between the inflaton and the matter sector generically fail to generate sizable cosmological collider signals [237]. In simple terms, this can be understood as follows: a large signal would typically require a large coupling between both sectors, which in turn induces large radiative corrections that make the massive field too heavy to leave any observable signal. One interesting possibility for which the exponential suppression can be alleviated is to consider a chemical potential.

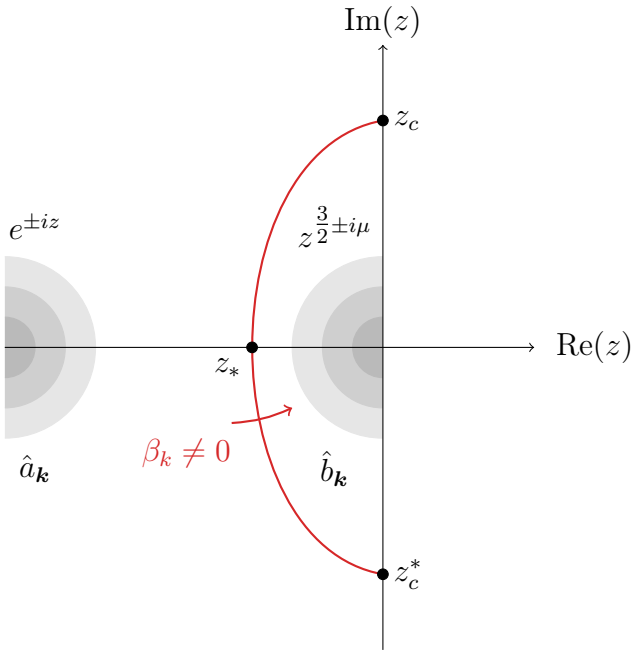


Figure 4.2: Analytic structure of the time-dependent frequency $\omega(z)$ of a scalar massive field in de Sitter, in the complex z-plane, with $z = k\tau$. The physical region lies on the negative real axis. The theory has two purely imaginary turning points z_c and z_c^*, coming in complex conjugate pairs. The Stokes line joining both turning points, which are surrounded by regions where adiabaticity is violated, is represented by the red line. On the left side of the Stokes line, i.e. in the infinite past, the solution is oscillatory $\sim e^{\pm iz}$, whereas on the right side, i.e. at later times, it is evanescent and non-analytic $\sim z^{3/2\pm i\mu}$. Particle production is maximal when the Stokes line crosses the real axis at z_*. The varying gray levels delineate the domain of validity for different orders of WKB approximations, both at early and late times. Being a local approximation, it fails to capture particle production which requires global information, i.e. necessitates crossing the Stokes line.

Generating a chemical potential can be achieved with an inflaton field ϕ coupled to massive fields through operators of the form $\partial_\mu\phi J^\mu$, where J^μ is a certain massive-field current. With the inflaton acquiring its slowly rolling vacuum expectation value $\phi = \phi_0 + \dot{\phi}_0 t + \ldots$, the chemical potential is typically identified with $\kappa = \dot{\phi}_0/\Lambda$ where Λ is some high-energy scale. Its effect on the massive-field dynamics is to produce a term *linear* in k in its time-dependent frequency. As a result, such a term can only appear from dotting the 3-momentum $\boldsymbol{k}$ with some other 3-vector, like the spin $\boldsymbol{s}$ of the heavy field. Since the quantity $\boldsymbol{k}\cdot\boldsymbol{s}$ is parity odd, it is expected that a chemical potential requires a coupling involving a conserved pseudo-vector current.

For spin-1 particles, it is natural to choose the Chern-Simons current $J^\mu = \frac{\epsilon^{\mu\nu\alpha\beta}}{\sqrt{-g}}\sigma_\nu\partial_\alpha\sigma_\beta$ which results in an enhanced production of vector bosons, see e.g. [238, 239, 240, 237, 241, 106, 242, 243] for more details. For massive spin-1/2 fermions, the chiral current $J^\mu = \bar{\psi}\gamma^5\gamma^\mu\psi$ leads to a chemical-potential assisted particle production, see e.g. [244, 245, 246, 237, 247]. Charged scalars can also generate a chemical potential when considering the current $J^\mu = i(\sigma^*\partial^\mu\sigma - \sigma\partial^\mu\sigma^*)$, see

e.g. [248, 249, 250, 237]. Recently, it has also been shown that a chemical potential from spin-2 massive fields is generated by the current $J^\mu = \frac{\epsilon^{\mu\nu\alpha\beta}}{\sqrt{-g}}\sigma_{\nu\lambda}\nabla_\alpha\sigma^\lambda_\beta$, see [251], and also e.g. [98, 237]. Chemical potential-assisted particle production is therefore a generic phenomenon that appears in many different models. A complete classification of chemical-potential enhancement of particle production for all type of particles can be found in [243], where the Stokes-line method is used to extract the production history of these models. We will see in Chap. 11 that these chemical-potential-assisted particle productions typically lead to (boost-breaking) parity-violating correlators.

In the presence of a chemical potential, the imprint of massive fields in correlators is rather insensitive to the details of the couplings, and the mean density of produced particle is found to be $|\beta_k|^2 \propto e^{-2\pi(\mu-\tilde{\kappa})}$ in the large-mass limit, where $\tilde{\kappa} = \kappa/H$ is the chemical potential in Hubble units. To prevent a transient phase of tachyonic instability for the massive fields that can eventually destabilise the inflationary background, we require $\kappa < m$, so that there is no exponential enhancement of particle production. However, we can easily accommodate for $\mathcal{O}(1)$ amplitude for the cosmological collider signal. These will be discussed in Chaps. 7 and 11.

Warm inflation. Another possibility to enhance particle production is that the produced degrees of freedom thermalise after the production. This is the paradigm of so-called warm inflation [252, 253] in which the inflaton coexists with a thermal plasma at a finite temperature $T \gg T_{\rm dS} = \frac{H}{2\pi}$. This model leads to a rich phenomenology of detectable non-Gaussian signals [254, 255, 256]. Using quasi-single field inflation as a model, it was shown in [257] that the resulting cosmological collider signal is not exponentially suppressed. At earlier times in the thermal bath, the propagation of massive fields is modified by thermal effects. Massive fields then acquire a temperature-dependent mass $m^2 \to m^2 + \Delta m^2(T)$, resulting in excited states that mimic thermal effects (this corresponds to a squeezing of the Bunch-Davies initial state). The mean density of produced particles is found to be $|\beta_k|^2 \propto (\Delta m(T)/H)^4$, which in turn leaves the cosmological collider signal unsuppressed.

Time-dependent mass. Motivated by axion monodromy [258, 259, 260], see also the references in [261], a time-dependent mass for the heavy field, generically leads to a large *resonant* production of heavy fields. It has been shown in [261] that the amount of particle production is given by $|\beta_k|^2 \propto e^{-\pi\tilde{m}^2/g\dot{\phi}_0}$, where $\dot{\phi}_0 \approx (60H)^2$, $\tilde{m}$ is the lightest value of the time-dependent mass, and the coupling g can be $\mathcal{O}(1)$. The associated cosmological collider signal is greatly enhanced compared to purely gravitational particle production from vacuum fluctuations, and can be detectable even when the massive fields are much larger than the Hubble scale.

4.2 Soft Limits of Cosmological Correlators

Cosmological collider signals are non-analytic momentum scalings in soft limits of correlators, which encode the propagation (and decay) of massive particles that have

been spontaneous produced.

4.2.1 Late-Time Non-Analytic Scaling

The presence of symmetries leads to precise and model-independent predictions for the soft limits of correlators, called consistency relations. This in turn reveals some general structure of these correlators in momentum space: in soft limits, they are *analytic* in the momentum ratio. However, the presence of additional massive fields during inflation violates consistency relations by inducing *non-analytic* deviations in the momentum ratio. In this sense, observing any deviation from these relations would rule out a large class of single-field inflationary models.

Local and non-local processes. To see the appearance of non-analytic scalings in soft limits of correlators, it is illuminating to look at the unequal-time two-point function of a scalar massive field σ for simplicity, as it is the building block of any process where this field is exchanged, see [262, 116, 263] for more details. For concreteness, we will assume the field σ to be heavy enough so that the parameter μ is real. The same reasoning also applies to the case of light fields. Using the quasi-normal mode expansion (4.3) in the late time limit, i.e. only considering the leading terms, we find

$$\begin{aligned}\langle\sigma_{\boldsymbol{k}}(\tau)\sigma_{-\boldsymbol{k}}(\tau')\rangle'_{\text{local}} &= \frac{H^2(\tau\tau')^{3/2}}{4\pi}\Gamma(i\mu)\Gamma(-i\mu)\left[e^{\pi\mu}\left(\frac{\tau}{\tau'}\right)^{i\mu}+e^{-\pi\mu}\left(\frac{\tau}{\tau'}\right)^{-i\mu}\right],\\ \langle\sigma_{\boldsymbol{k}}(\tau)\sigma_{-\boldsymbol{k}}(\tau')\rangle'_{\text{non-local}} &= \frac{H^2(\tau\tau')^{3/2}}{4\pi}\left[\Gamma(-i\mu)^2\left(\frac{k^2\tau\tau'}{4}\right)^{i\mu}+\Gamma(i\mu)^2\left(\frac{k^2\tau\tau'}{4}\right)^{-i\mu}\right],\end{aligned} \tag{4.17}$$

where we have distinguished contributions from *local* and *non-local* processes. The local part is independent of the momentum k, which, in a process, is identified as the exchanged momentum. In real space, the local part gives a propagator proportional to $\delta^{(3)}(\boldsymbol{x}-\boldsymbol{y})$, and is interpreted as the accumulated dynamical phase of a *single* particle propagating from τ' to τ, as

$$\left(\frac{\tau}{\tau'}\right)^{\pm i\mu} = e^{\pm im(t'-t)}\,, \tag{4.18}$$

where t is cosmic time. Conversely, the non-local part is non-analytic in the momentum k, which gives rise to non-trivial long-range correlations of the form $k^{2i\mu}\sim|\boldsymbol{x}-\boldsymbol{y}|^{i\mu+3/2}$. It is interpreted as the accumulated dynamical phase of *two* propagating particles as

$$(k^2\tau\tau')^{\pm i\mu}\propto\left(\frac{\tau}{\tau_\star}\right)^{\pm i\mu}\left(\frac{\tau'}{\tau_\star}\right)^{\pm i\mu} = e^{\pm im(t_\star-t)}e^{\pm im(t_\star-t')}\,, \tag{4.19}$$

where $\tau_\star$ (resp. $t_\star$) denotes the conformal (resp. cosmic) time at which the *pair* of particles is produced. Non-local processes therefore describe on-shell propagation of massive particles from their production to their decay. Notice that the non-local

part of the massive propagator is real in the late-time limit. This implies that the commutator of field operators does not contain any non-local terms

$$\langle[\sigma_{\boldsymbol{k}}(\tau), \sigma_{-\boldsymbol{k}}(\tau')]\rangle \supset [u_k^*(\tau)u_k(\tau') - u_k(\tau)u_k^*(\tau')]_{\text{non-local}} = 0\,. \tag{4.20}$$

In fact, it follows from microcausality, i.e. from requiring that operators commute outside the lightcone. This property implies some cutting rules for correlators enabling to directly extract signals associated to non-local processes, see [263] for more details, also see [264]. We will explicit use these cutting rules in Chap. 8. Physically, Eq. (4.20) means that two endpoints of a soft propagator are in space-like separation so that time ordering becomes irrelevant. Both signals are illustrated in Fig. 4.3.

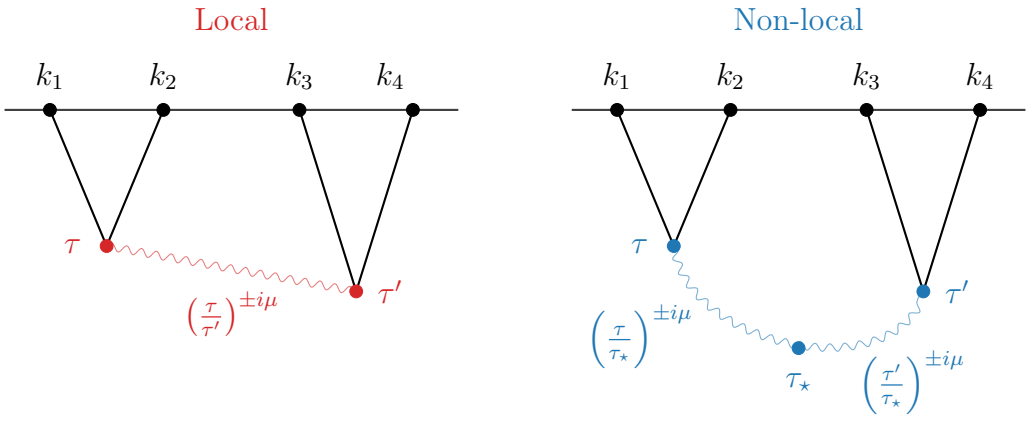


Figure 4.3: Schematic illustration of local and non-local processes in the case of the four-point (s-channel) exchange cosmological correlator. The local signal is analytic in the exchanged momentum $s = |\boldsymbol{s}| = |\boldsymbol{k}_1 + \boldsymbol{k}_2|$ but non-analytic in k_{34}/k_{12} where $k_{ij} \equiv k_i + k_j$. The non-local signal is non-analytic in $s^2/(k_{12}k_{34})$. Taking the soft limit $k_4 \to 0$ to recover the three-point correlator (and its shape), and therefore sending $k_{34} \to s$ due to momentum conservation, the local and non-local signals become indistinguishable.

Background. In a specific process, a third contribution is also present, which corresponds to contact terms that can be mimicked by adding a local operator in the low-energy theory after integrating the massive field out. This so-called *background* is associated to the particular solution to the equation of motion for the massive field σ sourced by a current of observable fields, i.e. $(-\Box + m^2)\sigma = J$, in the regime $m^2 \gg \Box$, see Chap. 10 for extensions beyond the usual gradient expansion. Its amplitude is given by $\mathcal{O}(1/\mu^{2n})$ with n is the order of the usual gradient expansion in the large-mass limit, and its form is fully analytic in all momentum ratios.

4.2.2 Cosmological Collider Signal

The detailed computation of the non-local signal in the tree-level four-point correlator of a conformally coupled external field φ mediated by the exchange of a massive field σ through the interaction $\mathcal{L}_{\text{int}}/a^3(t) = -\frac{g}{2}\varphi^2\sigma$ is performed in Chap. 7 using the

newly developed spectral representation method, and in App. A using bulk cutting rules. For light fields ($m/H < 3/2$), non-analytic scalings of the resulting correlator were first discovered in the seminal papers [58, 59] whereas cosmological collider signals for heavy fields were first exposed in [60]. Referring the reader to App. A for details, we directly quote the result. The leading-order late-time contribution to the four-point correlator encoding the non-local signal is

$$\begin{aligned}\langle \varphi_{\boldsymbol{k}_1}\varphi_{\boldsymbol{k}_2}\varphi_{\boldsymbol{k}_3}\varphi_{\boldsymbol{k}_4}\rangle' &= \frac{g^2H^2\tau_0^4}{32\pi k_1k_2k_3k_4(k_{12}k_{34})^{1/2}} \\ &\times \left[(1+i\sinh\pi\mu)\left(\frac{s^2}{4k_{12}k_{34}}\right)^{i\mu}\Gamma(-i\mu)^2\Gamma\left(\tfrac{1}{2}+i\mu\right)^2 + \text{c.c.}\right] .\end{aligned} \tag{4.21}$$

A remarkable property of this correlator is that it oscillates in the momentum ratio $s^2/(k_{12}k_{34})$ at a frequency set by μ. Measuring this so-called *cosmological collider signal* would in turn allow us to perform spectroscopy to probe the inflationary particle content, since μ is directly related to the mass of the exchanged (and decaying) particle. Higher-order corrections in the ratio $s^2/(k_{12}k_{34})$ can be computed systematically employing methods such as Mellin-Barnes techniques (see details in App. A) where leading contributions to the non-local signal correspond to the leading IR poles in Mellin space. These refined terms encode higher-order harmonics in the massive quasi-normal mode expansion (4.3), which are more suppressed.

Shape. Let us specify to the three-point correlator by taking the external soft limit $k_4 \to 0$. By momentum conservation, we have $k_{34} \to s = k_3$. This corresponds to the kinematic configuration in which k_3 is the long (i.e. soft) mode and k_1 and k_2 are the short (i.e. hard) modes. The cosmological collider signal of the correlator is valid in the squeezed limit $k_3 \ll k_{1,2}$. The corresponding shape reads

$$S(k_1,k_2,k_3) = \mathcal{A}\left(\frac{k_3}{k_1}\right)^{1/2}\cos\left[\mu\log\frac{k_3}{k_1}+\theta\right] , \tag{4.22}$$

where we specified to the isosceles kinematic configuration $k_1 = k_2$. The amplitude $\mathcal{A}$ and the phase θ dependent on the parameter μ (and on the interaction) and can be readily deduced from (4.21). The amplitude is Boltzmann suppressed $\mathcal{A} \sim \mathcal{O}(e^{-\pi\mu})$, which is reminiscent from the gravitational particle production and the on-shell propagation of the exchanged field. The part of the shape function that does not encode non-analytic scaling scales as $S \propto k_3/k_1$. This background part of the signal corresponds to the two permutations in which the exchange momentum is short (i.e. hard). In the case of a light exchange field, the cosmological collider signal is instead encoded in power-law scalings of the momentum ratio. The shape function takes the form $S \propto (k_1/k_3)(k_3/k_1)^{3/2-\nu}$ where $\nu \equiv i\mu$. The first term k_1/k_3 corresponds to the local shape, and the second term $(k_3/k_1)^{3/2-\nu}$ introduces an additional non-analytic scaling. In the strict massless limit $\nu = 3/2$, i.e. $m/H = 0$, we recover the local shape. However, for a light field $m/H > 0$, i.e. $\nu > 0$, the shape is suppressed in the squeezed limit. This modification is attributed to the super-horizon decay of the massive field. These scalings for the shape function have been derived in [265] without setting up the full calculation. It has been shown

in [262] that these scalings are universally controlled by (slightly broken conformal) symmetry, also see [266].

4.2.3 Particle Collider Analogy & Observational Prospects

In (flat-space) particle physics, the existence of new particles and determining their properties are inferred from collider experiments. Indeed, ground-based colliders bring two opposing particle beams together so that particles collide. These collisions leave some jets or energy deposit on the detectors, that enable us to study and reconstruct properties of the subatomic world and the laws governing it. More specifically, massive particles leave resonant signatures in the cross section of lighter particles' collisions when the center-of-mass energy coincides with the particle masses. Characteristics of these resonances, such as the height and the width, give information about the lifetime of the heavy particles and how they couple to other particles in the Standard Model. The angular distribution of the decay products on the detector enables to reconstruct the spin of the produced particles.

Analogy with terrestrial colliders. Cosmological collider signals offer promising detection channels to probe new physics at the highest reachable energies. In fact, as we have just seen, similar information—such as the masses of heavy particles—is encoded in cosmological correlators. By analogy, maps of energy deposits on the detectors translate into maps of LSS or temperature anisotropies in the CMB, and the peaks in the invariant mass distribution translate into specific patterns in cosmological correlators when varying the kinematic configuration. The spin information of the exchanged particle can also be inferred from the angular distribution. Probing high-energy aspects of inflation following the same approach as in particle physics now goes under the name of "cosmological collider physics" [262].

Fig. 4.4 illustrates the analogy between terrestrial and cosmological collider physics. The left panel represents the Higgs boson resonance in the cross section as function of the center-of-mass energy, as reported by the ATLAS Collaboration [268]. If the proton-proton beams at the LHC collide at sufficiently low energy, the Higgs boson cannot be produced on-shell. Consequently, we are probing the regime of the theory where the heavy particle can be integrated out, yielding local contact interactions. In the case of the electroweak theory, this corresponds to probing the Fermi theory. When increasing the center-of-mass energy, heavy particles start to be produced. Their existence prevents the violation of perturbative unitarity in the low-energy description of the theory and manifests as resonances. Analogously, the right panel shows the four-point cosmological correlator as function of the momentum ratio. Close to "equilateralish" configurations, the signal is smooth. This is because we are probing the "EFT" part of the signal, corresponding to a sum of contact interactions found after integrating out the intermediate field. Essentially, seeing the propagation of a massive particle for a sufficiently long time requires a large hierarchy of scales, and any signature of new particles is completely dwarfed by this "background" signal. In soft-enough configurations, as the (analytic) background signal vanishes, the signal starts to deviate from that produced by pure contact interactions: it is the (non-analytic) cosmological collider signal.

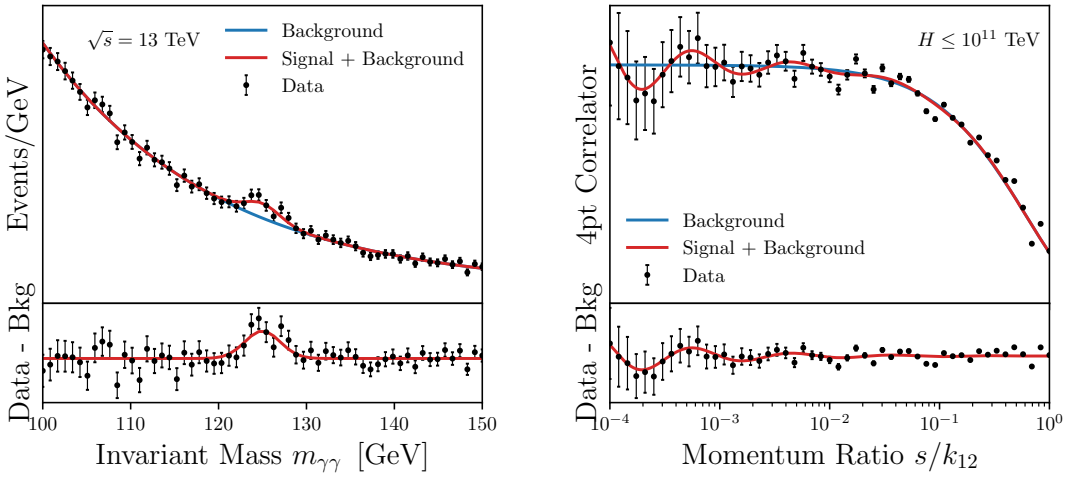


Figure 4.4: *Left panel:* The hadronic cross-section as a function of center-of-mass energy for the $H \to \gamma\gamma$ process, as measured by ATLAS [267]. The mass and the width of the Higgs boson are precisely measured after fitting a Breit-Wigner distribution: $m_H = 125.17 \pm 0.11$ GeV. Other parameters, such as the decay rate, branching fractions and the angular distribution of its decay products, would provide a complete description of the Higgs resonance. *Right panel:* Rescaled four-point cosmological correlator generated by the exchange of a single massive scalar field with $\mu = 2$. The correlator contains all terms and permutations, and is normalised to unity in the equilateral configuration. The non-local part of the signal is exponentially suppressed compared to the local one, and the precise form of the full signal is strongly model dependent. Being an on-shell effect, the cosmological collider signal is the reminiscence of the mass pole for scattering amplitudes. The fake data points and the error bars were artificially generated using Poisson noise for the particle physics case and Gaussian noise with a width that spreads in the soft limit to mimic limitation from cosmic variance.

Under the assumption of a specific type of coupling and the exchange of a single massive particle, detecting this signal (and fitting the smooth background part to find consistency) would be a measure of the underlying physics.

Observational challenges and opportunities. Delving into softer configurations of cosmological correlators requires an increasing level of precision, and a detection of new exchange particles requires both a precise measurement of the smooth signal as well as the cosmological collider signal.

Extracting the smooth "background" part of the signal from large-scale structure observations will be extremely challenging because equilateral-type non-Gaussianities are severely degenerated with late-time gravitational non-linearities, see [269] and the references therein. The complication of disentangling primordial signals from non-linear structure formation has been recently reconsidered in [161]. Because inflation produces correlations that appear non-local for a late-time observer, measur-

ing non-Gaussianities in position space—instead of Fourier space—makes the long-range property of primordial non-Gaussianities manifest, as late-time non-linearities only affect the physics locally and cannot influence correlations that span over large cosmological distances. Accordingly, a map-level analysis of large-scale structure correlations would significantly impact the quest for primordial non-Gaussianities.

The experimental challenge to observe cosmological collider signals is enormous. Nevertheless, recent studies suggest that prospects for detection are bright [270, 271, 272, 273, 274, 275, 276, 277]. Considering that the squeezed-limit of the bispectrum constitutes only a small fraction of the full bispectrum and that the signal shows significant overlap with equilateral-type shapes, conducting a dedicated search using CMB data would likely lead to a null outcome. This expectation arises from the fact that existing constraints on equilateral non-Gaussianities are aligned with zero [137]. Recently in [278], stringent constraints from temperature and polarisation CMB data on cosmological collider shapes (including distinctive oscillatory patterns, angular dependence from spinning fields, and non-trivial sound speed effects) were derived, see also [279] for related recent work. If one can fully exploit the potential of futuristic 21cm cosmology—i.e. analysing maps of neutral Hydrogen distribution in the redshift range $30 \leq z \leq 100$—, particles with masses $m \lesssim \mathcal{O}(H)$ and with large direct interactions with the observable sector have a realistic chance to be detected, see [273] for recent forecasts. The reasons are twofold. First, the (mostly) linear physics at play at these times in principle contains a very predictable signal. And second, the enormous amount of volume would drastically reduce cosmic variance. We refer to e.g. [276] for the latest forecasts addressing quantitatively the detectability of massive particles with non-zero spin in the galaxy bispectra for the spectroscopic galaxy surveys DESI [162] and Euclid [280]. Also see [281] for dedicated search of cosmological collider signals in the CMB temperature and polarisation trispectrum, yielding zero detection.

4.3 Phenomenology of Cosmological Colliders

Cosmological collider signals appear to be clean and distinct probes of the particle content of inflation. Although exponentially suppressed in the simplest canonical case, the oscillatory signature from the exchange of a heavy particle cannot be mimicked by late-time physics, contrary to the smooth background equilateral-type part of the signal. However, even though many features such as oscillatory (or power-law) behaviours in soft limits are rather general, the precise form (e.g. amplitude, phase) is highly sensitive to the exchange particle type (e.g. bosonic, fermionic), its coupling to the visible sector (e.g. weak/strong mixing, different cubic interactions), the type of exchange process (e.g. tree-level or loop-level), and also to some properties of the visible sector (e.g. various dispersion relations for curvature perturbation modes). The task of categorising cosmological collider signals presents a significant challenge, primarily attributed to the intricate algebraic complexity in computing them and to the vast landscape of inflationary theories. Here, we present the many phenomenological aspects of these cosmological collider signals, starting with the case of spinning fields, and then charting the landscape of different signals.

4.3.1 Spinning Particles

Consider a massive and spinning particle with integer spin s, described by a totally symmetric and traceless field $\sigma_{\mu_1\cdots\mu_s}$.[9] Only the longitudinal mode of this field can contribute to the scalar three-point exchange correlator at tree-level because this process requires a linear mixing between $\sigma_{\mu_1\cdots\mu_s}$ and the visible scalar sector. For the purpose of the discussion, let us consider the following interacting Lagrangian

$$\mathcal{L}/a^3(t) = \rho\,\partial_{i_1\cdots i_s}\varphi\,\hat{\sigma}_{i_1\cdots i_s} + \lambda\,\dot{\varphi}\,\partial_{i_1\cdots i_s}\varphi\,\hat{\sigma}_{i_1\cdots i_s}\,, \tag{4.23}$$

where ρ and λ are some coupling constants, $\partial_{i_1\cdots i_s} \equiv \partial_{i_1}\cdots\partial_{i_s}$, and the hat indicates the traceless part of the spinning field. Note that in general, the spinning field can also couple to the visible sector through interactions of the type $\dot{\varphi}\hat{\sigma}^2_{i_1\cdots i_s}$ and $\hat{\sigma}^3_{i_1\cdots i_s}$, leading to double- and triple-exchange processes at weak mixing. The exchange of a spinning particle leads to a pronounced distinctive angular dependence of the correlator when $\sigma_{\mu_1\cdots\mu_s}$ carries the highest angular momentum, i.e. when the polarisation indices are fully contracted with spatial derivative indices so that $\sigma_{\mu_1\cdots\mu_s}$ has the most number of spatial components.

Analytic signal. The analytic signal can be described by an effective theory of pure contact interactions after the heavy field is integrated out. The linear mixing in (4.23) generates a source term for the on-shell equation of motion for $\sigma_{\mu_1\cdots\mu_s}$ of the form[10]

$$(-\Box + m^2)\hat{\sigma}_{\mu_1\cdots\mu_s} = \rho\,\hat{\partial}_{i_1\cdots i_s}\varphi\,. \tag{4.24}$$

Note that the traceless property of the spinning field translates into a traceless spatial derivative structure for the source. At tree-level, integrating out the heavy field amounts to plugging back the solution to (4.24) in the original Lagrangian. If the squared mass m^2 of the field is larger than the typical energy scale (squared) of $\Box$, in this simple case the squared Hubble scale H^2, one can expand the particular solution in inverse powers of m^2. The leading term in this expansion reads[11]

$$\mathcal{L}/a^3(t) = \frac{\rho\lambda}{m^2}\,\dot{\varphi}(\hat{\partial}_{i_1\cdots i_s}\varphi)^2 + \cdots\,, \tag{4.25}$$

where the ellipses denote higher-order terms of order $\mathcal{O}((\Box/m^2)^n)$ with $n \geq 1$. As in any effective theory where heavy and spinning fields are integrated out, the effective

[9] There are different ways to define spinning particles during inflation. In [116], the spinning field is assumed to belong to a unitary irreducible representation of the dS group. Since these representations are in one-to-one correspondence with those of the Poincaré group (with the interesting exception of partially massless fields), this means in simple terms that a particle of spin-s is described by a totally symmetric rank-s field $\sigma_{\mu_1\cdots\mu_s}$, which is a tensor under 4-dimensional diffeomorphisms once coupled to dynamical gravity. In [282], a more general approach has been proposed in which the spinning particle arises as a "matter" field, with no further assumptions. Note that both references considered only integer-spin particles. To our knowledge, the study of fermions has not been tackled (with the exception of supersymmetric theories [265, 283, 284]).

[10] Note that it is sufficient to use the linear equation of motion as we are interested in the bispectrum. Non-linear corrections coming from cubic interactions identically vanish up to cubic order.

[11] We omit the modified quadratic term in the Lagrangian for the field φ due to the linear mixing as it in unimportant for the following general development.

Lagrangian does not contain the information about the mass m as it is absorbed in the coupling constant that only governs the overall size of the interaction. However, the information about the spin persists via the traceless structure of spatial derivatives, effectively emulating the polarisation structure exhibited by the integrated out particle. In the squeezed limit $k_3 \ll k_1 \approx k_2$, the scaling behaviour of the analytic part of the bispectrum shape accounting for all channels is analytic in the momentum ratio and reads [116]

$$\lim_{k_3\to 0} S(k_1,k_2,k_3) \propto \frac{k_3}{k_1} + \cdots + \left(\frac{k_3}{k_1}\right)^{s-1} P_s(\cos\theta)\,, \tag{4.26}$$

where $\cos\theta = \hat{\boldsymbol{k}}_1 \cdot \hat{\boldsymbol{k}}_3$ and P_s is the Legendre polynomial. The first term verifies the single-field consistency relation, and comes from the channel where the soft limit has been taken on the mode $\dot{\varphi}$ in the cubic vertex in Eq. (4.23). The last term stems from taking the soft limit on the spatial gradient mode $\partial_{i_1\cdots i_s}\varphi$ where the factor $(k_3/k_1)^{s-1}$ comes from s spatial derivatives (one factor k_3/k_1 is lost when going from the bispectrum to the shape). Notice that the specific contraction of spatial gradient indices with spinning indices gives an angular dependence. An important feature is that the factor $P_s(\cos\theta)$ is not exclusively attributed to the non-analytic part of the signal, as we will see in what follows, nor specific to the soft limit. This means that the spin dependence can in principle be inferred from the analytic part of the signal, although the signal is suppressed for higher-spin $s > 2$ compared to the leading-order term. When considering odd spins, the Legendre polynomial gains an additional factor k_3/k_1 when summing over permutations, and the term carrying the angular dependence remains suppressed.

Non-analytic signal. The cosmological collider signal comes from the channel where the exchange particle carries a soft momentum, equivalently when the external mode that directly mixes with the exchanged field is taken to be soft by momentum conservation. In the squeezed limit, the bispectrum shape from this channel takes the form

$$\lim_{k_3\to 0} S(k_1,k_2,k_3) \propto \left(\frac{k_3}{k_1}\right)^{1/2} P_s(\cos\theta)\cos\left[\mu_s \log\frac{k_3}{k_1} + \mathfrak{0}_s\right]\,, \tag{4.27}$$

for a heavy particle such that $m \geq (s-1/2)H$, where $\mu_s \equiv \sqrt{\frac{m^2}{H^2} - \left(s-\frac{1}{2}\right)^2}$, and $\mathfrak{0}_s$ is a phase that generically depends on the mass m and spin s. Note that the late-time behaviour of the massive spin-s particle in this case is fully determined by scaling symmetry and dictates the squeezed limit behaviour, see e.g. [116] for more details. This signal therefore contains both information on the mass and the spin of the intermediate particle, with the mass entering the frequency of the oscillations and the spin in the angular dependence, function of the angle between the short and long momenta. For odd spins, the scaling behaviour becomes $(k_3/k_1)^{3/2}$ after summing over permutations. Similarly for the case of an exchanged scalar particle, for light spinning particles such that $m \leq (s-1/2)H$, the scaling of the squeezed limit changes to

$$\lim_{k_3\to 0} S(k_1,k_2,k_3) \propto \left(\frac{k_3}{k_1}\right)^{1/2-\nu_s} P_s(\cos\theta)\,, \tag{4.28}$$

with $\nu_s \equiv i\mu_s$. Away from the squeezed limit, this angular dependence slightly deviates from a pure Legendre polynomial [116].

Phenomenology of exchanged spinning particles. Having reviewed the basic features of (integer) spinning fields, we now lead the reader through the vast literature on the matter. The imprint of spinning particles, defined from de Sitter representations, on cosmological correlators has been initiated in [262] where the angular dependence was first pointed out. This feature has been further studied in [116] where the assumption of (approximate) conformal invariance was dropped, leading to larger signals and allowing for a wider variety of couplings to the visible sector. Using bootstrap techniques and in particular spin-raising operators, these signals have been categorised in [198, 285, 286] for a set of de-Sitter invariant or boost-breaking interactions, in single-exchange processes. Probing heavy spinning particles based on the signs of the Wilson coefficients of the visible sector effective action has been considered in [287]. The unitarity bound in de Sitter $m^2/H^2 \geq s(s-1)$ for integer spins [288, 289], known as the Higuchi bound for $s = 2$, sets the smallest allowed mass value for massive and spinning particles during inflation. As such, the particle mass spectrum, identified with unitary irreducible representations of the spacetime isometry group, leaves small room for light particles with spin during inflation and the corresponding cosmological collider signals are oscillating rather than power-law. Interestingly, at some discrete mass points below the Higuchi bound, particles in de Sitter can gain a gauge symmetry which results in less propagating degrees of freedom. They are called partially massless fields [290, 291]. Being light, some of these partially massless particles can contribute to soft limits of correlators without any suppression, making their prospective detection easier [292], see [293] for an in-depth study of their imprints in cosmological correlators. As shown in [282], breaking de Sitter isometries allows for light spinning particles with sizeable couplings with the visible sector to be present during inflation and therefore extends the reach of cosmological collider signals, also see [284]. The phenomenology of bosonic spinning particle imprints on cosmological correlators has been actively reported in [294, 295, 296, 297, 298, 237, 241, 106, 299, 300, 287, 242, 301, 302, 303, 304, 305, 251, 306, 307]. Phenomenological aspects of fermions in cosmological collider signals can be found in [294, 295, 296, 245, 237, 241, 106, 246, 300, 299, 287, 308, 309]. Since fermions have to be created in pairs, the leading order contribution would be a 1-loop process. In this case, the characteristic non-local signals come from the channel in which the two internal fermionic propagators are attached to the soft external leg. Remarkably, massive fermions always show oscillatory signal rather than power-law. Also see [297] and [310] for cosmological collider signals in correlators involving both scalar and tensor perturbations, and only tensor perturbations, respectively. Known examples of the amplitude, the k_3/k_1 scaling and the frequency of the characteristic oscillatory signals have been categorised in the (not exhaustive) Table 1 of [302] for various spinning and massive particle exchange processes.

4.3.2 Charting Cosmological Colliders

Cosmological collider physics is a rapidly evolving field that brings together expertise from both cosmology and particle physics. here, we guide the reader through the vast literature on the subject.

Speed of sound. The curvature perturbation acquiring a speed of sound allows for modified cosmological collider signals and novel signatures in cosmological correlators. In a nutshell, a reduced speed of sound leads to an enhanced amplitude for the cosmological collider signal, where the Boltzmann suppression changes from $e^{-\pi\mu}$ to $e^{-\pi\mu/2}$. In Chap. 8, we will show that this can be physically understood with the Saddle point approximation. A reduced speed of sound also leads to so-called *cosmological low-speed collider signals* to which Chap. 11 is dedicated. We also refer to [311, 286] for more details.

Strong mixing. In order to generate a tree-level bispectrum, a linear conversion from the exchange particle to the visible sector in the form of a quadratic mixing is needed. When the mixing is large, it cannot be treated perturbatively and new methods, such as the cosmological flow (see Part IV), are needed to compute correlators. A consequence of a linear mixing is to renormalise the mass $\mu \to \mu_{\rm eff} = \sqrt{m^2_{\rm eff}/H^2 - 9/4}$ with $m^2_{\rm eff} = m^2 + \rho^2$ where ρ is the linear mixing. Therefore, a light but strongly mixed field, and a heavy but weakly mixed field cannot be distinguished based only on the signal frequency. This effective mass resummation was pointed out in [312, 313, 314, 315, 316]. An additional noticeable feature of the resulting cosmological collider signals is the strong dependence of its amplitude on the quadratic coupling ρ that is not monotonic, see Chap. 15 for more details. This phenomenon of cosmological colliders acquiring an effective mass has also been noticed in the context of loop processes [294, 295, 296], and in the presence of a chemical potential [237].

Multiple-exchange colliders. At weak mixing, various cubic couplings between the additional and the visible sectors can lead to single-, double-, and triple-exchange processes for the bispectrum. The algebraic complexity arising from the increasing number of nested time integrals makes it impossible to find analytical closed-form solutions for triple-exchange diagrams. Yet, these integrals have been solved numerically, see e.g. [58, 59, 60, 116, 313, 314, 315, 316]. It is known that quasi-single-field-type models of inflation, where all non-linearities arise from self-interactions in the hidden sector (e.g. σ^3) and are transfered to the visible sector by linear mixings, generically allow for large non-Gaussianities, as opposed to cubic interactions that mix both sectors. These theories ultimately lead to natural models, in the sense that they do not involve fine-tuning at tree- nor loop-level to generate large signals, see [265, 316].

Multiple-exchange processes can involve the exchange of different fields which leave characteristic signatures that differ from the (multiple) exchange of a single particle species. Extensions of quasi-single field inflation in the case of multiple additional heavy scalar fields were first studied in [317]. The bispectrum shape is

shown to be sensitive to the lightest field. Specific mixings between additional fields can lead to a local-type shape in the squeezed limit with oscillations [318]. Multiple light scalar fields that do not couple directly to the visible sector but to an intermediate heavy field were studied in [319]. Such models of "missing scalars" induce a mass correction—mimicking a thermal mass correction—entering the standard cosmological collider signal of the heavy field and lead to a $(k_3/k_1)^\alpha$ suppression of the amplitude of the non-analytic part of the correlator, where $\alpha \propto g^2$ with g the coupling constant between both hidden sectors. When several additional massive scalar fields, their representation in the *flavour basis* in general differs from the freely propagating *mass basis*, due to their specific mixings to the visible sector. These mixings in turn induce modulated cosmological collider signals, whose amplitudes depend on the mixing angles between the two basis and frequencies set by the mass eigenvalues [320]. Disentangling the mass spectrum of additional fields in the cosmological collider signal has been considered in [321]. The interesting case of particles with a continuous mass spectrum, i.e. $m^2 \to \rho(m^2)$ where ρ is the spectral density, was investigated in [322].

Standard Model signatures. Studying cosmological collider physics with the hope to detect new physics requires good knowledge of the signatures from known physics, in our case from Standard Model (SM) particles. A careful and complete study of this SM background in cosmological collider signals has been conducted in [295, 296], see also [300]. This requires both determining the SM spectrum during inflation in the electroweak unbroken phase, and evaluating loop corrections as SM particles contribute to the bispectrum at loop level. Accordingly, spin-0, 1/2, and 1 particles induce 1-loop corrections to Schwinger-Keldysh propagators, that have been computed, renormalised and resummed using dynamical renormalisation group methods in [294]. In particular, it was shown that SM particles can acquire large mass corrections from infrared-divergent loop diagrams, which significantly modify the SM spectrum. It was also shown that SM signatures can also enter the bispectrum at tree-level if the electroweak symmetry is broken [323, 324]. So-called *Cosmological Higgs Collider* signals were considered in [241, 246], exploiting the possibility that the visible sector originates from quantum fluctuations of the SM Higgs field through the modulated reheating process [325, 326, 75, 327]. Any deviation from these SM background signals can be considered as a baseline for probing new physics.

Beyond the Standard Model. With the SM background computed, beyond SM signatures can be investigated. Neutrino oscillations, due to their small non-zero masses introduced through a right-handed neutrino sector, are not described within the SM. The natural scale for right-handed neutrinos being around $\mathcal{O}(10^{13}\text{GeV})$, these beyond SM particles can be a target for cosmological collider physics. The spectrum of neutrinos during inflation and their signatures in correlators has been studied in [245]. Axion-like particles (including the QCD axion) were studied in [301]. Cosmological collider physics can also be a probe of leptogenesis with the non-analytic signal in correlators carying information about lepton-number violation [308]. Superheavy dark matter particles can be produced during inflation and

their impact on correlators has been studied in [228, 328]. Signatures from grand unified theories and imprints of higher-spin particles motivated by supersymmetry in cosmological collider signals have been considered in [303, 329, 298] and [299], respectively.

Alternatives to inflation. Non-analytic behaviours in soft limits of correlators can also be used to directly probe the time-evolution of the scale factor $a(t)$, therefore allowing to probe the primordial Universe evolution and possible alternatives to inflation. The idea stems from the realisation that quantum fluctuations of massive fields $\propto e^{imt}$ can be used as standard clocks. These fields undergo continuous quantum oscillations during inflation that are not a source of scale-invariance breaking, see [330, 331, 332, 333, 334] for classical primordial standard clocks generated by sharp features. The ever-present ticks of such clock fields allow $a(t)$ to be directly and model-independently encoded in the shape dependence of correlators. This was dubbed *quantum primordial standard clocks* [335, 336, 94, 337]. For inflation, non-analytic oscillations of correlators in the logarithm of momentum ratio crucially encodes $a(t) = e^{Ht}$, as $\log(k_\ell/k_s) = H\Delta t$ where Δt is the (cosmic) time elapsed between horizon crossing of the long and short modes. Changing the scale factor time dependence therefore amounts to change the functional form of the oscillatory pattern. For power-law cosmologies $a(t) \sim t^p$, the non-analytic part oscillates in $(k_s/k_\ell)^{1/p}$.

Loop-level cosmological colliders. Exact calculations of cosmological correlators, including analytic and non-analytic signals, at 1-loop order have been conducted in [302] with a numerical approach. Details on the direct numerical implementation of Feynman integrals, including integral ranges and gridding, Wick rotation, and integral divergences as well as regularisations can be found therein. Information about the particle content of inflation has been shown to be also encoded in the phase of cosmological collider signals [304]. Analytical results of full non-analytic signals (making use of cutting rules for propagators that factorises time-ordered diagrams [263]) at 1-loop order are presented, allowing for deriving cosmological collider templates also away from soft configurations. This enables to break potential degeneracies between two similar signals. The use of spectral decomposition in de Sitter allows to build loop-level diagrams out of tree-level ones [338]. Closed-form solutions for arbitrary non-analytic signals of 1-particle-irreducible 1-loop correlators using factorisation properties and cutting rules can be found in [307], see also [339].

Chemical potential. The chemical potential naturally enhances the amplitude of cosmological collider signals as it boosts particle production. An in-depth analysis of the size of the oscillatory signal generated by the exchange of scalars, spin-1/2 fermions, gauge bosons, and spin-2 particles with chemical potential is presented in [237], also see [242] and [340] for the calculation of the cosmological collider signal generated by gauge bosons and complex scalar fields, respectively. Exact analytical correlators—using Mellin-Barnes representation for the bulk-to-bulk propagator and bootstrap methods—in all kinematic configurations are presented in [305]. Hints of

a chemical potential assisted gauge bosons during inflation can also appear in gravitational waves at small scales [341]. In the SM, the so-called strong CP problem is solved by introducing a dynamical field known as the axion. During inflation, CP is spontaneously broken by the rolling background of this axion and is naturally described through a chemical potential. CP violation is then shown to be encoded in the parity-odd (imaginary) trispectrum as a distinctive angular dependence [106]. Interestingly, superconductivity can lead to Bardeen-Cooper-Schrieffer (BCS) condensate of Cooper pairs (binded electrons) at low temperature, which spontaneously breaks the electromagnetic $U(1)$ symmetry. Analogous BCS condensation has been studied in the context of primordial cosmology [309]. Cosmological collider signals then encode the BCS phase transition, since different momentum ratios effectively probe different energy scales, i.e. different temperatures. Further about the chemical potential will be discussed in Chap. 7, Chap. 8 and Chap. 11.

Primordial features. A breaking of scale-invariance leads to scale-dependent features in the power spectrum and in the scale dependence of higher-order correlators. However, features can also leave some imprints in the shape dependence of correlators, and more specifically on cosmological collider signals [342, 315, 316]. Since these features classically excite massive particles, the resulting signals are unsuppressed. Observable shapes, found after properly subtracting the consistency relation, are presented in Chap. 15. Ultimately, a time-dependent mass of the exchanged heavy particle is imprinted in a running of the scaling behaviour of the bispectrum squeezed limit [343, 344, 345].

Part II

Fundamental Aspects of Cosmological Correlators

5

Schwinger-Keldysh Formalism

Cosmological correlators provide an exciting probe of the physics governing the earliest moments of our Universe. Fortunately, we have well-established methods for computing them. In flat-space quantum field theory, perturbative calculations of S-matrix elements are efficiently performed using Feynman diagrams, whose rules follow directly from a classical Lagrangian. This approach circumvents the need to explicitly switch to the Hamiltonian formulation and manually perform field contractions, as reviewed in Chap. 12, which forms the foundation of the systematic cosmological flow framework exposed in Part IV. Similarly, cosmological correlators can be computed using the Schwinger-Keldysh formalism, a path integral approach particularly suited for systems with an evolving background, as illustrated in Fig. 5.1. For historical context, see [346, 347, 348]; for broader reviews, see [349, 350, 351]; and for applications in cosmology, refer to [352, 353, 354, 355, 356].

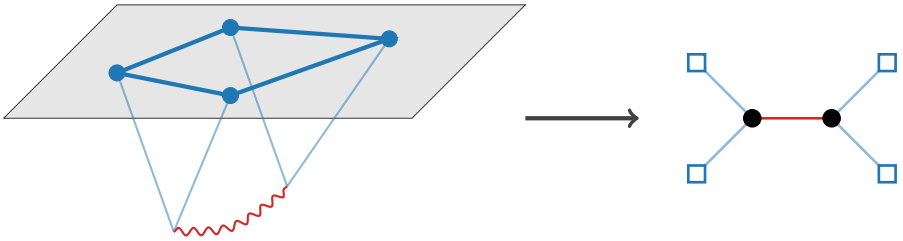


Figure 5.1: Cosmological correlators can be computed using handy Schwinger-Keldysh diagrammatic rules.

This chapter provides a comprehensive review of the Schwinger-Keldysh formalism, formulated within the path integral framework and naturally leading to a set of practical Feynman rules. Throughout the text, numerous worked-out examples illustrate key computations, making this material accessible for readers aiming to develop a solid foundation in first-principles calculations of cosmological correlation

functions.

5.1 Preliminaries

In the path integral formalism, the fundamental objects are *classical field configurations*, in contrast to the *field operators* of canonical quantisation. This approach is often more convenient to handle while remaining fully equivalent to the operator formalism. By relying on the Lagrangian—whose role will become clear in what follows—the path integral framework naturally leads to efficient diagrammatic rules for computing observables perturbatively. Moreover, working directly with the Lagrangian offers significant advantages: (i) most physical theories are formulated in this language, (ii) it allows for a broader range of gauge choices (e.g. simplifying the treatment of gauge fields), (iii) and it may even provide insights into non-perturbative effects.

In a nutshell, the fundamental leap of the path integral approach is to realise that the generating functional, i.e. the transition amplitude from an initial state with no particles at some time t_0 to a later state with no particles at $t > t_0$, can be expressed as a functional integral over all field configurations, each one being weighted by a factor determined by the Lagrangian. Coupling the theory to a fiducial current source, correlation functions are determined as the responses of the generating functional to this source. Ironically yet quite elegantly, the path integral formalism perfectly reflects our poor capability to only be able to compute Gaussian integrals.

5.1.1 Constructing Path Integrals

Keeping in mind that we eventually aim at computing cosmological correlators, we start by recalling how standard transition amplitudes can be recasted as path integral by adopting a constructionist approach.

In quantum mechanics. In elementary quantum mechanics, the amplitude that a particle starts at point q_0 at time t_0 and ends up at point q at time t (i.e. the propagator) is found by summing all possible trajectories subjected to appropriate boundary conditions[1]

$$\langle q;t|q_0;t_0\rangle = \int_{q(t_0)=q_0}^{q(t)} \mathcal{D}[q(t)]\, e^{i\int_{t_0}^{t} \mathrm{d}t\, L[q(t)]}\,. \tag{5.1}$$

The derivation is based on splitting the trajectory into N infinitesimal steps Δt and inserting a complete set of position eigenstates $\mathbb{1} = \int \mathrm{d}q_n\, |q_n\rangle\, \langle q_n|$ in between each tiny time-evolution operator. Then, each "mini" propagator is evaluated by replacing

[1] If the Hamiltonian $\hat{H}$ does *not* depend on time t, the transition amplitude simply reads $\langle q;t|q_0;t_0\rangle = \langle q|e^{-\hat{H}(t-t_0)}|q_0\rangle$. When it is time dependent, the trick is to solve for this matrix element on infinitesimal time intervals where $\hat{H}$ can be taken to be constant.

operators by eigenvalues, crucially removing all operators in favour of numbers. This requires expanding $|q_n\rangle$ in terms of momentum eigenstates. The integrals over the introduced momenta being Gaussian, it can be performed exactly which enables one to reconstruct the Lagrangian out of the Hamiltonian. Finally, the path integral is found by taking the continuous limit $N \to \infty$ and $\Delta t \to 0$. We refer to the textbooks [357, 358] (or any other elementary course on the matter) for the detailed derivation.

In QFT. We would like to explicitly construct the transition amplitude $\langle\varphi(t)|\varphi_0(t_0)\rangle$ between an initial state with field configuration $\varphi_0(\boldsymbol{x})$ at time t_0 to a final state with field configuration $\varphi(\boldsymbol{x})$ at time t. In standard quantum mechanics, the trick is to break the amplitude by inserting a complete set of eigenstates of the position operator $\hat{q}$. In QFT, we instead use a complete set of eigenstates of the field operator $\hat{\varphi}$. Working with the Schrödinger-picture field $\hat{\varphi}(\boldsymbol{x})$ and momentum $\hat{p}(\boldsymbol{x})$, a complete eigenbasis of the Hilbert space is defined by

$$\hat{\varphi}(\boldsymbol{x})\,|\varphi\rangle = \varphi(\boldsymbol{x})\,|\varphi\rangle \ , \quad \hat{p}(\boldsymbol{x})\,|p\rangle = p(\boldsymbol{x})\,|p\rangle \ . \tag{5.2}$$

The states $|\varphi\rangle$ are conjugate to the states $|p\rangle$, i.e. $\langle p|\varphi\rangle = \exp\left(-i\int \mathrm{d}^3x\, p(\boldsymbol{x})\varphi(\boldsymbol{x})\right)$,[2] which enables to define the overlap between two field states by using the completeness of the momentum basis $\langle\varphi'|\varphi\rangle = \int \mathcal{D}[p(\boldsymbol{x})]\,\langle\varphi'|p\rangle\,\langle p|\varphi\rangle$, where $\mathcal{D}[p(\boldsymbol{x})]$ (resp. $\mathcal{D}[\varphi(\boldsymbol{x})]$) is the measure in the space of momentum (resp. field) configurations which will be properly defined later.[3] Intuitively, it involves summing over all possible spatial field configurations. In order to make progress in evaluating $\langle\varphi(t)|\varphi_0(t_0)\rangle$, we now discretise time in N infinitesimal steps with duration $\Delta t \equiv (t-t_0)/N$, sufficiently small that $\hat{H}(t) \approx \hat{H}(t_n)$ during $t_n \leq t \leq t_{n+1}$. This way, the scalar product is easy to compute as the Hamiltonian can be assumed to be constant during Δt. Between two consecutive time steps, the Heisenberg-picture field operators evolve as

$$\hat{\varphi}(t_n) = e^{i\Delta t\hat{H}(t_{n-1})}\hat{\varphi}(t_{n-1})e^{-i\Delta t\hat{H}(t_{n-1})} \ , \tag{5.3}$$

which implies $|\varphi(t_n)\rangle = e^{i\Delta t\hat{H}(t_{n-1})}\,|\varphi(t_{n-1})\rangle$ for the states. By induction until reaching the time t_0 at which initial conditions are given, one can show that the Heisenberg-picture field operators are related to Schrödinger-picture ones via

$$\hat{\varphi}(t_n) = \bar{\mathcal{T}}\left\{\exp\left(i\Delta t\sum_{j=0}^{n-1}\hat{H}(t_j)\right)\right\}\hat{\varphi}(t_0)\,\mathcal{T}\left\{\exp\left(-i\Delta t\sum_{j=0}^{n-1}\hat{H}(t_j)\right)\right\} \ , \tag{5.4}$$

which implies $|\varphi(t_n)\rangle = \bar{\mathcal{T}}\left\{\exp\left(i\Delta t\sum_{j=0}^{n-1}\hat{H}(t_j)\right)\right\}|\varphi(t_0)\rangle$, where $\mathcal{T}$ (resp. $\bar{\mathcal{T}}$) is the time ordering (resp. anti-time ordering) operator. Recall that at the initial time t_0 both pictures coincide. Let us now insert a complete set of field eigenstates after the first time step $t_1 = t_0 + \Delta t$ that we call φ_1, i.e. $\mathbb{1} = \int \mathcal{D}[\varphi_1(\boldsymbol{x})]\,|\varphi_1(t_1)\rangle\,\langle\varphi_1(t_1)|$ (it should be clear here that φ_1 is simply a dummy integration field configuration).

[2] The quantum mechanical analogue of this conjugation condition is $\langle p|q\rangle = e^{-ipq}$.

[3] This inner product generalises $\langle q'|q\rangle = \delta(q-q') = \int \frac{\mathrm{d}p}{2\pi}\, e^{-ip(q-q')}$.

After infinitesimally propagating the state $\langle\varphi_1(t_1)|$ to t_0, we then obtain

$$\begin{aligned}\langle\varphi(t)|\varphi_0(t_0)\rangle &= \int \mathcal{D}[\varphi_1(\boldsymbol{x})]\,\langle\varphi(t)|\varphi_1(t_1)\rangle\,\langle\varphi_1(t_1)|\varphi_0(t_0)\rangle \\ &= \int \mathcal{D}[\varphi_1(\boldsymbol{x})]\,\langle\varphi(t)|\varphi_1\rangle\,\langle\varphi_1|e^{-i\Delta t\hat{H}(t_0)}|\varphi_0(t_0)\rangle\ .\end{aligned} \tag{5.5}$$

Repeating this procedure, we can insert $N-1$ copies of the complete set of field eigenstates, one at each time step t_n, which yields

$$\begin{aligned}&\langle\varphi(t)|\varphi_0(t_0)\rangle = \int \mathcal{D}[\varphi_1(\boldsymbol{x})]\ldots\int \mathcal{D}[\varphi_{N-1}(\boldsymbol{x})] \\ &\times\langle\varphi(t)|e^{-i\Delta t\hat{H}(t_{N-1})}|\varphi_{N-1}\rangle\,\langle\varphi_{N-1}|\ldots|\varphi_1\rangle\,\langle\varphi_1|e^{-i\Delta t\hat{H}(t_0)}|\varphi_0(t_0)\rangle\ .\end{aligned} \tag{5.6}$$

Note that discretising time this way enables us to neglect time ordering, which is in general the source of complication. Let us now evaluate each of the infinitesimal matrix elements $\langle\varphi_{n+1}|e^{-i\Delta t\hat{H}(t_n)}|\varphi_n\rangle$. To do this, we need to specify a form for the Hamiltonian. We take it to be $\hat{H}(t)=\int \mathrm{d}^3x\,\hat{\mathcal{H}}$ with the Hamiltonian density being $\hat{\mathcal{H}}=\frac{1}{2}\,\hat{p}^2(\boldsymbol{x})+\hat{V}[\hat{\varphi}(\boldsymbol{x})]$, where $\hat{V}$ includes interactions and the time dependence of $\hat{H}$ comes from how the operators change with time in the full interacting theory. At this stage, there is an important subtlety which is worth mentioning straight away. In cosmology, we usually have time-derivative interactions (e.g. $\dot{\varphi}^3$) which makes the potential term $\hat{V}$ depend on the conjugate momentum. Whenever interactions mix field and momentum operators, different orderings of the quantum Hamiltonian lead to different discretised versions of the path integral. For example, if a mixing term of the form φp is present in the *classical* Hamiltonian, there are infinitely many non-equivalent representations for the *quantum* Hamiltonian, e.g. $\hat{\varphi}\hat{p},\hat{p}\hat{\varphi},(\hat{\varphi}\hat{p}+\hat{p}\hat{\varphi})/2,\hat{\varphi}^{1/2}\hat{p}\hat{\varphi}^{1/2}$, etc. In this case, it is standard to define the quantum Hamiltonian to be *Weyl ordered* with the momentum operators all to the left of field operators. This subtlety being mentioned, we now insert a complete set of momentum eigenstates, i.e. $\mathbb{1}=\int\mathcal{D}[p_n(\boldsymbol{x})]\,|p_n\rangle\,\langle p_n|$ to obtain

$$\begin{aligned}&\langle\varphi_{n+1}|e^{-i\Delta t\hat{H}(t_n)}|\varphi_n\rangle = \int \mathcal{D}[p_n(\boldsymbol{x})]\,\langle\varphi_{n+1}|p_n\rangle\,\langle p_n|e^{-i\Delta t\int\mathrm{d}^3x\left[\frac{1}{2}\,\hat{p}^2(\boldsymbol{x})+\hat{V}[\hat{\varphi}(\boldsymbol{x})]\right]}|\varphi_n\rangle \\ &\approx \int \mathcal{D}[p_n(\boldsymbol{x})]\,\langle\varphi_{n+1}|p_n\rangle\,\langle p_n|e^{-i\frac{\Delta t}{2}\int\mathrm{d}^3x\hat{p}^2(\boldsymbol{x})}e^{-i\Delta t\int\mathrm{d}^3x\hat{V}[\hat{\varphi}(\boldsymbol{x})]}|\varphi_n\rangle \\ &= \int \mathcal{D}[p_n(\boldsymbol{x})]\,\langle\varphi_{n+1}|p_n\rangle\,\langle p_n|\varphi_n\rangle\,e^{-i\Delta t\int\mathrm{d}^3x\left(\frac{1}{2}\,p_n^2(\boldsymbol{x})+V[\varphi_n(\boldsymbol{x})]\right)} \\ &= \int \mathcal{D}[p_n(\boldsymbol{x})]\,e^{i\int\mathrm{d}^3x\,p_n(\boldsymbol{x})(\varphi_{n+1}(\boldsymbol{x})-\varphi_n(\boldsymbol{x}))}\,e^{-i\Delta t\int d^3x\left(\frac{1}{2}\,p_n^2(\boldsymbol{x})+V[\varphi_n(\boldsymbol{x})]\right)}\ ,\end{aligned} \tag{5.7}$$

where we have neglected $\mathcal{O}(\Delta t^2)$ contributions as we will anyway take the $\Delta t\to 0$ limit in the end. This important step is the upshot of the path integral construction: using the correct basis to expand the unity operator $\mathbb{1}$, we have completely traded operators for field and momentum configurations. Noticing that the functional in-

tegral over the momentum is Gaussian, it can be directly carried out, yielding[4]

$$\langle\varphi_{n+1}|e^{-i\Delta t\hat{H}(t_n)}|\varphi_n\rangle = \mathcal{N}\, e^{i\Delta t\int \mathrm{d}^3x\left[\frac{1}{2}\left(\frac{\varphi_{n+1}(\boldsymbol{x})-\varphi_n(\boldsymbol{x})}{\Delta t}\right)^2 - V[\varphi_n(\boldsymbol{x})]\right]}\,, \tag{5.9}$$

with $\mathcal{N} = (2\pi/i\Delta t)^{1/2}$. Of course, this only holds if the theory does not contain higher-order time-derivative interactions, as the Hamiltonian is simply quadratic in the momentum. If it is not the case, this integral cannot be exactly evaluated. However, it can still be carried out in a perturbative manner. It was shown in [356] that the result agrees with canonical perturbation theory (see Chap. 12) up to fourth order in the fields (in passing somehow suggesting that this statement might be correct at the non-perturbative level), which is enough for most of cosmological applications. In what follows, we will assume that (5.9) holds with higher-order time-derivative interactions. Coming back to the full transition amplitude, we now take the continuous limit $\Delta t \to 0$ and $N \to \infty$ while keeping the product $N\Delta t$ constant, to obtain

$$\langle\varphi(t)|\varphi_0(t_0)\rangle = \int_{\varphi_0(\boldsymbol{x})}^{\varphi(\boldsymbol{x})} \mathcal{D}[\varphi(t,\boldsymbol{x})]\, e^{i\int_{t_0}^{t}\mathrm{d}t\int\mathrm{d}^3x\,\mathcal{L}[\varphi(t,\boldsymbol{x})]}\,, \tag{5.10}$$

where we have defined a "continuous-time" measure for field configurations as

$$\int \mathcal{D}[\varphi(t,\boldsymbol{x})] \equiv \lim_{\substack{N\to 0\\ \Delta t\to 0}} \prod_{n=1}^{N-1} \frac{2\pi}{i\Delta t}\int \mathcal{D}[\varphi_n(\boldsymbol{x})]\,. \tag{5.11}$$

Although being over all field configurations, the path integral (5.10) is subject to boundary conditions that we have clearly written, i.e. from the field configuration $\varphi_0(\boldsymbol{x})$ at t_0 to $\varphi(\boldsymbol{x})$ at t.[5] It is rather remarkable that the Lagrangian appears explicitly. In fact, performing the functional integral over momenta effectively does the Legendre transform.

5.1.2 Generating Correlation Functions

The transition amplitude (5.10) is written as a path integral where the functions $\varphi(t,\boldsymbol{x})$ over which we integrate are constrained to the specific configurations $\varphi_0(\boldsymbol{x})$ at t_0 and $\varphi(\boldsymbol{x})$ at t. However, we really want access to all of the correlation functions

[4] The (one-dimensional) result we need is

$$\int_{-\infty}^{+\infty}\mathrm{d}x\, e^{-\frac{1}{2}ax^2+bx} = \sqrt{\frac{2\pi}{a}}\, e^{\frac{b^2}{2a}}\,, \tag{5.8}$$

with the replacement $a = i\Delta t$ and $b = i(\varphi_{n+1} - \varphi_n)$. This result straightforwardly generalises to functional integrals.

[5] Without performing the integral over momenta, we would have found that the final path integral over momentum configurations is unconstrained. This can be traced back to the fact that we are describing transition amplitudes between field eigenstates. Technically, this can also be seen in the discretised path integral where there is an additional integration over $p_0(\boldsymbol{x})$ (while $\varphi_0(\boldsymbol{x})$ is fixed).

for a theory, since these contain all of the physics. The relevant quantity is then the partition function $Z(t,t_0)$ which is defined as the sum of all possible transition amplitudes from one field configuration at time t_0 to the same field configuration at later time t, for any such field configuration. From the derived previous result (5.10), the partition function can be written as a path integral over all field configurations

$$Z(t,t_0) \equiv \int \mathcal{D}[\varphi(t,\boldsymbol{x})]\ \langle\varphi(t)|\varphi(t_0)\rangle = \int \mathcal{D}[\varphi(t,\boldsymbol{x})]\, e^{i\int_{t_0}^{t}\mathrm{d}t\int\mathrm{d}^3x\,\mathcal{L}[\varphi(t,\boldsymbol{x})]}\,, \tag{5.12}$$

where the initial and final field configurations are not constrained anymore, as we have integrated over the boundary conditions.

Generating functional and correlation functions. There is an easy way to work out correlation functions from the objects we have previously defined and constructed. The trick is to realise that all of the information about the theory can be generated by a single entity called the generating functional $Z[J]$, defined by $Z[J] = \langle\Omega|\hat{U}(t,t_0)|\Omega\rangle_J$, i.e. the transition amplitude of starting in the "in" vacuum at t_0 and ending up in the "out" vacuum at later time t, in the presence of a source $J(t,\boldsymbol{x})$ which couples linearly to the field $\varphi(t,\boldsymbol{x})$: $\mathcal{L}[\varphi(t,\boldsymbol{x})] \to \mathcal{L}[\varphi(t,\boldsymbol{x})] + J(t,\boldsymbol{x})\varphi(t,\boldsymbol{x})$. This object is a specific partition function for which the initial and final states have been meticulously chosen (the vacuum), and the theory slightly modified. We could actually call $Z[J]$ a "no particle propagator". The reason why J is referred to as a source is that this term generates particle excitations in the field φ. In fact, $Z[J]$ allows two classes of processes: (i) those where an excitation is created by J at t_0 and later absorbed by J at t, and (ii) those where an excitations spontaneously appears and then disappears without the aid of J. The latter class is generated by $Z[J=0]$ and corresponds to vacuum diagrams which need to be removed by normalisation. Correlation functions can be recovered from the generating functional by taking the functional derivatives with respect to the source

$$i^n\,\langle\Omega|\mathcal{T}\{\hat{\varphi}(t_1,\boldsymbol{x}_1)\dots\hat{\varphi}(t_n,\boldsymbol{x}_n)\}|\Omega\rangle = \frac{1}{Z[0]}\frac{\delta^n Z[J]}{\delta J(t_1,\boldsymbol{x}_1)\dots\delta J(t_n,\boldsymbol{x}_n)}\bigg|_{J=0}\,, \tag{5.13}$$

where the generating functional being explicitly written as

$$Z[J] = \int \mathcal{D}[\varphi(t,\boldsymbol{x})]\,\exp\left(i\int_{t_0}^{t}\mathrm{d}t\int\mathrm{d}^3x\,\left[\mathcal{L}[\varphi(t,\boldsymbol{x})] + J(t,\boldsymbol{x})\varphi(t,\boldsymbol{x})\right]\right)\,, \tag{5.14}$$

see standard textbooks e.g. [357, 359, 360] to see how the time ordering appears explicitly. In cosmology, we are interested in computing equal-time correlation functions, so time ordering here is unimportant. The generating functional (5.14) generates standard Feynman rules. So far, we have only reviewed the standard functional approach to QFT. Let us now apply the same path integral approach to cosmological correlators, the aim being to explicitly construct the generating functional for the objects $\langle\Omega|\hat{\mathcal{O}}(t)|\Omega\rangle$ of interest in cosmology, where operators are sandwiched in between two "in" vacua rather than an "in" and an "out" vacuum.

5.2 Schwinger-Keldysh Path Integral

Let us now derive the Schwinger-Keldysh path integral to compute expectation values by drawing Feynman-like diagrams in inflationary cosmology. We will closely follow the clear presentation of [356].

5.2.1 Forward & Backward Evolution

The in-in path integral we look for in cosmology differs from the transition amplitudes defined and constructed previously by the fact that both the initial and the final states should be the ground "in" state $|\Omega\rangle$, which in general is not a field eigenstate. We would like to continuously connect the state $|\Omega\rangle$ to the operator $\hat{\mathcal{O}}(t)$ at the time t, and then go back to $|\Omega\rangle$. Clearly, since the notion of vacuum can only be defined in the asymptotic past, we can only approach the state $|\Omega\rangle$ by taking the asymptotic limit $t_0 \to -\infty$, when primordial fluctuations have wavelengths (in Fourier space) much smaller than the size of the cosmological horizon. To address this point, we first divide the in-in transition amplitude $\langle\Omega|\Omega\rangle$ (which is trivially one by the normalisation of the state) into two standard transition amplitudes that we constructed previously, by inserting a complete set of field eigenstates at the time t at which we eventually want to evaluate the observables

$$\langle\Omega|\Omega\rangle = \int \mathcal{D}\varphi \, \langle\Omega|\varphi(t)\rangle\langle\varphi(t)|\Omega\rangle \,, \tag{5.15}$$

where, from now on, we do not write the explicit space-time dependence of the field in the integration measure, $\mathcal{D}\varphi \equiv \mathcal{D}[\varphi(t,\boldsymbol{x})]$, to avoid clutter. The two contributions in Eq. (5.15) are referred to as the two "branches" of the Schwinger-Keldysh path integral. From right to left, the second branch, denoted $(+)$, represents a forward evolution from t_0 to t, and the first branch, denoted $(-)$, represents a backward evolution from t to t_0. To make contact with transition amplitudes between field eigenstates, we now insert a complete set of field eigenstates at time t_0, and use the result (5.10) to obtain

$$\begin{aligned}\langle\varphi(t)|\Omega\rangle &= \int \mathcal{D}\varphi_0^+ \, \langle\varphi(t)|\varphi_0^+(t_0)\rangle \, \langle\varphi_0^+(t_0)|\Omega\rangle \\ &= \int \mathcal{D}\varphi_0^+ \, \langle\varphi_0^+(t_0)|\Omega\rangle \int_{\varphi_0^+(\boldsymbol{x})}^{\varphi(\boldsymbol{x})} \mathcal{D}\varphi_+ \, e^{i\int_{t_0}^t \mathrm{d}t\mathrm{d}^3x\,\mathcal{L}[\varphi_+]} \,,\end{aligned} \tag{5.16}$$

and

$$\begin{aligned}\langle\Omega|\varphi(t)\rangle &= \int \mathcal{D}\varphi_0^- \, \langle\Omega|\varphi_0^-(t_0)\rangle \, \langle\varphi_0^-(t_0)|\varphi(t)\rangle \\ &= \int \mathcal{D}\varphi_0^- \, \langle\Omega|\varphi_0^-(t_0)\rangle \int_{\varphi_0^-(\boldsymbol{x})}^{\varphi(\boldsymbol{x})} \mathcal{D}\varphi_- \, e^{-i\int_{t_0}^t \mathrm{d}t\mathrm{d}^3x\,\mathcal{L}[\varphi_-]} \,.\end{aligned} \tag{5.17}$$

The two branches can then be re-combined by noting that the boundary conditions at t impose both $|\varphi_\pm(t)\rangle = |\varphi(t)\rangle$. This is the only place where the field φ appears

explicitly, so the integration over φ can be done explicitly. The result is simply that the endpoints at t of each branch should coincide:

$$\begin{aligned}&\int \mathcal{D}\varphi\mathcal{D}\varphi_+\mathcal{D}\varphi_- \int \mathrm{d}^3x \prod_{\pm} \delta[\varphi_\pm(t,\boldsymbol{x}) - \varphi(t,\boldsymbol{x})] \\ &= \int \mathcal{D}\varphi_+\mathcal{D}\varphi_- \int \mathrm{d}^3x\, \delta[\varphi_+(t,\boldsymbol{x}) - \varphi_-(t,\boldsymbol{x})]\,,\end{aligned} \tag{5.18}$$

where δ here is the Kronecker functional distribution in the space of field configurations. We can therefore define a new integration contour as starting at t_0 with unconstrained field configuration (due to the integration over φ_0^+), evolving φ_+ until reaching the external time t, and then coming back independently by evolving φ_- (except that both $\varphi_\pm$ field configurations should coincide at t) until t_0 with again unconstrained field configuration (due to the integration over φ_0^-). This contour is illustrated in Fig. 5.2. Taking into account the integrations over $\varphi_0^\pm$ as we did for the standard partition function in Eq. (5.12) to leave the lower bounds on $\varphi_\pm$ unconstrained, we eventually find the in-in partition function

$$\begin{aligned}Z(t,t_0) \equiv \langle\Omega|\Omega\rangle = &\int \mathcal{D}\varphi_\pm\ \langle\Omega|\varphi_0^-(t_0)\rangle\,\langle\varphi_0^+(t_0)|\Omega\rangle \\ &\times \int \mathrm{d}^3x\, \delta[\varphi_+(t,\boldsymbol{x}) - \varphi_-(t,\boldsymbol{x})]\, \exp\left(i\int_{t_0}^{t} \mathrm{d}t\mathrm{d}^3x\, (\mathcal{L}[\varphi_+] - \mathcal{L}[\varphi_-])\right),\end{aligned} \tag{5.19}$$

where the path integrals over $\varphi_\pm$ are unconstrained at t_0 and t. This result contains two copies of the standard partition function (5.12) with the condition that both branches ($\pm$) are sewn at the time t. The apparent doubling of the degrees of freedom, simply corresponding to independent dummy variables for fields along both branches, is typical of the Schwinger-Keldysh formalism.

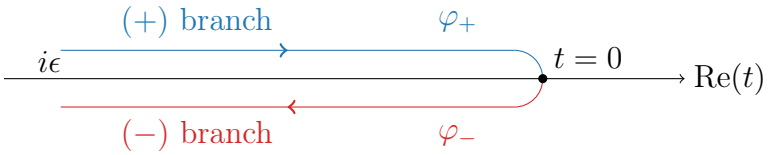


Figure 5.2: Illustration of the Schwinger-Keldysh contour in the complex time plane for the path integral (5.19). As only the initial state is available, i.e. the "in" vacuum $|\Omega\rangle$, the dynamics is first evolved forward in time from t_0 to t on the (+) branch with $\mathcal{L}[\varphi_+]$, and then backwards from t to t_0 on the (−) branch with $\mathcal{L}[\varphi_-]$. The two branches are sewn at t by imposing that both *a priori* independent field configurations $\varphi_\pm$ should coincide, i.e $\varphi_+(t,\boldsymbol{x}) = \varphi_-(t,\boldsymbol{x})$. In the limit $t_0 \to -\infty$, the vacuum wavefunctionals $\langle\varphi_0^+(t_0)|\Omega\rangle$ and $\langle\Omega|\varphi_0^-(t_0)\rangle$ provide the correct $i\epsilon$ prescription on the two branches $k \to k \pm i\epsilon$, leading to the in-in partition function (5.29) of interest for inflationary cosmology.

The expression (5.19) is almost in the desired form: two path integrals over $\varphi_\pm$ (which should coincide at t) weighted by a factor determined by the Lagrangian $\mathcal{L}[\varphi_\pm]$. The only non-explicit pieces are the remaining projection amplitudes of the

initial field eigenstates at t_0 onto the vacuum. Those factors are not specific to cosmology, and are ever-present in standard QFT. There are several ways to deal with these, which all lead to the same physical prescription. In particular, we will now show that these two inner products actually provide us with the correct $i\epsilon$ prescription.

5.2.2 $i\epsilon$ Prescription

Let us compute the so-called vacuum wave-functional $\Psi[\varphi](t_0) \equiv \langle\varphi(t_0)|\Omega\rangle$, i.e. transition amplitude from the vacuum of the full theory to a specific field configuration $\varphi(\boldsymbol{x})$ at some time t_0, following [357] (Sec. 9.2) but adapted to our case of interest, also see [361]. The idea is to look for an equation satisfied by $\Psi[\varphi](t_0)$ and then solve it. We keep in mind that we are eventually looking for the quantity $\Psi[\varphi_0^{\pm}](t_0)$ in the limit $t_0 \to -\infty$. Briefly coming back to the more fundamental Hamiltonian description, we make use of the free theory in the asymptotic past $t_0 \to \infty$ to canonically quantise the field and momentum operators in Fourier space

$$\hat{\varphi}_{\boldsymbol{k}}(t_0) = \varphi_k(t_0)\hat{a}_{\boldsymbol{k}} + \varphi_k^*(t_0)\hat{a}^\dagger_{-\boldsymbol{k}}\,, \quad \text{and} \quad \hat{p}_{\boldsymbol{k}}(t_0) = p_k(t_0)\hat{a}_{\boldsymbol{k}} + p_k^*(t_0)\hat{a}^\dagger_{-\boldsymbol{k}}\,, \tag{5.20}$$

where the creation and annihilation operators verify the usual commutation relation, together with $\hat{a}_{\boldsymbol{k}}\,|\Omega\rangle = 0$.[6] Together with the Wronskian condition $\varphi_k p_k^* - \varphi_k^* p_k = i$ (fixed by the commutation relation), the relations (5.20) can be inverted to find $\hat{a}_{\boldsymbol{k}} = \frac{1}{i}\left(p_k^*\,\hat{\varphi}_{\boldsymbol{k}} - \varphi_k^*\,\hat{p}_{\boldsymbol{k}}\right)$. Note that this relation holds at any time. We now want to write the annihilation operator in the field eigenbasis, so we use the field-space representation of the momentum operator $\hat{p}_{\boldsymbol{k}} \to -i\delta/\delta\varphi_{\boldsymbol{k}}$, with $\delta\varphi_{\boldsymbol{q}}/\delta\varphi_{\boldsymbol{k}} = (2\pi)^3\delta^{(3)}(\boldsymbol{q}+\boldsymbol{k})$.[7] The condition $\hat{a}_{\boldsymbol{k}}\,|\Omega\rangle = 0$ projected on the state $\langle\varphi(t_0)|$ gives the following functional differential equation for $\Psi[\varphi](t_0)$

$$0 = \langle\varphi(t_0)|\hat{a}_{\boldsymbol{k}}|\Omega\rangle = \left(\varphi_k^*\,\frac{\delta}{\delta\varphi_{\boldsymbol{k}}} - ip_k^*\varphi_{\boldsymbol{k}}\right)\Psi[\varphi](t_0)\,. \tag{5.21}$$

The analogous ordinary differential equation has a well-known Gaussian solution, so let's try the following functional Gaussian ansatz

$$\Psi[\varphi](t_0) = \mathcal{N}\,\exp\left(-\frac{1}{2}\int\frac{\mathrm{d}^3q}{(2\pi)^3}\frac{\mathrm{d}^3q'}{(2\pi)^3}\,\varphi_{\boldsymbol{q}}(t_0)\mathcal{E}_{\boldsymbol{q},\boldsymbol{q}'}(t_0)\varphi_{\boldsymbol{q}'}(t_0)\right)\,, \tag{5.22}$$

with kernel $\mathcal{E}$ in Fourier space and constant $\mathcal{N}$ to be determined. Substituting this ansatz in Eq. (5.21) and noting that the functional differential equation should be satisfied for all $\varphi_{\boldsymbol{k}}$, we obtain

$$\varphi_k^*\int\frac{\mathrm{d}^3q}{(2\pi)^3}\,\mathcal{E}_{\boldsymbol{q},-\boldsymbol{k}}(t_0)\varphi_{\boldsymbol{q}}(t_0) + ip_k^*\varphi_{\boldsymbol{k}}(t_0) = 0\,. \tag{5.23}$$

[6] In practice, it is not possible to find the mode functions defined with the creation and annihilation operators with respect to the vacuum of the full theory $|\Omega\rangle$. In this case, we have to resort to perturbation theory, and the mode functions are defined with respect to the vacuum of the free theory only $|0\rangle$. Here, we are not particularly careful about this distinction as we have in mind to work out the vacuum wave-functional in the infinite past limit, precisely when the free and interacting theories coincide.

[7] This is the functional generalisation of $\hat{p} \to -i\partial/\partial q$ in position representation for quantum mechanics.

This equation can be easily solved, yielding

$$\mathcal{E}_{\boldsymbol{q},\boldsymbol{q}'}(t_0) = (2\pi)^3\delta^{(3)}(\boldsymbol{q}+\boldsymbol{q}')\,\omega_q(\varphi,t_0)\,, \quad \text{with} \quad \omega_q(\varphi,t_0) = -i\,\frac{p_q^*}{\varphi_q^*}\,, \tag{5.24}$$

where the mode functions are evaluated at t_0. The constant $\mathcal{N}$ may be formally obtained from the normalisation condition for the vacuum state but we will not need this result in what follows. Eventually, we have found the vacuum wave-functional in a very general way to be

$$\Psi[\varphi](t_0) = \mathcal{N}\,\exp\left(-\frac{1}{2}\int\frac{\mathrm{d}^3k}{(2\pi)^3}\,\varphi_{\boldsymbol{k}}(t_0)\,\omega_k(\varphi,t_0)\,\varphi_{-\boldsymbol{k}}(t_0)\right)\,. \tag{5.25}$$

Let us now evaluate this solution for $\varphi = \varphi_0^+$ (we will simply take the complex conjugate for $\varphi = \varphi_0^-$) and take the limit $t_0 \to -\infty$. To do this, we introduce the following regularisation for any reasonably smooth function $f(t)$

$$f(-\infty) = \lim_{\epsilon\to 0}\,\epsilon\int_{-\infty}^{t}\mathrm{d}t' f(t')\,e^{\epsilon t'}\,, \tag{5.26}$$

with $\epsilon > 0$ an infinitesimal parameter, which at this stage is just a mathematical trick. This identity can be easily proved by integration by parts, and is valid for any upper bound t, in particular at the time we want to evaluate the correlators. Using Eqs. (5.25) and (5.26), the total contribution from vacuum wave-functionals in Eq. (5.19) is found to be

$$\lim_{t_0\to-\infty}\Psi[\varphi_0^+](t_0)\Psi^*[\varphi_0^-](t_0) =$$
$$\lim_{\epsilon\to 0}\,|\mathcal{N}|^2\,\exp\left(-\frac{\epsilon}{2}\int_{-\infty}^{t}\mathrm{d}t' e^{\epsilon t'}\int\frac{\mathrm{d}^3k}{(2\pi)^3}\left[\varphi_{0,\boldsymbol{k}}^+(t')\omega_k(\varphi_0^+,t')\varphi_{0,-\boldsymbol{k}}^+(t') + (+\leftrightarrow -)\right]\right)\,. \tag{5.27}$$

So far, we have avoided a discussion related to an explicit choice of vacuum state for the theory. In inflationary cosmology, a relevant notion of vacuum is the Bunch-Davies one which states that under the horizon, the fields should adiabatically converge to freely propagating flat-space plane waves, i.e. $\varphi_0(\tau) \sim e^{-ik\tau}$ in the limit $\tau \to -\infty$, where we momentarily switched to conformal time. From Eq. (5.24), we see that $\omega_k(\varphi_0^\pm) = k$, hence recovering the usual dispersion relation in the infinite past.[8] Taking the infinite past limit $t_0 \to -\infty$ in (5.19), we see that the net effect of the vacuum wave-functionals is therefore to add a contribution to the Lagrangian (written in Fourier space) in each branch[9]

$$\pm i\int_{-\infty}^{t}\mathrm{d}t\,\mathcal{L}[\varphi_{\boldsymbol{k},\pm}] \to \pm i\int_{-\infty}^{t}\mathrm{d}t\,\mathcal{L}[\varphi_{\boldsymbol{k},\pm}] - \lim_{\epsilon\to 0}\frac{\epsilon}{2}\int_{-\infty}^{t}\mathrm{d}t' e^{\epsilon t'}k\,\varphi_{\boldsymbol{k},\pm}(t')\varphi_{-\boldsymbol{k},\pm}(t')\,. \tag{5.28}$$

[8] Note that in general we have $\omega_k(\varphi_0^\pm) \propto k$ where the precise (possibly time-dependent) proportional constant depends on the theory. For example, for a canonically normalised scalar field with a sound speed in FLRW spacetime, i.e. $\mathcal{L}/a^3 = \frac{1}{2}\dot{\varphi}^2 - \frac{c_s^2}{2}\frac{(\partial_i\varphi)^2}{a^2}$, this gives $\omega_k(\varphi_0^\pm) = c_s k/a$.

[9] In flat-space QFT, note that the whole effect of the vacuum wave-functionals is to provide the usual $i\epsilon$ prescription in the denominator of the scalar field propagator in momentum space.

Clearly, these additional terms amount to adiabatically shut down interactions when going towards the infinite past, as the path integral now contains Gaussian weights in the fields with negative real values instead of purely imaginary ones. Independently of the precise form of the kinetic terms in the theory, in practice, the vacuum wave-functionals always amount to slightly shift the gradient contribution in the limit $t_0 \to -\infty$ as $k \to k \pm i\epsilon$ for the two branches. This is a good place to mention that the overall normalisation constant $|\mathcal{N}|^2$ is found to be unity due to the correct vacuum normalisation, i.e. $\langle\Omega|\Omega\rangle = 1$.[10]

Finally, after trading the vacuum wave-functional terms for the $i\epsilon$ prescription, the Schwinger-Keldysh partition function (5.19) reads

$$Z = \int_{\mathcal{C}} \mathcal{D}\varphi_{\pm} \exp\left(i \int_{-\infty}^{t} \mathrm{d}t\mathrm{d}^3x \left(\mathcal{L}[\varphi_+] - \mathcal{L}[\varphi_-] \right) \right) , \tag{5.29}$$

where the contour $\mathcal{C}$ goes in the upper-half complex plane from $-\infty^+$ to t where both branches are sewn and reverts towards $-\infty^-$ in the lower-half complex plane, with $-\infty^{\pm} \equiv -\infty(1 \mp i\epsilon)$, see Fig. 5.2. We have omitted writing explicitly the condition $\varphi_+(t, \boldsymbol{x}) = \varphi_-(t, \boldsymbol{x})$ as it should be understood as part of the integration contour.

5.3 Diagrammatic Rules

The derived in-in partition function (5.29) can be turned into a generating functional by adding sources to the fields. This allows us to compute cosmological correlators $\langle\Omega|\hat{\mathcal{O}}(t)|\Omega\rangle$ by taking functional derivatives, resulting in a set of diagrammatic rules analogous to Feynman rules in flat-space QFT. For simplicity in what follows, we will consider a single scalar real field $\varphi(t, \boldsymbol{x})$. Generalisations to multiple (spinning) fields is straightforward and is discussed when introducing propagators. A summary of Schwinger-Keldysh diagrammatic rules can be found by following the coloured link.

5.3.1 Generating Functional

The partition function (5.29) is an interesting formal object, but the normalisation of the "in" state $|\Omega\rangle$ imposes the trivial property $Z = 1$ for any final time t.[11] In order to compute correlation functions, we introduce external sources $J_{\pm}(t, \boldsymbol{x})$ for the fields $\varphi_{\pm}(t, \boldsymbol{x})$, and define the generating function $Z[J_+, J_-]$ as

$$Z[J_+, J_-] = \int_{\mathcal{C}} \mathcal{D}\varphi_{\pm} \exp\left(i \int_{-\infty}^{t} \mathrm{d}t\mathrm{d}^3x \left(\mathcal{L}[\varphi_+] + J_+\varphi_+ - \mathcal{L}[\varphi_-] - J_-\varphi_- \right) \right) . \tag{5.30}$$

[10] The usual argument to discard such constants for in-out matrix elements goes as follows: in calculating the connected part of vacuum expectation values of time-ordered products we eliminate the contribution of disconnected bubble diagrams by dividing by the in-out inner product $\langle\Omega|\Omega\rangle$, therefore cancelling any constant factors.

[11] Recall that the flat-space analogue is not automatically normalised to unity as the "in" vacuum may differ from the "out" vacuum.

This generating functional is the holy grail of any particular inflationary theory: if an exact closed-form expression for $Z[J_+, J_-]$ is known, then the theory is completely solved. A general equal-time n-point correlator $\langle\Omega|\varphi_{\mathsf{a}_1}(t,\boldsymbol{x}_1)\dots\varphi_{\mathsf{a}_n}(t,\boldsymbol{x}_n)|\Omega\rangle$ with $\mathsf{a}_1,\dots,\mathsf{a}_n=\pm$, can be computed by taking functional derivatives

$$\begin{aligned}\langle\varphi_{\mathsf{a}_1}(t,\boldsymbol{x}_1)\dots\varphi_{\mathsf{a}_n}(t,\boldsymbol{x}_n)\rangle &= \int_{\mathcal{C}}\mathcal{D}\varphi_\pm\,\varphi_{\mathsf{a}_1}(t,\boldsymbol{x}_1)\dots\varphi_{\mathsf{a}_n}(t,\boldsymbol{x}_n)\,\exp\left(i\int_{-\infty}^{t}\mathrm{d}t\mathrm{d}^3x\,(\mathcal{L}[\varphi_+]-\mathcal{L}[\varphi_-])\right)\\ &= \frac{1}{i\mathsf{a}_1\dots i\mathsf{a}_n}\,\frac{\delta^n Z[J_+,J_-]}{\delta J_{\mathsf{a}_1}(t,\boldsymbol{x}_1)\dots\delta J_{\mathsf{a}_n}(t,\boldsymbol{x}_n)}\bigg|_{J_\pm=0}\,,\end{aligned} \tag{5.31}$$

where from now on we omit the explicit reference to the vacuum. Unfortunately though, the full theory is often too complicated to allow for an exact calculation of the in-in generating functional. We therefore have to resort to perturbation theory by splitting the full Lagrangian into a free part $\mathcal{L}_0$ and an interacting part $\mathcal{L}_{\rm int}$, $\mathcal{L}=\mathcal{L}_0+\mathcal{L}_{\rm int}$. In general, $\mathcal{L}_0$ is taken to be the quadratic one that can be solved exactly, with $\mathcal{L}_{\rm int}$ containing higher-order interactions. Non-trivial quadratic mixings, almost ever-present in multi-field inflationary theories, are in general included in the interacting Lagrangian. The generating functional (5.30) can then be written

$$Z[J_+,J_-]=\exp\left(i\int_{-\infty}^{t}\mathrm{d}t\mathrm{d}^3x\left(\mathcal{L}_{\rm int}\left[\varphi_+\to\frac{\delta}{i\delta J_+}\right]-\mathcal{L}_{\rm int}\left[\varphi_-\to\frac{-\delta}{i\delta J_-}\right]\right)\right)Z_0[J_+,J_-]\,, \tag{5.32}$$

with

$$Z_0[J_+,J_-]=\int_{\mathcal{C}}\mathcal{D}\varphi_\pm\,\exp\left(i\int_{-\infty}^{t}\mathrm{d}t\mathrm{d}^3x\,(\mathcal{L}_0[\varphi_+]+J_+\varphi_+-\mathcal{L}_0[\varphi_-]-J_-\varphi_-)\right)\,. \tag{5.33}$$

This formula can be checked explicitly by applying successively the functional derivatives, thus generating the appropriate products of fields to reproduce the full Schwinger-Keldysh generating functional.[12] Then, as usual, provided the object Z_0 can be computed exactly, one can expand the exponential encoding interactions to some desired order, and, combined with (5.31), compute cosmological correlators.

[12] One subtelty concerns the presence of time-derivative interactions in $\mathcal{L}_{\rm int}$. In principle, those should be dealt with by keeping the action expressed in the Hamiltonian form (without performing the path integral over momenta), and by introducing currents both for fields J_φ and for momenta J_p. In the general case, the perturbative in-in generating functional reads

$$Z[J_\varphi^\pm,J_p^\pm]=\exp\left(-i\int_{-\infty}^{t}\mathrm{d}t\mathrm{d}^3x\left(\mathcal{H}_{\rm int}\left[\varphi_+\to\frac{\delta}{i\delta J_\varphi^+},p_+\to\frac{\delta}{i\delta J_p^+}\right]-(+\leftrightarrow-)\right)\right)Z_0[J_\varphi^\pm,J_p^\pm]\,, \tag{5.34}$$

with

$$Z_0[J_\varphi^\pm,J_p^\pm]=\int\mathcal{D}\varphi_\pm\mathcal{D}p_\pm\,\exp\left(i\int_{-\infty}^{t}\mathrm{d}t\mathrm{d}^3x\,(p_+\dot\varphi_+-\mathcal{H}_0[\varphi_+,p_+]+J_\varphi^+\varphi_++J_p^+p_+-(+\leftrightarrow-))\right)\,. \tag{5.35}$$

5.3.2 Propagators

Having defined the free theory $\mathcal{L}_0$, the *free* propagators $-i\Delta_{\mathsf{ab}}$ are defined as functional derivatives of the free generating functional

$$\begin{aligned} -i\Delta_{\mathsf{ab}}(t_1,\boldsymbol{x}_1;t_2,\boldsymbol{x}_2) &= \int_{\mathcal{C}} \mathcal{D}\varphi_{\pm}\, \varphi_{\mathsf{a}}(t_1,\boldsymbol{x}_1)\varphi_{\mathsf{b}}(t_2,\boldsymbol{x}_2) \exp\left(i\int_{-\infty}^{t} \mathrm{d}t\mathrm{d}^3x(\mathcal{L}_0[\varphi_+]-\mathcal{L}_0[\varphi_-])\right) \\ &= \frac{1}{(i\mathsf{a})(i\mathsf{b})}\frac{\delta^2 Z_0[J_+,J_-]}{\delta J_{\mathsf{a}}(t_1,\boldsymbol{x}_1)\,\delta J_{\mathsf{b}}(t_2,\boldsymbol{x}_2)}\bigg|_{J_\pm=0}, \end{aligned} \tag{5.36}$$

where $\mathsf{a},\mathsf{b}=\pm$. Various combinations for the indices a,b lead to 4 types of propagators. By carefully investigating the steps for constructing the in-in partition function, one realises that the time ordering of the fields' operators plays an important role when choosing whether it results in introducing fields on the (+) or (−) branch. In particular, it is found that

$$\begin{aligned} \langle \mathcal{T}\{\hat{\varphi}(t_1,\boldsymbol{x}_1)\hat{\varphi}(t_2,\boldsymbol{x}_2)\}\rangle &= -i\Delta_{++}(t_1,\boldsymbol{x}_1;t_2,\boldsymbol{x}_2)\,, \\ \langle \bar{\mathcal{T}}\{\hat{\varphi}(t_1,\boldsymbol{x}_1)\hat{\varphi}(t_2,\boldsymbol{x}_2)\}\rangle &= -i\Delta_{--}(t_1,\boldsymbol{x}_1;t_2,\boldsymbol{x}_2)\,. \end{aligned} \tag{5.37}$$

Note that once the external operators are evaluated as field configurations on a given branch in the right-hand side above, their order does not matter as they are dummy functional variables in the path integral, contrary to the field operators on the left-hand side. If the two-point function is not (anti)-time ordered, we can still derive

$$\begin{aligned} \langle \hat{\varphi}(t_1,\boldsymbol{x}_1)\hat{\varphi}(t_2,\boldsymbol{x}_2)\rangle &= -i\Delta_{-+}(t_1,\boldsymbol{x}_1;t_2,\boldsymbol{x}_2)\,, \\ \langle \hat{\varphi}(t_2,\boldsymbol{x}_2)\hat{\varphi}(t_1,\boldsymbol{x}_1)\rangle &= -i\Delta_{+-}(t_1,\boldsymbol{x}_1;t_2,\boldsymbol{x}_2)\,. \end{aligned} \tag{5.38}$$

The correct ordering always amounts to inserting fields (from right to left) along the integration contour from $-\infty^+$ to t and back to $-\infty^-$, see Fig. 5.2. Practical calculations being often carried out in Fourier space, we also define the Fourier-space free propagators as

$$\mathcal{G}_{\mathsf{ab}}(k;t_1,t_2) = -i\int \mathrm{d}^3x\, e^{-i\boldsymbol{k}\cdot\boldsymbol{x}}\Delta_{\mathsf{ab}}(t_1,\boldsymbol{x};t_2,\boldsymbol{0})\,, \tag{5.39}$$

where the factor $-i$ is simply a useful convention (see later when we derive the vertex diagrammatic rules). Explicitly, using (5.37) and (5.38), and replacing the (anti)-time ordering of operators in terms of Heaviside functions, we obtain

$$\begin{aligned} \mathcal{G}_{++}(k;t_1,t_2) &= \mathcal{G}_{>}(k;t_1,t_2)\Theta(t_1-t_2)+\mathcal{G}_{<}(k;t_1,t_2)\Theta(t_2-t_1)\,, \\ \mathcal{G}_{+-}(k;t_1,t_2) &= \mathcal{G}_{<}(k;t_1,t_2)\,, \\ \mathcal{G}_{-+}(k;t_1,t_2) &= \mathcal{G}_{>}(k;t_1,t_2)\,, \\ \mathcal{G}_{--}(k;t_1,t_2) &= \mathcal{G}_{<}(k;t_1,t_2)\Theta(t_1-t_2)+\mathcal{G}_{>}(k;t_1,t_2)\Theta(t_2-t_1)\,, \end{aligned} \tag{5.40}$$

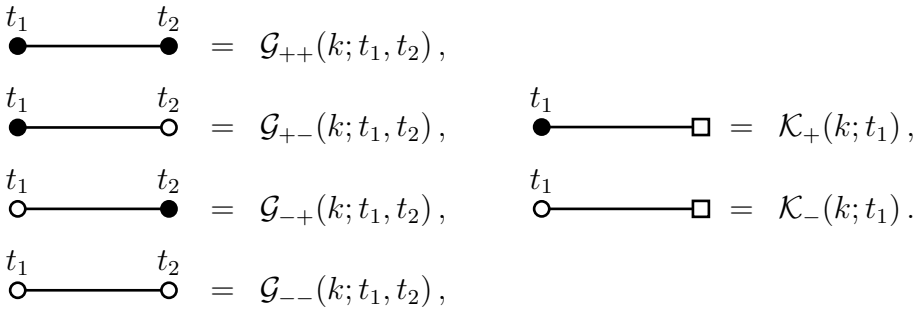
where the causal propagators (also sometimes referred to as the Wightman function) are defined in terms of the mode functions

$$\mathcal{G}_{>}(k;t_1,t_2) \equiv u_k(t_1)u_k^*(t_2)\,, \quad \mathcal{G}_{<}(k;t_1,t_2) \equiv u_k^*(t_1)u_k(t_2)\,. \tag{5.41}$$

The four propagators are not independent as they satisfy $\mathcal{G}^*_{>} = \mathcal{G}_{<}, \mathcal{G}^*_{++} = \mathcal{G}_{--}$ and $\mathcal{G}^*_{+-} = \mathcal{G}_{-+}$ (see e.g. [347] for another basis in which these propagators are represented). It is also useful to define propagators with an endpoint evaluated at the external time t at which correlation functions are sought for. These "bulk-to-boundary" propagators, as opposed to the previous "bulk-to-bulk" propagators, read (for $t_1 < t$)

$$\begin{aligned} \mathcal{K}_+(k;t_1) &\equiv \mathcal{G}_{++}(k;t_1,t) = \mathcal{G}_{+-}(k;t_1,t) = \mathcal{G}_{<}(k;t_1,t)\,, \\ \mathcal{K}_-(k;t_1) &\equiv \mathcal{G}_{--}(k;t_1,t) = \mathcal{G}_{-+}(k;t_1,t) = \mathcal{G}_{>}(k;t_1,t)\,, \end{aligned} \tag{5.42}$$

where we used the condition that the two in-in branches coincide at the external time $\varphi_+(t,\boldsymbol{x}) = \varphi_-(t,\boldsymbol{x})$. Following [356], we represent these propagators with a black dot ● denoting $+$, a white dot ○ denoting $-$, and a square □ denoting the boundary at external time t where $+$ and $-$ are indistinguishable:



(5.43)

5.3.3 List of Standard Free Propagators

We now gather some known propagators, referring the interested reader to the corresponding literature. We will only display $G_>$ (or just the mode function) for each cases as all kind of propagators can be easily constructed from it.

Scalar field in flat space. In flat-space, a freely propagating scalar field with mass m (and in Fourier space for the spatial coordinates) is described by a harmonic oscillator with the time-independent frequency $\omega_k = \sqrt{k^2+m^2}$, corresponding to the well-known energy of the field. The correctly normalised positive-frequency mode function is $u_k(t) = e^{-i\omega_k t}/\sqrt{2\omega_k}$ and the causal propagator reads

$$\mathcal{G}_{>}(k;t_1,t_2) = \frac{e^{-i\omega_k(t_1-t_2)}}{2\omega_k}\,. \tag{5.44}$$

Scalar field in de Sitter. For a massive scalar field with mass m in $(3+1)$-dimensional de Sitter space, the correctly-normalised positive-frequency mode function is given by

$$u_k(\tau) = -i\frac{H\sqrt{\pi}}{2}e^{i\pi/4}e^{i\pi\nu/2}(-\tau)^{3/2}H^{(1)}_\nu(-k\tau) \xrightarrow[k\tau\to-\infty]{} (iH\tau)\frac{e^{-ik\tau}}{\sqrt{2k}}\,, \tag{5.45}$$

where τ is conformal time, defined by $\mathrm{d}\tau = \mathrm{d}t/a$ with $a(\tau) = -1/(H\tau)$, $\nu \equiv \sqrt{9/4-(m/H)^2}$ is related to the mass, and $H^{(1)}_a(z)$ is the Hankel function of the

first kind. More details are given in App. A. In the case $m > 3H/2$, it is customary to define the parameter μ such that $\nu \equiv i\mu$. The causal propagator reads

$$\mathcal{G}_>(k;\tau_1,\tau_2) = \frac{\pi H^2}{4} e^{-\pi \mathrm{Im}(\nu)} (\tau_1\tau_2)^{3/2} H^{(1)}_\nu(-k\tau_1) H^{(2)}_{\nu^*}(-k\tau_2)\,. \tag{5.46}$$

In the heavy-field case $m > 3H/2$, it is customary to use the relation $H^{(2)}_{-i\mu}(z) = e^{\pi\mu} H^{(2)}_{i\mu}(z)$ to cancel the factor $e^{-\pi\mu}$. For a non-unit speed of sound $c_s \neq 1$, one just needs to make the replacement $k \to c_s k$ in the mode function. The massless case is found by setting $m = 0$, equivalently $\nu = 3/2$, and using $H^{(1)}_{3/2}(z) = -\frac{2i}{\pi}(1 - iz)e^{iz}/z^{3/2}$. Then, one finds the well-known result $u_k(\tau) = \frac{H}{\sqrt{2k^3}}(1 + ik\tau)e^{-ik\tau}$, and

$$\mathcal{G}_>(k;t_1,t_2) = \frac{H^2}{2k^3}(1 + ik\tau_1)(1 - ik\tau_2)e^{-ik(\tau_1-\tau_2)}\,. \tag{5.47}$$

This propagator in $(d+1)$-dimensional de Sitter space does not have a similar simple form, which makes dimensional regularisation difficult in this formalism. Another interesting case is the conformally coupled field $m = \sqrt{2}H$, equivalently $\nu = 1/2$, for which the mode function $u_k(\tau) = i\frac{H\tau}{\sqrt{2k}} e^{-ik\tau}$ and the propagator

$$\mathcal{G}_>(k;\tau_1,\tau_2) = \frac{H^2\tau_1\tau_2}{2k}\, e^{-ik(\tau_1-\tau_2)}\,, \tag{5.48}$$

resembles the flat-space ones.

Bosonic spinning fields in de Sitter. The generalisation of the previous mode functions to bosonic spinning fields is straightforward, and problems such as constraints and gauge redundancies can be treated with standard techniques. Let us emphasize that this was one of the motivations to introduce the path integral approach for cosmological correlators, as spinning fields are naturally described by Lagrangians. The proper canonical quantisation of a spin-s field $\varphi_{\mu_1\ldots\mu_s}$ (with s a positive integer) in terms of the mode functions reads

$$\hat{\varphi}_{\mu_1\ldots\mu_s}(\tau,\boldsymbol{x}) = \int \frac{\mathrm{d}^3k}{(2\pi)^3} \sum_\lambda \left[u_{\lambda,k}(\tau)\varepsilon^\lambda_{\mu_1\ldots\mu_s}(\boldsymbol{k})\,\hat{a}^\lambda_{\boldsymbol{k}} + u^*_{\lambda,k}(\tau)\varepsilon^{\lambda *}_{\mu_1\ldots\mu_s}(\boldsymbol{k})\,\hat{a}^{\lambda\dagger}_{-\boldsymbol{k}}\right] e^{i\boldsymbol{k}\cdot\boldsymbol{x}}\,, \tag{5.49}$$

where λ labels helicity states and $\varepsilon^\lambda_{\mu_1\ldots\mu_s}(\boldsymbol{k})$ is the polarisation tensor. Note that in general the equation of motion couples different components of the field. However, the different helicity components $u_{\lambda,k}(\tau)$ decouple, see [116] for more details and explicit solutions for mode functions of (de Sitter covariant) fields with arbitrary integer spin. Once the mode functions are known, the causal propagator (summed over helicity states) is then given by

$$(\mathcal{G}_>)_{\mu_1\ldots\mu_s,\nu_1\ldots\nu_s}(k;\tau_1,\tau_2) = \sum_\lambda \mathcal{G}^\lambda_>(k;\tau_1,\tau_2)\,\varepsilon^\lambda_{\mu_1\ldots\mu_s}(\boldsymbol{k})\varepsilon^{\lambda *}_{\nu_1\ldots\nu_s}(\boldsymbol{k})\,, \tag{5.50}$$

with the single-helicity propagator

$$\mathcal{G}^\lambda_>(k;\tau_1,\tau_2) = u_{\lambda,k}(\tau_1)u^*_{\lambda,k}(\tau_2)\,. \tag{5.51}$$

As an example, the two independent helicity states of the massless graviton can be described by the transverse and traceless part of a spatial rank-2 tensor γ_{ij}. The corresponding propagator is given by

$$\begin{aligned}(\mathcal{G}_{>})_{ij,k\ell}(k;\tau_1,\tau_2) &= \frac{2}{M_{\rm Pl}^2}\sum_{\lambda=\pm} u_{\lambda,k}(\tau_1)u^*_{\lambda,k}(\tau_2)\,\varepsilon^{\lambda}_{ij}(\boldsymbol{k})\varepsilon^{\lambda *}_{k\ell}(\boldsymbol{k}) \\ &= \frac{H^2}{M_{\rm Pl}^2 k^3}(1+ik\tau_1)(1-ik\tau_2)e^{-ik(\tau_1-\tau_2)}\sum_{\lambda=\pm}\varepsilon^{\lambda}_{ij}(\boldsymbol{k})\varepsilon^{\lambda *}_{k\ell}(\boldsymbol{k})\,.\end{aligned} \tag{5.52}$$

Gauge fields in de Sitter. Another concrete example of bosonic fields are gauge fields, of which we consider Abelian gauge fields for simplicity. Yang-Mills theories, i.e. the non-Abelian case, can be recovered by including appropriate group factors and color indices. The kinetic action

$$S = -\frac{1}{4}\int \mathrm{d}^4x\sqrt{-g}F_{\mu\nu}F^{\mu\nu}\,, \tag{5.53}$$

is Weyl invariant in 4-dimensional spacetime. Consequently, the action, the equation of motion and the mode functions for the corresponding vector field A_μ are the same ones as in flat space. After quantising the gauge fields à la Faddeev-Popov (see standard QFT textbooks, e.g. [360, 359, 362], for more details) and fixing the gauge,[13] the equation of motion for A_μ takes the very simple form $\partial_\nu^2 A_\mu = 0$. The solution is given by

$$\hat{A}_\mu(\tau,\boldsymbol{x}) = \int\frac{\mathrm{d}^3k}{(2\pi)^3}\frac{1}{\sqrt{2k}}\sum_{\lambda=\pm}\left[e^{-ik\tau}\varepsilon^{\lambda}_{\mu}(\boldsymbol{k})\,\hat{a}^{\lambda}_{\boldsymbol{k}} + e^{ik\tau}\varepsilon^{\lambda *}_{\mu}(\boldsymbol{k})\,\hat{a}^{\lambda\dagger}_{-\boldsymbol{k}}\right]e^{i\boldsymbol{k}\cdot\boldsymbol{x}}\,, \tag{5.55}$$

where λ labels physical polarisations of the field A_μ. The causal propagator is then given by

$$(\mathcal{G}_{>})_{\mu\nu}(k;\tau_1,\tau_2) = \eta_{\mu\nu}\,\frac{e^{-ik(\tau_1-\tau_2)}}{2k}\,, \tag{5.56}$$

where we have substituted the polarisation sum $\sum\varepsilon^{\lambda}_{\mu}(\boldsymbol{k})\varepsilon^{\lambda *}_{\nu}(\boldsymbol{k}) \to \eta_{\mu\nu}$ which holds as long as the photon couples to conserved sources. We refer to [294] for more details, in particular for extensions to arbitrary dimensions.

Massive fields with chemical potential in de Sitter. A natural extension of the gauge field case is to add a mass to the spin-1 field. For completeness and because we will use this in the following development of the thesis, we will also

[13] Fixing the gauge is performed by supplementing the action with the additional term

$$S \supset -\frac{1}{2\xi}\int \mathrm{d}\tau\mathrm{d}^3x\sqrt{-g}(g^{\mu\nu}\nabla_\mu A_\nu + \tfrac{2}{\tau}A_0)^2\,, \tag{5.54}$$

where ξ is the usual gauge parameter. The choice $\xi = 0$ is the Lorenz gauge whereas $\xi = 1$ is usually referred to as the Feynman-'t Hooft gauge. The additional time-dependent term is included so that the quantised action for the gauge field still resembles its flat-space counterpart.

add a chemical potential by adding to the theory the dimension-5 operator (Chern-Simons) $\phi F\tilde{F}$ that respects the shift symmetry of the (background) inflaton ϕ. We refer to Chap. 9 for further details. The action we consider is

$$S=\int \mathrm{d}t\mathrm{d}^3x\sqrt{-g}\left[-\frac{1}{4}F_{\mu\nu}F^{\mu\nu}-\frac{1}{2}m^2A_\mu A^\mu-\frac{1}{4}\frac{\phi}{\Lambda}F_{\mu\nu}\tilde{F}^{\mu\nu}\right], \tag{5.57}$$

where $\tilde{F}^{\mu\nu}=\frac{1}{2}\mathcal{E}^{\mu\nu\alpha\beta}F_{\alpha\beta}$ with $\mathcal{E}^{\mu\nu\alpha\beta}=\epsilon^{\mu\nu\alpha\beta}/\sqrt{-g}$ being the Levi-Civita tensor density. After imposing the gauge condition $\partial_\mu(\sqrt{-g}A^\mu)=0$ and canonically quantising the field A_μ, as in Eq. (5.49), the equations of motion for the mode functions in Fourier space read

$$u''_{\pm,k}(\tau)+(k^2\pm 2a\kappa k+a^2m^2)u_{\pm,k}(\tau)=0\,,\quad u''_{0,k}(\tau)+(k^2+a^2m^2)u_{0,k}(\tau)=0\,, \tag{5.58}$$

where $\lambda=\pm$ denote the transverse modes and $\lambda=0$ is the longitudinal mode. Here $\kappa\equiv\dot{\phi}_0/\Lambda$ is the chemical potential that only affects the free propagation of transverse modes. The properly-normalised solutions read

$$u_{\pm,k}(\tau)=\frac{e^{\mp\pi\kappa/2H}}{\sqrt{2k}}W_{\pm i\kappa/H,\nu}(2ik\tau)\,,\quad u_{0,k}(\tau)=\frac{\sqrt{\pi}}{2}e^{i\pi/4}e^{i\pi\nu/2}\sqrt{-\tau}H^{(1)}_\nu(-k\tau)\,, \tag{5.59}$$

where $W_{a,b}(z)$ is the Whittaker function. We refer the reader to e.g. [241, 106, 237, 251, 305, 363, 112] for more details and phenomenological implications, in particular see [237] for extensions to complex scalar fields, spin-1/2 fermions, and spin-2 particles.

Fermions in de Sitter. Fermions can also be well described within the Schwinger-Keldysh formalism. However, the anti-commuting Grassmannian nature of fermions forbids the mixing between the two in-in branches. When constructing the in-in path integral, it is important to keep the anti-time ordered contour to the left of the time-ordered contour. For a two-component Weyl spinor ψ, the generating functional reads

$$\begin{aligned}Z[I_\pm,I^\dagger_\pm]=&\int\mathcal{D}\psi^\dagger_-\mathcal{D}\psi_-\exp\left(-iS[\psi_-,\psi^\dagger_-]-i\int\mathrm{d}t\mathrm{d}^3x\left(I^\alpha_-\psi_{-\alpha}+I^\dagger_{-\dot\alpha}\psi^{\dagger\dot\alpha}_-\right)\right)\\&\times\int\mathcal{D}\psi^\dagger_+\mathcal{D}\psi_+\exp\left(iS[\psi_+,\psi^\dagger_+]+i\int\mathrm{d}t\mathrm{d}^3x\left(I^\alpha_+\psi_{+\alpha}+I^\dagger_{+\dot\alpha}\psi^{\dagger\dot\alpha}_+\right)\right),\end{aligned} \tag{5.60}$$

where the left-handed spinors $\psi_{\pm\alpha}$ and the right-handed ones $\psi^{\dagger\dot\alpha}_\pm$ are treated as independent variables, α and $\dot\alpha$ are the conventional spinor indices, and $I_\pm$ and $I^\dagger_\pm$ are external sources. The boundary condition reads $\psi_+(t,\boldsymbol{x})=\psi_+(t,\boldsymbol{x})$ and $\psi^\dagger_+(t,\boldsymbol{x})=\psi^\dagger_+(t,\boldsymbol{x})$ at the external time t, as usual. Free propagators are derived by taking two functional derivatives with respect to the corresponding sources. For example, in Fourier space, we have

$$\mathcal{G}_{\mathsf{ab}\alpha\beta}(k;t_1,t_2)=\int\mathrm{d}^3x e^{-i\boldsymbol{k}\cdot\boldsymbol{x}}\frac{1}{(i\mathsf{a})(i\mathsf{b})}\frac{\delta^2Z[I_\pm,I^\dagger_\pm]}{\delta I^\alpha_{\mathsf{a}}(t_1,\boldsymbol{x})\delta I^\beta_{\mathsf{b}}(t_2,\boldsymbol{0})}\bigg|_{I_\pm,I^\dagger_\pm=0}, \tag{5.61}$$

and similarly for $\mathcal{G}^{\dot{\beta}}_{\mathsf{ab}\alpha}$. Therefore, there are two types of propagators, $\langle\psi^{\dagger\dot{\alpha}}(t_1,\boldsymbol{x}_1)\psi_\beta(t_2,\boldsymbol{x}_2)\rangle$ and $\langle\psi_\alpha(t_1,\boldsymbol{x}_1)\psi_\beta(t_2,\boldsymbol{x}_2)\rangle$, each of them containing four types. Using standard notations (see [360, 359, 362]), the canonical quantisation of Weyl spinors reads

$$\hat{\psi}_\alpha(\tau,\boldsymbol{x}) = \int \frac{\mathrm{d}^3k}{(2\pi)^3}\sum_{s=\pm}\left[\xi_{\alpha,s}(\tau,\boldsymbol{k})\hat{a}^s_{\boldsymbol{k}} + \chi_{\alpha,s}(\tau,-\boldsymbol{k})\hat{a}^{s\dagger}_{-\boldsymbol{k}}\right]e^{i\boldsymbol{k}\cdot\boldsymbol{x}}\,, \tag{5.62}$$

where s is the helicity index, and $\hat{a}^s$ and $\hat{a}^{s\dagger}$ are annihilation and creation operators that satisfy the anticommutation relation $\{\hat{a}^s_{\boldsymbol{k}},\hat{a}^{s'\dagger}_{\boldsymbol{k}'}\} = (2\pi)^3\delta_{ss'}\delta^{(3)}(\boldsymbol{k}-\boldsymbol{k}')$. The mode functions ξ and χ can be further written in terms of normalised helicity eigenstates h_s as[14]

$$\xi_{\alpha,s}(\tau,\boldsymbol{k}) = u_s(\tau,\boldsymbol{k})h_s(\boldsymbol{k})\,,\quad \chi^{\dagger\dot{\alpha}}_s(\tau,\boldsymbol{k}) = v_s(\tau,\boldsymbol{k})h_s(\boldsymbol{k})\,, \tag{5.64}$$

where $\chi^\dagger$ was chosen instead of χ so that both u and v are positive-frequency mode functions. As a concrete example, let us consider a massive Weyl fermion with a chemical potential (see previous example) described by the following action

$$S = \int \mathrm{d}t\mathrm{d}^3x\sqrt{-g}\left[i\psi^\dagger\bar{\sigma}^\mu D_\mu\psi - \frac{1}{2}m(\psi\psi+\psi^\dagger\psi^\dagger) + \frac{(\partial_\mu\phi)}{\Lambda}\psi^\dagger\bar{\sigma}^\mu\psi\right]\,, \tag{5.65}$$

where $\bar{\sigma}^\mu = (1,-\boldsymbol{\sigma})$ and D_μ is the covariant derivative. The solutions for the corresponding mode functions with the usual initial conditions are found to be

$$\begin{aligned}
u_+(\tau,\boldsymbol{k}) &= \frac{(m/H)e^{+\pi\kappa/(2H)}}{\sqrt{-2k\tau}}W_{-1/2-i\kappa/H,i\tilde{\nu}}(2ik\tau)\,,\quad u_-(\tau,\boldsymbol{k}) = \frac{e^{-\pi\kappa/(2H)}}{\sqrt{-2k\tau}}W_{1/2+i\kappa/H,i\tilde{\nu}}(2ik\tau)\,,\\
v_+(\tau,\boldsymbol{k}) &= \frac{e^{+\pi\kappa/(2H)}}{\sqrt{-2k\tau}}W_{1/2-i\kappa/H,i\tilde{\nu}}(2ik\tau)\,,\quad v_-(\tau,\boldsymbol{k}) = \frac{(m/H)e^{-\pi\kappa/(2H)}}{\sqrt{-2k\tau}}W_{-1/2+i\kappa/H,i\tilde{\nu}}(2ik\tau)\,,
\end{aligned} \tag{5.66}$$

with $W_{a,b}(z)$ the Whittaker function, $\kappa = \dot{\phi}_0/\Lambda$ the chemical potential, and $\tilde{\nu} = \sqrt{m^2+\kappa^2}/H$. For more details about Weyl spinors in de Sitter or a slow-roll background, as well as their implementation within the Schwinger-Keldysh path integral formalism, we refer the reader to [245], see also [350, 246, 237]. The generalisation to Dirac fermions $\Psi = (\psi_\alpha,\psi^{\dagger\dot{\alpha}})^T$ is straightforward, see [294].

5.3.4 Vertices

From Eq. (5.32), interactions in $\mathcal{L}_{\rm int}$ should be understood as operators acting on the free generating function $Z_0[J_+,J_-]$. Functional derivatives will bring down powers of $\varphi_\pm$ with appropriate factors depending on the nature of the interactions. These interactions are typically of three kinds: (i) non-derivative, (ii) spatial derivative, and (iii) time derivative. Then, the resulting path integral can be expressed in

[14] The helicity eigenstates h_s satisfy

$$\boldsymbol{\sigma}\cdot\boldsymbol{k}\,h_s(\boldsymbol{k}) = 0\,,\quad h^\dagger_s(\boldsymbol{k})h_{s'}(\boldsymbol{k}) = \delta_{ss'}\,,\quad \sum_{s=\pm}h_s(\boldsymbol{k})h^\dagger_s(\boldsymbol{k}) = 1\,, \tag{5.63}$$

where $\boldsymbol{\sigma}$ are the usual Pauli matrices.

terms of the free propagators using Wick theorem. A particularity of the Schwinger-Keldysh path integral is that for each term in $\mathcal{L}_{\rm int}$, there are two vertices, one for $+$ fields coming with a factor of i, and one for $-$ fields coming with a factor of $-i$ (and the $i\epsilon$ prescriptions are opposite for the two branches). Let us separate the discussion in different kinds of possible interactions.

Non-derivative interactions. We start by considering the n-leg non-derivative interaction $\mathcal{L}_{\rm int}/a^3(t) = -\frac{g}{n!}\,\varphi^n$. These interactions act as simple functional derivatives with respect to the sources. Concretely, we have

$$\begin{aligned} Z[J_+,J_-] &= \left[1 - \frac{ig}{n!}\int \mathrm{d}t\mathrm{d}^3x a^3(t)\left(\frac{\delta^n}{i^n\delta J_+^n(t,\boldsymbol{x})} - \frac{\delta^n}{i^n\delta J_-^n(t,\boldsymbol{x})}\right) + \dots\right] Z_0[J_+,J_-] \\ &= Z_0[J_+,J_-] - \frac{ig}{n!}\int \mathcal{D}\varphi_\pm \int \mathrm{d}t\mathrm{d}^3x\left[\varphi_+^n(t,\boldsymbol{x}) - \varphi_-^n(t,\boldsymbol{x})\right] \\ &\times \exp\left(i\int \mathrm{d}t\mathrm{d}^3x\left(\mathcal{L}_0[\varphi_+] + J_+\varphi_+ - (+\leftrightarrow -)\right)\right) + \dots\,. \end{aligned} \tag{5.67}$$

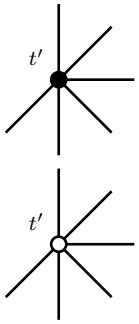
At this stage, we can hardly identify a propagator since there are only products of fields at the same space-time point. However, in practical calculations, the vertex presented above never comes alone and must be supplemented either by external fields to be directly introduced in the path integral and evaluated at the external time, or by other vertices which would similarly bring down powers of $\pm$ fields integrated over time. Given that the vertex has n legs attached to it, we consider n such other fields that will connect to this vertex in a generic way, $\varphi_{\mathsf{a}_1}(t_1,\boldsymbol{x}_1),\dots\varphi_{\mathsf{a}_n}(t_n,\boldsymbol{x}_n)$, that we insert in the path integral. We observe the appearance of a product of n free propagators

$$\left[-i\int \mathrm{d}^3x_1\Delta_{+\mathsf{a}_1}(t,\boldsymbol{x};t_1,\boldsymbol{x}_1)\right]\times\dots\times\left[-i\int \mathrm{d}^3x_n\Delta_{+\mathsf{a}_n}(t,\boldsymbol{x};t_n,\boldsymbol{x}_n)\right] - (+\leftrightarrow -)\,, \tag{5.68}$$

where we have considered integration over the spatial positions $\boldsymbol{x}_n$—that can either come from another vertex or from writing an external field in Fourier space in terms of its real-space mode function—but no integration over t_i since this depends on the fields being external or not. Using $\Delta_{\mathsf{ab}}(t,\boldsymbol{x};t_i,\boldsymbol{x}_i) = \Delta_{\mathsf{ab}}(t,\boldsymbol{x}-\boldsymbol{x}_i;t_i,\boldsymbol{0})$, we can switch to Fourier space to identify the free propagators $\mathcal{G}_{\pm\mathsf{a}_i}(k_i;t,t_i)$. This explains *a posteriori* the $-i$ convention in Eq. (5.36). Taking into account the combinatorial factors (there are $n!$ equivalent ways to connect the n fields to the n-vertex), we finally obtain

$$-ig\int_{-\infty^+}^{t}\mathrm{d}t' a^3(t')\,\mathcal{G}_{+\mathsf{a}_1}(k_1;t',t_1)\dots\mathcal{G}_{+\mathsf{a}_n}(k_n;t',t_n) - (+\leftrightarrow -)\,. \tag{5.69}$$

Diagrammatically, this reads

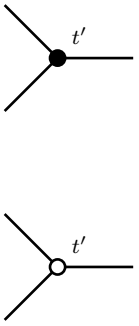


$$= -ig \int_{-\infty^+}^{t} \mathrm{d}t' a^3(t')\, \mathcal{G}_{+\mathsf{a}_1}(k_1;t',t_1)\ldots\mathcal{G}_{+\mathsf{a}_n}(k_n;t',t_n)\,,$$

$$= +ig \int_{-\infty^-}^{t} \mathrm{d}t' a^3(t')\, \mathcal{G}_{-\mathsf{a}_1}(k_1;t',t_1)\ldots\mathcal{G}_{-\mathsf{a}_n}(k_n;t',t_n)\,. \tag{5.70}$$

Of course, we could have derived the same diagrammatic rules by working directly in terms of the generating function expressed as a momentum integral. This turns out to be very convenient when treating spatial derivative interactions, to which we turn now.

Spatial derivative interactions. We consider the following spatial derivative interaction $\mathcal{L}_{\rm int}/a^3(t) = -\frac{g}{2}\frac{(\partial_i\varphi)^2}{a^2}\varphi$. This example should suffice to understand the rule, as it can be easily generalised to any order. In Fourier space, the spatial derivative operation simply becomes a multiplication. However, care needs to be taken due to non-equivalent permutations as well as the additional minus sign coming from two factors of $\partial_i \to i\boldsymbol{k}_i$. We obtain



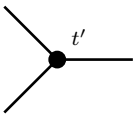
$$\begin{aligned} &= +ig\,(\boldsymbol{k}_1\cdot\boldsymbol{k}_2 + 2 \text{ perms.}) \\ &\quad\times\int_{-\infty^+}^{t}\mathrm{d}t' a(t')\mathcal{G}_{+\mathsf{a}_1}(k_1;t',t_1)\mathcal{G}_{+\mathsf{a}_2}(k_2;t',t_2)\mathcal{G}_{+\mathsf{a}_3}(k_3;t',t_3)\,, \\ &= -ig\,(\boldsymbol{k}_1\cdot\boldsymbol{k}_2 + 2 \text{ perms.}) \\ &\quad\times\int_{-\infty^-}^{t}\mathrm{d}t' a(t')\mathcal{G}_{-\mathsf{a}_1}(k_1;t',t_1)\mathcal{G}_{-\mathsf{a}_2}(k_2;t',t_2)\mathcal{G}_{-\mathsf{a}_3}(k_3;t',t_3)\,. \end{aligned} \tag{5.71}$$

Time derivative interactions. Interactions with time derivatives are more complicated as they should in principle be taken care of in a Hamiltonian formulation of the perturbative Schwinger-Keldysh path integral. We consider the interaction $\mathcal{L}_{\rm int}/a^3(t) = -\frac{g}{3!}\dot{\varphi}^3$. Contrary to flat-space Lorentz-invariant QFT, time derivatives cannot be considered as multiplications as no four-dimensional Fourier transform is defined. Therefore, they need to be kept as derivative operators acting on the free generating function

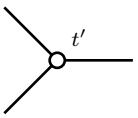
$$i\mathcal{L}_{\rm int}[\varphi_\pm] \to -ia^3(t)\frac{g}{3!}\left(\frac{\partial}{\partial t}\frac{1}{\pm i}\frac{\delta}{\delta J_\pm}\right)^3\,. \tag{5.72}$$

The difference compared to non-derivative interactions is that instead of bringing down powers of the $\pm$ fields, it will bring down time derivatives of these fields, which

then is transferred to the corresponding propagators. This gives



$$= -ig \int_{-\infty^+}^{t} \mathrm{d}t' a^3(t') \times \left[\partial_{t'}\mathcal{G}_{+\mathsf{a}_1}(k_1;t',t_1)\right]\left[\partial_{t'}\mathcal{G}_{+\mathsf{a}_2}(k_2;t',t_2)\right]\left[\partial_{t'}\mathcal{G}_{+\mathsf{a}_3}(k_3;t',t_3)\right] ,$$



$$= +ig \int_{-\infty^-}^{t} \mathrm{d}t' a^3(t') \times \left[\partial_{t'}\mathcal{G}_{-\mathsf{a}_1}(k_1;t',t_1)\right]\left[\partial_{t'}\mathcal{G}_{-\mathsf{a}_2}(k_2;t',t_2)\right]\left[\partial_{t'}\mathcal{G}_{-\mathsf{a}_3}(k_3;t',t_3)\right] . \tag{5.73}$$

Note that the time derivative acting on the propagators is non-trivial as it hits the causal propagators $\mathcal{G}_{\lessgtr}$ and the Heaviside functions (when applicable). We will come back to this point later with a concrete example.

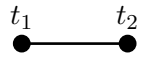
Computing a given diagram. A given diagram representing a correlator is the sum over all possible ways of colouring the dots representing vertices in black and white. A diagram with V vertices is actually composed of 2^V contributions. As a result, the doubling of fields in the Schwinger-Keldysh formalism drastically increases the number of diagrammatic contributions to evaluate as the number of vertices increases. However, some contributions are related to others by complex conjugation. Indeed, the complex conjugation of a diagram is obtained by switching black dots to white ones and vice versa. The actual number of independent diagrams to compute is then 2^{V-1}. For parity-even theories, an immediate consequence is that cosmological correlators $\langle\hat{\mathcal{O}}(t)\rangle$ are real. We summarise the Schwinger-Keldysh diagrammatic rules, keeping only the essential, in the insert below.

Schwinger-Keldysh diagrammatic rules.

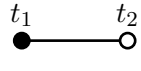
- *Perturbation theory*: Split the full Lagrangian $\mathcal{L}[\varphi]$ into a free exactly-solvable part $\mathcal{L}_0[\varphi]$ and an interaction part $\mathcal{L}_{\rm int}[\varphi]$ that can be treated perturbatively. Solve the equation of motion given by $\mathcal{L}_0[\varphi]$ with appropriate initial conditions to find the mode functions for the field φ. It is customary to Fourier transform the spatial coordinates but not the temporal one. Therefore, the mode function can be represented by $u_k(t)$, where $k = |\boldsymbol{k}|$ is the 3-momentum magnitude, and similarly for the field $\varphi_{\boldsymbol{k}}(t)$.

- *Diagram*: Draw a square □ for each field $\varphi_{\boldsymbol{k}_i}(t)$ in the correlator $\langle\mathcal{O}(t)\rangle$ evaluated at the external time t. These are boundary points. Draw interaction bulk vertices as read from $\mathcal{L}_{\rm int}[\varphi]$ as usual to desired order in perturbation theory, and associate a different (dummy) time t_i to each one. Then, connect all bulk vertices and boundary points with lines (without lines connecting boundary points) so that the diagram is fully connected. Decorate each bulk vertex by either a black dot ● (+ type vertex) or a white dot ○ (− type vertex) in all possible ways. There are 2^V distinct ways of decorating a diagram with V vertices.

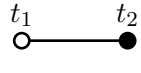
- *Free propagators*: From the free theory $\mathcal{L}_0[\varphi]$, the bulk-to-bulk propagators are given by



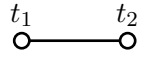
$$= \mathcal{G}_{++}(k;t_1,t_2) = \mathcal{G}_{>}(k;t_1,t_2)\Theta(t_1-t_2) + \mathcal{G}_{<}(k;t_1,t_2)\Theta(t_2-t_1)\,,$$



$$= \mathcal{G}_{+-}(k;t_1,t_2) = \mathcal{G}_{<}(k;t_1,t_2)\,,$$



$$= \mathcal{G}_{-+}(k;t_1,t_2) = \mathcal{G}_{>}(k;t_1,t_2)\,,$$

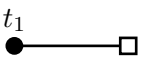


$$= \mathcal{G}_{--}(k;t_1,t_2) = \mathcal{G}_{<}(k;t_1,t_2)\Theta(t_1-t_2) + \mathcal{G}_{>}(k;t_1,t_2)\Theta(t_2-t_1)\,, \tag{5.74}$$

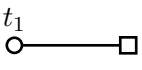
with

$$\mathcal{G}_{>}(k;t_1,t_2) \equiv u_k(t_1)u_k^*(t_2)\,, \quad \mathcal{G}_{<}(k;t_1,t_2) \equiv u_k^*(t_1)u_k(t_2)\,, \tag{5.75}$$

and the bulk-to-boundary propagators are given by



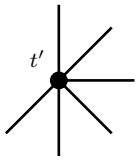
$$= \mathcal{K}_{+}(k;t_1) = \mathcal{G}_{<}(k;t_1,t)\,,$$



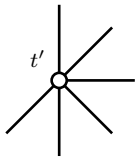
$$= \mathcal{K}_{-}(k;t_1) = \mathcal{G}_{>}(k;t_1,t)\,. \tag{5.76}$$

Associate the corresponding bulk-to-bulk propagator to each line connecting two bulk vertices, and the bulk-to-boundary propagator to each line connecting a bulk vertex to a boundary point. The momentum flowing in each propagator is chosen such that the total momentum is conserved at each vertex.

- *Vertices*: Associate appropriate factors to each vertex as derived from $\mathcal{L}_{\rm int}[\varphi]$. Integrate over all unconstrained and independent 3-momenta (for loop diagrams), and integrate each vertex over time from the initial time with the $i\epsilon$ prescription to the external time t. Here are some examples. A non-derivative interaction $\mathcal{L}_{\rm int}/a^3(t) = -\frac{g}{n!}\varphi^n$ reads

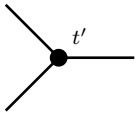


$$= -ig\int_{-\infty^+}^{t} \mathrm{d}t' a^3(t')\,,$$

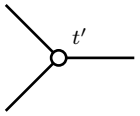


$$= +ig\int_{-\infty^-}^{t} \mathrm{d}t' a^3(t')\,. \tag{5.77}$$

with $-\infty^{\pm} \equiv -\infty(1\mp i\epsilon)$, i.e. the superscript $\pm$ matches the natural visualisation in the complex plane. A spatial-derivative interaction $\mathcal{L}_{\rm int}/a^3(t) = -\frac{g}{2}\frac{(\partial_i\varphi)^2}{a^2}\varphi$ reads

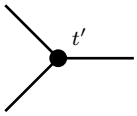


$$= +ig\,(\boldsymbol{k}_1\cdot\boldsymbol{k}_2 + 2 \text{ perms.})\int_{-\infty^+}^{t} \mathrm{d}t' a(t')\,,$$



$$= -ig\,(\boldsymbol{k}_1\cdot\boldsymbol{k}_2 + 2 \text{ perms.})\int_{-\infty^-}^{t} \mathrm{d}t' a(t')\,. \tag{5.78}$$

A time-derivative interaction such as $\mathcal{L}_{\rm int}/a^3(t) = -\frac{g}{2}\varphi\dot{\varphi}^2$ (with $\dot{} \equiv \frac{\rm d}{{\rm d}t}$) gives



$$= -ig\int_{-\infty^+}^{t} {\rm d}t' a^3(t') \times \left[\partial_{t'}\mathcal{G}_{+\mathsf{a}_1}(k_1;t',t_1)\right]\left[\partial_{t'}\mathcal{G}_{+\mathsf{a}_2}(k_2;t',t_2)\right]\mathcal{G}_{+\mathsf{a}_3}(k_3;t',t_3) + 2 \text{ perms.}\,, \tag{5.79}$$

where we have explicitly written the propagators attached to it, and $\mathsf{a}_i = \pm$. The corresponding $-$ type vertex is obtained from the $+$ one by including an additional minus sign (and turning $+ \to -$ in the propagators as well as modifying the $i\epsilon$ prescription).

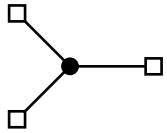
- *Symmetry factor*: The symmetry factor is as usual in ordinary Feynman diagrams.
- *Full correlator*: The final result for the correlator $\langle\mathcal{O}(t)\rangle$ is the sum of all 2^V diagrams.

These rules straightforwardly generalise to multiple fields.

5.3.5 Worked Out Examples

Let us illustrate the Schwinger-Keldysh diagrammatics with a few concrete example to show how the machinery works. Of course, the whole point of organising perturbation theory in a set of diagrams is that writing down the corresponding expressions for each diagram becomes an elementary task.

Contact diagram. We start by considering the time-derivative cubic interaction $\mathcal{L}_{\rm int}/a^3(t) = -\frac{g}{3!}\dot{\varphi}^3$ in FLRW spacetime, with g a coupling constant (with mass dimension -2) and $\varphi(t,\boldsymbol{x})$ a generic scalar field. This interaction leads to a three-point contact correlator composed of two contributions. The first one reads

$$I_+ \equiv$$  $$= -ig\int_{-\infty^+}^{0} {\rm d}\tau a(\tau)\left[\partial_\tau\mathcal{K}_+(k_1;\tau)\right]\left[\partial_\tau\mathcal{K}_+(k_2;\tau)\right]\left[\partial_\tau\mathcal{K}_+(k_3;\tau)\right]\,, \tag{5.80}$$

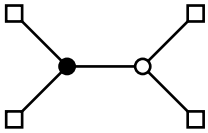
where we have switched to conformal time τ defined by ${\rm d}\tau \equiv {\rm d}t/a$. For concreteness, we specify to the case where φ is a massless field and consider the background to be de Sitter, i.e. $a(\tau) = -(H\tau)^{-1}$. This contribution then reads

$$I_+ = -\frac{g}{8}\frac{H^5}{k_1k_2k_3}\int_0^{+\infty}{\rm d}z z^2 e^{-k_t z} = -\frac{g}{4}\frac{H^5}{k_1k_2k_3k_t^3}\,, \tag{5.81}$$

with $k_t = k_1 + k_2 + k_3$. We have used $\partial_\tau(1 \pm ik\tau)e^{\mp ik\tau} = k^2\tau e^{\mp ik\tau}$, and have Wick rotated the integral on the positive imaginary axis, setting $\tau = iz$ (this is valid because the integrand is analytic everywhere in the complex plane and the arc at infinity vanishes due to Jordan's lemma). Since I_+ is real, the resulting

correlator is just twice the result (5.81). The corresponding shape resembles (but is not identical to) the equilateral template. In fact, it is a general statement that derivative contact interactions lead to equilateral-type primordial non-Gaussianities. This is a consequence of interactions being non-negligeable only around horizon crossing, hence selecting a single time and consequently a single scale.

Exchange diagram. The previous interaction also generates a non-vanishing four-point correlation function. Although for non-derivative or spatial-derivative interactions, writing down the integrals to compute is easy, the presence of time derivatives leads to slight complications as the double time derivatives of the internal propagator will be non-trivial. Let us compute the two contributions I_{+-} and I_{++} separately, the two others being found by adding the complex-conjugated results. From the diagrammatic rules, we find

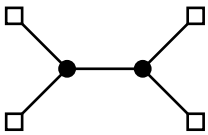
$I_{+-} \equiv$ 

$$\begin{aligned} &= g^2 \int_{-\infty^+}^{0} \mathrm{d}\tau_1 a(\tau_1) \int_{-\infty^-}^{0} \mathrm{d}\tau_2 a(\tau_2) \\ &\times [\partial_{\tau_1} \mathcal{K}_+(k_1;\tau_1)]\,[\partial_{\tau_1} \mathcal{K}_+(k_2;\tau_1)] \\ &\times [\partial_{\tau_1}\partial_{\tau_2} \mathcal{G}_{+-}(s;\tau_1,\tau_2)]\,[\partial_{\tau_2} \mathcal{K}_-(k_3;\tau_1)]\,[\partial_{\tau_2} \mathcal{K}_-(k_4;\tau_2)] \\ &+ 2 \text{ perms}\,. \end{aligned} \tag{5.82}$$

where $s \equiv |\boldsymbol{k}_1 + \boldsymbol{k}_2|$, and the two permutations correspond to the usual t- and u-channels, with $t = |\boldsymbol{k}_1 + \boldsymbol{k}_3|$ and $u = |\boldsymbol{k}_1 + \boldsymbol{k}_4|$. This diagram is in general easy to compute as the internal propagator is not time-ordered. Specifying to the case of a massless field in de Sitter, we obtain

$$\begin{aligned} I_{+-} &= \frac{g^2}{32} \frac{H^8 s}{k_1 k_2 k_3 k_4} \int_{-\infty^+}^{0} \mathrm{d}\tau_1 \tau_1^2 e^{i(k_{12}+s)\tau_1} \int_{-\infty^-}^{0} \mathrm{d}\tau_2 \tau_2^2 e^{i(k_{34}+s)\tau_2} + 2 \text{ perms} \\ &= \frac{g^2}{8} \frac{H^8 s}{k_1 k_2 k_3 k_4 E_L^3 E_R^3} + 2 \text{ perms}\,. \end{aligned} \tag{5.83}$$

where $k_{12} \equiv k_1 + k_2$ and $k_{34} = k_3 + k_4$, and $E_{L,R} \equiv k_{12,34} + s$ are the "energies" flowing in the left and right vertices. It is a general feature that the two integrals appearing in non-time ordered diagrams factorise. The second contribution reads

$I_{++} \equiv$ 

$$\begin{aligned} &= -g^2 \int_{-\infty^+}^{0} \mathrm{d}\tau_1 a(\tau_1) \int_{-\infty^+}^{0} \mathrm{d}\tau_2 a(\tau_2) \\ &\times [\partial_{\tau_1} \mathcal{K}_+(k_1;\tau_1)]\,[\partial_{\tau_1} \mathcal{K}_+(k_2;\tau_1)] \\ &\times [\partial_{\tau_1}\partial_{\tau_2} \mathcal{G}_{++}(s;\tau_1,\tau_2)]\,[\partial_{\tau_2} \mathcal{K}_+(k_3;\tau_1)]\,[\partial_{\tau_2} \mathcal{K}_+(k_4;\tau_2)] \\ &+ 2 \text{ perms}\,. \end{aligned} \tag{5.84}$$

The time-ordered bulk-to-bulk propagator $\mathcal{G}_{++}$ (as well as G_{--}) contains Heaviside Θ-functions so that the double time derivatives act non-trivially on propagators.

Using the identity (see [356] for the derivation)

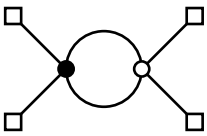
$$\partial_{\tau_1}\partial_{\tau_2}\mathcal{G}_{++}(k;\tau_1,\tau_2) = \Theta(\tau_1-\tau_2)\partial_{\tau_1}\partial_{\tau_2}\mathcal{G}_{>}(k;\tau_1,\tau_2) + \Theta(\tau_2-\tau_1)\partial_{\tau_1}\partial_{\tau_2}\mathcal{G}_{<}(k;\tau_1,\tau_2) + \frac{i}{c(\tau_1)}\delta(\tau_1-\tau_2)\,, \tag{5.85}$$

for a free Lagrangian of the form $\mathcal{L}_0 = c(\tau)[\varphi'^2/2 - (\partial_i\varphi)^2/2]$ in conformal time, we see that the contribution I_{++} actually contains three sub-contributions. The two first sub-contributions have nested time integrals. We will not write these ones explicitly, but instead focus on the third sub-contribution, which reads

$$I_{++}^{\text{contact}} = -3ig^2\int_{-\infty^+}^{0}\mathrm{d}\tau\frac{a^2(\tau)}{c(\tau)}\left[\partial_\tau\mathcal{K}_+(k_1;\tau)\right]\left[\partial_\tau\mathcal{K}_+(k_2;\tau)\right]\left[\partial_\tau\mathcal{K}_+(k_3;\tau)\right]\left[\partial_\tau\mathcal{K}_+(k_4;\tau)\right]\,, \tag{5.86}$$

with the symmetry factor coming from the 2 other identical permutations. Such contribution would arise from an effective quartic interaction $\mathcal{L}_{\text{int}} = -\frac{3}{4!}\frac{g^2}{c(\tau)}\varphi'^4$. Actually, the appearance of this effective interaction can be traced back to the fact that we are using the interacting Lagrangian instead of the interacting Hamiltonian as would be relevant for time-derivative interactions. Indeed, going from the Lagrangian to the Hamiltonian, we find $\mathcal{H}_{\text{int}}^{\mathcal{I}} = -\mathcal{L}_{\text{int}} + \frac{g^2}{8c}\varphi'^4$ for the particular interaction we consider here, see [356] for the general expression. Therefore, an exchange diagram in the path integral formalism actually contains a contact diagram for time-derivative interactions.

Loop diagram. Finally, we consider the simplest polynomial interaction $\mathcal{L}_{\text{int}}/a^3(t) = -\frac{g}{4!}\varphi^4$ to illustrate how loops are dealt with. This interaction contributes to the four-point correlation function at one-loop level and contains two independent diagrams to evaluate, I_{+-} and I_{++}, as in the previous case. The non-time ordered one reads

$I_{+-} \equiv$  $= g^2\int\frac{\mathrm{d}^3q}{(2\pi)^3}\int_{-\infty^+}^{0}\mathrm{d}\tau_1 a^4(\tau_1)\int_{-\infty^-}^{0}\mathrm{d}\tau_2 a^4(\tau_2)$

$\times\,\mathcal{K}_+(k_1;\tau_1)\mathcal{K}_+(k_2;\tau_1)\mathcal{G}_{+-}(q;\tau_1,\tau_2)\mathcal{G}_{+-}(|\boldsymbol{k}_{12}-\boldsymbol{q}|;\tau_1,\tau_2)\mathcal{K}_-(k_3;\tau_2)\mathcal{K}_-(k_4;\tau_2)$

$+\,2$ perms$\,,$ (5.87)

where the unconstrained momentum running in the loop should be integrated over, as usual. A similar expression can be found for the time-ordered diagram.

6

Spectral Representation

The complexity of real physical processes is often made simple when these processes are extended to the complex plane. While thinking about particles propagating with complex momenta and scattering at imaginary angles may seem grotesque, this perspective can offer profound insights into the real world. For instance, physical states are mapped onto to the analytic structure of scattering amplitudes (such as poles), which manifest as resonances in real physical observables. Even more remarkably, fundamental physical principles themselves can be read off from analytic properties of scattering amplitudes.

The development of off-shell methods for scattering amplitudes is deeply rooted in the power of complex analysis. This approach traces its origins back to the celebrated Kramers-Kronig relations, which link absorption and dissipation in a medium by relating the real and imaginary parts of the response function, thereby establishing the foundational connection between causality and analyticity. Building on this foundation, the complex deformation of momenta has led to significant developments, such as Berends-Giele recursion relations [364], recovering tree-level amplitudes by stitching together lower-point building blocks with one leg off-shell, or crossing symmetry, revealing that different processes are related through analytic continuation. From this perspective, further rethinking kinematic constraints and symmetries has led to the discovery of fascinating internal mathematical beauty of scattering amplitudes. Methods such as the use of spinor-helicity variables, improved on-shell recursion relations including BCFW [365, 366], or unitarity methods and generalised cuts [367, 368, 369] not only deepen our understanding of quantum field theory but also facilitate the computation of complicated physical processes, as evidenced by recent achievements in high-loop calculations (see [370, 371, 372, 373] for nice reviews).

Recently, a deeper understanding of the structure of cosmological correlators has begun to emerge as insights from flat-space scattering amplitudes are imported

to cosmology [374]. Essentially, flat-space amplitudes are embedded within cosmological correlators as residues on the total energy pole, when energies of the external particles add up to zero [127, 375]. Similarly, on partial energy poles, when the energy of a subdiagram vanishes, correlators factorise into a product of a (shifted) lower-point correlator and a lower-point scattering amplitude. Notably, these singularities can only be reached by analytically continuing (some) external energies to negative values. Perturbative unitarity leads to a set of cutting rules [376, 377, 378, 379, 380], while its non-perturbative counterpart is captured through the Källén–Lehmann representation in de Sitter space [381, 199, 382]. This opens up new possibilities to sew together simple building blocks to construct more complex correlators. Furthermore, simple cosmological correlators can be conceptualised as canonical forms of a polytope [383, 384, 385, 386, 387, 388, 389, 390] and progress has been made in understanding the differential equations they satisfy, from which "time emerges" [391, 392, 393, 394] (with related aspects discussed in [395, 396, 397]). As we will argue in this chapter and in Chap. 7, employing an *off-shell* formulation of cosmological correlators not only makes their analytic and factorisation properties more explicit, but also streamlines practical computational techniques.

In this chapter, we propose a systematic off-shell reformulation of cosmological correlation functions. Our approach relies on a spectral representation of massive bulk-to-bulk propagators in de Sitter. Essentially, time ordering is replaced by an appropriate contour integral. While spontaneous particle production makes it impossible to use the usual complex energy plane because of branch cuts, the key insight is instead to shift to the complex mass domain, where the dispersive integral takes the form of a split representation of off-shell bulk-to-boundary propagators. In this plane, mode functions are analytic and the integration contour can be safely closed. This approach uses a suitable $i\epsilon$ prescription to account for particle production. By incorporating particle production, unlike the usual Feynman propagator, the number of poles effectively doubles, with different Boltzmann weights that either suppress or enhance their effects. This encodes a crossing symmetry between incoming and outgoing modes separated by a Stokes line, fully capturing particle production. In the flat-space limit, where particle production is turned off, this propagator naturally reduces to the standard Feynman propagator. At the level of correlators, this off-shell propagator trivialises time integrals as they only appear in a factorised manner.

Additionally, we leverage the fundamental properties of in-in Schwinger-Keldysh diagrammatics to derive the largest-time equation satisfied by cosmological correlators. This equation relates processes occurring on different in-in branches through the analytic continuation of external energies, mirroring crossing symmetry in flat space. This relationship is universally applicable to all cosmological correlators, regardless of the order in perturbation theory or whether the theory is unitary, and it can serve as a consistency check when computing complicated diagrams. We conclude by illustrating how the largest-time equation is satisfied through a series of explicit examples.

6.1 From Time Ordering to Contour Integrals

Starting from Schwinger-Keldysh propagators, which have been introduced in Sec. 5.3, we present the associated spectral representations.

6.1.1 Multiple Propagators: a Matter of Contour

The key insight is to realise that these propagators are nothing but Green's functions of the free equation of motion with appropriate boundary conditions, and therefore can be written as contour integrals.

Feynman propagator. To illustrate how a frequency-space representation of the propagators can be constructed and for the sake of simplicity, let us first consider a massless scalar field φ in flat space. We will upgrade the presented integral representations of propagators to massive fields in de Sitter space in the next section. The corresponding positive-frequency mode function reads $u_k(t) = \frac{e^{-ikt}}{\sqrt{2k}}$. The generalisation to massive fields is straightforward after setting $k \to \omega_k = \sqrt{k^2+m^2}$. The key insight is to realise that time ordering can be written as a frequency-space integral using the mathematical identity

$$e^{-ik(t_1-t_2)}\Theta(t_1-t_2) + e^{+ik(t_1-t_2)}\Theta(t_2-t_1) = -2k\int_{-\infty}^{+\infty}\frac{\mathrm{d}\omega}{2i\pi}\frac{e^{i\omega(t_1-t_2)}}{(\omega^2-k^2)_{i\epsilon}}\,, \tag{6.1}$$

where the $i\epsilon$ prescription is implemented as follows

$$\frac{1}{(\omega^2-k^2)_{i\epsilon}} \equiv \frac{1}{2k}\left[\frac{1}{\omega-(k-i\epsilon)} - \frac{1}{\omega-(-k+i\epsilon)}\right] = \frac{1}{\omega^2-k^2+i\epsilon}\,, \tag{6.2}$$

with $\epsilon > 0$ an infinitesimal positive parameter, and where in the second equality we have dropped terms of order $\mathcal{O}(\epsilon^2)$ and set $2k\epsilon = \epsilon$, which is valid in the limit $\epsilon \to 0$. This procedure effectively sets the two poles slightly off the real axis in the complex plane. To see that we indeed recover the correct Feynman propagator, we suppose that $t_1 > t_2$ and close the contour in the upper-half complex plane. The first term in Eq. (6.2) gives zero and only the second term selects the residue, effectively setting the exponential on shell, i.e. $e^{i\omega(t_1-t_2)} \to e^{-ik(t_1-t_2)}$. One can proceed in the same way for $t_1 < t_2$, this way closing the contour in the lower-half complex plane, to find $e^{ik(t_1-t_2)}$. Importantly, this requires that the mode function should be analytic, which is valid here for the exponential in the entire complex plane, and that the integrand decays at least faster than $1/\omega$ when $\omega \to \infty$ so that the semi-circle at infinity does not contribute.

In the end, the time-ordered propagator $\mathcal{G}_{++}$ can be re-written as

$$\mathcal{G}_{++}(k;t_1,t_2) = i\int_{-\infty}^{+\infty}\frac{\mathrm{d}\omega}{2\pi}\frac{\tilde{u}^*_\omega(t_1)\tilde{u}_\omega(t_2)}{(\omega^2-k^2)_{i\epsilon}}\,, \tag{6.3}$$

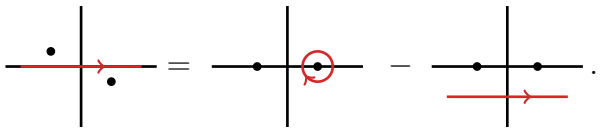
where $\tilde{u}_k(t) = e^{-ikt}$ is the mode function after stripping off the overall normalisation. Naturally, we have $\mathcal{G}_{--}(k;t_1,t_2) = \mathcal{G}^*_{++}(k;t_1,t_2)$. Some comments are in order.

First, the use of tilted mode functions $\tilde{u}_k(t)$ avoids introducing unnecessary branch cuts in the integrand coming from $\sqrt{k}$, thereby preserving its analytic property. Second, both times t_1 and t_2 appear factorised so that time integrals within correlators become trivial. Finally, the $i\epsilon$ prescription is just a simple way for representing time ordering and specifying a pole prescription. Equivalently, one may deform the contour slightly from $-\infty^- = -\infty(1+i\epsilon)$ to $+\infty^+ = +\infty(1+i\epsilon)$, while keeping the poles on the real axis. We have shown in Chap. 5 how this $i\epsilon$ prescription can be recovered directly from the Schwinger-Keldysh path integral.

Retarded and advanced propagators. Various Green's functions with different boundary conditions can be recovered from the usual integral representation of the Feynman propagator. This can be easily done by deforming and combining diverse integration contours. For example, using the standard identity satisfied by the Heaviside function $\Theta(t_1-t_2)+\Theta(t_2-t_1)=1$, the time-ordered propagator $\mathcal{G}_{++}$ can be written as

$$\mathcal{G}_{++}(k;t_1,t_2) = \mathcal{G}_{<}(k;t_1,t_2) + [\mathcal{G}_{>}(k;t_1,t_2) - \mathcal{G}_{<}(k;t_1,t_2)]\,\Theta(t_1-t_2)\,. \tag{6.4}$$

The first term is the non-time-ordered propagator $\mathcal{G}_{+-}(k;t_1,t_2)$ and therefore is factorised in time, whereas the second one is nothing but the causal retarded Green's function $\mathcal{G}_R(k;t_1,t_2)$. In terms of integration contours, Eq. (6.4) reads

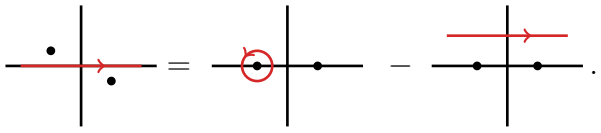


(6.5)

Importantly, non-local processes lead to a vanishing retarded Greens's function. This observation has consequences for the cosmological case, and enables to extract various signals from correlators with different origin. Similarly, one can flip the second Heaviside function in the expression of $\mathcal{G}_{++}$ to obtain

$$\mathcal{G}_{++}(k;t_1,t_2) = \mathcal{G}_{>}(k;t_1,t_2) + [\mathcal{G}_{<}(k;t_1,t_2) - \mathcal{G}_{>}(k;t_1,t_2)]\,\Theta(t_2-t_1)\,, \tag{6.6}$$

which, in terms of integration contours, reads



(6.7)

6.1.2 Spectral Representation of Massive Propagators

We now show how the previous integration contour prescription is modified when taking into account spontaneous particle production. For concreteness in what follows, we consider a real massive scalar field in de Sitter. We consider fields in the principal series $m/H \geq 3/2$ so that $\mu \equiv \sqrt{m^2/H^2 - 9/4}$ is real. In particular, we will not deal with late-time secular divergences appearing when exchanging light fields.

Contour prescription. Spontaneous particle production manifests itself as non-analyticity in the complex energy domain $k \to \omega$ once the momentum is set off shell. This renders impossible to construct an integral representation of massive cosmological propagators for the reason that implementing time ordering requires crossing the branch cut. This challenge can be alleviated by instead analytically continuing the massive mode function to the complex μ plane, allowing the field to acquire any complex mass, as shown in [398]. The integral representation of the time-ordered massive cosmological propagator reads[1]

$$\mathcal{G}_{++}(k;\tau_1,\tau_2) = i\int_{-\infty}^{+\infty} \mathrm{d}\nu\, \mathcal{N}_\nu \frac{u_k^*(\tau_1,\nu)u_k^*(\tau_2,\nu)}{(\nu^2-\mu^2)_{i\epsilon}}\,, \tag{6.8}$$

where $\mathcal{N}_\nu \equiv \frac{\nu}{\pi}\sinh(\pi\nu)$ is the de Sitter density of states, $u_k^*(\tau,\mu)$ is the negative-frequency massive mode function defined in (A.3), and the contour prescription to select the correct pole structure is given by[2]

$$\frac{1}{(\nu^2-\mu^2)_{i\epsilon}} \equiv \frac{1}{2\sinh(\pi\mu)}\left[\frac{e^{+\pi\mu}}{\nu^2-\mu^2+i\epsilon} - \frac{e^{-\pi\mu}}{\nu^2-\mu^2-i\epsilon}\right]. \tag{6.10}$$

Naturally, the anti-time ordered propagator is given by $\mathcal{G}_{--}(k;\tau_1,\tau_2) = \mathcal{G}_{++}^*(k;\tau_1,\tau_2)$. The detailed derivation of (6.8) is presented in the next section. The integral over the spectral parameter ν can be viewed as an integration over the scaling dimension $\Delta = \frac{3}{2} + i\nu$ in the principal series that labels infinite-dimensional (scalar) representations of the de Sitter group, which defines eigenvalues of the quadratic Casimir operator $\Delta(3-\Delta)$, see e.g. [399, 400, 401, 402]. In this sense, this integral is closely related to the de Sitter Källén–Lehmann representation albeit in spatial Fourier space [199, 382]. Such spectral representation has its analogue in anti-de Sitter space, see e.g. [403], and in other spacetimes [404, 405].

Flat-space limit. The spectral representation (6.8) extends the familiar flat-space prescription (6.2) by capturing spontaneous particle production while at the same time having a well-defined flat-space limit. Indeed, in the limit $H \to 0$, the Boltzmann suppression is turned off $e^{-\pi\mu} \to 0$ as $\mu \sim m/H$ for a fixed mass. The additional unusual poles $\nu = \pm\mu \pm i\epsilon$ vanish and the contour prescription reduces to the flat-space one (6.2)

$$\frac{1}{(\nu^2-\mu^2)_{i\epsilon}} \xrightarrow[\mu\to\infty]{} \frac{1}{\nu^2-\mu^2+i\epsilon}\,. \tag{6.11}$$

[1] The spectral parameter ν should not be confused with $\nu = i\mu$ that is commonly used to label light fields in the complementary series.

[2] The explicit pole structure (and the corresponding residues) can be immediately obtained from the usual flat-space prescription (6.2) or by noticing that

$$\frac{1}{\nu^2-\mu^2+i\epsilon} = \frac{\Gamma(i\nu-i\mu-\epsilon)\Gamma(-i\nu-i\mu-\epsilon)}{\Gamma(i\nu-i\mu-\epsilon+1)\Gamma(-i\nu-i\mu-\epsilon+1)}\,. \tag{6.9}$$

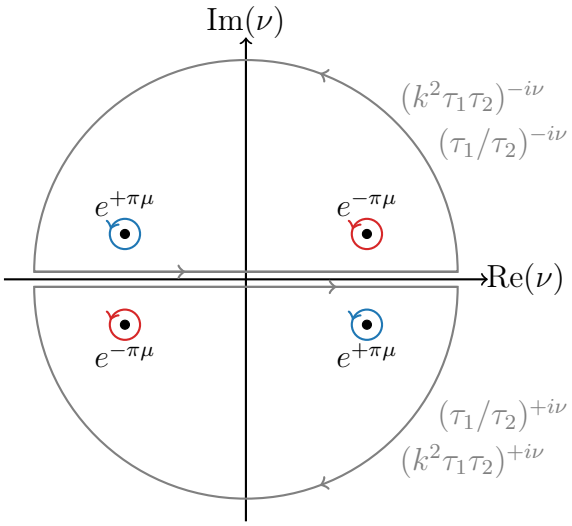


Figure 6.1: Illustration of the contour prescription (6.10) in the complex ν plane. The usual poles $\nu = \pm\mu \mp i\epsilon$ effectively project the off-shell mode onto late-time positive-frequency modes, whereas taking the residues at the Boltzmann suppressed poles $\nu = \pm\mu \pm i\epsilon$ projects the off-shell mode onto the late-time negative-frequency modes. This interchange of ingoing and outgoing modes captures particle production. In the late-time limit, the $\nu \leftrightarrow -\nu$ symmetry of the off-shell modes completely fixes the contour prescription both for the local and non-local contributions, leading to the disappearance of time ordering.

Following the derivation of the next section, for τ_1 being in the future of τ_2, the massive propagator reduces to

$$\begin{aligned}\mathcal{G}_{++}(k;\tau_1,\tau_2) &= \frac{i}{2}\int_{-\infty}^{+\infty} \mathrm{d}\nu\, \frac{\nu J_{i\nu}(-k\tau_1)H^{(2)}_{i\nu}(-k\tau_2)}{\nu^2-\mu^2+i\epsilon} \\ &= \frac{\pi}{2} J_{i\mu}(-k\tau_1)H^{(2)}_{i\mu}(-k\tau_2) \\ &\xrightarrow[\mu\to\infty]{} \frac{e^{-i\mu(t_1-t_2)}}{\sqrt{2\mu}}\,,\end{aligned} \tag{6.12}$$

where we have selected the *single* pole at $\nu = \mu - i\epsilon$ by closing the contour in the lower-half complex plane, and have set $H = 1$. We recover the properly-normalised flat-space propagator composed of plane waves oscillating in cosmic time t. In the flat-space limit, this propagator captures the free super-horizon evolution of the massive field when spatial gradients are negligible, leading to a dispersion relation dominated by the mass $\omega_k \sim \mu$. This provides insight into why analytically continuing the mass, rather than the momentum, allows for defining a spectral representation of massive fields.

Local and non-local parts. The $i\epsilon$ prescription (6.10) projects ingoing particle states onto outgoing states, which enables the mixing of positive- and negative-frequency mode functions. This is made manifest by rewriting the off-shell ingoing mode function in terms of off-shell outgoing ones using the connection for-

mula (A.10), so that the propagator can be written

$$\mathcal{G}_{++}(k;\tau_1,\tau_2) = \mathcal{G}^{\text{local}}_{++}(k;\tau_1,\tau_2) + \mathcal{G}^{\text{non-local}}_{++}(k;\tau_1,\tau_2)\,, \tag{6.13}$$

where both contributions read

$$\begin{aligned}
\mathcal{G}^{\text{local}}_{++}(k;\tau_1,\tau_2) &= \frac{+i\pi}{4}\int_{-\infty}^{+\infty}\mathrm{d}\nu\,\frac{\mathcal{N}_\nu}{\sinh^2(\pi\nu)}\,\frac{J_{i\nu}(-k\tau_1)J^*_{i\nu}(-k\tau_2)+(\nu\leftrightarrow-\nu)}{(\nu^2-\mu^2)_{i\epsilon}}\,,\\
\mathcal{G}^{\text{non-local}}_{++}(k;\tau_1,\tau_2) &= \frac{-i\pi}{4}\int_{-\infty}^{+\infty}\mathrm{d}\nu\,\frac{\mathcal{N}_\nu}{\sinh^2(\pi\nu)}\,\frac{e^{-\pi\nu}J_{i\nu}(-k\tau_1)J_{i\nu}(-k\tau_2)+(\nu\leftrightarrow-\nu)}{(\nu^2-\mu^2)_{i\epsilon}}\,.
\end{aligned} \tag{6.14}$$

As seen in Chap. 4, the local part is interpreted as the accumulated dynamical phase of a single particle propagating since in the late-time limit we have

$$J_{i\nu}(-k\tau_1)J^*_{i\nu}(-k\tau_2) \sim \frac{\sinh(\pi\nu)}{\pi\nu}\left(\frac{\tau_1}{\tau_2}\right)^{i\nu} \propto e^{-i\nu(t_1-t_2)}\,. \tag{6.15}$$

Notably, the local part is independent of the momentum so that it describes correlation at coincident points in position space. Assuming $\tau_1 > \tau_2$, we close the contour in the lower-half complex plane for the term $J_{i\nu}(-k\tau_1)J^*_{i\nu}(-k\tau_2)$ and in the upper-half complex plane for the complex conjugate piece, which leads to

$$\begin{aligned}
\mathcal{G}^{\text{local}}_{++}(k;\tau_1,\tau_2) &= \frac{\pi}{4\sinh^2(\pi\mu)}\left[e^{+\pi\mu}J_{i\mu}(-k\tau_1)J^*_{i\mu}(-k\tau_2)+e^{-\pi\mu}J^*_{i\mu}(-k\tau_1)J_{i\mu}(-k\tau_2)\right]\\
&\xrightarrow[\tau_1,\tau_2\to0]{} \frac{\Gamma(+i\mu)\Gamma(-i\mu)}{4\pi}\left[e^{+\pi\mu}\left(\frac{\tau_1}{\tau_2}\right)^{+i\mu}+e^{-\pi\mu}\left(\frac{\tau_1}{\tau_2}\right)^{-i\mu}\right].
\end{aligned} \tag{6.16}$$

For the reverse time ordering, the contours should be closed in the opposite directions for both contributions. The doubling of poles projects the off-shell positive-frequency mode into positive- and negative-frequency ones as $(\frac{\tau_1}{\tau_2})^{\pm i\nu} \to e^{\pm\pi\mu}(\frac{\tau_1}{\tau_2})^{\pm i\mu}+e^{\mp\pi\mu}(\frac{\tau_1}{\tau_2})^{\mp i\mu}$, which then combine to reconstruct the correct mode mixing. This is illustrated in Fig. 6.1. On the other hand, the non-local part corresponds to the creation and the propagation of two particles since

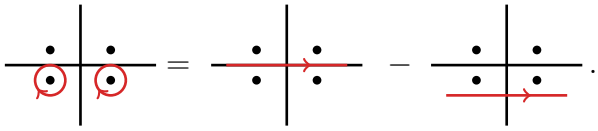
$$J_{i\nu}(-k\tau_1)J_{i\nu}(-k\tau_2) \sim \frac{1}{\Gamma(1+i\nu)^2}\left(\frac{k^2\tau_1\tau_2}{4}\right)^{i\nu} \propto e^{-i\nu(t_1-t_\star)}e^{-i\nu(t_2-t_\star)}\,, \tag{6.17}$$

in the late-time limit, where $t_\star = \log k$ is the pair production (cosmic) time. Being non-analytic in the momentum, this piece describes long-range non-local correlations in position space. Similarly to the local contribution, we close the contour in the lower-half complex plane for the term $e^{-\pi\nu}J_{i\nu}(-k\tau_1)J_{i\nu}(-k\tau_2)$ and in the opposite direction for the second one. We obtain

$$\begin{aligned}
\mathcal{G}^{\text{non-local}}_{++}(k;\tau_1,\tau_2) &= \frac{\pi}{4\sinh^2(\pi\mu)}\left[J_{i\mu}(-k\tau_1)J_{i\mu}(-k\tau_2)+J^*_{i\mu}(-k\tau_1)J^*_{i\mu}(-k\tau_2)\right]\\
&\xrightarrow[\tau_1,\tau_2\to0]{} \frac{1}{4\pi}\left[\Gamma(-i\mu)^2\left(\frac{k\tau_1\tau_2}{4}\right)^{+i\mu}+\Gamma(+i\mu)^2\left(\frac{k\tau_1\tau_2}{4}\right)^{-i\mu}\right].
\end{aligned} \tag{6.18}$$

Importantly, at late times, the choice of closing the contour is completely fixed so that time ordering does not matter. The Feynman propagator $\mathcal{G}_{++}$ effectively reduces to the Wightman function $\mathcal{G}_{>}$. Non-local processes being real, as can be explicitly seen from the last equation, they do not enter the advanced or retarded Green's functions. This reflects the fact that the endpoints of a soft propagator are in space-like separation. With the spectral representation of the time-ordered propagator, subtracting the commutator of field operators simply amounts to selecting the residues at the poles in the contour prescription

$$\mathcal{G}^{\text{non-local}}_{++}(k;\tau_1,\tau_2) = \mathcal{G}_{++}(k;\tau_1,\tau_2) \;-\; \mathcal{G}_{R}(k;\tau_1,\tau_2)\,, \tag{6.19}$$



Of course, selecting the poles in upper-half complex plane requires subtracting the advanced Green's function $\mathcal{G}_A$. This contour deformation is completely equivalent to the bulk cutting rules that extract non-local signals [263].

Conformally coupled field. The special case of a conformally coupled field in de Sitter $m^2 = 2H^2$ is related to the flat-space one by a conformal transformation. Physically, particle production of a conformally coupled field in de Sitter is effectively turned off so that its mode function is analytic in the entire complex k plane. Therefore, from the flat-space propagator (6.3), one immediately obtains

$$\mathcal{G}_{++}(k;\tau_1,\tau_2) = i\,\tau_1\tau_2 \int_{-\infty}^{+\infty} \frac{\mathrm{d}\omega}{2\pi} \frac{\tilde{u}^*_\omega(\tau_1)\tilde{u}_\omega(\tau_2)}{(\omega^2-k^2)_{i\epsilon}}\,, \tag{6.20}$$

where $\tilde{u}_k(\tau) = e^{-ik\tau}$ and where we have set $H = 1$.

6.1.3 Derivation

Here, we present the proof of the spectral representation of massive scalar field in de Sitter, closely following [398]. Let us first consider the case where the time τ_1 is in the future of τ_2, i.e. $-k\tau_1 < -k\tau_2$, so that the time-ordered propagator reduces to $\mathcal{G}_{++}(k;\tau_1,\tau_2) = u_k(\tau_1,\mu)u^*_k(\tau_2,\mu)$. Expanding the first Hankel function $H^{(2)}_{i\nu}(-k\tau_1)$ in (6.8) in terms of Bessel functions using (A.10), using Eq. (A.5), and the symmetry of the pole prescription with respect to $\nu \leftrightarrow -\nu$, the integral can be written

$$\mathcal{G}_{++}(k;\tau_1,\tau_2) = \frac{i}{2}\int_{-\infty}^{+\infty} \mathrm{d}\nu\, \frac{\nu J_{i\nu}(-k\tau_1)H^{(2)}_{i\nu}(-k\tau_2)}{(\nu^2-\mu^2)_{i\epsilon}}\,. \tag{6.21}$$

The crucial stage is to observe that the numerator $\nu J_{i\nu}(-k\tau_1)H^{(2)}_{i\nu}(-k\tau_2)$ is analytic in the entire complex ν plane, so that we choose to close the integration contour in the lower-half complex plane [406]. Since the large-ν expansion (A.14) gives

$$\nu J_{i\nu}(z_1)H^{(2)}_{i\nu}(z_2) \sim \frac{e^{i\nu\log(z_1/z_2)}}{\pi}\,, \tag{6.22}$$

the arc at infinity does not contribute for $z_1 < z_2$ and $\mathrm{Im}(\nu) \to -\infty$. By Cauchy's residue theorem, only the two poles located at $\nu = \pm\mu - i\epsilon$ are selected by the closed contour integral, which yields

$$\begin{aligned}\mathcal{G}_{++}(k;\tau_1,\tau_2) &= \frac{\pi}{4\sinh(\pi\mu)}\left(e^{+\pi\mu}J_{+i\mu}(-k\tau_1)H^{(2)}_{+i\mu}(-k\tau_2) - e^{-\pi\mu}J_{-i\mu}(-k\tau_1)H^{(2)}_{-i\mu}(-k\tau_2)\right)\\ &= u_k(\tau_1,\mu)u_k^*(\tau_2,\mu)\,,\end{aligned} \tag{6.23}$$

where we have again used Eqs. (A.5) and (A.10). For the case where the time τ_2 is in the future of τ_1, i.e. $-k\tau_2 < -k\tau_1$, one needs to expand the second Hankel function $H^{(2)}_{i\nu}(-k\tau_2)$ in (6.8) in terms of Bessel functions and then close the contour, picking up the corresponding residues.

6.2 Cosmological Largest-Time Equation

Unitarity at the quantum level, often described as the conservation of probability, imposes powerful constraints on observables, even when the full set of states in the Hilbert space is unknown. At a perturbative level, unitarity implies relations between cosmological correlators [376] and conserved quantities under unitary time evolution [377]. These relations are analogous to the flat-space optical theorem [362, 360]. It has been shown that these relations can be organised into a set of cutting rules [407, 379, 380, 378, 408], which stem from the Hermitian analytic nature of propagators and the straightforward factorisation of a combination of bulk-to-bulk propagators, bearing resemblance to the standard S-matrix Cutkosky rules, see e.g. [409] for a recent review. However, these cutting rules were derived for the quantum mechanical wavefunction of the universe, as relations satisfied by the corresponding wavefunction coefficients.

In this section, we derive similar relations directly at the level of cosmological correlators, and relaxing the assumption of unitarity. We show that individual in-in branch components of cosmological correlators, once external legs are properly analytically continued to negative energies on the negative branch, satisfy the largest-time equation [410]. We then showcase how this equation is satisfied for relatively simple diagrams.

6.2.1 Propagator Identity from an Off-Shell Perspective

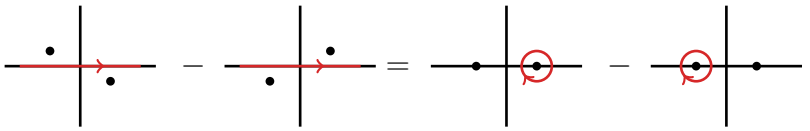
Using the spectral representation of bulk-to-bulk propagators presented in the previous section, deriving the largest-time equation exactly parallels that for the flat-space S-matrix [411, 412, 410]. The essence of this equation lies in a specific trivial identity satisfied by propagators. Using the standard distributional identity

$$\frac{1}{x+i\epsilon} - \frac{1}{x-i\epsilon} = -2i\pi\delta(x)\,, \tag{6.24}$$

in the limit $\epsilon \to 0$, which follows from the Sokhotski-Plemelj identity, the flat-space bulk-to-bulk propagators (6.3) satisfy the known relation[3]

$$\mathcal{G}_{++}(k;t_1,t_2)+\mathcal{G}_{--}(k;t_1,t_2)=\mathcal{G}_{+-}(k;t_1,t_2)+\mathcal{G}_{-+}(k;t_1,t_2)\,, \tag{6.26}$$

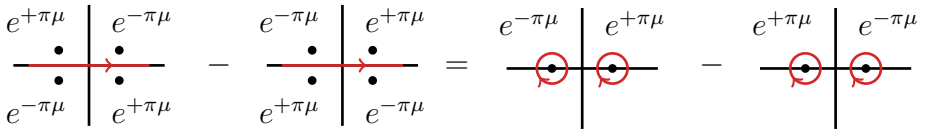
that is, since $\mathcal{G}_{--}(k;t_1,t_2) = \mathcal{G}^*_{++}(k;t_1,t_2)$, the real part does not contain time ordering. In terms of integration contour, this identity reads



(6.27)

with the additional factor i imposing the correct closed contour orientation. Without branch cuts in the energy domain, the additional identity $\mathcal{G}_{--}(k;t_1,t_2) = -\mathcal{G}_{++}(-k;t_1,t_2)$—which can be found directly from the frequency-space representation using $\frac{1}{(\omega^2-k^2)_{i\epsilon}} \to \frac{1}{\omega^2-k^2-i\epsilon}$ as $k \to -k$ or from the explicit split representation in terms of mode functions—enables us to interpret the combination of propagators (6.26) as cutting the internal line of a diagram on the same in-in branch since time integrals factorise. At the level of correlators, the additional input of unitarity relates individual diagrams to their complex conjugate version (with flipped external energies) *on the same branch*. Consequently, the latest-time equation we derive should be understood as only a direct outcome of locality, as it is fundamentally determined by the structure of propagators. This general property remains valid in the presence of dissipation, fluctuations and non-unitary time evolution.

In de Sitter space, we have seen that the effect of particle production amounts to double the usual poles while assigning distinct weights $e^{\pm\pi\mu}$ to the associated residues. From the spectral representation (6.8), it is easy to observe that bulk-to-bulk propagators also satisfy the identity (6.26), which, in terms of integration contours, is illustrated by



(6.28)

Crucially, note that particle production poles change their respective weight under complex conjugation. Sending $\mu \to \infty$, one immediately recovers the flat-space limit (6.27).[4] The identity (6.26) can of course be recovered from the form of prop-

[3] In addition, we have used the following identity for the delta Dirac function

$$\delta(\omega^2-k^2)=\frac{1}{2k}[\delta(\omega+k)+\delta(\omega-k)]\,, \tag{6.25}$$

for $k>0$.

[4] The combination $\mathcal{G}_K \equiv \mathcal{G}_{++}+\mathcal{G}_{--}$ is nothing but the standard Keldysh propagator. The advanced, retarded and Keldysh propagators can be recovered after performing a rotation in the $\varphi_\pm$ field basis, introducing a new pair of fields $\varphi_r = \frac{1}{\sqrt{2}}(\varphi_+ + \varphi_-)$ and $\varphi_a = \frac{1}{\sqrt{2}}(\varphi_+ - \varphi_-)$, which is referred to the Keldysh basis [347]. The advantage of this basis is that the physical interpretation of various propagators become transparent. Indeed, $\mathcal{G}_R$ and $\mathcal{G}_A$ characterise the dynamical properties of the particles in the system under consideration, while $\mathcal{G}_K$ characterises their statistical distribution and encodes the mean particle density [413].

agators written with the time-ordered usual representation using $\Theta(t_1-t_2)+\Theta(t_2-t_1)=1$. Here, we have derived this identity from an off-shell perspective.

6.2.2 Largest-Time Equation

Our aim is to translate the propagator identity (6.26) at the level of correlators, resulting in an identity satisfied by individual branch contributions of cosmological correlators. In the context of flat-space scattering amplitudes, this identity is known as the largest-time equation [414].[5]

Graph. Computing correlators boils down to evaluating a set of multi-nested time integrals, whose number equals the number of vertices. Thus, instead of working with correlators, we define a *graph* with V vertices and N internal lines by its collection of external energies $\{E_i\}$ $(i=1,\ldots,V)$ and internal energies $\{K_j\}$ $(j=1,\ldots,N)$. The resulting graph integrals are found after removing all overall factors of $1/2k$ from bulk-to-boundary and bulk-to-bulk propagators, hence defining the rescaled propagators

$$\tilde{\mathcal{K}}_{\mathsf{a}}(k;t)\equiv 2k\,\mathcal{K}_{\mathsf{a}}(k;t)\,,\quad \tilde{\mathcal{G}}_{\mathsf{ab}}(k;t,t')\equiv 2k\,\mathcal{G}_{\mathsf{ab}}(k;t,t')\,, \tag{6.30}$$

and overall coupling constants. We also multiply each graph integral by $(-i)^V$. Of course, in practice, the external energies are function of external momentum magnitudes. The main motivation is that the number of bulk-to-boundary propagators attached to a vertex, which we take to be massless in flat space and conformally coupled in de Sitter, does not matter, as they satisfy the trivial relation

$$\prod_{i=1}^{n}\tilde{\mathcal{K}}_{\mathsf{a}}(k_i;t)=\tilde{\mathcal{K}}_{\mathsf{a}}\left(\sum_{i=1}^{n}k_i;t\right)\,, \tag{6.31}$$

[5] Consider $F(\{x_i\})$ an amputated (real-space) Feynman diagram with n vertices in flat space. Let us perform the following manipulations on this diagram:

- Duplicate the Feynman diagram 2^n times by colouring vertices either in black or in white in all possible ways.
- For each vertex, a black-coloured vertex brings a factor i, and a white-coloured one brings a factor $(-i)$.
- The propagator between two black vertices is the usual Feynman propagator $\Delta_F(x-y)=\Theta(x^0-y^0)\Delta^+(x-y)+\Theta(y^0-x^0)\Delta^-(x-y)$, where $\Delta^{\pm}(x-y)$ are the usual positive and negative frequency commutation functions, while the propagator between two white vertices is taken to be $\Delta^*_F(x-y)$. The propagator between black and white vertices is replaced by $\Delta^+(x-y)$, and $\Delta^-(x-y)$ for white and black vertices. Clearly, the all-black diagram is the usual Feynman diagram while the all-white one is its complex conjugate.

The flat-space largest-time equation states that the sum of all these contributions must vanish

$$F(\{x_i\})+F^*(\{x_i\})+\boldsymbol{F}(\{x_i\})=0\,, \tag{6.29}$$

where F denotes the usual Feynman diagram, F^* its complex conjugate, and $\boldsymbol{F}$ all other 2^n-2 contributions. This is often taken as the starting point to derive recursion relations, see e.g. [364, 365, 369], or cutting rules, see e.g. [411, 415, 414]. From the above colouring rules, it comes at no surprise that the Schwinger-Keldysh diagrammatic rules, and therefore cosmological correlators, are the most suited objects to phrase the largest-time equation.

where n is the number of external legs of a vertex. The sum of all external momentum magnitudes is defined to be the energy of the vertex, i.e. $k_1 + \ldots + k_n = E$. Diagrammatically, we represent a graph the same way as a correlator (with each vertex carrying a Schwinger-Keldysh index) albeit with external legs removed, and instead labelling each vertex with its energy. For example, a one-site graph integral in flat space reads

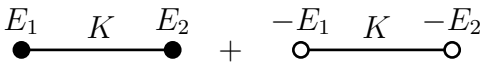


$$\equiv (-i) \sum_{\mathsf{a}=\pm} \mathsf{a} \int_{-\infty^{\mathsf{a}}}^{0} \mathrm{d}t\, e^{i\mathsf{a}Et}\,, \tag{6.32}$$

which represents any contact correlator with arbitrary number of external legs. We also label internal lines with their corresponding internal energies.

A simple illustrative example. Before stating the general largest-time equation, we illustrate the consequence of the identity (6.26) on a simple example, namely the two-site chain. Even though the precise nature of the field φ, interactions, and the background is unimportant for what follows, we consider polynomial self-interactions in flat space and set coupling constants to unity.

First, let us consider the sum of both time-ordered contributions with flipped external energies on the negative branch



(6.33)

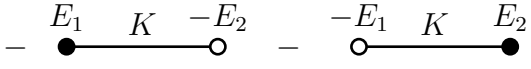
It is given by

$$-\int_{-\infty^+}^{0} \mathrm{d}t_1 \int_{-\infty^+}^{0} \mathrm{d}t_2\, e^{iE_1 t_1} \left[\tilde{\mathcal{G}}_{++}(K;t_1,t_2) + \tilde{\mathcal{G}}_{--}(K;t_1,t_2)\right] e^{iE_2 t_2}\,. \tag{6.34}$$

Note that flipping external energies amounts to exchanging both in-in branches. As such, the $i\epsilon$ prescription that makes the integrals converge needs to be modified. Therefore, we have also deformed the lower bound of the time integrals accordingly so that both graph integrals can be combined. Using the propagator identity (6.26) and flipping the external energies (and the corresponding lower bound of the time integral) for each integral appearing on the negative branch, we directly obtain

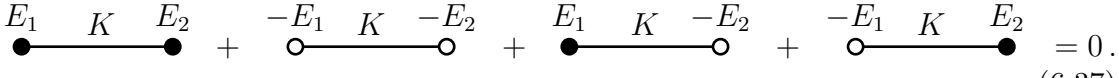
$$-\int_{-\infty^+}^{0} \mathrm{d}t_1 \int_{-\infty^-}^{0} \mathrm{d}t_2\, e^{iE_1 t_1} \tilde{\mathcal{G}}_{+-}(K;t_1,t_2) e^{-iE_2 t_2} - \int_{-\infty^-}^{0} \mathrm{d}t_1 \int_{-\infty^+}^{0} \mathrm{d}t_2\, e^{-iE_1 t_1} \tilde{\mathcal{G}}_{-+}(K;t_1,t_2) e^{iE_2 t_2}\,, \tag{6.35}$$

which we recognise as



(6.36)

Finally, let us group the factorised contributions in (6.35) with the nested ones on the same side. The resulting diagrammatic formula reads



(6.37)

Note that in this simple flat-space example, the rotation direction to negative energies does not matter as the mode functions are analytic. However, for massive fields in de Sitter space, one needs to specify the analytic continuation to negative energies so that it does not cross any branch cuts. In particular, energies should be rotated in opposite directions for the two branches

$$\tilde{\mathcal{K}}_+(e^{-i\pi}k;t) = \tilde{\mathcal{K}}_-(k;t)\,, \quad \tilde{\mathcal{K}}_-(e^{+i\pi}k;t) = \tilde{\mathcal{K}}_+(k;t)\,. \tag{6.38}$$

In most of the cases, we are interested in graphs with analytic external mode functions so that this prescription to evade the branch cut and define negative energies remains implicit.

Largest-time equation. The previous simple example actually generalises to arbitrary graphs. In words, *the sum of all individual graph contributions with negative external energies on the negative branch vanishes*. More formally and at tree-level, individual graph integral contributions can be written as

$$\mathcal{I}_{\mathsf{a}_1\ldots\mathsf{a}_V}(\{E_i\},\{K_j\}) \equiv (-i)^V \int \prod_{i=1}^{V} \mathrm{d}t_i\, f_i(t_i)\, \tilde{\mathcal{K}}_{\mathsf{a}_i}(E_i;t_i) \prod_{j=1}^{I} \tilde{\mathcal{G}}_{\mathsf{a}_j\mathsf{a}_{j+1}}(K_j;t_j,t_{j+1})\,, \tag{6.39}$$

where V is the number of vertices, $I \equiv V-1$ is the number of internal lines (at tree-level), E_i and K_j denote external and internal energies, respectively, and $f_i(t_i)$ are form factors associated to each vertex that account for possible (time-dependent) couplings. We leave the dependence on momenta implicit. The labels a_j and a_{j+1} are to be understood as two consecutive Schwinger-Keldysh vertex indices that match those of the bulk-to-boundary propagators a_i (for a_j) and a_{i+1} (for a_{j+1}). Taking the values $\pm$, they indicate on which in-in branch the corresponding vertices are located. With these definitions, the latest-time equation can be simply stated as the following schematic identity

$$\sum_{\mathsf{a}_1,\ldots,\mathsf{a}_V=\pm} \mathcal{I}_{\mathsf{a}_1\ldots\mathsf{a}_V}(\{\mathsf{a}_i E_i\},\{K_j\}) = 0\,. \tag{6.40}$$

The above sum contains 2^V terms. In the presence of spatial derivative interactions, parity-violating interactions, or with external spinning fields, correlators can explicitly depend on external momenta $\boldsymbol{k}_i$, that can be contracted with e.g. polarisation tensors. In such cases, analytically continuing the energies $k_i \to -k_i$ also implies flipping the signs of the corresponding momenta $\boldsymbol{k}_i \to -\boldsymbol{k}_i$.[6]

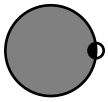
[6]It should be pointed out that the latest-time equation can be understood as a consequence of the following combinatoric operator identity [416, 417, 418, 407]

$$\sum_{k=0}^{n}(-1)^k \sum_{\sigma\in\Pi(k,n-k)} \bar{\mathcal{T}}\left[\mathcal{O}(t_{\sigma_1})\cdots\mathcal{O}(t_{\sigma_k})\right] \mathcal{T}\left[\mathcal{O}(t_{\sigma_{k+1}})\cdots\mathcal{O}(t_{\sigma_n})\right] = 0\,, \tag{6.41}$$

where $\bar{\mathcal{T}}$ and $\mathcal{T}$ are the (anti-)time-ordering operators, and $\Pi(k,n-k)$ denotes the set of bi-partitions of $\{1,\ldots,n\}$ with size k and $n-k$. This "operator optical theorem" can be proved by induction. This means that the identity relating various in-in branches holds more generally at the operator level.

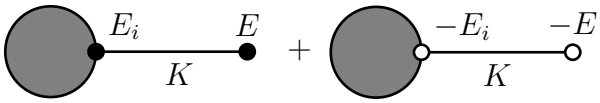
Proof at tree-level. To prove this identity for tree-level graphs, we use an inductive approach, as any tree graph can be constructed iteratively by successively adding internal lines. We follow the same lines as in the original work [414] where Cutkosky rules were derived for amputated Feynman diagrams, also see [419, 407, 378].

As seen above, the largest-time equation is satisfied for the simple two-site graph (the even more simple case of a one-site graph is trivial). We now assume that the latest-time equation (6.40) is valid for a tree-level graph with V vertices and prove that it still remains valid when we add an additional vertex to the graph. Therefore, given a graph with V vertices, we choose a vertex (say the farthest right one) and denote its corresponding external energy by E_i. Of course, this vertex carries $\pm$ labels. For what follows, it is useful to introduce some diagrammatic notation. We denote by the grey circle



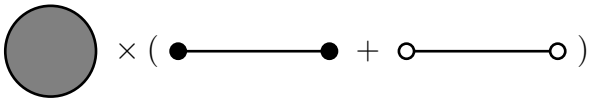
, (6.42)

the sum of all individual graph contributions with V vertices, where the picked vertex ◐ has been brought forward. We now attach to it an additional vertex with external energy E and we label the internal energy flowing through the bulk-to-bulk propagator by K. This increases the number of individual contributions by a factor 2, i.e. from 2^V to 2^{V+1}. Similarly to the simple illustrative example that we have treated above, we now consider the special combination of attaching both time-ordered bulk-to-bulk propagators with negative energies on the negative branch, which pictorially is represented by



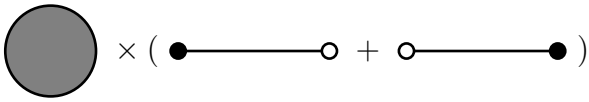
. (6.43)

Note that we have added an additional factor of i (which we include in the grey circle as it does not spoil the argument). Adding this vertex also brings an additional time integral. Flipping the external energies on the negative branch allows us to factor out all the information about external lines (and group both terms under same time integrals after also flipping the $i\epsilon$ prescription). Internal energies remain untouched. This manipulation isolates the bulk-to-bulk propagators to give



. (6.44)

This way, we can use the propagator identity (6.26) to replace all time-ordered propagators with non-time-ordered ones, yielding



. (6.45)

These terms can then be redistributed to generate two individual graphs. At this stage, we recognise the two factorised contributions with flipped external energies on the negative branch, up to an overall minus sign coming from the Schwinger-Keldysh

vertex indices. We obtain



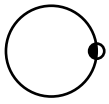
(6.46)

Combining all terms on the same side, we finally obtain the desired diagrammatic identity. Since the simplest graph explicitly verifies this identity, the largest-time equation is proved for all tree-level graphs.

Loop-level diagrams. Cuts, in the broad sense, are at the heart of modern flat-space scattering amplitude methods, especially at the loop level. For cosmological correlators, we will see here that the largest-time equation naturally generalises to loop graphs, as this identity stems from general properties of bulk-to-bulk propagators.

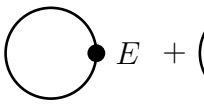
A loop diagram can essentially be generated from a tree-level diagram by merging two vertices. However, this process involves addressing two key points. First, the propagator identity (6.26), which lies at the core of the largest-time equation at tree-level, must be extended to accommodate products of propagators. Second, loop diagrams contain unconstrained momenta flowing in the loops that need to be integrated over, which often results in divergences. As we are not primarily interested in loops, we will not explicitly perform loop integrals nor paying attention to regularising them. Instead, we will show how the largest-time equation holds at the loop level for a few simple graphs.

One-site graph. Let us consider the following simplest one-site graph at one-loop level with the vertex energy E



(6.47)

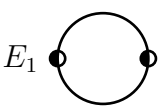
This diagram consists of two distinct contributions that are complex conjugate to each other. As usual, we sum these contributions after flipping the energy on the negative branch, resulting in



$$= -i \int_{-\infty^+}^{0} \mathrm{d}t\, e^{iEt} \int \frac{\mathrm{d}^3\ell}{(2\pi)^3} \Big[\tilde{\mathcal{G}}_{++}(\ell;t,t) - \tilde{\mathcal{G}}_{--}(\ell;t,t)\Big] \,. \tag{6.48}$$

This combination of graphs vanishes as both propagators are indistinguishable at equal times, i.e. $\tilde{\mathcal{G}}_{++}(\ell;t,t) = \tilde{\mathcal{G}}_{--}(\ell;t,t)$. Notice that this straightforwardly extends to all one-site graphs to any loop order.

Two-site graph. We then consider the two-site graph at one-loop level



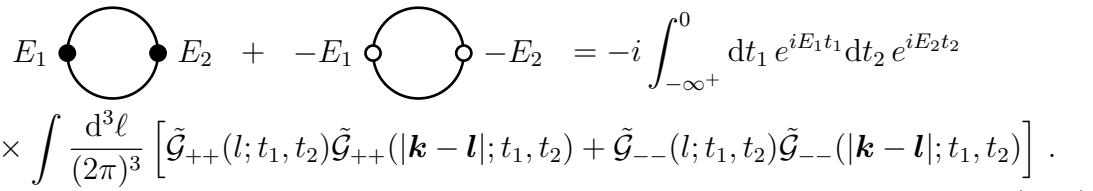
(6.49)

Each contribution contains a product of bulk-to-bulk propagators. The key insight

is to realise that bulk-to-bulk propagators satisfy

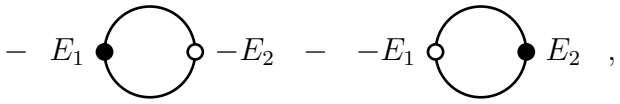
$$\prod_{i=1}^{L+1}\mathcal{G}_{++}(k_i,t_1,t_2)+\prod_{i=1}^{L+1}\mathcal{G}_{--}(k_i,t_1,t_2)=\prod_{i=1}^{L+1}\mathcal{G}_{+-}(k_i,t_1,t_2)+\prod_{i=1}^{L+1}\mathcal{G}_{-+}(k_i,t_1,t_2)\,, \tag{6.50}$$

where L denotes the number of loops. Of course, this relation is also valid for the rescaled (tilted) propagators. For $L=0$, we recover the identity (6.26) that was used in the tree-level case. Proving this identity is simply a matter of manipulating and rearranging time orderings. For unequal times $t_1\neq t_2$, one further requires the use of the trivial formula $\Theta(t_1-t_2)\Theta(t_2-t_1)=0$, and at equal times $t_1=t_2$, one should notice that the Wightman function is real $\mathcal{G}(k_i,t,t)=\mathcal{G}^*(k_i,t,t)$. The special value $\Theta(0)=1/2$ is used. At one-loop order $L=1$, we therefore have



$$\times\int\frac{\mathrm{d}^3\ell}{(2\pi)^3}\left[\tilde{\mathcal{G}}_{++}(l;t_1,t_2)\tilde{\mathcal{G}}_{++}(|\boldsymbol{k}-\boldsymbol{l}|;t_1,t_2)+\tilde{\mathcal{G}}_{--}(l;t_1,t_2)\tilde{\mathcal{G}}_{--}(|\boldsymbol{k}-\boldsymbol{l}|;t_1,t_2)\right]. \tag{6.51}$$

Using (6.50), we recognise the sum of non-time-ordered contributions with flipped energies on the negative branch



(6.52)

albeit with an overall minus sign. Putting all terms on the same side, we recover the largest-time equation. Using (6.50) for $L>2$, this naturally generalises to any loop order.

6.2.3 Application to Simple Diagrams

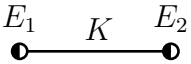
The primary challenge in performing perturbative calculations of cosmological correlators lies in the presence of nested time integrals, which are generally difficult to evaluate. However, as we have seen previously, time-ordering can be interpreted as a specific choice of contour to set the exchanged fields on shell. We can do this by considering a suitable integral representation for the bulk-to-bulk propagators, so that the off-shell propagators appear explicitly factorised.

Here, before turning to correlators in a cosmological background which are of primary interest in Chap. 7, we first consider correlators in flat space.[7] In this case, the corresponding mode functions are analytic in the time (or energy) domain, and the frequency-space representation of the bulk-to-bulk propagator takes the exact same form as the usual Feynman propagator. Therefore, conventional flat-space methods

[7] In flat-space, we are interested in computing equal-time correlators at a fixed time $t=0$ so that interactions are building up during the time interval $-\infty<t<0$. For concreteness, we consider a theory containing a single self-interacting massless scalar field φ. At tree level, the generalisation to (possible different) massive fields is straightforward after setting $k\to\sqrt{k^2+m^2}$. However, adding a mass to a mediated particle inside a loop is much more complicated.

can be used to compute correlators and reveal their analytic structure. In practice, once the factorised time integrals are evaluated, the remaining frequency integral can be finished with the residue theorem. We illustrate this off-shell factorisation with the simplest of all exchanged diagrams, and explicitly show that the computed correlators consistently satisfy the largest-time equation.

Two-site chain. Let us start with the simplest two-chain diagram[8]



$$= \sum_{\mathsf{a},\mathsf{b}=\pm} \mathcal{I}_{\mathsf{ab}}\,, \qquad \text{with} \quad \mathcal{I}_{\mathsf{ab}} = -\mathsf{ab}\int_{-\infty^{\mathsf{a}}}^{0} \mathrm{d}t_1 \int_{-\infty^{\mathsf{b}}}^{0} \mathrm{d}t_2\, e^{i\mathsf{a}E_1 t_1}\tilde{\mathcal{G}}_{\mathsf{ab}}(K;t_1,t_2)e^{i\mathsf{b}E_2 t_2}\,. \tag{6.54}$$

In order to compute the time integrals, the $i\epsilon$ prescription in the in-in contour can be translated to a shift in energy through the formula

$$\int_{-\infty^{\pm}}^{0} \mathrm{d}t\, e^{\pm izt} = \int_{-\infty}^{0} \mathrm{d}t\, e^{\pm i(z\mp i\epsilon)t} = \frac{\mp i}{z\mp i\epsilon}\,, \tag{6.55}$$

for a real positive energy $z>0$. This is equivalent to Wick rotating time, as is usually done. However, it gives the correct pole prescription for the later frequency integration when computing the nested contribution. In the limit $\epsilon\to 0$, the unnested integral is simply given by

$$\mathcal{I}_{+-} = \int_{-\infty^{+}}^{0} \mathrm{d}t_1 e^{i(E_1+K)t_1}\int_{-\infty^{-}}^{0} \mathrm{d}t_2 e^{-i(E_2+K)t_2} = \frac{1}{E_L E_R}\,, \tag{6.56}$$

where $E_L\equiv E_1+K$ and $E_R\equiv E_2+K$ are the sum of energies at the left and right vertices. Note that this contribution has only partial energy poles when $E_{L,R}\to 0$, which emerge from the factorised form. Since the result is purely real, we have $\mathcal{I}_{-+}=\mathcal{I}_{+-}$. Similarly, introducing the frequency-space representation of the time-ordered bulk-to-bulk propagator (6.3) and performing the time integrals using (6.55), the time-ordered contribution reads

$$\mathcal{I}_{++} = -2K\int_{-\infty}^{+\infty}\frac{\mathrm{d}\omega}{2i\pi}\frac{1}{(E_1+\omega-i\epsilon)(\omega^2-K^2)_{i\epsilon}(E_2-\omega-i\epsilon)}\,. \tag{6.57}$$

This representation makes it explicit that both time integrals factorise and that time ordering is encoded in the additional frequency integral. The symmetry under $E_1\leftrightarrow E_2$ can be restored after changing variables $\omega\to-\omega$. The analytic structure of the integrand in the complex ω plane exhibits several interesting features that we show in Fig. 6.2: (i) the pole $\omega=+E_2-i\epsilon$ is the off-shell collinear (folded)

[8] Concretely, for the interaction $\mathcal{L}=-\frac{g}{3!}\varphi^3$, the s-channel tree-level exchange correlator reads

$$\langle\varphi_{\boldsymbol{k}_1}\varphi_{\boldsymbol{k}_2}\varphi_{\boldsymbol{k}_3}\varphi_{\boldsymbol{k}_4}\rangle' = \frac{g^2}{16k_1k_2k_3k_4}\sum_{\mathsf{a},\mathsf{b}=\pm}\mathcal{I}_{\mathsf{ab}}(E_1=k_{12},E_2=k_{34},K=s)\,, \tag{6.53}$$

where $s=|\boldsymbol{k}_1+\boldsymbol{k}_2|$ is the magnitude of the exchange momentum, and $k_{ij}=k_i+k_j$.

limit, (ii) the pole $\omega = -E_1 + i\epsilon$ is the off-shell (left) partial energy pole, and (iii) the poles $\omega = \pm(K - i\epsilon)$ are the on-shell conditions. Notice that poles that can only be reached after analytically continuing the energies to the unphysical kinematic configuration (after setting the exchanged particle on shell) are located in the upper-half complex ω plane. Therefore, selecting for example the *physical* on-shell condition requires closing the contour in the lower-half complex plane, picking the residues at $\omega = +K - i\epsilon$ and $\omega = +E_2 - i\epsilon$, we obtain

$$\mathcal{I}_{++} = \frac{1}{E}\left(\frac{1}{E_L} + \frac{1}{E_R}\right) , \tag{6.58}$$

where $E \equiv E_1 + E_2$ is the total energy of the graph. Of course, closing the contour upwards yields the same result. This shows that partial energy singularities reached for *unphysical* kinematic configurations are related to folded singularities reached for *physical* ones by different time ordering choices. In this representation, the total energy pole $E \to 0$ is made explicit through the identity

$$\frac{1}{(E_1 + \omega - i\epsilon)(E_2 - \omega - i\epsilon)} = \frac{1}{E}\left(\frac{1}{E_1 + \omega - i\epsilon} + \frac{1}{E_2 - \omega - i\epsilon}\right) , \tag{6.59}$$

and partial energy poles are reconstructed from the frequency integral. By reality of the result, we have $\mathcal{I}_{--} = \mathcal{I}_{++}$. Summing all contributions, the final result reads

$$\mathcal{I}(\{E_i\}, K) = \frac{f(\{E_i\}, K)}{E E_L E_R} , \quad \text{with} \quad f(\{E_i\}, K) = 4(E_1 + E_2 + K) . \tag{6.60}$$

This graph integral is a rational function of the energies and has a singularity when

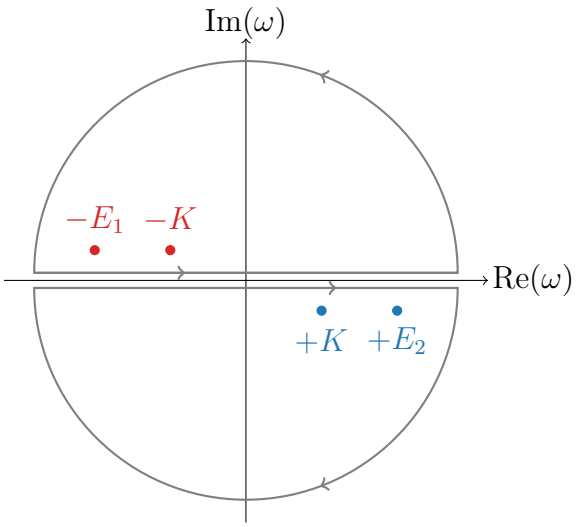


Figure 6.2: Illustration of the analytic structure of the integrand of $\mathcal{I}_{++}$ in the complex ω plane. Different choices of closing the contour, or equivalently different time orderings, relate physical poles in the lower-half plane to unphysical poles in the upper-half plane.

the total energy vanishes $E \to 0$, and when partial energies flowing into the left

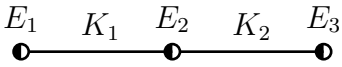
or right vertices add up to zero $E_{L,R} \to 0$, see e.g. [383, 384, 385, 198, 378] for more details. The residue at the total energy poles is the corresponding scattering amplitude [127, 375]. Indeed, using the identity $E_L + E_R = 2K$ in the limit $E \to 0$, the graph integral can be written

$$\lim_{E\to 0} \tfrac{1}{4K}\, \mathcal{I}(\{E_i\}, K) = \frac{\mathcal{A}}{E}\,, \tag{6.61}$$

where $\mathcal{A} = \frac{1}{-\mathcal{S}}$ is the corresponding s-channel scattering amplitude with $\mathcal{S} = -(k_1^\mu + k_2^\mu)^2 = E_1^2 - K^2$ being the usual Mandelstam variable. Note that in order to extract the scattering amplitude in Eq. (6.60), we have imposed the energy conservation condition $E_1 + E_2 = 0$—valid in the asymptotic past—to write $K^2 - E_1^2 = E_L E_R$. Eventually, the identity (6.59) makes it explicit that the graph integrals $\mathcal{I}_{\mathsf{ab}}$ satisfy the largest-time equation

$$\mathcal{I}_{++}(E_1, E_2, K) + \mathcal{I}_{--}(-E_1, -E_2, K) + \mathcal{I}_{+-}(E_1, -E_2, K) + \mathcal{I}_{-+}(-E_1, E_2, K) = 0\,. \tag{6.62}$$

Three-site chain. We now examine the three-site chain, which presents additional complexities compared to the two-site chain. Notably, this requires evaluating two frequency integrals for the fully nested contribution. The corresponding graph reads



$$= \sum_{\mathsf{a,b,c}=\pm} \mathcal{I}_{\mathsf{abc}}\,, \quad \text{with}$$

$$\mathcal{I}_{\mathsf{abc}} = i\mathsf{abc} \int_{-\infty^{\mathsf{a}}}^{0} \mathrm{d}t_1 \int_{-\infty^{\mathsf{b}}}^{0} \mathrm{d}t_2 \int_{-\infty^{\mathsf{c}}}^{0} \mathrm{d}t_3\, e^{i\mathsf{a}E_1 t_1} \tilde{\mathcal{G}}_{\mathsf{ab}}(K_1; t_1, t_2) e^{i\mathsf{b}E_2 t_2} \tilde{\mathcal{G}}_{\mathsf{bc}}(K_2; t_2, t_3) e^{i\mathsf{c}E_3 t_3}\,. \tag{6.63}$$

We have in total $2^3 = 8$ integrals to evaluate, among which half of them are related by complex conjugation. Using Eq. (6.55) and the previous result for evaluating a single frequency integral, the fully factorised and partially nested contributions read

$$\mathcal{I}_{+-+} = \frac{-1}{E_L E_M E_R}\,, \quad \mathcal{I}_{++-} = \frac{-1}{\bar{E}_L E_R}\left(\frac{1}{E_L} + \frac{1}{E_M}\right), \quad \mathcal{I}_{-++} = \frac{-1}{E_L \bar{E}_R}\left(\frac{1}{E_M} + \frac{1}{E_R}\right), \tag{6.64}$$

where $E_L \equiv E_1 + K_1, E_M \equiv E_2 + K_1 + K_2$ and $E_R \equiv E_3 + K_2$ are the sum of energies at the left, middle and right vertices, respectively, and $\bar{E}_L \equiv E_1 + E_2 + K_2$ and $\bar{E}_R \equiv E_2 + E_3 + K_1$ are the energies of the joined two left and right vertices, respectively. Similar integrals were computed in [383] for the corresponding wavefunction coefficient. After using the frequency-space representation for the time-ordered bulk-to-bulk propagators and evaluating the time integrals, the fully nested contribution reads

$$\begin{aligned}\mathcal{I}_{+++} = -(2K_1)(2K_2) \int_{-\infty}^{+\infty} \frac{\mathrm{d}\omega_1}{2i\pi} \frac{\mathrm{d}\omega_2}{2i\pi} \frac{1}{(\omega_1^2 - K_1^2)_{i\epsilon}(\omega_2^2 - K_2^2)_{i\epsilon}} \\ \times \frac{1}{(E_1 + \omega_1 - i\epsilon)(E_2 - \omega_1 + \omega_2 - i\epsilon)(E_3 - \omega_2 - i\epsilon)}\,.\end{aligned} \tag{6.65}$$

This double integral can be evaluated after expanding the integrand into partial fractions, rendering the off-shell poles manifest, and then picking up residues. We obtain

$$\begin{aligned}\mathcal{I}_{+++} = &-\frac{1}{E}\left(\frac{1}{E_2+E_3+K_1}-\frac{1}{E_2+E_3-K_1}\right)\left(\frac{1}{E_3+K_2}-\frac{1}{E_3-K_2}\right)\\ &-\frac{1}{(E_3-K_2)(E_1+E_2+K_2)}\left(\frac{1}{E_2+K_1+K_2}-\frac{1}{E_2-K_1+K_2}\right)\\ &-\frac{1}{(E_1+K_1)(E_2+E_3-K_1)}\left(\frac{1}{E_3+K_2}-\frac{1}{E_3-K_2}\right)\\ &-\frac{1}{(E_1+K_1)(E_2-K_1+K_2)(E_3-K_2)}\,.\end{aligned} \tag{6.66}$$

Notice that it is important to keep track of the correct $i\epsilon$ pole prescription to collect the correct residues. Eventually, since all contributions are real, the remaining ones are identical. Summing all contributions, the graph integral is

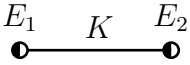
$$\begin{aligned}&\mathcal{I}(\{E_i\},\{K_i\}) = \frac{f(\{E_i\},\{K_i\})}{EE_L\bar{E}_LE_M\bar{E}_RE_R}\,,\\ &\text{with}\quad f(\{E_i\},\{K_i\}) = -8\left[\bar{E}_LE_M\bar{E}_R+E_M(E_1\bar{E}_L+E_3\bar{E}_R)+E_1E_3(\bar{E}_L+\bar{E}_R)\right]\,.\end{aligned} \tag{6.67}$$

The fairly non-trivial form factor f is well symmetric under $(E_1 \leftrightarrow E_3, K_1 \leftrightarrow K_2)$, and the final result displays the correct $E_L, E_M, E_R, \bar{E}_L, \bar{E}_R$ and E poles, as expected. One can explicitly verify that individual contributions satisfy the largest-time equation

$$\begin{aligned}0 = &\,\mathcal{I}_{+++}(E_1,E_2,E_3,K_1,K_2)+\mathcal{I}_{---}(-E_1,-E_2,-E_3,K_1,K_2)\\ &+\mathcal{I}_{++-}(E_1,E_2,-E_3,K_1,K_2)+\mathcal{I}_{--+}(-E_1,-E_2,E_3,K_1,K_2)\\ &+\mathcal{I}_{-++}(-E_1,E_2,E_3,K_1,K_2)+\mathcal{I}_{+--}(E_1,-E_2,-E_3,K_1,K_2)\\ &+\mathcal{I}_{+-+}(E_1,-E_2,E_3,K_1,K_2)+\mathcal{I}_{-+-}(-E_1,E_2,-E_3,K_1,K_2)\,,\end{aligned} \tag{6.68}$$

providing a non-trivial check of the final result. In principle, this procedure can be generalised to arbitrary tree-level diagrams. However, the number of required integrals and the complexity of multi-dimensional frequency integrals rapidly become intractable.

Conformal two-site chain in de Sitter. As a last example, we consider the two-site chain of conformally coupled scalar fields (with mass $m^2 = 2H^2$) in de Sitter, whose computation conceptually follows the same line as in flat space, as the corresponding time-ordered bulk-to-bulk propagators can be recasted as frequency-space integrals.[9] The corresponding graph integrals are



$$= \sum_{\mathsf{a},\mathsf{b}=\pm}\mathcal{I}_{\mathsf{ab}}\,,\quad \mathcal{I}_{\mathsf{ab}} = -\mathsf{ab}\int_{-\infty^{\mathsf{a}}}^{\tau_0}\frac{\mathrm{d}\tau_1}{\tau_1^2}\int_{-\infty^{\mathsf{b}}}^{\tau_0}\frac{\mathrm{d}\tau_2}{\tau_2^2}\,e^{i\mathsf{a}E_1\tau_1}\tilde{\mathcal{G}}_{\mathsf{ab}}(K;\tau_1,\tau_2)e^{i\mathsf{b}E_2\tau_2}\,, \tag{6.69}$$

[9] It is possible to map correlators of conformally coupled fields to correlators of massive scalars with half-integer values of ν by applying a set of weight-shifting operators. This procedure follows from the property of the Hankel function that drastically simplifies for $\nu = n/2$ with n integer ($n = 1$ is the conformally coupled case).

where $\tau_0 < 0$ is a small late-time cutoff. Shifting the energy and neglecting analytic terms in the late-time limit, we use the formula

$$\int_{-\infty^{\pm}}^{\tau_0} \frac{\mathrm{d}\tau}{\tau} e^{\pm iz\tau} = \int_{-\infty}^{\tau_0} \frac{\mathrm{d}\tau}{\tau} e^{\pm i(z\mp i\epsilon)\tau} = \log\left[\pm i(z\mp i\epsilon)\tau_0\right] , \tag{6.70}$$

for a real positive energy $z > 0$, to write the factorised contribution as

$$\mathcal{I}_{+-} = \log(+iE_L\tau_0)\log(-iE_R\tau_0) . \tag{6.71}$$

Similarly, after performing the time integrals for the nested contribution, we obtain

$$\mathcal{I}_{++} = 2K\int_{-\infty}^{+\infty} \frac{\mathrm{d}\omega}{2i\pi} \frac{\log[i(E_1+\omega-i\epsilon)]\log[i(E_2-\omega-i\epsilon)]}{(\omega^2-K^2)_{i\epsilon}} . \tag{6.72}$$

This integral, besides being formally divergent, is hard to evaluate because of the branch cuts spanning over $\omega \in (-E_1+i\epsilon-i\infty, -E_1+i\epsilon)$ and $\omega \in (E_2-i\epsilon+i\infty, E_2-i\epsilon)$ (choosing the log branch cut to be the principal one). These branch cuts notably cross the real axis, and arise from the cancellation of would-be IR divergences, as explicitly shown in footnote 10, that are otherwise absent in the presence of derivative interactions. As first noticed in [262], this integral can be written as an energy integral over the flat-space result

$$\begin{aligned}\mathcal{I}_{++} &= 2K\int_{-\infty}^{+\infty} \frac{\mathrm{d}\omega}{2i\pi} \frac{1}{(\omega^2-K^2)_{i\epsilon}} \int_{E_1+\omega-i\epsilon}^{\infty}\int_{E_2-\omega-i\epsilon}^{\infty} \frac{\mathrm{d}x\mathrm{d}y}{xy} \\ &= 2K\int_{E_1}^{\infty}\mathrm{d}x\int_{E_2}^{\infty}\mathrm{d}y\int_{-\infty}^{+\infty} \frac{\mathrm{d}\omega}{2i\pi} \frac{1}{(x+\omega-i\epsilon)(\omega^2-K^2)_{i\epsilon}(y-\omega-i\epsilon)} ,\end{aligned} \tag{6.73}$$

where we have shifted the kinematic integrals so that their limits do not depend on the off-shell frequency. We recognise the flat-space frequency integral that we previously computed. The energy integrals were first computed in [262] and the result reads[10]

$$\begin{aligned}\mathcal{I}_{++} = {} & \mathrm{Li}_2\left(\frac{E-E_L}{E}\right) + \mathrm{Li}_2\left(\frac{E-E_R}{E}\right) + \log\left(\frac{E_L}{E}\right)\log\left(\frac{E_R}{E}\right) - \frac{\pi^2}{6} \\ & - \log(iE_L\tau_0)\log(iE_R\tau_0) ,\end{aligned} \tag{6.76}$$

[10] In order to extract the divergence, one can subtract and add the term

$$\int_{-\infty^+}^{\tau_0} \frac{\mathrm{d}\tau_1}{\tau_1}\frac{\mathrm{d}\tau_2}{\tau_2} e^{i(E_L\tau_1+E_R\tau_2)} = \log(iE_L\tau_0)\log(iE_R\tau_0) = \int_{E_1}^{\infty}\mathrm{d}x\int_{E_2}^{\infty}\mathrm{d}y\,\frac{1}{(x+K-i\epsilon)(y+K-i\epsilon)} , \tag{6.74}$$

which can either be written as a product of logarithms (hence isolating the divergence) or as energy integrals that can be combined with the original ones. This effectively mimics the corresponding wavefunction coefficient calculation. The remaining convergent integral to be computed is

$$\int_0^{\infty} \frac{\mathrm{d}x\mathrm{d}y}{(x+y+E)(x+E_L)(y+E_R)} . \tag{6.75}$$

Sophisticated techniques to evaluate such integrals are detailed in [391, 392, 393, 394].

where Li_2 is the dilogarithm function. When summing all contributions, the kinematic parts of divergent pieces cancel against each other thanks to the property $\log(iz) - \log(-iz) = -i\pi$ for $z < 0$. Using the Euler's identity

$$\mathrm{Li}_2(z) + \mathrm{Li}_2(1-z) + \log(z)\log(1-z) = \frac{\pi^2}{6}\,, \tag{6.77}$$

both nested contributions combine to give

$$\begin{aligned}\mathcal{I}_{++}(E_1, E_2, K) + \mathcal{I}_{--}(-E_1, -E_2, K) = &- \log[i(E_1 - K)\tau_0]\log[i(E_2 + K)\tau_0] \\ &- \log[i(E_1 + K)\tau_0]\log[i(E_2 - K)\tau_0]\,,\end{aligned} \tag{6.78}$$

which is exactly minus the combination $\mathcal{I}_{+-}(E_1, -E_2, K) + \mathcal{I}_{-+}(-E_1, E_2, K)$. Consequently, the graph integrals $\mathcal{I}_{\mathsf{ab}}$ satisfy the largest-time equation.

7

Bootstrapping Cosmological Correlators

Pushing forward the state-of-the-art of computational techniques, even at first order in perturbation theory, demands gruelling mathematical dexterity, for at least three interrelated reasons. First, computing cosmological correlators requires integrating over the entire bulk time evolution, as time translation symmetry is lost and an asymptotically free future is absent. Second, the curved geometry of the cosmological background distorts the free propagation of particles. Finally, unlike tree-level scattering amplitudes, which are meromorphic functions of complex kinematics with branch cuts appearing only at the loop level, tree-level cosmological correlators already exhibit branch cuts. This crucial distinction arises from spontaneous particle production.

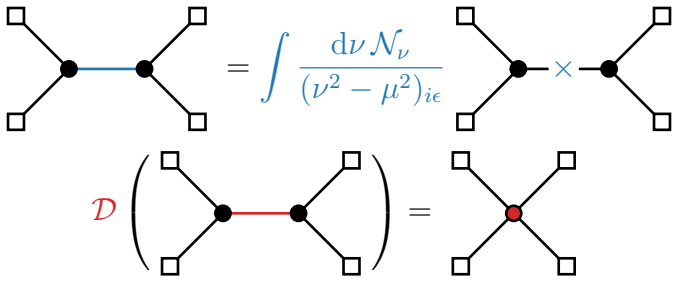


Figure 7.1: Schematic illustration of the two approaches used in this chapter to bootstrap cosmological correlators: (*top*) performing a spectral integration that unnests time integrals, (*bottom*) solving a boundary kinematic differential equation satisfied by cosmological correlators.

Despite these challenges, several powerful techniques have recently been developed. At tree level, approaches such as bootstrapping correlators by solving bound-

ary kinematic equations [262, 198, 286, 311, 305, 306, 420] and reformulating perturbative diagrammatic rules in Mellin space [421, 422, 381, 423] have proven effective. The use of partial Mellin-Barnes representations [304, 305, 424], leveraging the global dilatation symmetry of de Sitter space that replaces time translations, has further improved these methods. Additionally, numerical techniques that trace the time evolution of correlation functions have been developed to explore and carve out the space of most correlators, see Part IV. At the loop order, dispersive integrals have been used to tame loop diagrams [338, 425] (also see [294, 296, 245, 302, 426, 307, 339] for other techniques).[1]

In this chapter, we "bootstrap" cosmological correlators using two different approaches. First, we explicitly compute the four-point function of conformally coupled scalars mediated by the tree-level exchange of massive scalars using the newly introduced spectral representation, and present a new, partially resummed representation for this correlator. This novel approach also offers a more intuitive understanding of the underlying physics. For example, the single tower of poles that we find maps directly to the quasi-normal modes of the exchanged massive field. Fundamentally, as we will show, this dispersive representation of cosmological correlators clearly illustrates the analytic structure of individual contributions and their factorisation properties. It makes explicit that exchange correlators are constructed by gluing lower-point off-shell correlators with a sewing kernel that encodes both particle production (from the off-shell leg) and a tower of EFT contributions that emerge after integrating out the exchanged field. By explicitly performing this spectral integral, we set the exchanged particle on-shell, allowing us to reconstruct more complex diagrams. Second, we explicitly compute the most general boost-breaking tree-level four-point correlator with external legs having reduced speed of sounds exchanging a massive field which additionally contains linear terms in its dispersion relation $\omega^2 \propto k$. This mediated field can be thought of as a massive particle coupled to a helical chemical potential whose mode function is given by a Whittaker function. To do this, we solve a boundary kinematic equation satisfied by the correlator and fix unconstrained coefficients using physical inputs.

7.1 Via Spectral Representation

Using the spectral representation of bulk-to-bulk cosmological correlators introduced in Chap. 6, we now compute the two-site chain of conformally coupled scalars mediated by the tree-level exchange of massive scalars in de Sitter. By explicitly performing the spectral integral, we derive a new closed-form expression for this correlator. As we will show, the branch cut in the energy domain due to particle production translates into a tower of poles in the complex mass domain. Summing over these residues leads to a new simple and partially resummed series solution.

[1] The resummation of massless loops in de Sitter space—and the associated secular infrared divergences—has a rich and extensive story that goes beyond our focus in this thesis.

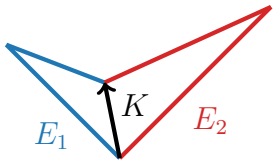
We are interested in computing the de Sitter tree-level exchange graph[2]

$$\begin{tikzpicture}[baseline=(current bounding box.center)]
\node[above] at (0,0.15) {E_1};
\node[above] at (1.2,0.15) {K};
\node[above] at (2.4,0.15) {E_2};
\draw (0,0) -- (2.4,0);
\fill (0,0) circle (0.08);
\fill (2.4,0) circle (0.08);
\end{tikzpicture} = \sum_{\mathsf{a},\mathsf{b}=\pm} F_{\mathsf{ab}}\,,$$

$$\text{with}\quad F_{\mathsf{ab}} = -\mathsf{ab}K\int_{-\infty^{\mathsf{a}}}^{0}\frac{\mathrm{d}\tau'}{(-\tau')^{1/2}}e^{i\mathsf{a}E_1\tau'}\int_{-\infty^{\mathsf{b}}}^{0}\frac{\mathrm{d}\tau''}{(-\tau'')^{1/2}}e^{i\mathsf{b}E_2\tau''}\mathcal{G}_{\mathsf{ab}}(K;\tau',\tau'')\,. \tag{7.2}$$

Recall that $\mathcal{G}_{\mathsf{ab}}$ are the propagators for the canonically normalised field $\sigma(\tau,\boldsymbol{x}) \equiv (-\tau)^{-3/2}\phi(\tau,\boldsymbol{x})$, hence the unusual power for the conformal time within the integral. We define the usual dimensionless kinematic variables (represented on the right)

$$u \equiv \frac{K}{E_1}\,,\qquad v \equiv \frac{K}{E_2}\,, \tag{7.3}$$



which lie in the unit disk, i.e. $|u|,|v| \leq 1$, and the three-point function

$$F^{(3)}(z,\mu) = \tfrac{1}{\sqrt{2}}|\Gamma(\tfrac{1}{2}+i\mu)|^2\,P_{i\mu-1/2}(z)\,, \tag{7.4}$$

where $P_{i\mu-1/2}$ is the Legendre function defined in Eq. (A.15). The non-time-ordered contribution, for which both time integrals factorise, is therefore given by

$$F_{+-} = F^{(3)}(u^{-1},\mu)\,F^{(3)}(v^{-1},\mu)\,. \tag{7.5}$$

We have used the useful formula (A.17) to perform the time integrals. Notice that the Legendre P function is real, i.e. $[P_{i\mu-1/2}(z)]^* = P_{i\mu-1/2}(z)$ for $z \geq 0$ and μ real. Therefore, the on-shell three-point function $F^{(3)}(z,\mu)$ is real. As a consequence, we obtain the same expression for F_{-+}. However, anticipating what follows, the off-shell function $F^{(3)}(z,\nu)$ where the mass parameter ν is analytically continued to the complex plane is not real.

7.1.1 Off-Shell Three-Point Function

For pedagogical reasons, before computing the spectral integral for the time-ordered contribution F_{++}, we first study the following simpler integral

$$\bar{F}^{(3)}(z) = \int_{-\infty}^{+\infty}\mathrm{d}\nu\,\mathcal{N}_\nu\,\frac{F^{(3)}(z,\nu)}{(\nu^2-\mu^2)_{i\epsilon}}\,, \tag{7.6}$$

with $z \geq 1$, and $F^{(3)}$ defined in Eq. (7.4). The object $\bar{F}^{(3)}$ is typically proportional to F_{++} in the folded limit $E_2 \to K$ (or $E_1 \to K$ by symmetry), equivalently $v \to 1$

[2]Concretely, considering a conformally coupled scalar field φ coupled to a massive scalar field σ by $\mathcal{L}_{\rm int}/a^3(t) = -\frac{g}{2}\sigma\varphi^2$ in de Sitter, the full correlator reads

$$\langle\varphi_{\boldsymbol{k}_1}\varphi_{\boldsymbol{k}_2}\varphi_{\boldsymbol{k}_3}\varphi_{\boldsymbol{k}_4}\rangle' = \frac{g^2\tau_0^4}{16k_1k_2k_3k_4}\,F(E_1=k_{12},E_2=k_{34},K=s)+t+u\text{ channels}\,, \tag{7.1}$$

where we have introduced a late-time cutoff τ_0 and defined $F \equiv \sum_{\mathsf{a},\mathsf{b}=\pm}F_{\mathsf{ab}}$. Notice that we have defined the integrals F_{ab} without the factor 2 to ease comparison with the literature.

(or $u \to 1$), and already exhibits an interesting analytic structure. To be able to perform the spectral integral, it is essential to understand the analytic structure of the function $F^{(3)}(z,\nu)$ in the complex ν plane, as well as its behaviour at infinity, to appropriately determine how to close the contour.

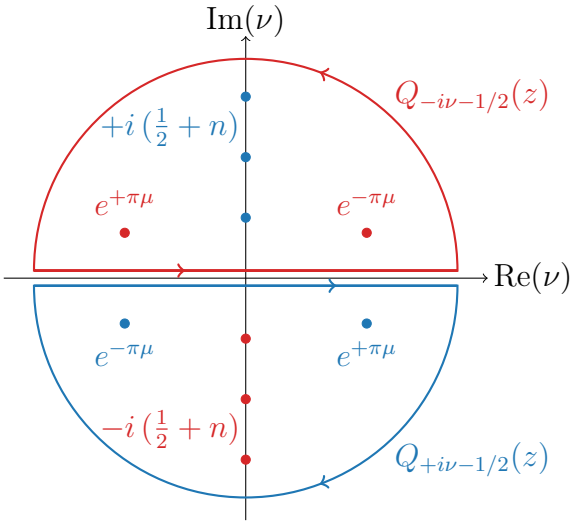


Figure 7.2: Illustration of the analytic structure of the off-shell three-point function integrand in (7.6) in the complex ν plane, written in the Legendre Q basis. The contour prescription avoids the infinite tower of poles lying on the imaginary axis and only picks up particle production poles.

The crucial observation is that the off-shell three-point function $F^{(3)}$ is a meromorphic function in the complex ν plane. At a fixed kinematic configuration z, the function $F^{(3)}(z,\nu)$ has poles at $\nu = \pm i\,(\frac{1}{2}+n)$ with integer $n \geq 0$, which corresponds to the poles of $|\Gamma(\frac{1}{2}+i\nu)|^2 = \Gamma(\frac{1}{2}+i\nu)\Gamma(\frac{1}{2}-i\nu)$, since the Legendre function P is analytic in the entire complex ν plane. However, the Legendre P representation of $F^{(3)}$ makes the large-ν asymptotic form not neat, i.e. it depends on the phase of z. In order to disentangle both behaviours at infinity, we project the off-shell three point function onto the Legendre Q basis using the connection formula (A.18), yielding

$$F^{(3)}(z,\nu) = \frac{e^{-\frac{i\pi}{2}}}{\sqrt{2}\sinh(\pi\nu)}\left[Q_{-i\nu-1/2}(z) - Q_{+i\nu-1/2}(z)\right] . \tag{7.7}$$

The function $Q_{\pm i\nu-1/2}(z)$ has purely imaginary poles located at $\nu = \pm i\,(\frac{1}{2}+n)$ (which come from $\Gamma(\frac{1}{2}\pm i\mu)$ in Eq. (A.15)), and should be closed in the lower (upper) complex plane since $Q_{\pm i\nu-1/2}(z) \sim e^{\mp i\nu\xi}$ with $\xi > 0$. Therefore, when performing the spectral integral, we never need to pick up these poles because the contour is closed to avoid the infinite tower.[3] We illustrate the analytic structure of the integrand (7.6) and the contour prescription in Fig 7.2. Eventually, picking up only the particle production poles, we obtain

$$\bar{F}^{(3)}(z) = F^{(3)}(ze^{+i\pi},\mu)\,, \tag{7.8}$$

[3]The factor $1/\sinh(\pi\nu) = |\Gamma(1+i\nu)|^2/(\pi\nu)$ also brings additional poles to the integrand. However, they are precisely cancelled by the density of states $\mathcal{N}_\nu$.

where we have used the analytic continuation of the Legendre function (A.19) to re-express the result in the Legendre P basis. As already seen in Chap. 6, the particle production pole structure projects ingoing modes on outgoing ones and vice versa. At the level of the three-point function, this amounts to rotate the kinematic configuration $z \to ze^{+i\pi}$. Actually, we show in the next section that the function $F^{(3)}(z,\mu)$ and its analytic continuation $F^{(3)}(ze^{+i\pi},\mu)$, viewed as functions of z for fixed μ, are related by a dispersive integral in the complex energy domain. Anticipating what follows, for the time-ordered contribution F_{++}, the infinite tower of poles cannot be evaded by the integration contour, and will result in series solution for the correlator.

7.1.2 Dispersive Integral in the Energy Domain

By performing the spectral integral in the mass domain, the effect of the particle production poles on the off-shell three-point function is to rotate its external energy $F^{(3)}(z,\mu) \to F^{(3)}(ze^{+i\pi},\mu)$. We now show that this connection is manifested through a dispersive integral in the energy domain.

Complex energy domain. Let us define the off-shell three-point function by its integral representation only

$$F^{(3)}(z,\mu) \equiv -i\frac{\sqrt{\pi}}{2}\, e^{\frac{\pi\mu}{2}+\frac{i\pi}{4}}\sqrt{K}\int_{-\infty}^{0}\frac{\mathrm{d}\tau\, e^{iE\tau}}{(-\tau)^{1/2}}\, H^{(2)}_{i\mu}(-K\tau)\,, \tag{7.9}$$

where $z \equiv E/K$, with E and K denoting the external and internal energies, respectively. The physical kinematic region is given by $z \geq 1$. We now want to analytically continue this function in the entire complex z plane, and in particular outside the physical region, without actually evaluating the integral explicitly (the result is given in (7.4)). First, from the asymptotic form of the Hankel function, we notice that the UV convergence as $\tau \to -\infty$ is controlled by the phase of $E+K$, i.e. the sum of the energies entering this three-point function. The integral converges only when $E+K$ has a negative imaginary part. The integral can be regularised by deforming the contour $-\infty \to -\infty^+(E+K)^{-1}$, with $-\infty^+ \equiv -\infty(1-i\epsilon)$, so that the lower bound $\tau = -\infty$ is approached from a direction that depends on the argument of $E+K$. Then, we note that the integrand exhibits a branch cut, from the Hankel function and the square root, that we choose to be on the positive real axis $\tau \in (0,+\infty)$, as usual. This gives rise to a discontinuity in the energy domain along $E+K \in (-\infty,0)$, equivalently along $z \in (-\infty,-1)$.

Discontinuity. We now show that the full function $F^{(3)}(z,\mu)$ can be recovered from the knowledge of its discontinuity only. By slightly deforming the time integration, the discontinuity of the integral along the branch cut $z \in (-\infty,-1)$ is given by the discontinuity of the integrand itself

$$\begin{aligned}\underset{z}{\mathrm{Disc}}\left[F^{(3)}(z,\mu)\right] &= \lim_{\epsilon\to 0}\left[F^{(3)}(ze^{-i\epsilon},\mu) - F^{(3)}(ze^{+i\epsilon},\mu)\right] \\ &= i\frac{\sqrt{\pi}}{2}\, e^{\frac{\pi\mu}{2}+\frac{i\pi}{4}}\sqrt{K}\int_{\infty}^{0}\mathrm{d}\tau\,\underset{\tau}{\mathrm{Disc}}\left[\frac{e^{iE\tau}}{\tau^{1/2}}\, H^{(2)}_{i\mu}(K\tau)\right]\,.\end{aligned} \tag{7.10}$$

Using the known analytic continuation of the Hankel function (A.7) and (A.9), the discontinuity of the integrand is given by

$$\underset{\tau}{\text{Disc}}\left[\frac{e^{iE\tau}}{\tau^{1/2}}\,H^{(2)}_{i\mu}(K\tau)\right] = -2i\cosh(\pi\mu)\,\frac{e^{iE\tau}}{\tau^{1/2}}\,H^{(2)}_{i\mu}(K\tau)\,. \tag{7.11}$$

Eventually, after changing variables, we obtain

$$\underset{z}{\text{Disc}}\left[F^{(3)}(z,\mu)\right] = -2i\cosh(\pi\mu)\,F^{(3)}(-z,\mu)\,. \tag{7.12}$$

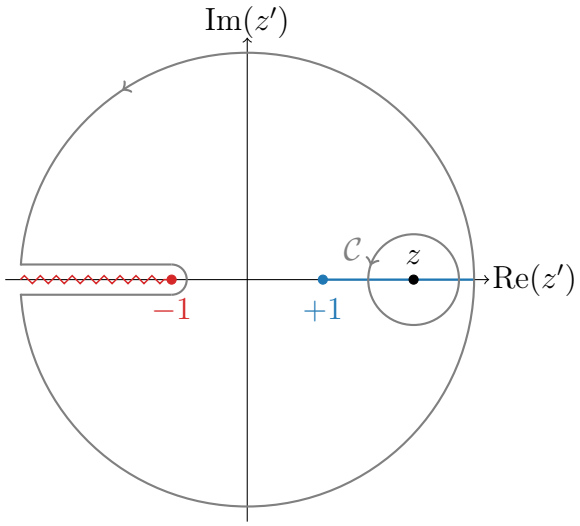


Figure 7.3: Illustration of the contour deformation used in (7.13) in the complex z' plane. At fixed mass μ, the off-shell three-point function $F^{(3)}(z,\mu)$ in the physical kinematic region $z \geq 1$ is related to its discontinuity along the branch cut $z \leq -1$ through a dispersive integral. At a fixed internal energy K flowing in the off-shell leg, the point $z = +1$ is the folded limit $E \to K$ whereas the branch point $z = -1$ is the standard early-time energy singularity $E + K \to 0$.

Dispersive integral. At fixed μ, since the function $F^{(3)}(z,\mu)$ is analytic everywhere except on the branch cut, we can use Cauchy's integral formula to write

$$F^{(3)}(z,\mu) = \oint_{\mathcal{C}} \frac{\mathrm{d}z'}{2i\pi}\,\frac{F^{(3)}(z',\mu)}{z'-z} = \int_{-\infty}^{-1} \frac{\mathrm{d}z'}{2i\pi}\,\frac{\text{Disc}_{z'}\left[F^{(3)}(z',\mu)\right]}{z'-z}\,, \tag{7.13}$$

where the integral contour $\mathcal{C}$ encircles z counterclockwise. The second equality is found by deforming the contour as shown in Fig. 7.3, as the integral along the large arc vanishes. Using the found discontinuity of the three-point function (7.12), we finally get

$$F^{(3)}(z,\mu) = -2i\cosh(\pi\mu)\int_{-\infty}^{-1} \frac{\mathrm{d}z'}{2i\pi}\,\frac{F^{(3)}(-z',\mu)}{z'-z}\,. \tag{7.14}$$

Inversely, $F^{(3)}(-z,\mu)$ is obtained from $F^{(3)}(z,\mu)$ in the same way. The same approach can be employed to reconstruct the complete four-point correlator, including the tower of EFT poles, using only the non-local signal. This powerful method was used and further explored in [425].

7.1.3 Bootstrapping via the Spectral Representation

We now explicitly compute the integral

$$F_{++} = -\int_{-\infty}^{+\infty} \mathrm{d}\nu\, \mathcal{N}_\nu \, \frac{F^{(3)}(u^{-1},\nu)F^{(3)}(v^{-1},\nu)}{(\nu^2-\mu^2)_{i\epsilon}} \,. \tag{7.15}$$

This spectral representation makes it explicit that the time-ordered contribution F_{++} is the spectral integral of the off-shell function F_{+-} given in Eq. (7.5). In practice, it means that solutions for the time-ordered contributions are of higher-transcendentality than the factorised ones. We expect that the result contains a local and non-local contributions which take a simple resummed form, as well as an EFT series contribution coming from infinite towers of poles. Proceeding the same way as previously for the three-point function, we decompose the functions $F^{(3)}$ in the Legendre Q basis to isolate well-behaved asymptotic forms at large ν. The integrand takes the form

$$\begin{aligned}\mathcal{N}_\nu\, F^{(3)}(u^{-1},\nu)F^{(3)}(v^{-1},\nu) &= \frac{-\nu}{2\pi\sinh(\pi\nu)} \\ \times \left[Q_{-i\nu-1/2}(u^{-1})Q_{-i\nu-1/2}(v^{-1}) - Q_{-i\nu-1/2}(u^{-1})Q_{+i\nu-1/2}(v^{-1}) + (\nu\leftrightarrow-\nu)\right] &.\end{aligned} \tag{7.16}$$

First, we immediately observe that both terms related by the shadow transformation $\nu \leftrightarrow -\nu$ contribute equally to the integral. Thus, it suffices to evaluate only one of these terms. Second, we notice that that the term $Q_{-i\nu-1/2}(u^{-1})Q_{-i\nu-1/2}(v^{-1})$ has a well-defined large-ν behaviour that is independent of the hierarchy between the kinematic variables u and v. However, the choice of whether to close the contour upwards of downwards for the term $Q_{-i\nu-1/2}(u^{-1})Q_{+i\nu-1/2}(v^{-1})$ depends on the relative magnitude between u and v. As such, we will obtain a solution for $|u|<|v|$ and another one for $|u|>|v|$. The matching condition at $u=v$ is inherently satisfied, as it is encoded in the spectral integral. Therefore, we decompose the spectral integral into two pieces

$$F_{++} = F^0_{++} + F^{<,>}_{++} \,, \tag{7.17}$$

with (we have accounted for the factor 2 coming from the $\nu\leftrightarrow-\nu$ symmetry)

$$\begin{aligned} F^0_{++} &= \frac{1}{\pi}\int_{-\infty}^{+\infty} \frac{\mathrm{d}\nu\,\nu}{\sinh(\pi\nu)} \frac{Q_{-i\nu-1/2}(u^{-1})Q_{-i\nu-1/2}(v^{-1})}{(\nu^2-\mu^2)_{i\epsilon}} \,, \\ F^{<,>}_{++} &= \frac{-1}{\pi}\int_{-\infty}^{+\infty} \frac{\mathrm{d}\nu\,\nu}{\sinh(\pi\nu)} \frac{Q_{-i\nu-1/2}(u^{-1})Q_{+i\nu-1/2}(v^{-1})}{(\nu^2-\mu^2)_{i\epsilon}} \,. \end{aligned} \tag{7.18}$$

Despite the appearance, the contribution $F^{<,>}_{++}$ is well symmetric under $u\leftrightarrow v$, which can be explicitly checked after changing variables $\nu\leftrightarrow-\nu$. The analytic structure of these integrands reveals the presence of several poles with different origins:

- A first tower of poles comes from the factor $\nu/\sinh(\pi\nu) = \Gamma(1+i\nu)\Gamma(1-i\nu)/\pi$. They are located on the entire imaginary axis $\nu = \pm i\,(1+n)$ with $n\geq 0$, and cannot be evaded by the contour prescription.

- The factor $Q_{-i\nu-1/2}(u^{-1})Q_{-i\nu-1/2}(v^{-1})$ also generates an infinite tower of (second-order) poles located on the imaginary axis $\nu = -i\,(\frac{1}{2}+n)$ with $n \geq 0$. However, at large ν, the integrand behaves as $\sim e^{+i\nu(\xi_u+\xi_v)}$ with $\xi_u = \cosh^{-1}(u^{-1}) \geq 0$ for $u^{-1} \geq 1$ (and similarly for ξ_v), so the contour should be closed in the upper-half complex plane. As a result, we do not collect these poles. This case is similar to the off-shell three-point function case seen in the previous section. Here, both off-shell exchanged modes interfere constructively so that their spectrum spans only over half the imaginary axis, with residues doubling their weight.

- Poles of the term $Q_{-i\nu-1/2}(u^{-1})Q_{+i\nu-1/2}(v^{-1})$ are located at $\nu = \pm i\,(\frac{1}{2}+n)$ with $n \geq 0$. At large ν, it behaves as $\sim e^{+i\nu(\xi_u-\xi_v)}$. For $|u| < |v|$, we have $\xi_u - \xi_v \geq 0$ and we close the contour in the upper-half complex plane, picking the tower of (first-order) poles. This case reflects the destructive interference between off-shell exchanged modes, resulting in the spectrum spanning over the entire imaginary axis.

- Eventually, we also have the usual particle production poles coming from the $i\epsilon$ prescription.

Let us now collect these various poles in turn.

Particle production residues. The poles coming from the $i\epsilon$ prescription are the easiest to evaluate. We obtain

$$F^0_{++} \supset \frac{-i}{2\sinh^2(\pi\mu)}\left[e^{+\pi\mu}Q_{+i\mu-1/2}(u^{-1})Q_{+i\mu-1/2}(v^{-1}) + (\mu \leftrightarrow -\mu)\right] . \tag{7.19}$$

For the contribution $F^<_{++}$ for which $|u| < |v|$, collecting both poles on the upper-half complex plane results in

$$F^<_{++} \supset \frac{i}{2\sinh^2(\pi\mu)}\left[e^{+\pi\mu}Q_{+i\mu-1/2}(u^{-1})Q_{-i\mu-1/2}(v^{-1}) + (\mu \leftrightarrow -\mu)\right] . \tag{7.20}$$

Combining both contributions, and projecting back onto the Legendre P basis using (A.18) and (A.19) yields

$$F^{\text{collider}}_{++} = -F^{(3)}(-u^{-1},\mu)F^{(3)}(v^{-1},\mu)\,, \tag{7.21}$$

for $|u| < |v|$. The contribution for which $|u| > |v|$ is simply found after swapping u and v. The found factorised form is not surprising as in the late-time limit time ordering vanishes, as seen in Chap. 4. The result (7.21) can be directly found by performing the time integrals after substituting $\mathcal{G}_{++} \to \mathcal{G}_{-+}$.

EFT residues. Contributions coming from EFT residues are analytic in both u and v as $u, v \to 0$, and therefore admits series representations. We first sum over the residues from the factor $1/\sinh(\pi\nu)$. The integration contour picks up only half of this tower of first-order poles on the imaginary axis. Explicitly, we obtain

$$F^0_{++} \supset -\frac{2}{\pi}\sum_{n=0}^{+\infty}(-1)^n\,\frac{(n+1)}{(n+1)^2+\mu^2}\,Q_{n+1/2}(u^{-1})Q_{n+1/2}(v^{-1})\,, \tag{7.22}$$

where we have used that the residue of $\Gamma(1+i\nu)$ at $\nu = +i(1+n)$ is $\frac{(-1)^n}{n!}$. The terms in $1/\mu^2$, characteristic of an EFT expansion, come from

$$\frac{1}{(\nu^2-\mu^2)_{i\epsilon}} \xrightarrow[\nu\to+i(n+1)]{} \frac{-1}{(n+1)^2-\mu^2}\,. \tag{7.23}$$

The large n behaviour of the series coefficients is given by

$$\left|\frac{(n+1)}{(n+1)^2+\mu^2}\,Q_{n+1/2}(u^{-1})Q_{n+1/2}(v^{-1})\right| \sim \frac{1}{(n+1)^2+\mu^2}\frac{e^{-(n+1)(\xi_u+\xi_v)}}{\sqrt{\sinh\xi_u\sinh\xi_v}}\,, \tag{7.24}$$

which is well convergent. Notice that close to $u, v = 1$, the exponential damping becomes less efficient and the series converges slower, i.e. as $1/n^2$. Similarly, the contribution of these residues to $F^{<}_{++}$ is found to be

$$F^{<}_{++} \supset \frac{2}{\pi}\sum_{n=0}^{+\infty}(-1)^n\,\frac{(n+1)}{(n+1)^2+\mu^2}\,Q_{n+1/2}(u^{-1})Q_{-n-3/2}(v^{-1})\,. \tag{7.25}$$

Quite interestingly, the two towers of residues (7.22) and (7.25) exactly cancel each other. Indeed, both contributions can be combined in a single series, and using (A.18), each series coefficient is proportional to

$$Q_{-n-3/2}(v^{-1}) - Q_{n+1/2}(v^{-1}) \propto \sin[\pi(n+1)]\,. \tag{7.26}$$

This effect, which generally occurs in odd spatial dimensions, was previously noted in [421] and is applicable to contact diagrams as well. Notably, while this phenomenon was initially understood as interference between the two branches of the in-in contour, we show here that this cancellation happens within a single branch. We finish with the poles located at $\nu = \pm i\,(\frac{1}{2}+n)$ which only enter the contribution $F^{<,>}_{++}$. They are the only ones contributing to the final expression. For $|u| < |v|$, we obtain the rather simple expression

$$F^{\text{EFT}}_{++} = u\sum_{n=0}^{+\infty}\frac{(-1)^n}{(n+\frac{1}{2})^2+\mu^2}\left(\frac{u}{v}\right)^n {}_2F_1\left[\begin{matrix}\frac{1+n}{2} & 1+\frac{n}{2}\\ \frac{3}{2}+n\end{matrix};u^2\right]{}_2F_1\left[\begin{matrix}\frac{1-n}{2} & -\frac{n}{2}\\ \frac{1}{2}-n\end{matrix};v^2\right]. \tag{7.27}$$

The Legendre Q function being not defined for negative integer order, the above expression is found after evaluating the residue of the Γ function entering (A.15).

Full result. The full result is found by summing all contributions, namely the non-time ordered pieces (7.5) and the time-ordered pieces combining the collider signal (7.21) with the EFT series (7.27). A few comments are in order. First, this method yields a convergent result in all kinematic configurations. Although not obvious from the analytical expression, we have checked numerically that the found result perfectly matches the one originally found in [198]. Fig. 7.4 shows the full closed-form result when keeping only a few terms in the series. We observe that the series convergence rate is the same as the bootstrap result but slower than the series solution found using the partial Mellin-Barnes method [305]. Second, compared to the bootstrap result of [198], the spectral integration naturally resums one of the

two series, which in practice makes the evaluation much faster. Lastly, since the spectral representation is solution to the bootstrap equation, there is a one-to-one correspondence between the basis of functions onto which the homogeneous solution of the bootstrap equation is expanded and the Legendre P or Q basis. Additionally, when solving the boundary differential equation, fixing the free coefficients requires two boundary conditions for specific values (or limits) of u and v. Here, these coefficients are fully encoded in the spectral integral. Eventually, the spectral method does not requires matching different solutions at $u = v$ because the transition of closing the contour, whether upwards or downwards, is continuous. However, the first derivative of the result is discontinuous at the transition, resulting in a noticeable kink. In short, rather than integrating the boundary differential equation, we directly perform the spectral integral, with the bounds inherently determining the free integration constants.

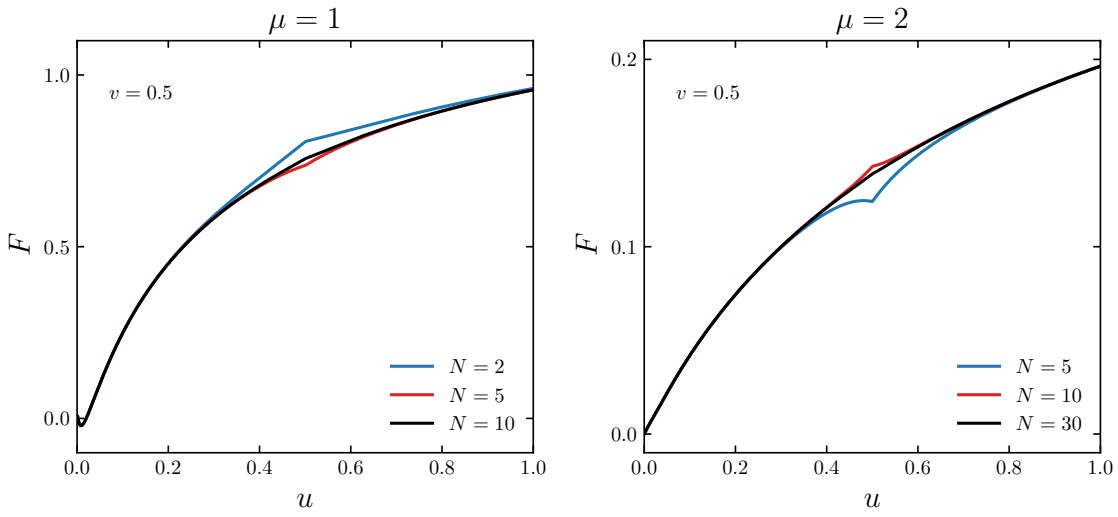


Figure 7.4: The four-point correlation function $F(u, v) = \sum_{\mathsf{a},\mathsf{b}=\pm} F_{\mathsf{ab}}$, as defined in Eq. (7.2), as function of the dimensionless kinematic variable u with fixed $v = 0.5$, for $\mu = 1$ (*left panel*) and $\mu = 2$ (*right panel*). We include terms in the series from $n = 1, \ldots, N$. These results reproduce those presented in [198] (Fig. 6) and in [305] (Fig. 6). The Mathematica notebook with the analytical expression for F is available on the Github repository [].

Largest-time equation. Assuming $|u| < |v|$, it is trivial to observe that

$$F_{++}(u, v) + F_{--}(-u, -v) + F_{+-}(u, -v) + F_{-+}(-u, v) = 0\,, \tag{7.28}$$

from their explicit forms in (7.5), (7.21) and (7.27). Indeed, both EFT series cancel against each other thanks to the overall factor u, i.e. $F^{\text{EFT}}_{--}(-u, -v) = -F^{\text{EFT}}_{++}(u, v)$. Similarly, $F^{\text{collider}}_{++}(u, v)$ cancels against $F_{-+}(-u, v)$, and $F^{\text{collider}}_{--}(-u, -v)$ against $F_{+-}(u, -v)$. Of course, swapping u and v yields the same result. This provides an additional consistency check for the derived formula.

Convergence outside the unit circle. By triangle inequality, the allowed region for the kinematics variables u and v is the unit circle $0 \leq |u|, |v| \leq 1$ (the physical region corresponding to the inscribed real line). However, when the external field has a reduced speed of sound, one needs to analytic continue the seed correlator beyond the physical domain implied by momentum conservation [311]. Indeed, by rescaling the external energies $E_{1,2} \to c_s E_{1,2}$ with $c_s \leq 1$ and leaving the internal momentum K unchanged, we now have $0 \leq |u|, |v| \leq c_s^{-1}$. Known convergent series for the seed correlator inside the unit disk need to be analytically continued outside it, which is in general very challenging. In Fig. 7.5, we show the seed four-point correlator as function of the kinematic variables extended outside the unit circle up to $u = 10$ (which describes the case $c_s = 0.1$). A remarkable feature of the found result (7.5), (7.21) and (7.27) is that it automatically encodes the analytic continuation of the correlator outside the unit disk. However, the convergence rate is much slower than inside the unit disk, especially for a larger mass. Notice the "resonance" around $u \sim 1$ for $\mu = 1$. This is the low-speed collider signal whose most of Part III of the thesis is dedicated.

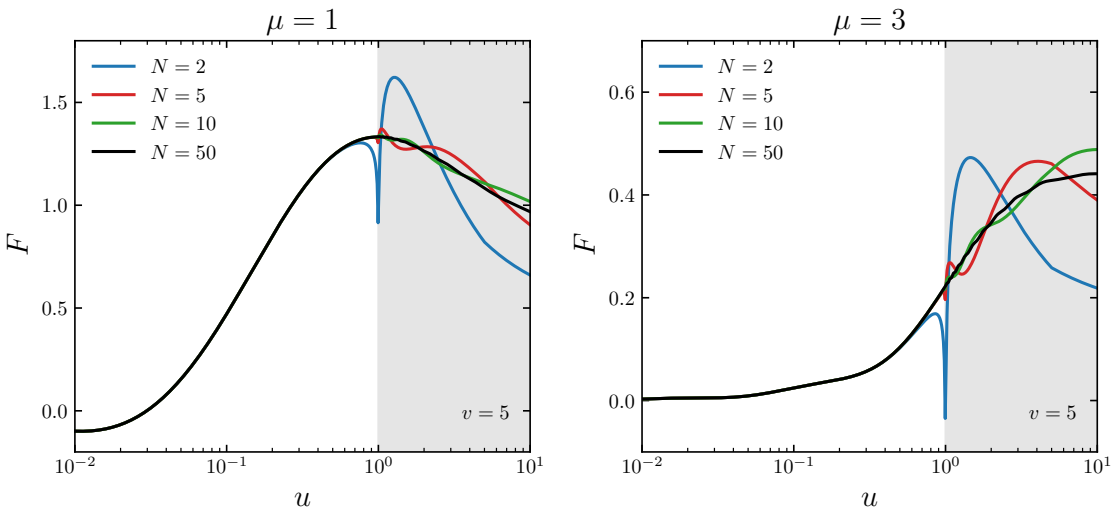


Figure 7.5: The four-point correlation function $F(u, v)$, as function of the dimensionless kinematic variable u with fixed $v = 5$, for $\mu = 1$ (*left panel*) and $\mu = 3$ (*right panel*). We include terms in the series from $n = 1, \ldots, N$. The shaded gray region corresponds to kinematic configurations outside the unit circle which covers the case of a reduced sound speed (here $c_s = 0.1$) for the external field.

7.1.4 Singularities & Analytic Structure

The spectral representation of the four-point function enables straightforward examination of various limits by directly inspecting the spectral integral. A first observation is that removing the dynamical part of the propagating exchanged field—that is, discarding the $i\epsilon$ prescription encoding particle production—, the spectral integral reduces to a contact four-point function generated by the leading bulk interaction φ^4 in a gradient expansion. This simplification is revealed through the generalised

Mehler-Fock transformation (Eq. (14.20.14) of [427])

$$\int_{-\infty}^{+\infty} \mathrm{d}\nu\, \mathcal{N}_\nu\, F^{(3)}(u^{-1},\nu) F^{(3)}(v^{-1},\nu) = \frac{uv}{u+v}\,. \tag{7.29}$$

This identity is analogous to setting the differential operator of the bootstrap equation to unity and therefore recovering the usual source term. Let us now probe the following limits: (i) collapsed limit $u, v \to 0$, i.e. internal soft momentum $K \to 0$ while keeping all external momenta hard, and (ii) the partial-energy pole $u \to -1$ while keeping v fixed. We illustrate the analytic structure of the seed correlator in the energy domain in Fig. 7.6.

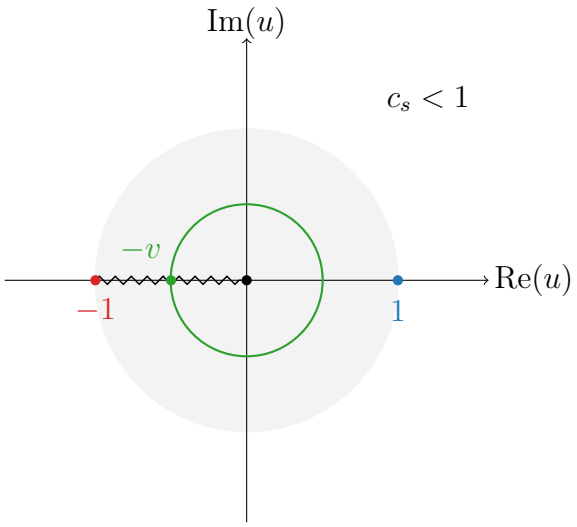


Figure 7.6: Analytic structure of the seed correlator $F(u,v)$ in the complex u plane for a fixed v. The shaded gray region is the unit disc, within which lie both dimensionless momentum ratios. The folded limit ($u \to +1$), the factorisation limit ($u \to -1$), and the flat-space limit ($u \to -v$) are displayed. The branch point at $u = 0$ (and its corresponding branch cut on the negative real axis) is due to non-perturbative particle production and corresponds to the internal soft limit, see Chap. 4. When the external field has a reduced sound speed $c_s \neq 1$, the range for the kinematic variables extends outside the unit disk.

Collapsed limit. In the limit $u, v \to 0$, we use the asymptotic behaviour of the Legendre P function (A.21) for large argument to easily obtain

$$\lim_{u,v\to 0} F_{+-} = \left(\frac{uv}{4}\right)^{\frac{1}{2}+i\mu} \frac{\Gamma(\frac{1}{2}+i\mu)^2\Gamma(-i\mu)^2}{2\pi}\,. \tag{7.30}$$

Taking the limit inside the spectral integral, we obtain

$$\lim_{u,v\to 0} F_{++} = -\frac{1}{2\pi}\left(\frac{uv}{4}\right)^{\frac{1}{2}} \int_{-\infty}^{+\infty} \frac{\mathrm{d}\nu}{(\nu^2-\mu^2)_{i\epsilon}} \left(\frac{uv}{4}\right)^{+i\nu} \Gamma(\tfrac{1}{2}+i\nu)^2\, \frac{\Gamma(-i\nu)}{\Gamma(+i\nu)}\,. \tag{7.31}$$

At large ν, the integrand scales as $\sim e^{i\nu\log(uv/4)}$ (up to a phase) so that the contour is closed in the lower-half complex plane (recall $\log(uv/4) \leq 0$). The usual particle production poles give

$$\lim_{u,v\to 0} F_{++} \supset \frac{i}{2}\left[e^{+\pi\mu}\left(\frac{uv}{4}\right)^{\frac{1}{2}+i\mu}\frac{\Gamma(\frac{1}{2}+i\mu)^2\Gamma(-i\mu)^2}{2\pi} + (\mu \leftrightarrow -\mu)\right] . \tag{7.32}$$

Notice that two infinite towers of poles arise: one from $\Gamma(\frac{1}{2}+i\nu)$ located at $\nu = +i\,(\frac{1}{2}+n)$ that we do not collect as they lie in the upper-half complex plane, and another from $\Gamma(-i\nu)$ located at $\nu = -i\,n$ with $n \geq 0$ integer, which we do collect. By definition, this EFT signal is analytic in both u and v as it admits a series representation. Its $u, v \to 0$ limit can be directly recovered from its full expression (7.27). Eventually, keeping only the terms which are non-analytic in uv as $u, v \to 0$ (and therefore also non-analytic in K), we obtain

$$\lim_{u,v\to 0} F = \left(\frac{uv}{4}\right)^{\frac{1}{2}+i\mu}(1+i\sinh\pi\mu)\frac{\Gamma(\frac{1}{2}+i\mu)^2\Gamma(-i\mu)^2}{2\pi} + \text{c.c.}\,, \tag{7.33}$$

which exactly reproduces the expression found in [262].

Partial-energy pole. At fixed v, let us probe the limit $u \to -1$. The three-point function $F^{(3)}(z,\mu)$ has a branch point at $z = -1$ so we analyse its behaviour directly at the level of the time integral. The limit $E_1 + K \to 0$ probes the early time-limit of the left vertex, so we can take the early-time limit of the Hankel function inside the integral

$$F^{(3)}(u^{-1},\mu) \sim \frac{1}{\sqrt{2}}\lim_{z\to 0}\int_z^{+\infty}\frac{\mathrm{d}x}{x}\,e^{-ix\left(1+u^{-1}\right)} = \frac{1}{\sqrt{2}}\lim_{z\to 0}\mathrm{E}_1\left[\left(1+u^{-1}\right)iz\right] , \tag{7.34}$$

where E_1 is the exponential integral, which has a logarithmic branch. Isolating the leading term, we obtain

$$\lim_{u\to -1} F^{(3)}(u^{-1},\mu) = -\tfrac{1}{\sqrt{2}}\log(1+u)\,. \tag{7.35}$$

The non-time-ordered contributions give

$$\lim_{u\to -1}(F_{+-}+F_{-+}) = -\sqrt{2}\log(1+u)\times F^{(3)}(v^{-1},\mu)\,. \tag{7.36}$$

Similarly, the time-ordered contribution is found to be

$$\lim_{u\to -1} F_{++} = \frac{1}{\sqrt{2}}\log(1+u)\int_{-\infty}^{+\infty}\mathrm{d}\nu\,\mathcal{N}_\nu\,\frac{F^{(3)}(v^{-1},\nu)}{(\nu^2-\mu^2)_{i\epsilon}} = \frac{1}{\sqrt{2}}\log(1+u)\times F^{(3)}(-v^{-1},\mu)\,, \tag{7.37}$$

where we have used (7.8). Summing all contributions, we eventually obtain

$$\lim_{u\to -1} F = -\sqrt{2}\log(1+u)\times\left[F^{(3)}(v^{-1},\mu) - F^{(3)}(-v^{-1},\mu)\right] . \tag{7.38}$$

In this limit, the residue of the partial-energy pole is proportional to the *shifted* three-point function. This behaviour generalises to any exchanged process where the sum of all "energies" entering a vertex vanishes, see e.g. [383, 384, 385]. Similarly, the correlator has a singularity in the flat-space limit $u \to -v$, i.e. $E = E_1 + E_2 \to 0$ or equivalently $\mu \to \infty$, with a coefficient that is related to the flat-space scattering amplitude [127, 375].

7.2 Via Boundary Kinematic Differential Equation

The general strategy of the cosmological bootstrap resides in the ability to find simple-enough differential equations in the external momenta (therefore termed "kinematic differential equations") satisfied by cosmological correlators. These equations follow from the bulk equations of motion (hence locality) for the propagating fields in an exchanged process and encode how the strength of correlations changes when varying the external momenta. Essentially, as a consequence of scale invariance, time evolution can be traded for momentum configurations. Solving these differential equations with the correct physical input (e.g. singularity structure) uniquely fixes consistent inflationary processes.

7.2.1 Cosmological Bootstrap: Light Review

The cosmological bootstrap is a very active area of current research, one that regrettably exceeds the scope of this thesis. Here, we will mostly focus on the practical computational technique to obtain analytical expressions for correlators using the cosmological bootstrap philosophy. We leave some parallel conceptual developments to a subsequent paragraph and mainly focus on illustrating the method with a concrete example.

Literature. The cosmological bootstrap is a recent technique. This strategy has been initiated in [262] where it has been shown that symmetries (e.g. conformal Ward identities for exact de Sitter spacetime) or bulk equations of motion lead to boundary equations for cosmological correlators, whose solutions can be systematically classified. Partial solutions, mostly non-analytic parts contributing to cosmological collider signals, are presented. Extensions to intermediate bosonic spinning fields have also been considered. An exact closed-form solution for the four-point correlation function of conformally coupled scalar field exchanging a massive scalar field in de Sitter has been derived in [198]. This correlator was shown to act as a *seed correlator* to generate other correlators. By acting on the seed with *weight-shifting operators*, conformally coupled external fields can be turned into massless ones, and using *spin-raising operators*, the mediated scalar field can acquire an integer spin. A systematic construction of de Sitter invariant weight-shifting operators working within the embedding-space formalism is presented in [285]. Inflationary three-point correlation functions are recovered from the seed after taking suitable *soft limits* of an external leg. Extension to external massless integer spinning fields, focusing on spin-1 and spin-2, are presented in [428]. Although initially designed for de Sitter invariant correlators with de Sitter covariant interactions, in passing recovering vanilla slow-roll suppressed primordial non-Gaussianities, this technique has been extended to boost-breaking interactions and including a reduced speed of sound for the external scalar fields in [286, 311]. Dealing with IR divergences arising from the exchange of massless fields were treated in [429]. Cosmological correlators arising from the exchange of massive particles carrying a chemical potential, most notably spin-1 fields, have been bootstrapped in [305]. These solutions have been improved in [306] with a suitable change of variables that speeds up the series convergence,

and full solutions for an intermediate massive particle having arbitrary mass, spin, chemical potential, and arbitrary non-derivative or derivative couplings to the external field are presented. Double-exchange diagrams were computed in [430] and solutions which converge in all kinematic configurations were found, which requires solving much more involved differential equations.

Kinematic differential equation. First, let us find a differential equation of the external energies satisfied by the correlator (7.2). The starting point of finding closed-form solutions to this correlator is to realise that the propagators $\mathcal{G}_{\pm\pm}$ satisfy the inhomogeneous differential equations

$$\mathcal{O}_\tau \mathcal{G}_{\pm\pm}(k;\tau,\tau') = \mp iH^2\tau^2\tau'^2\delta(\tau-\tau')\,, \quad \mathcal{O}_\tau \equiv \tau^2\partial_\tau^2 - 2\tau\partial_\tau + k^2\tau^2 + \frac{m^2}{H^2}\,, \tag{7.39}$$

and a similar equation after the replacement $\tau \leftrightarrow \tau'$, while the propagators $\mathcal{G}_{\pm\mp}$ satisfy the same homogenous equations. These are the key equations that are used to derive equations for the correlator and directly follow from the equation of motion of the exchanged field, i.e. these are nothing but the Green's function equations. The differential operator $\mathcal{O}_\tau$ in Eq. (7.39) can be placed in front of the propagators $\mathcal{G}_{\mathsf{ab}}$ in the integrals (7.2) to obtain the identity

$$-\frac{\mathsf{ab}}{2}\int_{-\infty}^{0}\frac{\mathrm{d}\tau'}{\tau'^2}\frac{\mathrm{d}\tau''}{\tau''^2}\,e^{i\mathsf{a}E_1\tau'+i\mathsf{b}E_2\tau''}\mathcal{O}_{\tau'}\mathcal{G}_{\mathsf{ab}}(K;\tau',\tau'') = \frac{\delta_{\mathsf{ab}}}{2E}\,, \tag{7.40}$$

with $E \equiv E_1 + E_2$. Then, the differential operator $\mathcal{O}_\tau$ can be pulled out of the integral after performing integrations by parts and using the relation $\tau\partial_\tau e^{\pm iE\tau} = E\partial_E e^{\pm iE\tau}$. After some algebra and combining the found equations for F_{ab}, we obtain the following equations[4]

$$\left[(E_1^2-K^2)\partial_{E_1}^2 + 2E_1\partial_{E_1} + \frac{m^2}{H^2} - 2\right]F = \frac{1}{E}\,, \quad \text{and} \quad (E_1 \leftrightarrow E_2)\,. \tag{7.41}$$

Time evolution in the bulk of spacetime has been traded for a differential operator in terms of the external energies E_1 and E_2, i.e. the entire dynamics of the exchanged field is reflected in the correlator kinematics. As such, kinematic differential equations follow from locality. When this operator acts on the exchange correlator it produces a contact solution. We can therefore think of this operator as effectively collapsing an internal propagator. Notably, there is no need to know the precise massive field mode function to solve for the correlator as Eq. (7.41) contains the same physical information. In terms of the dimensionless momentum variables u and v, defined in Eq. (7.3), and defining $\hat{F} = sF$, these equations can be turned into

$$\left[\Delta_u + \left(\mu^2 + \frac{1}{4}\right)\right]\hat{F} = \frac{uv}{u+v}\,, \quad \text{and} \quad (u \leftrightarrow v)\,, \tag{7.42}$$

[4]The boundary terms appearing when doing this procedure can be discarded because they represent three-point correlators of the form $\langle\varphi\varphi\sigma\rangle$ which vanish on the boundary if the field σ is massive enough. In the case where σ is massless, these induce additional source terms in (7.41) which reflect secular IR divergences of the correlator, see [429] for more details.

where $\mu^2 \equiv \frac{m^2}{H^2} - \frac{9}{4}$, and where the introduced hypergeometric differential operator reads

$$\Delta_u \equiv u^2\left(1-u^2\right)\partial_u^2 - 2u^3\partial_u\,. \tag{7.43}$$

It was shown in [262] and [198] that Eq. (7.42) follows from the special conformal Ward identity as it has a hidden conformal symmetry. However, the strategy of turning integrals into differential equations is applicable in a wider range of situations, e.g. with broken de Sitter invariance, for three-point correlators, or for different dispersion relations for internal and external fields.

Contact solutions. Before explicitly solving Eq. (7.42), it is instructing to see that is also encodes contact diagrams that emerge after integrating out the exchanged massive field. Indeed, both ordinary differential equations in u and v can be combined into the single homogeneous partial differential equation

$$(\Delta_u - \Delta_v)\hat{F} = 0\,, \tag{7.44}$$

which removes the explicit mass-dependent term and the source term. The simplest solution to this equation is

$$\hat{F}_{c,0} = \frac{uv}{u+v}\,, \tag{7.45}$$

which actually corresponds to a contact four-point correlator emerging from the non-derivative interaction φ^4. Solutions corresponding to higher-order derivative contact interactions can be constructed by recursively applying the operator Δ_u, i.e. $\hat{F}_{c,n} = \Delta_u^n \hat{F}_{c,0}$. It is easy to see that $\hat{F}_{c,n}$ is a solution to Eq. (7.44) as the initial seed is symmetric under u and v.

Exchange solution. The general solution to Eq. (7.42) is the sum of the homogeneous solution $\hat{\mathcal{H}}$ and a particular solution $\hat{\mathcal{S}}$. As (7.42) is a second-order ordinary differential equation with three singular points $u = 0, \pm 1$, $\hat{\mathcal{H}}$ can be expressed in terms of hypergeometric functions, as a linear combination of two independent solutions

$$\hat{\mathcal{H}}(u) = \sum_{\pm} \mathcal{A}_{\pm}\left(\frac{iu}{2\mu}\right)^{\frac{1}{2}\pm i\mu} {}_2F_1\left[\begin{matrix}\frac{1}{4}\pm\frac{i\mu}{2} & \frac{3}{4}\pm\frac{i\mu}{2} \\ 1\pm i\mu\end{matrix}; u^2\right], \tag{7.46}$$

with two free coefficients $\mathcal{A}_{\pm}$. Equivalent solutions are chosen for the differential equation in terms of v. Of course, the precise basis of functions onto which the solution is expanded is a matter of choice, and usually is taken to satisfy specific properties e.g. location of branch cuts or convenient analytic structure, see [311, 305, 306] for different choices of basis. To completely fix the free coefficients, one needs to add two boundary conditions for specific values of u and v, for example at the singular points of the differential equation, that are represented in Fig. 7.6. Let us discuss their physical meaning.

- *Folded limit*: The limit $u \to +1$ corresponds to the case where the external momenta become collinear. As explained in Chap. 3, the found solution should be regular in this limit when considering Bunch-Davies initial conditions, i.e. only selecting positive-frequency modes. However, the solutions have a logarithmic

singularity $\propto \log(1-u)$. Cancelling this singularity can be taking as one constraint to partially fix the coefficients $\mathcal{A}_\pm$.

- *Factorisation limit*: The limit $u \to -1$ corresponds to the situation where the total energy flowing in one vertex vanishes (and similarly for the other vertex in the limit $v \to -1$). The singularity of the correlator is allowed in this limit, and the four-point correlator factorises into a product of three-particle amplitudes. Correctly normalising this limit can also be taken as a physical input to fix the general solution.

- *Internal soft limit*: The limit $u \to 0$ corresponds to the internal momentum becoming soft, and is where non-analytic scaling in u contained in the correlator is dominant. Since in this limit the correlator can be computed exactly, matching the general solution to its form in the soft limit can also be taken as a boundary condition supplementing Eq. (7.42).

- *Flat-space limit*: The limit $u \to -v$ corresponds to the total energy pole where the residue is found to be the corresponding flat-space scattering amplitude [127, 375]. Similarly, fixing the correlator to the known behaviour in this limit also enables us to partially fix the coefficients $\mathcal{A}_\pm$.

Determining which boundary conditions to apply in order to determine the free coefficients is a matter of choice, and various possibilities were considered in the literature, e.g. imposing the absence of folded singularity and the correct factorisation limit in [198, 311], or matching to the soft limit behaviour in [286, 305, 306].

One should also find a particular solution to the inhomogeneous equation (7.42). The general method that has been initiated in [198] is to look for a double series solution. Around $u = 0$, one solution is found to be

$$\hat{\mathcal{S}}_<(u,v) = \sum_{m,n=0}^{\infty} c_{mn}(\mu)\, u^{2m+1}(u/v)^n\,, \tag{7.47}$$

where the coefficients $c_{mn}(\mu)$ have explicit expressions, see [198] for the detailed derivation. For $u > v$, the solution takes the form $\hat{\mathcal{S}}_>(u,v) = \hat{\mathcal{S}}_<(v,u)$. Matching both asymptotic solutions at $u = v$ completely fixes the particular solution $\hat{\mathcal{S}}(u,v)$. The complete closed-form solution for the considered correlator $\hat{F}(u,v) = \hat{\mathcal{H}}(u)\hat{\mathcal{H}}(v) + \hat{\mathcal{S}}(u,v)$ can be found in Eq. (3.36) of [198] and its analytic structure is represented in Fig. 7.6. It is worth mentioning that in some cases the series can be (partially) resummed to known generalised hypergeometric series, see e.g. [306].

Weigh-shifting and spin-raising operators. From the seed four-point correlator, one can obtain a vast class of other correlators. External conformally coupled scalars can be mapped to massless fields by acting on the seed with a set of weight-shifting operators which were first constructed in the study of conformal field theories, see e.g. [431, 432]. These differential operators in the external momenta can be easily found using the relation $(1+ik\tau)e^{-ik\tau} = (1-k\partial_k)e^{-ik\tau}$. Correlators arising from spatial derivative interactions (e.g. $(\partial_i\varphi)^2\sigma$) can also be found by multiplying

the seed with appropriate momentum dependence, and time derivative interactions (when applied to external fields) can all the same be recasted as differential operators in the external momenta acting on the seed. Note that recovering correlators with time derivatives hitting the exchanged field is more intricate. Inflationary three-point correlators, which are of phenomenological interest, can be found by taking suitable soft limits on the external legs. Adding spin to the exchanged field can also be done by acting on the seed correlator with specific spin-raising operators.

Some parallel theoretical developments. The cosmological bootstrap philosophy has spurred significant advancements in analysing cosmological correlators solely through consistency requirements, such as unitarity, locality, and symmetries. These advancements mirror the S-matrix program, where fundamental principles alone provide substantial insights (see [370, 433, 372, 373] for some recent reviews). In what follows, we will provide a brief overview of recent efforts in this direction without delving into extensive details. For a more comprehensive understanding, we direct the reader to the thorough review [374] and the references therein.

- *Singularity structure*: Much as in the case of tree-level scattering amplitudes that e.g. can only have poles when intermediate particles go on-shell, the singularity structure of correlators (and that of the more fundamental wavefunction coefficients from which correlators can be recovered, at least in perturbation theory,[5] see [376]) has been studied in [383, 198, 385, 384, 428, 378, 436]. It has been shown that the analytic structure in some cases enables to fully fix the entire form of certain correlators, whereas in other cases additional information must be supplied.

  Correlator (or wavefunction) singularities manifest at specific locations where a particular combination of external momentum magnitudes vanishes. At the *total energy singularity* $\sum_n k_i \to 0$ (whose order is determined by details about the interactions and fields), the residue is the corresponding flat-space scattering amplitude [127, 375]. Correlators can also have *partial energy singularities* when the sum of momentum magnitudes flowing into a subdiagram vanishes. Similarly, the residues at this poles are related to lower-point flat-space scattering amplitudes. Note that accessing these singularities requires analytically continuing the momenta into the complex plane as these configurations are not physical.

- *Unitarity*: Imposing unitarity as a consistency requirement for correlators results in the *Cosmological Optical Theorem* (COT) [376]. Consequences of the COT are the associated *cutting rules* [378, 379, 380] which relate the discontinuity of a diagram to the sum over all its possible "cuts", see [437] for related work. Generalising unitarity cuts, we have presented cosmological largest-time equations in Chap. 6. The COT is a powerful tool to reconstruct tree-level exchange diagrams by fixing the residues of partial energy singularities in terms

[5] See e.g. [434, 435, 376] for details about computing perturbative wavefunction coefficients, which is similar to diagrammatic rules to compute scattering amplitudes.

of lower-order diagrams, see e.g. [438]. Although the COT is valid to all orders in perturbation theory including any number of loops, it still relies on a perturbative diagrammatic approach. On the other hand, non-perturbative implications of unitarity, such as the Källén-Lehmann representation of the two-point function in de Sitter, are discussed in [381, 199, 439, 423, 382].

- *Locality*: If interactions are products of fields and their derivatives at the same point in spacetime, wavefunction coefficients must satisfy the *Manifestly Local Test* (MLT) [438]. Its derivation is based on a simple property satisfied by the mode function of massless fields in de Sitter. This condition enables to reconstruct some three- and four-point correlators [440]. Notably, a manifestly local theory satisfies the MLT, but satisfying the MLT does not offer a diagnosis of the underlying theory being manifestly local, see e.g. [441].

- *Bootstrapping massless correlators*: Correlators of massless spinning fields were derived from kinematic conformal invariance and current conservation in [428, 442]. The treel-level (hence contact) bispectrum arising from the EFT of inflation (see Chap. 9) was reconstructed using the MLT to all orders in the derivative expansion in [443, 378, 408, 438] (see [440] for the contact trispectrum and [444] for resonant non-Gaussianities). With similar methods, the treel-level graviton bispectrum and trispectrum have been computed in [142] and [146], respectively.

- *Polytopes*: The effort to completely remove the explicit time dependence, therefore focusing solely on kinematics, has driven the exploration of cosmological correlators via co-called polytopes, closely paralleling similar works within the dual space of kinematic configurations for scattering amplitudes. These polytopes are geometric objects whose volume gives the wavefunction coefficients of a conformally coupled scalar, therefore rational [383, 384, 385, 386, 387, 445, 389, 390], see [446] for a review.

- *Structure of kinematic differential equations*: Inspired by the mathematical tools readily available for studying and computing Feynman integrals [447, 448, 449, 450, 451] (see [452, 453] for nice reviews and the references therein), these techniques are gradually being adapted in cosmology to investigate the structure and origin of kinematic differential equations satisfied by cosmological correlators. This approach has been applied to cosmological correlators of conformally coupled scalars in [391, 392, 393, 454, 394, 455, 456, 457], with related aspects discussed in [458, 388, 395, 396, 397, 459, 460]. This active field of research is opening up new connections between cosmological correlators and areas of mathematics such as positive geometry (see e.g. [461]), cohomology (see e.g. [462, 463]), and twisted intersection theory from twisted integrals appearing in dimensional regularisation of loop amplitudes (see e.g. [464, 465, 466, 467, 468, 469]).

7.2.2 Helical Seed Correlator & Boundary Equation

We now turn to computing the seed correlator exchanging a massive field coupled to a helical chemical potential, with the external field having a possible reduced sound speed, using the bootstrap technique.[6] The motivations are two-fold. First, the chemical potential is known to enhance particle production (see Chap. 4) and is the most natural extension (in the EFT sense) to the canonical de Sitter invariant case. Indeed, chemical potential operators are the lowest dimension operators that couple massive spinning fields to the inflaton field and respect the inflaton shift symmetry. The chemical potential strongly breaks de Sitter boosts and spatial parity, leading to a rich phenomenology. Second, a reduced sound speed is known to enhance the amplitude of cosmological correlator non-analytic scalings (also see Chap. 4), and is a natural feature of observed inflationary fluctuations, see Chap. 9. In the end, bootstrapping this correlator is the final milestone for carving out the space of all boost-breaking correlators up to second-order in derivative expansion.

From the free propagating solutions of a massive spin-1 field with a chemical potential that has been properly quantised, see Chap. 5, we define the following boost-breaking helical seed correlator

$$F^{(\lambda)}_{\mathsf{ab}} \equiv -\mathsf{ab}\, K \int_{-\infty^{\mathsf{a}}}^{0} \frac{\mathrm{d}\tau'}{\tau'}\, e^{i\mathsf{a}c_s E_1 \tau'} \int_{-\infty^{\mathsf{b}}}^{0} \frac{\mathrm{d}\tau''}{\tau''}\, e^{i\mathsf{b}c_s E_2 \tau''}\, \mathcal{G}^{\lambda}_{\mathsf{ab}}(K;\tau',\tau'')\,, \tag{7.48}$$

where $\lambda \equiv \pm 1$ denote the two transverse modes, which are affected by the chemical potential κ, see Eq. (5.59). To avoid clutter, we define the dimensionless chemical potential $\tilde{\kappa} \equiv \kappa/H$. We have used the same kinematics as defined in Sec. 7.1. The prefactor K is included to ensure that the integral is dimensionless. Following the strategy outlined in the previous section, the seed correlator satisfies the following boundary differential equations:

$$\begin{aligned} \left[\Delta^{(\lambda)}_{\pm,\tilde{u}} + \left(\mu^2 + \frac{1}{4}\right)\right] F^{(\lambda)}_{\pm\mp} &= 0\,, \\ \left[\Delta^{(\lambda)}_{\pm,\tilde{u}} + \left(\mu^2 + \frac{1}{4}\right)\right] F^{(\lambda)}_{\pm\pm} &= \frac{1}{2}\frac{\tilde{u}\tilde{v}}{\tilde{u}+\tilde{v}-\tilde{u}\tilde{v}}\,, \end{aligned} \tag{7.49}$$

with the differential operator for different helicities defined by

$$\Delta^{(\lambda)}_{\pm,\tilde{u}} \equiv \tilde{u}^2(1-\tilde{u})\partial^2_{\tilde{u}} - (2 \pm i\lambda\tilde{\kappa})\tilde{u}^2\partial_{\tilde{u}}\,, \tag{7.50}$$

and similar equations for $\tilde{u} \leftrightarrow \tilde{v}$, with the newly defined dimensionless kinematic variables

$$\tilde{u} \equiv \frac{2K}{c_s E_1 + K} = \frac{2u}{1+u}\,, \quad \tilde{v} \equiv \frac{2K}{c_s E_2 + K} = \frac{2v}{1+v}\,. \tag{7.51}$$

In the case of a unit sound speed, these two variables are always constrained to be less than unity due to triangle inequality. However, where the sound speed is small, $\tilde{u}, \tilde{v}$ may exceed unity which makes the series solution presented in [305] superficially divergent. The new kinematic variables $(\tilde{u}, \tilde{v})$ turn out to be more convenient than (u, v) for the helical seed correlator (7.48) as the exchanged mode is the transverse part of the massive spinning particle.

[6] I thank Zhehan Qin and Yuhang Zhu for performing this heroic calculation.

Example. Building on the boost-breaking helical seed correlator defined above, we can derive a wide range of correlators involving the exchange of massive spinning fields with non-unit sound speeds and chemical potentials. A particularly interesting example is generated by the interaction

$$S_{\rm int} = \int {\rm d}^3x{\rm d}\tau \left(\frac{a^{-1}}{\Lambda^3}\partial_j\varphi'\partial_i\partial_j\varphi A_i\right) . \tag{7.52}$$

The corresponding four-point exchange correlator can be expressed as

$$\begin{aligned}\langle\varphi_{\boldsymbol{k}_1}\varphi_{\boldsymbol{k}_2}\varphi_{\boldsymbol{k}_3}\varphi_{\boldsymbol{k}_4}\rangle' = \frac{-1}{\Lambda^6}\sum_{\lambda=\pm1}\sum_{\mathsf{a},\mathsf{b}=\pm}\frac{(\boldsymbol{k}_1\cdot\boldsymbol{k}_2)(\boldsymbol{k}_3\cdot\boldsymbol{k}_4)}{16k_1k_2k_3k_4}\frac{\left[\boldsymbol{k}_1\cdot\varepsilon^\lambda(\boldsymbol{s})\right]^*\left[\boldsymbol{k}_3\cdot\varepsilon^\lambda(\boldsymbol{s})\right]}{k_1^2k_3^2s^7}\\ \times(1-k_1\partial_{k_1})(1-k_3\partial_{k_3})[\mathcal{D}^{\mathsf{a}}_{k_{12}}]^3[\mathcal{D}^{\mathsf{b}}_{k_{34}}]^3F^{(\lambda)}_{\mathsf{ab}} + 3\,\text{perms.}\\ + (t\text{-channel}) + (u\text{-channel})\,,\end{aligned} \tag{7.53}$$

where $\boldsymbol{s} = \boldsymbol{k}_1 + \boldsymbol{k}_2$ is the exchanged momentum in the s-channel, and $\mathcal{D}^{\mathsf{a}}_k \equiv is/(\mathsf{a}c_s)\partial_k$. The polarisation factor can be further explicitly written as

$$[\boldsymbol{k}_1\cdot\varepsilon^\lambda(\boldsymbol{s})]^*[\boldsymbol{k}_3\cdot\varepsilon^{(\lambda)}(\boldsymbol{s})] = \frac{1}{2}\left[\boldsymbol{k}_1\cdot\boldsymbol{k}_3 - (\boldsymbol{k}_1\cdot\hat{\boldsymbol{s}})(\boldsymbol{k}_3\cdot\hat{\boldsymbol{s}}) + i\lambda\hat{\boldsymbol{s}}\cdot(\boldsymbol{k}_1\times\boldsymbol{k}_3)\right] . \tag{7.54}$$

It is clear from the expression that, although the interaction is parity-conserving, the presence of the chemical potential causes the four-point correlator to contain both parity-even (real part) and parity-odd (imaginary part) components.

7.2.3 Boost-Breaking Helical Massive Exchange Solution

We now compute the helical seed correlator and apply analytic continuation to extend the region of validity of the solutions, thereby encompassing the domains of our interest.

Homogeneous solution. The homogeneous equation takes the same form as in the unit sound speed case. Here, we will adhere to the derivation provided in previous works and present only the key results relevant to our discussion, readers interested in details are encouraged to read [305]. There are two differential operators that are related to each other through the helicity reflection condition:

$$\Delta^{(\lambda)}_{-,\tilde{u}} = \Delta^{(-\lambda)}_{+,\tilde{u}} . \tag{7.55}$$

Since the equation is second order, each differential operator possesses two linearly independent solutions such that

$$\left[\Delta^{(\lambda)}_{\pm,\tilde{u}} + \left(\mu^2+\frac{1}{4}\right)\right]\mathcal{H}_\pm(\tilde{u}) = 0\,. \tag{7.56}$$

The homogeneous solutions are explicitly given by

$$\mathcal{H}_\pm(\tilde{u}) = \tilde{u}^{\frac{1}{2}\pm i\mu}\,{}_2\bar{F}_1\left[\begin{matrix}\frac{1}{2}\pm i\mu & \frac{1}{2}+i\lambda\tilde{\kappa}\pm i\mu\\ 1\pm 2i\mu\end{matrix};\tilde{u}\right] . \tag{7.57}$$

where ${}_2\bar{F}_1\left[\begin{smallmatrix} a & b \\ & c \end{smallmatrix}; z\right] \equiv \frac{\Gamma(a)\Gamma(b)}{\Gamma(c)} {}_2F_1\left[\begin{smallmatrix} a & b \\ & c \end{smallmatrix}; z\right]$ is the dressed hypergeometric function. The hypergeometric functions exhibit a branch cut along $\tilde{u} \geq 1$. In the case where $c_s = 1$, $\tilde{u}$ remains strictly less than unity, ensuring that the branch point (specifically, the folded pole singularity) is never encountered in the physical region. However, when $c_s < 1$, the variable $\tilde{u}$ can exceed unity in certain kinematic regions, thereby crossing the branch point. Since the evaluation of the hypergeometric function ${}_2F_1$ for $\tilde{u} > 1$ is well-established, the homogeneous solution remains valid even in this regime. In other words, the homogeneous solution can be smoothly continued from the unit sound speed case to the small sound speed case, owing to the known analytic continuation properties of hypergeometric series. For the factorised contribution, the general solution is then expressed as

$$\begin{aligned} F^{(\lambda)}_{+-}(\tilde{u},\tilde{v}) = {} & \mathcal{A}^{+-}_{++}\mathcal{H}_+(\tilde{u})\mathcal{H}^*_-(\tilde{v}) + \mathcal{A}^{+-}_{+-}\mathcal{H}_+(\tilde{u})\mathcal{H}^*_+(\tilde{v}) \\ & + \mathcal{A}^{+-}_{-+}\mathcal{H}_-(\tilde{u})\mathcal{H}^*_-(\tilde{v}) + \mathcal{A}^{+-}_{--}\mathcal{H}_-(\tilde{u})\mathcal{H}^*_+(\tilde{v})\,, \end{aligned} \tag{7.58}$$

and $\mathcal{A}$ represents some coefficients that will be determined through the boundary conditions later. We naturally have $F^{(\lambda)}_{-+} = F^{(\lambda)*}_{+-}$. Also for the nested contribution, we can express it as

$$\begin{aligned} F^{(\lambda)}_{++}(\tilde{u},\tilde{v}) = {} & \mathcal{A}^{++}_{++}\mathcal{H}_+(\tilde{u})\mathcal{H}_+(\tilde{v}) + \mathcal{A}^{++}_{+-}\mathcal{H}_+(\tilde{u})\mathcal{H}_-(\tilde{v}) \\ & + \mathcal{A}^{++}_{-+}\mathcal{H}_-(\tilde{u})\mathcal{H}_+(\tilde{v}) + \mathcal{A}^{++}_{--}\mathcal{H}_-(\tilde{u})\mathcal{H}_-(\tilde{v}) \\ & + \mathcal{S}^{(\lambda)}_{\pm}(\tilde{u},\tilde{v})\,, \end{aligned} \tag{7.59}$$

where $\mathcal{S}^{(\lambda)}_{\pm}$ is the particular solution for the inhomogeneous differential equation which we solve now.

Particular solution. To find the particular solution, we assume $\tilde{u} < \tilde{v}$ without loss of generality. The result for the other region is obtained by swapping the relevant variables. Note that this procedure is highly non-trivial for higher-point correlators as one needs to analytically continue correlators to other kinematic regions, picking up a homogeneous solution along the way. In this discussion, we focus on $\mathcal{S}_+$ as an illustrative example, while the corresponding result for $\mathcal{S}_-$ can be derived straightforwardly using the conjugate relation $\mathcal{S}_- = [\mathcal{S}_+]^*$. The source term in Eq. (7.49) can be systematically expanded as follows

$$\frac{\tilde{u}\tilde{v}}{\tilde{u}+\tilde{v}-\tilde{u}\tilde{v}} = \sum_{n=0}^{\infty} \tilde{u}^{n+1}\left(1-\frac{1}{\tilde{v}}\right)^n = \tilde{u}\sum_{n=0}^{\infty}(-1)^n\left(\frac{\tilde{u}}{\tilde{v}}\right)^n(1-\tilde{v})^n\,. \tag{7.60}$$

We propose the following ansatz for the particular solution, assuming a functional form that resembles the structure of the source:

$$\mathcal{S}^{(\lambda)}_{+} = \sum_{m,n=0}^{\infty} \mathcal{A}^{(\lambda)}_{m,n}\,(-1)^n\,\tilde{u}^{m+1}\left(\frac{\tilde{u}}{\tilde{v}}\right)^n(1-\tilde{v})^n\,. \tag{7.61}$$

Substituting the proposed ansatz into the differential equation, we obtain a recurrence relation that governs the coefficients

$$\begin{aligned}\mathcal{A}^{(\lambda)}_{m+1,n} &= \frac{(m+n+1)(m+n+1+i\lambda\tilde{\kappa})}{(m+n+1+\frac{1}{2})^2+\mu^2}\,\mathcal{A}^{(\lambda)}_{m,n}\,,\\ \mathcal{A}^{(\lambda)}_{0,n} &= \frac{1}{2}\frac{1}{(n+\frac{1}{2})^2+\mu^2}\,.\end{aligned} \tag{7.62}$$

Using this recurrence relation, the coefficients can be iteratively solved. Explicitly, the coefficients are given by

$$\mathcal{A}^{(\lambda)}_{m,n} = \frac{1}{2}\frac{(n+1)_m(n+1+i\lambda\tilde{\kappa})_m}{(n+\frac{1}{2}+i\mu)_{m+1}(n+\frac{1}{2}-i\mu)_{m+1}}\,, \tag{7.63}$$

where $(a)_m \equiv \Gamma(a+n)/\Gamma(a)$ denotes the Pochhammer symbol. This series expansion is well-behaved only within the region $\tilde{u} < 1$, indicating that the solution derived here appears to be valid exclusively for the case of unit sound speed. In the kinematic region where $\tilde{u} > 1$, the series fails to converge, suggesting that the ansatz employed here is unsuitable for this range. To address this, it seems that modifying the ansatz similarly to that adopted in e.g. [311] (with negative powers of $\tilde{u}$) should be used for $\tilde{u} > 1$. However, the current series admits a resummation, which facilitates its analytic continuation to the $\tilde{u} > 1$ regions directly. To illustrate this process, we observe that the m-layer of the series can be resummed, and the particular solution becomes

$$\mathcal{S}^{(\lambda)}_{\pm} = \frac{\tilde{u}}{2}\sum_{n=0}^{\infty}\frac{(-1)^n}{(n+\frac{1}{2})^2+\mu^2}\left(\frac{\tilde{u}}{\tilde{v}}\right)^n(1-\tilde{v})^n\,{}_3F_2\left[\begin{matrix}1 & n+1 & n+1\pm i\lambda\tilde{\kappa}\\ \frac{3}{2}+n-i\mu & \frac{3}{2}+n+i\mu\end{matrix};\tilde{u}\right]. \tag{7.64}$$

Note the similarity with the series found directly from the spectral representation (7.27). Here, we have summed the series with respect to $\tilde{u}$, which is then packaged into a generalised hypergeometric function. This allows us to evaluate the series even for $\tilde{u} > 1$. Given that we have assumed $\tilde{u} < \tilde{v}$ and by definition $0 < \tilde{v} < 2$, it can be explicitly verified that this resummed single-layer series converges throughout the entire kinematic region under consideration. One aspect we have not yet addressed is the branch cut of the hypergeometric series, where $\tilde{u} > 1$ along the real axis. Taking $F^{(\lambda)}_{++}$ as an example, the appropriate branch involves selecting the lower-half plane prescription, specifically $\tilde{u} = \tilde{u} - i\epsilon$ with the infinitesimal $\epsilon > 0$ (vice versa, for $F^{(\lambda)}_{--}$ the appropriate choice, consistent with the complex conjugate relation, is to take $\tilde{u} = \tilde{u} + i\epsilon$). This branch choice can be justified by analysing the corresponding bulk integral, which will be discussed in detail later.

Boundary condition. We have nearly completed the calculation of the analytical expressions, except for the unfixed coefficients $\mathcal{A}$. Several approaches can be used to impose the boundary conditions, such as requiring the absence of spurious poles or considering the factorised limit as discussed previously. For simplicity, here the coefficients are directly determined by matching the expression in the soft limit $\tilde{u}, \tilde{v} \to 0$, where the bulk integral can be evaluated easily through the IR expansion

of the integrand or using the Mellin-Barnes transformation. The final expressions are found to be

$$\begin{aligned}
\mathcal{A}^{+-}_{++} &= -\mathcal{A}^{+-}_{+-} = -\mathcal{A}^{+-}_{-+} = \mathcal{A}^{+-}_{--} = \frac{-e^{-\pi\lambda\tilde{\kappa}}}{4\sinh^2(2\pi\mu)}\left[\cosh(2\pi\tilde{\kappa})+\cosh(2\pi\mu)\right], \\
\mathcal{A}^{++}_{++} &= -\mathcal{A}^{++}_{+-} = \frac{-i\pi e^{-\pi(\lambda\tilde{\kappa}-\mu)}\cosh[\pi(\mu+\lambda\tilde{\kappa})]}{2\sinh^2(2\pi\mu)\Gamma(\frac{1}{2}+i\lambda\tilde{\kappa}+i\mu)\Gamma(\frac{1}{2}+i\lambda\tilde{\kappa}-i\mu)}, \\
\mathcal{A}^{++}_{--} &= -\mathcal{A}^{++}_{-+} = \frac{-i\pi e^{-\pi(\lambda\tilde{\kappa}+\mu)}\cosh[\pi(-\mu+\lambda\tilde{\kappa})]}{2\sinh^2(2\pi\mu)\Gamma(\frac{1}{2}+i\lambda\tilde{\kappa}+i\mu)\Gamma(\frac{1}{2}+i\lambda\tilde{\kappa}-i\mu)}.
\end{aligned} \tag{7.65}$$

This concludes the derivation of the helical seed correlator involving two boost-breaking effects: (i) the sound speed, and (ii) the chemical potential. These results are valid for all physical kinematic regions and exhibit rapid convergence. In Fig. 7.7, we show the boost-breaking helical seed correlator at a fixed mass μ but varying the chemical potential $\tilde{\kappa}$ and for both helicities $\lambda = \pm 1$. We note that the chemical potential essentially modifies the signal contribution, boosting the amplitude and changing the phase of the cosmological collider signal, but barely affects the background signal. Also, note that the signal coming from one transverse helicity ($\lambda = -1$) is enhanced compared to the other one.

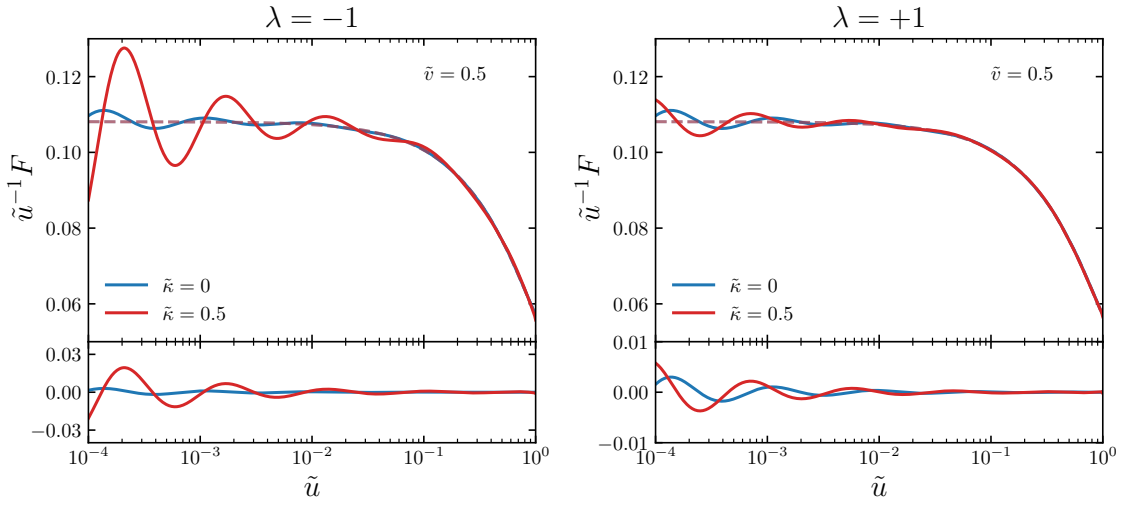


Figure 7.7: The (rescaled) boost-breaking helical seed correlator $F(\tilde{u},\tilde{v})$, as function of the dimensionless kinematic variable $\tilde{u}$ with fixed $\tilde{v} = 0.5$ and at fixed mass $\mu = 3$ for both $\tilde{\kappa} = 0$ and $\tilde{\kappa} = 0.5$, for $\lambda = -1$ (*left panel*) and $\lambda = +1$ (*right panel*). We include terms in the series from $n = 1, \ldots, 5$. In the upper panel, we show both the full correlator (*solid line*) and the background contribution (*dashed line*). In the lower panel, we only show the signal contribution. The kinematic variables being inside the unit circle, this case corresponds to a unit sound speed $c_s = 1$.

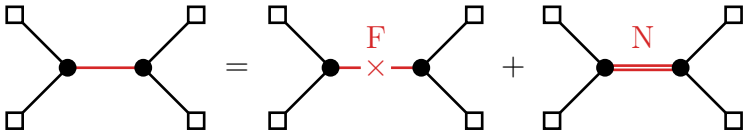
7.2.4 Discussion

Let us make a few remarks concerning the full solution for the boost-breaking helical massive exchange correlator.

- *Bulk cutting rules revisited*: We have introduced bulk cutting rules for extracting non-analytic processes in Chap. 4, with a concrete and simple application in App. A. To briefly revisit these cutting rules, as an illustrative example, consider the integral $F_{++}^{(\lambda)}$. First, assuming that $E_1 > E_2$, by manipulating one of the Heaviside theta functions, $\Theta(\tau' - \tau'') = 1 - \Theta(\tau'' - \tau')$, the bulk propagator can be decomposed into two distinct terms

$$\mathcal{G}_{++}^{\lambda}(K;\tau',\tau'') = \mathcal{G}_{-+}^{\lambda}(K;\tau',\tau'') + \left[\mathcal{G}_{+-}^{\lambda}(K;\tau'',\tau') - \mathcal{G}_{-+}^{\lambda}(K;\tau',\tau'')\right]\Theta(\tau''-\tau')\,, \tag{7.66}$$

where the first term is factorised in time, while the second term is still nested. Consequently, the integral $F_{++}^{(\lambda)}$ can be expressed as the sum of two components, $F_{++}^{(\lambda)} = F_{\rm F}^{(\lambda)} + F_{\rm N}^{(\lambda)}$, that can be schematically represented as



(7.67)

Here, the first term on the right-hand side of (7.66) is the *factorised* part, which is straightforward to evaluate due to the time-integral factorisation property. The second term is *nested*. The remarkable aspect of the bulk cutting rule is that the purest signatures are often the simplest. These oscillatory cosmological collider signals, which include both local and non-local types, entirely stem from the factorised piece, while the nested term contributes to the background, which is analytic in the momentum ratio.

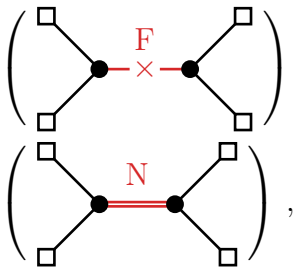
This cutting rule works perfectly in the case of a unit sound speed, even when the chemical potential effects are taken into account. However, it seems to break down in certain kinematical regions when we have a small sound speed. To illustrate this more concretely, let us focus on the integral associated with the factorised part, which contains terms of the form

$$F_{\rm F}^{(\lambda)} \supset \int_{-\infty^+}^{0} {\rm d}\tau\, e^{ic_sE_1\tau}\sigma_K^{(\lambda)}(\tau) \sim \int_{-\infty^+}^{0} {\rm d}\tau\, e^{i(c_sE_1-K)\tau}\,, \tag{7.68}$$

where we have evaluated the UV behaviour of the massive mode function $\tau \to -\infty$. When $c_s = 1$, although the integral contains a spurious folded pole, which should be cancelled by the integral $F_{\rm N}^{(\lambda)}$, the overall integral remains convergent in the physical kinematic regions due to the triangle inequality $E_1 > K$. However, a small sound speed changes the situation significantly, as in certain kinematic regions, c_sE_1 can become smaller than K, leading to a divergence when $\tau \to -\infty^+$. What we are doing here is actually the analytic continuation of the bulk cutting rule. Since the term $F_{\rm F}^{(\lambda)}$ is factorised, it must satisfy the homogeneous boundary equations and contains all the information about the cosmological collider signals. In contrast, $F_{\rm N}^{(\lambda)}$ satisfies the inhomogeneous part, as the Heaviside step function generates the source term in the bootstrap differential equation. For regions where $c_sE_1 > K$, (7.59) and (7.67) are in one-to-one correspondence, as all terms are convergent. When $c_sE_1 < K$, the resummation of the series allows us to analytically continue

each term in (7.59) for a small sound speed, ensuring convergence. This is why we should choose the branch $\tilde{u} = \tilde{u} - i\epsilon$ (or equivalently, $K = K - i\epsilon$, $E_i = E_i - i\epsilon$) in the analytical expression when $\tilde{u} > 1$. From the bulk time integral, this corresponds to deforming the contour such that in the UV it behaves as $\sim e^{(K-c_s E_1)\tau}$ when $\tau \to -\infty$, then it is convergent for cases with a small sound speed. In other words, this process generalises the bulk cutting rule by analytically continuing each term in the bulk time integrals, which can be represented schematically as:

$$\mathcal{A}\cdot\mathcal{H}\cdot\mathcal{H} = \text{P.V.}\left(\quad\right), \qquad \mathcal{S} = \text{P.V.}\left(\quad\right), \tag{7.69}$$



where the operation P.V. represents extracting the finite part (Cauchy principal value) of the corresponding bulk integral.

- *Parity-odd correlator factorisation*: Exchanging massive spin-1 fields with a chemical potential can give rise to a large parity-odd four-point correlator. We refer the reader to Chap. 11 for more details. Remarkably, parity-odd parts of correlators must factorise, and the total energy singularity ($E \equiv \sum_i E_i \to 0$) should be absent at tree-level [112]. This result was derived from the properties of bulk-to-bulk propagators under a set of mild assumptions, which are applicable to spin-1 fields with a chemical potential and sound speed. With the complete analytical expressions now available, we are in a position to perform an explicit consistency check. Consider the example previously discussed, with the interaction (7.52), the parity-odd component is proportional to

$$\begin{aligned}\langle\varphi_{\boldsymbol{k}_1}\varphi_{\boldsymbol{k}_2}\varphi_{\boldsymbol{k}_3}\varphi_{\boldsymbol{k}_4}\rangle'_{\text{PO}} \propto\ & i\hat{\boldsymbol{s}}\cdot(\boldsymbol{k}_1\times k_3)(1-k_1\partial_{k_1})(1-k_3\partial_{k_3}) \\ & \times\sum_{\substack{\mathsf{a},\mathsf{b}=\pm\\ \lambda=\pm1}}\lambda\,[\mathcal{D}^{\mathsf{a}}_{k_{12}}]^3[\mathcal{D}^{\mathsf{b}}_{k_{34}}]^3 F^{(\lambda)}_{\mathsf{ab}}\,.\end{aligned} \tag{7.70}$$

Given that the parity-odd part is purely imaginary, we have omitted certain real prefactors for the sake of simplicity. The homogeneous solution is already factorised and does not exhibit any E singularity. The theorem asserts that the contribution from the particular solution to the parity-odd correlator must vanish, as it originates from the fully connected part of the bulk integral, and also contains the total-energy singularity. To verify this, we note that the particular solution (7.64) satisfies the following property

$$\mathcal{S}^{(\lambda)}_{+} = [\mathcal{S}^{(\lambda)}_{-}]^* = \mathcal{S}^{(-\lambda)}_{-}\,. \tag{7.71}$$

Then, the summation over helicity gives

$$\sum_{\substack{\mathsf{a}=\pm\\ \lambda=\pm1}}\lambda\,\mathcal{S}^{(\lambda)}_{\mathsf{a}} = \mathcal{S}^{(+1)}_{+} + \mathcal{S}^{(+1)}_{-} - \mathcal{S}^{(-1)}_{+} - \mathcal{S}^{(-1)}_{-} = 0\,, \tag{7.72}$$

which is indeed consistent with the parity-odd factorisation theorem.

- *Comparison with the cosmological low-speed collider result*: There is an alternative approach to obtaining the convergent solution besides the continuation method employed here. For example, in previous studies involving low sound speed without considering chemical potential, the ansatz for the particular solution was formulated as $\sum_{m,n=0}^{\infty}(a_{mn}+b_{mn}\log(u))\,u^{-m}\,(u/v)^n$ when $u<v$ [311]. The inverse power of u here ensures the convergence of series when $v>u>1$. We can adopt a modified ansatz similar to those used in previous studies. However, deriving and solving the recurrence relations for the coefficients proves to be non-trivial. This raises the question: how are these two different methods connected? To facilitate a comparison between both methods, we set the chemical potential to zero. In this case, the solutions for the particular case with unit sound speed reads

$$\mathcal{S}_+=\sum_{m,n=0}^{\infty}\frac{(-1)^n(n+1)_{2m}}{2^{2m+1}(\frac{n}{2}+\frac{1}{4}+\frac{i\mu}{2})_{m+1}(\frac{n}{2}+\frac{1}{4}-\frac{i\mu}{2})_{m+1}}u^{2m+1}\left(\frac{u}{v}\right)^n. \tag{7.73}$$

This series is convergent for $u<1$, but we can still perform the resummation along the m-direction. After resummation, the series becomes

$$\mathcal{S}_+=2u\sum_{n=0}^{\infty}\frac{(-1)^n}{(n+\frac{1}{2})^2+\mu^2}\left(\frac{u}{v}\right)^n{}_3F_2\left[\begin{matrix}1 & \frac{n+1}{2} & \frac{n}{2}+1\\ \frac{5}{4}+\frac{n}{2}-\frac{i\mu}{2} & \frac{5}{4}+\frac{n}{2}+\frac{i\mu}{2}\end{matrix};u^2\right]. \tag{7.74}$$

The two layers of infinite series are now reorganised into a single series involving a hypergeometric function. It can be explicitly checked that the result remains valid even for $c_s<1$. To connect to the results derived in [311], one can expand the hypergeometric function around $u\to\infty$. This reveals a structure consistent with $[a+b\log(u)]u^{-m}$, where the coefficients involve harmonic numbers. In summary, we started here with a series ansatz expansion around $u\to 0$ but after summation, the result converges at the significantly larger radius. The previously obtained result corresponds to the $u\to\infty$ expansion of this expression. The correspondence is quite natural, as the ansatz $[a+b\log(u)]u^{-m}$ was originally formulated based on an analysis of the bootstrap equations in the UV limit ($u,v\to\infty$).

8

Classifying Non-Analyticities

Cosmological correlators exhibit a far greater complexity than their flat-space counterparts, such as tree-level scattering amplitudes. As discussed in Chap. 7, while the latter possess a simple analytic structure with well-defined factorisation properties, cosmological correlators develop branch cuts and are expressed through complicated mathematical expressions, often involving hypergeometric functions and infinite series. Despite their generality and exactness, these analytical solutions are nevertheless complicated and offer little physical insight. It is striking that even the simplest processes require highly advanced techniques to be computed. More concerning, however, is that the physical mechanisms underlying these correlators remain obscured, and intuitive explanations for their distinct behaviours across different kinematic regimes are difficult to discern. To make manifest the bulk evolution physics, we actually need *approximate* solutions instead of exact ones.

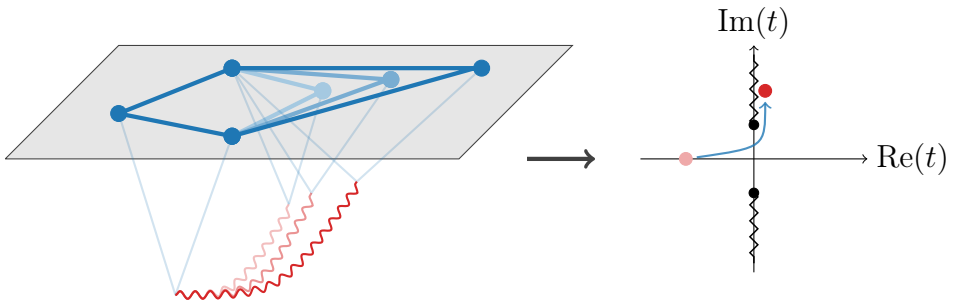


Figure 8.1: Schematic representation of the saddle point method to classify cosmological collider signals and obtain approximate solutions for correlators. The production and decay of massive particles in the bulk of spacetime are in one-to-one correspondence with resonant times (saddle points) that move in the complex time plane according to external kinematics.

In this chapter, we introduce the saddle point method supplemented with the WKB approximation, as a powerful tool to classify and gain physical insight into various cosmological collider signals.[1] This approach relies solely on analysing the location of saddle points in the complex time plane, providing a natural explanation for the behaviour of these signals by tracking the motion of these saddles driven by external kinematics. By evaluating the time integrals using the saddle point method, we obtain approximate solutions for a range of correlators, expressed entirely in terms of elementary functions. These simplified expressions are not only easy to implement but also offer practical templates for observational searches.

8.1 Extracting & Approximating Cosmological Collider Signals

We first outline the general strategy to classify non-analyticities of correlators and approximating cosmological collider signals. Without loss of generality, we will work with the exchange four-point seed correlators F, whose kinematics is described by external energies $E_{1,2}$ and the internal momentum K. We refer to Chap. 7 for more details. In full generality, we include a reduced speed of sound for external legs and a helical chemical potential for the exchanged massive particle. These boost-breaking effects will be turned on in turn lately.

- *Apply bulk cutting rules*: As discussed in Chap. 4, non-analytic scalings of cosmological correlators—and therefore cosmological collider signals—come from factorised contributions. We limit ourselves to the kinematic region $E_1 > E_2$ and focus on the factorised contribution

$$F_{\rm F} = \int_{-\infty^+}^{0} \mathrm{d}\tau' \, e^{ic_s E_1 \tau'} \int_{-\infty^+}^{0} \mathrm{d}\tau'' \, e^{ic_s E_2 \tau''} \, \mathcal{G}_{-+}(K;\tau',\tau'') \,. \tag{8.1}$$

  Here, we have removed powers of conformal time. We stress that this choice simplifies our technical discussion later on, but not at the cost of generality nor physicality. Note that we have also dropped overall kinematic factors to make the integral dimensionless. These prefactors can easily be restored at the end. Factorising the Wightman function $\mathcal{G}_{-+} \equiv \mathcal{G}_{>}$ into mode functions, we can separate the integral into two parts $F_{\rm F} = F_L^{(3)} \times \tilde{F}_R^{(3)}$ with

$$F_L^{(3)} = \int_{-\infty^+}^{0} \mathrm{d}\tau' \, e^{ic_s E_1 \tau'} \sigma_K(\tau') \,, \quad \tilde{F}_R^{(3)} = \int_{-\infty^+}^{0} \mathrm{d}\tau'' \, e^{ic_s E_2 \tau''} \sigma_K^*(\tau'') \,, \tag{8.2}$$

  where σ_K is the mode function of the exchanged field. In most of the cases, these integrals can be easily computed and result in hypergeometric functions.

- *Apply the WKB approximation*: After canonically normalising the massive field $\sigma \to \sigma/a(\tau)$, the mode function satisfies an equation of motion of the form

$$\sigma_K'' + \omega_K^2(\tau)\sigma_K = 0 \,, \tag{8.3}$$

[1] I thank Xi Tong for brilliantly designing this method and carrying out these calculations.

where ω is an effective frequency for the K-mode that is theory-dependent. Instead of directly solving the exact mode function, we write the solution as a time-dependent superposition of positive- and negative-frequency parts, both solved via the WKB approximation

$$\sigma_K(\tau) \approx \alpha_K(\tau) f_K(\tau) + \beta_K(\tau) f_K^*(\tau)\,, \quad \text{with} \quad f_K(\tau) \equiv \frac{e^{-i\int_{\tau_0}^{\tau} \mathrm{d}\tau' \omega_K(\tau')}}{\sqrt{2\omega_K(\tau)}}\,, \tag{8.4}$$

where τ_0 is an arbitrary reference (conformal) time. The integration contour follows the negative real axis with a slight shift towards the positive imaginary direction due to the $i\epsilon$ prescription. The time-dependent Bogolyubov coefficients are approximately given by

$$\alpha_K(\tau) \approx 1\,, \quad \beta_K(\tau) \approx \frac{i}{2}[1 + \mathrm{erf}(\Gamma_K(\tau))] e^{-F_K(\tau_0)}\,, \tag{8.5}$$

where

$$\Gamma_K(\tau) = \frac{-\mathrm{Im}(F_K(\tau))}{\sqrt{2\mathrm{Re}(F_K(\tau))}}\,, \quad F_K(\tau) = -2i\int_{\tau_c}^{\tau} \mathrm{d}\tau' \omega_K(\tau')\,, \tag{8.6}$$

with τ_c being the turning points such that $\omega_K^2(\tau_c) = 0$ with $\mathrm{Im}(\tau_c) < 0$. In the early-time limit $\tau \to -\infty$, $\omega > 0$ and the Stokes multiplier $\frac{1}{2}[1 + \mathrm{erf}(\Gamma_K(\tau))]$ asymptotes to zero, thereby recovering the Bunch-Davies initial condition. However, it asymptotes to unity in the late-time limit, indicating the emergence of the negative-frequency mode signalling spontaneous particle production. More details are presented in Chap. 4. The exact moment of particle production can be read from the Stokes line crossing time $\tau = \tau_*$ where $\mathrm{Im}(F_K(\tau_*)) = 0$ and $\frac{1}{2}[1 + \mathrm{erf}(\Gamma_K(\tau_*))] = 1/2$.

- *Use the saddle point method to find resonant times*: Plugging the WKB approximation (8.4) in the bulk time integrals $F_L^{(3)}$ and $\tilde{F}_R^{(3)}$, all integrals are of the form

$$\int_{\mathcal{C}} \mathrm{d}\tau\, g(\tau) e^{\mu f(\tau)}\,, \tag{8.7}$$

where g and f are theory-dependent functions of the complex conformal time τ, and μ denotes the dimensionless mass parameter of the exchanged particle. Here, $\mathcal{C}$ denotes the specific contour on the complex plane that encodes the $i\epsilon$ prescription. Integrals of this type are known to be solvable as an asymptotic expansion in μ^{-1} via the saddle-point method, also capturing non-perturbative effects. We give details about this method in App. B. Solving for the saddle point $\tau_\bullet$ such that $f'(\tau_\bullet) = 0$, the integration contour $\mathcal{C}$ is continuously deformed to a new contour $\mathcal{C}'$ that passes through the saddle point in the steepest direction. Note that whether or not $\mathcal{C}'$ has to pass exactly along the steepest descent direction is unimportant, since the integrand is often analytic around $\tau_\bullet$ and small deformations are allowed. Expanding the integrand around the saddle, the Gaussian integral can be finished, leading to

$$\int_{\mathcal{C}} \mathrm{d}\tau\, g(\tau) e^{\mu f(\tau)} \approx g(\tau_\bullet) e^{\mu f(\tau_\bullet)} \left[\sqrt{\frac{-2\pi}{\mu f''(\tau_\bullet)}} + \dots\right]\,. \tag{8.8}$$

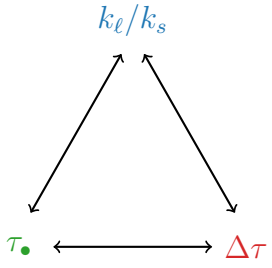
Note that higher-order terms are small due to the small variance of the Gaussian. These terms scale as μ^{-1}. Therefore, at leading order, the resulting integral is fully controlled by the location of the saddle, which is a function of the external kinematics, i.e. $\tau_\bullet = \tau_\bullet(E_{1,2}, K)$.

- *Classify cosmological collider signals*: To relate the mathematical notion of saddle points to the physical bulk evolution, we note that massive fields are constantly produced and decay. Due to the lack of time-translational symmetry and hence the non-conservation of energy, particles can be produced either in pairs from the propagator, or in singlet from the interaction vertices, before decaying. These production and decay events happen in the form of resonant transitions or saddles. The time spent by the particle between these saddles is thus recorded in the resultant cosmological collider signals. One can also estimate the size of the cosmological signal by inspecting the location of the saddle. The rule of thumb is

$$\begin{aligned} &\text{Saddle points lying in the physical region i.e. } \tau_\bullet \in \mathbb{R}_- \\ &\to \mu^{-\#} \text{ suppression}\,, \\ &\text{---} \\ &\text{Saddle points lying in the unphysical region i.e. } \tau_\bullet \notin \mathbb{R}_- \\ &\to e^{-\#\mu} \text{ suppression}\,, \end{aligned} \tag{8.9}$$

  where # denotes an order-one positive number. One can intuitively understand this as an "on-shell" versus "off-shell" effect. In conclusion, by studying the kinematic dependence of the saddle point $\tau_\bullet = \tau_\bullet(E_{1,2}, K)$, we can classify cosmological collider signals into different categories with distinct shapes and sizes.

Through this procedure, we have learned a beautiful correspondence between the observational, the mathematical, and the physical aspect of cosmological collider signals: (i) the momentum ratio k_ℓ/k_s, where k_ℓ is a long-wavelength mode and k_s is a short-wavelength one, reflects the kinematic control (more precisely the internal soft limit) of the boundary cosmological correlator on the observational side, (ii) the location of the complex saddle point $\tau_\bullet$ dictates the dominant sources of the time integrals on the mathematical side, and (iii) the lifetime of the massive particle $\Delta\tau$ traces the origin of the cosmological collider signal on the physical side. Modifying any one of the three variables is equivalent to changing the other two, as represented in the picture below.



8.2 Application to Tree-Level Exchange Correlators

We now apply the strategy previously outlined to concrete examples with increasing complexity.

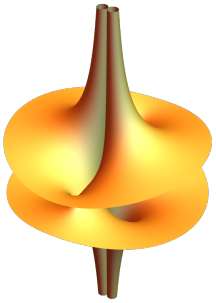
8.2.1 Unit Sound Speed & No Chemical Potential

Let us first consider the minimal scenario of an exchanged massive scalar field with zero chemical potential $\tilde{\kappa} = 0$ and with a trivial sound speed for the external field $c_s = 1$. The effective frequency in this case is given by

$$\omega_K^2(\tau) = K^2 + \frac{\mu^2}{\tau^2}\,, \tag{8.10}$$

which has a pole at $\tau = 0$ and two simple zeros at $\tau_c, \tau_c^* = \mp i\mu/K$. Taking the square root gives a double-valued function defined on two Riemann sheets $\mathbb{C}_{\rm I,II}$ that we define by

$$\omega_K(\tau) = +\sqrt{K^2 + \frac{\mu^2}{\tau^2}}\,,\ \ \tau \in \mathbb{C}_{\rm I}\,, \quad \text{and} \quad \omega_K(\tau) = -\sqrt{K^2 + \frac{\mu^2}{\tau^2}}\,,\ \ \tau \in \mathbb{C}_{\rm II}\,, \tag{8.11}$$



where $\sqrt{\cdot}$ denotes the standard principal-valued square root function. On either sheets, there is a branch cut that joins $\tau_c, 0$ and τ_c^*, but there are no discontinuities between $\tau_c, 0$ and τ_c^* across different sheets. Instead, the discontinuities are from τ_c, τ_c^* to $\mp i\infty$. The corresponding surface is represented on the right. We now follow the recipe outlined in the previous section. The first factorised time integral $F_L^{(3)}$ is given by

$$\begin{aligned} F_L^{(3)} &\approx \int_{-\infty^+}^{0} \frac{\mathrm{d}\tau'}{\sqrt{2\omega_K(\tau')}} \left[e^{i\left(E_1\tau' - \int_{\tau_0}^{\tau'} \mathrm{d}\tau\omega_K(\tau)\right)} + \beta_K(\tau') e^{i\left(E_1\tau' + \int_{\tau_0}^{\tau'} \mathrm{d}\tau\omega_K(\tau)\right)} \right] \\ &\equiv F_L^{(3),\alpha} + F_L^{(3),\beta}\,, \end{aligned} \tag{8.12}$$

where the superscripts α and β keep track of the positive- and negative-frequency parts of the massive mode functions. Here, τ_0 is an arbitrary reference time which can be taken to be $\tau_0 \to -\infty$ without loss of generality. To find the saddle points, we solve

$$\frac{\mathrm{d}}{\mathrm{d}\tau'}\left(E_1\tau' \mp \int_{\tau_0}^{\tau'} \mathrm{d}\tau\omega_K(\tau)\right) = 0\,. \tag{8.13}$$

For the integral $F_L^{(3),\alpha}$, the nearest saddle—which contributes the most—lies in the physical domain of $\mathbb{C}_{\rm I}$

$$\tau_\bullet'^{(\alpha)} = \frac{-\mu}{\sqrt{E_1^2 - K^2}} \in \mathbb{C}_{\rm I}\,. \tag{8.14}$$

Although $\tau_\bullet'$ and $-\tau_\bullet'$ are both solutions of the saddle-point equation (8.18), according to the rule of thumb, we always pick up the one closest to the physical region

since its contribution is the largest. For the integral $F_L^{(3),\beta}$, there are no saddle points in the physical domain. Instead, the nearest saddle point lies in $\mathbb{C}_{\rm II}$

$$\tau_\bullet^{\prime(\beta)} = \frac{+\mu}{\sqrt{E_1^2 - K^2}} \in \mathbb{C}_{\rm II}\,. \tag{8.15}$$

In addition, the Bogolyubov coefficient is suppressed by $|\beta_K| = e^{-\pi\mu}$. Therefore, we can completely discard this term. In fact, one can show that this term evaluated at the saddle $\tau_\bullet^{\prime(\beta)}$ is of order $\mathcal{O}(e^{-2\pi\mu})$. Its cousin at $-\tau_\bullet^{\prime(\beta)} \in \mathbb{C}_{\rm II}$ is unreachable from the original contour on the first Riemann sheet and therefore does not contribute. For pedagogical reasons, we gather a pedagogical introduction to Riemann surfaces and the saddle point method (as well as concrete worked out examples) in App. B. Performing the saddle-point approximation for the positive-frequency integral, we obtain

$$F_L^{(3)} \approx F_L^{(3),\alpha} \approx \frac{\sqrt{\pi\mu}}{(E_1^2 - K^2)^{3/4}} e^{-i\pi/4} \exp\left[-i\mu \operatorname{arccosh}\frac{E_1}{K}\right]. \tag{8.16}$$

We give more details of the derivation in App. B, and represent the complex τ' plane in Fig. 8.2. Note that keeping the dependence on τ_0 gives an unphysical phase that will eventually be cancelled in the final result, after multiplying by $\tilde{F}_R^{(3)}$. The factorised time integral $\tilde{F}_R^{(3)}$ turns out to be more complicated. Again, let us

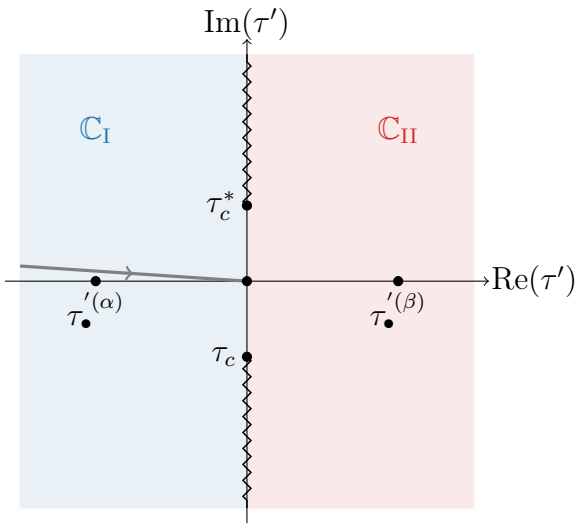


Figure 8.2: Analytic structure of the effective frequency ω_K in the complex τ' plane, together with both Riemann sheets $\mathbb{C}_{\rm I}$ and $\mathbb{C}_{\rm II}$ for the case $c_s = 1$ and $\tilde{\kappa} = 0$ to compute $F_L^{(3)}$. We also represent the turning points τ_c, τ_c^*, and the saddle points $\tau_\bullet^{\prime(\alpha)}, \tau_\bullet^{\prime(\beta)}$. The original integration contour is in gray, which encodes the early-time $i\epsilon$ prescription.

separate the integral into positive- and negative-frequency modes

$$\begin{aligned}\tilde{F}_R^{(3)} &\approx \int_{-\infty^+}^{0} \frac{\mathrm{d}\tau''}{\sqrt{2\omega_K(\tau'')}} \left[e^{i\left(E_2\tau'' + \int_{\tau_0}^{\tau''} \mathrm{d}\tau\omega_K(\tau)\right)} + \beta_K^*(\tau'') e^{i\left(E_2\tau'' - \int_{\tau_0}^{\tau''} \mathrm{d}\tau\omega_K(\tau)\right)}\right] \\ &\equiv \tilde{F}_R^{(3),\alpha} + \tilde{F}_R^{(3),\beta}\,.\end{aligned} \tag{8.17}$$

The saddle points now are solutions to the following equation

$$\frac{\mathrm{d}}{\mathrm{d}\tau''}\left(E_2\tau'' \pm \int_{\tau_0}^{\tau''} \mathrm{d}\tau\omega_K(\tau)\right) = 0\,. \tag{8.18}$$

The integral $\tilde{F}_R^{(3),\beta}$, despite being suppressed by $|\beta_K| = e^{-\pi\mu}$, has a saddle in the physical domain

$$\tau_\bullet^{''(\beta)} = \frac{-\mu}{\sqrt{E_1^2 - K^2}} \in \mathbb{C}_{\mathrm{I}}\,, \tag{8.19}$$

while the saddle of the positive-frequency integral $\tilde{F}_R^{(3),\alpha}$ lies unphysically on the second Riemann sheet

$$\tau_\bullet^{''(\alpha)} = \frac{+\mu}{\sqrt{E_1^2 - K^2}} \in \mathbb{C}_{\mathrm{II}}\,. \tag{8.20}$$

Consequently, we expect the contribution from both terms to be comparable, i.e. both are of order $\mathcal{O}(e^{-\#\mu})$. Computing $\tilde{F}_R^{(3),\beta}$ is identical to that of $F_L^{(3),\alpha}$ and we directly write the result

$$\tilde{F}_R^{(3),\beta} \approx \frac{\sqrt{\pi\mu}\,e^{-\pi\mu}}{(E_2^2 - K^2)^{3/4}} e^{-i\pi/4} \exp\left[-i\mu\,\mathrm{arccosh}\frac{E_2}{K}\right] S(\tau_\bullet^{''(\beta)})\,, \tag{8.21}$$

where $S(\tau) \equiv \frac{1}{2}[1 + \mathrm{erf}(\Gamma_K(\tau))]$ is the Stokes multiplier, and where we have used the relation $F_K(\tau_0) = \pi\mu - 2iK\tau_0$. As for the positive-frequency integral $\tilde{F}_R^{(3),\alpha}$, we need to continuously deform the integration contour so that it crosses the saddle point $\tau_\bullet^{''(\alpha)}$ on the second Riemann sheet $\mathbb{C}_{\mathrm{II}}$. According to the saddle-point method, the complete integral is proportional to the integrand evaluated at the saddle point. Therefore, the size of the integral is estimated by

$$|\tilde{F}_R^{(3),\alpha}| \sim \left|\exp\left(iE_2\tau_\bullet^{''(\alpha)} + i\int_{-\infty}^{\tau_\bullet^{''(\alpha)}} \mathrm{d}\tau\omega_K(\tau)\right)\right| = \exp\left(-\mathrm{Im}\int_{-\infty}^{\tau_\bullet^{''(\alpha)}} \mathrm{d}\tau\omega_K(\tau)\right)\,. \tag{8.22}$$

The original integral contour is now deformed to pass through the saddle $\tau_\bullet^{''(\alpha)} \in \mathbb{C}_{\mathrm{II}}$. The new contour consists of three portions

$$\int_{-\infty}^{\tau_\bullet^{''(\alpha)}} = \int_{\mathcal{C}_1} + \int_{\mathcal{C}_2} + \int_{\mathcal{C}_3}\,, \tag{8.23}$$

where the various contours are depicted in Fig. 8.3. Both $\mathcal{C}_1$ and $\mathcal{C}_3$ give purely real contributions, which directly drop out of our estimation. The only contribution to the imaginary part is from the semicircle $\mathcal{C}_2$, which can be nicely written as half the residue at the origin

$$|\tilde{F}_R^{(3),\alpha}| \sim \exp\left(-\mathrm{Im}\int_{\mathcal{C}_2} \mathrm{d}\tau\omega_K(\tau)\right) = e^{\pi \underset{\tau=0}{\mathrm{Res}}\,\omega_K(\tau)} = e^{-\pi\mu}\,. \tag{8.24}$$

Interestingly, the price to pay for an "off-shell" vertex resonance is an exponential factor closely related to the location of the saddle point and the late-time behaviour

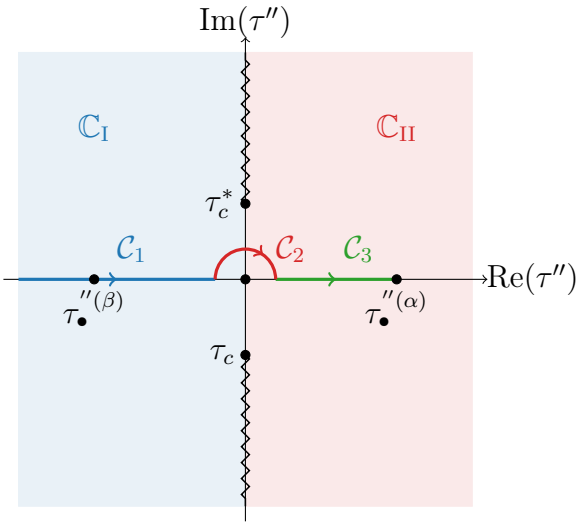


Figure 8.3: Analytic structure of the effective frequency ω_K in the complex τ'' plane to compute $\tilde{F}_R^{(3)}$. For the positive-frequency integral $\tilde{F}_R^{(3),\alpha}$, the original integration contour is deformed to pass through the saddle point on the second Riemann sheet $\mathbb{C}_{\rm II}$, which results in three different portions.

of the effective frequency. We will later that this is a universal feature. We can now finish the saddle-point approximation by performing the rest of the Gaussian integral. This yields

$$\tilde{F}_R^{(3),\alpha} \approx \frac{-\sqrt{\pi\mu}\, e^{-\pi\mu}}{(E_2^2-K^2)^{3/4}} e^{-i\pi/4} \exp\left[-i\mu \operatorname{arccosh}\frac{E_2}{K}\right] . \tag{8.25}$$

Combining (8.16), (8.21) and (8.25), and setting $S(\tau_\bullet''^{(\beta)}) = 1$ in the soft limit, we obtain the full approximate solution for the cosmological collider signal

$$\begin{aligned} F_{\rm F} + \text{c.c.} \approx \frac{2\pi\mu}{\left[(E_1^2-K^2)(E_2^2-K^2)\right]^{3/4}} \Bigg\{ & e^{-\pi\mu} \sin\mu \left[\operatorname{arccosh}\frac{E_1}{K} - \operatorname{arccosh}\frac{E_2}{K}\right] \\ & + e^{-\pi\mu}\cos\mu\left[\operatorname{arccosh}\frac{E_1}{K} + \operatorname{arccosh}\frac{E_2}{K}\right]\Bigg\} , \end{aligned} \tag{8.26}$$

for $E_1 > E_2$. The opposite regime $E_1 < E_2$ is obtained by swapping $E_1 \leftrightarrow E_2$. In Fig. 8.4, we show the approximate solution against the exact one given in terms of hypergeometric functions. We stress that this method gives amazingly accurate results already for $\mu \gtrsim 2$. The small phase shift for the non-local signal—oscillating in the K^2/E_1E_2 direction—can be fixed by considering higher-order corrections in μ^{-1}.

Discussion. Let us make a few comments regarding the found approximate solution.

- The first line in (8.26) comes from the positive-frequency integral $\tilde{F}_R^{(3),\alpha}$ and asymptotes to $\sin[\mu\log(E_1/E_2)]$ in the collapsed limit $K \to 0$. This term

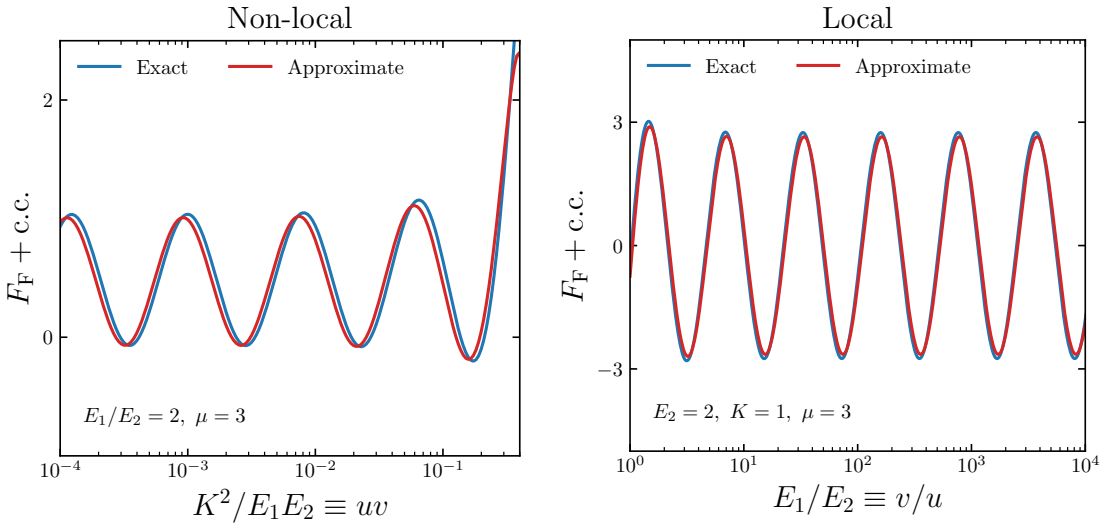


Figure 8.4: Exact and approximate four-point correlator $F_{\rm F}+\text{c.c}\equiv F_L^{(3)}\tilde{F}_R^{(3)}+\text{c.c}$ for $\mu=3$ both in the non-local direction oscillating as function of $K^2/E_1E_2\equiv uv$ (*left panel*) and in the local direction oscillating as function of $E_1/E_2\equiv v/u$ (*right panel*). Details about the kinematics can be found in Sec. 7.1.

is known as the local cosmological collider signal as it is analytic in K, see Chap. 4. We recall that it captures the propagation of massive particles from one vertex to the other one. More specifically, we see that the local signal is given by the time elapsed between the saddle point $\tau_\bullet^{''(\alpha)}$ that creates the particle and the saddle $\tau_\bullet^{'(\alpha)}$ that destroys the particle.

- The second line in (8.26) comes from the negative-frequency integral $\tilde{F}_R^{(3),\beta}$ and asymptotes to $\sin[\mu\log(E_1E_2/K^2)]$ in the collapsed limit $K\to 0$. These oscillations are known as the non-local cosmological collider signal due to their non-analyticity in K. In contrast to the local signal, this one represents the propagation effect of massive particles from vacuum pair production to their subsequent decay at $\tau_\bullet^{'(\alpha)}$ and $\tau_\bullet^{''(\beta)}$.

- In this minimal setup, both signals are suppressed by *half* the Boltzmann factor $e^{-\pi\mu}=e^{-m/(2T_{\rm dS})}$, but due to different reasons. For the local signal, it is due to the *semi-circle* we take to reach the saddle in the unphysical domain, whereas for the non-local signal, it is essentially the Bogolyubov coefficient. We will see in more general scenarios that the size of these signals can be drastically different.

- The seed integral we started with does not correspond to any physical coupling. However, all physical interaction vertices respecting the shift symmetry of external legs come with higher conformal time weights in the integrand, and their effects can be derived by differentiating the found result with respect to external kinematics. For instance, acting with $E_1\partial_{E_1}$ on (8.26) raises the conformal time power from zero to one. In the large-mass limit, the leading effect of such derivatives is to bring out powers of μ from the waveform while

shifting its phase,

$$(E_1\partial_{E_1})^{p_1}\,(E_2\partial_{E_2})^{p_2}\,(F_{\rm F}+\text{c.c.}) \approx \left(\frac{\mu E_1}{\sqrt{E_1^2-K^2}}\right)^{p_1}\left(\frac{\mu E_2}{\sqrt{E_2^2-K^2}}\right)^{p_2} \times (F_{\rm F}+\text{c.c.})_{\text{shifted phase}}\,, \tag{8.27}$$

with

$$\text{shifted phase} = \begin{cases} \dfrac{\pi(p_1-p_2)}{2}\,, & \text{local signal} \\ \dfrac{\pi(p_1+p_2)}{2}\,, & \text{non-local signal} \end{cases}\,. \tag{8.28}$$

This feature does not alter the qualitative properties of the cosmological collider signals discussed above. In particular, the waveforms are unchanged modulo discrete phase shifts.

- Readers looking for mathematical rigour may have noticed that our "steepest" contour is strictly speaking not valid for the integral $\tilde{F}_R^{(3)}$. This is because the contour is restricted by the branching point τ_c^*, and is in fact not a path for which the saddle-point approximation is justified. Namely, there exist points along this contour where the size of the integrand is actually larger than the height of the saddle at $\tau_\bullet^{\prime\prime(\alpha)}$. To remedy this seemingly fatal mathematical flaw, we note that the defining integrand given in terms of the exact mode function is analytic in the upper-half complex τ''-plane without branching points. Moreover, the Bunch-Davies $i\epsilon$ prescription ensures that the integrand vanishes for the upper arc at infinity. Therefore, we can Wick rotate the contour from the very beginning, and then insert the WKB approximation. This way, the saddle can be picked up by the Wick rotated contour directly, eventually giving the same result as in (8.25).

8.2.2 Turning on a Non-Trivial Sound Speed

Let us now introduce a non-trivial sound speed. We rescale the spacetime coordinates such that the speed of sound of the massive field remains unity while the external legs acquire a sound speed c_s, which is the ratio of both sound speeds. For $c_s > 1$, i.e. the exchanged massive field propagating slower than the external one, the analysis from the previous section applies and one only needs to replace $E_{1,2} \to c_s E_{1,2}$. The case $c_s < 1$ needs to be treated with care. Indeed, applying the bulk cutting rules requires that both factorised integrals converge. However, for $E_1 > E_2$, convergence is achieved only if $E_1/K < c_s^{-1}$ as seen in Chap. 7. In the opposite kinematic regime $E_2 > E_1$, one needs to flip the other theta function, therefore requiring $E_2/K < c_s^{-1}$ for convergence. In the end, the convergence of the factorised time integrals for a reduced sound speed carves out a diamond-shape region in kinematic space to which our approximation scheme no longer applies, see the region in red in Fig. 8.5. Moreover, two new "edge" regions in green defined by $E_2/K < c_s^{-1} < E_1/K$ and $E_1/K < c_s^{-1} < E_2/K$ emerge where our approximate procedure still applies. From now on, we will assume $c_s < 1$ and focus on the edge

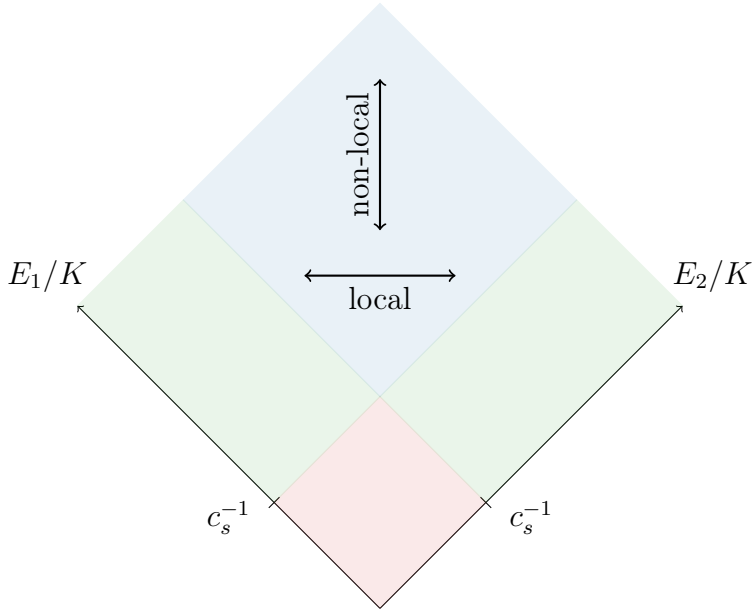


Figure 8.5: Kinematic space of the four-point function in the presence of a reduced sound speed for the external legs $c_s < 1$. The local signal direction is horizontal and the non-local signal direction is vertical.

region $E_2/K < c_s^{-1} < E_1/K$. The integral $F_L^{(3)}$ can again be separated into two pieces

$$\begin{aligned} F_L^{(3)} &\approx \int_{-\infty^+}^{0} \frac{\mathrm{d}\tau'}{\sqrt{2\omega_K(\tau')}} \left[e^{i\left(c_s E_1 \tau' - \int_{\tau_0}^{\tau'} \mathrm{d}\tau \omega_K(\tau)\right)} + \beta_K(\tau') e^{i\left(c_s E_1 \tau' + \int_{\tau_0}^{\tau'} \mathrm{d}\tau \omega_K(\tau)\right)} \right] \\ &\equiv F_L^{(3),\alpha} + F_L^{(3),\beta} \,, \end{aligned} \tag{8.29}$$

Since the massive field remained untouched by the external reduced sound speed, the negative-frequency integral $F_L^{(3),\beta}$ remains subdominant and can be neglected. The saddle point for the positive-frequency integral $F_L^{(3),\alpha}$ is found to be

$$\tau_\bullet^{\prime(\alpha)} = \frac{-\mu}{\sqrt{c_s^2 E_1^2 - K^2}} \in \mathbb{C}_{\mathrm{I}} \,. \tag{8.30}$$

Because we placed ourselves in the edge region where $E_1/K > c_s^{-1}$, the saddle $\tau_\bullet^{\prime(\alpha)}$ lies in the physical region. Therefore, we can directly apply the result (8.16) after replacing $E_1 \to c_s E_1$. Similarly, the second integral $\tilde{F}_R^{(3)}$ is also well approximated by (8.21) and (8.25) with $E_2 \to c_s E_2$. However, in the edge region $E_2/K < c_s^{-1}$, the saddle points for the integral

$$\begin{aligned} \tilde{F}_R^{(3)} &\approx \int_{-\infty^+}^{0} \frac{\mathrm{d}\tau''}{\sqrt{2\omega_K(\tau'')}} \left[e^{i\left(c_s E_2 \tau'' + \int_{\tau_0}^{\tau''} \mathrm{d}\tau \omega_K(\tau)\right)} + \beta_K^*(\tau'') e^{i\left(c_s E_2 \tau'' - \int_{\tau_0}^{\tau''} \mathrm{d}\tau \omega_K(\tau)\right)} \right] \\ &\equiv \tilde{F}_R^{(3),\alpha} + \tilde{F}_R^{(3),\beta} \,, \end{aligned} \tag{8.31}$$

lie along the imaginary axis

$$\tau_\bullet^{\prime\prime(\alpha)} = \frac{+i\mu}{\sqrt{K^2 - c_s^2 E_2^2}} \in \mathbb{C}_{\mathrm{II}} \,, \quad \tau_\bullet^{\prime\prime(\beta)} = \frac{+i\mu}{\sqrt{K^2 - c_s^2 E_2^2}} \in \mathbb{C}_{\mathrm{I}} \,. \tag{8.32}$$

Now, $\tau_\bullet^{''(\beta)}$ is moved away from the physical regime. Using the rule of thumb, we expect $\tilde{F}_R^{(3),\beta}$ to be suppressed by $\mathcal{O}(e^{-(\pi+\#)\mu})$, making it negligible compared to $\tilde{F}_R^{(3),\alpha}$, expected to be of size $\mathcal{O}(e^{-\#\mu})$. We therefore drop the negative-frequency integral and focus on $\tilde{F}_R^{(3),\alpha}$. Following the saddle point approximation method, we deform the integration contour to pass through $\tau_\bullet^{''(\alpha)}$. The size of the integral is given by

$$\begin{aligned} |\tilde{F}_R^{(3),\alpha}| &\sim \left| \exp\left(i c_s E_2 \tau_\bullet^{''(\alpha)} + i \int_{-\infty}^{\tau_\bullet^{''(\alpha)}} \mathrm{d}\tau \omega_K(\tau) \right) \right| \\ &= \exp\left(-c_s E_2 \, \mathrm{Im}\tau_\bullet^{''(\alpha)} \right) \exp\left(-\mathrm{Im} \int_{-\infty}^{\tau_\bullet^{''(\alpha)}} \mathrm{d}\tau \omega_K(\tau) \right) . \end{aligned} \tag{8.33}$$

To reach the imaginary saddle point on the second Riemann sheet, we need to rotate around the pole at the origin only a quarter of circle, plus an imaginary contour from the branching point to the saddle point. The new contour consists now of four portions

$$\int_{-\infty}^{\tau_\bullet^{''(\alpha)}} = \int_{\mathcal{C}_1} + \int_{\mathcal{C}_2} + \int_{\mathcal{C}_3} + \int_{\mathcal{C}_4} , \tag{8.34}$$

where the various contours are depicted in Fig. 8.6. Picking up a quarter of residue at the origin, we obtain

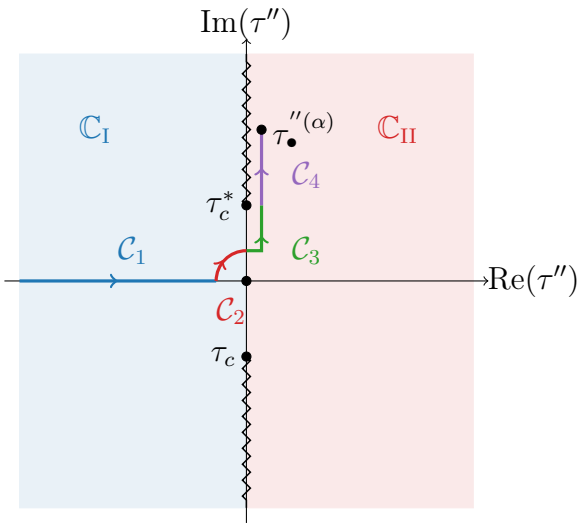


Figure 8.6: Analytic structure of the effective frequency ω_K in the complex τ'' plane to compute $\tilde{F}_R^{(3)}$ in the case of a reduced sound speed $c_s < 1$.

$$
\begin{aligned}
|\tilde{F}_R^{(3)}| &\sim \exp\left(-\mathrm{Im}\int_{\mathcal{C}_2} \mathrm{d}\tau\omega_K(\tau)\right)\exp\left(-\mathrm{Im}\int_{\mathcal{C}_4} \mathrm{d}\tau\omega_K(\tau)\right)\exp\left(-c_sE_2\,\mathrm{Im}\tau_\bullet^{''(\alpha)}\right)\\
&= e^{\frac{\pi}{2}\mathrm{Res}_{\tau=0}\omega_K(\tau)}\exp\left(\int_{\mu/K}^{\mu/\sqrt{K^2-c_s^2E_2^2}}\sqrt{K^2-\frac{\mu^2}{x^2}}\mathrm{d}x-\frac{c_sE_2\mu}{\sqrt{K^2-c_s^2E_2^2}}\right)\\
&= e^{-\pi\mu/2}\exp\left(-\mu\arcsin\frac{c_sE_2}{K}\right)\,.
\end{aligned}
\tag{8.35}
$$

Applying the full saddle point approximation yields

$$
\tilde{F}_R^{(3)} = \frac{-i\sqrt{\pi\mu}\,e^{-\pi\mu/2}}{(K^2-c_s^2E_2^2)^{3/4}}\exp\left[-\mu\arcsin\frac{c_sE_2}{K}\right]\,. \tag{8.36}
$$

Combining all found solutions, we obtain the full approximate solution for the cosmological collider signal

$$
\begin{aligned}
F_{\mathrm{F}}+\mathrm{c.c.} \approx\ & \frac{2\pi\mu}{[(c_s^2E_1^2-K^2)(K^2-c_s^2E_2^2)]^{3/4}}\\
&\times e^{-\pi\mu/2}\exp\left[-\mu\arcsin\frac{c_sE_2}{K}\right]\cos\left[\mu\,\mathrm{arccosh}\frac{c_sE_1}{K}+\frac{3\pi}{4}\right]\,.
\end{aligned}
\tag{8.37}
$$

Again, the signal in the edge region $E_1/K < c_s^{-1} < E_2/K$ is obtained by swapping the kinematic variables $E_1 \leftrightarrow E_2$.

Discussion. A few comments are in order.

- In contrast to the conventional cosmological collider signal, the one with a reduced sound speed is suppressed by only a quarter of the usual Boltzmann factor $e^{-\pi\mu/2} = e^{-m/(4T_{\mathrm{dS}})}$ due to the quarter circle we take to reach the saddle. Such amplified oscillations have long been known in the literature but without much explanation nor interpretation [116, 311].

- The behaviour of the cosmological collider signal is intimately related to the location of the saddle $\tau_\bullet^{''(\alpha)}$. In the edge region of kinematic space, $\tau_\bullet^{'(\alpha)}$ is real, and it shifts in the real direction when we vary the ratio E_1/K, giving rise to oscillations. On the other hand, $\tau_\bullet^{''(\alpha)}$ is purely imaginary. Hence when we vary the ratio E_2/K, the saddle point shifts in the imaginary direction, giving rise to smooth exponential attenuation instead of oscillations. In addition, the arcsin function nicely produces a smooth interpolation between $e^{-\pi\mu/2}$ (reduced sound speed) and $e^{-\pi\mu}$ (conventional collider), as c_sE_2/K increases from zero to one.

- Interestingly, we notice that (8.37) can be derived from (8.26) via direct analytic continuation. To see this, note that the $\mathrm{arccosh}(z)$ function has a branching point at $z \equiv c_sE_2/K = 1$. To consistently continue beyond this singularity, we recall that $E_2 = |E_2| - i\epsilon$ is defined with a negative imaginary part to ensure the convergence of $\tilde{F}_R^{(3)}$. Therefore, the correct transformation of the $\mathrm{arccosh}(z)$ function is

$$
\mathrm{arccosh}(z) \to -i\arccos(z)\,,\quad 0<\mathrm{Re}(z)<1\,,\quad \mathrm{Im}(z)<0\,. \tag{8.38}
$$

The power law prefactor transforms as

$$(c_s^2 E_2^2 - K^2)^{3/4} \to e^{-3i\pi/4}(K^2 - c_s^2 E_2^2)^{3/4} \,. \tag{8.39}$$

Expansion of the trigonometric functions yields terms of higher order in $\mathcal{O}(e^{-\#\mu})$ which can be dropped. This allows us to directly land on the correct result (8.37) without repeating the entire saddle point analysis. It is intriguing why this should be the case since approximate solutions are not expected to enjoy precise analytic continuations in general. We leave this pleasant yet seemingly coincidental phenomenon for future work.

- Similar to the case with no unit sound speed, realistic correlators with more derivatives in the interaction vertices can be obtained by differentiating the seed integral with respect to the external kinematics. In the large-μ asymptotic limit, we can approximate

$$\begin{aligned}(E_1\partial_{E_1})^{p_1}\,(E_2\partial_{E_2})^{p_2}\,(F_{\rm F}+\text{c.c.}) \approx \left(\frac{c_s\mu E_1}{\sqrt{c_s^2E_1^2-K^2}}\right)^{p_1}\left(\frac{-c_s\mu E_2}{\sqrt{K^2-c_s^2E_2^2}}\right)^{p_2} \\ \times\,(F_{\rm F}+\text{c.c.})_{\text{shifted phase}}\,.\end{aligned} \tag{8.40}$$

Again, the waveform changes at most by a discrete phase shift,

$$\text{shifted phase} = \frac{\pi p_1}{2}\,, \quad (c_s<1)\,. \tag{8.41}$$

Consequently, the phase of the low-speed collider signal is fixed at $\pm\pi/4, \pm 3\pi/4$ at leading order in μ^{-1}, which is a unique prediction of the approximated signal.

8.2.3 Further Turning on the Chemical Potential

We now turn to the most general case where a non-zero chemical potential $\tilde{\kappa} \equiv \kappa/H$ is turned on. Since the superadiabatic approximation of the mode function is valid only when $|\beta_K(\tau)| \ll 1$, we will only consider the parameter regime with weak particle production, i.e. $\tilde{\kappa} < \mu$. This avoids large backreaction from massive particle loops. Without loss of generality, we set $E_1 > E_2$ and $\lambda = -1$. The result for the $\lambda = +1$ mode can be found via a simple flip of the chemical potential $\tilde{\kappa} \to -\tilde{\kappa}$. We also require $E_1/K > c_s^{-1}$ to ensure the bulk cutting rule yields convergent time integrals. The effect of the chemical potential is to add a linear term in the massive effective frequency

$$\omega_K^2(\tau) = K^2 + \frac{2K\tilde{\kappa}}{\tau} + \frac{\mu^2}{\tau^2}\,. \tag{8.42}$$

This additional linear term does not alter the leading late-time pole at $\tau = 0$, but it shifts the turning points away from the imaginary axis

$$\tau_c = \frac{1}{K}\left(-\tilde{\kappa} - i\sqrt{\mu^2-\tilde{\kappa}}\right)\,. \tag{8.43}$$

The branch cut at $\omega_K^2(\tau) < 0$ joins τ_c, τ_c^* and 0, separating the complex plane into different Riemann sheets. The effective frequency is therefore defined as double-valued function

$$\begin{aligned}\omega_K(\tau) &= +\sqrt{K^2 + \frac{2K\tilde{\kappa}}{\tau} + \frac{\mu^2}{\tau^2}}\,, \quad \tau \in \mathbb{C}_{\rm I}\,, \\ \omega_K(\tau) &= -\sqrt{K^2 + \frac{2K\tilde{\kappa}}{\tau} + \frac{\mu^2}{\tau^2}}\,, \quad \tau \in \mathbb{C}_{\rm II}\,.\end{aligned} \tag{8.44}$$

The singulant function admits a closed-form expression

$$\begin{aligned}F_K(\tau) = -2i\Bigg[&\tau\omega_K(\tau) + \mu\,\text{arctanh}\left(\frac{K\tau\tilde{\kappa}+\mu^2}{-\mu\tau\omega_K(\tau)}\right) \\ &-\tilde{\kappa}\,\text{arctanh}\left(\frac{K\tau+\tilde{\kappa}}{-\tau\omega_K(\tau)}\right)\Bigg] + \pi(\mu-\tilde{\kappa})\,.\end{aligned} \tag{8.45}$$

The chemical potential assists spontaneous particle production by alleviating the effective mass in the Boltzmann factor $|\beta_K|^2 = e^{-2\pi(\mu-\tilde{\kappa})}$. Following the same procedure as in previous sections, we start with the left time integral

$$\begin{aligned}F_L^{(3)} &\approx \int_{-\infty^+}^{0} \frac{\mathrm{d}\tau'}{\sqrt{2\omega_K(\tau')}}\left[e^{i\left(E_1\tau' - \int_{\tau_0}^{\tau'}\mathrm{d}\tau\omega_K(\tau)\right)} + \beta_K(\tau')e^{i\left(E_1\tau' + \int_{\tau_0}^{\tau'}\mathrm{d}\tau\omega_K(\tau)\right)}\right] \\ &\equiv F_L^{(3),\alpha} + F_L^{(3),\beta}\,.\end{aligned} \tag{8.46}$$

Solving for the saddle points, we find

$$\tau_\bullet^{\prime(\alpha)} = \frac{K(\tilde{\kappa}-\mu\Delta_L)}{c_s^2E_1^2-K^2} \in \mathbb{C}_{\rm I}\,, \quad \tau_\bullet^{\prime(\beta)} = \frac{K(\tilde{\kappa}+\mu\Delta_L)}{c_s^2E_1^2-K^2} \in \mathbb{C}_{\rm II}\,, \tag{8.47}$$

with $\Delta_L = \sqrt{c_s^2E_1^2/K^2 - (1-\tilde{\kappa}^2/\mu^2)}$. Again, the integral $F_L^{(3),\alpha}$ has a physical saddle point, and thereby dominates over $F_L^{(3),\beta}$. Finishing the Gaussian integral around $\tau_\bullet^{\prime(\alpha)}$, we obtain

$$\begin{aligned}F_L^{(3)} \approx \frac{\sqrt{\pi}\mu^{3/2}}{K^{3/2}(\tilde{\kappa}+\mu\Delta_L)\sqrt{\Delta_L}}e^{-i\pi/4-i\theta}\exp\Bigg[&-i\mu\left(\text{arccosh}\frac{c_sE_1/K}{\sqrt{1-\tilde{\kappa}^2/\mu^2}}\right) \\ &-i\tilde{\kappa}\left(\text{arccosh}\frac{c_sE_1}{K} - \text{arctanh}\frac{c_sE_1\tilde{\kappa}}{K\mu\Delta_L}\right)\Bigg]\,,\end{aligned} \tag{8.48}$$

where θ is a kinematic-independent phase, given by

$$\theta(\mu,\tilde{\kappa}) \equiv \frac{\mu+\tilde{\kappa}}{2}\log(\mu+\tilde{\kappa}) - \frac{\mu-\tilde{\kappa}}{2}\log(\mu-\tilde{\kappa}) - \tilde{\kappa}\,. \tag{8.49}$$

As usual, the integral $\tilde{F}_R^{(3)}$ is more complicated. We define

$$\begin{aligned}\tilde{F}_R^{(3)} &\approx \int_{-\infty^+}^{0} \frac{\mathrm{d}\tau''}{\sqrt{2\omega_K(\tau'')}}\left[e^{i\left(c_sE_2\tau'' + \int_{\tau_0}^{\tau''}\mathrm{d}\tau\omega_K(\tau)\right)} + \beta_K^*(\tau'')e^{i\left(c_sE_2\tau'' - \int_{\tau_0}^{\tau''}\mathrm{d}\tau\omega_K(\tau)\right)}\right] \\ &\equiv \tilde{F}_R^{(3),\alpha} + \tilde{F}_R^{(3),\beta}\,.\end{aligned} \tag{8.50}$$

The location of the saddle points are

$$\tau_\bullet^{''(\alpha)} = \frac{K(\tilde{\kappa}+\mu\Delta_R)}{c_s^2E_2^2-K^2} \in \mathbb{C}_{\rm II}\,, \quad \tau_\bullet^{''(\beta)} = \frac{K(\tilde{\kappa}-\mu\Delta_R)}{c_s^2E_2^2-K^2} \in \mathbb{C}_{\rm I}\,, \tag{8.51}$$

with $\Delta_R = \sqrt{c_s^2E_2^2/K^2-(1-\tilde{\kappa}^2/\mu^2)}$. For $E_2/K > c_s^{-1}\sqrt{1-\tilde{\kappa}^2/\mu^2}$, we have $\Delta_R \in \mathbb{R}$ and the saddle points lie on the real axis. For $E_2/K < c_s^{-1}\sqrt{1-\tilde{\kappa}^2/\mu^2}$, Δ_R is purely imaginary and the saddle points can move around in the complex plane. The point $E_2 = K/c_s$ also distinguishes the position of $\tau_\bullet^{''(\alpha)}$ relative to infinity. As the qualitative behaviour of cosmological collider signals dramatically depends on the location of the saddle points, we separate the discussion according to kinematic regions.

Interior region $E_2/K > c_s^{-1}$. This region is depicted in blue in Fig. 8.5 (recall that $E_1 > E_2$). In this region, $\tau_\bullet^{''(\alpha)}$ is along the positive real axis on the second Riemann sheet $\mathbb{C}_{\rm II}$, whereas $\tau_\bullet^{''(\beta)}$ is along the negative real axis on $\mathbb{C}_{\rm I}$. The integral $\tilde{F}_R^{(3),\beta}$ picks up the saddle in the physical region, which leads to

$$\begin{aligned}\tilde{F}_R^{(3),\beta} \approx \frac{\sqrt{\pi}\mu^{3/2}e^{-\pi(\mu-\tilde{\kappa})}}{K^{3/2}(\tilde{\kappa}+\mu\Delta_R)\sqrt{\Delta_R}}e^{i\pi/4+i\theta}\exp\left[-i\mu\left(\operatorname{arccosh}\frac{c_sE_2/K}{\sqrt{1-\tilde{\kappa}^2/\mu^2}}\right)\right.\\ \left.-i\tilde{\kappa}\left(\operatorname{arccosh}\frac{c_sE_2}{K}-\operatorname{arctanh}\frac{c_sE_2\tilde{\kappa}}{K\mu\Delta_R}\right)\right]\,.\end{aligned} \tag{8.52}$$

In order to apply the saddle-point approximation for the integral $\tilde{F}_R^{(3),\alpha}$, we deform the initial integration contour such that it dives under the branch cut, passing through $\tau_\bullet^{''(\alpha)}$ in the steepest direction. As represented in Fig. 8.7, we again need to rotate around the origin, therefore picking up the same suppression power

$$|\tilde{F}_R^{(3),\alpha}| \sim \exp\left(-{\rm Im}\int_{\mathcal{C}_2}{\rm d}\tau\omega_K(\tau)\right) = e^{\pi\underset{\tau=0}{\rm Res}\,\omega_K(\tau)} = e^{-\pi\mu}\,. \tag{8.53}$$

Finishing the Gaussian integral, we obtain

$$\begin{aligned}\tilde{F}_R^{(3),\alpha} \approx \frac{-\sqrt{\pi}\mu^{3/2}e^{-\pi\mu}}{K^{3/2}(\tilde{\kappa}-\mu\Delta_R)\sqrt{\Delta_R}}e^{i\pi/4+i\theta}\exp\left[i\mu\left(\operatorname{arccosh}\frac{c_sE_2/K}{\sqrt{1-\tilde{\kappa}^2/\mu^2}}\right)\right.\\ \left.-i\tilde{\kappa}\left(\operatorname{arccosh}\frac{c_sE_2}{K}+\operatorname{arctanh}\frac{c_sE_2\tilde{\kappa}}{K\mu\Delta_R}\right)\right]\,.\end{aligned} \tag{8.54}$$

Combining all found results, we obtain the leading approximation of the local and non-local signals in the interior region $E_1/K < E_2/K > c_s^{-1}$

$$\begin{aligned}F_{\rm F}+{\rm c.c.} \approx \frac{2\pi\mu^3}{K^3(\tilde{\kappa}+\mu\Delta_L)\sqrt{\Delta_L\Delta_R}}\\ \times\left\{\frac{e^{-\pi\mu}}{\mu\Delta_R-\tilde{\kappa}}\sin\left[\mu\left(\operatorname{arccosh}\frac{c_sE_1/K}{\sqrt{1-\tilde{\kappa}^2/\mu^2}}-\operatorname{arccosh}\frac{c_sE_2/K}{\sqrt{1-\tilde{\kappa}^2/\mu^2}}\right)+\Xi\right]\right.\\ \left.+\frac{e^{-\pi(\mu-\tilde{\kappa})}}{\mu\Delta_R+\tilde{\kappa}}\cos\left[\mu\left(\operatorname{arccosh}\frac{c_sE_1/K}{\sqrt{1-\tilde{\kappa}^2/\mu^2}}+\operatorname{arccosh}\frac{c_sE_2/K}{\sqrt{1-\tilde{\kappa}^2/\mu^2}}\right)+\Upsilon\right]\right\}\,,\end{aligned} \tag{8.55}$$

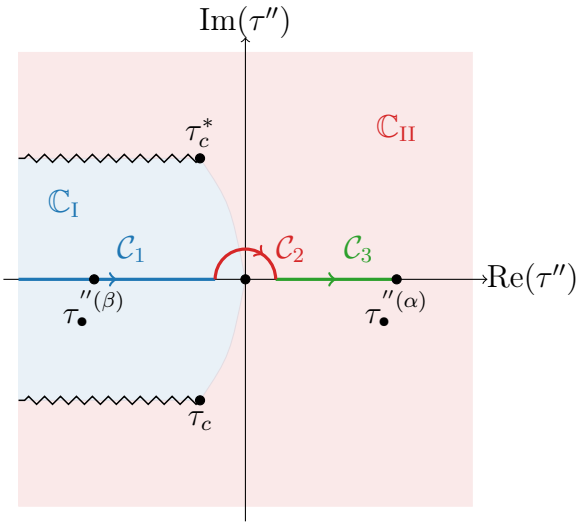


Figure 8.7: Analytic structure of the effective frequency ω_K in the complex τ'' plane to compute $\tilde{F}_R^{(3)}$ in the case of a non-unity sound speed and non-zero chemical potential in the interior region.

where the dephasing functions are given by

$$\begin{aligned}\Xi &\equiv \tilde{\kappa}\left(\operatorname{arccoth}\frac{c_s E_1}{K}+\operatorname{arccoth}\frac{c_s E_2}{K}-\operatorname{arctanh}\frac{c_s E_1\tilde{\kappa}}{K\mu\Delta_L}+\operatorname{arctanh}\frac{c_s E_2\tilde{\kappa}}{K\mu\Delta_R}\right),\\ \Upsilon &\equiv \Xi-2\tilde{\kappa}\operatorname{arctanh}\frac{c_s E_2\tilde{\kappa}}{K\mu\Delta_R}\,.\end{aligned} \tag{8.56}$$

Let us now comment on the result.

- In the interior region, the cosmological collider signals here behave qualitatively the same way as those in the case $c_s = 1$ and $\tilde{\kappa} = 0$. The first line in (8.55) represents the local signal. Its size is dictated only by the mass $\mathcal{O}(e^{-\pi\mu})$ coming from the semicircle around the origin. In the soft limit, the dephasing function approaches zero $\Xi \to 0$ and the waveform approaches $\sin\mu\log(E_1/E_2)$. In other words, the phase of the local cosmological collider signal is *universally* zero, independent of any parameters of the theory.
- The second line in (8.55) gives the non-local signal, whose size is amplified by the chemical potential $\mathcal{O}(e^{-\pi(\mu-\tilde{\kappa})})$. The corresponding dephasing function asymptotes to a constant that does depend on the parameters of the theory $\Upsilon \to -2\tilde{\kappa}\operatorname{arctanh}\tilde{\kappa}/\mu$. In general, the presence of the dephasing function implies that the waveform can significantly deviate from a simple logarithmically oscillating pattern.

Edge region $E_2/K < c_s^{-1}\sqrt{1-\tilde{\kappa}^2/\mu^2}$. This region is depicted in green in Fig. 8.5. Here, both saddle points are complex. Using the rule of thumb, the saddle at $\tau_\bullet^{''(\beta)}$ can then be dropped due to its additional suppression. We then focus on the saddle located at

$$\tau_\bullet^{''(\alpha)} = \frac{K(-\tilde{\kappa}+i\mu|\Delta_R|)}{K^2-c_s^2E_2^2} \in \mathbb{C}_{\rm II}\,. \tag{8.57}$$

To reach this saddle, we again need to dive under the branch cut to enter the second Riemann sheet $\mathbb{C}_{\rm II}$. The size of the integral is estimated from the exponent

$$\begin{aligned}|\tilde{F}_R^{(3),\alpha}| &\sim \left|\exp\left(ic_sE_2\tau_\bullet''^{(\alpha)} + i\int_{-\infty}^{\tau_\bullet''^{(\alpha)}} \mathrm{d}\tau\omega_K(\tau)\right)\right| \\ &= \exp\left(-c_sE_2\,\mathrm{Im}\tau_\bullet''^{(\alpha)}\right)\exp\left(-\mathrm{Im}\int_{-\infty}^{\tau_\bullet''^{(\alpha)}} \mathrm{d}\tau\omega_K(\tau)\right)\,.\end{aligned} \tag{8.58}$$

As depicted in Fig. 8.8, the path to reach the saddle consists of four segments

$$\int_{-\infty}^{\tau_\bullet''^{(\alpha)}} = \int_{\mathcal{C}_1} + \int_{\mathcal{C}_2} + \int_{\mathcal{C}_3} + \int_{\mathcal{C}_4}\,. \tag{8.59}$$

The contour $\mathcal{C}_1$ is purely real and drops out of the imaginary part. The contour $\mathcal{C}_4$ part is negligible if $E_2/K \ll c_s^{-1}$ because both the integrand and the length of the integration path ten to zero in this regime. We are left with an integral along a quarter circle around the origin, which gives

$$\mathrm{Im}\int_{\mathcal{C}_2}\mathrm{d}\tau\omega_K(\tau) = -\mathrm{Im}\left(\frac{i\pi}{2}\operatorname*{Res}_{\tau=0}\omega_K(\tau)\right) = \frac{\pi\mu}{2}\,, \tag{8.60}$$

and a quarter circle around the branch cut on $\mathbb{C}_{\rm II}$, whose imaginary part can be computed from the residue at infinity

$$\mathrm{Im}\int_{\mathcal{C}_3}\mathrm{d}\tau\omega_K(\tau) = \mathrm{Im}\left(-\frac{i\pi}{2}\operatorname*{Res}_{\tau=\infty}\omega_K(\tau)\right) = -\frac{\pi\tilde{\kappa}}{2}\,. \tag{8.61}$$

We obtain the neat size $|\tilde{F}_R^{(3),\alpha}| \sim e^{-\pi(\mu-\tilde{\kappa})/2}$. We note in passing that it is remarkable to behold the intimate connection between the cosmological collider signal strength, which reflects the amount of kinematic non-analyticities in boundary correlators, and the residue of the dispersion relation at early and late times, which reflects the amount of temporal non-analyticities of the bulk Lagrangian. Completing the Gaussian integral, we then have

$$\begin{aligned}\tilde{F}_R^{(\alpha)} \approx{}& \frac{\sqrt{\pi}\mu^{3/2}e^{-\pi(\mu-\tilde{\kappa})/2}}{K^{3/2}(\tilde{\kappa}+i\mu|\Delta_R|)\sqrt{|\Delta_R|}}e^{i\theta}\exp\left[-\mu\,\arcsin\frac{c_sE_2/K}{\sqrt{1-\tilde{\kappa}^2/\mu^2}}\right.\\ &\left.+\tilde{\kappa}\arctan\frac{c_sE_2\tilde{\kappa}}{K\mu|\Delta_R|} - i\tilde{\kappa}\mathrm{arctanh}\frac{c_sE_2}{K}\right]\,.\end{aligned} \tag{8.62}$$

Combining all found results, we obtain the leading approximation of the local and non-local signals in the edge region

$$\begin{aligned}F_{\rm F} + \text{c.c.} \approx{}& \frac{2\pi\mu^3e^{-\pi(\mu-\tilde{\kappa})/2}}{K^3(\tilde{\kappa}+\mu\Delta_L)[(\tilde{\kappa}^2+\mu^2|\Delta_R|^2)\Delta_L|\Delta_R|]^{1/2}}\\ &\times\exp\left[-\mu\arcsin\frac{c_sE_2/K}{\sqrt{1-\tilde{\kappa}^2/\mu^2}}+\tilde{\kappa}\arctan\frac{c_sE_2\tilde{\kappa}}{K\mu|\Delta_R|}\right]\\ &\times\cos\left[\mu\,\mathrm{arccosh}\frac{c_sE_1/K}{\sqrt{1-\tilde{\kappa}^2/\mu^2}}+\tilde{\kappa}\mathrm{arctanh}\frac{c_sE_R}{K}+\frac{3\pi}{4}+\Omega\right]\,,\end{aligned} \tag{8.63}$$

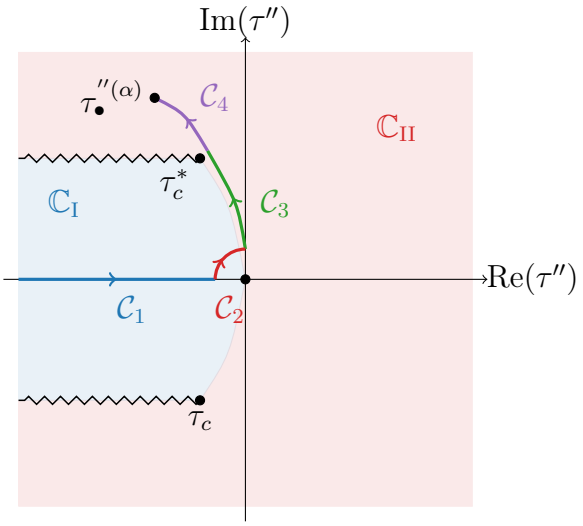


Figure 8.8: Analytic structure of the effective frequency ω_K in the complex τ'' plane to compute $\tilde{F}_R^{(3)}$ in the case of a non-unity sound speed and non-zero chemical potential in the edge region.

where the dephasing function reads

$$\Omega \equiv \tilde{\kappa}\left(\operatorname{arccoth}\frac{c_s E_1}{K} - \operatorname{arctanh}\frac{c_s E_1 \tilde{\kappa}}{K\mu\Delta_L}\right) - \arctan\frac{\tilde{\kappa}}{\mu|\Delta_R|}\,. \tag{8.64}$$

- In the edge region of the kinematics space, the cosmological collider signal has important chemical-potential-dependent corrections. Apart from the overall enhancement, the corrected attenuation factor renders the signal amplitude to smoothly interpolate between $e^{-\pi(\mu-\tilde{\kappa})/2}$ and $e^{-\pi(\mu-\tilde{\kappa})}$ when $c_s E_2/K$ varies from 0 to $\sqrt{1-\tilde{\kappa}^2/\mu^2}$. This corresponds to the shift of the saddle $\tau_\bullet''^{(\alpha)}$ in the imaginary direction.

- The waveform is also corrected by the dephasing function Ω, which tends to a constant in the hierarchical soft limit $c_s E_1/K \to \infty$, $c_s E_2/K \to 0$,

$$\lim_{\substack{c_s E_1/K\to\infty \\ c_s E_2/K\to 0}} \Omega = -\tilde{\kappa}\operatorname{arctanh}\frac{\tilde{\kappa}}{\mu} - \arctan\frac{\tilde{\kappa}}{\sqrt{1-\tilde{\kappa}^2/\mu^2}}\,. \tag{8.65}$$

  Interestingly, in addition to the dephasing function, the waveform acquires a term proportional to the chemical potential (the second term in the second line of (8.63)). With E_1 held fixed, there is an intermediate stage where $E_2 \ll c_s^{-1}$ and the waveform is approximated by

$$F_{\rm F} + \text{c.c.} \supset \exp\left(-c_s\sqrt{\mu^2-\tilde{\kappa}^2}\,\frac{E_2}{K} + \cdots\right)\cos\left(c_s\tilde{\kappa}\,\frac{E_2}{K} + \cdots\right)\,. \tag{8.66}$$

  Consequently, a *new type of cosmological collider signal* arises. Drastically distinct from all other more standard signals above, this new signal oscillates linearly with respect to the momentum ratio E_2/K with a frequency $c_s\tilde{\kappa}$ determined by the sound speed and the chemical potential. Meanwhile, the

amplitude of the oscillations decays exponentially at a rate $c_s\sqrt{\mu^2-\tilde{\kappa}^2}$ which is often comparable to oscillation frequency. Due to its large decay rate, we name this new signal the *transient cosmological collider signal*. Such a transient signal was found previously in the parity-odd sector of non-local EFT description of the same system [363], but without apparent physical interpretation. Here we see clearly that the origin of the transient signal is the curvilinear motion of the saddle point $\tau_\bullet^{''(\alpha)}$ on the complex plane. When the ratio c_sE_2/K increases from nearly zero, the saddle point $\tau_\bullet^{''(\alpha)}$ moves away from τ_c^* and shifts simultaneously in the real and imaginary direction, leading to the damped oscillations in the transient signal. The oscillations stop exponential decaying when $\tau_\bullet^{''(\alpha)}$ hits the negative real axis on the second Riemann sheet $\mathbb{C}_{\rm II}$, which corresponds to the boundary of the edge region where $E_2/K=c_s^{-1}\sqrt{1-\tilde{\kappa}^2/\mu^2}$ and our approximation fails.

- Similar to the previous case, the found result can be derived from direct analytic continuation from that in the interior region, upon utilising the following continuation rules,

$$\begin{aligned}\operatorname{arccosh}\frac{c_sE_2/K}{\sqrt{1-\tilde{\kappa}^2/\mu^2}} &\to -i\arccos\frac{c_sE_2/K}{\sqrt{1-\tilde{\kappa}^2/\mu^2}}\,,\\ \Delta_R &\to -i|\Delta_R|\,,\\ \operatorname{arccoth}\frac{c_sE_2}{K} &\to \operatorname{arctanh}\frac{c_sE_2}{K}+\frac{i\pi}{2}\,.\end{aligned}\tag{8.67}$$

Joint region $c_s^{-1}\sqrt{1-\tilde{\kappa}^2/\mu^2}<E_2/K<c_s^{-1}$. Entering the join region from above, $E_2>K/c_s\to E_2<K/c_s$, the location of $\tau_\bullet^{''(\alpha)}$ switches from $+\infty$ to $-\infty$, while the location of $\tau_\bullet^{''(\beta)}$ changes continuously. In principle, we can run the same reasoning as before and perform the same saddle-point analysis. To avoid technical repetitions, instead of computing the approximate results from scratch, we shall take advantage of the analyticity property we discovered above. The continued results are then checked against the exact results. We observe that the dephasing functions contain singularities at $E_2=K/c_s$ (where $\Delta_R=\tilde{\kappa}/\mu$) for different terms. In Υ, the singularities of two trigonometrical functions cancel out, leaving a straightforward analytic continuation rule

$$\Upsilon\ :\ \begin{cases}\operatorname{arccoth}\dfrac{c_sE_2}{K}\to\operatorname{arctanh}\dfrac{c_sE_2}{K}+\dfrac{i\pi}{2}\\ \operatorname{arctanh}\dfrac{c_sE_2\tilde{\kappa}}{K\mu\Delta_R}\to\operatorname{arccoth}\dfrac{c_sE_2\tilde{\kappa}}{K\mu\Delta_R}+\dfrac{i\pi}{2}\end{cases}.\tag{8.68}$$

In Ξ, the singularities add up, suggesting that the consistent continuation rule is

$$\Xi\ :\ \begin{cases}\operatorname{arccoth}\dfrac{c_sE_2}{K}\to\operatorname{arctanh}\dfrac{c_sE_2}{K}+\dfrac{i\pi}{2}\\ \operatorname{arctanh}\dfrac{c_sE_2\tilde{\kappa}}{K\mu\Delta_R}\to\operatorname{arccoth}\dfrac{c_sE_2\tilde{\kappa}}{K\mu\Delta_R}-\dfrac{i\pi}{2}\end{cases}.\tag{8.69}$$

All other terms remain unchanged.

Part III

Physics at Low Speed & Non-Locality

9

EFT of Inflationary Fluctuations

Cosmology is about observing inhomogeneities and studying their statistical properties. According to the inflationary paradigm, these perturbations emerge from quantum fluctuations of the inflationary fields, which ultimately provide the seeds for small density fluctuations in the late Universe. Remarkably, these fluctuations during inflation can be studied in a systematic manner through the effective field theory (EFT) of inflationary fluctuations, which provides a model-independent framework to study the physics of degrees of freedom that are directly linked to observations, making manifest the implications of symmetries.

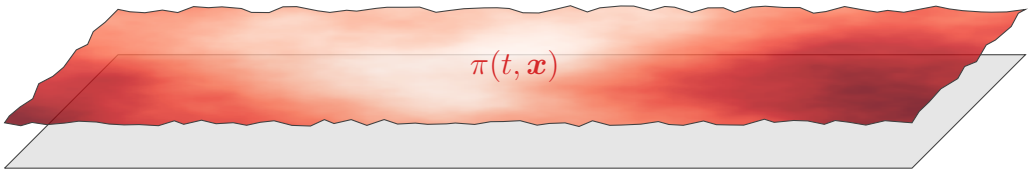


Figure 9.1: Schematic representation of the Goldstone boson of broken time translations $\pi(t, \boldsymbol{x})$ describing scalar fluctuations during inflation, whose effective field theory can be constructed without specifying the underlying inflationary mechanism. These fluctuations of quantum origin ultimately seed the large-scale structure of the Universe.

In this chapter, we first review the standard formulation of the EFT describing a single inflationary fluctuation [470].[1] We then extend this framework by coupling the visible sector to hidden sectors, which include a massive scalar field and a spin-1 particle interacting with a helical chemical potential. Along the way, we establish

[1] Prior to its full development in [470], the general logic of the EFT of inflation was discussed earlier in [471, 472, 473]. An excellent and more comprehensive review may be found in [474]. We will assume that the reader is familiar with the elementary aspects of EFTs in general; for pedagogical introductions we recommend [362, 475, 476].

constraints on the couplings to ensure the theory remains weakly coupled and discuss naturalness.

9.1 Adopting the EFT Philosophy

Adopting an EFT language to describe the physics of inflation has several motivations.

- *Observing fluctuations*: First, we do not have direct experimental access to the mechanism that gives rise to inflation. What we infer through observations is instead the dynamics of the perturbations which, being weakly coupled, provide only limited information about the background physics. The situation is even worse because so far we are only able to probe perturbations most robustly in a narrow range of energies corresponding to wavelengths of the order of the Hubble scale during inflation. Fundamental models of inflation are therefore bound to be hugely degenerate as to their detectable predictions. This invites us to rethink inflation in more agnostic terms, where the homogeneous and isotropic background is taken as given, and instead focus directly on the perturbations. This is the point of view afforded for by the EFT formalism. It is a completely general approach within the context of its minimal assumptions and regime of validity, encompassing in principle *all* models of inflation.

- *Powerful computational and organising principle*: Second, the EFT description serves as a powerful computational and organisational tool. The problems of deriving the Lagrangian for the perturbations from the covariant theory and the identification of the variables of interest (e.g. the adiabatic perturbation) are largely bypassed in the EFT framework. The construction of the EFT proceeds by simply writing the most general Lagrangian for the degrees of freedom of interest and consistent with the symmetries of the system, organised as a series expansion in perturbations and number of derivatives. The truncation of this series is then dictated by the accuracy one seeks to achieve in the calculation of observables, which can be estimated directly if one knows the typical size of the relevant coupling constants and the energy scale of the "experiment". Such description is valid up to a UV cutoff scale, beyond which the UV physics become important. However, at energies below the UV cutoff, higher-order terms in the series expansion become irrelevant as they are suppressed by increasing powers of the UV cutoff. In the end, only a finite number of terms is sufficient to accurately describe the physics of these fluctuations.

- *Physical principles*: Lastly, adopting the EFT perspective provides direct insight into a number of physically important questions. On the one hand, the built-in symmetries of the EFT Lagrangian translate into robust, model-independent relations among observable quantities. The most celebrated example of this type of predictions in the EFT of inflation is the relation between large non-Gaussianities and a reduced speed of sound of the curvature perturbation. Another advantage of the formalism is to make transparent the roles

played by the different scales of interest, allowing one to understand and hence focus on the physics that is relevant at a given energy. An important example is the so-called decoupling limit regime in which the dynamics is well-described by the interactions of Nambu-Goldstone (NG) bosons, with important simplifications that often provide valuable analytical insight. Once again, the EFT description makes it clear that this behaviour is predictable and universal: according to the NG boson equivalence theorem [477, 478, 479], a decoupling limit *must* exist whenever gauge symmetries are broken.

9.2 Constructing the Action for Adiabatic Perturbations

Let us start by deriving the EFT for the observed adiabatic perturbations.[2]

9.2.1 Geometric Construction

Perturbations in inflation propagate in a quasi-de Sitter FLRW background spacetime. This background, or vacuum state, spontaneously breaks the 4-dimensional diffeomorphism group down to its 3-dimensional spatial part. Flat FLRW spacetime enjoys fewer isometries than Minkowski spacetime, breaking boosts and time translations, but preserving rotations and spatial translations.

The task is to determine the most general set of operators built out of the metric tensor—the relevant gauge field during inflation—which respect 3-dimensional spatial diffeomorphism invariance on the constant-time hypersurfaces, as illustrated in Fig. 9.2 with the corresponding geometric objects. This assumes a foliation of spacetime with space-like hypersurfaces, consistent with the physics being described by an FLRW background plus small fluctuations, and we choose cosmic time $t \equiv x^0$ as the parameter of the foliation, so that

$$n_\mu = -(-g^{00})^{-1/2}\delta^0_\mu \,, \tag{9.1}$$

is the future-directed ($n^0 > 0$) unit vector normal to the hypersurfaces. This covariant vector, or alternatively δ^0_μ itself, is invariant under spatial diffeomorphisms, $x^i \to \tilde{x}^i(t, \boldsymbol{x})$, and so it can be used to contract indices of 4-dimensional tensors in order to build singlets. In practice, given any 4-dimensional tensor we can define lower-rank spatially-covariant objects simply by setting one or more of its contravariant indices equal 0. For example g^{00}, R^{00} and $R^{0\mu0\nu}R^0{}_\mu{}^0{}_\nu$ are valid invariant operators. Note that we may choose to take two inequivalent types of covariant derivatives of such tensors, the usual 4-dimensional one and a covariant differentiation in which we ignore the upper 0 indices. This is so because $\Gamma^0_{\mu\nu}$ transforms covariantly under spatial diffeomorphisms.[3] In particular $\partial_\mu g^{00}$ is a valid covari-

[2] This section was originally written by Sebastian Garcia-Saenz and is included in the forthcoming review to which I have contributed.

[3] For example,

$$\nabla_\mu X^{\nu 0} = \partial_\mu X^{\nu 0} + \Gamma^\nu_{\mu\rho}X^{\rho 0} + \Gamma^0_{\mu\rho}X^{\nu\rho}\,, \quad \text{and} \quad \partial_\mu X^{\nu 0} + \Gamma^\nu_{\mu\rho}X^{\rho 0}\,, \tag{9.2}$$

ant object. Using the normal vector n_μ we can define the induced metric on the constant-time hypersurfaces (also called the first fundamental form),

$$h_{\mu\nu} \equiv g_{\mu\nu} + n_\mu n_\nu \,, \tag{9.3}$$

which acts as a projector operator onto the hypersurfaces ($h_{\mu\nu}n^\nu = 0$, $h^\mu{}_\rho h^\rho{}_\nu = h^\mu{}_\nu$), and may also be used to construct spatially-covariant tensors. Most important among these are the geometric objects built out of the induced metric, in particular the covariant derivative D_μ compatible with $h_{\mu\nu}$, which in turn defines the Riemann tensor on the hypersurface via

$$[D_\mu, D_\nu]X^\rho = {}^{(3)}R^\rho{}_{\sigma\mu\nu}X^\sigma \,. \tag{9.4}$$

Equivalently, D_μ and ${}^{(3)}R^\rho{}_{\sigma\mu\nu}$ may be defined in terms of the Christoffel connection constructed out of $h_{\mu\nu}$. We remark that D_μ is actually redundant for our present purposes, since it is easy to show that when acting on any tensor it equals the projection of the 4-dimensional covariant derivative, for example $D_\mu X^\nu = h_\mu{}^\rho h^\nu{}_\sigma \nabla_\rho X^\sigma$. Lastly we have the option to take covariant derivatives of n_μ. When projected onto the hypersurfaces this defines their extrinsic curvature (or second fundamental form),

$$K_{\mu\nu} \equiv D_\mu n_\nu = h_\mu{}^\rho \nabla_\rho n_\nu = \frac{1}{2}\mathcal{L}_n h_{\mu\nu} \,, \tag{9.5}$$

where $\mathcal{L}_n$ denotes the Lie derivative with respect to n^μ. The last equality gives the interpretation of the extrinsic curvature as the rate of change of the induced metric in the direction normal to the hypersurfaces, and also makes manifest that $K_{\mu\nu}$ is symmetric. The covariant derivatives of n_μ may also be contracted with n^μ itself. Note however that $n^\nu \nabla_\mu n_\nu = 0$ and

$$n^\mu \nabla_\mu n_\nu = -\frac{1}{2g^{00}}\, h_\nu{}^\mu \partial_\mu g^{00} \,, \tag{9.6}$$

so that such terms are dispensable as they can be traded for derivatives of g^{00}. It follows therefore that n_μ, and so likewise $h_{\mu\nu}$, need not be used explicitly as it is redundant with δ^0_μ, while all its derivatives are captured by the extrinsic curvature and g^{00} (and derivatives thereof). Note that 3-dimensional tensor densities are also unnecessary since the determinant of h_{ij} can be written as ${}^{(3)}g = g^{00}g$. With $K_{\mu\nu}$ at hand we may also dispense of the 3-dimensional Riemann tensor (or rather the 3-dimensional Ricci tensor, since ${}^{(3)}R^\rho{}_{\sigma\mu\nu}$ is not independent of ${}^{(3)}R_{\mu\nu}$ thanks to the vanishing of the Weyl tensor in three dimensions). Indeed the first Gauss-Codazzi equation,

$${}^{(3)}R_{\rho\sigma\mu\nu} = h_\rho{}^\alpha h_\sigma{}^\beta h_\mu{}^\gamma h_\nu{}^\delta R_{\alpha\beta\gamma\delta} - K_{\rho\mu}K_{\sigma\nu} + K_{\rho\nu}K_{\sigma\mu} \,, \tag{9.7}$$

allows us to write it in terms of the full Riemann tensor and the extrinsic curvature.[4] Finally, the additional options for taking covariant derivatives that we mentioned

are both tensors under spatial diffeomorphisms.

[4]For completeness we also mention the second Gauss-Codazzi equation:

$$D_{[\mu}K_{\nu]}{}^\mu = \frac{1}{2}h^\rho{}_\nu R_{\rho\sigma}n^\sigma \,.$$

This shows that derivatives of the extrinsic curvature are not all independent.

above are also unnecessary since $\Gamma^0_{\mu\nu}$ is not independent of $K_{\mu\nu}$,

$$\Gamma^0_{\mu\nu} = \sqrt{-g^{00}}K_{\mu\nu} - \frac{1}{g^{00}}\delta^0_{(\mu}\partial_{\nu)}g^{00} + \frac{1}{(g^{00})^2}\delta^0_\mu\delta^0_\nu g^{0\rho}\partial_\rho g^{00}\,, \tag{9.8}$$

again provided we include $\partial_\mu g^{00}$ in our basis of covariant objects.

To summarise, a complete set of spatially-covariant tensors is given by all possible 4-dimensional geometric tensors, where we allow every tensor to have free contravariant 0 indices, together with the extrinsic curvature and $\partial_\mu g^{00}$, and covariant derivatives of all these objects. Furthermore, in the Lagrangian each invariant operator may be multiplied by a coefficient that is allowed to be an explicit function of time, so that the most general action describing the EFT of single-field inflation is schematically given by [470]

$$S = \int \mathrm{d}^4x\sqrt{-g}\,F\left(g^{00}, \partial_\mu g^{00}, R_{\mu\nu\rho\sigma}, K_{\mu\nu}; \nabla_\mu; t\right)\,. \tag{9.9}$$

Note that, among all the components of the metric and its inverse, only g^{00} needs to appear explicitly. Let us emphasise that the "basis" of covariant tensors one uses is of course a matter of choice, and different choices may be more suitable for certain applications. For instance, in the context of the EFT of dark energy [480] (which is formally equivalent to the EFT of inflation as discussed here) it is convenient to classify certain higher-derivative operators by using both ${}^{(3)}R_{\mu\nu}$ and $K_{\mu\nu}$ [481].

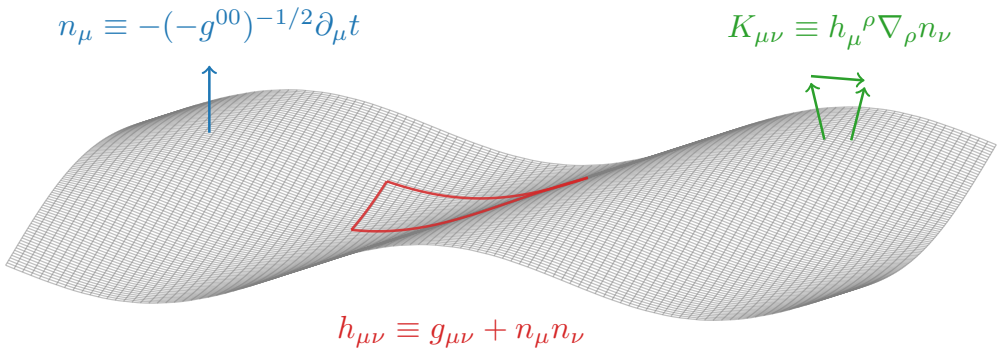


Figure 9.2: Illustration of a constant-time (spacelike) hypersurface parameterised by the cosmic time t with associated geometric objects and their definitions: future-directed unit normal vector n_μ, induced metric $h_{\mu\nu}$, and extrinsic curvature $K_{\mu\nu}$. These objects respect 3-dimensional spatial diffeomorphism invariance.

9.2.2 Tadpole Cancellation

The action (9.9) is actually more general than what we need, as we have only demanded that the hypersurfaces of the foliation be spacelike. Further constraints arise from requiring the theory to admit the FLRW metric as a background solution (assumed here flat for simplicity). This is achieved by imposing tadpole cancellation, i.e. expanding the action in perturbations around this background and asking for the linear terms to vanish.

To this end it is convenient to subtract the background part of the basis tensors, for instance

$$\begin{aligned}\delta g^{00} &\equiv g^{00} - \overline{g}^{00} = g^{00} + 1\,,\\ \delta K_{\mu\nu} &\equiv K_{\mu\nu} - \overline{K}_{\mu\nu} = K_{\mu\nu} - H\overline{h}_{\mu\nu}\,,\\ \delta R_{\mu\nu} &\equiv R_{\mu\nu} - \overline{R}_{\mu\nu} = R_{\mu\nu} - \left[(\dot{H}+3H^2)\overline{h}_{\mu\nu} - 3(\dot{H}+H^2)\delta^0_\mu\delta^0_\nu\right]\,,\end{aligned} \tag{9.10}$$

and note that $\overline{h}_{ij} = a^2\delta_{ij}$, $\overline{h}_{0\mu} = 0$. With these definitions one can then show that the action may be written as [470]

$$\begin{aligned}S = \int \mathrm{d}^4x\sqrt{-g}\,\Big[&\frac{M_{\rm Pl}^2}{2}\left(f(t)R - 2\Lambda(t)\right) - c(t)g^{00}\\ &+F^{(2)}\left(\delta g^{00}, \partial_\mu\delta g^{00}, \delta R_{\mu\nu\rho\sigma}, \delta K_{\mu\nu}; \nabla_\mu; t\right)\Big]\,,\end{aligned} \tag{9.11}$$

where the function $F^{(2)}$ is at least quadratic in the tensors δg^{00}, $\delta R_{\mu\nu\rho\sigma}$ and $\delta K_{\mu\nu}$ and hence does not affect the background equations of motion. In the absence of matter fields (by which we mean, in the present construction, any other field beyond the metric) the function $f(t)$ may be set to one by performing a conformal rescaling, $g_{\mu\nu} \to \frac{1}{f}g_{\mu\nu}$, and an appropriate redefinition of the coefficient functions, in particular $\Lambda(t)$ and $c(t)$, which are anyway arbitrary at this stage. We then expand the action to first order in $\delta g_{\mu\nu}$ and ask for the coefficients of the independent linear terms to vanish. This fixes $\Lambda(t)$ and $c(t)$ as

$$\Lambda(t) = \dot{H} + 3H^2\,, \qquad c(t) = -M_{\rm Pl}^2\dot{H}\,. \tag{9.12}$$

If matter fields are present the function $f(t)$ is of physical importance and one may prefer to work in the Jordan frame as in (9.11). This is often done in the EFT of dark energy and gives rise to additional scalar-tensor couplings in the action; see e.g. [480] for details.

9.2.3 Derivative Expansion

A consistent EFT will in general contain an infinite number of operators of arbitrarily high mass dimension. This means that observables can only be calculated after expanding the Lagrangian in number of derivatives and truncating at some given order. Although in principle one may compute non-perturbative effects in an EFT, in practice one will typically also carry out an expansion in field perturbations, which in inflation is validated by the fact that fluctuations are expected to be weakly coupled.

To zeroth order in derivatives the function $F^{(2)}$ in (9.11) contains

$$F^{(2)} \supset \sum_{n=2}^{\infty}\frac{M_n^4(t)}{n!}(\delta g^{00})^n\,, \tag{9.13}$$

where M_n is an arbitrary time-dependent coefficient of mass-dimension one. Truncated at this order the Lagrangian reproduces the complete theory of perturbations derived from the $P(X,\phi)$ class of covariant scalar models.

At first order in derivatives of the metric and quadratic order in fluctuations one encounters terms such as

$$F^{(2)} \supset -\frac{\bar{M}_1^3}{2}\delta g^{00}\delta K^{\mu}{}_{\mu} - \frac{\bar{M}_2^2}{2}(\delta K^{\mu}{}_{\mu})^2 - \frac{\bar{M}_3^2}{2}\delta K^{\mu\nu}\delta K_{\mu\nu} + \cdots , \tag{9.14}$$

which are of particular interest as they arise in Galileon type models [482] and in the ghost condensate [471, 483, 484]. This is however only a partial list, see e.g. [481] for complete classifications of operators at this order. What we would like to emphasise here is that this way of organising the effective action by counting derivatives of the metric is not necessarily the only one. This is so because there may be additional symmetries protecting certain relations among Wilson coefficients that would otherwise be unnatural. Examples include DBI inflation [485, 486], which enforces a technically natural relation among the M_n scales in (9.13), and a class of Horndeski theories [487, 488, 489] which enjoy a so-called weakly-broken Galileon symmetry [490] (see also [491, 492, 493]), which implies for instance that there exists a technically natural relation between M_2 and $\bar{M}_1$ such that the corresponding operators are of similar importance on an inflationary background.

9.2.4 Stückelberg Procedure

The result (9.11) corresponds to the effective action in the so-called unitary gauge. By construction, the full gauge symmetry of the microscopic theory, i.e. 4-dimensional diffeomorphisms, is explicitly absent. Because we assume that this symmetry will be recovered at high energies, we interpret its breaking in the action (9.11) as arising from a gauge fixing or, equivalently, from the fact that the symmetry breaking is spontaneous rather than explicit. We therefore expect one or more NG bosons to be present in the gauge-invariant description of the EFT. The unitary gauge is by definition the choice of gauge in which the NGs are set to zero. However, a gauge-invariant formulation of a theory is more desirable. Indeed, the NG field will turn out to be directly related to the variable of most interest for the aim of calculating observables, namely the curvature perturbation ζ. Moreover, various sizes of interactions are made explicit. In the case of spontaneously broken gauge theories, as a rule of thumb we will have three different scales: one for the operators that respect the symmetry (let us denote it by Λ_A), one for the ones that break it (denoted Λ_π), and one corresponding to the mass of the gauge bosons (denoted m). It is clear that the gauge-breaking sector will not contain the scale Λ_A, since gauge invariant operators cannot generate gauge-breaking terms, but the converse is not true. Furthermore, it is *a priori* unclear how to combine the scales m and Λ_π to suppress the gauge non-invariant operators. It is an advantage of the formulation of the EFT with explicit NG bosons to elucidate this question of power counting.

Gauge theory analogy. The procedure of restoring gauge invariance by reintroducing the NG fields in a spontaneously broken gauge theory is known as the Stückelberg formalism, see [494] for a review. The method is best illustrated with the simple example of a $U(1)$ gauge theory [495]. The unitary gauge Lagrangian involves only the vector field A_μ. We can undo this gauge fixing by performing the

replacement

$$A_\mu \to A_\mu + \frac{\partial_\mu \pi}{m} \equiv \frac{\mathcal{D}_\mu \pi}{m}\,, \tag{9.15}$$

where the scalar field π is the NG—also called the "Stückelberg fields"—associated to the breaking of the $U(1)$ symmetry. The new Stückelberg Lagrangian is now invariant under the gauge transformation

$$\delta A_\mu = \partial_\mu \alpha\,, \qquad \delta\pi = -m\alpha\,, \tag{9.16}$$

and so must be a function of the invariant building blocks $F_{\mu\nu}$ and $\mathcal{D}_\mu\pi$ (and their derivatives). A technically natural effective Lagrangian is then given by

$$\mathcal{L} = \mathcal{L}_A[F_{\mu\nu}] + \mathcal{L}_\pi[\mathcal{D}_\mu\pi] = \Lambda_A^4 F_A\left(F_{\mu\nu}/\Lambda_A^2; \partial_\mu/\Lambda_A\right) + \Lambda_\pi^4 F_\pi\left(\mathcal{D}_\mu\pi/\Lambda_\pi^2; \partial_\mu/\Lambda_\pi\right)\,. \tag{9.17}$$

Consistency of the EFT requires $m \ll \Lambda_\star \sim \min\{\Lambda_A, \Lambda_\pi\}$ but the ratio between Λ_A and Λ_π is *a priori* arbitrary. From a UV perspective, however, we should have $\Lambda_A \gg \Lambda_\pi$ if the gauge theory is to be weakly coupled at energies above the symmetry breaking scale. The gauge-breaking sector will generically contain gauge invariant terms because $\partial_\mu\mathcal{D}_\nu\pi - \partial_\nu\mathcal{D}_\mu\pi = mF_{\mu\nu}$, so for instance $\mathcal{L}_\pi$ will contain

$$\mathcal{L}_\pi \supset \Lambda_\pi^4 \frac{\mathcal{D}^\rho\pi\mathcal{D}_\rho\pi}{\Lambda_\pi^4}\frac{m^2F^{\mu\nu}F_{\mu\nu}}{\Lambda_\pi^6} \supset \frac{m^4}{\Lambda_\pi^6}A^\rho A_\rho F^{\mu\nu}F_{\mu\nu}\,. \tag{9.18}$$

Whence we see that the operators of the schematic form A^2F^2, which are present in the unitary gauge, are suppressed by the scale Λ_π^3/m^2. This precise ratio would have been far from obvious had we written the Lagrangian directly in the gauge-fixed formalism. The moral is that power counting can be obscure in unitary gauge and it is therefore often advisable to employ the Stückelberg procedure for the purpose of the derivative expansion. It should be clear from the way the field π is introduced that couplings between A_μ and π will be proportional to powers of the scale m. Indeed the leading mixing comes from a relevant quadratic coupling given by

$$\mathcal{L}_\pi \supset -\frac{1}{2}\mathcal{D}^\rho\pi\mathcal{D}_\rho\pi \supset -m\partial^\mu\pi A_\mu\,, \tag{9.19}$$

while higher-dimension operators will be more suppressed by scales of the form $(\Lambda_\pi^n/m)^{1/(n-1)} \gg \Lambda_\pi \gg m$ with $n > 1$. Therefore, the smallest scale controlling the mutual interactions between A_μ and π is $\Lambda_{\rm mix} = m$, and so it follows that all scalar-vector couplings will be negligible at energies $\Lambda_{\rm mix} \ll E \ll \Lambda_\pi$. This is the decoupling limit we had previously advertised, applied here to this simple $U(1)$ model.

It is important to emphasise that in this regime the theory is not necessarily trivial since we may still retain the self-interactions of the NG boson. Indeed, because of the hierarchy $(\Lambda_\pi^n/m)^{1/(n-1)} \gg \Lambda_\pi$, it is consistent to neglect the mutual scalar-vector interactions while keeping the scalar self-couplings sizeable but subleading in the derivative expansion. In practice this can be achieved by taking the formal limit $\Lambda_{\rm mix} \to 0$ in the Lagrangian. Note that in doing so it is crucial to use the Stückelberg formulation of the theory, for otherwise the limit is ill-defined because

the number of degrees of freedom is not maintained (a massive spin-1 particle has three polarisations, a massless one has two). Another way to see this is by noting from (9.16) that π becomes gauge-invariant in the limit $m \to 0$ so that choosing unitary gauge is no longer possible. Regarding the self-interactions of the gauge field A_μ, while in principle we do not need to assume them negligible, it is consistent and often convenient to do so given the hierarchy $\Lambda_A \gg \Lambda_\pi$.

Application to inflation. With these lessons in mind, we are now ready to apply the Stückelberg procedure to the inflationary case. We introduce a Stückelberg field $\pi(t, \boldsymbol{x})$ via the replacement

$$t \to \tilde{t} = t + \pi(t, \boldsymbol{x})\,, \tag{9.20}$$

so that the effective action becomes invariant under the full 4-dimensional diffeomorphism group, provided π also transforms:

$$x^\mu \to \tilde{x}^\mu = x^\mu + \xi^\mu(t, \boldsymbol{x})\,, \quad \pi(t, \boldsymbol{x}) \to \tilde{\pi}(\tilde{t}(t, \boldsymbol{x}), \tilde{\boldsymbol{x}}(t, \boldsymbol{x})) = \pi(t, \boldsymbol{x}) - \xi^0(t, \boldsymbol{x})\,. \tag{9.21}$$

We emphasise that ξ^μ here is not assumed to be infinitesimal. Notice also that, despite its appearance, π is not a true scalar under diffeomorphisms. Because (9.20) (together with $x^i \to \tilde{x}^i = x^i$) has the form of a diffeomorphism, any 4-dimensional scalar in the action (in particular the volume element $\mathrm{d}^4x\sqrt{-g}$ and the curvature scalar R) are unaffected by the Stückelberg replacement. However, this is not true for the perturbation of a scalar about its background part, e.g. $\delta R \to \delta R + \overline{R}(t) - \overline{R}(t + \pi)$. Quantities with free upper 0 indices are replaced according to the usual transformation rule of contravariant tensors, e.g.

$$V^0 \to \frac{\partial(t + \pi)}{\partial x^\mu} V^\mu = \left(\delta^0_\mu + \partial_\mu \pi\right) V^\mu\,. \tag{9.22}$$

The extrinsic curvature on the other hand does not change covariantly upon introducing π, as the Stückelberg replacement represents a change of the spacetime foliation. It is straightforward to work out the replacement rule of K_{ij} from its definition in terms of the metric[5] (note that $K_{0\mu} = 0$ in FLRW coordinates; more generally $K_{\mu\nu} n^\nu = 0$), and while the full expression is rather cumbersome, to linear order in π one finds [63, 474, 496]

$$K_{ij} \to K_{ij} - \partial_i \partial_j \pi + \mathcal{O}(\pi^2)\,. \tag{9.23}$$

Slow-roll inflation and EFT resummation. As a concrete and very simple application let us consider the standard scenario of slow-roll inflation in which the function $F^{(2)}$ in Eq. (9.11) vanishes. The Stückelberg replacement of g^{00} is given by

$$g^{00} \to g^{00} + 2g^{0\mu}\partial_\mu \pi + g^{\mu\nu}\partial_\mu \pi \partial_\nu \pi = -1 - 2\dot{\pi} - \dot{\pi}^2 + \frac{(\partial_i \pi)^2}{a^2} + \cdots\,, \tag{9.24}$$

where the ellipses denote terms proportional to metric perturbations. We will ignore these here for simplicity, although in the next section we shall justify this to be a

[5] See Eq. (9.8) or Ref. [60].

valid approximation. In this event, we may replace the curvature scalar in the Einstein-Hilbert term by its background value, $R = 6\dot{H} + 12H^2$, so as to obtain the Stückelberg action

$$S = \int \mathrm{d}t\mathrm{d}^3x\, a^3 M_{\rm Pl}^2 \Big[3\dot{H}(t) + 6H^2(t) - 3H^2(t+\pi) - 2(1+\dot{\pi})\dot{H}(t+\pi) + \dot{H}(t+\pi)(\partial_\mu \pi)^2 \Big] , \tag{9.25}$$

where $(\partial_\mu \pi)^2 \equiv -\dot{\pi}^2 + \partial_i \pi \partial_i \pi / a^2$. Given a generic function H, this effective action *a priori* includes an infinite series of self-interactions for π. Eq. (9.25) may thus be thought of as a resummation of the perturbative expansion of the EFT. The fact that the NG field enters in a non-linear but resummed form is a general feature of effective theories for spontaneously broken non-abelian symmetries.

Interestingly, the action (9.25) admits an even simpler resummation [497]. Noting that the fourth term may be written as $-2\mathrm{d}H(t+\pi)/\mathrm{d}t$ and integrating by parts one gets

$$S = \int \mathrm{d}t\mathrm{d}^3x\, a^3 M_{\rm Pl}^2 \dot{H}(t+\pi)(\partial_\mu \pi)^2 \, . \tag{9.26}$$

We have also dropped a term proportional to $(H(t+\pi) - H(t))^2$ which is proportional to $\mathcal{O}(\epsilon^2)$, therefore slow-roll suppressed compared to the term depicted in (9.26).

9.2.5 Decoupling Limit

Mixing scales. In order to understand the scales controlling the mixing between the Stückelberg field and the metric fluctuation we start by canonically normalising the fields. Since the Einstein-Hilbert term contains $M_{\rm Pl}^2 R \supset M_{\rm Pl}^2 (\partial_0 \delta g^{00})^2$, we have $\delta g_c^{00} \equiv M_{\rm Pl} \delta g^{00} / \sqrt{2}$. Other operators contributing to this kinetic term (e.g. $M^2 g^{\mu\nu} \partial_\mu \delta g^{00} \partial_\nu \delta g^{00}$) will not affect this as we assume the new physics associated to the UV completion of the EFT enters at a scale parametrically below the Planck scale, i.e. $M \ll M_{\rm Pl}$. The first operator contributing to the kinetic term of π is given by $-c(t) g^{00}$, which contains $\epsilon M_{\rm Pl}^2 H^2 \dot{\pi}^2$ upon introducing the Stückelberg field, so we infer the canonical normalisation of π as $\pi_c \equiv (2\epsilon M_{\rm Pl}^2 H^2)^{1/2} \pi$.

Performing the Stückelberg procedure and expanding the Lagrangian in terms of these canonically normalised variables one finds

$$\begin{aligned} &\int \mathrm{d}^4x \sqrt{-g} \Big[- M_{\rm Pl}^2 \Lambda(t) - c(t) g^{00} \Big] \\ &\to \frac{1}{2} \int \mathrm{d}t\mathrm{d}^3x\, a^3 \Big[\dot{\pi}_c^2 - \frac{(\partial_i \pi_c)^2}{a^2} - \sqrt{\epsilon} H \delta g_c^{00} \dot{\pi}_c + \cdots \Big] . \end{aligned} \tag{9.27}$$

From this expression we infer that the mixing between the metric fluctuation $\delta g^{\mu\nu}$ and the NG boson π is controlled by the scale $\Lambda_{\rm mix} \equiv \sqrt{\epsilon} H$. Since $\delta g_c^{00} \dot{\pi}_c$ is a relevant operator, it becomes unimportant at energies $E \gtrsim \Lambda_{\rm mix}$.

What about irrelevant operators? These terms are instead unimportant at energies below the scale that suppresses them. Consider for concreteness a coupling of the form $(\delta g^{00})^m \dot{\pi}^n$ with $m + n > 2$ and assume for simplicity that all the scales M_n as well as $\epsilon^{1/4} (M_{\rm Pl} H)^{1/2}$ are of the same order, i.e. of order $(M_{\rm Pl} \Lambda_{\rm mix})^{1/2}$. The

suppression scale of this operator is then $\left(M_{\rm Pl}^{m+n-2}\Lambda_{\rm mix}^{n-2}\right)^{1/(m+2n-4)}$. This is arbitrarily large provided we take $M_{\rm Pl}$ to be much greater than all scales of interest in the theory, so that once again these interactions mixing π and gravity may be neglected. Similar conclusions may be shown to apply for other mixings arising from operators of higher order in the derivative expansion as well as for terms coming from time derivatives of the Wilson coefficients (or H) which we assume to be slow-roll suppressed. In practice, therefore, we may get rid of mixings between gravity and the Goldstone boson π by taking the formal limit $M_{\rm Pl} \to \infty$ and $\epsilon \to 0$ with the product $\epsilon M_{\rm Pl}^2 H^2$ kept fixed. The latter condition ensures, as we will see, that the self-interactions of π do not become trivial in the decoupling limit.

ADM analysis. We may verify the above argument by explicitly integrating out the auxiliary components of the metric fluctuation. The calculation is most conveniently done using the ADM parametrisation of the metric [498],

$$\mathrm{d}s^2 = -N^2\mathrm{d}t^2 + h_{ij}(\mathrm{d}x^i + N^i\mathrm{d}t)(\mathrm{d}x^j + N^j\mathrm{d}t)\,, \tag{9.28}$$

where N is the lapse function and N^i is the shift vector. A convenient gauge fixing is given by the choice $h_{ij} = a^2(\delta_{ij} + \gamma_{ij})$, i.e. the spatially flat gauge, where γ_{ij} is a tensor perturbation and we ignore vector-type fluctuations for simplicity.

The effective action is again expanded in perturbations, where we write $N = 1+\alpha$ and $N^i = \partial^i\theta$ (note that spatial indices are raised with the 3-dimensional metric h_{ij}). Working at quadratic order in fluctuations one finds that α and θ are indeed auxiliary, i.e. they appear without time derivatives in the action. One may therefore solve for them from their equations of motion and substitute back in the Lagrangian without modifying the dynamics. At linear order the result is

$$\alpha = \epsilon H\pi\,, \qquad \partial^2\theta = -\epsilon H\left(\dot\pi - \epsilon H\pi\right)\,. \tag{9.29}$$

If we now imagine plugging this back into the action and canonically normalising the fields, we see that the gravity-π couplings produce self-interactions for the NG which are always suppressed by at least a factor of $\sqrt{\epsilon}$ relative to the ones coming from the π sector. Interactions with the tensor mode γ_{ij} by construction only appear at cubic and higher orders and are therefore suppressed by extra powers of $M_{\rm Pl}$. This argument shows, now without ambiguities related to field redefinitions, gauge freedom and auxiliary variables, that the decoupling limit is indeed obtained by taking $M_{\rm Pl} \to \infty$ and $\epsilon \to 0$.

Before proceeding to discuss the non-linearities of π in the decoupling regime, let us mention an important aspect of the decoupling limit, namely that π only becomes exactly massless in this limit. Upon substituting α and θ back into the Lagrangian one finds, at quadratic order in fluctuations and at next-to-leading order in slow-roll,

$$S_\pi = \int \mathrm{d}t\mathrm{d}^3x\, a^3\epsilon M_{\rm Pl}^2 H^2\left[\dot\pi^2 - \frac{(\partial_i\pi)^2}{a^2} + 3\epsilon H^2\pi^2 + \cdots\right], \tag{9.30}$$

so that π has a "mass" given by $m_\pi^2 = -3\epsilon H^2$. One might worry that $m_\pi^2 < 0$, which in standard QFT would signal an instability. However, in this case, we would interpret the "particle" as having a Compton wavelength that is larger than the Hubble horizon.

Action in the decoupling limit. Let us now consider the strict decoupling limit, $M_{\rm Pl} \to \infty$ and $\epsilon \to 0$, with $\epsilon M_{\rm Pl}^2$ held fixed. All other scales entering in the effective action, such as the M_n, are also assumed finite in this limit. We may verify explicitly that the resulting π dynamics is not trivial, i.e. that π cannot be gauged away anymore and that it retains some self-interactions. A calculation of the effective action up to fourth order in perturbations and first order in derivatives yields the result

$$\begin{aligned} S_\pi = \int \mathrm{d}t \mathrm{d}^3x\, a^3 \frac{\epsilon M_{\rm Pl}^2 H^2}{c_s^2} \Bigg[\dot\pi^2 - c_s^2 \frac{(\partial_i \pi)^2}{a^2} - (1-c_s^2) \left(\dot\pi \frac{(\partial_i\pi)^2}{a^2} + \frac{A}{c_s^2} \dot\pi^3 \right) \\ + (1-c_s^2) \left(\frac{1}{4} \frac{(\partial_i\pi)^4}{a^4} + \left(1 + \frac{3A}{2c_s^2} \right) \dot\pi^2 \frac{(\partial_i\pi)^2}{a^2} + \frac{B}{c_s^4} \dot\pi^4 \right) + \cdots \Bigg] . \end{aligned} \tag{9.31}$$

Note that this neglects the time variation of the coefficients and we defined

$$\begin{aligned} \frac{1}{c_s^2} &\equiv 1 + \frac{2M_2^4}{\epsilon M_{\rm Pl}^2 H^2} , \\ \frac{A}{c_s^2} &\equiv -1 + \frac{2}{3} \left(\frac{M_3}{M_2} \right)^4 , \\ \frac{B}{c_s^4} &\equiv \frac{1}{4} - \left(\frac{M_3}{M_2} \right)^4 + \frac{1}{3} \left(\frac{M_4}{M_2} \right)^4 , \end{aligned} \tag{9.32}$$

in terms of the scales M_n introduced in Eq. (9.13). The rationale for factoring out a power of c_s^2 in these parameters is that it is A and B, rather than the combinations A/c_s^2 and B/c_s^4, which receive order-one quantum corrections upon renormalisation, see e.g. [64].

From the result (9.31) we discover that, in the strict decoupling limit or equivalently to leading order in the slow-roll approximation, the scalar action S_π becomes invariant under the shift symmetry $\pi \to \pi + c$. This property is easy to understand: in the limit of exact dS the background part of the action (9.11) is invariant under time translations, and so it is consistent to impose this symmetry on the dynamics of the perturbations [470], i.e. we may choose all the coefficients M_n and so on as time independent, and thus upon performing the Stückelberg procedure the field π will always appear differentiated. We remark that this shift symmetry is unrelated to the gauge symmetry of the full Stückelberg action; although the global part of (9.21) does shift π, here neither the coordinates nor the metric are being transformed. Moreover, the action (9.31) is not gauge invariant: after taking the decoupling limit, π has turned into a scalar field propagating on a fixed quasi-dS background; the diffeomorphism symmetry is present only in the gravitational sector, which thus reduces in this limit to standard Einstein gravity plus higher-derivative corrections, all in close analogy with the $U(1)$ gauge theory example discussed previously. The coefficient c_s^2 is of special interest and corresponds to the squared "speed of sound" of the π quanta.

Let us also mention that there exists an alternative to the decoupling limit we have discussed so far. This is the limit of exact dS, i.e. $\epsilon \to 0$, but with $M_{\rm Pl}$ kept finite. We see that this implies that the speed of sound goes to zero maintaining a

finite ratio ϵ/c_s^2 (provided $M_2 \neq 0$). In this situation π loses its standard gradient term $\propto (\partial_i\pi)^2$ and thus "dispersive" terms $\propto (\partial_i^2\pi)^2$, arising from operators such as those in Eq. (9.14), become relevant. This corresponds to the regime of Ghost Inflation [483].

Turning to the cubic operators in Eq. (9.31), we observe that they are multiplied by $(1-c_s^2)$ and hence vanish when $M_2 = 0$, as is the case of vanilla-type models of inflation driven by a scalar field with standard kinetic term. In this context the leading cubic interactions arise from operators that are slow-roll suppressed, omitted in (9.31), implying a very small bispectrum of scalar fluctuations, $f_{\rm NL} = \mathcal{O}(\epsilon)$. However this is not true as soon as $c_s^2 < 1$ and in fact one finds in general $f_{\rm NL} = (1-c_s^{-2})\,\mathcal{O}(1)$, which can be significantly large if c_s^2 is small. It is worth emphasising that this result is universal since the operator $\propto \dot\pi(\partial_i\pi)^2$ does not have an independent Wilson coefficient in front, as $\dot\pi^3$ does, and hence cannot be tuned to zero. This unambiguous prediction of a large bispectrum in fact generalises to all higher point correlation functions and is one of the celebrated successes of the EFT formalism.

9.3 From Fluctuations to Observables

After constructing the action for the Goldstone boson π, it is crucial to link it with observables for the EFT to be predictable and useful in practice.

9.3.1 Scalar Power Spectrum: from π to ζ

Let us next explain the relationship between the Goldstone boson π and the comoving curvature perturbation ζ. The calculation is most straightforwardly done by considering two gauges [42]: the spatially flat gauge

$$g_{ij} = a^2\delta_{ij}\,, \qquad \pi \neq 0\,, \tag{9.33}$$

and the comoving or ζ-gauge

$$g_{ij} = a^2 e^{2\zeta}\delta_{ij}\,, \qquad \pi = 0\,. \tag{9.34}$$

Going from the first gauge to the second amounts to performing a time reparametrisation $t \to \tilde t = t + \xi(t,\boldsymbol{x})$ such that

$$\zeta(t,\boldsymbol{x}) = \log\left(\frac{a(t+\xi(t,\boldsymbol{x}))}{a(t)}\right)\,, \quad \text{with} \quad \pi(t+\xi(t,\boldsymbol{x}),\boldsymbol{x}) + \xi(t,\boldsymbol{x}) = 0\,. \tag{9.35}$$

This equation implicitly determines ξ in terms of π. Beyond linear order, a spatial diffeomorphism is also requires for the mapping, but its effect is negligible when all modes are well outside the horizon. Solving for π to second order, one obtains

$$\zeta = -H\pi + H\pi\dot\pi + \frac{\dot H}{2}\pi^2 + \mathcal{O}(\pi^3)\,. \tag{9.36}$$

At linear level and leading order in slow-roll we thus obtain the simple proportionality relation $\zeta \simeq -H_\star \pi$, where H is evaluated at sound horizon crossing for concreteness, i.e. $k = (aH/c_s)_\star$. This relationship is easy to understand intuitively [63]: on super-horizon scales ζ quantifies the relative expansion among separate unperturbed FLRW universes while π measures the time delay among these universes, implying that $\zeta \simeq -H\pi$ in the dS limit (the minus sign is due to the definition of π). Beyond linear order in perturbations and at next-to-leading order in slow-roll we see that the conservation of ζ, i.e. $\dot{\zeta} = 0$ in the super-horizon limit, does *not* translate into the constancy of π. In other words, π evolves on super-horizon scales and therefore cannot be interpreted as an exactly massless field. This is in precise agreement with the fact that the effective action includes mass-like terms for the Goldstone boson beyond the strict decoupling limit.

At leading order we then have a very simple relation between the power spectra of ζ and the NG π: $\mathcal{P}_\zeta = H_\star^2 \mathcal{P}_\pi$. From the effective action of Eq. (9.31) a standard calculation yields the well-known result

$$\mathcal{P}_\zeta = \frac{1}{8\pi^2 \epsilon_\star c_{s\star}} \left(\frac{H^2}{M_{\rm Pl}^2} \right)_\star . \tag{9.37}$$

9.3.2 Graviton Power Spectrum

The power spectrum of primordial tensor modes, i.e. gravitational waves, famously fixes the ratio between the Hubble scale during inflation and the Planck mass [41]. This robust and model-independent prediction of inflation means that a detection of a primordial stochastic background of gravitational waves would ultimately determine the scale of inflation. Using the ADM parametrisation of the metric (9.28), tensor fluctuations are described as $h_{ij} = a^2(\delta_{ij} + \gamma_{ij})$ with $\gamma_{ii} = 0$ (traceless) and $\partial_i \gamma_{ij} = 0$ (transverse). The field $\gamma_{ij}(t, \boldsymbol{x})$ describes the graviton two degrees of freedom. Inserting this decomposition in the usual Einstein-Hilbert action and keeping only terms quadratic in γ, we obtain

$$S = \frac{M_{\rm Pl}^2}{8} \int {\rm d}^4x \sqrt{-g} \left[\dot{\gamma}_{ij}^2 - \frac{(\partial_k \gamma_{ij})^2}{a^2} \right] . \tag{9.38}$$

Note that the γ_{ij} field is dimensionless. Naturally, the field $\gamma_{ij}(t, \boldsymbol{x})$ can be expanded in plane waves with corresponding polarisation tensors as

$$\gamma_{ij}(t, \boldsymbol{x}) = \int \frac{{\rm d}^3k}{(2\pi)^3} \sum_{\lambda=\pm} \varepsilon_{ij}^\lambda \gamma_{\boldsymbol{k}}^\lambda \, e^{i\boldsymbol{k}\cdot\boldsymbol{x}} , \tag{9.39}$$

where $\varepsilon_{ij}^\lambda = k^i \varepsilon_{ij}^\lambda = 0$ and $\varepsilon_{ij}^\lambda \varepsilon_{ij}^{\lambda'} = 2\delta_{\lambda\lambda'}$. Each polarisation mode $\gamma_{\boldsymbol{k}}^\lambda$ has the equation of motion of a massless scalar field. The solution is similar to that for scalar fluctuations, except the important difference being the overall amplitude (the relation to the canonically normalised field does not depend on ϵ). In simple terms, at linear order, tensor fluctuations are not sensitive to the symmetry breaking of the background evolution. In particular, the modes $\gamma_{\boldsymbol{k}}^\lambda$ being massless, they become

constant after horizon crossing and therefore survive after inflation. The graviton power spectrum from the Einstein-Hilbert action is given by [4]

$$\langle \gamma^{\lambda}_{\boldsymbol{k}_1} \gamma^{\lambda'}_{\boldsymbol{k}_2} \rangle = (2\pi)^3 \delta^{(3)}(\boldsymbol{k}_1 + \boldsymbol{k}_2) \frac{1}{k^3} \left(\frac{H^2}{M_{\rm Pl}^2} \right)_\star \delta_{\lambda\lambda'} \,, \tag{9.40}$$

where $\star$ denotes that the quantity is evaluated at horizon crossing. The dimensionless power spectrum of tensor modes is given by

$$\mathcal{P}_t = \frac{2}{\pi^2} \left(\frac{H^2}{M_{\rm Pl}^2} \right)_\star \,, \tag{9.41}$$

where the factor 2 accounts for the sum over polarisation modes.

Scale of inflation. Observational constraints on primordial tensor modes are usually expressed in terms of its relative amplitude compared to scalar fluctuations. It is therefore customary to define the tensor-to-scalar ratio

$$r = \frac{\mathcal{P}_t}{\mathcal{P}_\zeta} = 16 \, (\epsilon c_s)_\star \,, \tag{9.42}$$

where its expression follows from (9.37) and (9.41). Since the amplitude of scalar fluctuations have been measured on large scales, the quantity r quantifies the size of tensor fluctuations. Using Eq. (9.41) and $\mathcal{P}_\zeta(k_\star) = 2.2 \times 10^{-9}$ [499], the Hubble scale during inflation is found to be

$$H_\star = 3 \times 10^{-5} \left(\frac{r}{0.1} \right)^{1/2} M_{\rm Pl} \,. \tag{9.43}$$

As of 2025, there has been no detection of primordial tensor modes. We have the upper bound $r < 0.036$ (at $k_\star = 0.05\,\text{Mpc}^{-1}$ and at 95% confidence level) from latest combined BICEP/Keck/Planck data [500]. Combined with BICEP2/Keck Array BK15 data, the *Planck* observational bound is $r < 0.056$ (at $k_\star = 0.002\,\text{Mpc}^{-1}$ and at 95% confidence level) [499].

Speed of sound. The action (9.38) describes the completely standard and minimal dynamics of gravitons. In fact, this form of the quadratic action is hard to modify or extend, contrary to the scalar sector. For example, working in the unitary gauge where inflaton perturbations are set to zero, the leading correction to the Einstein-Hilbert action can be written as

$$S = \frac{M_{\rm Pl}^2}{2} \int \mathrm{d}^4x \sqrt{-g} \left[R + \hat{M}_2^2(t) (\delta K^{\mu\nu} \delta K_{\mu\nu} - \delta K^2) \right] \,. \tag{9.44}$$

The precise combination $\delta K^{\mu\nu} \delta K_{\mu\nu} - \delta K^2$ does not change the sound speed of scalar fluctuations. However, this correction leads to a non-luminal speed of sound for the gravitons

$$S = \frac{M_{\rm Pl}^2}{8} \int \mathrm{d}^4x \sqrt{-g} \frac{1}{c_\gamma^2} \left[\dot{\gamma}_{ij}^2 - c_\gamma^2 \frac{(\partial_k \gamma_{ij})^2}{a^2} \right] \,, \quad \text{with} \quad c_\gamma^{-2} = 1 + \frac{2\hat{M}_2^2}{M_{\rm Pl}^2} \,. \tag{9.45}$$

Nevertheless, as discussed in [501], the sound speed c_γ can always be set to unity by the following suitable redefinitions of the metric:

$$g_{\mu\nu} \to g_{\mu\nu} + \left(1 - c_\gamma^2\right) n_\mu n_\nu \,, \quad \text{then} \quad g_{\mu\nu} \to c_\gamma^{-1} g_{\mu\nu} \,. \tag{9.46}$$

The first redefinition corresponds to a disformal transformation that leaves the shift vector N^i and h_{ij} unchanged but rescales the lapse function N. This essentially restores on equal footing the time and the spatial kinetic term of the graviton, and the speed of sound only appears as an overall normalisation of the action. The second conformal transformation restores the standard normalisation by going to the Einstein frame.[6] As such, the power spectrum of tensor modes cannot be modified at leading order in derivatives, and its detection unambiguously fixes the Hubble scale during inflation.

9.3.3 Scales of Inflation

Determining the regime of validity of an EFT requires one to understand the energy scales that control the dynamics at both the classical and quantum levels. An insightful discussion on the scales of inflation is given in [502] (see also [64, 503]) which we summarise in Fig. 9.3 and below.

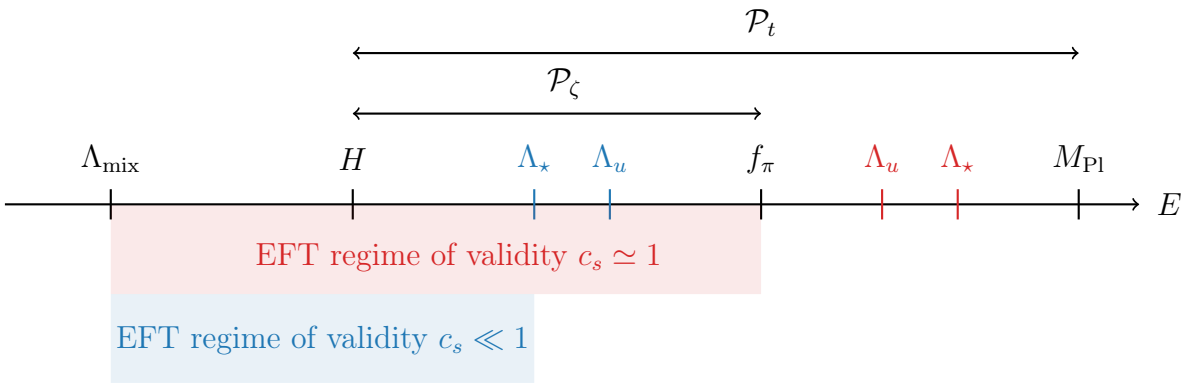


Figure 9.3: Illustration of the scales of inflation in the case $c_s \simeq 1$ and in scenarios with reduced speed of sound $c_s \ll 1$. Below $\Lambda_{\rm mix} \equiv \sqrt{\epsilon} H$, mixing between the Stückelberg field π and dynamical gravity, i.e. metric fluctuations, cannot be neglected. Above f_π, invariance under time diffeomorphisms is restored. The scalar power spectrum controls the hierarchy between the Hubble scale H and the symmetry breaking scale f_π while the tensor power spectrum determines the energy scale of inflation in terms of the Planck mass.

- *Symmetry breaking scale* f_π: At energies above f_π the invariance under time diffeomorphisms becomes unbroken.[7] Since it is the background that is re-

[6] Notably, since disformal and conformal transformations change the way fields are coupled to the metric, restoring $c_\gamma = 1$ induces corrections to the scalar sector. However, such changes do not enter in the predictions of inflation, i.e. it redefines the speed of sound for scalar fluctuations which cannot be disentangled from the slow-roll parameter from the power spectrum measurement.

[7] The notation f_π is meant to emphasise the analogy with the role played by the "pion decay constant" in the Standard Model chiral Lagrangian.

sponsible for the symmetry breaking, it is intuitive that fluctuations of frequency/wavelength much shorter than those characterising the background should be insensitive to the breaking of the symmetry. Applying this logic to the EFT of inflation one finds

$$f_\pi^4 = 2\epsilon c_s H^2 M_{\rm Pl}^2 \,. \tag{9.47}$$

Two useful checks can be made to see that this result is sensible. First we may consider the simplest scenario of slow-roll inflation driven by a scalar field ϕ. In this case, $c_s = 1$ and $f_\pi^4 = 2\epsilon H^2 M_{\rm Pl}^2 = \dot{\overline{\phi}}^2$, in agreement with the expectation that the breaking of time translations is produced by the "clock" defined by the background field. Second, the scalar power spectrum may be expressed in terms of f_π as $\mathcal{P}_\zeta \sim (H/f_\pi)^4$. In the simplest single-field slow-roll scenario, we find $f_\pi \simeq 60H$. We thus see that cosmological perturbation theory can only be trusted when the "energy of the experiment" H is smaller than f_π, again in accordance with our intuition.

- *Strong coupling scale* $\Lambda_\star$: This is the scale at which the theory becomes strongly coupled. That this must occur at some scale is simply a consequence of the fact that EFTs are non-renormalisable, i.e. they include irrelevant interactions whose importance grows with energy. As the energy approaches $\Lambda_\star$ an infinite set of operators in the effective action become important and so perturbative control is lost. The strong coupling scale may therefore be identified by the scale that suppresses the leading irrelevant operators in the effective action. For the EFT of inflation this turns out to be

$$\Lambda_\star^4 = 2\epsilon H^2 M_{\rm Pl}^2 c_s^5 (1 - c_s^2)^{-2} \,. \tag{9.48}$$

For $c_s \simeq 1$, this is parametrically larger than the symmetry breaking scale f_π, but the hierarchy is reversed in scenarios with reduced speed of sound.

- *Unitarity scale* Λ_u: A closely related scale, which may be alternatively used to define the cutoff for the regime of validity of the EFT, is the unitarity scale Λ_u, that is the energy at which scattering amplitudes computed from a given interaction violate perturbative unitarity. For the cubic operators in the EFT of inflation this is

$$\Lambda_u^4 = \frac{24\pi}{5}(1 - c_s^2)\Lambda_\star^4 \,. \tag{9.49}$$

We see that this is similar to $\Lambda_\star$ in models with reduced speed of sound, while for $c_s \simeq 1$ it is again parametrically above the background scale f_π.

- *Scale of new physics* $\Lambda_{\rm new}$: The cutoff scale, corresponding to the limit of validity of the EFT, is given by the smallest among the scales f_π, $\Lambda_\star$ and Λ_u. In reality however the EFT may cease to serve as an accurate description of the physical system at energies far below this scale. This will be the case if "new physics" starts to play a role above some scale $\Lambda_{\rm new} \ll \Lambda_{\rm cutoff}$ characterising the change in the physical description. Such "new physics" may be due to heavy degrees of freedom becoming active (as for example the massive gauge bosons

in Fermi theory) or to a modification in the dynamics of the light fields that results in the cutoff scale being raised (for instance a change in the dispersion relation).

When this happens, the EFT admits a UV completion by a weakly coupled theory, as opposed to entering a strongly coupled regime when no such "new physics" occurs below the cutoff scale. Notice that, unlike the scales f_π, $\Lambda_\star$ and Λ_u which are calculable within the EFT and thus define the regime of self-consistency of the theory, the scale $\Lambda_{\rm new}$ is completely determined by the UV completion and is *a priori* unknown.

9.4 Additional Hidden Sectors

The previous section reviewed an EFT for a single scalar dynamical degree of freedom coupled to gravity. As we explained, this set of variables is the most minimal one required to describe the physics of inflation, and is universal in the sense that these fields (the Goldstone boson of broken time translations π and the graviton γ_{ij}) are guaranteed to be present as follows from the general principles of EFT and symmetry breaking. Obviously, however, they need not be the only fields in the theory. Certainly, and again following the general EFT logic, there will be additional *heavy* fields, with masses $m \sim H$, associated to the new physics responsible for the UV completion of the theory.

Additional light fields. Before coupling the visible sector to a massive hidden one, it is worth emphasising that the EFT of inflationary fluctuations may well be extended to include additional *light* fields with masses $m \lesssim H$, whose dynamics is fully described within the EFT without reference to the UV completion of the theory. These fields can be classified into three types: (i) Nambu-Goldstone fields as, in the case of spontaneous breaking of spacetime symmetries, there is no one-to-one correspondence between the Goldstone fields and the broken symmetries (unlike for internal symmetries), (ii) matter fields, referring to any field with a vanishing vacuum expectation value, (iii) gauge fields, which appear if the broken symmetries are local.[8]

In what follows, we will couple the Goldstone boson of broken time translations to a massive scalar field σ, and a spin-1 massive field coupled to a helical chemical potential σ_μ. These two hidden sectors will be extensively studied in the remaining chapters of the thesis.

9.4.1 Massive Scalar Field

We are interested in coupling the adiabatic mode π to an additional massive scalar degree of freedom σ which may have significant self-interactions. We consider the

[8] In fact, in the presence of gauge fields, one can dispense of the Goldstone fields altogether by choosing the unitary gauge, in which case the gauge fields carry additional degrees of freedom, i.e. they "eat" the Goldstone bosons and become "massive".

Lagrangian up to dimension-4 operators for the σ-sector

$$\mathcal{L}_\sigma/a^3 = -\frac{1}{2}(\partial_\mu\sigma)^2 - \frac{1}{2}m^2\sigma^2 - \mu\sigma^3\,. \tag{9.50}$$

At cubic order, the σ self-interactions are completely characterised by μ.

Mixing interactions. Our interest is the coupling between the two sectors, both converting intrinsic non-linearities of σ to the π sector via a quadratic mixing, and generating non-linear interactions amongst them. In the unitary gauge, we consider the following mixing action

$$S_{\pi\sigma} = -\int \mathrm{d}^4x\sqrt{-g}\left[\tilde{M}_1^3(t)\delta g^{00}\sigma + \tilde{M}_2^2(t)\delta g^{00}\sigma^2 + \tilde{M}_3^3(t)\left(\delta g^{00}\right)^2\sigma + \dots\right], \tag{9.51}$$

where $\tilde{M}_{1,2,3}$ are some—in general time-dependent—mass scales. The most general mixing operators are of the form $(\delta g^{00})^m\,\mathcal{O}_n$ where $\mathcal{O}_n$ is an operator of dimension n function of the following combinations: σ, $g^{0\mu}\partial_\mu\sigma$ and $g^{\mu\nu}\partial_\mu\partial_\nu\sigma$. These operators have been fully classified in [265] up to dimension-6 operators. Note that we do not impose additional symmetries on the σ field to make it naturally light because we will be mostly interested in the cases where σ is (effectively) heavier than the Hubble scale. Theories with additional symmetries imposed on the σ-sector have been treated in [504]. Taking the decoupling limit and introducing π, the theory up to cubic interactions reads

$$\mathcal{L}_{\pi-\sigma}/a^3 = 2\tilde{M}_1^3\dot{\pi}\sigma + \tilde{M}_1^3(\partial_\mu\pi)^2\sigma + 2\tilde{M}_2^2\dot{\pi}\sigma^2 - 4\tilde{M}_3^3\dot{\pi}^2\sigma\,. \tag{9.52}$$

Similarly to the π-sector treated previously, we note that the Wilson coefficient of the $(\partial_i\pi)^2\sigma$ operator is completely fixed by the $\dot{\pi}\sigma$ operator that appears in the quadratic Lagrangian, again a consequence of the fact that π non-linearly realises time diffeomorphisms.

Full theory. Up to cubic order including self-interactions in the π-sector, the complete Lagrangian for the coupled π-σ system is then

$$\begin{aligned}\mathcal{L}/a^3 = &-\frac{1}{2}\left[-\dot{\pi}_c^2 + c_s^2\frac{(\partial_i\pi_c)^2}{a^2}\right] - \frac{1}{2}\left[(\partial_\mu\sigma)^2 + m^2\sigma^2\right] + \rho\dot{\pi}_c\sigma \\ &- \lambda_1\dot{\pi}_c\frac{(\partial_i\pi_c)^2}{a^2} - \lambda_2\dot{\pi}_c^3 - \mu\sigma^3 - \frac{1}{2}\alpha\dot{\pi}_c\sigma^2 - \frac{1}{2\Lambda_1}\frac{(\partial_i\pi_c)^2}{a^2}\sigma - \frac{1}{2\Lambda_2}\dot{\pi}_c^2\sigma\,,\end{aligned} \tag{9.53}$$

where we have defined the canonically normalised field $\pi_c^2 = c_s^{-3}f_\pi^4\,\pi^2$ with $f_\pi^4 \equiv 2M_{\rm pl}^2|\dot{H}|c_s$ being the symmetry breaking scale, and redefined the coupling constants

$$\begin{aligned}&\rho \equiv 2c_s^{3/2}\frac{\tilde{M}_1^3}{f_\pi^2}, \quad \lambda_1 \equiv c_s^{3/2}\frac{c_s^2-1}{2f_\pi^2}, \quad \lambda_2 \equiv -\frac{c_s^{3/2}}{2f_\pi^2}\left[1 - c_s^2 - \frac{8}{3}\frac{M_3^4}{f_\pi^4}c_s^3\right], \\ &\alpha \equiv -4c_s^{3/2}\frac{H^2}{f_\pi^2}\,\tilde{\alpha}^2, \quad \Lambda_1^{-1} \equiv c_s^{3/2}\frac{\rho}{f_\pi^2}, \quad \Lambda_2^{-1} \equiv c_s^{3/2}\frac{\tilde{\rho}}{f_\pi^2}\,,\end{aligned} \tag{9.54}$$

with $\tilde{\alpha} = \frac{\tilde{M}_2}{H}$ and $\tilde{\rho} = 8c_s^{3/2}\frac{\tilde{M}_3^3}{f_\pi^2} - \rho$. These couplings have mass dimensions $[\Lambda_{1,2}] = [\mu] = [\rho] = 1, [\alpha] = 0$, and $[\lambda_{1,2}] = -2$. As we will see in Chap. 15, the couplings $\rho, \tilde{\rho}$ and $\tilde{\alpha}$ enter in the genuine typical size of each contribution to the dimensionless shape function of the bispectrum in the case $c_s = 1$. Both ρ and Λ_1 are correlated since they are determined by the same parameter $\tilde{M}_1$, which is a consequence of the non-linearly realised time-diffeomorphism invariance. Similarly, M_2 governs both the Goldstone boson sound speed c_s and λ_1. Note that there is a priori no model-building requirement on the size of the quadratic coupling ρ/H, and we crucially allow this mixing parameter to be order one or larger, which we call the strong mixing regime.

9.4.2 Spin-1 Helical Field

Let us now introduce a massive vector field σ_μ with a chemical potential that breaks parity, hence leaving distinctive signatures in cosmological correlators.

Unitary gauge. In the unitary gauge, we take the action for the spin-1 massive field to be of Proca type supplemented by a Chern-Simons term

$$S_\sigma = \int \mathrm{d}^4x\sqrt{-g}\left[-\frac{1}{4}F_{\mu\nu}^2 - \frac{m^2}{2}\sigma_\mu^2 + \frac{\kappa t}{4}F_{\mu\nu}\tilde{F}^{\mu\nu}\right], \tag{9.55}$$

where $\tilde{F}^{\mu\nu} = \mathcal{E}^{\mu\nu\alpha\beta}F_{\alpha\beta}$ with $\mathcal{E}^{\mu\nu\alpha\beta} = \frac{\epsilon^{\mu\nu\alpha\beta}}{\sqrt{-g}}$ being the Levi-Civita tensor density, and κ is the chemical potential. It is clear that all the terms in the action are invariant under spatial diffeomorphisms. After reintroducing the Goldstone boson, that transforms as $\pi \to \pi - \xi^0(\boldsymbol{x}, t)$ under a time-diffeomorphism $t \to t + \xi^0(\boldsymbol{x}, t)$, the specific coupling of σ_μ to the time foliation of spacetime prevents the last term in (9.55) from being a total derivative. This term respects the shift symmetry for the Goldstone boson.

From a model-building perspective, the chemical potential naturally arises from the dimension-5 coupling $\phi F\tilde{F}$ between the inflaton field ϕ and the spin-1 field σ_μ [505, 240, 506, 507, 508]. This coupling respects the shift symmetry of the scalar field $\phi \to \phi + c$, since the constant c contributes to a total derivative. With the inflaton acquiring its slowly rolling vacuum expectation value, i.e. $\phi = \phi_0 + \dot{\phi}_0 t + \cdots$, the chemical potential term is identified as $\kappa = \dot{\phi}_0/\Lambda_\kappa$ where Λ_κ is some higher-energy cutoff. Higher-order terms are slow-roll suppressed. From an EFT point of view, the chemical potential is a direct consequence of broken time diffeomorphism invariance by the background inflaton field.

Equation of Motion. Varying the action (9.55) yields the equation of motion

$$\Box\sigma^\nu - \nabla_\mu\nabla^\nu\sigma^\mu - m^2\sigma^\nu - \kappa\mathcal{E}^{0\nu\alpha\beta}F_{\alpha\beta} = 0\,, \tag{9.56}$$

where $\Box \equiv g^{\mu\nu}\nabla_\mu\nabla_\nu = -\partial_t^2 - 3H\partial_t + \partial_i^2/a^2$ denotes the d'Alembert operator on four-dimensional de Sitter spacetime. The time-like component of the field σ_μ is solved in terms of the spatial components using the constraint equation $\nabla^\mu\sigma_\mu = 0$,

which is found after taking the divergence of the equation of motion. Substituting the constraint back into (9.56) gives the following on-shell equation of motion

$$\left[\Box - (m^2 + 3H^2)\right] \sigma^\nu = 2\kappa \mathcal{E}^{0\nu\alpha\beta} \nabla_\alpha \sigma_\beta \,. \tag{9.57}$$

Being massive, the field σ_μ has three degrees of freedom, a longitudinal mode and two transverse modes. Decomposing the spatial components in 3-dimensional Fourier space $\sigma_i(\boldsymbol{x}, \tau) = \int \frac{\mathrm{d}^3 k}{(2\pi)^3} e^{i\boldsymbol{k}\cdot\boldsymbol{x}} \sigma_{i,\boldsymbol{k}}(\tau)$ into helicity eigenstates, one can write

$$\sigma_{i,\boldsymbol{k}}(\tau) = \sum_{\lambda=0,\pm} \varepsilon_i^\lambda \left[\sigma_{\lambda,k}(\tau)\, a_{\boldsymbol{k}}^\lambda + \sigma_{\lambda,k}^*(\tau)\, a_{-\boldsymbol{k}}^{\lambda\dagger}\right] , \tag{9.58}$$

where $\sigma_{\lambda,k}(\tau)$ are the helicity eigenstates, with $\lambda = 0$ being the longitudinal mode and $\lambda = \pm$ denoting the transverse modes. In terms of these mode functions, the equations of motion for different helicities decouple from each other. As we are mostly interested in parity violation in what follows, and the chemical potential only affects the transverse modes, we only consider the transverse modes equation of motion that reads

$$\sigma_{\pm,k}'' + \left[k^2 \pm 2ak\kappa + a^2 m^2\right] \sigma_{\pm,k} = 0 \,. \tag{9.59}$$

We refer to Chap. 5 for the corresponding mode functions.

Dynamics of transverse modes. Concentrating on transverse modes, it is instructive to directly read the physics from the equation of motion (9.59). In particular, in the flat-space limit $H \to 0$, neglecting Hubble friction for simplicity, the equation of motion can be solved with plane waves, leading to the following dispersion relation

$$\omega_\pm^2(k_\mathrm{p}) = (k_\mathrm{p} \pm \kappa)^2 + m^2 - \kappa^2 \,, \tag{9.60}$$

where $k_\mathrm{p} = k/a$ is the physical momentum. The effect of the chemical potential appears as a constant shift of k_p, or equivalently as a time-dependent mass term owing to the redshift of the physical momentum. This phenomenon assists the spontaneous particle production of $\sigma_\pm$ by the exponentially expanding spacetime, enhancing the cosmological collider signal, see Chap. 4. However, the latter effect does not manifest itself in the single-field EFT treatment of interest in this work. Instead, what is of direct relevance for our purpose is simply the *asymmetry* between the different helicities, as it is this parity violation that gets imprinted in the four-point correlator of the Goldstone boson. Considering $\kappa > 0$ without loss of generality, the dispersion relation (9.60) shows that for $\kappa > m$, each σ_- mode experiences a transient tachyonic instability in the time interval with $\omega_-^2(k_\mathrm{p}) < 0$. The energy carried by these modes can lead to a strong backreaction on the inflationary background and we restrict our discussion to the situation with $\kappa \leq m$. In this regime, the behaviour of each helicity mode is qualitatively similar, with modes beginning to decay around the mass-shell horizon $k_\mathrm{p}/H = |k\tau| \sim m/H$. Nonetheless, the chemical potential does affect differently the two helicities, with important consequences as we will see.

Mixing interactions. In the unitary gauge, Lorentz invariant operators constructed out of the spin-1 field, e.g. $\sigma_\mu\sigma^\mu$, are of course invariant under all diffeomorphisms and therefore are invariant under spatial ones. However, they do not lead to mixing interactions with the Goldstone boson. The time-like component σ^0 is a scalar under spatial diffeomorphisms, hence it constitutes a building block to construct mixing interactions. Performing a spacetime-dependent time diffeomorphism, reintroducing the Goldstone boson, leads to

$$\sigma^0(\boldsymbol{x},t) \to \tilde{\sigma}^0(\tilde{\boldsymbol{x}},\tilde{t}) = \partial_\mu(t+\pi)\,\sigma^\mu(\boldsymbol{x},t) = \left[\delta^0_\mu + \partial_\mu\pi\right]\sigma^\mu(\boldsymbol{x},t)\,. \tag{9.61}$$

In order to generate a parity-odd trispectrum via the (single) exchange of σ_μ, one needs to determine mixing interactions of the schematic form $\sim \pi^2\sigma$, compatible with the symmetry and with an odd number of spatial derivatives.[9] There are two ways to generate such interactions: (i) couple the time-like component σ^0 to index-free building blocks invariant under spatial diffeomorphisms, and (ii) couple σ_μ with building blocks carrying a free (spacetime) index. Up to dimension seven, the corresponding lowest-dimension cubic interactions are therefore given by the following operators

$$S_{\pi\sigma} = \int \mathrm{d}^4x\sqrt{-g}\left[\omega_1^3\delta g^{00}\sigma^0 + \omega_2\nabla_\mu\delta g^{00}\delta K^\mu_\nu\sigma^\nu + \omega_3 n^\mu\nabla_\mu\delta g^{00}\nabla_\nu\delta g^{00}\sigma^\nu\right], \tag{9.62}$$

where $\omega_{1,2,3}$ are constant mass-dimension couplings. Reintroducing the Goldstone boson leads to

$$S_{\pi\sigma} = \int \mathrm{d}t\mathrm{d}^3x a^3\left[\rho a^{-2}\partial_i\pi_c\sigma_i - \frac{a^{-2}}{\tilde{\Lambda}}\dot{\pi}_c\partial_i\pi_c\sigma_i + \frac{a^{-4}}{\Lambda^3}\partial_j\dot{\pi}_c\partial_i\partial_j\pi_c\sigma_i + \frac{a^{-2}}{\bar{\Lambda}^3}\ddot{\pi}_c\partial_i\dot{\pi}_c\sigma_i\right], \tag{9.63}$$

where the couplings are defined by $\rho \equiv 2c_s^{3/2}\omega_1^3/f_\pi^2$, $\tilde{\Lambda}^{-1} \equiv c_s^{3/2}\rho/f_\pi^2$, $\Lambda^{-3} \equiv 2c_s^3\omega_2/f_\pi^4$, and $\bar{\Lambda}^{-3} \equiv 4c_s^3\omega_3/f_\pi^4$. Here we have kept cubic terms in the fields relevant for the parity-odd trispectrum. Note that the size of the cubic interaction $\dot{\pi}_c\partial_i\pi_c\sigma_i$ is completely fixed by the size of the quadratic mixing $\partial_i\pi_c\sigma_i$. This is a consequence of the Goldstone boson non-linearly realizing time diffeomorphism, as both interactions are governed by the same coupling ω_1.[10] We will see later that the two operators with coupling proportional to ω_1 are tightly constrained by mixing perturbativity, leading to undetectably small parity-violating non-Gaussianities. However, the two dimension-7 operators originating from ω_2 and ω_3 can lead to sizable signals. Note that by putting the Goldstone boson on shell, namely using its equation of motion, and observing that $\partial_i(\dot{\pi}_c^2)$ does not couple to the transverse mode of the vector field, the cubic interaction governed by the coupling ω_3 is of the same form as that fixed by ω_2, albeit with a different spatial gradient structure.

[9] Note that the chemical potential term itself generates a $\pi\sigma^2$ coupling after reintroducing the Goldstone of time diffeomorphism. This can in principle produce parity-violating correlators at 1-loop level, but with a small signal strength due to the heavy scale Λ_κ and an extra $(4\pi)^{-2}$ loop suppression. Instead, in this thesis, we work with tree-level diagrams produced by $\sim \pi^2\sigma$ couplings.

[10] Notice that we could have considered manifestly parity-violating interactions by contracting spatial derivatives with ϵ_{ijk}. The leading operator in this case would be a dimension-8 operator and the corresponding exchange diagram would typically give a smaller signal compared to the one we compute using parity-even vertices only.

9.5 Strong Coupling Scales & Naturalness

It is important to ensure that the effective description of fluctuations that we study is under theoretical control and identify the natural hierarchy of scales of the system. Because the theory contains non-renormalisable interactions, the theory will become strongly coupled at a certain energy scale.[11] In this section, we derive the strong coupling scale, or unitarity bound, in the weak and strong quadratic mixing regimes. These bounds translate into bounds on the size of non-Gaussianities, see Chap. 15, but only give a parametric estimation, possibly missing large dimensionless numbers. We also discuss naturalness.

Theoretical lower bound on the sound speed. As we have discussed in Sec. 9.3.3, the effective description of primordial fluctuations is valid up to some UV cutoff scale $\Lambda_\star$ beyond which the perturbative description breaks down. When $c_s = 1$, analogous to the chiral Lagrangian describing the dynamics of pions, the strong coupling scale of the effective theory is $\Lambda_\star = 4\pi f_\pi$.[12] However, when the sound speed c_s is sufficiently small, it is well-known that $\Lambda_\star$ is not too far from the Hubble scale. Indeed, it is given by [470, 502][13]

$$\Lambda_\star^4 = 2\pi f_\pi^4 \frac{c_s^4}{1-c_s^2}\,, \tag{9.64}$$

which, in the limit $c_s \ll 1$, gives $\Lambda_\star \sim c_s f_\pi$. Imposing $\Lambda_\star > H$ for the EFT to be valid—otherwise fluctuations cannot be initialised in the proper vacuum inside the horizon—and assuming the single-field limit (i.e. $\rho/H = 0$) gives a theoretical lower bound on the sound speed $c_s \geq 0.0087$.[14] The additional degree of freedom σ changes the physical description, and interactions between π_c and σ will modify $\Lambda_\star$. Yet, the quadratic mixing $\dot\pi_c\sigma$ makes the analysis more subtle. Therefore, we examine separately the weak and strong mixing regimes.

9.5.1 Weak Mixing

In the weak mixing regime, the quadratic theory is dominated by the standard kinetic terms. The free fields can then be considered decoupled as a first approximation. Usually, the strong coupling scale $\Lambda_\star$ is derived from operators constructed out of canonically-normalised fields with a Lorentz invariant kinetic term. Here, the non-relativistic dispersion relation of π_c makes it impossible to put time and

[11] This scale can be derived by finding the maximum energy at which the tree-level scattering of the fields is unitary, through partial wave expansion. Here, we give an heuristic derivation of these strong coupling scales based on power counting which, of course, misses order-one factors.

[12] After reintroducing the Goldstone boson, the action (9.31) without truncating to a certain order in fields is an expansion in π_c/f_π with $\pi_c \sim \omega$, and higher dimensional operators become relevant if the effective dimensionless coupling constant ω/f_π is of order one.

[13] This strong coupling scale is associated with the operator $(\partial_i\pi_c)^4$.

[14] Assuming pure single-field c_s-theory, Planck constraints on primordial non-Gaussianities give a more stringent lower bound on the speed of sound: $c_s \geq 0.021$ (95% CL) [137].

space on the same footing, so that one needs to consider energy and momentum separately.[15]

Let us first consider the cubic interaction coming from $\delta g^{00}\sigma$ in the unitary gauge, so that the action we examine—together with the quadratic part but neglecting the quadratic mixing—reads

$$S \supset \frac{1}{2}\int \mathrm{d}t\,\mathrm{d}^3x\,a^3\left[\dot{\pi}_c^2 - c_s^2\frac{(\partial_i\pi_c)^2}{a^2} + \dot{\sigma}^2 - \frac{(\partial_i\sigma)^2}{a^2} - m^2\sigma^2 - c_s^{3/2}\frac{\rho}{f_\pi^2}\frac{(\partial_i\pi_c)^2}{a^2}\sigma\right]. \tag{9.65}$$

In order to estimate how various terms in this action scale with energy and momentum, we need to chose a reference. Let us fix the (physical) momentum k_p carried by the propagating modes, whose energies should be understood as derived concepts depending on their dispersion relations. The energy of π_c then reads $\omega_\pi = c_s k_\mathrm{p}$, whereas the energy of σ is $\omega_\sigma = k_\mathrm{p}$, from which we deduce that $\omega_\pi = c_s\omega_\sigma$. In the following, we will express all quantities in terms of the energy of the Goldstone boson $\omega \equiv \omega_\pi$ because it is the energy probed experimentally at the Hubble scale $\omega \sim H$. Therefore, the kinetic term $\dot{\pi}_c^2$ scales as $\sim \omega^2\pi_c^2$—so does the gradient term—, and the kinetic term $\dot{\sigma}^2$ scales as $\sim \omega_\sigma^2\sigma^2 \sim c_s^{-2}\omega^2\sigma^2$, and likewise for the gradient term. Yet, a question needs to be answered. What is the typical size of the fluctuations? By dimensional analysis, π_c scales as $\omega^{-1/2}k_\mathrm{p}^{3/2} \sim c_s^{-3/2}\omega$. Similarly, σ scales as $\omega_\sigma \sim c_s^{-1}\omega$. Combining all scalings, we obtain that the Goldstone boson kinetic term scales as $\sim c_s^{-3}\omega^4$, and that of σ scales as $c_s^{-4}\omega^4$. We notice that, at small sound speed, the kinetic term of σ is the dominant one in the quadratic action.[16] No strong coupling scale is associated with the quadratic mixing operator $\dot{\pi}_c\sigma$ because it is of dimension 3. However, the theory is under control in the weak mixing regime if this interaction can be treated perturbatively. Requiring that this interaction—that scales as $c_s^{-5/2}\rho\,\omega^3$—is smaller than the kinetic term of the Goldstone boson gives

$$\frac{\rho}{H} \lesssim c_s^{-1/2}. \tag{9.66}$$

Now, the cubic interaction scales as $c_s^{-9/2}\rho/f_\pi^2\,\omega^5$. Requiring that this term should be smaller than the kinetic term of the Goldstone boson—giving the more stringent bound—sets the strong coupling scale to[17]

$$\Lambda_\star = c_s^{3/2}\,\frac{f_\pi^2}{\rho}. \tag{9.67}$$

[15] In single-field theories, up to a redefinition of spacetime coordinates, fake Lorentz invariance can be restored and standard dimensional analysis can then be applied, see [502]. However, this trick does not work in our situation with several degrees of freedom propagating at different sound speeds.

[16] Note also that this hierarchy is reversed when the massive fluctuations propagate slower than the Goldstone boson fluctuations, $c_\sigma < c_\pi$.

[17] Let us comment on the mass term $m^2\sigma^2$, that we neglected so far. This term changes the dispersion relation of σ to $\omega_\sigma^2 = k_\mathrm{p}^2 + m^2$, which leads to $\omega_\sigma^2 = \omega^2/c_s^2 + m^2$. The kinetic term of σ including this mass term therefore scales as $\sim (\omega^2/c_s^2 + m^2)\sigma^2$. The typical size of σ is found to be $\sigma \sim \omega/c_s\left[1+(c_s m/\omega)^2\right]^{-1/4}$. In the end, the kinetic term of σ scales as $\sim c_s^{-4}\omega^4\left[1+(c_s m/\omega)^2\right]^{1/2}$. Note that we recover the scaling presented in the main text in the limit $\omega \gg c_s m$. Fixing the energy scale to the Hubble scale, we deduce that the mass term is negligible when $m/H \ll c_s^{-1}$. Still, we note that properly taking into account the mass term increases the size of the kinetic term of σ. For $c_s < 1$ and including the mass of σ, the smallest contribution

Imposing $H \lesssim \Lambda_\star$ leads to $\rho/H \lesssim c_s^{3/2}/2\pi\Delta_\zeta$, where $2\pi\Delta_\zeta \equiv (H/f_\pi)^2$ (we measure $\Delta_\zeta = 2.2 \times 10^{-9}$). This bound is less stringent that the previous one, and therefore (9.66) defines the weak mixing regime. Additionally, it has been shown that $\rho \lesssim m$ is also required in order to treat the quadratic mixing perturbatively, see Chap. 10. Depending on the value of c_s, this bound can be stronger.

Next, we consider the interactions coming from $\delta g^{00}\sigma^2$. After introducing the Goldstone boson, the interactions we examine are

$$S \supset \frac{1}{2}\int \mathrm{d}t\,\mathrm{d}^3x\,a^3\left[-\alpha\dot{\pi}_c\sigma^2 + \frac{c_s^{3/2}}{2}\frac{\alpha}{f_\pi^2}(\partial_\mu\pi_c)^2\sigma^2\right]. \tag{9.68}$$

The interaction $\dot{\pi}_c\sigma^2$ is of dimension 4 so no strong coupling scale is associated with it. However, requiring that the size of this term in the action be smaller than the kinetic term of π_c to be in the perturbative regime leads[18] to

$$\alpha \lesssim c_s^{1/2}\,, \quad \text{i.e.} \quad \tilde{\alpha}^2 \lesssim c_s^{-1}/4 \times (2\pi\Delta_\zeta)^{-1}\,. \tag{9.69}$$

Repeating the power counting for the dimension-6 operator gives the following strong coupling scale[19]

$$\Lambda_\star = c_s^{5/4}\frac{f_\pi}{\sqrt{\alpha}}\,. \tag{9.70}$$

Requiring that primordial fluctuations are weakly coupled at the Hubble scale $\Lambda_\star > H$ gives the constraint $\alpha \lesssim \frac{c_s^{5/4}}{2\pi\Delta_\zeta}$, equivalently $\tilde{\alpha}^2 \lesssim c_s^{-1/4}\,(4\pi\Delta_\zeta)^{-2}$, on the coupling constant, which is less stringent than the previous one.

Lastly, we consider the interactions coming from $\left(\delta g^{00}\right)^2\sigma$, which in terms of the Goldstone boson gives the following interactions

$$\begin{aligned} S \supset \frac{1}{2}\int \mathrm{d}t\,\mathrm{d}^3x\,a^3\Bigg[&-\frac{1}{\Lambda_2}\dot{\pi}_c^2\sigma + \frac{c_s^{3/2}}{f_\pi^2}\dot{\pi}_c\frac{(\partial_\mu\pi_c)^2}{\Lambda_2}\sigma - \frac{c_s^3}{4f_\pi^4}\frac{1}{\Lambda_2}\dot{\pi}_c^4\sigma \\ &+\frac{c_s^3}{2f_\pi^4}\frac{1}{\Lambda_2}\dot{\pi}_c^2\frac{(\partial_i\pi_c)^2}{a^2}\sigma - \frac{c_s^3}{4f_\pi^4}\frac{1}{\Lambda_2}\frac{(\partial_i\pi_c)^4}{a^4}\sigma\Bigg]\,, \end{aligned} \tag{9.71}$$

where we have defined $\Lambda_2^{-1} = 8c_s^3\tilde{M}_3^3/f_\pi^4$. Note that this definition differs from (9.54). The reason is that the interaction $\dot{\pi}_c^2\sigma$ is also generated by $\delta g^{00}\sigma$, so that its coupling constant depends on both $\tilde{M}_1$ and $\tilde{M}_3$. Here, we isolate interactions coming from $\left(\delta g^{00}\right)^2\sigma$ only, effectively setting $\tilde{M}_1 = 0$. Estimating the size of all the interactions

of the quadratic theory is still the kinetic term of the Goldstone boson. Therefore, we can safely discard the mass term in our analysis because it would play no role in the derivation of the strong coupling scales.

[18] In the standard Lorentz invariant case, the perturbative criteria on marginal operators is that the dimensionless couplings have to be less than unity. Here, the non-relativistic dispersion relation makes things more subtle, introducing a sound speed dependence in the perturbative criterion.

[19] Note that, for $c_s \ll 1$, the gradient term in $(\partial_\mu\pi_c)^2$ dominates over the $\dot{\pi}_c^2$ term, hence giving the strong coupling scale by requiring that it should be smaller than the kinetic term of π_c. However, if $c_s > 1$, the hierarchy is reversed and the strong coupling scale is found by comparing the time derivative interaction term to the kinetic term of σ. This gives $\Lambda_\star = c_s^{-1/4}f_\pi/\sqrt{\alpha}$.

in (9.71) gives several strong coupling scales. The smallest one is associated with the interaction $\dot{\pi}_c^2\sigma$ and reads

$$\Lambda_\star = c_s\Lambda_2\,. \tag{9.72}$$

Requiring $H < \Lambda_\star$ gives the bound $H/\Lambda_2 \lesssim c_s$, equivalently $\tilde{\rho}/H \lesssim c_s^{-1/2}(2\pi\Delta_\zeta)^{-1}$.

Finally, the operator σ^3 being relevant and the field σ having a relativistic dispersion relation, the criteria for a perturbative treatment of this interaction is simply $\mu/H \lesssim 1$.

Spin-1 massive helical field. The introduced couplings in the mixing action (9.63) are free parameters of the theory. We now derive bounds on them by requiring that the dimension-3 quadratic mixing term can be treated perturbatively, and that the dimension-5 and -7 interactions are suppressed by scales larger than H, ensuring weak coupling of fluctuations.

Following the same strategy as previously, noting that the dispersion relation for the transverse modes of the massive spin-1 field is $\omega_\sigma^2 = k_{\rm p}^2 \pm 2\kappa k_{\rm p} + m^2$, we have $c_s^2\omega_\sigma^2 = \omega^2 \pm 2c_s\kappa\omega + c_s^2m^2$. The spin-1 field kinetic term then scales as $\sim (\omega^2/c_s^2)\,\sigma^2\gamma(\omega)$, where we have defined $\gamma(\omega) \equiv 1 \pm 2\alpha_\kappa(\omega) + \alpha_m^2(\omega)$ in terms of the dimensionless energy-dependent quantities $\alpha_\kappa(\omega) \equiv c_s\kappa/\omega$ and $\alpha_m(\omega) \equiv c_sm/\omega$. As we will see in the next chapter, the regime of interest, where physical effects of a reduced speed of sound become important, is characterised by $\alpha_\kappa \ll 1$ and $\alpha_m \ll 1$, hence $\gamma \sim 1$, where the parameters are evaluated at the Hubble scale $\omega = H$. We nevertheless keep these terms for consistency. Note that the mass term of the additional field and the chemical potential term are already taken into account in the dispersion relation. For a reduced sound speed, they do not significantly contribute to the quadratic action for both fields and can be consistently neglected. By dimensional analysis, we obtain $\sigma \sim \omega/c_s\,\gamma^{-1/4}(\omega)$. Combining these scalings with those of the free quadratic terms in the action, the kinetic term of the spin-1 field scales as $\sim c_s^{-4}\omega^4\gamma^{1/2}(\omega)$. It becomes again clear that the Goldstone boson kinetic term is smaller than that of the massive field for $c_s \ll 1$.

Using the same dimensional analysis arguments, the mixing interactions scale as

$$\begin{aligned}
\rho\,\partial_i\pi_c\sigma_i &\sim c_s^{-1/2}\rho\,\frac{\omega^3}{c_s^3}\,\gamma^{-1/4}(\omega)\,,\\
\frac{1}{\tilde{\Lambda}}\dot{\pi}_c\partial_i\pi_c\sigma_i &\sim c_s^{-7}\frac{\omega^5}{\tilde{\Lambda}}\,\gamma^{-1/4}(\omega)\,,\\
\frac{1}{\Lambda^3}\partial_j\dot{\pi}_c\partial_i\partial_j\pi_c\sigma_i &\sim c_s^{-7}\frac{\omega^7}{\Lambda^3}\,\gamma^{-1/4}(\omega)\,,\\
\frac{1}{\bar{\Lambda}^3}\ddot{\pi}_c\partial_i\dot{\pi}_c\sigma_i &\sim c_s^{-5}\frac{\omega^7}{\bar{\Lambda}^3}\,\gamma^{-1/4}(\omega)\,.
\end{aligned} \tag{9.73}$$

Let us now require that these scalings should be smaller than the Goldstone kinetic term which is of order $c_s^{-3}\omega^4$, and evaluate the above expressions at $\omega = H$. For the quadratic coupling ρ, which also fixes the size of the cubic interactions $\dot{\pi}_c\partial_i\pi_c\sigma_i$, one obtains

$$\frac{\rho}{H} \lesssim c_s^{1/2}\gamma^{1/4}\,,\quad \text{and}\quad \frac{\rho}{H} \lesssim c_s^{5/2}\frac{\gamma^{1/4}}{2\pi\Delta_\zeta}\,. \tag{9.74}$$

Within our regime of interest, $c_s \ll 1$ and $\gamma \sim 1$, the first inequality gives the most stringent bound and is taken to be the perturbative criterion.[20] Performing the same procedure for the remaining interactions gives

$$\frac{H}{\Lambda} \lesssim c_s^{4/3}\gamma^{1/12}\,, \quad \text{and} \quad \frac{H}{\bar{\Lambda}} \lesssim c_s^{2/3}\gamma^{1/12}\,. \tag{9.75}$$

We will see in the next chapter that both $\partial_j\dot{\pi}_c\partial_i\partial_j\pi_c\sigma_i$ and $\ddot{\pi}_c\partial_i\dot{\pi}_c\sigma_i$ can lead to a large parity-odd trispectrum. In fact, the generated trispectrum shapes are similar, and we will mainly focus on the former one without loss of generality. Note that the way the spin-1 field couples to the time foliation through the chemical potential term $\kappa t F_{\mu\nu}\tilde{F}^{\mu\nu}$ introduces an additional mixing of the form $\sim \pi\sigma^2$. The same scaling analysis as previously gives the bound $\kappa/H \lesssim c_s\gamma^{-1/2}/(2\pi\Delta_\zeta)$ on the chemical potential. However, this mixing contributes to the (double-exchange) bispectrum and the (triple-exchange) trispectrum, and typically leads to no observable non-Gaussianity. We therefore discard this mixing interaction from our analysis.

9.5.2 Strong Mixing

At large quadratic mixing in the Lagrangian (9.53), the mixing term $\dot{\pi}_c\sigma$ dominates over the kinetic terms $\dot{\pi}_c^2$ and $\dot{\sigma}^2$. In the next chapter, we will study in detail this regime where the Goldstone boson acquires a modified dispersion relation. In the general case with $c_s \leq 1$, the condition of validity for this regime is

$$\frac{\rho}{H} \gtrsim c_s^{-1}\,, \quad \text{and} \quad c_s\,\frac{m^2}{\rho} \lesssim H\,. \tag{9.76}$$

The theory being effectively described by a single degree of freedom, it is possible to rescale the spatial coordinates and the fields to canonically normalise the propagating degree of freedom. This is completely equivalent to the power counting method used previously. By performing the rescaling $x \to \tilde{x} = \rho^{1/2}c_s^{-1/2}x$, $\pi_c \to \tilde{\pi}_c = \rho^{-1/4}c_s^{5/4}\pi_c$, and $\sigma \to \tilde{\sigma} = \rho^{-1/4}c_s^{1/4}\sigma$, we obtain for the interactions coming from $\delta g^{00}\sigma$—and the quadratic part but neglecting the time derivative terms—the following action

$$S \supset \frac{1}{2}\int \mathrm{d}t\,\mathrm{d}^3\tilde{x}\,a^3\left[\dot{\tilde{\pi}}_c\tilde{\sigma} - \frac{(\tilde{\partial}_i\tilde{\pi}_c)^2}{a^2} - \frac{(\tilde{\partial}_i\tilde{\sigma})^2}{a^2} - M^2\tilde{\sigma}^2 - c_s^{-3/4}\frac{\rho^{5/4}}{f_\pi^2}\frac{(\tilde{\partial}_i\tilde{\pi}_c)^2}{a^2}\tilde{\sigma}\right]\,, \tag{9.77}$$

where $M \equiv c_s\frac{m^2}{\rho}$. By dimensional analysis, we have $[\tilde{\partial}] = 1/2$ and $[\tilde{\pi}_c] = [\tilde{\sigma}] = 3/4$ in mass units. This implies that the strong coupling scale is

$$\Lambda_\star = c_s\left(\frac{f_\pi^8}{\rho^5}\right)^{1/3}\,, \tag{9.78}$$

[20] In the case of a vanishing chemical potential, a more stringent bound on the quadratic mixing strength ρ can be found by requiring that the spin-1 field propagates subluminally [116]. This bound enforces the coupling ρ to be almost vanishing if the longitudinal mode of the massive vector field propagates almost relativistically, and therefore puts severe theoretical constraints on the size of non-Gaussianities. In practice, this leads to undetectable parity-even and parity-odd non-Gaussian signals generated by mixings fixed by the coupling ρ.

which generalises the strong coupling scale found in [502] for the $c_s = 1$ case. Using $\Delta_\zeta^2 = \frac{2\Gamma(5/4)^2}{\pi^3}\left(\frac{H}{f_\pi}\right)^4\left(\frac{\rho}{H}\right)^{1/2}$ (see next chapter) and imposing $H \lesssim \Lambda_\star$, we obtain the following constraint[21]

$$\frac{\rho}{H} \lesssim c_s^{3/4}\frac{\kappa^{1/2}}{\Delta_\zeta}\,, \tag{9.79}$$

where $\kappa = 2\Gamma(5/4)^2/\pi^3 \approx 0.053$. Importantly, this bound shows that the theory can be strongly mixed without being strongly coupled.

Let us now consider the interactions coming from $\delta g^{00}\sigma^2$. After performing the same rescaling, the action we examine is

$$S \supset -\frac{1}{2}\int \mathrm{d}t\,\mathrm{d}^3\tilde{x}\,a^3\left[c_s^{-1/4}\alpha\rho^{-3/4}\dot{\tilde{\pi}}_c\tilde{\sigma}^2 + \frac{1}{2}\frac{\alpha}{f_\pi^2}\left(\rho^{-1/2}\dot{\tilde{\pi}}_c^2\tilde{\sigma}^2 - c_s^{-1}\rho^{1/2}\frac{(\tilde{\partial}_i\tilde{\pi}_c)^2}{a^2}\tilde{\sigma}^2\right)\right]. \tag{9.80}$$

We notice that the would-be Lorentz invariant interaction $(\partial_\mu\pi_c)^2\sigma^2$ is broken due to the rescaling of spatial (but not time) coordinates. Therefore, we expect that different strong coupling scales will be associated with $\dot{\tilde{\pi}}_c^2\tilde{\sigma}^2$ and $(\tilde{\partial}_i\tilde{\pi}_c)^2\tilde{\sigma}^2$. The interaction $\dot{\tilde{\pi}}_c\tilde{\sigma}^2$ can be treated as a perturbative correction to the quadratic action as long as

$$\alpha \lesssim c_s^{1/4}\left(\frac{\rho}{H}\right)^{3/4}, \quad \text{i.e.} \quad \tilde{\alpha}^2 \lesssim \frac{c_s^{-1/2}}{4}\frac{\kappa}{\Delta_\zeta^2}\,. \tag{9.81}$$

The smallest strong coupling scale—associated with the interaction $(\tilde{\partial}_i\tilde{\pi}_c)^2\tilde{\sigma}^2$—is

$$\Lambda_\star = \left(\frac{c_s}{\alpha}\right)^{2/3}\left(\frac{f_\pi^4}{\rho}\right)^{1/3}, \tag{9.82}$$

which gives the following constraint to be in the perturbative regime at energies $\omega \sim H$

$$\alpha \lesssim c_s\left(\frac{\rho}{H}\right)^{-1/2}\left(\frac{f_\pi}{H}\right)^2, \quad \text{i.e.} \quad \tilde{\alpha}^2 \lesssim \frac{c_s^{-1/2}}{4}\frac{\kappa}{\Delta_\zeta^2}\,. \tag{9.83}$$

Interestingly, both conditions (9.81) and (9.83) give the same perturbativity bounds. Therefore, it is taken to be the criteria for a consistent perturbative treatment of all interactions coming from $\delta g^{00}\sigma^2$.

Next, we consider the interactions coming from $(\delta g^{00})^2\sigma$. Following the same strategy as we did previously, we find that the smallest strong coupling scale is the one associated with the interaction $\dot{\tilde{\pi}}_c^2\sigma$, which is

$$\Lambda_\star = \left(c_s^5\rho^3\Lambda_2^4\right)^{1/7}. \tag{9.84}$$

Requiring $H \lesssim \Lambda_\star$ gives us the following condition

$$\frac{H}{\Lambda_2} \lesssim c_s^{5/4}\left(\frac{\rho}{H}\right)^{3/4}, \quad \text{i.e.} \quad \frac{\tilde{\rho}}{H} \lesssim c_s^{1/2}\frac{\kappa}{\Delta_\zeta^2}\,. \tag{9.85}$$

[21] Note that imposing the validity of the decoupling limit—that is neglecting the mixing with gravity through terms like $\delta g^{00}\dot{\pi}$—also gives a lower bound on ρ/H.

Lastly, the condition for perturbativity of the interaction σ^3 is found to be $\mu/H \lesssim c_s^{-3/4}\,(\rho/H)^{3/4}$.[22]

9.5.3 Radiative Corrections

Finally, we derive bounds on the size of the coupling constants based on the requirement that the theory is stable under radiative corrections, hence requiring the theory to be *technically natural*. These bounds are not strict, and rely on several assumptions: (i) we only require that the mass of the field σ does not receive large loop corrections[23] $\delta m^2 \lesssim m^2 \sim H^2$, (ii) we restrict ourselves to one-loop order, therefore neglecting self-interactions of π_c. Because the UV-divergent diagrams are dominated by the UV dynamics of the system $\omega > H$, the fields—even at strong mixing provided that the loops mostly receive contributions for energies $\omega > \rho$—are considered decoupled. Moreover, this enables us to use flat-space propagators. Divergent diagrams are cut off (in energy) at the scale where the theory breaks down, namely the strong coupling scale associated with the Goldstone sector $\Lambda_\star \sim c_s f_\pi$.[24]

- The interaction σ^3 generates the following mass shift

$$\delta m^2 = \quad \sim \mu^2 \int \frac{\mathrm{d}\omega \mathrm{d}^3 k}{(\omega^2 - k^2 - m^2)^2} \sim \mu^2\,, \tag{9.86}$$

  hence giving a finite loop correction. Naturalness of the mass of the field σ therefore requires $\mu \lesssim H$.

- Let us now consider the mass correction arising from the interaction fixed by the non-linearly realised symmetry $(\partial_i \pi_c)^2 \sigma$. It reads

$$\delta m^2 = \quad \sim c_s^3 \frac{\rho^2}{f_\pi^4} \int \mathrm{d}\omega \mathrm{d}^3 k \, \frac{k^4}{(\omega^2 - c_s^2 k^2)^2} \sim \rho^2\,, \tag{9.87}$$

  where we have set the cutoff in energy to $\Lambda_\omega = c_s f_\pi$ and the cutoff in momentum to $\Lambda_k = c_s^{-1}\Lambda_\omega$ to take into account the non-relativistic dispersion relation of π_c. Hence, the naturalness criterion we consider requires the quadratic mixing to be weak $\rho/H \lesssim 1$. We see that a large quadratic mixing *and* a small mass—and consequently the modified dispersion relation regime—is *not* technically natural, and can only be reached with fine-tuning.

- Next, we consider the interaction $\dot\pi_c^2 \sigma$ which gives the following mass correction

$$\delta m^2 = \quad \sim \frac{1}{\Lambda_2^2} \int \mathrm{d}\omega \mathrm{d}^3 k \, \frac{\omega^4}{(\omega^2 - c_s^2 k^2)^2} \sim c_s \frac{f_\pi^4}{\Lambda_2^2}\,. \tag{9.88}$$

[22] We have checked that the requirement that no group velocity exceeds the speed of light gives no further constraints on the parameters.

[23] Similar bounds were derived in [265, 116]. Of course, all couplings receive corrections under renormalisation but the entire analysis is beyond the scope of this thesis.

[24] In principle, the UV-divergent integrals should be cut off at the most stringent strong coupling scale. However, these scales are strongly parameter dependent, and we consider to set the UV-cutoff to $\Lambda_\star \sim c_s f_\pi$ for definiteness [265]. Note that in the case of a reduced sound speed $c_s \ll 1$, it is the most stringent bound. Let us reiterate that the naturalness conditions we derive here are contingent upon several assumptions, and therefore, they should not be regarded as absolute.

In the weak mixing regime, we write the condition for radiative stability in term of the dimensionless power spectrum. It reads

$$\frac{H}{\Lambda_2} \lesssim \frac{2\pi\Delta_\zeta}{c_s^{1/2}}\,, \qquad \text{i.e.} \qquad \frac{\tilde{\rho}}{H} \lesssim c_s^{-2}\,. \tag{9.89}$$

- Finally, we consider the radiative correction induced by the interaction $\dot{\pi}_c\sigma^2$. This reads

$$\delta m^2 = \quad \sim \alpha^2 \int \mathrm{d}\omega \mathrm{d}^3k \, \frac{\omega^2}{(\omega^2 - c_s^2 k^2)(\omega^2 - k^2 - m^2)} \sim \alpha^2 \frac{f_\pi^2}{c_s}\,. \tag{9.90}$$



In the weak mixing regime, the naturalness condition reads

$$\alpha \lesssim c_s^{1/2}\,(2\pi\Delta_\zeta)^{1/2}\,, \qquad \text{i.e.} \qquad \tilde{\alpha}^2 \lesssim c_s^{-1}\,(2\pi\Delta_\zeta)^{-1/2}\,. \tag{9.91}$$

10

Going Non-Local

The primordial fluctuations in any theory of inflation are at least of two types: the Goldstone boson associated with the spontaneous breaking of time translations π, and the transverse dynamical part of the metric γ_{ij}. As reviewed in the previous chapter, the Lagrangian for the Goldstone boson can be constructed without any knowledge of the specific mechanism that led to this symmetry breaking. This places inflaton fluctuations on the same footing as e.g. pions of the chiral Lagrangian, phonons of solids, or longitudinal polarisations of the W and Z bosons. The field π being gapless in the decoupling limit, it is fully characterised at leading order in a gradient expansion by its speed of sound c_s, that is, its dispersion relation reads $\omega = c_s k_{\rm p} + \mathcal{O}(k_{\rm p}^2)$, where $k_{\rm p} = k/a$ is the physical momentum. As a consequence of π non-linearly realising Lorentz symmetry, the size of non-linearities is correlated to the amount of symmetry breaking at the linear level. This generates well-known equilateral non-Gaussianities whose amplitude is related to the speed of sound by symmetry, $f_{\rm NL}^{\rm eq} \sim 1/c_s^2$. Possibly arising from a fundamental non-perturbative UV description of inflation, a reduced sound speed can also be commonly generated by integrating out heavy fields with masses above the scale $\Lambda_\star$ beyond which primordial fluctuations become strongly coupled. Accordingly, c_s is the primary parameter to be constrained by observations that encodes UV physics.

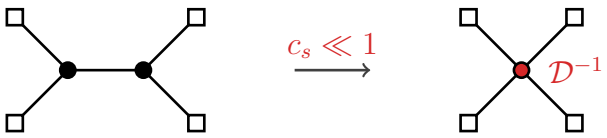


Figure 10.1: When the Goldstone boson of broken time translations has a reduced sound speed, the hidden massive sector can be integrated out albeit in a non-local (in space) manner. This leads to simpler correlators to compute that accurately reproduce the rich physics at low speed.

In this chapter, we show that the theory describing inflationary fluctuations drastically simplifies when the Goldstone boson propagates with a reduced speed of sound, to become *non-local in space*. This arises after integrating out heavy fields, therefore becoming effectively non-dynamical, as illustrated in Fig. 10.1. This theory accurately describes the full dynamics of the Goldstone boson and captures all multi-field physical effects distinct from the non-perturbative particle production leading to the conventional cosmological collider signal. As such, this theory provides a systematic and tractable way to study the imprint of massive fields on cosmological correlators.

10.1 Low-Speed Yukawa Limit

In de Sitter, dealing with massive fields even in perturbation theory is notoriously challenging, see Chap. 7. However, the picture drastically simplifies when π has a reduced speed of sound $c_s \ll 1$. To better appreciate the underlying physics behind this simplicity, let us imagine the two-to-two scattering of Goldstone bosons at the energy scale ω and consider a particle with mass $m \lesssim \omega/c_s$ mediating a force between them. In this exchange process, the energy and the momentum of the off-shell particle are of order ω and ω/c_s, respectively, implied by energy and momentum conservation. As a result, similar to the low-speed limit of the Yukawa theory, the massive field propagator can be simplified as

$$\frac{1}{\omega^2 - \boldsymbol{k}^2 - m^2} \sim \frac{-1}{\boldsymbol{k}^2 + m^2}\,. \tag{10.1}$$

This approximation corresponds to replacing the real-space Feynman propagator of the massive field $D_{\rm F}$ by a Yukawa potential

$$D_{\rm F}(\boldsymbol{x}, t; \boldsymbol{y}, t') \to \delta(t - t')\,\frac{e^{-m|\boldsymbol{x}-\boldsymbol{y}|}}{4\pi|\boldsymbol{x}-\boldsymbol{y}|}\,, \tag{10.2}$$

reflecting the instantaneous propagation of the massive field. Notice that the *local* EFT limit is recovered from the non-local one when the massive field is heavier than the transferred momentum $m \gtrsim \omega/c_s$. In this limit, the real-space propagator becomes $D_{\rm F}(\boldsymbol{x}, t; \boldsymbol{y}, t') \to m^{-2}\delta(t - t')\,\delta^{(3)}(\boldsymbol{x} - \boldsymbol{y})$. Similarly, for the computation of cosmological correlators, we show that the relativistic heavy field can be integrated out, albeit in a non-local manner in space, resulting in a *non-local single-field EFT* for the Goldstone boson. This non-local EFT comes extremely handy when computing cosmological correlators for mainly two reasons. First, the only dynamical field in this EFT is the massless field π which has a simple mode function, at least when the effect of the mixing with the additional field is weak. Second, exchange diagrams reduce to contact ones, which drastically simplify computations. Corrections to the leading non-local EFT can also be systematically captured by adding extra higher-order time-derivative terms.

10.2 Integrating out Heavy Fields

It is the most essential aspect of the EFT program that heavy degrees of freedom manifest in low-energy observables through small effects proportional to powers of E/M, with E the energy of the "experiment" and M the mass scale of the heavy fields, and where by definition of "heavy" one has $E \ll M$. In standard QFT in flat spacetime, this statement is made explicit in the so-called decoupling theorem [509]: given a scattering process with only light fields in the external states, Feynman diagrams containing internal heavy fields are suppressed by powers of E/M, with E the typical energy of the external particles. In the Wilsonian approach to QFT, one is not interested in the fully decoupled low-energy theory, but instead considers the effects of the heavy fields as providing an infinite set of effective interaction vertices for the light particles. Once again, the contribution of these to observables are controlled by positive powers of E/M, which at the level of the Lagrangian implies the presence of irrelevant operators. This is nothing but the standard logic of the derivative expansion.

For the sake of pedagogy, we begin this section with a brief review of the procedure of integrating out heavy fields in flat spacetime. We focus for simplicity on a simple scalar field model, the generalisation to spinning fields and more general interactions (e.g. non-canonical kinetic terms) being fairly straightforward. We then explicitly derive the non-local EFT for π.[1]

10.2.1 Time-Independent Backgrounds

Consider the following theory describing a heavy field σ coupled to a light field φ

$$S[\varphi,\sigma] = S_\varphi + \int \mathrm{d}^4x \bigg[-\frac{1}{2}(\partial\sigma)^2 - \frac{M^2}{2}\sigma^2 + \sigma F[\varphi] \bigg] , \tag{10.3}$$

where S_φ does not contain σ. If the energy of the experiment is much smaller than the mass scale M, $E \ll M$, then the kinetic term of σ will be negligible relative to the mass term: $(\partial\sigma)^2 \sim E^2\sigma^2 \ll M^2\sigma^2$ (recall that we are working here in flat spacetime and assume a standard relativistic dispersion relation). It is therefore consistent to drop derivatives of the heavy field and thus obtain an action in which σ only appears algebraically. Of course, strictly speaking, the statement that the kinetic term is small is only true on-shell and not at the level of the Lagrangian. Ignoring derivatives in the Lagrangian is however justified if we are only interested in tree-level effects, because the equation of motion thereby obtained obviously coincides with the one we would get by dropping derivatives in the full equation of motion.

Solving this approximate form of the σ equation, we find $\sigma_c \simeq \frac{1}{M^2}F[\varphi]$, where the subscript stands for 'classical', i.e. σ_c is the solution to its *classical* equation of motion. Substituting into (10.3), one gets the effective action for φ

$$S_{\rm eff}[\varphi] \simeq S[\varphi,\sigma_c] \simeq S_\varphi + \frac{1}{2M^2}\int \mathrm{d}^4x F[\varphi]^2 \, . \tag{10.4}$$

[1] Secs. 10.2.1 and 10.2.2 were originally written by Sebastian Garcia-Saenz and are included in the forthcoming review to which I have contributed.

This result is of course not exact, for two reasons. The first approximate sign is because we are working at tree level, which will be enough for the purpose of this thesis, although we will briefly mention loop corrections later on. The second approximate sign is because we did not actually substitute the full classical solution but only its first approximation in the low-energy expansion. Before continuing, let us emphasise that everything we have said so far applies to more general theories. Had we included self-interactions for σ, or more general couplings between σ and φ, then we would follow the same steps as above, the only added complication is that the equation of motion of σ would now be non-linear (although still algebraic at this order in the derivative expansion).

Let us next improve upon this approximation by calculating the full classical solution for σ. The simple assumed form of Eq. (10.3) allows us to carry this out explicitly, but once again the procedure could in principle be done for a more general theory, although in practice we would usually need to solve the non-linear equations of motion perturbatively. The quadratic terms for σ in (10.3) can be written as

$$S_\sigma = -\frac{1}{2}\int \mathrm{d}^4x\mathrm{d}^4y\,\sigma(x)\mathcal{K}(x-y)\sigma(y)\,, \qquad \mathcal{K}(x) \equiv (M^2-\Box)\delta(x)\,. \tag{10.5}$$

Defining the inverse $\mathcal{K}^{-1}$ of the distribution $\mathcal{K}$ via $\int \mathrm{d}^4z\,\mathcal{K}(x-z)\mathcal{K}^{-1}(z-y) = \delta(x-y)$, we may write the solution of the equation of motion of σ as

$$\sigma_c(x) = \int \mathrm{d}^4z\mathcal{K}^{-1}(x-z)F[\varphi(z)]\,. \tag{10.6}$$

Notice that $\mathcal{K}^{-1}(x)$ is nothing but the propagator of the heavy field,[2] defined via

$$(M^2-\Box)\mathcal{K}^{-1}(x) = \delta(x)\,. \tag{10.7}$$

If we now substitute the classical solution (10.6) into S_σ we obtain the full tree-level effective action $S_{\text{eff}}[\varphi] \simeq S[\varphi,\sigma_c]$. The result is however non-local as is clear from the above expression for σ_c. But let us again consider the low-energy limit $E \ll M$ and expand the propagator as a power series in $\Box/M^2$:

$$\mathcal{K}^{-1}(x) = \frac{1}{M^2}\left[\delta(x) + \sum_{n=1}^{\infty}\left(\frac{\Box}{M^2}\right)^n\delta(x)\right]\,, \tag{10.8}$$

so that

$$S_{\text{eff}}[\varphi] \simeq S_\varphi + \frac{1}{2M^2}\int \mathrm{d}^4x\left[F[\varphi]^2 + \sum_{n=1}^{\infty}F[\varphi]\left(\frac{\Box}{M^2}\right)^n F[\varphi]\right]\,. \tag{10.9}$$

[2]The explicit expression for $\mathcal{K}^{-1}$, using the Feynman prescription, is

$$\mathcal{K}^{-1}(x) = \int\frac{\mathrm{d}^4p}{(2\pi)^4}\frac{e^{-ip\cdot x}}{p^2+M^2-i\epsilon} = \frac{iM}{8\pi\sqrt{-x^2}}H_1^{(1)}(M\sqrt{-x^2})\,,$$

where $x^2 \equiv \eta_{\mu\nu}x^\mu x^\nu$. The expressions for space-like and null x^μ may be obtained respectively via analytic continuation and by taking a limit.

The low-energy expansion has produced a series of manifestly local operators. The full result is of course still non-local because it is an infinite series, but the fact that we are considering physical processes with $E \ll M$ means that we are justified to truncate this expansion. The order of the truncation is dictated by the precision one seeks in the calculation of observables, which will be naturally organised as series in powers of E/M.

Since the truncated action is now local, calculating observables is a straightforward task, although one must consistently make use of the low-energy approximation. This point is relevant in particular because of the fact that, beyond the lowest order, the effective theory expansion will necessarily produce operators with more than one derivative acting on the light fields. According to the well-known Ostrogradsky theorem [510], such higher-derivative terms are typically associated with instabilities as they produce Hamiltonians which are unbounded from below. At the quantum level these pathologies manifest themselves as additional poles in the propagators of the light fields which have negative residues, signaling the presence of ghost particles. These extra poles will however occur at energies of order M, and are therefore to be consistently ignored in the EFT.

10.2.2 Integrating out via the Path Integral

Having understood the general procedure for integrating out heavy fields at the classical level, let us make a brief aside to review the question of integrating out via the path integral and how one may go beyond the tree level approximation in the calculation of the effective action. The generating functional or path integral is given by (see Chap. 5)

$$Z[j,J] = \int \mathcal{D}\varphi \mathcal{D}\sigma \exp\left[i \int \mathrm{d}^4x \left(\mathcal{L}[\varphi,\sigma] + j\varphi + J\sigma \right) \right] . \tag{10.10}$$

The quantum effective action (not to be confused with the Wilsonian effective action S_{eff}) is defined as the Legendre transform of $\log Z$ with respect to the sources j and J:

$$\Gamma[\varphi_j, \sigma_J] = -i \log Z[j,J] - \int \mathrm{d}^4x \left[j\varphi_j + J\sigma_J \right] , \tag{10.11}$$

where

$$\varphi_j(x) = -i \frac{\delta \log Z[j,J]}{\delta j(x)} , \qquad \sigma_J(x) = -i \frac{\delta \log Z[j,J]}{\delta J(x)} , \tag{10.12}$$

correspond to the solutions of the quantum equations of motion with sources j and J, respectively [362]. Recall that $Z[j,J]$ is the generator of all the correlation functions of φ and σ. By setting $J = 0$ we obtain the generator of the correlation functions of the light fields only, which must match the generating functional of the EFT

$$Z_{\text{eff}}[j] = \int \mathcal{D}\varphi \exp\left[i \int \mathrm{d}^4x \left(\mathcal{L}_{\text{eff}}[\varphi] + j\varphi \right) \right] , \tag{10.13}$$

so that the effective Lagrangian $\mathcal{L}_{\text{eff}}[\varphi]$ is defined by the condition

$$Z[j,0] = Z_{\text{eff}}[j]\Big|_{\text{on-shell}} , \tag{10.14}$$

where we have emphasised that this equality need only hold on-shell, i.e. we only require the equality of S-matrix elements. While this result is exact, it is hardly useful since in general the path integral of the heavy field cannot be performed explicitly. We therefore consider the loop expansion, i.e. the saddle-point approximation of the generating functionals.

Consider first expanding Z_{eff} about a saddle point $\varphi_{c,j}$, i.e. a solution of the classical equation of motion with source j. Defining $\varphi' = \varphi - \varphi_{c,j}$ one finds, at next-to-leading order in the loop expansion,

$$Z_{\text{eff}}[j] = \exp\left[i\int \mathrm{d}^4x\,(\mathcal{L}_{\text{eff}}[\varphi_{c,j}] + j\varphi_{c,j})\right]\int \mathcal{D}\varphi \exp\left[\frac{i}{2}\int \mathrm{d}^4x\,\varphi\hat{Q}_{\text{eff}}\varphi\right] + \cdots\,, \tag{10.15}$$

where the differential operator $\hat{Q}_{\text{eff}}$ is defined via

$$\hat{Q}_{\text{eff}}\varphi(x) = \int \mathrm{d}^4y \frac{\delta^2 S_{\text{eff}}}{\delta\varphi(x)\delta\varphi(y)}\Big|_{\varphi=\varphi_{c,j}}\varphi(y)\,, \tag{10.16}$$

and we have dropped the prime on the field fluctuation. For a real scalar field, the above path integral gives $\int \mathcal{D}\varphi \exp\left[\frac{i}{2}\int \mathrm{d}^4x\,\varphi\hat{Q}_{\text{eff}}\varphi\right] \propto (\det \hat{Q}_{\text{eff}})^{-1/2}$, with a constant of proportionality that is irrelevant for our purposes. Legendre transforming we find

$$\Gamma_{\text{eff}}[\varphi] = S_{\text{eff}}[\varphi] + \frac{i}{2}\log\det\hat{Q}_{\text{eff}} + \cdots\,. \tag{10.17}$$

This is the familiar result that the quantum effective action equals the usual action up to loop corrections. Notice that we have relabeled $\varphi_{c,j} \to \varphi$ in the final result, which is justified since the source j is arbitrary, and therefore $\varphi_{c,j}$ is essentially unconstrained.

We can next perform the same expansion for the UV generating functional $Z[j,0]$, the important difference being that $\sigma_c \equiv \sigma_{c,J}\big|_{J=0}$ is defined here with zero source. It is therefore not unconstrained but rather determined in terms of φ by its classical equation of motion. The Legendre transform is then

$$\Gamma[\varphi,\sigma_c] = S[\varphi,\sigma_c] + \frac{i}{2}\log\det\hat{Q}\Big|_{\sigma=\sigma_c} + \cdots\,, \tag{10.18}$$

where $\hat{Q}$ is defined analogously to (10.16) in terms of the UV action S. Equality of $\Gamma_{\text{eff}}[\varphi]$ and $\Gamma[\varphi,\sigma_c]$ then immediately yields

$$S^{(0)}_{\text{eff}}[\varphi] = S[\varphi,\sigma_c]\,, \tag{10.19}$$

at zeroth order in the loop expansion, i.e. at tree level, while at one-loop we find[3]

$$S^{(1)}_{\text{eff}}[\phi] = \frac{i}{2}\log\det\hat{Q}\Big|_{\sigma=\sigma_c} - \frac{i}{2}\log\det\hat{Q}^{(0)}_{\text{eff}}\,, \tag{10.20}$$

where $\hat{Q}^{(0)}_{\text{eff}}$ is given by Eq. (10.16) upon substituting $S^{(0)}_{\text{eff}}$.

[3]The resulting determinants can be computed using the formula $\log\det\hat{O} = \mathrm{tr}\log\hat{O}$. The trace here involves an integral over spacetime (if one works in the position basis) and one therefore eventually arrives at a local action.

10.2.3 Non-Local Effective Action

Starting from the full theory of the (canonically normalised) Goldstone π_c coupled to a massive scalar field σ, see Eq. (9.53), let us now derive an effective single-field theory that captures the physics at low sound speed in an uninvolved way. We discuss how one can obtain an accurate single-field, albeit non-local, effective description of the full dynamics, in the almost entire quadratic parameter space, by integrating out the heavy degree of freedom from the mass spectrum.

Working at tree level, varying the action (9.53) with respect to $\sigma_{\rm cl}$ gives the following equation of motion

$$(-\Box + m^2)\,\sigma_{\rm cl} = \rho\dot{\pi}_c + \dots\,, \tag{10.21}$$

where $\Box \equiv g^{\mu\nu}\nabla_\mu\nabla_\nu = -\partial_t^2 - 3H\partial_t + \tilde{\partial}_i^2$ denotes the d'Alembert operator on dS_4, and the ellipses denote non-linear corrections. Here, we define $\tilde{\partial}_i \equiv \partial_i/a$. Note that it is sufficient to use the *linear* equation of motion for $\sigma_{\rm cl}$ and to plug it back in the original Lagrangian. Indeed, non-linear corrections to $\sigma_{\rm cl}$ coming from cubic interactions identically vanish up to cubic order.[4] Inverting the equation of motion for $\sigma_{\rm cl}$ gives

$$\sigma_{\rm cl} = \rho\,(-\Box + m^2)^{-1}\dot{\pi}_c\,. \tag{10.22}$$

As long as the low-energy modes described by the effective action obey a non-relativistic dispersion relation $\omega^2 \ll k_{\rm p}^2$, which is the case when the intrinsic speed of sound of the Goldstone boson is (significantly) reduced, the d'Alembert operator is dominated by spatial gradients. We will give the precise regime of validity of this approximation later on. Therefore, one can write the non-local operator in Eq. (10.22) as a time derivative expansion[5]

$$\frac{1}{-\Box + m^2} = \frac{1}{-\tilde{\partial}_i^2 + m^2}\sum_{n=0}^{\infty}(-1)^n\left[(\partial_t^2 + 3H\partial_t)(-\tilde{\partial}_i^2 + m^2)^{-1}\right]^n\,. \tag{10.23}$$

Plugging back Eq. (10.22) in the action (9.53) and keeping only the leading order term in (10.23) leads to the following non-local single-field theory

$$\begin{aligned} S_{\rm eff} = \int \mathrm{d}^4x\sqrt{-g}\,\Bigg(&\frac{1}{2}\dot{\pi}_c\left[1 + \rho^2\,\mathcal{D}^{-1}\right]\dot{\pi}_c - \frac{c_s^2}{2}(\tilde{\partial}_i\pi_c)^2 - \lambda_1\dot{\pi}_c(\tilde{\partial}_i\pi_c)^2 - \lambda_2\dot{\pi}_c^3 \\ &- \frac{\rho}{\Lambda_1}(\tilde{\partial}_i\pi_c)^2\,\mathcal{D}^{-1}\dot{\pi}_c - \frac{\rho}{\Lambda_2}\dot{\pi}_c^2\,\mathcal{D}^{-1}\dot{\pi}_c - \lambda\rho^2\dot{\pi}_c\left[\mathcal{D}^{-1}\dot{\pi}_c\right]^2 - \mu\rho^3\left[\mathcal{D}^{-1}\dot{\pi}_c\right]^3\Bigg)\,, \end{aligned} \tag{10.24}$$

[4] This can be shown in general terms as follows. The Lagrangian we are interested in schematically reads $\mathcal{L} = -\frac{1}{2}\sigma O\sigma + \sigma J(\pi)$ with the equation of motion $O\sigma = J$ for the field σ. Replacing σ by $O^{-1}J$ in the action gives $\mathcal{L} = \frac{1}{2}(O^{-1}J)J$, which, upon splitting $J = J_1 + J_2 + \dots$ into terms linear in π, quadratic etc, gives the Lagrangian $\mathcal{L} = \frac{1}{2}(O^{-1}J_1)J_1 + \frac{1}{2}(O^{-1}J_1)J_2 + \frac{1}{2}(O^{-1}J_2)J_1$ up to cubic order. Instead, if one simply replaces σ by the solution to its linear equation of motion $O^{-1}J_1$, one obtains $\mathcal{L} = \frac{1}{2}(O^{-1}J_1)J_1 + (O^{-1}J_1)J_2$. It is easy to see that both actions agree in the regime of validity of the single-field EFT. For instance, in the local EFT where O^{-1} is written as a series of $\Box^n/m^{2(n+1)}$ terms, the identification follows from $\int \mathrm{d}^4x\sqrt{-g}J_2\Box^n J_1 = \int \mathrm{d}^4x\sqrt{-g}J_1\Box^n J_2$ upon integrations by parts. Analogous arguments hold in the non-local EFT regime when considering $\int \mathrm{d}^3x J_2\mathcal{D}^{-1}J_1 = \int \mathrm{d}^3x J_1\mathcal{D}^{-1}J_2$, see the definition of $\mathcal{D}^{-1}$ after Eq. (10.24), which is transparent in Fourier space.

[5] Note that $\tilde{\partial}_i = \partial_i/a$ bears a hidden (cosmic) time dependence in the scale factor $a(t)$. As a result, the order of the operators matters.

where we have introduced the *non-local* differential operator $\mathcal{D}^{-1} = (-\tilde{\partial}_i^2 + m^2)^{-1}$. This effective theory should be understood as the leading order contribution in the time derivative expansion (10.23) where higher-order terms are encoded in an infinite number of operators, in fact, all possible terms that are compatible with the shift symmetry of the Goldstone boson. As we will see in the next section, the non-local theory (10.24) accurately describes the dynamics of the Goldstone boson in the almost entire parameter space i.e. for almost all ranges of ρ/H and m/H. However, because this theory is intrinsically single-field, it does not capture the non-perturbative particle production hence does not describe the conventional cosmological collider signal, visible in ultra-soft limits of cosmological correlators. Indeed, the effects of the massive field are encoded in (non-local) contact interactions which reflect the fact it propagates instantaneously. As such, the theory (10.24) does not describe long-range interactions coming from the exchange of an additional massive field.

Let us make an important comment. Inflationary fluctuations become strongly coupled at energies above $\Lambda_\star \sim c_s f_\pi$, see Chap. 9. Heavy particles with masses above the strong coupling scale cannot be produced on-shell. However, they can be consistently coupled to the massless mode π_c as long as the energy carried by the Goldstone boson does not exceed $\Lambda_\star$. This is analogous to the chiral Lagrangian where pions can be coupled to heavy baryons, see the insert below.[6] However, in our case of interest, heavy particles with masses far above the Hubble scale can be integrated out in the usual local manner. We will see in the following that interesting physics at low sound speed appears when $m/H \lesssim 1/c_s$, which is roughly compatible with the criterion that the additional field mass should not exceed the strong coupling scale $m \lesssim \Lambda_\star$.

Chiral Lagrangian.—In this insert, we allow ourselves a small digression to highlight similarities between the construction of the effective field theory of inflationary fluctuations and the chiral Lagrangian, especially when the Goldstone boson of broken time translations is coupled to heavy fields. Consider the QCD Lagrangian with N_f quark flavours. The action has an approximate $SU(N_f)_L \times SU(N_f)_R$ chiral symmetry that is spontaneously broken to the vector $SU(N_f)_V$ subgroup. As a consequence, there is a manifold of vacua with the same energy connected by spacetime-independent transformations along the direction of broken symmetry, analogous to the breaking time diffeomorphism invariance by the background inflaton field. These vacua are parametrised by the quark condensate $\langle \bar{q}_{Rj} q_{Li} \rangle = \sigma U_{ij}$ with $U \in SU(N_f)$. Goldstone's theorem tells us that there are $N_f - 1$ massless particles in the spectrum, one for each broken generator. These are thought of as long-wavelength ripples of the condensate, where it's value now varies in space and time $U \to U(t, \boldsymbol{x})$. These excitations are parametrised by

$$U(t, \boldsymbol{x}) = \exp\left(\frac{2i}{f_\pi}\, \pi^a(t, \boldsymbol{x}) T^a\right) , \tag{10.25}$$

where T^a are generators of $SU(N_f)$. The modes π^a for $a = 1, \dots N_f^2 - 1$ are called pions. The dimensionful constant f_π ensures that pions have canonical dimensions

[6] We thank Paolo Creminelli for helpful discussions on this topic.

for scalar fields in four dimensions. At leading order in derivatives, there is a unique Lagrangian describing the dynamics of pions that is invariant under chiral symmetry

$$\mathcal{L} = -\frac{f_\pi^2}{4}\,\mathrm{tr}(\partial^\mu U^\dagger \partial_\mu U)\,. \tag{10.26}$$

Although this chiral Lagrangian is very simple, it does not describe a free theory because U is valued in $SU(N_f)$. The beauty of the chiral Lagrangian is that it contains an infinite series of non-renormalisable interactions whose couplings are all determined by a single parameter f_π: this is a consequence of non-linear realisation of chiral symmetry.

Let us now specify to the strong nuclear interaction keeping only the two lightest quarks u and d whose masses are well below the QCD strong coupling scale $\Lambda_{\rm QCD} = 4\pi f_\pi \sim 1$ GeV. The parameter f_π is therefore identified with the chiral symmetry-breaking scale above which a description in terms of weakly coupled Goldstone bosons alone is appropriate. Considering $N_f = 2$ quarks implies the existence of three pseudo-Goldstone bosons, i.e. the $\pi^\pm$ and π^0 pions. Although heavy baryons—the proton and the neutron in this case—have masses close (or above) the QCD strong coupling scale, they can couple to pions through for example a pseudo-vector coupling $g\bar{N}\gamma^5\gamma_\mu T^a \partial^\mu \pi^a N$. Being stable, they cannot decay to light pions nor being produced on-shell from pion excitations. However, the proton and the neutron can scatter by mediating a pion. We refer to [511, 512] for more details.

10.3 Dispersion Relation

The quadratic part of the non-local action (10.24) describes various phenomenologically interesting regimes for the Goldstone boson dynamics, that can be deciphered through its dispersion relation. Here, we clarify the dynamics of the Goldstone boson by looking at extreme regimes. We explicitly show that the non-local theory interpolates between the *reduced speed of sound* regime and the *modified dispersion relation* regime.

When the energy of the Goldstone boson is above the Hubble scale $\omega \gg H$, its dynamics is well described by plane-wave solutions. This motivated approximation can be extended up to horizon crossing where Hubble friction kicks in and π_c starts to freeze. The quadratic part of the non-local action (10.24) leads to the following dispersion relation

$$\omega^2 = \frac{c_s^2 k_{\rm p}^2}{1 + \frac{\rho^2}{k_{\rm p}^2 + m^2}}\,, \tag{10.27}$$

where $k_{\rm p} = k/a$ is the physical momentum carried by the Goldstone boson. Fixing $c_s = 1$, the quadratic theory depends on two variables m and ρ. To get some physical intuition, one can understand the qualitative behaviour of the quadratic theory in some asymptotic limits that we summarise in Fig. 10.2. In the following, we give insights on these regimes, i.e. we take the large mass and the large quadratic mixing limits.

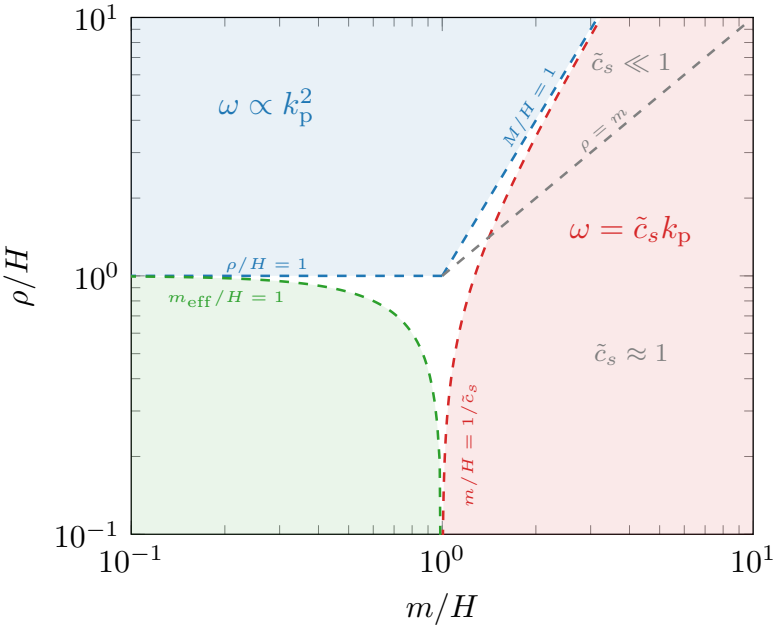


Figure 10.2: Phase diagram of the quadratic theory in the $(m/H, \rho/H)$ plane, for $c_s = 1$, that delimits three distinct regions: (i) the modified dispersion relation regime ($M \ll H$ and $\rho \gg H$ where $M = m^2/\rho$), (ii) the reduced speed of sound regime ($m \gg H/\tilde{c}_s$ with $\tilde{c}_s^{-2} = 1 + \rho^2/m^2$), and (iii) the light field regime ($m_{\rm eff} \ll H$ where $m_{\rm eff}^2 \equiv m^2 + \rho^2$). One should notice that the regime with a significantly reduced speed of sound, $\tilde{c}_s \ll 1$, is rather limited as it requires $\rho \gg m$ in region (ii). This is shown by the grey dashed line $\rho = m$. Of course, the borderlines of these regions should not be taken as exact but rather as faint boundaries: the deeper in the regions, the better the approximations.

10.3.1 Reduced Effective Sound Speed

When the mass of the heavy field becomes large, it dominates the gradient term in the non-local differential operator $\mathcal{D}^{-1} \approx 1/m^2$. The heavy field therefore leaves its imprint in the dynamics of the Goldstone boson in the form of an induced speed of sound

$$\tilde{c}_s^{-2} = c_s^{-2}\left(1 + \frac{\rho^2}{m^2}\right) . \tag{10.28}$$

The massless mode then freezes at the *effective* sound horizon $|\tilde{c}_s k\tau| \sim 1$ while having a linear dispersion relation $\omega \approx \tilde{c}_s k_{\rm p}$. Clearly, this limiting regime is valid as long as the physical momentum $k_{\rm p}$ of the Goldstone boson satisfies $k_{\rm p} \ll m$. Using the dispersion relation, one can see that this regime is an accurate description of the quadratic dynamics if $\omega \ll \omega_{\rm new} = \tilde{c}_s m$, where $\omega_{\rm new}$ marks the energy scale at which higher-order terms in the derivative $-\tilde{\partial}_i^2/m^2$ expansion should be taken into account. In order to be able to initialise the mode functions in the proper vacuum, one must require that $\omega_{\rm new}$ be well above the Hubble scale i.e. $\omega_{\rm new} \gg H$. Therefore, the reduced effective speed of sound regime is valid if

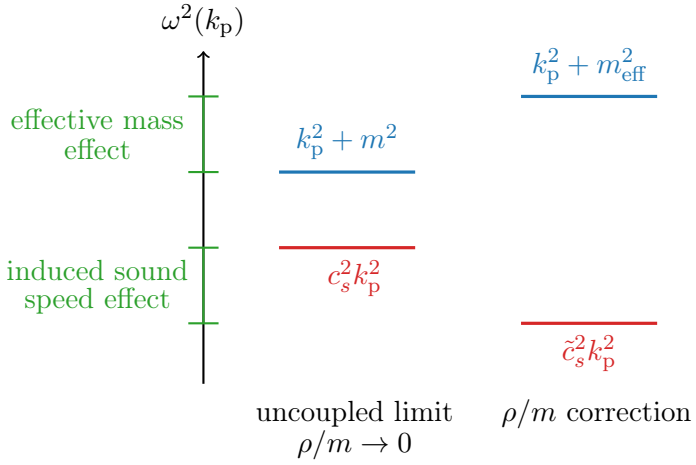
$$\frac{H}{\tilde{c}_s} \ll m\,. \tag{10.29}$$

It should be noted that the region with a significantly reduced effective speed of sound compared to the "bare" one $\tilde{c}_s \ll c_s$ is rather limited as it requires $\rho \gg m$ while maintaining (10.29). In the two-field picture of this regime, we show in the insert below that the energy gap between the heavy and the light modes increases due to the quadratic mixing.

Reduced effective sound speed energy gap.—In this insert, we examine the energy gap between the heavy and the massless modes in the reduced effective speed of sound regime when $c_s \ll 1$. In flat space, the quadratic two-field dynamics can be solved analytically, see Chap. 11. The leading-order solution at weak mixing, corresponding to the completely decoupled case $\rho/m \to 0$, is given by $\omega_-^2 = c_s^2 k_\mathrm{p}^2$ and $\omega_+^2 = k_\mathrm{p}^2 + m^2$. Let us now examine the perturbative limit $\rho \lesssim m$. Taking this limit in the exact dispersion relations (11.23) at next-to-leading order leads to

$$\omega_-^2 \approx c_s^2 k_\mathrm{p}^2 - \rho^2 \frac{c_s^2 k_\mathrm{p}^2}{(1-c_s^2)k_\mathrm{p}^2 + m^2} \quad \text{and} \quad \omega_+^2 \approx k_\mathrm{p}^2 + m^2 + \rho^2 \frac{k_\mathrm{p}^2 + m^2}{(1-c_s^2)k_\mathrm{p}^2 + m^2} \,. \tag{10.30}$$

At reduced sound speed, $c_s \ll 1$, the heavy mode dispersion relation reduces to $\omega_+^2 \approx k_\mathrm{p}^2 + m_\mathrm{eff}^2$ where $m_\mathrm{eff}^2 = m^2 + \rho^2$. For the massless mode, assuming $(1-c_s^2)k_\mathrm{p}^2 \ll m^2$, the dispersion relation boils down to $\omega_-^2 \approx c_s^2\,(1-\rho^2/m^2)k_\mathrm{p}^2$, recovering the induced sound speed $\tilde{c}_s^2 = c_s^2\,(1+\rho^2/m^2)^{-1} \approx c_s^2\,(1-\rho^2/m^2)$ in the limit $\rho \lesssim m$, see Eq. (10.28). Note that the Goldstone boson cannot acquire an effective mass from the quadratic mixing because it is protected by shift symmetry. We summarise the effect of the quadratic coupling at weak mixing in the following energy-level diagram



10.3.2 Modified Dispersion Relation

In the regime where $k_\mathrm{p} \gg m$, the gradient term dominates the mass in the non-local differential operator $\mathcal{D}^{-1} \approx -\tilde{\partial}_i^{-2}$. Additionally, for $\rho \gg k_\mathrm{p}$, the second term containing $\mathcal{D}^{-1}$ in the quadratic part of the action (10.24) dominates over the usual $\dot{\pi}_c^2$ term. This regime is similar, but still different from ghost inflation [513], and describes the dynamics of the Goldstone boson having a modified dispersion relation

$\omega \approx c_s k_{\rm p}^2/\rho$. Evaluating this dispersion relation at the Hubble scale $\omega = H$, one can see that the Goldstone boson freezes at the time scale set by $c_s^{1/2}|k\tau| \sim \sqrt{\rho/H}$, before the usual horizon crossing $|k\tau| \sim 1$. In this regime, the quadratic theory can be fully solved analytically. The equation of motion is found to be

$$\ddot{\pi}_c + 5H\dot{\pi}_c + \frac{c_s^2}{\rho^2}\, k_{\rm p}^4\, \pi_c = 0\,. \tag{10.31}$$

After quantising the theory and imposing Bunch-Davies initial conditions, the mode functions are completely determined in term of the Hankel function

$$\pi_{c,k}(\tau) = \sqrt{\frac{\pi}{4}}\frac{H}{\rho}\frac{H}{\sqrt{2k^3}}(-k\tau)^{5/2} H^{(1)}_{5/4}\left(\frac{c_s}{2}\frac{H}{\rho}(k\tau)^2\right)\,. \tag{10.32}$$

This regime leads to the amplification of the power spectrum

$$\mathcal{P}_\zeta = \frac{\Gamma(5/4)^2}{\pi^3 M_{\rm Pl}^2}\left(\frac{H^2}{\epsilon c_s}\right)\left(\frac{\rho}{H}\right)^{1/2}\,. \tag{10.33}$$

Let us now derive the precise regime of validity of this regime. Using the dispersion relation, the first condition $k_{\rm p} \gg m$ evaluated at the Hubble scale gives $c_s m^2/\rho \ll H$. This defines a new energy scale $M \equiv c_s m^2/\rho$. When M approaches the Hubble scale, the dynamics becomes sensitive to higher-order powers of $m^2/\tilde{\partial}_i^2$, i.e. these terms are no longer irrelevant and the effective description of the Goldstone boson having a non-linear dispersion relation breaks down. The second condition $\rho/k_{\rm p} \gg 1$, upon using the dispersion relation at $\omega = H$, gives $\rho/H \gg 1/c_s$. To sum up, the modified dispersion relation regime is valid as long as

$$M \equiv \frac{c_s m^2}{\rho} \ll H\,, \quad \text{and} \quad \frac{\rho}{H} \gg \frac{1}{c_s}\,. \tag{10.34}$$

From the two asymptotic regimes above, it is clear that the dispersion relation (10.27) gives a unified description in the (c_s, m, ρ) parameter space of the full quadratic dynamics, except in the regime where $m < H$ and $\rho < H$, where the non-local EFT is not valid. Indeed, if the additional field is light and weakly mixed to π_c, the Goldstone boson is continuously sourced by σ on super-Hubble scales. The dynamics is then sensitive to the amount of e-folds elapsed from the moment at which the mode crosses the horizon to the end of inflation. In the next section, we derive the precise regime of validity of the non-local single-field theory (10.24).

10.4 Regimes of Validity

It is important to determine the precise regime of validity of the non-local theory (10.24), as the leading-order term in the derivative expansion (10.23). Indeed, we wish to treat higher-order terms as perturbative corrections to the effective action.

10.4.1 Flat-space Intuition

Before considering cosmological correlators, for pedagogical reasons, it is instructive to analyse the dynamics in the flat-space limit $H \to 0$. Let us come back to the full two-field picture (9.53) and consider the four-point amplitude of Goldstone bosons due to the exchange of a σ field, with interactions $g\pi_c^2\sigma$ for definiteness. This amplitude is given by

$$\mathcal{A} = \mathcal{A}_s + \mathcal{A}_t + \mathcal{A}_u \,, \tag{10.35}$$

where the three contributions are the s, t and u channels, respectively. We denote the particle four-momenta as $p_a^\mu = (\omega_a, \boldsymbol{p}_a)$, where $a \in \{1, \dots, 4\}$ labels the momentum of each particle. Importantly, since boost invariance is broken, the scattering amplitude is no longer a function of the Lorentz-invariant momentum inner products. Instead, the s-channel amplitude is given by

$$\mathcal{A}_s = \frac{-g^2}{(\omega_1 + \omega_2)^2 - (\boldsymbol{p}_1 + \boldsymbol{p}_2)^2 - m^2} \,, \tag{10.36}$$

where we use all incoming particles convention, so that $\sum_a \omega_a = 0$ and $\sum_a \boldsymbol{p}_a = 0$. When writing the non-local effective theory (10.24), we have precisely considered that the term $(\omega_1 + \omega_2)^2$ is negligible compared to the term $(\boldsymbol{p}_1 + \boldsymbol{p}_2)^2$, which is equivalent to considering that the time derivative is negligible compared to the gradient term in the equation of motion of σ. Because the Goldstone boson propagates with a reduced sound speed, we have $(\omega_1 + \omega_2)^2 = c_s^2(p_1 + p_2)^2 \approx 4c_s^2k^2$, where k is the characteristic momentum carried by incoming particles.

Let us now consider two situations. The first one is when the transfer momentum carried by the exchanged particle, denoted $q = |\boldsymbol{q}|$, is of the same magnitude as the incoming particle, that is $q^2 \equiv (\boldsymbol{p}_1 + \boldsymbol{p}_2)^2 \approx 4k^2$. If the sound speed of the Goldstone boson is sufficiently reduced $c_s \ll 1$, then we always have $(\omega_1 + \omega_2)^2 \ll (\boldsymbol{p}_1 + \boldsymbol{p}_2)^2$ and the non-local theory correctly describes the dynamics for this kinematic configuration. The second case is that of the transfer momentum being soft. In this case, k is the hard momentum. We immediately see that in the ultra-soft limit—i.e. when $q/k \ll 2c_s$—, the term $(\omega_1 + \omega_2)^2$ is no longer negligible compared to $(\boldsymbol{p}_1 + \boldsymbol{p}_2)^2$. In other words, the propagator is no longer dominated by the gradient term and the non-local theory (10.24) breaks down. Crucially, this means that the regime of validity of the non-local effective theory not only depends on the parameters of the theory but also on the *kinematics*, and fails to correctly describe ultra-soft limits of scattering amplitudes or—as we will see in the next paragraph—cosmological correlators.

10.4.2 Soft Limits of Cosmological Correlators

We now extend this picture to cosmological correlators. The time dependence of the background and of the physical momenta makes the analysis more intricate. However, when the energy of the Goldstone boson is above the Hubble scale $\omega \gtrsim H$, we still can use the notion of dispersion relation to derive the precise regime of validity of the non-local effective theory. It should be noted that when $\omega \lesssim H$, corrections due to Hubble friction become important. Although these corrections

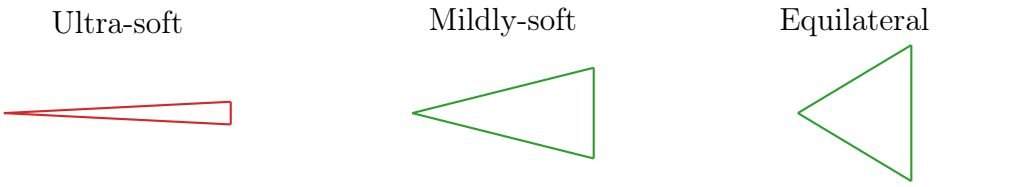


Figure 10.3: Summary of the regimes of validity of the effective action (10.24) for cosmological correlators, in the low-speed collider regime $\rho \lesssim H/c_s$ (*top*) and in the modified dispersion relation regime (*bottom*). We have coloured in red the kinematic configuration that is not accurately described by the non-local effective theory and in green those that are. When the massive field is heavy $m \gg H$, the effective description is valid in all configurations. For purpose of illustration, we have displayed the regimes of validity for the three-point correlators as they are our main interest in this work, but the same conditions should be verified for higher-point correlators.

can be accounted for systematically by working at the level of the mode functions, we do not follow this path for simplicity of presentation.

In the full two-field picture, let us consider a generic cubic interaction describing the decay of a massive field σ into two Goldstone bosons appearing on the external legs of a correlator. We are intentionally being agnostic on the precise form of this interaction because it is unimportant for the following argument. Such a process is described by $(-\Box + m^2)\sigma = J(\pi_c)$, where the sourcing J is quadratic in the field π_c. Depending on the precise channel that we consider, the massive field σ can carry a hard (i.e. short) or a soft (i.e. long) momentum. In the following, we examine the most constraining situation, where the Goldstone bosons are the short modes $k_{\rm p} = k_s/a$ and the massive field is the long mode $q_{\rm p} = k_\ell/a$. Considering only the leading order term in the time derivative expansion (10.23) enforces the following inequality to hold for the effective action to be correct:

$$\omega^2(k_{\rm p}) \lesssim q_{\rm p}^2 + m^2\,. \tag{10.37}$$

Here, $\omega^2(k_{\rm p})$ should be understood as the sum of the energies of both Goldstone bosons. Of course, we stress that the stronger the inequality is, the better the approximation of working with the effective action will be. The complication when dealing with cosmological correlators is that (10.37) depends on time, which is hidden in the physical momenta. In order for the non-local EFT to give an accurate description of cosmological correlators, we do not need this inequality to hold at all times (the fields are effectively decoupled deep inside the horizon $\omega \gg H$ where the system asymptotically reaches the vacuum state), but it should be valid at the critical time of horizon crossing of the Goldstone boson $\omega \sim H$. Let us now examine the cases of weak and strong mixing separately.

At weak mixing, the Goldstone boson dynamics is described by a linear dispersion

relation $\omega^2(k_{\rm p}) = c_s^2 k_{\rm p}^2$. Evaluating this expression for energies of order the Hubble scale gives $c_s k_{\rm S} = aH$. Plugging back this condition in (10.37) gives

$$1 \lesssim \frac{1}{c_s^2}\left(\frac{k_\ell}{k_s}\right)^2 + \left(\frac{m}{H}\right)^2 . \tag{10.38}$$

Two situations appear. If the field σ is heavy $m \gtrsim H$, then (10.38) is always valid. If the mass of the field σ is of order the Hubble scale $m \sim H$, then one needs to ensure that the first term on the right-hand side of the inequality is greater than unity, i.e. $k_\ell/k_s \gtrsim c_s$. As a result, the momentum carried by σ cannot be arbitrarily soft.[7] Notice that within the regime of the low-speed collider, i.e. for masses such that $m \lesssim H/c_s$, one can neglect the mass term for $\omega(k_{\rm p}) \sim H$, as the non-local dynamics is dominated by the gradients. Also, from (10.38), it is clear that close to equilateral configurations $k_\ell \sim k_s$, the effective action is valid as long as the sound speed is reduced.

At strong enough mixing, the Goldstone boson dynamics is described by the non-linear dispersion relation $\omega^2(k_{\rm p}) = c_s^2 k_{\rm p}^4/\rho^2$. For energies around the Hubble scale, this gives $c_s k_s^2 = a^2 H\rho$. Substituting this in (10.37) yields

$$1 \lesssim \frac{1}{c_s}\left(\frac{k_\ell}{k_s}\right)^2 \frac{\rho}{H} + \left(\frac{m}{H}\right)^2 . \tag{10.39}$$

If $m \gtrsim H$, this inequality is always satisfied. Likewise the weak mixing case, if $m \sim H$, one needs to require $k_\ell/k_s \gtrsim \sqrt{c_s H/\rho}$. Certainly, as we have illustrated in the flat-space picture, ultra-soft limits of cosmological correlators are not accurately described by the non-local effective theory. For the reader's convenience, we have collected the established regimes of validity in Fig. 10.3.

10.5 Non-locally Integrating out the Chemical Potential

We now generalise the above analysis to the case of a spin-1 field coupled to a helical chemical potential. Of course, the physics at low sound speed is entirely described by the local theory presented previously in Sec. 9.4.2. However, computations in this theory are complicated and the relevant physics is obscured by technicalities, see Chap. 7. For this reason, analogously to the case of a massive scalar field, we now introduce a simplified and natural picture that captures well the physics at play. Indeed, the vector field response in the bulk of the inflationary spacetime can be treated as instantaneous. This results in a non-local single-field EFT description that captures well the underlying physics. This non-locality, although mild as we will see, turns out to be critical for bringing out the parity violation to the final observables.

[7] We now see that if we had chosen one of the Goldstone boson to be the long mode and the other one to be the short mode, then the massive field would have been a short mode. Therefore, ω on the left-hand side of (10.37) would have been the sum of the energies of a long and a short mode, therefore completely dominated by the short mode, ultimately creating no hierarchy of scales.

Explicitly writing the mixing of the vector field with the Goldstone boson through its coupling to a current $J_i(\pi_c)$, the action reads

$$S_{\rm UV} = \int {\rm d}t{\rm d}^3x a^3 \left[\frac{1}{2}\dot{\pi}_c^2 - \frac{c_s^2}{2}(\tilde{\partial}_i\pi_c)^2 \right. \\ \left. - \frac{1}{2a^2}\sigma_i \left[\delta_{ij}(\partial_t^2 + H\partial_t) + \mathcal{D}_{ij}\right]\sigma_j + \frac{\sigma_i}{a^2}J_i(\pi_c) \right], \tag{10.40}$$

where we have introduced the spatial component of the quadratic kinetic operator of the massive spinning field

$$\mathcal{D}_{ij} \equiv \left(-\tilde{\partial}_i^2 + m^2\right)\delta_{ij} - 2\kappa\epsilon_{ijl}\tilde{\partial}_l \,, \tag{10.41}$$

that can be identified as the effective frequency of the vector field in Fourier space, and the Goldstone currents (up to a total derivative) from the operators in (9.63)

$$J_i(\pi_c) \equiv -\frac{1}{\tilde{\Lambda}}\dot{\pi}_c\partial_i\pi_c + \frac{a^{-2}}{\Lambda^3}\partial_j\dot{\pi}_c\partial_i\partial_j\pi_c + \frac{1}{\bar{\Lambda}^3}\ddot{\pi}_c\partial_i\dot{\pi}_c \,. \tag{10.42}$$

The Gaussian form of the vector sector in the UV Lagrangian (10.40) allows one to directly integrate out σ_i and obtain an effective theory, if the massive vector field is not excited on-shell. The effective theory is necessarily non-local in time and space, and can be formally written as

$$S_{\rm EFT} = \int {\rm d}t{\rm d}^3x a^3 \left[\frac{1}{2}\dot{\pi}_c^2 - \frac{c_s^2}{2}(\tilde{\partial}_i\pi_c)^2 + \frac{1}{2a^2}J_i(\pi_c)\left[(\partial_t^2 + H\partial_t) + \mathcal{D}\right]^{-1}_{ij} J_j(\pi_c) \right]. \tag{10.43}$$

Since the vector response is much faster than the relaxation of the Goldstone, one can expand the second line in powers of $-(\partial_t^2 + H\partial_t)/\mathcal{D} \sim \omega_\pi^2/\omega_\sigma^2 \sim c_s^2 \ll 1$. The fully non-local differential operator becomes effectively non-local in space only, and reads

$$\left[(\partial_t^2 + H\partial_t) + \mathcal{D}\right]^{-1}_{ij} = \mathcal{D}^{-1}_{il}\sum_{n=0}^{\infty}\left[-(\partial_t^2 + H\partial_t)\,\mathcal{D}^{-1}\right]^n_{lj} \,. \tag{10.44}$$

This allows one to construct a non-local single-field EFT organized as a *time-derivative expansion*, whose first leading terms are

$$S_{\rm EFT} = \int {\rm d}t{\rm d}^3x a^3 \left[\frac{1}{2}\dot{\pi}_c^2 - \frac{c_s^2}{2}(\tilde{\partial}_i\pi_c)^2 + \frac{1}{2a^2}J_i(\pi_c)\mathcal{D}^{-1}_{ij}J_j(\pi_c) \right. \\ \left. - \frac{1}{2a^2}J_i(\pi_c)\mathcal{D}^{-1}_{il}(\partial_t^2 + H\partial_t)\,\mathcal{D}^{-1}_{lj}J_j(\pi_c) + \mathcal{O}(\partial_t^4) \right]. \tag{10.45}$$

Here, only the Leading-Order (LO) and the Next-to-Leading-Order (NLO) non-local EFT operator are spelled out explicitly. The non-local differential operator $\mathcal{D}^{-1}$ can be projected onto parity-even and parity-odd parts

$$\mathcal{D}^{-1}_{ij} = [\mathcal{D}^{-1}_{\rm PE}]_{ij} + [\mathcal{D}^{-1}_{\rm PO}]_{ij} \,, \tag{10.46}$$

with

$$[\mathcal{D}_{\rm PE}^{-1}]_{ij} \equiv \frac{(-\tilde{\partial}_i^2+m^2)\left[\delta_{ij}+\frac{4\kappa^2\tilde{\partial}_i\tilde{\partial}_j}{(-\tilde{\partial}_i^2+m^2)^2}\right]}{(-\tilde{\partial}_i^2+m^2)^2+4\kappa^2\tilde{\partial}_i^2}\,,$$
$$[\mathcal{D}_{\rm PO}^{-1}]_{ij} \equiv \frac{2\kappa\epsilon_{ijl}\tilde{\partial}_l}{(-\tilde{\partial}_i^2+m^2)^2+4\kappa^2\tilde{\partial}_i^2}\,. \tag{10.47}$$

Let us make a few comments on the non-local single-field theory (10.45).

- The appearance of inverse spatial derivatives in $\mathcal{D}_{ij}^{-1}$ implies that the action actually contains terms evaluated at distinct spatial positions, i.e. that the action is spatially non-local. This does not signal any pathological behaviour, as such form of non-locality is mild: the effect of the action at distance that this describes is confined within the Compton wavelength of the massive spin-1 field, analogous to the non-local Yukawa force after integrating out the pions in nuclear theory. For the same reason, correlators generated by (contact) interactions in the theory (10.45) satisfy the Manifest Locality Test (MLT) [438]. Indeed, $\mathcal{D}_{ij}^{-1}$, once expressed in Fourier space, has no singularity in the long wavelength limit $k \to 0$, due to the displacement of its pole away from $\partial_i^2 = 0$ by the presence of the finite mass. More details will be given in the following chapter.

- The formal series in Eq. (10.44) is actually divergent. For $\mathcal{D}$ being a rational function of the scale factor, the time derivatives bring a factorial contribution $\partial_t^{2n} \sim (2n)!$, which always dominates over the EFT expansion $\mathcal{D}^{-2n}$ in the large-order limit. Such a divergence is not a surprise, since we expect non-perturbative effects that are not captured by the $\mathcal{D}^{-1}$ expansion to kick in at large orders, and indeed cosmological collider signals coming from on-shell particle propagation are *not* captured by the non-local EFT.[8] For our purpose, apart from internal ultra-soft limits of correlators $k_\ell/k_s \lesssim c_s$ where this effective description breaks down for $m \sim H$, it suffices to truncate the time-derivative expansion (10.44) at LO or NLO.

- Note that the non-local EFT contains a single massless degree of freedom with a Bunch-Davies vacuum. It is also invariant under a global dilation transformation $(t, \boldsymbol{x}) \to (t + \Delta t, \boldsymbol{x}e^{-H\Delta t})$, which is equivalent to scale invariance. Additionally, the whole tower of interactions in Eq. (10.45) generates IR-finite correlators. Thus the non-local EFT satisfies all the assumptions of the no-go theorem on parity violation except the implicit locality requirement [106, 107]. This *emergent* non-locality is derived from the fact that the UV theory contains an extra massive spinning field.

[8] Another perspective on this can be gained by examining the time-dependence of the vector field equation of motion. Namely, the time dependence in $\mathcal{D}$—hidden in the physical momenta $k_{\rm p} = k/a(t)$—leads to $[\partial_t^2 + H\partial_t, \mathcal{D}^{-1}] \neq 0$, which is the cause of the $(2n)!$ behavior at large orders. Physically this corresponds to the Stokes phenomenon for time-dependent equation of motions with particle production, see Chap. 4.

From the UV picture, it is clear that the origin of parity-violating observables stems from the intrinsic chemical-potential induced parity-odd dynamics of the vector field. This parity-odd dynamics subsequently propagates to the visible sector through parity-even mixing interactions. From the non-local single-field EFT, after inspecting the structure of the non-local parity-odd operator $\mathcal{D}_{\rm PO}^{-1}$ in Eq. (10.47), it becomes manifest that the theory leads to a non-vanishing parity-violating trispectrum even without any explicit reference to the UV massive field.

11

Boost-Breaking Cosmological Correlators

In this chapter, we present a new discovery channel to detect additional heavy particles during inflation when they are coupled to the Goldstone boson that propagates with a reduced speed of sound $c_s \ll 1$. These so-called *cosmological low-speed collider signals* are characterised by a distinct *resonance* in mildly-soft (internal) kinematic configurations of cosmological correlators, signalling the presence of a massive particle lighter than H/c_s, as illustrated in Fig. 11.1. In analogy with terrestrial collider experiments in which massive particles leave resonant signatures in the cross section of lighter particles' collisions when the center of mass energy coincides with the particle masses $\sqrt{s} \sim m$, the low-speed collider resonance is located at $k_\ell/k_s \sim c_s m/H$, where k_ℓ and k_s are the long and short modes. After the detection of equilateral-type non-Gaussianities and hence the measurement of c_s, we would enter an era of precision measurements, analogous to electroweak precision physics in colliders. Measuring the low-speed collider peak would reveal the existence of an additional field coupled to the Goldstone boson and would give indications about its mass, which could be later confirmed by the measurement of the conventional cosmological collider signal in ultra-soft limits.

In addition, when coupling the Goldstone boson to a spin-1 massive field coupled to a helical chemical potential, we show that a large parity-violating primordial trispectrum can be produced while remaining under perturbative control, and that its amplitude is enhanced to $\mathcal{O}(e^{-c_s m/H})$. We show that the resulting parity-odd component of the trispectrum is completely fixed by the singularity of the non-local interactions. The derived parity-odd template consists of simple rational and exponential functions, thereby greatly reducing the computational costs of future non-Gaussianity data analysis. We then conduct a thorough analysis of the kinematic dependence of the identified signal. In particular, we show that the internal

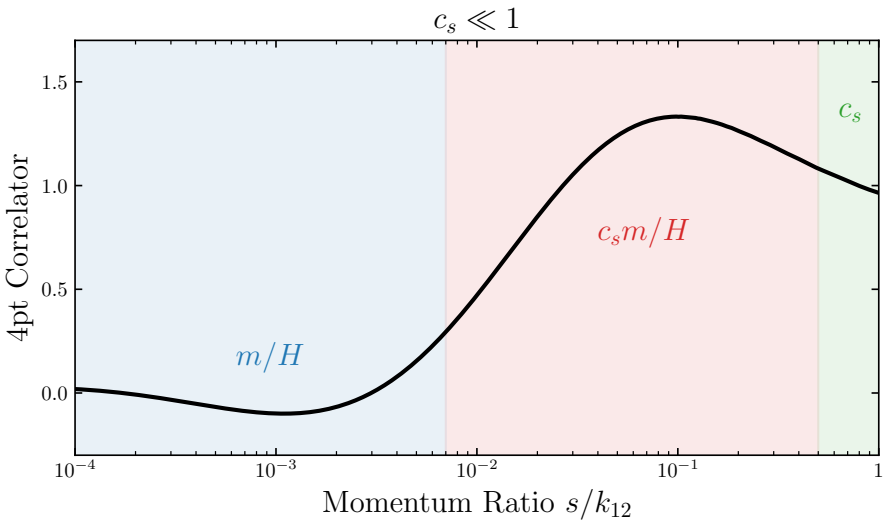


Figure 11.1: Schematic illustration of the four-point cosmological correlator—representative of any correlator, in particular the bispectrum shape for observational interest—as function of the momentum ratio in the low-speed regime. A strong breaking of de Sitter boosts during inflation leads to large equilateral-type non-Gaussianities, whose size in regular configurations, $s/k_{12} \sim k_\ell/k_s \sim 1$ (green), fixes the speed of sound c_s of the Goldstone bosons π. The presence of an extra heavy particle is imprinted in the low-speed collider signal in mildly-soft configurations, $s/k_{12} \sim k_\ell/k_s \sim c_s m/H$ (red). Together with the detection of equilateral non-Gaussianities, this distinctive resonance provides a clean detection channel to pinpoint the mass of additional particles. In ultra-soft configurations, $s/k_{12} \sim k_\ell/k_s \ll c_s m/H$ (blue), the spontaneous production of these particles by the expanding spacetime is imprinted in the conventional cosmological collider signal, i.e. characteristic oscillatory patterns whose frequency is set by m/H and amplitude is suppressed by $e^{-\pi m/2H}$. As we delve into softer configurations of cosmological correlators, one requires an increasing level of precision. Therefore, it is highly probable that we will first detect the low-speed collider resonance before detecting any indication of a cosmological collider signal.

mildly-soft kinematic configurations exhibit a resonance peak that is identified as the low-speed collider signal. Its location is fixed by a combination of the sound speed, the mass and the chemical potential. Moreover, we find a new family of oscillatory signals that are periodic in the momentum ratio rather than its logarithm as in conventional cosmological collider signals. The frequency of this oscillatory pattern is determined by the sound speed and the chemical potential, but not the mass of the exchanged vector field. Consequently, detecting a parity-violating trispectrum provides an interesting detection channel for extra massive and spinning particles, as well as for reconstructing parameters governing inflationary fluctuations.

11.1 Cosmological Correlators at Low Speed

The various cubic interactions in the full theory (9.53) gives rise to single-, double-, and triple-exchange diagrams for the bispectrum. Not being interested in the cosmological collider signal here, but rather in the more striking low-speed collider signature, we will extract it by using the effective single-field theory (10.24), within which all diagrams collapse into simple (non-local) contact ones.

Following the bootstrap approach discussed in Chap. 7, we will first trade the Goldstone boson for an auxiliary field φ with mass $m_\varphi^2 = 2H^2$ that propagates with a speed of sound c_s, and identify a set of seed correlators that serve as building blocks for all desired correlators. We then introduce well-chosen weight-shifting operators that map correlators of φ to correlators of Goldstone bosons as external fields, which is the case of interest in this work. This strategy enables one to obtain a complete set of correlators, regardless of the precise interactions. In a second phase, we will see that the seed correlators collapse into simple contact diagrams when the exchanged massive field is integrated out in a non-local manner. Eventually, within the framework of the non-local EFT (10.24), we will give explicit solutions for single-, double- and triple-exchange correlators of massless external fields.

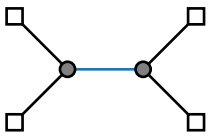
11.1.1 Weight-Shifting Operators

Let us introduce an auxiliary scalar field $\varphi(t, \boldsymbol{x})$ with mass $m_\varphi^2 = 2H^2$ that propagates with a speed of sound c_s. For $c_s = 1$, φ reduces to a conformally coupled field in dS_4. The fundamental objects that generate *all* correlators—regardless of the precise form of the interactions—are the equal-time four- and six-point correlation functions of φ generated by the interactions

$$\mathcal{L}/a(t)^3 = -g_1\varphi^2\sigma - g_2\varphi^2\sigma^2 - g_3\sigma^3\,, \tag{11.1}$$

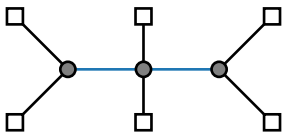
where g_i are arbitrary coupling constants. Let us stress that by considering this proxy theory—which may seem over-complicated at first sight—we are able to easily obtain all correlators generated by arbitrary interactions, even beyond those considered in (10.24), see App. C for more details. Using scaling symmetry, we define the seed functions $F_{1,2,3}$ as the corresponding solutions of the following diagrams

$$\langle\varphi_{\boldsymbol{k}_1}\varphi_{\boldsymbol{k}_2}\varphi_{\boldsymbol{k}_3}\varphi_{\boldsymbol{k}_4}\rangle'_{(1)} \equiv$$



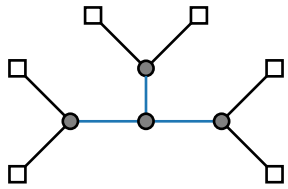
$$= g_1^2\left(\prod_{i=1}^{4}\frac{\tau_0}{c_s k_i}\right)\times\frac{1}{s_{12}}F_1\left(\frac{c_s k_{12}}{s_{12}},\frac{c_s k_{34}}{s_{12}}\right). \tag{11.2}$$

$$\langle\varphi_{\boldsymbol{k}_1}\varphi_{\boldsymbol{k}_2}\varphi_{\boldsymbol{k}_3}\varphi_{\boldsymbol{k}_4}\varphi_{\boldsymbol{k}_5}\varphi_{\boldsymbol{k}_6}\rangle'_{(2)} \equiv$$



$$= g_1^2 g_2\left(\prod_{i=1}^{6}\frac{\tau_0}{c_s k_i}\right)\times\frac{1}{s_{12}^3}F_2\left(\frac{c_s k_{12}}{s_{12}},\frac{c_s k_{34}}{s_{12}},\frac{c_s k_{56}}{s_{12}},\frac{s_{56}}{s_{12}}\right), \tag{11.3}$$

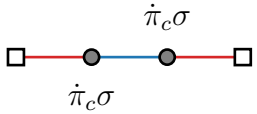
$$\langle \varphi_{\boldsymbol{k}_1}\varphi_{\boldsymbol{k}_2}\varphi_{\boldsymbol{k}_3}\varphi_{\boldsymbol{k}_4}\varphi_{\boldsymbol{k}_5}\varphi_{\boldsymbol{k}_6}\rangle'_{(3)} \equiv$$



$$= g_1^3 g_3 \left(\prod_{i=1}^{6} \frac{\tau_0}{c_s k_i}\right) \times \frac{1}{s_{12}^3} F_3\left(\frac{c_s k_{12}}{s_{12}}, \frac{c_s k_{34}}{s_{12}}, \frac{c_s k_{56}}{s_{12}}, \frac{s_{34}}{s_{12}}, \frac{s_{56}}{s_{12}}\right). \tag{11.4}$$

where $s_{ij} = |\boldsymbol{k}_i + \boldsymbol{k}_j|$, $k_{ij} = k_i + k_j$, and τ_0 marks the end of inflation surface. A gray dot ● means the sum of both (+) and (−) branch vertices. Having defined these seed functions, we now derive correlators of the Goldstone boson by introducing a set of weight-shifting operators that map diagrams with external fields φ to those with external fields π_c. The reason why this procedure is universal, regardless of the form of the considered interactions, is because the mode functions of both fields can be easily related by simple differential operators. Importantly, as the weight-shifting operators only act on external fields of a specific diagram, they are valid for any bulk theory, i.e. be it the full two-field picture or within the effective single-field theory. To avoid clutter, we leave their precise derivation in App. C.

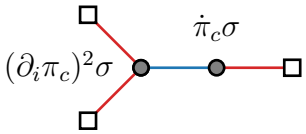
Power spectrum correction. The effect of the quadratic mixing $\dot{\pi}_c\sigma$ can be obtained from the cubic interaction $\varphi^2\sigma$ after taking a suitable soft limit on the external field. From this, one obtains the leading correction to the two-point correlator of π_c as



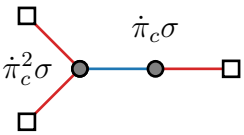
$$= \frac{\rho^2}{2c_s^2}\frac{1}{k_1^3} F_1(c_s, c_s)\,. \tag{11.5}$$

The corresponding weight-shifting operator simply consists in taking the soft limit of two external legs k_2 and k_4 while keeping the diagram connected.

Single-exchange diagrams. Both single-exchange diagrams arising from the interactions $\dot{\pi}_c^2\sigma$ and $(\partial_i\pi_c)^2\sigma$ can be obtained from the same seed function F_1. They read

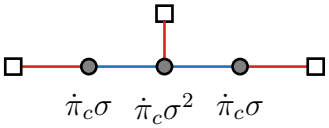


$$= -\frac{\rho}{2c_s^3}\frac{H}{\Lambda_1}\frac{1}{(k_1k_2k_3)^2}\frac{\boldsymbol{k}_1\cdot\boldsymbol{k}_2}{k_1k_2} \times \left(1 - k_{12}\frac{\partial}{\partial k_{12}} + k_1k_2\frac{\partial^2}{\partial k_{12}^2}\right) F_1\left(\frac{c_s k_{12}}{k_3}, c_s\right), \tag{11.6}$$



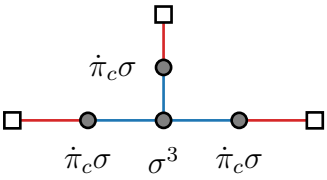
$$= -\frac{\rho}{4c_s^5}\frac{H}{\Lambda_2}\frac{k_1k_2}{(k_1k_2k_3)^2}\frac{\partial^2}{\partial k_{12}^2} F_1\left(\frac{c_s k_{12}}{k_3}, c_s\right). \tag{11.7}$$

Double-exchange diagram. The double-exchange diagram is related to the double-exchange six-point function F_2 by the relation



$$= -\lambda \frac{\rho^2}{c_s^3} \frac{1}{k_1^4 k_2 k_3} F_2\left(c_s, \frac{c_s k_2}{k_1}, \frac{c_s k_3}{k_1}, \frac{k_3}{k_1}\right) . \tag{11.8}$$

Triple-exchange diagram. The triple-exchange diagram is related to the seed function F_3 after taking suitable soft limits. It is given by



$$= -\mu \frac{\rho^3}{c_s^3} \frac{1}{k_1^4 k_2 k_3} F_3\left(c_s, \frac{c_s k_2}{k_1}, \frac{c_s k_3}{k_1}, \frac{k_2}{k_1}, \frac{k_3}{k_1}\right) . \tag{11.9}$$

The seed function F_1 is fully computed in Chap. 7. Determining a closed-form solution for $F_{2,3}$ in the full two-field theory requires more sophisticated tools and is beyond the scope of this thesis. However, when the heavy field is integrated out, the seed functions $F_{2,3}$ collapse into contact interactions that can be easily computed.

11.1.2 Non-local EFT Seed Integrals

The non-local single-field EFT at leading-order in the time-derivative expansion (10.24) has a remarkable property: the two- and three-point correlators can be derived from of a single *EFT seed integral* by applying a set of bespoke weight-shifting operators. Exploiting this feature, in this section, we give closed form expressions for the power spectrum correction and all three-point correlators.

As illustrated in Fig. 11.2, within the non-local single-field EFT framework, interactions that mix φ and σ become effective contact interactions $\mathcal{L}_{\rm eff}/a^3 = -g_1^2\varphi^2\mathcal{D}^{-1}\varphi^2 - g_1^2 g_2 \varphi^2[\mathcal{D}^{-1}\varphi^2]^2 - g_1^3 g_3[\mathcal{D}^{-1}\varphi^2]^3$. The seed functions $F_{1,2,3}$ take the following simple forms

$$F_1 = \frac{c_s k_t}{s_{12}} \mathcal{I}_1\left(\frac{c_s k_t}{s_{12}} \frac{m}{H}\right) , \tag{11.10a}$$

$$F_2 = \frac{c_s k_T s_{12}}{2 s_{56}^2} \mathcal{I}_2\left(\frac{c_s k_T}{s_{12}} \frac{m}{H}, \frac{c_s k_T}{s_{56}} \frac{m}{H}\right) , \tag{11.10b}$$

$$F_3 = \frac{3 c_s^3 k_T^3 s_{12}}{2 s_{34}^2 s_{56}^2} \mathcal{I}_3\left(\frac{c_s k_T}{s_{12}} \frac{m}{H}, \frac{c_s k_T}{s_{34}} \frac{m}{H}, \frac{c_s k_T}{s_{56}} \frac{m}{H}\right) , \tag{11.10c}$$

with $k_t = \sum_{i=1}^4 k_i$, $k_{\rm T} = \sum_{i=1}^6 k_i$, and where we have defined the *EFT seed integrals*

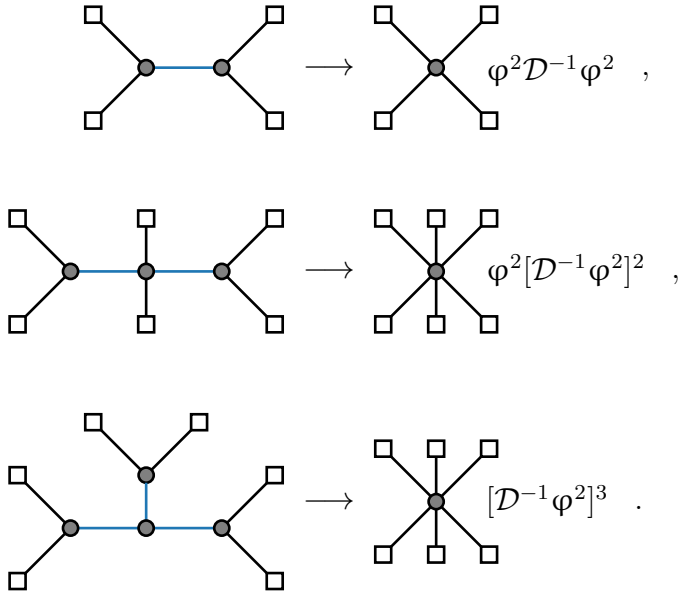


Figure 11.2: Schematic representation of the single-, double-, and triple-exchange correlators of φ in the full local fundamental theory that we consider (*left*), and the resulting (non-local) contact correlators of φ after integrating out the field σ (*right*). These diagrams provide the seeds for the complete set of correlation functions of the Goldstone boson, that are derived by acting on the seed diagrams with weight-shifting operators.

as

$$\begin{aligned}\mathcal{I}_1(x) &= \int_{-\infty}^{0} \mathrm{d}u\, \frac{\sin(u)}{u^2+x^2}\,,\\ \mathcal{I}_2(x,y) &= \int_{-\infty}^{0} \mathrm{d}u\, \frac{u^2\sin(u)}{(u^2+x^2)(u^2+y^2)}\,,\\ \mathcal{I}_3(x,y,z) &= \int_{-\infty}^{0} \mathrm{d}u\, \frac{u^2\sin(u)}{(u^2+x^2)(u^2+y^2)(u^2+z^2)}\,.\end{aligned} \tag{11.11}$$

All correlators can therefore be derived by acting with weight-shifting operators on these building-block integrals.

Properties of the EFT seed integrals. Anticipating the following development, it is useful to give some properties of the seed integrals. First, the integral $\mathcal{I}_1$ can be readily integrated analytically, giving

$$\mathcal{I}_1(x) = \frac{e^x\mathrm{Ei}(-x) - e^{-x}\mathrm{Ei}(x)}{2x}\,, \tag{11.12}$$

where Ei is the exponential integral. Note that one uses $\mathrm{Ei}(-x) = \frac{1}{2}[\mathrm{Ei}(-x+\epsilon) + \mathrm{Ei}(-x-\epsilon)]$ due to the branch cut on the negative real axis. Remarkably, the integrals $\mathcal{I}_2$ and $\mathcal{I}_3$ can be written in terms of $\mathcal{I}_1$, which therefore constitutes the building block of all correlators. Indeed, decomposing the rational functions of u^2 in the integrands as sums of simple poles, one obtains

$$\mathcal{I}_2(x,y) = \frac{x^2\,\mathcal{I}_1(x) - y^2\,\mathcal{I}_1(y)}{x^2-y^2}\,,$$
$$\mathcal{I}_3(x,y,z) = \frac{x^2\,\mathcal{I}_1(x)}{(x^2-z^2)(y^2-x^2)} + \frac{y^2\,\mathcal{I}_1(y)}{(y^2-z^2)(x^2-y^2)} + \frac{z^2\,\mathcal{I}_1(z)}{(z^2-y^2)(x^2-z^2)}\,. \tag{11.13}$$

It is straightforward to see that the apparent singularities when some arguments coincide are artificial, and to deduce the expressions

$$\begin{aligned}
\mathcal{I}_2(x,x) &= \mathcal{I}_1(x) + \frac{x}{2}\frac{\partial\mathcal{I}_1}{\partial x}(x)\,,\\
\mathcal{I}_3(x,x,x) &= -\frac{3}{8x}\frac{\partial\mathcal{I}_1}{\partial x}(x) - \frac{1}{8}\frac{\partial^2\mathcal{I}_1}{\partial x^2}(x)\,,\\
\mathcal{I}_3(x,x,y) &= \frac{x}{2(x^2-y^2)}\frac{\partial\mathcal{I}_1}{\partial x}(x) + y^2\,\frac{\mathcal{I}_1(x)-\mathcal{I}_1(y)}{(x^2-y^2)^2}\,.
\end{aligned} \tag{11.14}$$

These forms of the integrals, as we have seen, all related to $\mathcal{I}_1$, appear in the correlators of the Goldstone boson.

We have previously explained that the differential operator $\mathcal{D}^{-1}$ should be considered as a building block on its own, and that any expansion either has pitfalls (in the large mass regime) or is doomed to fail (in the low-speed collider regime). Let us now explain how these statements translate into properties of the seed integral $\mathcal{I}_1$, respectively for $x \gg 1$, and $x \ll 1$. As the rapid oscillations of the $\sin(u)$ term in the integrand of (11.11) implies that most of the contribution to the integral comes from $|u| \lesssim 1$, it is natural, for $x \gg 1$, to simply Taylor expand the denominator $(u^2+x^2)^{-1}$ for large x. After proper Wick rotations of the different frequencies in $\sin(u)$, one then obtains the asymptotic expansion $\mathcal{I}_1 = -\sum_{n=0}^{\infty}(2n)!/x^{2(n+1)}$, corresponding to the local EFT expansion in the large mass regime. Naturally, what this computation misses is the contribution from $|u| \geq x$, and hence the poles of the Wick-rotated integrand at the Euclidean times $u = \pm ix$. As for $x \ll 1$, the naive expansion of the denominator $(u^2+x^2)^{-1} = \sum_{n=0}^{\infty}(-1)^n x^{2n}/u^{2(n+1)}$, valid for $x < |u|$, cannot work simply because the integrand gets most of its contribution precisely from $|u| \sim x$.[1] In the end, only the full function can reproduce the logarithmic behaviour $\mathcal{I}_1 = \log(x) + \gamma - 1 + \ldots$ for small x.

11.1.3 Bispectrum

Using Eqs. (11.10) as the corresponding forms of the seed functions within the single-field EFT and using the weight-shifting operators, we now explicitly give analytical expressions of the two- and three-point correlators generated by (10.24). The curvature perturbation dimensionless power spectrum is given by

$$\Delta^2_\zeta = \Delta^2_{\zeta,0}\left[1 + 2c_s^2\left(\frac{\rho}{H}\right)^2\mathcal{I}_1\left(2c_s\frac{m}{H}\right)\right]\,, \tag{11.15}$$

[1] Note that the corresponding integrals, divergent near $u = 0$, could be regularized by an IR cutoff, but this would not change the fact that the corresponding expansion is anyway not valid for $|u| \leq x$, and hence cannot provide a reliable estimate of $\mathcal{I}_1$.

where $\Delta^2_{\zeta,0}$ is the zeroth order dimensionless power spectrum. The three-point correlator of the Goldstone boson associated with the interaction $(\tilde{\partial}_i\pi_c)^2\mathcal{D}^{-1}\dot{\pi}_c$ is

$$\begin{aligned}\frac{\langle\pi_{c,\boldsymbol{k}_1}\pi_{c,\boldsymbol{k}_2}\pi_{c,\boldsymbol{k}_3}\rangle'}{H^3} &= \frac{1}{2c_s^6}\frac{\rho}{\Lambda_1}\frac{k_1k_2}{(k_1k_2k_3)^3}\frac{\boldsymbol{k}_1\cdot\boldsymbol{k}_2}{K}\\ &\times\left[1+\left(\frac{K^2}{k_1k_2}-\frac{K(k_1+k_2)}{k_1k_2}+c_s\frac{m}{H}\frac{K}{k_3}\right)\mathcal{I}_1\left(c_s\frac{m}{H}\frac{K}{k_3}\right)\right.\\ &\left.-c_s\frac{m}{H}\frac{K}{k_3}\frac{K(k_1+k_2)}{k_1k_2}\mathcal{I}_1'\left(c_s\frac{m}{H}\frac{K}{k_3}\right)\right]+\ 2\ \text{perms}\,,\end{aligned}\tag{11.16}$$

where we have defined $K=k_1+k_2+k_3$, and that associated with $\dot{\pi}_c^2\mathcal{D}^{-1}\dot{\pi}_c$ reads

$$\frac{\langle\pi_{c,\boldsymbol{k}_1}\pi_{c,\boldsymbol{k}_2}\pi_{c,\boldsymbol{k}_3}\rangle'}{H^3}=\frac{1}{4c_s^4}\frac{\rho}{\Lambda_2}\frac{1}{(k_1k_2k_3)^2}\frac{k_1k_2}{Kk_3}\left[1+\left(c_s\frac{m}{H}\frac{K}{k_3}\right)^2\mathcal{I}_1\left(c_s\frac{m}{H}\frac{K}{k_3}\right)\right]+2\ \text{perms}\,.\tag{11.17}$$

The double-exchange correlator of Goldstone bosons is

$$\frac{\langle\pi_{c,\boldsymbol{k}_1}\pi_{c,\boldsymbol{k}_2}\pi_{c,\boldsymbol{k}_3}\rangle'}{H^3}=-\frac{\lambda}{2}\left(\frac{\rho}{H}\right)^2\frac{k_3^2K}{c_s^2(k_1k_2k_3)^3}\mathcal{I}_2\left(c_s\frac{m}{H}\frac{K}{k_1},c_s\frac{m}{H}\frac{K}{k_2}\right)+\ 2\ \text{perms}\,,\tag{11.18}$$

while the triple-exchange correlator of Goldstone bosons is

$$\frac{\langle\pi_{c,\boldsymbol{k}_1}\pi_{c,\boldsymbol{k}_2}\pi_{c,\boldsymbol{k}_3}\rangle'}{H^3}=-\frac{3}{2}\frac{\mu}{H}\left(\frac{\rho}{H}\right)^3\frac{K^3}{(k_1k_2k_3)^3}\mathcal{I}_3\left(c_s\frac{m}{H}\frac{K}{k_1},c_s\frac{m}{H}\frac{K}{k_2},c_s\frac{m}{H}\frac{K}{k_3}\right)\,.\tag{11.19}$$

With these expressions at hand, using $\zeta=-Hc_s^{3/2}f_\pi^{-2}\pi_c$, one can obtain the corresponding correlators of ζ.

Non-locality. Before moving on, let us make some comments on (non)-locality. Loosely speaking, locality is related to the effects of a field decreasing with distance. For instance, in the non-relativistic limit, a massive scalar field with mass m generates the well-known Yukawa potential $V(r)=\frac{e^{-mr}}{4\pi r}$ when sourced by a point-like charge. This action at a distance is non-local, but its effect is confined in a region $r\lesssim 1/m$, i.e. it is a mild form of non-locality. In contrast, an inverse gradient term of the form $\frac{m^2}{-\tilde{\partial}_i^2}\sim m^2r^2$ becomes increasingly important for $r\gtrsim 1/m$ and represents a severe violation of locality. Our single-field effective theory is non-local, as can be seen from the presence of the non-local differential operator $\mathcal{D}^{-1}=(-\tilde{\partial}_i^2+m^2)^{-1}$ in cubic and quadratic interactions. The action in real space indeed contains terms evaluated at two distinct positions, i.e. $S\sim\int\mathrm{d}t\int\mathrm{d}^3x\,\mathcal{D}^{-1}J(\boldsymbol{x})=-\int\mathrm{d}t\int\mathrm{d}^3x\int\mathrm{d}^3y\,\Pi(\boldsymbol{x},\boldsymbol{y})J(\boldsymbol{y})$ where $\Pi(\boldsymbol{x},\boldsymbol{y})=\frac{e^{-m|\boldsymbol{x}-\boldsymbol{y}|}}{4\pi|\boldsymbol{x}-\boldsymbol{y}|}$ and $J(\boldsymbol{x})$ is a general source term. However, being of Yukawa-type, we see that this represents a mild form of non-locality.

Recently, the Manifestly Local Test (MLT) was proposed as a check of correlators arising from a manifestly-local theory [438]. It is stated at the level of wavefunction coefficients [434, 435], and reads in our case

$$\frac{\partial}{\partial k_i}\psi_3(k_1,k_2,k_3)\bigg|_{k_i=0}=0\,.\tag{11.20}$$

Its derivation is based on a simple property satisfied by the mode function of a massless field in de Sitter. We have explicitly checked that our correlators satisfy the MLT for $\mathrm{Re}\,\psi_3$, and extends to the full wavefunction coefficient ψ_3 by inspecting the MLT derivation from a bulk perspective. The reason is that the non-local differential operator $\mathcal{D}^{-1}$ appearing in the diagram vertices cannot be singular as the momentum is taken to be soft due to the non-zero mass, which is naturally related to the mild non-locality that we have just discussed. To put it short, a manifestly local theory satisfies the MLT, but satisfying the MLT does not offer a diagnosis of the underlying theory being manifestly local.

11.2 Low-Speed Collider Phenomenology

The presence of a reduced sound speed for the propagation of the Goldstone boson leads to a striking signature of heavy fields—referred to as the *low-speed collider signal*—that is captured by the single-field non-local EFT (10.24). For heavy particles lighter than H/c_s, this signal manifests itself as a resonance in the squeezed limit of the bispectrum. In this section, we discuss in detail both the size and the shape dependence of this signal, both in the weak and the strong mixing regimes. In the strong mixing regime, we compute the corresponding correlators using the cosmological flow, see Part IV.

11.2.1 Physics of the Low-Speed Collider

Before diving in the phenomenology, it is worth highlighting that the low-speed collider signal has a simple physical explanation, related to the presence of two characteristic time scales in the dynamics. Because modes of different wavelength freeze or decay at different times, these time scales are encoded in the momentum dependence of primordial correlators. Indeed, due to a reduced sound speed c_s, a given short Goldstone boson mode freezes when it exits the sound horizon $c_s k_s/a(t_1) \sim H$. Likewise, a long mode of the massive field starts to decay when it crosses the mass-shell horizon $k_\ell/a(t_2) \sim m$. When $m \ll H/c_s$, the time t_1 occurs before t_2 and the Goldstone boson interacts with the massive field during the period of time $t_1 < t < t_2$ as if the latter were massless. This effect leads to the amplification of the bispectrum and mimics local non-Gaussianities close to equilateral configurations for $c_s m/H \lesssim k_\ell/k_s$, equivalent to the condition $t_1 \lesssim t_2$. In the ultra-squeezed limit $k_\ell/k_s \lesssim c_s m/H$, equivalent to $t_2 \lesssim t_1$, the bispectrum fades away due to the decay of the massive field, which is then encoded in the conventional cosmological collider signal. When $k_\ell/k_s \sim c_s m/H$, equivalent to both time scales coinciding $t_1 \sim t_2$, the bispectrum displays a characteristic resonance. Instead, for $m \gg H/c_s$, the time t_1 occurs after t_2 for all kinematic configurations, and the situation qualitatively resembles the one with $c_s = 1$. Namely, the heavy field can be integrated out in the usual local manner, corresponding to the regime "Reduced effective speed of sound" in Sec. 10.3, and the bispectrum shapes generated by all interactions are of the conventional equilateral type. Consequently, the low-speed

collider phenomenology is governed by the dimensionless parameter

$$\alpha \equiv c_s \frac{m}{H} \,, \tag{11.21}$$

with $\alpha \gtrsim 1$ corresponding to usual equilateral shapes, and $\alpha \lesssim 1$ to the genuine low-speed collider regime, on which we focus from now on.

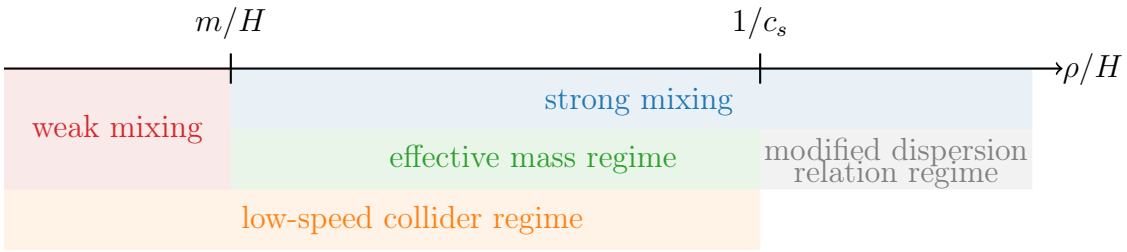


Figure 11.3: Schematic illustration of the different regimes for a reduced Goldstone boson intrinsic sound speed $c_s \lesssim 1$ and $m/H \lesssim 1/c_s$, varying the mixing strength ρ/H. Of course, the boundaries of these regions are not meant to be taken as strict demarcations, but rather as faint delimitations.

The physics of the low-speed collider explained above is valid in the weak mixing regime, i.e. when the quadratic mixing $\rho\dot{\pi}_c\sigma$ can be treated perturbatively. This corresponds to $\rho \lesssim m$, as we show in the insert below. A natural question is how this description is changed at strong mixing. We show in the insert that the effect of the mixing beyond perturbative treatments is to induce an effective mass $m^2 \to m^2_{\rm eff} = m^2 + \rho^2$ for the heavy mode, see also Chap. 15. Moreover, we show that the mixing, despite having this important effect for the dynamics of the heavy mode, has a small effect on the dynamics of the Goldstone boson inside the horizon as long as $m_{\rm eff} \lesssim H/c_s$, corresponding to the parameter

$$\alpha_{\rm eff} \equiv c_s \frac{m_{\rm eff}}{H} \,, \tag{11.22}$$

being less than unity. This entails that the physics of the low-speed collider valid at weak mixing $\rho \lesssim m$, also holds qualitatively in the regime $m \lesssim \rho \lesssim H/c_s$, simply upon considering the effective mass $m_{\rm eff}$, i.e with $\alpha \to \alpha_{\rm eff}$. If the mixing is further increased to $\rho/H \gtrsim 1/c_s$, corresponding to $\alpha_{\rm eff} \gtrsim 1$, the dynamics of the system enters the regime where the Goldstone boson has a modified dispersion relation, see Sec. 10.3 and the conditions (10.34),[2] giving rise to standard equilateral-type shapes. In Fig. 11.3, we summarise the low-speed collider phenomenology at weak and strong mixing.

We will see that the strong mixing regime of the low-speed collider, i.e. the effective mass regime depicted in green in Fig. 11.3, is particularly interesting. Indeed, the low-speed collider signal can be observationally large and is not dwarfed by the ever-present equilateral-type non-Gaussianities coming from self-interactions of the Goldstone boson. With this in mind, one aspect is worth highlighting: fluctuations

[2]Note that when $m/H \lesssim 1/c_s$ and $1/c_s \lesssim \rho/H$, the condition $m^2/\rho \lesssim H/c_s$ is automatically satisfied.

in this regime can be strongly mixed without being strongly coupled. Strong mixing refers to the fact that the quadratic mixing $\rho\dot{\pi}_c\sigma$ cannot be treated in perturbation theory. At the same time, because of the non-linearly realised time diffeomorphism invariance, this interaction is necessarily accompanied by the dimension-5 cubic interaction $\propto \rho(\tilde{\partial}_i\pi)^2\sigma$. Hence, one can wonder whether large values of ρ in this regime are such that this interaction becomes strongly coupled at energies of order the Hubble scale, making the theory strongly coupled. This is not the case. As the arguments above show, all reasonings in the weak mixing regime approximately hold also in the effective mass regime upon considering the effective mass $m_{\rm eff}$. Thus, the bound on ρ coming from avoiding strong coupling reads $\rho/H \lesssim c_s^{3/2}(2\pi\Delta_\zeta)^{-1} \sim 100$ for the representative value $c_s \sim 0.1$, showing that the theory remains healthy in the strong mixing regime of the low-speed collider $\rho/H \lesssim 1/c_s$.

Dispersion relation analysis.—In this insert, we examine the full two-field quadratic dynamics. First, we give the corresponding dispersion relations and we show that $\rho \lesssim m$ is required in order to treat the quadratic mixing perturbatively. Then, we explain that in the parameter space of interest $c_s m/H \lesssim 1$ for the low-speed collider, $m_{\rm eff}$ plays the role of the mass of the heavy mode. Furthermore, going beyond weak mixing, we show that $\alpha_{\rm eff} \equiv c_s m_{\rm eff}/H \lesssim 1$ is the correct non-perturbative criterion for the existence of the low-speed collider, giving rise to the "effective mass" regime of Fig. 11.3. Remarkably, this regime is amenable to an approximate analytical understanding.

Taking the flat-space limit $H \to 0$ of the full theory (9.53), the quadratic dynamics can be solved exactly after injecting plane-wave solutions. The dispersion relations for both degrees of freedom are given by

$$\omega_\pm^2 = \frac{1+c_s^2}{2}\,k_{\rm p}^2 + \frac{m_{\rm eff}^2}{2} \pm \frac{1}{2}\sqrt{m_{\rm eff}^4 + (1-c_s^2)^2 k_{\rm p}^4 + 2(1+c_s^2)k_{\rm p}^2\left[\rho^2 + \frac{1-c_s^2}{1+c_s^2}\,m^2\right]}\,, \tag{11.23}$$

where $m_{\rm eff}^2 = m^2 + \rho^2$ is simply a short-hand notation at this stage. We will look below at physically interesting limits in which this exact solution simplifies, but first, as a sanity check, we note that the uncoupled limit $\rho/H = 0$ gives $\omega_-^2 = c_s^2 k_{\rm p}^2$ and $\omega_+^2 = k_{\rm p}^2 + m^2$. We recover that the spectrum is then composed of a massless mode propagating with a speed of sound c_s and a relativistic heavy mode with mass m.

We now explain the criterion $\rho \lesssim m$ as the perturbativity bound on the quadratic coupling, directly at the level of the non-local EFT (10.24). To do this, we need to estimate the propagator $\mathcal{D}^{-1} = (k_{\rm p}^2+m^2)^{-1}$ at the relevant time scales of the dynamics, which includes sound-horizon crossing but also mass-shell crossing and beyond. At the sound-horizon crossing of the massless mode $k_{\rm p} \sim H/c_s$ and in the parameter space of interest with $c_s m/H \lesssim 1$, the propagator scales as $\mathcal{D}^{-1} \approx c_s^2/H^2$. Therefore, the correction to the quadratic Lagrangian scales as $c_s^2(\rho/H)^2 \lesssim c_s^2(m/H)^2 \lesssim 1$ in the would-be weak mixing regime, and is indeed negligible. At and after the mass-shell crossing of the heavy mode $k_{\rm p} \lesssim m$, it scales as $\mathcal{D}^{-1} \approx m^{-2}$, giving a correction of order $(\rho/m)^2$, which is consistently negligible as long as $\rho \lesssim m$. From the exact dispersion relations (11.23), it is then interesting to consider the first correction to the decoupled dynamics of the heavy mode in this weak mixing regime

$$\omega_+^2 \approx k_{\rm p}^2 + m^2 + \rho^2\,\frac{k_{\rm p}^2+m^2}{(1-c_s^2)k_{\rm p}^2+m^2}\,. \tag{11.24}$$

One can appreciate that for a low sound speed $c_s \ll 1$, the last term in the heavy mode dispersion relation ω_+^2 is given by ρ^2, and therefore combines with the mass parameter to generate the combination $m_{\rm eff}^2$, which indeed appears as the physical mass of the heavy excitations. This effect is small by definition in the weak mixing regime. However, remarkably, this picture holds beyond weak mixing for $\alpha \equiv c_s m/H \lesssim 1$. Indeed, in the regime of small α, the exact dispersion relations boil down to

$$\omega_-^2 \approx c_s^2 k_{\rm p}^2 \, \frac{k_{\rm p}^2 + m^2}{k_{\rm p}^2 + m_{\rm eff}^2} \,, \quad \text{and} \quad \omega_+^2 \approx k_{\rm p}^2 + m_{\rm eff}^2 + c_s^2 \rho^2 \frac{k_{\rm p}^2}{k_{\rm p}^2 + m_{\rm eff}^2} \,. \tag{11.25}$$

These relations are non-perturbative in the quadratic mixing as they do not assume weak mixing. Notice that the last term, $c_s^2\rho^2 \frac{k_{\rm p}^2}{k_{\rm p}^2+m_{\rm eff}^2} \lesssim c_s^2\rho^2$, is negligible compared to the term ρ^2 appearing in $m_{\rm eff}^2$. Therefore, in the regime $\alpha \lesssim 1$, the heavy mode dynamics is governed by $\omega_+^2 = k_{\rm p}^2 + m_{\rm eff}^2$. This explains why the low-speed collider resonance occurs also at strong mixing as long as $\alpha_{\rm eff} \equiv c_s \, m_{\rm eff}/H \lesssim 1$. Indeed, in this regime, the mixing between the massless and the heavy mode is important enough to generate an effective mass different from the bare one, but it does not appreciably affect the dynamics of the Goldstone boson, and the heavy mode can still be considered as effectively massless at sound horizon crossing for π_c. To see this, let us recall that the massless mode dispersion relation is only valid for $\omega_- \gtrsim H$ as Hubble friction becomes important at smaller energies. The requirement that the dispersion relation is not affected by the mixing even at this energy, corresponding to momenta $k_{\rm p} \sim H/c_s$ (the two modes obviously decouple in the large $k_{\rm p}$ limit), is equivalent to $\frac{1+\alpha^2}{1+\alpha_{\rm eff}^2} \simeq 1$, which is satisfied for $\alpha_{\rm eff} \ll 1$. This condition also guarantees that the effective mass in $\omega_+^2 = k_{\rm p}^2 + m_{\rm eff}^2$ is negligible for $k_{\rm p} \sim H/c_s$, giving rise to the peculiar local-like behaviour of the bispectrum for near equilateral configurations. Furthermore, one can check that in this effective mass regime, the corrections to the dispersion relation of the Goldstone mode around sound horizon crossing, $\omega_-^2/(c_s^2 k_{\rm p}^2) - 1 \simeq -c_s^2\rho^2/H^2$, takes exactly the same form as in the weak mixing regime. Eventually, as $m_{\rm eff}$ also controls the dynamics at late times, i.e the quasi-normal modes of the coupled system (a statement that does not depend on sound speeds), the decay of the heavy mode starts at effective mass crossing $k_{\rm p} \sim m_{\rm eff}$, hence giving rise to the low-speed collider resonance at the location $k_\ell/k_s \sim c_s m_{\rm eff}/H$. This analysis suggests that, to a good approximation, the analytical results of the low-speed collider in the weak mixing regime can be transposed to the effective mass regime $m/H \lesssim \rho/H \lesssim 1/c_s$, simply upon considering the "dressed" effective mass $m^2 \to m_{\rm eff}^2 = m^2 + \rho^2$, with any small discrepancy attributed to the intermediate regime $m_{\rm eff} \lesssim k_{\rm p} \lesssim H/c_s$.

In this thesis, we are interested in the low-speed collider signatures of effectively heavy fields, corresponding to $m_{\rm eff} \gtrsim H$, a situation that is amenable to a description in terms of a single-field (non-local) description. But interesting signatures also arise in the complementary regime of a light field weakly mixed to the Goldstone boson. The low-speed collider signal still manifests itself as a resonance in mildly-squeezed configurations, with the usual quasi-single field scalings taking over in the ultra-squeezed configuration, and with the resonance ultimately fading away as the field

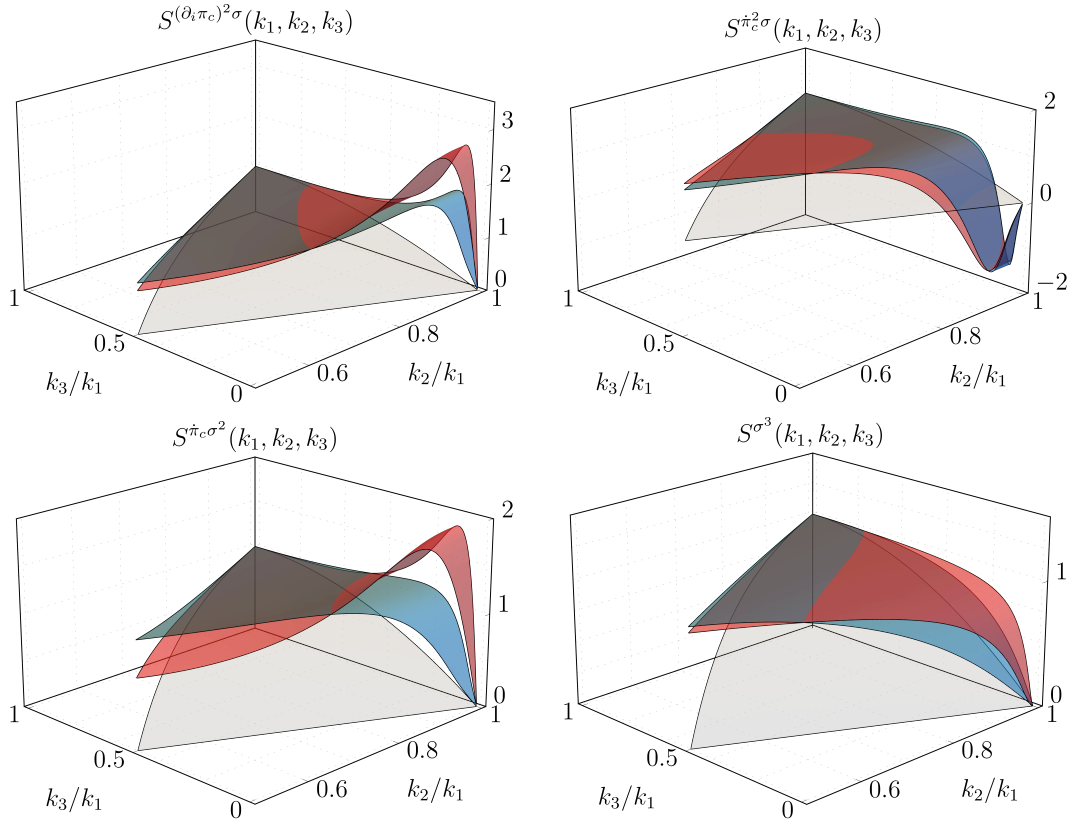


Figure 11.4: The dimensionless shape functions $S(k_1, k_2, k_3)$ normalised to unity in the equilateral configuration $k_1 = k_2 = k_3$ at weak mixing in blue for $\alpha = 0.1$ and at strong mixing in red for $\alpha_{\rm eff} = 0.1$. The different panels represent the shapes generated by the interactions $(\partial_i\pi_c)^2\sigma$, $\dot\pi_c^2\sigma$, $\dot\pi_c\sigma^2$ and σ^3. The shapes in the strong mixing regime have been computed with the cosmological flow approach described in Part IV for $c_s = 0.05, m/H = 0.1, \rho/H = 2$. We have represented in transparent gray the standard equilateral shape for comparison.

becomes massless.

11.2.2 Shapes of the Low-Speed Collider

In this section, we describe the low-speed collider shapes, as defined in Chap. 3. Without loss of generality, we order the momenta such that $k_3 \leq k_2 \leq k_1$ and fix k_1 by virtue of scale invariance. Therefore, the shape information only depends on the two dimensionless ratios k_2/k_1 and k_3/k_1 that satisfy $0 \leq k_3/k_1 \leq k_2/k_1 \leq 1$ and $k_1 \leq k_2 + k_3$. We show the shape functions, using this parametrization, in Fig. 11.4 and 11.5 for the four interactions $(\partial_i\pi_c)^2\sigma$, $\dot\pi_c^2\sigma$, $\dot\pi_c\sigma^2$ ad σ^3, both at weak and strong mixing, for $\alpha_{\rm eff} = 0.1$ and $\alpha_{\rm eff} = 0.05$, respectively. The shapes are normalised to unity in the equilateral configuration to ease comparison with the standard equilateral template, represented in gray.

As we understood previously, the striking feature of the low-speed collider is the presence of a resonance in the squeezed limit. This resonance is readily visible in the shape generated by the interaction $(\partial_i\pi_c)^2\sigma$. At weak mixing, the location

and the amplitude of the peak are governed by α. For smaller α, the resonance is visible in more squeezed configurations and has a larger amplitude, proportional to α^{-1}. The shape generated by the interaction $\dot{\pi}_c^2\sigma$—whose amplitude is not fixed by the quadratic coupling—presents a more complex resonance characterised by a double-peak structure, i.e. a first small peak and a second one more noticeable. The shape generated by the interaction $\dot{\pi}_c\sigma^2$—which leads to double-exchange diagrams at weak mixing—have a resonance less pronounced than those generated by $(\partial_i\pi_c)^2\sigma$ and $\dot{\pi}_c^2\sigma$. As for the interaction σ^3, it does not lead to resonances, which can be traced back to the presence of additional propagators in the corresponding interactions once the heavy field σ has been non-locally integrated out. This is particular though to the situation considered here for simplicity of one additional heavy field, and it is straightforward to generalise our results to more generic setups.[3] An interesting case then is the shape generated by the triple-exchange diagram of several heavy fields having different masses, say m_1, m_2 and m_3. When $m_2/H, m_3/H \geq 1/c_s$, the corresponding fields can be integrated out in a local manner, and the shape therefore resembles the one generated by $\dot{\pi}_c^2\sigma$, with an amplitude suppressed by $(H/m_2)^2(H/m_3)^2$. In this case, the interaction only consists of the propagator associated with the field of mass m_1 and the shape displays a resonance around $k_3/k_1 \sim c_s m_1/H$. Similarly, if only one field is heavier than $1/c_s$, the resonance would be sensitive to the lightest field. In essence, the low-speed collider resonance is a natural discovery channel to detect heavy fields with masses not far from the Hubble scale when the Goldstone boson has a reduced speed of sound, in analogy with resonance peaks in ground-based colliders proving the existence of new particles.

At strong mixing, in the "effective mass regime" depicted in Fig. 11.3, the low-speed collider physics leads to a similar phenomenology of shapes, though the resonances are more pronounced. We have understood that this regime can be qualitatively described by the weak mixing shapes after replacing α by α_{eff}. Here, the exact computation using the cosmological flow approach gives a quantitative measure of the quality of this approximation. Indeed, if this substitution was exactly accurate, the shapes at weak and strong mixing in Fig. 11.4 and 11.5 would coincide. The slight mismatch signals that non-trivial physics occurs between sound-horizon crossing of π_c and mass-shell crossing of σ in the strong mixing regime that cannot be inferred from the dispersion relation analysis. As such, only an exact numerical calculation can in turn be decisive. Remarkably, substituting $\alpha \to \alpha_{\text{eff}}$ in the analytical shape generated by $\dot{\pi}_c^2\sigma$ at weak mixing gives an excellent match, and the "effective mass regime" still provides an accurate description of the low-speed collider physics at strong mixing. In this respect, note that we have checked that this also applies to

[3] More specifically, the natural generalisation of (9.53) is obtained by introducing the operators $\sum_a \rho_a\sigma_a\dot{\pi}_c$, $\sum_a(\Lambda_{1,a})^{-1}\,\sigma_a(\tilde{\partial}_i\pi_c)^2$, $\sum_a(\Lambda_{2,a})^{-1}\sigma_a\dot{\pi}_c^2$, $\sum_{ab}\lambda_{ab}\sigma_a\sigma_b\dot{\pi}_c$ and $\sum_{a,b,c}\mu_{abc}\sigma_a\sigma_b\sigma_c$, with $\sigma_{a=1,\dots,N}$ standing for N heavy scalars with masses m_a, and $\rho_a, (\Lambda_{1,a})^{-1}, (\Lambda_{2,a})^{-1}, \lambda_{ab}, \mu_{abc}$ for flavour-indexed coupling constants. At weak mixing, these interactions induce single-, double- and triple-exchange diagrams, incorporating internal lines with different masses for the last two ones. The computation is then identical to the case with only one heavy field, mutatis mutandis. In fact, the expressions for the correlators become identical to Eqs. (11.15)-(11.19), after a trivial adjustment for the coupling constants and accounting for the mass of each propagator inside the arguments of $\mathcal{I}_{1,2,3}$ in Eq. (11.10).

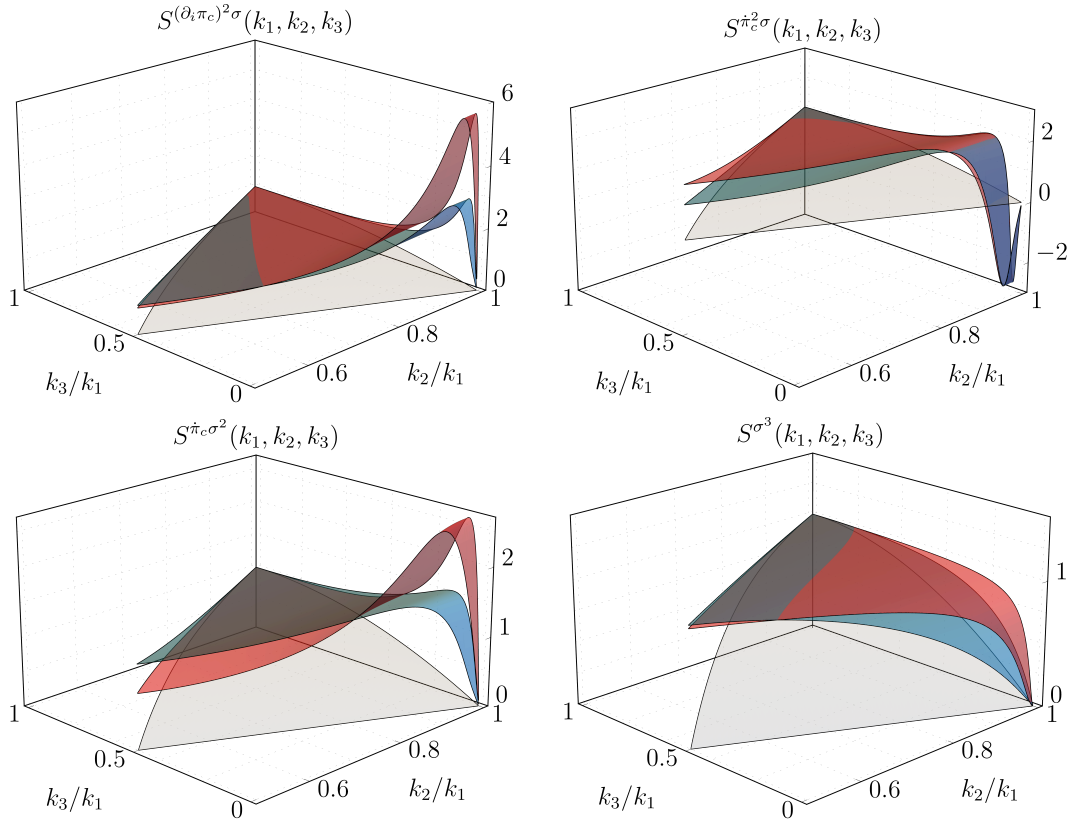


Figure 11.5: The dimensionless shape functions $S(k_1, k_2, k_3)$ normalised to unity in the equilateral configuration $k_1 = k_2 = k_3$ at weak mixing in blue for $\alpha = 0.05$ and at strong mixing in red for $\alpha_{\rm eff} = 0.05$, generated by the interactions $(\partial_i\pi_c)^2\sigma$, $\dot\pi_c^2\sigma$, $\dot\pi_c\sigma^2$ and σ^3. We have set $c_s = 0.025, m/H = 0.1, \rho/H = 2$ in the strong mixing regime, and have represented in transparent gray the standard equilateral shape.

the amplitude of the signal, and not only to the shape information as shown in the figures. In the following, we give a quantitative analysis of the low-speed collider shapes by inspecting their overlap with the standard templates.

11.2.3 Shape Correlation

To further characterise the low-speed collider shapes, we now compute their correlations with the standard local, equilateral and orthogonal shapes used in data analysis, that are defined and discussed in Chap. 3. For definiteness, we only focus on the shape (11.16) generated by the interaction $(\partial_i\pi_c)^2\sigma$, that leads to the most sizeable low-speed collider resonance. We show in Fig. 11.6 the correlations with the standard templates as functions of α. As anticipated, for $\alpha \approx 1$, the shape is strongly correlated with the equilateral template. As the parameter α decreases, the low-speed collider resonance appears and becomes more pronounced. As a consequence, the shape correlation with $S^{\rm eq}$ decreases while that with $S^{\rm loc}$ increases. For sufficiently small α, it is interesting to notice that we obtain a non-negligible correlation with $S^{\rm loc}$, commonly attributed to the presence of multiple light fields during inflation. In contrast, the low-speed collider shape has been derived from an

(effective) *single*-field theory after integrating out a *heavy* field. Overall though, in the bulk of the low-speed collider parameter space $0.01 \lesssim \alpha \lesssim 0.1$, there is a poor overlap between the representative shape $S^{(\partial_i\pi_c)^2\sigma}$ and the conventional templates.

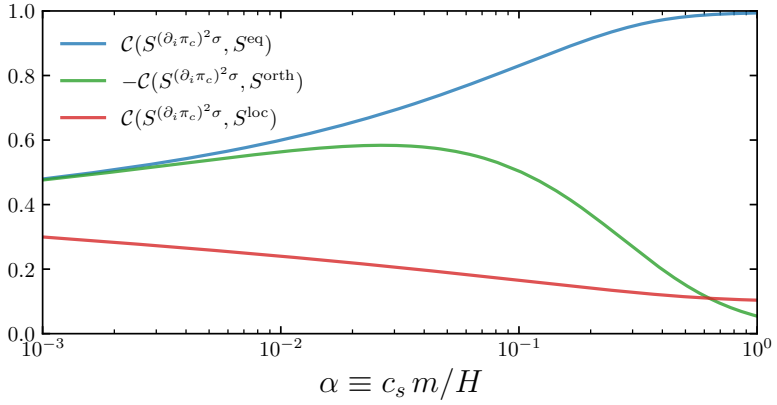


Figure 11.6: Correlations of the shape $S^{(\partial_i\pi_c)^2\sigma}$ with the standard equilateral template $S^{\rm eq}$ in blue, orthogonal template $S^{\rm orth}$ in green, and local template $S^{\rm loc}$ in red, as functions of $\alpha \equiv c_s m/H$ in the weak mixing regime.

This analysis thus reveals that probing the bispectrum using only the standard templates $S^{\rm loc}, S^{\rm eq}$ and $S^{\rm orth}$ could lead to a biased interpretation of data about the physics active in the primordial universe. Namely, conventional templates would not be blind to the low-speed collider signal, but a non-zero response to the equilateral/orthogonal and local templates could then be wrongly attributed to a scenario with multiple light fields endowed with a non-trivial sound speed. Therefore, it appears essential to give a proper treatment to the low-speed collider shapes.

11.2.4 Low-Speed Collider Template

For convenience of data analysis, we give a simple and universal template for the shape that captures the low-speed collider resonance. The derived analytical shapes are not convenient to deal with numerically because of fine cancellations appearing in Eq. (11.12). For this reason, we give a simpler template expressed in terms of elementary functions. To construct it, we realise that the low-speed collider shape behaves like the local one close to equilateral configurations and like the equilateral one in the squeezed limit, resulting in the low-speed collider resonance located in mildly-squeezed configurations. Naturally, the peak is shifted from the equilateral configuration to the squeezed limit as the parameter α decreases. A simple template for such a shape is given by

$$S^{\alpha}(k_1,k_2,k_3) = S^{\rm eq}(k_1,k_2,k_3) + \frac{1}{3}\frac{k_1^2}{k_2k_3}\left[1+\left(\alpha\,\frac{k_1^2}{k_2k_3}\right)^2\right]^{-1} + \text{ 2 perms}\,, \quad (11.26)$$

where permutations only apply to the second term and the equilateral shape $S^{\rm eq}$ is defined in Chap. 3. By construction, the shape S^{α} interpolates between the usual equilateral and local shapes, and can be used for the observational search of

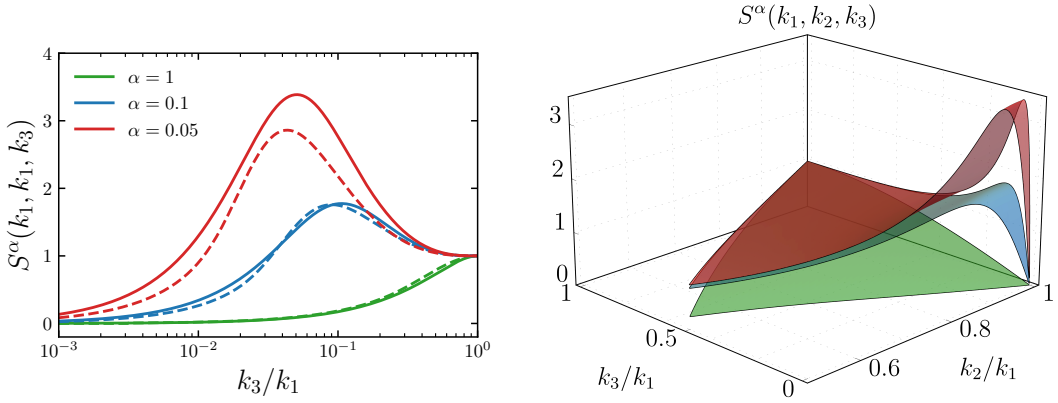


Figure 11.7: The low-speed collider shapes $S^\alpha(k_1, k_2, k_3)$ for $\alpha = 1$ in green, $\alpha = 0.1$ in blue and $\alpha = 0.05$ in red. *Left*: The template S^α (*solid line*) and the shape $S^{(\partial_i \pi_c)^2 \sigma}$ (*dashed line*) in the isosceles-triangle configuration $k_1 = k_2$. *Right*: The template S^α given in Eq. (11.26) in all triangular configurations. For illustration purposes, we have normalised the amplitudes of the signals to unity in the equilateral configuration.

primordial non-Gaussianity. As illustrated in Fig. 11.7, it captures well the location and the amplitude of the low-speed collider resonance for the α range of interest. Remarkably, this simple template also reproduces the qualitative properties of the shapes generated by the non-universal single- and double-exchange diagrams, with $\dot{\pi}_c^2 \sigma$ and $\dot{\pi}_c \sigma^2$ interactions respectively, albeit replacing α by effective parameters $\alpha_{\rm eff}^{\dot{\pi}_c^2 \sigma} = 2\alpha \log_{10}(\alpha)$ and $\alpha_{\rm eff}^{\dot{\pi}_c \sigma^2} = \alpha/2$. Note that this template is different from the one obtained in the context of multiple light fields with different sound speeds where resonances were already noticed [514, 429]. In this case, when adjusting parameters of such a template to reproduce the location of the peak, the template misses the relative amplitude of the equilateral signal compared to the resonant one. Contrariwise, the shape (11.26) results from the exchange of a massive field. One can therefore observationally distinguish, despite similar features, the exchange of light fields from signatures of massive fields.

It is well known that the computational complexity is drastically reduced when looking for a template that is *product separable*, as discussed in Sec. 3.1.3. This is due to numerical challenges of integrating highly oscillating functions that arise when projecting cosmological observables onto two-dimensional redshift surfaces [49, 74, 515, 62]. One might rightly worry that the second term in Eq. (11.26) ruins factorisability. However, this apparent problem can be solved by introducing a Mellin parameter

$$\left[1 + \left(\alpha \frac{k_1^2}{k_2 k_3}\right)^2\right]^{-1} = \frac{1}{2i\pi} \int_{c-i\infty}^{c+i\infty} \mathrm{d}s\, \Gamma(s)\Gamma(1-s)\, \alpha^{-2s} \left(\frac{k_1^2}{k_2 k_3}\right)^{-2s}, \qquad (11.27)$$

where $0 < c < 1$ such that the contour separates poles of $\Gamma(s)$ from those of $\Gamma(1-s)$. The integrand is manifestly product separable in the momenta.[4] Along the contour,

[4]Note that it is not possible to write the term that ruins factorisability as a geometric series

e.g. by setting $s \to 1/2 + i\tilde{s}$, the Mellin-Barnes integral can be accurately computed numerically. More generally, a similar trick can also be used when the shape has a non-trivial pole structure.

11.2.5 Self-Interaction Contamination

In the presence of a reduced speed of sound, the non-linearly realised time diffeomorphism invariance unavoidably generates large Goldstone boson self-interactions which contaminate the low-speed collider signature. This is attributed to the cubic interaction $\dot{\pi}_c(\partial_i\pi_c)^2$ in Eq. (9.53), whose size is fixed by c_s and that generates an equilateral-type bispectrum of amplitude $\sim 1/c_s^2$ at weak mixing. Naturally, by tuning the Wilson coefficient setting the size of the other self-interaction $\dot{\pi}_c^3$, it is possible to lower the amplitude of the total self-interaction signal precisely at the location of the low-speed collider resonance, making it more visible.[5] We do not allow this in the following: we concentrate on the signal fixed by symmetries, so that our assessment of the observability of the low-speed collider resonance is conservative.

Let us first estimate the relative size of the low-speed collider resonance with respect to the self-interaction contamination at weak mixing. Focusing on the interaction $(\partial_i\pi_c)^2\sigma$, the shape in the squeezed limit around $k_3/k_1 \sim \alpha$ scales as $S^{(\partial_i\pi_c)^2\sigma} \sim \alpha^{-1}(\rho/H)^2$, where the α^{-1} is attributed to the resonance. The standard equilateral-type shape decreases like k_3/k_1 so that $S^{\dot{\pi}_c(\partial_i\pi_c)^2} \sim c_s^{-2}\alpha$. Therefore, the ratio of both signals is $S^{(\partial_i\pi_c)^2\sigma}/S^{\dot{\pi}_c(\partial_i\pi_c)^2} \sim (\rho/m)^2 \lesssim 1$. In the strict weak mixing regime $\rho \ll m$, the low-speed collider resonance is dwarfed by the ever-present self-interaction signal. In Fig. 11.8, we show the exact low-speed collider signal and the corresponding self-interaction contamination, as well as the total shape, for different scenarios. At weak mixing (top left), the low-speed collider is indeed not visible in the total signal one would measure. As a consequence, it can only be detected after properly subtracting the equilateral-type contamination, considered as a "background noise" in this case. Although the scalings above miss $\mathcal{O}(1)$ coefficients, the two contributions become comparable for $\rho \sim m$, which motivates to consider strong mixing where the situation is more interesting. In the "effective mass regime", as discussed previously, replacing m by the effective mass m_{eff} gives an accurate description of the low-speed collider physics at strong mixing. The low-speed collider resonance therefore scales as $S^{(\partial_i\pi_c)^2\sigma} \sim \alpha_{\text{eff}}^{-1}(\rho/H)^2$, where $\alpha_{\text{eff}} \approx c_s\rho/H$, while the equilateral-type shape is $S^{\dot{\pi}_c(\partial_i\pi_c)^2} \sim c_s^{-2}\alpha_{\text{eff}}$. The ratio leads to $S^{(\partial_i\pi_c)^2\sigma}/S^{\dot{\pi}_c(\partial_i\pi_c)^2} \sim 1$. It means that the resonance is not suppressed, and is well visible in the total shape, as seen in the top right panel of Fig. 11.8. Note that the estimates of the self-interaction signal parametrically hold, as the propagation of π_c is not much affected by its mixing with σ for the regime of interest $\alpha_{\text{eff}} \lesssim 1$. However, the full dynamics is taken into account in the numerical results of Fig. 11.8.

It is straightforward to generalise these estimates to the other interactions, which can lead to low-speed collider signals with even larger amplitude as their correspond-

because it does not converge close to equilateral configurations for some permutations.

[5] In that respect, note that the "multi-speed" shapes put forth in [429] are not observable without a severe fine-tuning, as they are necessarily accompanied by a much larger equilateral-type shape that dwarfs it.

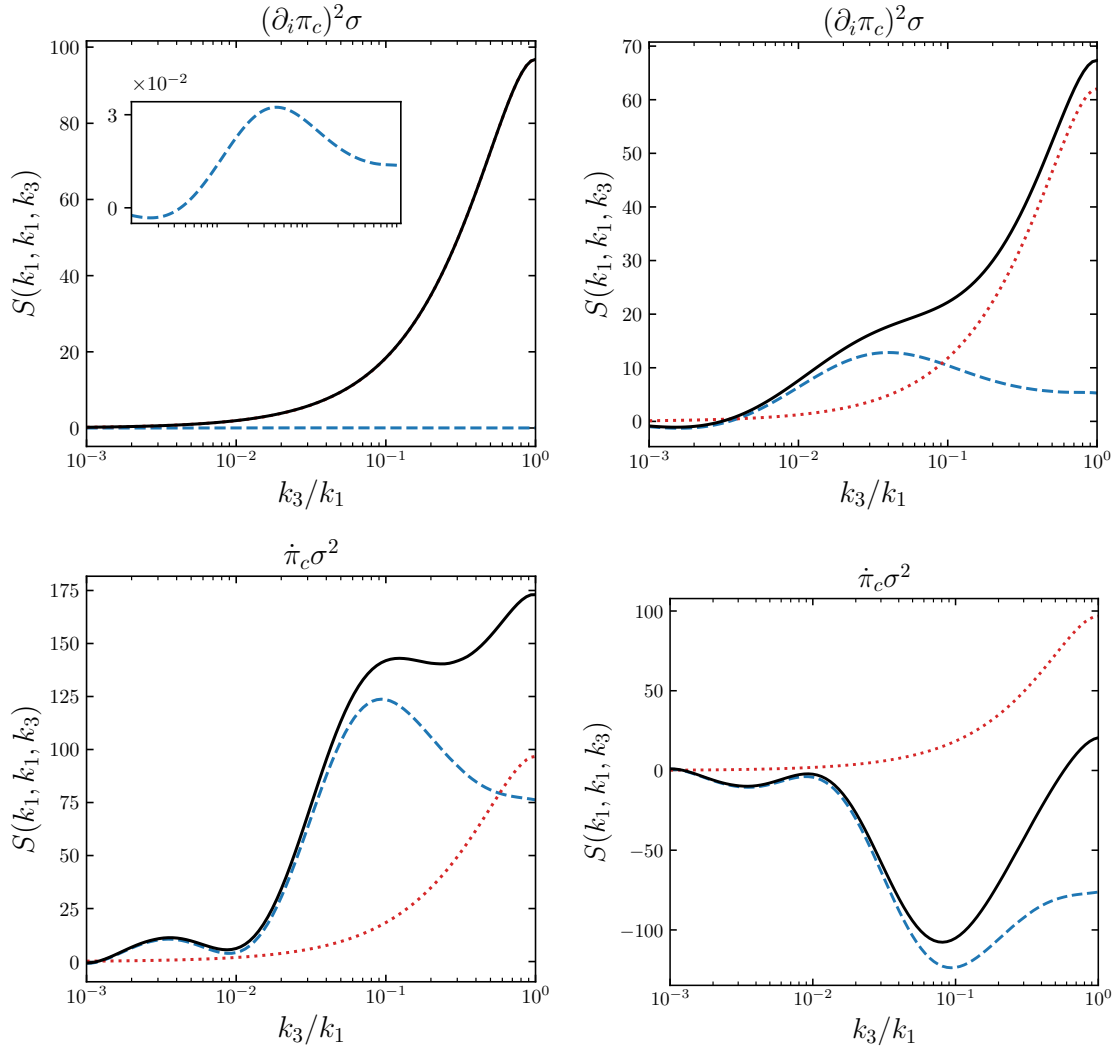


Figure 11.8: Shape functions generated by $(\partial_i\pi_c)^2\sigma$ (*top*) and $\dot{\pi}_c\sigma^2$ (*bottom*) in dashed blue line and self-interactions of the Goldstone boson $\dot{\pi}_c(\partial_i\pi_c)^2$ fixed by the speed of sound c_s in dotted red line, and the sum of both signals in solid black line, in the isosceles-triangle configuration $k_1 = k_2$. *Top panel*: In the weak mixing regime (*left*), we have set $m/H = 2, \rho/H = 0.1$ and $c_s = 0.05$ so that $\alpha = 0.1$. At strong mixing in the "effective mass regime" (*right*), we have set $m/H = 0.1, \rho/H = 2$ and $c_s = 0.05$ so that $\alpha_{\rm eff} = 0.1$. *Bottom panel*: We have set $\rho/H = m/H = 2, c_s = 0.05$ with $\lambda = 0.01$ (*left*) and $\lambda = -0.01$ (*right*).

ing cubic couplings are not tied to ρ/H. For definiteness, the case of the interaction $\dot{\pi}_c\sigma^2$ is considered on the bottom panels of Fig. 11.8, for two different values $\lambda = \pm 0.01$ of the coupling constant in Eq. (9.53) ensuring perturbative control. The low-speed collider resonance is well visible, notably due to the enhancement of the signal by Δ_ζ^{-1}. Additionally, note that when the signal generated by the mixing cubic interaction and the one generated by self-interactions have opposite signs, the low-speed collider signature is well distinct in the total shape.

Measuring equilateral-type non-Gaussianities would constrain the speed of sound

c_s, and the position of the low-speed collider resonance would then pinpoint the (effective) mass of the additional heavy field. While this picture is correct at weak mixing, it is in general more subtle at strong mixing. Indeed, the total signal near equilateral configurations is not entirely fixed by c_s, as the low-speed collider and self-interaction signals can have a comparable amplitude there, see for instance the situations in the bottom panels in Fig. 11.8.

11.3 Parity Violation from Emergent Non-Locality

We now extend the above analysis to correlators exchanging a spin-1 particle with a chemical potential, working at the level of the single-field non-local theory (10.45). Notably, this gives rise to a sizeable parity-violating trispectrum, a neat signature of new physics during inflation. In this section, we will use the notations of Sec. 10.5.

11.3.1 Size of Parity-odd Signals

The (non-local) single-field theory (10.45) provides a handy way for estimating the size of the parity-odd trispectrum, denoted $\tau_{\rm NL,\,PO}$, generated by the exchange of a massive spinning field σ_i. The theory contains only one dynamical degree of freedom, the Goldstone boson, and a simple estimate of the parity-odd trispectrum is then given by $\tau_{\rm NL,\,PO} \sim \frac{\mathcal{L}_{4,\rm PO}}{\mathcal{L}_2}\Delta_\zeta^{-2}$, where all dimensionful quantities in the Lagrangian, which crucially depend on time, are evaluated at sound horizon crossing $c_s k_{\rm p} \sim H$, or equivalently at the Hubble scale $\omega \sim H$.[6] The quadratic Lagrangian $\mathcal{L}_2$ is taken to be the Goldstone boson kinetic term that scales as $\sim c_s^{-3}\omega^4$, as seen in Sec. 9.5. Evaluating the parity-odd non-local differential operator $\mathcal{D}_{\rm PO}^{-1}$ in Eq. (10.47) at the relevant time scale leads to

$$\mathcal{D}_{\rm PO}^{-1} \sim \left(\frac{c_s}{H}\right)^2 \frac{\alpha_\kappa}{(1+\alpha_m^2)^2+4\alpha_\kappa^2}\,, \tag{11.28}$$

where $\alpha_m = c_s m/H$ and $\alpha_\kappa = c_s\kappa/H$ are small in the regime of interest $c_s \ll 1$, also corresponding to the domain of validity of the non-local EFT. In the following, for simplicity, we will estimate the size of the parity-odd exchange trispectra involving the same two vertices, although the procedure analogously extends to all contributions.

Dimension-5 operator. After integrating out the massive spinning field in a non-local manner, the dimension-5 interaction in the Lagrangian reads $\mathcal{L}_4/a^3 = -\frac{a^{-2}}{\tilde{\Lambda}^2}\dot\pi_c\partial_i\pi_c[\mathcal{D}_{\rm PO}^{-1}]_{ij}\dot\pi_c\partial_j\pi_c$ and the size of the parity-odd trispectrum is given by

$$\tau_{\rm NL,\,PO}^{\dot\pi_c\partial_i\pi_c\sigma_i} \sim \left(\frac{\rho}{H}\right)^2 \frac{\alpha_\kappa}{(1+\alpha_m^2)^2+4\alpha_\kappa^2}\,, \tag{11.29}$$

where we recall that the energy-scale $\tilde\Lambda$ is fixed by the quadratic mixing strength ρ due to the non-linearly realized symmetry. Using the perturbativity bound (9.74),

[6] This estimate does not take into account the interactions outside the sound horizon, characteristic of the low-speed collider physics, that give rise to additional dependencies on $\alpha_{m,\kappa}$. However, it is sufficient for our purpose here to estimate the size of the signals.

and in the regime of interest $\alpha_m, \alpha_\kappa \ll 1$ and $\gamma \sim 1$, we find $\tau_{\rm NL,\,PO}^{\dot\pi_c\partial_i\pi_c\sigma_i} \lesssim c_s\alpha_\kappa$, i.e. negligible parity-odd non-Gaussianities. Henceforth, we will discard the contribution from the dimension-5 operator in the following calculations.

Dimension-7 operators. Remarkably, the considered higher-order operators can generate large parity-odd non-Gaussianities. Indeed, integrating out the field σ_i for the interactions fixed by the scale Λ leads to $\mathcal{L}_4/a^3 = \frac{a^{-6}}{\Lambda^6}\partial_l\dot\pi_c\partial_i\partial_l\pi_c[\mathcal{D}_{\rm PO}^{-1}]_{ij}\partial_k\dot\pi_c\partial_j\partial_k\pi_c$. The size of the resulting parity-odd trispectrum reads

$$\tau_{\rm NL,\,PO}^{\partial_j\dot\pi_c\partial_i\partial_j\pi_c\sigma_i} \sim c_s^{-7}\left(\frac{H}{\Lambda}\right)^6 \frac{\alpha_\kappa\,\Delta_\zeta^{-2}}{(1+\alpha_m^2)^2+4\alpha_\kappa^2}\,. \tag{11.30}$$

We will see in what follows that the actual size of the trispectrum presents an additional c_s^4 suppression. This results from a careful analysis of the dimensionless integral entering in the size of the trispectrum, and can be traced back to the residue at the pole of the non-local differential operator $\mathcal{D}_{\rm PO}^{-1}$. Accordingly, using the perturbativity bound (9.75) gives $\tau_{\rm NL,\,PO}^{\partial_j\dot\pi_c\partial_i\partial_j\pi_c\sigma_i} \lesssim c_s^5\alpha_\kappa\Delta_\zeta^{-2} = \mathcal{O}(500)$ for a representative value $c_s = 0.1$. For comparison, the parity-even trispectrum has been constrained to be $\tau_{\rm NL,\,PE} \lesssim 2800$ and $g_{\rm NL,\,PE} \lesssim 10^4$ [71, 137]. Let us stress that the estimated parity-odd signal is free from large contaminations coming from self-interactions of the Goldstone boson. Although it might seem counter-intuitive, as the signal is generated by higher-derivative interactions, the reason for the apparent sound-speed enhancement in Eq. (11.30) can be traced back to the large number of spatial derivatives $\tilde\partial_i \sim k_{\rm p} \sim H/c_s$, which are boosted in the case of a reduced sound speed $c_s \ll 1$. However, we stress that this enhancement is dummy when applying perturbativity bounds on the couplings. In fact, these mixings can generate large parity-odd signals due to the Δ_ζ^{-2} enhancement as these interactions are not tied to the strength of the quadratic mixing. Following the same procedure for the interaction fixed by the energy scale $\bar\Lambda$ leads to the same bound $\tau_{\rm NL,\,PO}^{\ddot\pi_c\partial_i\dot\pi_c\sigma_i} \lesssim c_s^5\alpha_\kappa\Delta_\zeta^{-2}$, which also gives rise to a potentially large amount of parity-odd non-Gaussianity. In what follows, we will focus on the interaction $\partial_j\dot\pi_c\partial_i\partial_j\pi_c\sigma_i$ fixed by Λ as both dimension-7 operators lead to qualitatively similar shapes with comparable sizes.

11.3.2 Parity Violation as a Residue

We now show explicitly that the singularity structure in the complex plane of the operator $\mathcal{D}^{-1}$ enables one to derive simple analytical expressions for the parity-odd trispectrum. With the non-local single-field EFT (10.45), one can readily work out the resulting trispectrum, whose parity-odd part will be of our main interest. For the s-channel contribution and at leading-order in time derivatives, the 4-point

correlator is simply computed as a tree-level contact diagram

$$\langle \pi_c^4 \rangle'_{s,\mathrm{PO}} = \quad \mathcal{D}_{\mathrm{PO}}^{-1} \quad = -\frac{1}{\Lambda^6}\, \boldsymbol{s}\cdot(\boldsymbol{k}_1\times\boldsymbol{k}_3)(\boldsymbol{k}_1\cdot\boldsymbol{k}_2)(\boldsymbol{k}_3\cdot\boldsymbol{k}_4)$$
$$\times\, 2i\,\mathrm{Im}\left[\int_{-\infty}^{0}\frac{\mathrm{d}\tau}{a^2}\mathcal{K}_+(k_1;\tau)\overleftrightarrow{\partial_\tau}\mathcal{K}_+(k_2;\tau)\frac{2\kappa a}{(s^2+m^2a^2)^2-4\kappa^2a^2s^2}\right. \tag{11.31}$$
$$\left.\times\mathcal{K}_+(k_3;\tau)\overleftrightarrow{\partial_\tau}\mathcal{K}_+(k_4;\tau)\right]\,,$$

where $f\overleftrightarrow{\partial_\tau}g \equiv f\partial_\tau g - g\partial_\tau f$. Notice that the integrand in Eq. (11.31) is analytic in the entire τ-complex plane except at the root of the denominator

$$[s^2+m^2a^2(\tau_c)]^2 - 4\kappa^2a^2(\tau_c)s^2 = 0\,. \tag{11.32}$$

This singularity in the upper left half complex plane lies at

$$\tau_c \equiv \frac{1}{s}\left(-\frac{\kappa}{H}+\frac{im}{H}\sqrt{1-\frac{\kappa^2}{m^2}}\right)\,. \tag{11.33}$$

In the limit $\kappa/H \to 0$, this pole is purely imaginary. As a result, the effect of the chemical potential is to shift the location of this pole away from the imaginary axis, as shown in Fig. 11.9. At LO, τ_c is a simple pole of the integrand while it is a double pole for the NLO term. In the next section, we show that all higher-order terms in the non-local EFT (10.45) share the same pole location at τ_c, except that these poles are of increasing orders. As mentioned before, this essential singularity at τ_c is the manifestation of emergent non-locality in the IR theory.

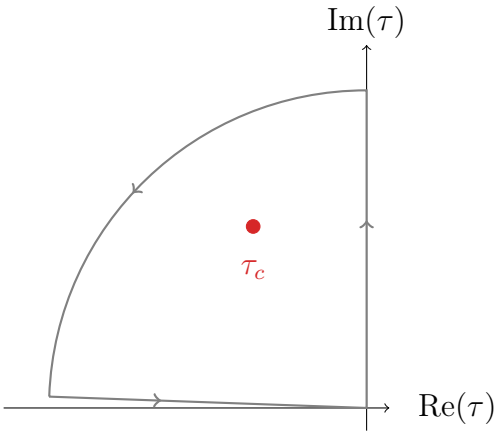


Figure 11.9: Representation of the τ-complex plane and the Wick rotation in the non-local EFT. The original integration contour specified by the $i\epsilon$-prescription is Wick-rotated to the imaginary axis, picking up the pole at τ_c. The contour integral along the imaginary axis is purely real and drops out of the result. The only non-zero contribution to the parity-odd trispectrum emerges from the residue at the pole $\tau = \tau_c$.

Implementing the $i\epsilon$-prescription, we now perform a Wick rotation on the upper half τ-complex plane, $\tau = -e^{-i(\frac{\pi}{2}-\epsilon)}x$ with $x > 0$, while taking into account the residue at τ_c. This procedure is illustrated in Fig. 11.9. The arc at infinity vanishes due to the exponential decay of the integrand. It is easy to check that the various ingredients transform as follows under the Wick rotation

$$\begin{aligned}
\int_{-\infty}^{0} \mathrm{d}\tau &\to -i \int_{0}^{\infty} \mathrm{d}x \in i\,\mathbb{R}\,, \\
\partial_\tau &\to -i\partial_x \in i\,\mathbb{R}\,, \\
a(\tau) &\to a(ix) = \frac{i}{Hx} \in i\,\mathbb{R}\,, \\
\mathcal{K}_{\mathsf{a}}(\tau) &\to \mathcal{K}_{\mathsf{a}}(ix) = \frac{H^2}{2c_s^3 k_{\mathsf{a}}^3}(1 + c_s k_{\mathsf{a}} x) e^{-c_s k_{\mathsf{a}} x} \in \mathbb{R}\,.
\end{aligned} \tag{11.34}$$

Interestingly, the Wick rotated integral is purely real and therefore vanishes from $\langle \pi_c^4 \rangle'_{s,\mathrm{PO}}$. The only remaining contribution comes from the *residue* at the singularity τ_c, which reads

$$\begin{aligned}
\langle \pi_c^4 \rangle'_{s,\mathrm{PO}} &= -\frac{1}{\Lambda^6}\, \boldsymbol{s}\cdot(\boldsymbol{k}_1 \times \boldsymbol{k}_3)(\boldsymbol{k}_1\cdot\boldsymbol{k}_2)(\boldsymbol{k}_3\cdot\boldsymbol{k}_4) \\
&\times 2i\,\mathrm{Im}\left[\frac{2i\pi}{a^2}\operatorname*{Res}_{\tau_c}\mathcal{K}_+(k_1;\tau)\overleftrightarrow{\partial_\tau}\mathcal{K}_+(k_2;\tau)\right. \\
&\left.\times\frac{2\kappa a}{(s^2+m^2a^2)^2-4\kappa^2a^2s^2}\mathcal{K}_+(k_3;\tau)\overleftrightarrow{\partial_\tau}\mathcal{K}_+(k_4;\tau)\right]\,.
\end{aligned} \tag{11.35}$$

The vanishing of the Wick rotated integral can be understood as a consequence of the no-go theorem of parity violation in single-field theories. After Wick rotation but before actually computing the integral, one can perform a further spatial gradient expansion in powers of $s/(ma)$, $s/(\kappa a)$, which corresponds to a *local* single-field EFT. The no-go theorem forbids the presence of parity violation in such local single-field EFTs, thus the spatial gradient expansion must vanish term-by-term upon performing the integral and taking the imaginary part. Our result bypasses the no-go theorem precisely via *emergent non-locality* at the singularity, which is derived from the fact that the UV theory is multi-field in nature.

To proceed to the final trispectrum, we relate the Goldstone boson to the curvature perturbation by using $\zeta = -Hc_s^{3/2}f_\pi^{-2}\pi_c$, and introduce the dimensionless trispectrum $\mathcal{T}$ by

$$\langle \zeta_{\boldsymbol{k}_1}\zeta_{\boldsymbol{k}_2}\zeta_{\boldsymbol{k}_3}\zeta_{\boldsymbol{k}_4}\rangle' = (2\pi)^6\Delta_\zeta^6\frac{(k_t/4)^3}{(k_1k_2k_3k_4)^3}\mathcal{T}(\boldsymbol{k}_1,\boldsymbol{k}_2,\boldsymbol{k}_3,\boldsymbol{k}_4)\,, \tag{11.36}$$

where $k_t \equiv \sum_i k_i$ is the total energy. The parity-odd dimensionless trispectrum at LO can be written as

$$\mathcal{T}_{\mathrm{PO}}(\boldsymbol{k}_1,\boldsymbol{k}_2,\boldsymbol{k}_3,\boldsymbol{k}_4) = \mathcal{A}_{\mathrm{PO}}\,\Pi_s(\{\boldsymbol{k}_i\})\,F_s(\{k_i\},s) + t,u\text{ channels}\,, \tag{11.37}$$

where the amplitude $\mathcal{A}_{\rm PO}$, the polarisation factor Π_s and the function F_s read

$$\begin{aligned}
\mathcal{A}_{\rm PO} &\equiv \frac{i}{(2\pi)^2 c_s^2 \Delta_\zeta^2}\left(\frac{H}{\Lambda}\right)^6\left(\frac{\kappa}{H}\right)\left(\frac{m}{2H}\right)^4 , \\
\Pi_s(\{\boldsymbol{k}_i\}) &\equiv \boldsymbol{s}\cdot(\boldsymbol{k}_1\times\boldsymbol{k}_3)\,(\boldsymbol{k}_1\cdot\boldsymbol{k}_2)\,(\boldsymbol{k}_3\cdot\boldsymbol{k}_4)\,, \\
F_s(\{k_i\},s) &\equiv \frac{64(k_1-k_2)(k_3-k_4)}{k_t^3 s^2}\,\mathrm{Im}\Big[e^{ic_s k_t\tau_c} \\
&\quad\times\frac{i\pi(H\tau_c)^6(ik_{12}+c_s k_1 k_2\tau_c)(ik_{34}+c_s k_3 k_4\tau_c)}{m^4\kappa\,(\kappa+sH\tau_c)}\Big] ,
\end{aligned} \tag{11.38}$$

where $k_{12}\equiv k_1+k_2$, $k_{34}\equiv k_3+k_4$ and τ_c is the location of the singularity given in Eq. (11.33). The function F_s, when combined with Π_s, has been defined to be of order unity in regular kinematic configurations when $c_s\kappa, c_s m \ll H$. As such, it can be identified as a shape function for the parity-odd trispectrum. Note though that one cannot simply treat the prefactor $\mathcal{A}_{\rm PO}$ as the amplitude of the parity-odd trispectrum, due to the dependence of $F_s(\{k_i\},s)$ on the parameters m and κ. The overall size of the signal should rather be determined by looking at the full dimensionless trispectrum $\mathcal{T}_{\rm PO}$.

We now make a few comments on the analytical structure of the non-local EFT result. First, we see that the prefactor $\mathcal{A}_{\rm PO}$ is imaginary[7] and the kinematic factor Π_s enforces the parity-odd trispectrum to vanish in non-planar configurations, as for any n-point correlators with parity violation. Second, the function $F_s(\{k_i\},s)$ encoding the inflationary dynamics is a combination of simple rational functions and exponential factors, which originates from products of Goldstone mode functions in the vertex integrand. This outcome is of course attributed to the residue theorem. Importantly, there is no total energy k_t-pole in the correlator $\langle\zeta^4\rangle' \propto k_t^3 F_s(\{k_i\},s)$, suggesting that the parity-odd correlator can be written as a sum of factorised terms on the singularity at τ_c.

11.3.3 Singularity at Higher Orders

At LO, the location τ_c (11.33) in the τ-complex plane appears to be the only singularity of the integrand (11.31), where it manifests as a simple pole. Here, we show that τ_c is the only singularity at *any* finite order in the parity-odd sector of the series expansion (10.44), so that the parity-odd trispectrum is, to all orders, fixed by the singularity at τ_c. In Fourier space, consider a further decomposition of $\mathcal{D}_{\rm PE}^{-1}$ in Eq. (10.47) into an identity part and a longitudinal part,

$$\mathcal{D}_{\rm PE}^{-1} = \mathcal{D}_{\rm I}^{-1} + \mathcal{D}_{\rm L}^{-1} , \tag{11.39}$$

with

$$\begin{aligned}
[\mathcal{D}_{\rm I}^{-1}]_{ij} &\equiv \frac{s^2/a^2+m^2}{(s^2/a^2+m^2)^2-4\kappa^2 s^2/a^2}\,\delta_{ij} , \\
[\mathcal{D}_{\rm L}^{-1}]_{ij} &\equiv \frac{-4\kappa^2}{(s^2/a^2+m^2)^2-4\kappa^2 s^2/a^2}\,\frac{s_i s_j/a^2}{s^2/a^2+m^2} .
\end{aligned} \tag{11.40}$$

[7] When splitting the trispectrum signal into parity-even and parity-odd contributions $\mathcal{T}=\mathcal{T}_{\rm PE}+\mathcal{T}_{\rm PO}$, the parity-odd contribution is identified as the imaginary part of the trispectrum $\mathcal{T}_{\rm PO}=i\,\mathrm{Im}\mathcal{T}$.

Now both $\mathcal{D}_{\rm I}^{-1}$ and $\mathcal{D}_{\rm PO}^{-1}$ possess a pole at τ_c, while the longitudinal part $\mathcal{D}_{\rm L}^{-1}$ has an extra pole at $\tau_L \equiv \frac{im}{sH}$. Thus, we need to show that in the full expansion[8]

$$\left(\frac{\partial_\tau^2}{a^2}+\mathcal{D}\right)^{-1} = \left(\mathcal{D}_{\rm I}^{-1}+\mathcal{D}_{\rm L}^{-1}+\mathcal{D}_{\rm PO}^{-1}\right)\sum_{n=0}^{\infty}\left\{-\frac{\partial_\tau^2}{a^2}\left(\mathcal{D}_{\rm I}^{-1}+\mathcal{D}_{\rm L}^{-1}+\mathcal{D}_{\rm PO}^{-1}\right)\right\}^n , \quad (11.41)$$

this extra pole never appears in the parity-odd sector. In fact, this is simply guaranteed by the tensorial structure. Namely, the parity-odd sector must have at least one factor of $\mathcal{D}_{\rm PO}^{-1}$:

$$\cdots \frac{\partial_\tau^2}{a^2}\,\mathcal{D}_{\rm PO}^{-1}\,\frac{\partial_\tau^2}{a^2}\cdots . \quad (11.42)$$

Now one can always find the *closest* insertion of $[\mathcal{D}^{-1}]_{\rm L}$, with a sequence of $[\mathcal{D}^{-1}]_{\rm I}$ inserted in between,

$$\cdots \mathcal{D}_{\rm PO}^{-1}\,\frac{\partial_\tau^2}{a^2}\,\mathcal{D}_{\rm I}^{-1}\cdots\mathcal{D}_{\rm I}^{-1}\,\frac{\partial_\tau^2}{a^2}\,\mathcal{D}_{\rm L}^{-1}\cdots . \quad (11.43)$$

The tensor structure then reads

$$\cdots 2i\kappa\epsilon_{ijl}s_l\,\delta_{jm_1}\cdots\delta_{m_{2q}n}\,s_n s_k\cdots = 0\,. \quad (11.44)$$

Therefore, any insertion of $\mathcal{D}_{\rm L}^{-1}$ with its extra pole is eliminated by the nearest factor $\mathcal{D}_{\rm PO}^{-1}$. Henceforth, there is no extra τ_L-singularity in the parity-odd sector of the non-local EFT. Since finite steps of summation, multiplication and taking derivatives also do not generate new singularities, but only serve to increase the order of the τ_c-pole, we conclude that τ_c is the only singularity of the non-local EFT at any finite order, and that the resulting parity-odd trispectrum only receives contribution from the τ_c-pole.

11.3.4 Shape Characteristics

The parity-odd trispectrum in the non-local EFT exhibits several interesting features. They are based on the observation that the dynamical function $F_s(\{k_i, s)$ contains an exponential factor $e^{ic_s k_t \tau_c}$ with both real and imaginary parts,

$$e^{ic_s k_t\tau_c} = \exp\left(-\frac{k_t}{s}\sqrt{\alpha_m^2-\alpha_\kappa^2}\right)\exp\left(\frac{-i\alpha_\kappa k_t}{s}\right) . \quad (11.45)$$

This exponential factor is inherited from the Goldstone dynamical phase at the singularity, and leads to both a low-speed resonance peak and a new family of oscillatory signals:

- First, the real part of the exponent dictates that the overall amplitude of the parity-odd trispectrum is $\mathcal{O}(e^{-c_s m/H})$, which is non-perturbative in m^{-1} (recall that $\alpha_\kappa < \alpha_m = c_s m/H$). Consistent with the no-go theorem, if we were to locally integrate out the massive spinning field, it would lead to a vanishing

[8] Notice that we have applied the identity $a^{-2}\partial_\tau^2 = \partial_t^2 + H\partial_t$ to Eq. (10.44).

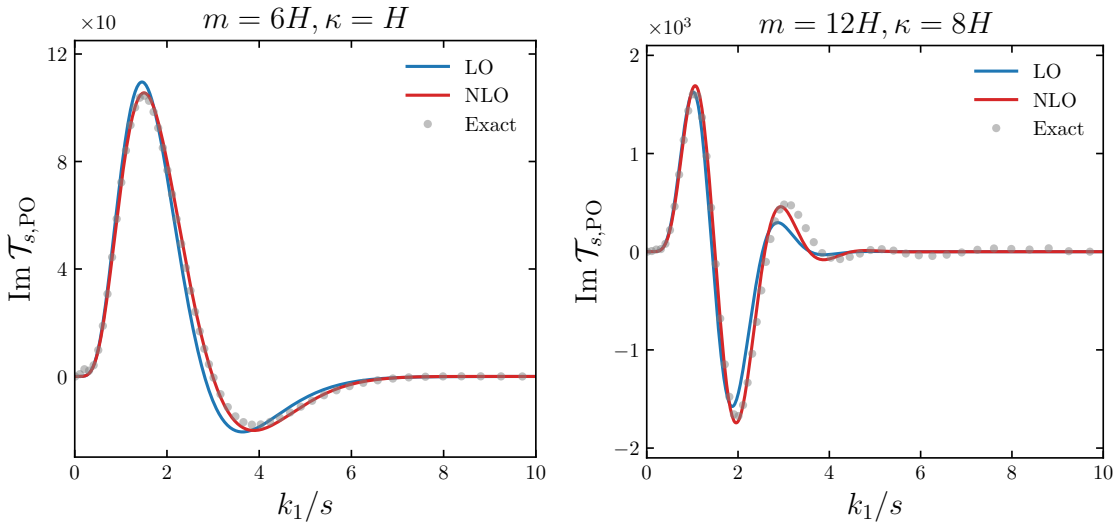


Figure 11.10: The s-channel parity-odd trispectrum shape $\mathrm{Im}\mathcal{T}_{s,\mathrm{PO}}$ as defined in Eq. (11.37) for the $\partial_j\dot{\pi}_c\partial_i\partial_j\pi_c\sigma_i$ interaction in the non-planar tetrahedron kinematics configuration, with $k_1 = k_3$, $k_2 = k_4 = \sqrt{s^2 + k_1^2}$ and $\psi = \pi/3$ being the dihedral angle from the $(\boldsymbol{k}_1, \boldsymbol{k}_2)$-plane to the $(\boldsymbol{k}_3, \boldsymbol{k}_4)$-plane. The parameters are chosen as $m/H = 6, \kappa/H = 1$ *(left)* and $m/H = 12, \kappa/H = 8$ *(right)*, together with a common sound speed $c_s = 0.1$ and $\Lambda = 30H$. The blue and red curves show the leading-order (LO) and the next-to-leading-order (NLO) non-local EFT results, respectively, and the gray dotted line shows the exact result in the two-field UV theory. The first visible resonance peak near the regular kinematics configuration is the low-speed collider signature, see Eq. (11.47). The second peak (valley) and the subsequent ones in the exponentially attenuated tail are attributed to the new class of oscillatory signals, periodic in k_1/s, see Eq. (11.45). For t and u channels, the exchanged momenta are not soft, the low-speed collider resonance is absent, and the corresponding signals are suppressed.

parity-odd contribution. Alternatively, a non-vanishing parity-odd signal arising from the exchange of a massive field must be non-perturbative in the mass. Now that the sound speed is reduced, the signal strength becomes considerably larger than the Boltzmann suppression $\mathcal{O}(e^{-\pi m/H})$ in the conventional case with a unit sound speed. Note also that the shape function is exponentially attenuated in the internal ultra-soft limit $s \to 0$, creating a resonance in the mildly-soft kinematic configuration. More explicitly, a resonance peak emerges in the trispectrum as a result of the interplay between a polynomial rising head and a exponentially attenuating tail:

$$|\mathcal{T}_{s,\mathrm{PO}}| \sim \left(\frac{k_s}{k_\ell}\right)^n e^{-\sqrt{\alpha_m^2 - \alpha_\kappa^2}\,\frac{4k_s}{k_\ell}}\,, \tag{11.46}$$

where $n \simeq 2$ is a power-law proxy for the polynomial dependence, while $k_\ell \sim s$ is the long mode and $k_s \sim k_1, \cdots, k_4$ represents the short modes. Demanding

$\partial|\mathcal{T}_{s,\mathrm{PO}}|/\partial(k_s/k_\ell) = 0$ yields the location of the resonance peak, given by

$$\frac{k_\ell}{k_s} \sim \frac{4}{n}\sqrt{\alpha_m^2 - \alpha_\kappa^2}\,. \tag{11.47}$$

This is essentially the same resonance peak as in the original low-speed collider framework, which lies at $k_\ell/k_s \sim \alpha_m = c_s m/H$ in the absence of chemical potential.

- On the other hand, the imaginary part in the exponential (11.45) gives a new class of oscillatory signals. The oscillation is periodic when expressed in the momentum ratio k_t/s, rather than logarithmic as in conventional cosmological collider signals. The oscillation frequency is determined not by the mass, but by the Goldstone sound speed and chemical potential through the dimensionless parameter $\alpha_\kappa = c_s\kappa/H$. Such oscillations are accompanied by the exponential decay in the limit $k_t/s \to \infty$, as noted above. It is interesting that even after integrating out the massive vector field, oscillatory features still appear within the IR non-local EFT. In contrast, conventional cosmological collider signals are *not* captured by the non-local EFT result, as they encode the super-horizon *on-shell* dynamics of the heavy field. One can think of the difference between the two types of oscillatory signals as a consequence of different dynamical phases in the complex τ-plane.

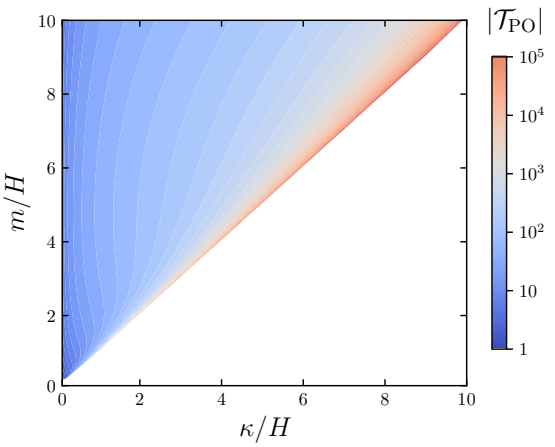


Figure 11.11: The size of the parity-odd trispectrum $|\mathcal{T}_{\mathrm{PO}}|$ generated by the interaction $\partial_j\dot{\pi}_c\partial_i\partial_j\pi_c\sigma_i$. The contours give the peak value of $\mathcal{T}_{\mathrm{PO}}$ in logarithmic scale. The horizontal axis is the chemical potential κ/H while the vertical axis shows the mass of the vector field m/H, both in Hubble units. The sound speed is chosen to be $c_s = 0.1$, along with the cutoff scale $\Lambda/H = 30$. The region $\kappa > m$ is excluded as the massive spinning particle develops a tachyonic instability.

To confirm the two features above, we present the s-channel dimensionless parity-odd trispectrum $\mathrm{Im}\,\mathcal{T}_{s,\mathrm{PO}}$ in Fig. 11.10 along with the numerical exact result computed with the UV theory, see Chap. 7. As one can clearly see from the figure, there are multiple peaks and valleys among which the first one is the low-speed collider

resonance and the others come from the new family of oscillatory signals. For a small sound speed $c_s \ll 1$ and chemical potential $\kappa/H \ll 1$, the LO non-local EFT result perfectly agrees with the exact one. Deviations start to appear when the chemical potential becomes comparable to the mass $\kappa \lesssim m$. In this case, the conventional cosmological collider signal becomes larger, dominating the collapsed limit (see the oscillating tail present in the exact result that is absent in the non-local EFT in the right panel of Fig. 11.10). The non-local EFT result nonetheless predicts well the other features of the signal. We also show the signal strength of the parity-odd trispectrum in Fig. 11.11, where we find that our model can give sizable signals within the reach of future LSS observations.

Part IV

Cosmological Flow

12

In-in Operator Formalism

An alternative approach to calculating cosmological correlators is the in-in operator formalism, which resembles the operator approach to S-matrix. Based on the Hamiltonian, as opposed to the Lagrangian for the Schwinger-Keldysh diagrammatic rules presented in Chap. 5, the operator (canonical) formalism requires performing field contractions by hand after expanding the Dyson series in perturbation theory, as illustrated in Fig. 12.1.

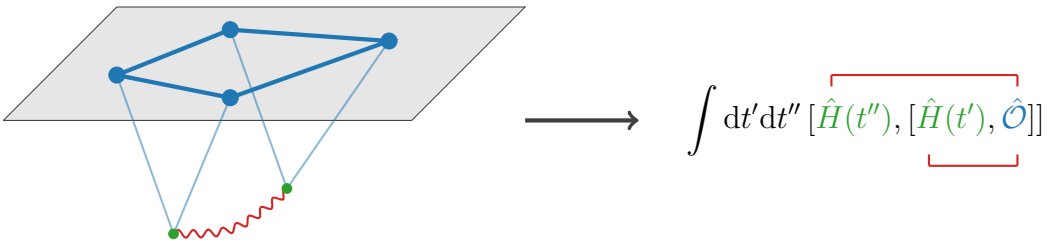


Figure 12.1: Cosmological correlators can be computed using the in-in operator formalism which consists of expanding the Dyson series in perturbation theory and performing Wick contractions by hand.

Before delving deeper, it is essential to pause and reflect on what exactly we aim to compute. In cosmology, we are interested in predicting—and observing—the (time-dependent) correlation functions of cosmological fluctuations. These differ fundamentally from cross sections in particle physics, which describe the probability of an event *localised* in spacetime. In contrast, our aim is to compute the *vacuum expectation value* of operators $\hat{\mathcal{O}}\left[\hat{\varphi}(t,\boldsymbol{x}),\hat{p}(t,\boldsymbol{y})\right]$, made up of products of various fields and their conjugate momenta at a given same time t,

$$\langle\Omega|\hat{\mathcal{O}}(t)|\Omega\rangle \equiv \langle\Omega|\hat{\mathcal{O}}\left[\hat{\varphi}(t,\boldsymbol{x}),\hat{p}(t,\boldsymbol{y})\right]|\Omega\rangle\ , \tag{12.1}$$

where the state $|\Omega\rangle$ is taken to be the vacuum of the fully interacting theory. The object defined in (12.1) is the answer to the question: what is the quantum-mechanical expectation value of (product of) fluctuations at some time t given that the Universe was prepared in some initial state in the infinite past that has been evolved to t? As such, these cosmological correlation functions are the central objects that link theory to observations: they can be readily computed from first principles given a theoretical description of the early Universe, and they can be observed as they correspond to (late-time or at least super-horizon) statistical correlation functions of fluctuations we see in the sky.[1]

In this chapter, we provide a detailed review of the in-in operator approach that forms the foundation for developing a systematic and automated method for computing cosmological correlators: the cosmological flow, to which the entire Part. IV of the thesis is dedicated.[2]

12.1 Preliminaries: a Matter of Picture

Let us first recall how standard scattering processes are treated in flat-space quantum field theory. Even though this discussion has some similarities with the cosmological case, major differences will arise.

S-matrix. In a typical collider experiment, one is interested in colliding particles that are in approximate momentum eigenstates at $t = -\infty$, and measuring the probability of finding certain outgoing momentum eigenstates at $t = +\infty$. The overlap between such an initial "in" state $|\alpha\rangle$ and a final "out" state $|\beta\rangle$ defines the S-matrix with elements $S_{\beta\alpha} = \langle\beta|\alpha\rangle$. The crucial assumption in scattering processes is that interactions happen in some finite time $-T < t < T$. This way, at $t = -\infty$ (resp. $t = +\infty$), we can define free-particle states $|\alpha_0\rangle$ (resp. $|\beta_0\rangle$) as eigenstates of the free Hamiltonian, known as asymptotic states. Instead of dealing with the S-matrix elements, it is often more convenient to work with the corresponding operator $\hat{S}$ such that $S_{\beta\alpha} \equiv \langle\beta_0|\hat{S}|\alpha_0\rangle$. Using the evolution unitary operator $\hat{U}(t,t')$ whose precise expression will be given in the following paragraph, and the properties $\hat{U}(t,t')\hat{U}(t',t'') = \hat{U}(t,t'')$ and $\hat{U}(t,t) = \mathbb{1}$, we have that $S_{\beta\alpha} = \langle\beta|\alpha\rangle = \langle\beta_0|\hat{U}^\dagger(0,+\infty)\hat{U}(0,-\infty)|\alpha_0\rangle = \langle\beta_0|\hat{U}(+\infty,-\infty)|\alpha_0\rangle$ so that

$$\hat{S} = \hat{U}(+\infty,-\infty)\,. \tag{12.2}$$

Note that the S-matrix elements, being "in-out" objects, are not observable. Only their modulus squared, producing a "in-in" object, gives the probability of a pro-

[1] Note that the link between quantum expectation values of operators we compute and statistical averages of fluctuations we observe is far from obvious and is still not completely understood.

[2] Historically, this formalism has been developed for the study of out-of-equilibrium or thermal open quantum systems [346, 348, 347] (see e.g. [516, 413] for textbooks) to account for the exchange of energy between an open system and its environment. More generally, it can be used whenever only the initial state of the system is known or can be prepared. It has been later used in cosmology for the first time in [42] and further systematised in [353]. Reviews on the in-in formalism in cosmology can be found in e.g. [517, 518].

cess to occur. The explicit expression for the $\hat{S}$-operator requires introducing the interaction picture.

Interaction picture and Dyson's formula. There exist several ways to derive the expression for the operator $\hat{U}$, of which we are going to choose to follow the Hamiltonian (canonical) derivation, see e.g. [359]. We assume that the dynamics of operators $\hat{\mathcal{O}}(t, \boldsymbol{x})$ is determined by a Hamiltonian $\hat{H}$ through the Heisenberg equation of motion $\frac{\mathrm{d}}{\mathrm{d}t}\hat{\mathcal{O}} = i[\hat{H}, \hat{\mathcal{O}}]$. This is the dynamical equation in the so-called *Heisenberg picture* where states (including the vacuum state of the full theory $|\Omega\rangle$) are time independent and operators are time dependent. To define a new picture in time-dependent perturbation theory, we write the Hamiltonian as

$$\hat{H} = \hat{H}_0 + \hat{H}_{\mathrm{int}}\,, \tag{12.3}$$

where the time evolution induced by $\hat{H}_0$ can be solved exactly. Importantly, this splitting is arbitrary as long as the interactions induced by $\hat{H}_{\mathrm{int}}$ can be treated perturbatively. We now define the *interaction picture* where the leading time evolution generated by $\hat{H}_0$ is factored out. From the operators $\hat{\mathcal{O}}$, we define the interaction-picture operators $\hat{\mathcal{O}}_{\mathrm{I}}$ as evolving according to the interaction-picture exactly solvable Hamiltonian $\hat{H}_0^{\mathrm{I}}$, i.e.

$$\frac{\mathrm{d}}{\mathrm{d}t}\hat{\mathcal{O}}_{\mathrm{I}} = i[\hat{H}_0^{\mathrm{I}}, \hat{\mathcal{O}}_{\mathrm{I}}]\,. \tag{12.4}$$

Thus, we can write $\hat{\mathcal{O}}_{\mathrm{I}}(t) = e^{i\hat{H}_0^{\mathrm{I}}(t-t_0)}\hat{\mathcal{O}}(t_0)e^{-i\hat{H}_0^{\mathrm{I}}(t-t_0)}$. Here, t_0 corresponds to the time when the interaction-picture operators $\hat{\mathcal{O}}_{\mathrm{I}}$ are matched onto the Heisenberg ones $\hat{\mathcal{O}}$. Let us now find the time evolution operator $\hat{U}(t, t_0)$ such that it relates the full Heisenberg-picture operators to the interaction-picture ones at the *same time* t, $\hat{\mathcal{O}}_{\mathrm{I}}(t) = \hat{U}^\dagger(t, t_0)\hat{\mathcal{O}}(t)\hat{U}(t, t_0)$. Differentiating this relation with respect to t and using the dynamical equations for $\hat{\mathcal{O}}_{\mathrm{I}}$ and $\hat{\mathcal{O}}$, one finds that a necessary condition is that the operator $\hat{U}(t, t_0)$ satisfies

$$\frac{\mathrm{d}}{\mathrm{d}t}\hat{U}(t, t_0) = i\hat{U}(t, t_0)\hat{H}_{\mathrm{int}}^{\mathrm{I}}(t)\,, \tag{12.5}$$

and where $\hat{H}_{\mathrm{int}}^{\mathrm{I}}$ is the interaction Hamiltonian expressed in the interaction picture. If everything commuted, the solution to Eq. (12.5) would trivially be $\hat{U}(t, t_0) = \exp\left(i\int_{t_0}^{t}\hat{H}_{\mathrm{int}}^{\mathrm{I}}(t')\mathrm{d}t'\right)$. However, $\hat{H}_{\mathrm{int}}^{\mathrm{I}}(t)$ does not necessarily commute with $\hat{H}_{\mathrm{int}}^{\mathrm{I}}(t')$ at different times $t \neq t'$. The correct solution is given, at least formally, by

$$\hat{U}(t, t_0) = \bar{\mathcal{T}}\left\{\exp\left(i\int_{t_0}^{t}\hat{H}_{\mathrm{int}}^{\mathrm{I}}(t')\mathrm{d}t'\right)\right\}\,, \tag{12.6}$$

where $\bar{\mathcal{T}}$ (with $\bar{\mathcal{T}}^\dagger = \mathcal{T}$) is the anti-time ordering operator. The expression (12.6) is known as the Dyson's formula, and works because time ordering effectively makes everything inside commute. Upon the correct boundary condition $\hat{U}(t_0, t_0) = \mathbb{1}$, this solution is unique.

What goes wrong in cosmology. So far, our discussion was centered around scattering processes. There, one is able to asymptotically define the vacuum of the theory by simply considering the system in the infinite past and future. In cosmology, inflation provides a mechanism that enables one to consistently define an asymptotic vacuum, "in", in the past: because fluctuations emerge from very small scales under the horizon, they were effectively behaving as in Minkowksi spacetime in which the notion of vacuum is well defined. However the "out" vacuum cannot be properly defined. Cosmological fluctuations never stop interacting, at least gravitationally, and their dynamics on super-horizon scales are very different from what could exist in flat spacetime for actual particles. Moreover, when a background gravitational field is present, as it is the case in cosmology, the very concept of particles is ill-defined. Indeed, any change in the gravitational background (more generally if the background is time-dependent) would spontaneously create particles, see Chap. 4. Therefore, one needs to use the in-in formalism that correctly takes into account the transfer of energy between fields and the background.

12.2 From Heisenberg to Interaction Picture

Let us now derive the master formula for in-in correlators in cosmology. The dynamics is governed by the Hamiltonian $\hat{H}$ which is a functional of the full Heisenberg-picture fields $\hat{\varphi}(t,\boldsymbol{x})$ and their conjugate momenta $\hat{p}(t,\boldsymbol{x})$. The operators $\hat{\varphi}$ and $\hat{p}$ evolve with the full Hamiltonian. After splitting the Hamiltonian into a free $\hat{H}_0$ and an interacting part $\hat{H}_{\rm int}$, the interaction-picture operators $\hat{\varphi}_{\rm I}$ and $\hat{p}_{\rm I}$ satisfy Eq. (12.4). By definition, at some initial time—that we denote for now as t_0—both the full fields and the interaction-picture ones coincide: $\hat{\varphi}(t_0) = \hat{\varphi}_{\rm I}(t_0)$, and similarly for the momenta. At some later time $t > t_0$, the interaction-picture fields and momenta are related to the full ones by

$$\hat{\varphi}_{\rm I}(t) = \hat{U}^\dagger(t,t_0)\hat{\varphi}(t)\hat{U}(t,t_0)\,, \quad \hat{p}_{\rm I}(t) = \hat{U}^\dagger(t,t_0)\hat{p}(t)\hat{U}(t,t_0)\,, \tag{12.7}$$

where the unitary operator $\hat{U}(t,t_0)$ is given by the Dyson's formula (12.6). Assuming that the operator $\hat{\mathcal{O}}$ of interest can be formally written as a series in terms of the fields and their momenta, one has

$$\hat{\mathcal{O}}_{\rm I}(t) = \hat{U}^\dagger(t,t_0)\hat{\mathcal{O}}(t)\hat{U}(t,t_0)\,. \tag{12.8}$$

The solution for the operator $\hat{\mathcal{O}}(t)$ in terms of the free fields and momenta in the interaction picture is then given by

$$\hat{\mathcal{O}}(t) = \bar{\mathcal{T}}\left\{\exp\left(i\int_{t_0}^{t}\hat{H}^{\rm I}_{\rm int}(t')\mathrm{d}t'\right)\right\}\hat{\mathcal{O}}_{\rm I}(t)\mathcal{T}\left\{\exp\left(-i\int_{t_0}^{t}\hat{H}^{\rm I}_{\rm int}(t')\mathrm{d}t'\right)\right\}\,. \tag{12.9}$$

We now want to express the expectation value of the operator $\hat{\mathcal{O}}(t)$ as evaluated in the vacuum of the full theory $|\Omega\rangle$. To do this, one needs to specify the time t_0 at which interactions are shut down and the theory is free, therefore trading the $|\Omega\rangle$ for the vacuum of the free theory $|0\rangle$. This allows concrete computations using Wick's theorem. In cosmological applications, the free theory can only be unambiguously defined in the asymptotic past $t_0 \to -\infty$. As we see now, reaching this limit requires introducing the $i\epsilon$ prescription.

12.2.1 $i\epsilon$ Prescription

The state $|\Omega\rangle$ asymptotically reaches the free theory vacuum $|0\rangle$ in the far past. Heuristically following [359] (chap. 4), let us evolve $|0\rangle$, i.e. the ground state of $\hat{H}_0$, using the full Hamiltonian $\hat{H}$

$$e^{-i\hat{H}(t_0-t)}\,|0\rangle = e^{-i\hat{H}(t_0-t)}\sum_n |n\rangle\,\langle n|0\rangle = \sum_n e^{-i\omega_n(t_0-t)}\,|n\rangle\,\langle n|0\rangle\ , \tag{12.10}$$

where ω_n are eigenvalues of $\hat{H}$ and with $|n\rangle$ ($n \geq 0$) being a complete set of states of $\hat{H}$. We have introduced an arbitrary constant shift in time t_0 whose purpose will be clearer later on. In order for the free dynamics dictated by $\hat{H}_0$ to be the dominant one (otherwise signaling a breakdown of perturbation theory), $|\Omega\rangle$ must have some overlap with $|0\rangle$, i.e. $\langle\Omega|0\rangle \neq 0$. Therefore, we can isolate the state $|\Omega\rangle$

$$e^{-i\hat{H}(t_0-t)}\,|0\rangle = e^{-i\omega_0(t_0-t)}\,|\Omega\rangle\,\langle\Omega|0\rangle + \sum_{n\neq 0} e^{-i\omega_n(t_0-t)}\,|n\rangle\,\langle n|0\rangle\ , \tag{12.11}$$

where $\hat{H}\,|\Omega\rangle = \omega_0\,|\Omega\rangle$. Since $\omega_n > \omega_0$ for $n \neq 0$, assuming that the ground state is not degenerate and that energy levels do not cross (which holds as long as interactions are switched off adiabatically), we can slightly tilt time in the imaginary direction

$$t \to t(1-i\epsilon)\,, \tag{12.12}$$

with $\epsilon > 0$ an infinitesimal constant, so that the limit $t \to -\infty$ effectively makes all terms with $n \neq 0$ in the series vanish. We obtain that $|\Omega\rangle$ can be mapped to $|0\rangle$ via

$$|\Omega\rangle = \lim_{t\to-\infty(1-i\epsilon)} \left(e^{-i\omega_0(t_0-t)}\,\langle\Omega|0\rangle\right)^{-1} e^{-i\hat{H}(t_0-t)}\,|0\rangle\ . \tag{12.13}$$

Splitting the full Hamiltonian $\hat{H}$ into $\hat{H}_0$ and $\hat{H}_{\rm int}$ and using $\hat{H}_0\,|0\rangle = |0\rangle$ (which defines the zero energy), a few elementary manipulations lead to

$$|\Omega\rangle = \lim_{\epsilon\to 0} \mathcal{N}_\epsilon\,\hat{U}^\dagger_\epsilon(t_0,-\infty)\,|0\rangle\ , \quad \text{with} \quad \mathcal{N}_\epsilon = \lim_{t\to-\infty(1-i\epsilon)} \left(e^{-i\omega_0(t_0-t)}\,\langle\Omega|0\rangle\right)^{-1}\ , \tag{12.14}$$

and where we define the time evolution operator with a deformed contour as

$$\hat{U}^\dagger_\epsilon(t_0,-\infty) = \mathcal{T}\left\{\exp\left(-i\int_{-\infty(1-i\epsilon)}^{t_0} \hat{H}^{\rm I}_{\rm int}(t')\mathrm{d}t'\right)\right\}\ . \tag{12.15}$$

Eventually, one obtains

$$\langle\Omega|\hat{\mathcal{O}}(t)|\Omega\rangle = \langle\Omega|\hat{U}(t,t_0)\hat{\mathcal{O}}_{\rm I}(t)\hat{U}^\dagger(t,t_0)|\Omega\rangle = \lim_{\epsilon\to 0} |\mathcal{N}_\epsilon|^2\,\langle 0|\hat{U}_\epsilon(t,-\infty)\hat{\mathcal{O}}_{\rm I}(t)\hat{U}^\dagger_\epsilon(t,-\infty)|0\rangle\ , \tag{12.16}$$

where in the limit $\epsilon \to 0$, we have $|\mathcal{N}_\epsilon|^2 = |\,\langle\Omega|0\rangle\,|^{-2}$. This normalisation can be evaluated by choosing $\hat{\mathcal{O}} = \mathbb{1}$, i.e. $1 = \langle\Omega|\mathbb{1}|\Omega\rangle = |\,\langle\Omega|0\rangle\,|^{-2}\,\langle 0|\hat{U}_\epsilon(t,-\infty)\hat{U}^\dagger_\epsilon(t,-\infty)|0\rangle = |\,\langle\Omega|0\rangle\,|^{-2}\,\langle 0|0\rangle = |\,\langle\Omega|0\rangle\,|^{-2}$.

12.2.2 In-in Master Formula

After including the $i\epsilon$ prescription to project the full theory vacuum $|\Omega\rangle$ onto the vacuum of the free theory $|0\rangle$, we obtain the master in-in formula

$$\langle\Omega|\hat{\mathcal{O}}(t)|\Omega\rangle = \langle 0|\bar{\mathcal{T}}\left\{\exp\left(i\int_{-\infty^-}^{t}\hat{H}^{\rm I}_{\rm int}(t')\mathrm{d}t'\right)\right\}\hat{\mathcal{O}}_{\rm I}(t)\mathcal{T}\left\{\exp\left(-i\int_{-\infty^+}^{t}\hat{H}^{\rm I}_{\rm int}(t')\mathrm{d}t'\right)\right\}|0\rangle\ , \tag{12.17}$$

where $-\infty^{\pm} \equiv -\infty(1\mp i\epsilon)$. This notation matches the visualisation in the complex plane. Although the master in-in formula is correct, this implementation of the $i\epsilon$ prescription has some major caveats, recently pointed out in [361]:

- We have crucially assumed that the (interacting) Hamiltonian is time independent in the manipulations (12.14) (and that $\hat{H}_0$ commutes with $\hat{H}_{\rm int}$) by writing
$$\mathcal{T}\left\{\exp\left(-i\int_{t}^{t_0}\hat{H}^{\rm I}_{\rm int}(t')\mathrm{d}t'\right)\right\} \approx e^{-i\hat{H}^{\rm I}_{\rm int}(t_0-t)}\ , \tag{12.18}$$
in passing completely neglecting the time ordering. This hand-wavy manipulation is often justified with some adiabaticity condition when all modes are well inside the horizon, therefore reaching the flat-space limit where the standard derivation is applicable. This infinite past limit has also allowed us to replace $\hat{H}_{\rm int} \to \hat{H}^{\rm I}_{\rm int}$ to recover the evolution operator.

- After projection, the produced state is not correctly normalised since the time evolution operator is non-unitary, i.e. we do not in general have $\hat{U}_\epsilon(t,-\infty)\hat{U}^\dagger_\epsilon(t,-\infty) = \mathbb{1}$. This is because the contours of integration are different in $\hat{U}_\epsilon(t,-\infty)$ and $\hat{U}^\dagger_\epsilon(t,-\infty)$, producing a commutator and not the identity.[3] Precisely specifying the complex contour is essential since the integrand can be non-analytic in time (for example when massive fields are present). Moreover, cancelling the overall phase in the normalisation implicitly assumes that both the limits $\epsilon \to 0$ and $t \to -\infty$ commute, which is not the case in general.

A more technical and rigorous derivation of this prescription that solves the mentioned issues is presented Chap. 5. Using the operator formalism, circumventing these issues is possible by deforming energy instead of time $\hat{H} \to \hat{H}_\epsilon = \hat{H}e^{\epsilon t}$ which is clearly Hermitian, see e.g. [361, 520, 521]. This way, the in-in formalism is exactly equivalent to perturbatively solving the quantum equations of motion with an appropriate $i\epsilon$-deformed Hamiltonian.

12.3 Perturbative Expansion

In practice, the master in-in formula (12.17) cannot be solved as it is: the aim of splitting the full Hamiltonian into a free part and an interacting one was to treat

[3] This property is even more explicit when dealing with non-unitary theories in which dissipation is induced as interferences between the two branches of the in-in contour, see e.g. the textbooks [516] for a canonical approach. The complex contour being not invariant under conjugation is a direct consequence of the lack of time-reversal invariance of the physics in cosmology, also see [519] that raises the issue of infinite localisation of fields in time for equal-time correlators.

interactions in a perturbative way.

12.3.1 Factorised Forms

Assuming interactions are small, we can consistently expand the exponentials in powers of $\hat{H}^{\mathrm{I}}_{\mathrm{int}}$. This results in the perturbative expansion

$$\langle\Omega|\hat{\mathcal{O}}(t)|\Omega\rangle = \sum_{n=0}^{\infty} \langle\Omega|\hat{\mathcal{O}}(t)|\Omega\rangle^{(n)} \,, \tag{12.19}$$

where the superscript (n) refers to the number of $\hat{H}^{\mathrm{I}}_{\mathrm{int}}$ insertions.

- To zeroth order, the leading term in the series (12.19) easily reads

$$\langle\Omega|\hat{\mathcal{O}}(t)|\Omega\rangle^{(0)} = \langle 0|\hat{\mathcal{O}}_{\mathrm{I}}(t)|0\rangle \,. \tag{12.20}$$

- To first order, carefully accounting for the operator ordering, we obtain

$$\langle\Omega|\hat{\mathcal{O}}(t)|\Omega\rangle^{(1)} = i\int_{-\infty^-}^{t} \mathrm{d}t' \, \langle 0|\hat{H}^{\mathrm{I}}_{\mathrm{int}}(t')\hat{\mathcal{O}}_{\mathrm{I}}(t)|0\rangle - i\int_{-\infty^+}^{t} \mathrm{d}t' \, \langle 0|\hat{\mathcal{O}}_{\mathrm{I}}(t)\hat{H}^{\mathrm{I}}_{\mathrm{int}}(t')|0\rangle \,. \tag{12.21}$$

  This expression can be further simplified if one assumes that the operator $\hat{\mathcal{O}}$ is Hermitian, $\hat{\mathcal{O}}^\dagger = \hat{\mathcal{O}}$ (and the Hamiltonian). In this case, using $\langle 0|\hat{\mathcal{O}}_{\mathrm{I}}(t)\hat{H}^{\mathrm{I}}_{\mathrm{int}}(t')|0\rangle^* = \langle 0|\hat{H}^{\mathrm{I}}_{\mathrm{int}}(t')\hat{\mathcal{O}}_{\mathrm{I}}(t)|0\rangle$, one obtains

$$\langle\Omega|\hat{\mathcal{O}}(t)|\Omega\rangle^{(1)} = 2\,\mathrm{Im}\left[\int_{-\infty^-}^{t} \mathrm{d}t' \, \langle 0|\hat{\mathcal{O}}_{\mathrm{I}}(t)\hat{H}^{\mathrm{I}}_{\mathrm{int}}(t')|0\rangle\right] \,. \tag{12.22}$$

  Note that applying the conjugation operation also changes the integration contour which allows us to write the formula in a compact way with a single integral. This expression captures the leading-order effect of interactions that are treated perturbatively.

- To second order, expanding (12.17) produces three contributions

$$\begin{aligned}\langle\Omega|\hat{\mathcal{O}}(t)|\Omega\rangle^{(2)} = &-\frac{1}{2}\langle 0|\bar{\mathcal{T}}\left\{\int_{-\infty^-}^{t}\mathrm{d}t'\int_{-\infty^-}^{t}\mathrm{d}t''\hat{H}^{\mathrm{I}}_{\mathrm{int}}(t')\hat{H}^{\mathrm{I}}_{\mathrm{int}}(t'')\right\}\hat{\mathcal{O}}_{\mathrm{I}}(t)|0\rangle \\ &-\frac{1}{2}\langle 0|\hat{\mathcal{O}}_{\mathrm{I}}(t)\mathcal{T}\left\{\int_{-\infty^-}^{t}\mathrm{d}t'\int_{-\infty^-}^{t}\mathrm{d}t''\hat{H}^{\mathrm{I}}_{\mathrm{int}}(t')\hat{H}^{\mathrm{I}}_{\mathrm{int}}(t'')\right\}|0\rangle \\ &+\int_{-\infty^-}^{t}\mathrm{d}t'\int_{-\infty^+}^{t}\mathrm{d}t''\,\langle 0|\hat{H}^{\mathrm{I}}_{\mathrm{int}}(t')\hat{\mathcal{O}}_{\mathrm{I}}(t)\hat{H}^{\mathrm{I}}_{\mathrm{int}}(t'')|0\rangle \,.\end{aligned} \tag{12.23}$$

  The (anti-)time ordering can be simplified as follows

$$\bar{\mathcal{T}}\left\{\int_{-\infty^-}^{t}\mathrm{d}t'\int_{-\infty^-}^{t}\mathrm{d}t''\hat{H}^{\mathrm{I}}_{\mathrm{int}}(t')\hat{H}^{\mathrm{I}}_{\mathrm{int}}(t'')\right\} = 2\int_{-\infty^-}^{t}\mathrm{d}t'\int_{-\infty^-}^{t'}\mathrm{d}t''\hat{H}^{\mathrm{I}}_{\mathrm{int}}(t'')\hat{H}^{\mathrm{I}}_{\mathrm{int}}(t') \,, \tag{12.24}$$

upon relabelling time $t' \leftrightarrow t''$. One finally obtains

$$\begin{aligned}\langle\Omega|\hat{\mathcal{O}}(t)|\Omega\rangle^{(2)} = &-\int_{-\infty^-}^{t}\mathrm{d}t'\int_{-\infty^-}^{t'}\mathrm{d}t''\,\langle 0|\hat{H}^{\mathrm{I}}_{\mathrm{int}}(t'')\hat{H}^{\mathrm{I}}_{\mathrm{int}}(t')\hat{\mathcal{O}}_{\mathrm{I}}(t)|0\rangle\\ &-\int_{-\infty^+}^{t}\mathrm{d}t'\int_{-\infty^+}^{t'}\mathrm{d}t''\,\langle 0|\hat{\mathcal{O}}_{\mathrm{I}}(t)\hat{H}^{\mathrm{I}}_{\mathrm{int}}(t')\hat{H}^{\mathrm{I}}_{\mathrm{int}}(t'')|0\rangle\\ &+\int_{-\infty^-}^{t}\mathrm{d}t'\int_{-\infty^+}^{t}\mathrm{d}t''\,\langle 0|\hat{H}^{\mathrm{I}}_{\mathrm{int}}(t')\hat{\mathcal{O}}_{\mathrm{I}}(t)\hat{H}^{\mathrm{I}}_{\mathrm{int}}(t'')|0\rangle\ .\end{aligned} \tag{12.25}$$

Note that the time ordering appears in the bounds of the time integrals which become nested. Similarly to the first-order contribution, in the case of $\hat{\mathcal{O}}$ being Hermitian, the second-order contribution can be written in a compact form

$$\begin{aligned}\langle\Omega|\hat{\mathcal{O}}(t)|\Omega\rangle^{(2)} = &\int_{-\infty^-}^{t}\mathrm{d}t'\int_{-\infty^+}^{t}\mathrm{d}t''\,\langle 0|\hat{H}^{\mathrm{I}}_{\mathrm{int}}(t')\hat{\mathcal{O}}_{\mathrm{I}}(t)\hat{H}^{\mathrm{I}}_{\mathrm{int}}(t'')|0\rangle\\ &-2\,\mathrm{Re}\left[\int_{-\infty^+}^{t}\mathrm{d}t'\int_{-\infty^+}^{t'}\mathrm{d}t''\,\langle 0|\hat{\mathcal{O}}_{\mathrm{I}}(t)\hat{H}^{\mathrm{I}}_{\mathrm{int}}(t')\hat{H}^{\mathrm{I}}_{\mathrm{int}}(t'')|0\rangle\right]\ .\end{aligned} \tag{12.26}$$

The expressions (12.20), (12.22) and (12.26) are known as factorised forms. Importantly, the compact forms (12.22) and (12.26) are the ones used in practice if the theory is parity invariant. Although operators in Fourier space are not Hermitian, in practical calculations one can simply flip the sign of all momenta to obtain these forms. In principle, these expressions can be evaluated explicitly using Wick's theorem, i.e. performing contractions. Expanding (12.17) to higher-order is somehow cumbersome but can be done following the same procedure.

12.3.2 Commutator Forms

There is an equivalent expression for in-in correlators that can be written to all order in $\hat{H}^{\mathrm{I}}_{\mathrm{int}}$ in a compact form, which reads[4]

$$\begin{aligned}\langle\Omega|\hat{\mathcal{O}}(t)|\Omega\rangle^{(n)} = i^n\int_{-\infty}^{t}\mathrm{d}t_1\int_{-\infty}^{t_1}\mathrm{d}t_2\ldots\int_{-\infty}^{t_{n-1}}\mathrm{d}t_n\\ \times\langle 0|[\hat{H}^{\mathrm{I}}_{\mathrm{int}}(t_n),\ldots[\hat{H}^{\mathrm{I}}_{\mathrm{int}}(t_2),[\hat{H}^{\mathrm{I}}_{\mathrm{int}}(t_1),\hat{\mathcal{O}}(t)]]\ldots]|0\rangle\ .\end{aligned} \tag{12.27}$$

This formula can be proved by mathematical induction [353] (also see [522]). However, there are some caveats. Indeed, already at first order $n = 1$, one can notice that constructing a commutator out of the expression (12.21) implicitly requires integrating both terms along the same contour, hence neglecting the $i\epsilon$ prescription [523, 524]. At any order, this complication in practice boils down to evaluating the right-hand side of (12.27) for $|\Omega\rangle$ and not $|0\rangle$. This way, proving the commutator form is just a reorganisation of the operator algebra. A more rigorous proof can be found in [520] where the trick is to deform energy instead of time.

[4] The $n = 0$ case should be understood as just $\langle\Omega|\hat{\mathcal{O}}(t)|\Omega\rangle^{(0)} = \langle 0|\hat{\mathcal{O}}_{\mathrm{I}}(t)|0\rangle$.

Each form presents distinct computational benefits and drawbacks. The factorised forms are mostly used to achieve convergence of the time integrals in the infinite past. Indeed, the time integrals in the commutator form are divergent or ill-defined in the UV because they require the integral contour to be deformed both in the positive and negative directions. On the contrary, the commutator form is convenient to deal with IR behaviours, as spurious different leading contributions are explicitly cancelled before the multiple time integrals are performed. This representation is often used when analytically estimating in-in contributions. Introducing an intermediate cutoff t_0, it is possible to mix both representations to achieve convergence in the UV and in the IR (especially if the integrals are performed numerically) [58].

12.4 In-in Formalism in Action

From first principles, we have introduced the in-in formalism to compute cosmological correlation functions. Let us now see how to use it in practice to obtain concrete results.

12.4.1 Wick Contractions

To make progress in evaluating the integrands, we now review Wick's theorem. The integrands take the general form $\langle 0|\hat{A}_{\rm I}\hat{B}_{\rm I}\dots|0\rangle$, which is hard to evaluate. On the other hand, the vacuum expectation value of a *normal-ordered* string of operators $\langle 0|\mathcal{N}\{\hat{A}_{\rm I}\hat{B}_{\rm I}\dots\}|0\rangle$ identically vanishes, as the normal ordering operation $\mathcal{N}$ places all creation operators $\hat{a}^\dagger_{\boldsymbol{k}}$ on the left of all annihilation operators $\hat{a}_{\boldsymbol{k}}$. Let us now give the simplest non-trivial example of a string of two (same) field operators. In Fourier space, the mode expansion of an operator contains two parts, an annihilation part and a creation part, and so can be written

$$\hat{\varphi}_{\rm I}(\boldsymbol{k},t) \equiv \hat{\varphi}^-_{\boldsymbol{k}}(t) + \hat{\varphi}^+_{\boldsymbol{k}}(t) = u_k(t)\hat{a}_{\boldsymbol{k}} + u^*_k(t)\hat{a}^\dagger_{-\boldsymbol{k}}\,. \tag{12.28}$$

Expressing both the simple product and the normal-ordered version of the string $\hat{\varphi}_{\rm I}(\boldsymbol{k},t)\hat{\varphi}_{\rm I}(\boldsymbol{q},t')$ in terms of $\hat{\varphi}^-$ and $\hat{\varphi}^+$, one can notice that these expressions only differ by a commutator

$$\hat{\varphi}_{\rm I}(\boldsymbol{k},t)\hat{\varphi}_{\rm I}(\boldsymbol{q},t') = \mathcal{N}\{\hat{\varphi}_{\rm I}(\boldsymbol{k},t)\hat{\varphi}_{\rm I}(\boldsymbol{q},t')\} + [\hat{\varphi}^-_{\boldsymbol{k}}(t),\hat{\varphi}^+_{\boldsymbol{q}}(t')]\,. \tag{12.29}$$

Subtracting out a normal-ordered string of operators from its simple product version defines a *contraction*

$$\begin{aligned}\overbrace{\hat{\varphi}_{\rm I}(\boldsymbol{k},t)\hat{\varphi}_{\rm I}(\boldsymbol{q},t')} &\equiv \hat{\varphi}_{\rm I}(\boldsymbol{k},t)\hat{\varphi}_{\rm I}(\boldsymbol{q},t') - \mathcal{N}\{\hat{\varphi}_{\rm I}(\boldsymbol{k},t)\hat{\varphi}_{\rm I}(\boldsymbol{q},t')\}\\ &= u_k(t)u^*_k(t')\,(2\pi)^3\delta^{(3)}(\boldsymbol{k}+\boldsymbol{q})\,,\end{aligned} \tag{12.30}$$

where we have used $[\hat{a}_{\boldsymbol{k}},\hat{a}^\dagger_{-\boldsymbol{q}}] = (2\pi)^3\delta^{(3)}(\boldsymbol{k}+\boldsymbol{q})$. Therefore, contractions turn field operators into simple complex numbers. This generalises to an arbitrary string of field operators

$$\langle 0|\hat{\varphi}_{\rm I}(\boldsymbol{k}_1,t_1)\dots\hat{\varphi}_{\rm I}(\boldsymbol{k}_n,t_n)|0\rangle \;=\; \begin{pmatrix}\text{all possible combinations involving}\\ \text{contractions of every pair of operators}\end{pmatrix}\,, \tag{12.31}$$

with $n \geq 1$. Note that all terms must be contracted. If the string is composed of an odd number of operators, fully contracting the chain gives zero, as only one operator having zero vacuum expectation value is left.

12.4.2 Worked out Examples

Contact diagram. First, we compute the equal-time three-point correlation function in Fourier space $\langle \varphi_{\boldsymbol{k}_1}(t)\varphi_{\boldsymbol{k}_2}(t)\varphi_{\boldsymbol{k}_3}(t)\rangle$ of an arbitrary scalar field $\varphi(t,\boldsymbol{x})$ in FLRW spacetime coming from a cubic interaction. The interacting Lagrangian is taken to be $\mathcal{L}_{\rm int}/a^3(t) = -\frac{g}{3!}\varphi^3$ where g is a coupling constant. Note that from now on, we will drop hats on operators, the explicit reference to the vacuum $|\Omega\rangle$, and the reference to the picture to avoid cluttered notations. In Fourier space, the interacting Hamiltonian reads

$$\begin{aligned} H_{\rm int}(t) &= \frac{g}{3!}\int \mathrm{d}^3\boldsymbol{x}\, a^3(t)\varphi^3(t,\boldsymbol{x}) \\ &= \frac{g}{3!}\,a^3(t)\int \left(\prod_{i=1}^{3}\frac{\mathrm{d}^3\boldsymbol{q}_i}{(2\pi)^3}\right)\varphi_{\boldsymbol{q}_1}(t)\varphi_{\boldsymbol{q}_2}(t)\varphi_{\boldsymbol{q}_3}(t)\,(2\pi)^3\delta^{(3)}(\boldsymbol{q}_1+\boldsymbol{q}_2+\boldsymbol{q}_3)\,, \end{aligned} \tag{12.32}$$

where the second line is obtained after performing the integral over space. The first contribution in Eq. (12.21) then reads

$$\begin{aligned} \langle \varphi_{\boldsymbol{k}_1}(t)\varphi_{\boldsymbol{k}_2}(t)\varphi_{\boldsymbol{k}_3}(t)\rangle \supset\, & i\,\frac{g}{3!}\int \left(\prod_{i=1}^{3}\frac{\mathrm{d}^3\boldsymbol{q}_i}{(2\pi)^3}\right)(2\pi)^3\delta^{(3)}(\boldsymbol{q}_1+\boldsymbol{q}_2+\boldsymbol{q}_3) \\ & \times\int_{-\infty^-}^{t}\mathrm{d}t' a^3(t')\,\langle 0|\varphi_{\boldsymbol{q}_1}(t')\varphi_{\boldsymbol{q}_2}(t')\varphi_{\boldsymbol{q}_3}(t')\varphi_{\boldsymbol{k}_1}(t)\varphi_{\boldsymbol{k}_2}(t)\varphi_{\boldsymbol{k}_3}(t)|0\rangle\,, \end{aligned} \tag{12.33}$$

where we have highlighted in blue the contributions coming from the single insertion of $H_{\rm int}$. Using Wick's theorem, we now perform all possible contractions of every pair of operators. However, being interested in the *connected* part of the correlator, we only contract internal legs ($\varphi_{\boldsymbol{q}_i}$) with external legs ($\varphi_{\boldsymbol{k}_i}$). An example of such contractions using (12.30) is

$$\langle 0|\varphi_{\boldsymbol{q}_1}(t')\varphi_{\boldsymbol{q}_2}(t')\varphi_{\boldsymbol{q}_3}(t')\varphi_{\boldsymbol{k}_1}(t)\varphi_{\boldsymbol{k}_2}(t)\varphi_{\boldsymbol{k}_3}(t)|0\rangle = \prod_{i=1}^{3}u_{k_i}(t')u^*_{k_i}(t)\,(2\pi)^3\delta^{(3)}(\boldsymbol{q}_i+\boldsymbol{k}_i)\,. \tag{12.34}$$

Integrating over the internal momenta $\boldsymbol{q}_i$ turns $\delta^{(3)}(\boldsymbol{q}_1+\boldsymbol{q}_2+\boldsymbol{q}_3)$ into $\delta^{(3)}(\boldsymbol{k}_1+\boldsymbol{k}_2+\boldsymbol{k}_3)$ in (12.33). Noticing that all possible contractions lead to the same result (this simply corresponds to a relabelling of the $\boldsymbol{q}_i$), there are 3! ways of pairing contracted fields. Thus, we obtain

$$\langle \varphi_{\boldsymbol{k}_1}(t)\varphi_{\boldsymbol{k}_2}(t)\varphi_{\boldsymbol{k}_3}(t)\rangle' \supset ig\,u^*_{k_1}(t)u^*_{k_2}(t)u^*_{k_3}(t)\int_{-\infty^-}^{t}\mathrm{d}t' a^3(t')u_{k_1}(t')u_{k_2}(t')u_{k_3}(t')\,, \tag{12.35}$$

where the prime denotes that we drop the overall momentum conserving delta function. Following the same manipulations for the second contribution in (12.21), it is

possible to recast the final expression for the correlator as

$$\langle\varphi_{\boldsymbol{k}_1}(t)\varphi_{\boldsymbol{k}_2}(t)\varphi_{\boldsymbol{k}_3}(t)\rangle' = 2g\,\mathrm{Im}\left[u^*_{k_1}(t)u^*_{k_2}(t)u^*_{k_3}(t)\int_{-\infty^-}^{t}\mathrm{d}t'a^3(t')u_{k_1}(t')u_{k_2}(t')u_{k_3}(t')\right], \tag{12.36}$$

where we recover Eq. (12.22). In order to do so, we have implicitly flipped the sign of momenta, which is a valid procedure if the theory preserves parity.[5] For a given function $a(t)$ and a mode function $u_k(t)$ found by solving the linear equation of motion, the time integral in Eq. (12.36) can be explicitly evaluated.

Exchange diagram. Let us now compute the equal-time four-point correlator of $\varphi_{\boldsymbol{k}}(t)$ coming from the exchange of a field σ. We take the interacting Lagrangian to be $\mathcal{L}_{\rm int}/a^3(t) = -\frac{g}{2}\varphi^2\sigma$, which results in a tree-level exchange diagram. Following the same steps as previously, the interacting Hamiltonian in Fourier space reads

$$H_{\rm int}(t) = \frac{g}{2}\,a^3(t)\int\left(\prod_{i=1}^{3}\frac{\mathrm{d}^3\boldsymbol{q}_i}{(2\pi)^3}\right)\varphi_{\boldsymbol{q}_1}(t)\varphi_{\boldsymbol{q}_2}(t)\sigma_{\boldsymbol{q}_3}(t)\,(2\pi)^3\delta^{(3)}(\boldsymbol{q}_1+\boldsymbol{q}_2+\boldsymbol{q}_3)\,. \tag{12.37}$$

Because the theory we consider preserves parity, and anticipating the result, we directly use Eq. (12.26) even though field operators in Fourier space are not Hermitian (we would anyway flip the sign of all momenta at some final stage). The full correlator is composed of two contributions, a factorised part (first line of (12.26)) and a nested part (second line of (12.26)), which we evaluate in turn. The factorised contribution explicitly reads

$$\begin{aligned}\langle\varphi_{\boldsymbol{k}_1}(t)\varphi_{\boldsymbol{k}_2}(t)\varphi_{\boldsymbol{k}_3}(t)\varphi_{\boldsymbol{k}_4}(t)\rangle \supset\ & \frac{g}{2}\int\left(\prod_{i=1}^{3}\frac{\mathrm{d}^3\boldsymbol{q}_i}{(2\pi)^3}\right)\times\frac{g}{2}\int\left(\prod_{i=1}^{3}\frac{\mathrm{d}^3\boldsymbol{p}_i}{(2\pi)^3}\right)\\ &\times(2\pi)^3\delta^{(3)}(\boldsymbol{q}_1+\boldsymbol{q}_2+\boldsymbol{q}_3)\,(2\pi)^3\delta^{(3)}(\boldsymbol{p}_1+\boldsymbol{p}_2+\boldsymbol{p}_3)\int_{-\infty^-}^{t}\mathrm{d}t'a^3(t')\int_{-\infty^-}^{t}\mathrm{d}t''a^3(t'')\\ &\times\langle 0|\varphi_{\boldsymbol{q}_1}(t')\varphi_{\boldsymbol{q}_2}(t')\sigma_{\boldsymbol{q}_3}(t')\varphi_{\boldsymbol{k}_1}(t)\varphi_{\boldsymbol{k}_2}(t)\varphi_{\boldsymbol{k}_3}(t)\varphi_{\boldsymbol{k}_4}(t)\varphi_{\boldsymbol{p}_1}(t'')\varphi_{\boldsymbol{p}_2}(t'')\sigma_{\boldsymbol{p}_3}(t'')|0\rangle\,,\end{aligned} \tag{12.38}$$

where we have highlighted in blue and red the contributions coming from the two insertions of $H_{\rm int}$. For simplicity, let us focus on the s-channel only in which the exchanged momentum is $\boldsymbol{s}\equiv\boldsymbol{k}_1+\boldsymbol{k}_2$. Using (12.30), an example of contractions contributing to this channel is

$$\begin{aligned}&\langle 0|\varphi_{\boldsymbol{q}_1}(t')\varphi_{\boldsymbol{q}_2}(t')\sigma_{\boldsymbol{q}_3}(t')\varphi_{\boldsymbol{k}_1}(t)\varphi_{\boldsymbol{k}_2}(t)\varphi_{\boldsymbol{k}_3}(t)\varphi_{\boldsymbol{k}_4}(t)\varphi_{\boldsymbol{p}_1}(t'')\varphi_{\boldsymbol{p}_2}(t'')\sigma_{\boldsymbol{p}_3}(t'')|0\rangle\\ &= v_{q_3}(t')v^*_{q_3}(t'')(2\pi)^3\delta^{(3)}(\boldsymbol{q}_3+\boldsymbol{p}_3)\\ &\times u_{k_1}(t')u^*_{k_1}(t)(2\pi)^3\delta^{(3)}(\boldsymbol{q}_1+\boldsymbol{k}_1)\,u_{k_2}(t')u^*_{k_2}(t)(2\pi)^3\delta^{(3)}(\boldsymbol{q}_2+\boldsymbol{k}_2)\\ &\times u_{k_3}(t)u^*_{k_3}(t'')(2\pi)^3\delta^{(3)}(\boldsymbol{k}_3+\boldsymbol{p}_1)\,u_{k_4}(t)u^*_{k_4}(t'')(2\pi)^3\delta^{(3)}(\boldsymbol{k}_4+\boldsymbol{p}_2)\,.\end{aligned} \tag{12.39}$$

There are 4 ways of doing such contractions keeping σ as the exchanged field. Performing the integrals over the $\boldsymbol{q}_i$ turns $(2\pi)^3\delta^{(3)}(\boldsymbol{q}_1+\boldsymbol{q}_2+\boldsymbol{q}_3)$ into $(2\pi)^3\delta^{(3)}(\boldsymbol{k}_1+\boldsymbol{k}_2+$

[5] It is nonetheless true for all (scalar) bispectra as in this case invariance under rotations implies parity.

$\boldsymbol{p}_3$), and the integrals over $\boldsymbol{p}_1$ and $\boldsymbol{p}_2$ turn $(2\pi)^3\delta^{(3)}(\boldsymbol{p}_1+\boldsymbol{p}_2+\boldsymbol{p}_3)$ into $(2\pi)^3\delta^{(3)}(\boldsymbol{k}_3+\boldsymbol{k}_4-\boldsymbol{p}_3)$. Eventually performing the integral over $\boldsymbol{p}_3$ gives the overall momentum conserving condition $(2\pi)^3\delta^{(3)}(\boldsymbol{k}_1+\boldsymbol{k}_2+\boldsymbol{k}_3+\boldsymbol{k}_4)$ with the exchanged mode carrying the momentum $s=|\boldsymbol{s}|=|\boldsymbol{k}_1+\boldsymbol{k}_2|$. For the factorised part, we obtain

$$\begin{aligned}\langle\varphi_{\boldsymbol{k}_1}(t)\varphi_{\boldsymbol{k}_2}(t)\varphi_{\boldsymbol{k}_3}(t)\varphi_{\boldsymbol{k}_4}(t)\rangle &\supset g^2u^*_{k_1}(t)u^*_{k_2}(t)u_{k_3}(t)u_{k_4}(t)\\ &\times\int_{-\infty^-}^{t}\mathrm{d}t'a^3(t')u_{k_1}(t')u_{k_2}(t')v_s(t')\times\int_{-\infty^+}^{t}\mathrm{d}t''a^3(t'')u^*_{k_3}(t'')u^*_{k_4}(t'')v^*_s(t'')\,.\end{aligned}\tag{12.40}$$

Notice that the two time integrals of this contribution factorise, hence the name. Following the same steps, the nested contribution is given by

$$\begin{aligned}\langle\varphi_{\boldsymbol{k}_1}(t)\varphi_{\boldsymbol{k}_2}(t)\varphi_{\boldsymbol{k}_3}(t)\varphi_{\boldsymbol{k}_4}(t)\rangle &\supset -2g^2\,\mathrm{Re}\Bigg[u_{k_1}(t)u_{k_2}(t)u_{k_3}(t)u_{k_4}(t)\\ &\times\int_{-\infty^+}^{t}\mathrm{d}t'a^3(t')u^*_{k_1}(t')u^*_{k_2}(t')v_s(t')\times\int_{-\infty^+}^{t'}\mathrm{d}t''a^3(t'')u^*_{k_3}(t'')u^*_{k_4}(t'')v^*_s(t'')\Bigg]\,.\end{aligned}\tag{12.41}$$

Loop diagram. The cubic interaction $\mathcal{L}_{\rm int}/a^3(t)=-\frac{g}{3!}\varphi^3$ that we have previously considered to compute the three-point contact diagram also induces a one-loop correction to the two-point correlator $\langle\varphi_{\boldsymbol{k}_1}(t)\varphi_{\boldsymbol{k}_2}(t)\rangle$. Let us illustrate how the usual integral over the momentum running in the loop appears in practice, focusing solely on the factorised part in Eq. (12.26) for simplicity. Grouping all pieces together, one gets

$$\begin{aligned}\langle\varphi_{\boldsymbol{k}_1}(t)\varphi_{\boldsymbol{k}_2}(t)\rangle &\supset \frac{g}{3!}\int\left(\prod_{i=1}^{3}\frac{\mathrm{d}^3\boldsymbol{q}_i}{(2\pi)^3}\right)\times\frac{g}{3!}\int\left(\prod_{i=1}^{3}\frac{\mathrm{d}^3\boldsymbol{p}_i}{(2\pi)^3}\right)\\ &\times(2\pi)^3\delta^{(3)}(\boldsymbol{q}_1+\boldsymbol{q}_2+\boldsymbol{q}_3)\,(2\pi)^3\delta^{(3)}(\boldsymbol{p}_1+\boldsymbol{p}_2+\boldsymbol{p}_3)\int_{-\infty^-}^{t}\mathrm{d}t'a^3(t')\int_{-\infty^-}^{t}\mathrm{d}t''a^3(t'')\\ &\times\langle0|\varphi_{\boldsymbol{q}_1}(t')\varphi_{\boldsymbol{q}_2}(t')\varphi_{\boldsymbol{q}_3}(t')\varphi_{\boldsymbol{k}_1}(t)\varphi_{\boldsymbol{k}_2}(t)\varphi_{\boldsymbol{p}_1}(t'')\varphi_{\boldsymbol{p}_2}(t'')\varphi_{\boldsymbol{p}_3}(t'')|0\rangle\,.\end{aligned}\tag{12.42}$$

We now want to contract fields such that it produces a connected diagram. The field $\varphi_{\boldsymbol{k}_1}$ can either be contracted with one of the $\varphi_{\boldsymbol{q}_i}$ or $\varphi_{\boldsymbol{p}_i}$. For this choice, we pick up a factor 2. Then, for each say $\varphi_{\boldsymbol{q}_i}$ there are 3 different options. The other external field $\varphi_{\boldsymbol{k}_2}$ therefore has also 3 options for the $\varphi_{\boldsymbol{p}_i}$. We are left with four internal legs that should be contracted among themselves in such a way that we only contract $\varphi_{\boldsymbol{q}_i}$ with $\varphi_{\boldsymbol{p}_i}$ (to make the diagram connected). There are 2 such ways. In total, this gives $2\times3\times3\times2=36$ possible contractions, which precisely cancel the factor $3!\times3!$. An example of such contractions is

$$\begin{aligned}&\langle0|\varphi_{\boldsymbol{q}_1}(t')\varphi_{\boldsymbol{q}_2}(t')\varphi_{\boldsymbol{q}_3}(t')\varphi_{\boldsymbol{k}_1}(t)\varphi_{\boldsymbol{k}_2}(t)\varphi_{\boldsymbol{p}_1}(t'')\varphi_{\boldsymbol{p}_2}(t'')\varphi_{\boldsymbol{p}_3}(t'')|0\rangle\\ &=u_{k_1}(t')u^*_{k_1}(t)(2\pi)^3\delta^{(3)}(\boldsymbol{q}_1+\boldsymbol{k}_1)\,u_{k_2}(t)u^*_{k_2}(t'')(2\pi)^3\delta^{(3)}(\boldsymbol{k}_2+\boldsymbol{p}_1)\\ &\times u_{q_2}(t')u^*_{q_2}(t'')(2\pi)^3\delta^{(3)}(\boldsymbol{q}_2+\boldsymbol{p}_2)\,u_{q_3}(t')u^*_{q_3}(t'')(2\pi)^3\delta^{(3)}(\boldsymbol{q}_3+\boldsymbol{p}_3)\,.\end{aligned}\tag{12.43}$$

Now comes the crucial step. Integrating over $\boldsymbol{q}_i$ sets $\boldsymbol{q}_1=-\boldsymbol{k}_1$, $\boldsymbol{q}_2=-\boldsymbol{p}_2$ and $\boldsymbol{q}_3=-\boldsymbol{p}_3$. Integrating over $\boldsymbol{p}_1$ and $\boldsymbol{p}_2$ sets $\boldsymbol{p}_1=-\boldsymbol{k}_2$ and $\boldsymbol{p}_2=\boldsymbol{k}_2-\boldsymbol{p}_3$ which

makes all delta functions collapse into a single momentum conservation condition $(2\pi)^3\delta^{(3)}(\boldsymbol{k}_1+\boldsymbol{k}_2)$ as it should. However, there is still one integral over the momentum $\boldsymbol{p}_3$ that we relabel $\boldsymbol{q}$. This is precisely the momentum running in the loop. Notice that performing all the previous momentum integrals sets $q_2 \to |\boldsymbol{k}_2 - \boldsymbol{q}|$ and $q_3 \to q$ for the corresponding internal mode functions. Eventually, the factorised part is found to be

$$\begin{aligned}&\langle\varphi_{\boldsymbol{k}_1}(t)\varphi_{\boldsymbol{k}_2}(t)\rangle' \supset g^2\, u^*_{k_1}(t)u_{k_2}(t)\\ &\times \int \frac{\mathrm{d}^3\boldsymbol{q}}{(2\pi)^3}\int_{-\infty^-}^{t}\mathrm{d}t' a^3(t')u_{k_1}(t')u_{|\boldsymbol{k}_2-\boldsymbol{q}|}(t')u_q(t') \times \int_{-\infty^+}^{t}\mathrm{d}t'' a^3(t'')u^*_{k_2}(t'')u^*_{|\boldsymbol{k}_2-\boldsymbol{q}|}(t'')u^*_q(t'')\,,\end{aligned} \tag{12.44}$$

where we have denoted in blue the loop integration over the momentum $\boldsymbol{q}$. The explicit form for the nested contribution can be derived in the same way.

Through these worked out examples, the readers can observe that employing the operator in-in formalism entails arduous manual contractions, which are tedious to set up in practice. However, in-in perturbation theory conceals a beautiful underlying structure: cosmological correlators satisfy simple and universal differential equations in time.

13

Following the Time Evolution

Cosmology is about understanding time. Indeed, the physics governing the Universe is deciphered through the *time evolution* of density perturbations, from their emergence from quantum zero-point fluctuations during inflation to the late-time galaxy distribution. Tracking down the cosmological flow of inflationary fluctuations thus connects the quantum laws of physics at a fundamental level to the largest observable scales.

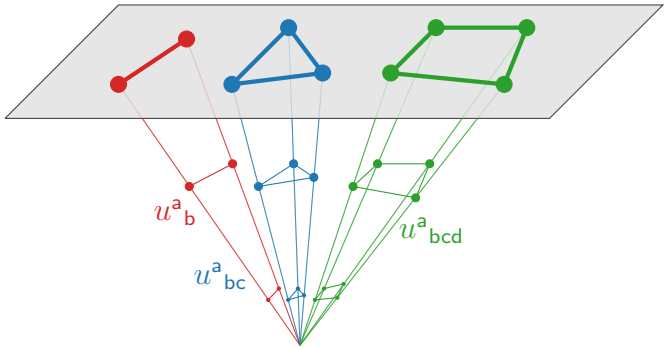


Figure 13.1: Schematic representation of the cosmological flow. The time evolution of cosmological correlators is tracked from initial quantum fluctuations in the infinite past to the end of inflation. The systematic resolution of their bulk time evolution is achieved by solving universal differential equations in time satisfied by the correlators. All the theory dependence is left in the precise form of the tensors $u^{a}{}_{b}, u^{a}{}_{bc}$ and $u^{a}{}_{bcd}$ driving this flow.

From first principles, cosmological correlators can be computed to arbitrary orders of perturbation theory, as discussed in Chap. 12. However, in practice, computations hide a daunting complexity: perturbation theory becomes intractable for realistic situations. The root of this difficulty resides in the challenge to track the

detailed time evolution of the physics in the bulk of spacetime. Yet, hidden within in-in perturbation theory is a *remarkable underlying structure*—one that is intrinsically shaped by time itself.

In this chapter, we present the cosmological flow, a systematic framework to compute cosmological correlators. This method is based on solving universal differential equations in time governing their time evolution throughout the entirety of spacetime during inflation, from their origin as quantum fluctuations in the deep past to the end of inflation. It takes into account all physical effects at tree-level without approximation. Systematically solving the cosmological flow does not require far-past UV regulators as correlators are evolved on the real-time axis, eliminates the need for mode functions, and bypasses the computation of intricate bulk time integrals.

13.1 Equal-Time Correlators

Our focus is be to derive differential equations in time satisfied by cosmological correlators, starting from the in-in formalism. We start by setting up relevant notations and definitions. We consider a generic theory of N degrees of freedom $\boldsymbol{\varphi}^\alpha$ (with Greek letters running from 1 to N) and remain voluntarily agnostic throughout this section on the precise form of the theory. It may contain arbitrary interactions and time-dependent coupling constants. The theory is described by a Hamiltonian $H(\boldsymbol{\varphi}^\alpha, \boldsymbol{p}^\beta)$ which is a functional of the phase-space coordinates i.e. the field-space coordinates $\boldsymbol{\varphi}^\alpha$ and their conjugate momenta $\boldsymbol{p}^\beta$. We introduce the interaction-picture operators φ^α and p^β defined in terms of the Heisenberg-picture operators $\boldsymbol{\varphi}^\alpha$ and $\boldsymbol{p}^\beta$ by $\varphi^\alpha \equiv U^\dagger \boldsymbol{\varphi}^\alpha U$ and $p^\alpha \equiv U^\dagger \boldsymbol{p}^\alpha U$.[1] For practical purposes, we gather all fields $\boldsymbol{\varphi}^\alpha$ and conjugate momenta $\boldsymbol{p}^\beta$ in a phase-space vector $\boldsymbol{X}^a \equiv (\boldsymbol{\varphi}^\alpha, \boldsymbol{p}^\beta)$, and we do the same for the interaction-picture operators $X^a \equiv (\varphi^\alpha, p^\beta)$. The Latin index a runs over all phase-space coordinates from 1 to $2N$. We will also assume that such indices are organised so that a block of field labels is followed by a block of momentum labels, in the same order. Interacting-picture operators evolve with the free Hamiltonian (12.4).

13.1.1 Equations of Motion

We now specify a certain form for the Hamiltonian. Since we are going to essentially work in Fourier space, we will adopt the extended Fourier summation convention that consists in using sans serif indices to denote a sum including integrals over Fourier modes, making the following expressions compact and manageable. Hence, in what follows, an index contraction reads

$$A_{\mathsf{a}} B^{\mathsf{a}} = \sum_a \int \frac{\mathrm{d}^3 k_a}{(2\pi)^3} A_a(\boldsymbol{k}_a) B^a(\boldsymbol{k}_a) \,. \tag{13.1}$$

[1] Compared to the previous chapter, we have removed hats on operators, and now use bold variables to denote Heisenberg-picture operators. We also have removed the subscript I for interaction-picture operators to avoid clutter.

We give more details in App. D. Using this notation, we take the Hamiltonian to be

$$H = \frac{1}{2!}H_{\mathsf{ab}}\boldsymbol{X}^{\mathsf{a}}\boldsymbol{X}^{\mathsf{b}} + \frac{1}{3!}H_{\mathsf{abc}}\boldsymbol{X}^{\mathsf{a}}\boldsymbol{X}^{\mathsf{b}}\boldsymbol{X}^{\mathsf{c}} + \frac{1}{4!}H_{\mathsf{abcd}}\boldsymbol{X}^{\mathsf{a}}\boldsymbol{X}^{\mathsf{b}}\boldsymbol{X}^{\mathsf{c}}\boldsymbol{X}^{\mathsf{d}} + \dots \,. \tag{13.2}$$

Without loss of generality, we take $H_{\mathsf{ab}}, H_{\mathsf{abc}}, \dots$ to be symmetric under the exchange of any indices.[2] These tensors encode the various interactions in the theory, and conventionally encompass functions of time and of the various momenta for derivative interactions. It is worth emphasising that this form of the Hamiltonian is completely general and captures *all* known theories of inflationary fluctuations.[3] The fully non-linear equations of motion then read

$$\begin{aligned}\frac{\mathrm{d}\boldsymbol{X}^{\mathsf{a}}}{\mathrm{d}t} &= i\left[H, \boldsymbol{X}^{\mathsf{a}}\right] \\ &= \epsilon^{\mathsf{ac}}H_{\mathsf{cb}}\boldsymbol{X}^{\mathsf{b}} + \frac{1}{2!}\epsilon^{\mathsf{ad}}H_{\mathsf{dbc}}\boldsymbol{X}^{\mathsf{b}}\boldsymbol{X}^{\mathsf{c}} + \frac{1}{3!}\epsilon^{\mathsf{ae}}H_{\mathsf{ebcd}}\boldsymbol{X}^{\mathsf{b}}\boldsymbol{X}^{\mathsf{c}}\boldsymbol{X}^{\mathsf{d}} + \dots \\ &= u^{\mathsf{a}}{}_{\mathsf{b}}\boldsymbol{X}^{\mathsf{b}} + \frac{1}{2!}u^{\mathsf{a}}{}_{\mathsf{bc}}\boldsymbol{X}^{\mathsf{b}}\boldsymbol{X}^{\mathsf{c}} + \frac{1}{3!}u^{\mathsf{a}}{}_{\mathsf{bcd}}\boldsymbol{X}^{\mathsf{b}}\boldsymbol{X}^{\mathsf{c}}\boldsymbol{X}^{\mathsf{d}} + \dots \,,\end{aligned} \tag{13.3}$$

where in the second line we have introduced the tensor ϵ^{ab} that is defined so that the commutation relation is written in the following compact form

$$\left[\boldsymbol{X}^{\mathsf{a}}, \boldsymbol{X}^{\mathsf{b}}\right] = i\epsilon^{\mathsf{ab}}\,, \tag{13.4}$$

where $\epsilon^{\mathsf{ab}} \equiv (2\pi)^3\delta^{(3)}(\boldsymbol{k}_a + \boldsymbol{k}_b)\,\epsilon^{ab}$ and the $2N \times 2N$ matrix can be written in block form

$$\epsilon^{ab} = \begin{pmatrix} \mathbf{0} & \mathbf{1} \\ -\mathbf{1} & \mathbf{0} \end{pmatrix}. \tag{13.5}$$

The third line of (13.3) should be seen as a definition for the tensors $u^{\mathsf{a}}{}_{\mathsf{b}}, u^{\mathsf{a}}{}_{\mathsf{bc}}, u^{\mathsf{a}}{}_{\mathsf{bcd}}, \dots$. We also have used the fact that the Hamiltonian has been taken to be fully symmetric[4] and ϵ^{ab} is antisymmetric. Written in this form, it is clear that the equations of motion (13.3) encode both the full evolution of $\boldsymbol{X}^{\mathsf{a}}$ *and* the commutation relations. In practice though, they are hard—if not impossible—to solve. One must therefore choose a simpler "free" Hamiltonian H_0 to evolve the interaction-picture operators, thus resorting to a perturbative description of the interactions.

[2] In a quantum theory, operator ordering of the Hamiltonian a priori matters. Canonical quantisation consisting in promoting the phase-space variables of the classical Hamiltonian to quantum operators is ambiguous, as an infinite number of quantum theories that reduce to the classical one in the limit $\hbar \to 0$ may be defined. In the context of QFT though, ambiguities in the operator ordering eventually show up as different types of UV divergences to be renormalised. Since we will not perform renormalisation explicitly—which amounts to assume we directly work with the renormalised theory—we will overlook the operator ordering ambiguity here. We can therefore safely and without loss of generality symmetrise the classical Hamiltonian and then promote the fields and momenta to quantum operators. We wish to especially thank David Mulryne and David Seery for helpful discussions on this matter.

[3] Higher-order time derivative interactions can lead to equations of motion with more than two time derivatives. As this situation signals the presence of an additional dynamical degree of freedom in the theory, one can introduce it in Eq. (13.2) so that the Hamiltonian always leads to equations of motion with no more than two time derivatives.

[4] Note that this implies that the tensors $u^{\mathsf{a}}{}_{\mathsf{bc}}, u^{\mathsf{a}}{}_{\mathsf{bcd}}, \dots$ are symmetric under the exchange of any lower indices.

13.1.2 Tree-Level Cosmological Correlators

We choose the free Hamiltonian to be the *full quadratic Hamiltonian*, $H_0 = \frac{1}{2!} H_{\mathsf{ab}} \boldsymbol{X}^{\mathsf{a}} \boldsymbol{X}^{\mathsf{b}}$, with the interacting part of the Hamiltonian being given by the cubic and higher orders. Doing so, the equations of motion verified by the interaction-picture fields and momenta are linear. Still, all quadratic mixings between the various fields and momenta are taken into account in a non-perturbative manner, as we will show more clearly later. With this splitting choice, the equations of motion for the interaction-picture operators read

$$\frac{\mathrm{d}X^{\mathsf{a}}}{\mathrm{d}t} = u^{\mathsf{a}}{}_{\mathsf{b}} X^{\mathsf{b}} \,, \tag{13.6}$$

which makes it explicit that X^{a} evolves with the full quadratic Hamiltonian. By now, we have derived all the necessary fundamental elements to write all possible n-point correlation functions. Up to three-point correlators and working at tree-level yields (see Chap. 12)

$$\begin{aligned} \langle\Omega|\, \boldsymbol{X}^{\mathsf{a}} \boldsymbol{X}^{\mathsf{b}} \,|\Omega\rangle &= \langle 0|\, X^{\mathsf{a}} X^{\mathsf{b}} \,|0\rangle \,, \\ \langle\Omega|\, \boldsymbol{X}^{\mathsf{a}} \boldsymbol{X}^{\mathsf{b}} \boldsymbol{X}^{\mathsf{c}} \,|\Omega\rangle &= \langle 0|\, \frac{i}{3!} \int_{-\infty}^{t} \mathrm{d}t' H_{\mathsf{def}} \left[X^{\mathsf{d}} X^{\mathsf{e}} X^{\mathsf{f}}, X^{\mathsf{a}} X^{\mathsf{b}} X^{\mathsf{c}} \right] |0\rangle \,. \end{aligned} \tag{13.7}$$

From now on, we will not write $|\Omega\rangle$ nor $|0\rangle$ to make the notations less cluttered, assuming it is clear from the context whether the operators are in the Heisenberg ($\boldsymbol{X}^{\mathsf{a}}$) or interaction picture (X^{a}). We retain the commutator form of the correlators because it will be more convenient in the following development. Note that no mention of mode functions is needed in this language.

13.2 Two- & Three-point Correlators

We now have all the necessary ingredients to derive the cosmological flow.

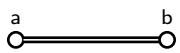
13.2.1 Two-Point Correlators

We start by deriving the flow equations for the two-point functions $\langle \boldsymbol{X}^{\mathsf{a}} \boldsymbol{X}^{\mathsf{b}} \rangle$. This object is the equal-time tree-level two-point correlator, taking into account the full quadratic Hamiltonian. In what follows, it will be more convenient to adopt a diagrammatic representation of such objects. We use a white dot to denote an external field insertion at the time t



$$= \boldsymbol{X}^{\mathsf{a}}(t) \,, \tag{13.8}$$

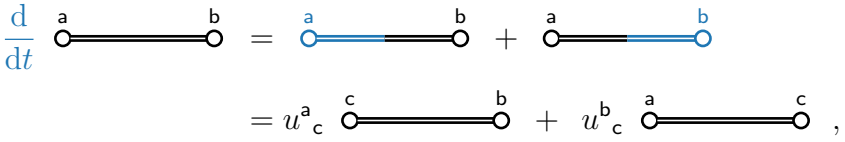
and a black dot to denote a single vertex insertion in the bulk at a time $t' < t$ which needs to be integrated over. The two-point correlator can be represented as

$\langle \boldsymbol{X}^{\mathsf{a}} \boldsymbol{X}^{\mathsf{b}} \rangle =$ 

. (13.9)

We will discuss various choices of interaction schemes and the resummation of quadratic mixings in 13.2.3, which will make the double-line notation clear. Since

the states are time independent, one can formally differentiate (13.9) with respect to time by acting on the interaction-picture operators X^{a} inside the correlator in (13.7). We then use the equation of motion (13.6) to find the following closed system



(13.10)

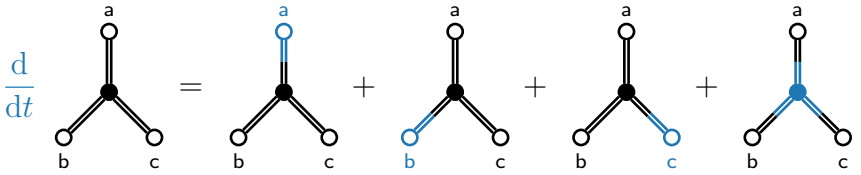
where we have colored in blue the parts of the correlator that have been differentiated with respect to time. Note that the introduced diagrammatic representation follows the usual Leibniz product rule of differentiation. The sum over repeated indices makes it explicit that—as usual in quantum physics—we sum over all possible diagrams. The flow equations for the two-point correlators are then

$$\frac{\mathrm{d}}{\mathrm{d}t}\langle \boldsymbol{X}^{\mathsf{a}}\boldsymbol{X}^{\mathsf{b}}\rangle = u^{\mathsf{a}}{}_{\mathsf{c}}\langle \boldsymbol{X}^{\mathsf{c}}\boldsymbol{X}^{\mathsf{b}}\rangle + u^{\mathsf{b}}{}_{\mathsf{c}}\langle \boldsymbol{X}^{\mathsf{a}}\boldsymbol{X}^{\mathsf{c}}\rangle\,. \tag{13.11}$$

Of course, these equations are completely equivalent—in the sense that they encode the same physics—to the linear equations of motion supplemented by the quantisation condition. Consequently, they correctly capture all physical effects arising from quadratic operators in the theory. Note also that (13.11) couples all two-point correlators through the tensor $u^{\mathsf{a}}{}_{\mathsf{b}}$, including mixed propagators and correlators which contain conjugate momenta.

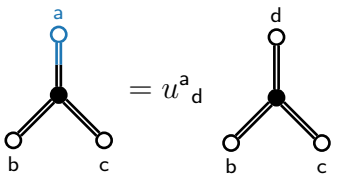
13.2.2 Three-Point Correlators

Let us now derive the flow equations for the three-point correlators. From (13.7), we see that such correlators carry two time dependencies: (i) the external operators, and (ii) the upper limit of the integral over a bulk vertex, in the following denoted by a black dot. Diagrammatically, differentiating the three-point correlators with respect to time is then represented by



(13.12)

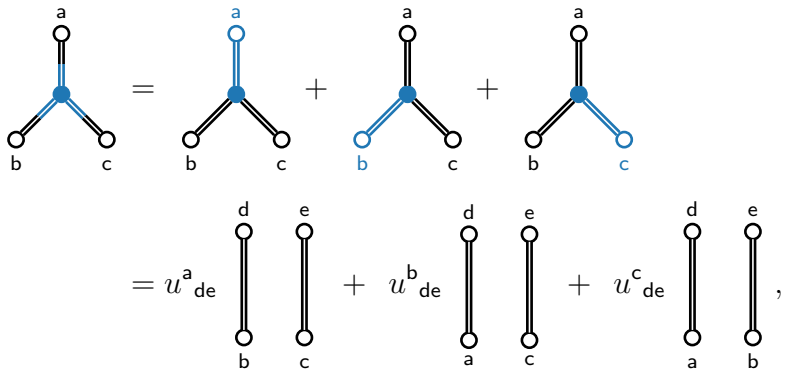
Similar to the case of two-point correlators in the previous section, using the equation of motion (13.6), differentiating an external operator leads to



(13.13)

The other term—coming from deriving the cubic bulk vertex—requires a few manipulations. We give a formal derivation of this contribution in the insert below.

In terms of diagrams, one needs to differentiate all combinations of a bulk vertex together with an external operator insertion, resulting in cutting the diagram in two-point correlators. The resulting two-point correlators should then be contracted with a $u^{\mathsf{a}}{}_{\mathsf{bc}}$ tensor. This leads to



(13.14)

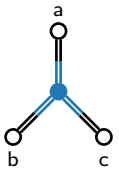
which should be regarded as the diagrammatic rule corresponding to differentiating a cubic bulk vertex. Collecting the various terms, the flow equations for the three-point correlators are

$$\frac{\mathrm{d}}{\mathrm{d}t}\langle \boldsymbol{X}^{\mathsf{a}}\boldsymbol{X}^{\mathsf{b}}\boldsymbol{X}^{\mathsf{c}}\rangle = u^{\mathsf{a}}{}_{\mathsf{d}}\langle \boldsymbol{X}^{\mathsf{d}}\boldsymbol{X}^{\mathsf{b}}\boldsymbol{X}^{\mathsf{c}}\rangle + u^{\mathsf{a}}{}_{\mathsf{de}}\langle \boldsymbol{X}^{\mathsf{b}}\boldsymbol{X}^{\mathsf{d}}\rangle\langle \boldsymbol{X}^{\mathsf{c}}\boldsymbol{X}^{\mathsf{e}}\rangle + (2 \text{ perms})\,. \tag{13.15}$$

Similar to Eq. (13.11), these equations couple all correlators, including mixed correlators and those involving conjugate momenta. A few comments are in order.

Cosmological flow. These equations are quantum in nature, as they evolve correlators in time including the effects of quantum interactions. Therefore, they provide an alternative way of computing correlators, following the "cosmological flow": instead of directly computing the in-in integrals, the correlators are transported from a finite time in the past to any time of interest on the *real time axis*. Importantly, the use of the $i\epsilon$ prescription is transferred to the derivation of initial conditions (we will of course come back to this point).

Cubic bulk vertex.—From (13.7), the term coming from differentiating the cubic bulk vertex formally reads



$$= \frac{i}{3!}\langle H_{\mathsf{def}}\left[X^{\mathsf{d}}X^{\mathsf{e}}X^{\mathsf{f}}, X^{\mathsf{a}}X^{\mathsf{b}}X^{\mathsf{c}}\right]\rangle\,. \tag{13.16}$$

Rearranging the commutator, introducing the commutation relation, and using the definition of the $u^{\mathsf{a}}{}_{\mathsf{bc}}$ tensor, this term can be rewritten

$$\frac{i}{3!}\langle H_{\mathsf{def}}\left[X^{\mathsf{d}}X^{\mathsf{e}}X^{\mathsf{f}}, X^{\mathsf{a}}X^{\mathsf{b}}X^{\mathsf{c}}\right]\rangle = \frac{1}{2!}u^{\mathsf{a}}{}_{\mathsf{de}}\langle X^{\mathsf{b}}X^{\mathsf{c}}X^{\mathsf{d}}X^{\mathsf{e}}\rangle + (2 \text{ perms})\,. \tag{13.17}$$

The right-hand side involves products of interaction-picture operators obeying Gaussian statistics. Consequently, one can use Wick's theorem to contract the various operators. Retaining only connected three-point functions, one obtains

$$\frac{i}{3!}\langle H_{\mathsf{def}}\left[X^{\mathsf{d}}X^{\mathsf{e}}X^{\mathsf{f}}, X^{\mathsf{a}}X^{\mathsf{b}}X^{\mathsf{c}}\right]\rangle = u^{\mathsf{a}}{}_{\mathsf{de}}\langle \boldsymbol{X}^{\mathsf{b}}\boldsymbol{X}^{\mathsf{d}}\rangle\langle \boldsymbol{X}^{\mathsf{c}}\boldsymbol{X}^{\mathsf{e}}\rangle + (2 \text{ perms})\,, \tag{13.18}$$

which, in the end, is given by the diagrammatic representation in (13.14).

Linearity. These equations are linear. This specific structure allows the flow of each kinematic configuration to be tracked independently. However, the source terms of these equations are non-linear, in the sense that the three-point correlators are sourced by a product of two two-point correlators. As a result, Eq. (13.15) does not form a closed system and one needs to solve for both the two- and three-point correlators. Intuitively, solving the two-point correlators is equivalent to solving the mode functions that are needed to compute higher-point correlators. The non-linear structure of the source is directly related to the fact that fields are quantum operators. Indeed, going from a three-point correlator—that is composed of six interaction-picture operators—to a product of two-point correlators—each composed of two operators—, we have used the commutation relation to reduce the number of operator insertions. We also remind the reader that working at tree-level means that non-linearities of the three-point correlators on the two-point correlators are neglected.

13.2.3 Resumming Quadratic Mixings

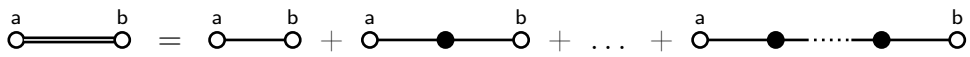
The flow equations previously derived encode an exact treatment of possible quadratic interactions appearing in $H_{\mathsf{ab}}\boldsymbol{X}^{\mathsf{a}}\boldsymbol{X}^{\mathsf{b}}$. We argue here that this is equivalent to dressing the two-point correlators with an infinite number of quadratic mixing insertions, when using an interaction scheme where quadratic mixings are treated perturbatively. Instead of choosing the "free" Hamiltonian to be the full quadratic one, a commonly used choice of interaction scheme is to split the quadratic Hamiltonian into two contributions

$$\frac{1}{2!}H_{\mathsf{ab}}\boldsymbol{X}^{\mathsf{a}}\boldsymbol{X}^{\mathsf{b}} = \frac{1}{2!}H^{\mathrm{diag}}_{\mathsf{ab}}\boldsymbol{X}^{\mathsf{a}}\boldsymbol{X}^{\mathsf{b}} + \frac{1}{2!}H^{\mathrm{mix}}_{\mathsf{ab}}\boldsymbol{X}^{\mathsf{a}}\boldsymbol{X}^{\mathsf{b}}\,, \tag{13.19}$$

with $H^{\mathrm{diag}}_{\mathsf{ab}}$ being diagonal. One can then define new interaction-picture operators $\bar{X}^{\mathsf{a}}$ that evolve with $H^{\mathrm{diag}}_{\mathsf{ab}}$ and derive approximate analytical forms for them. Assuming that quadratic mixings can be treated perturbatively, one can derive analytical expressions for correlators in this regime. The *fully dressed* two-point correlator can be formally written as an infinite sum of nested integrals

$$\begin{aligned}\langle \boldsymbol{X}^{\mathsf{a}}\boldsymbol{X}^{\mathsf{b}}\rangle = \sum_{n=0}^{\infty}\frac{i^n}{(2!)^n}\int_{-\infty}^{t}\mathrm{d}t'\int_{-\infty}^{t'}\mathrm{d}t''\ldots\int_{-\infty}^{t^{(n-1)}}\mathrm{d}t^{(n)} \\ \left\langle\left[H^{\mathrm{mix}}_{\mathsf{cd}}\bar{X}^{\mathsf{c}}\bar{X}^{\mathsf{d}}, \left[H^{\mathrm{mix}}_{\mathsf{ef}}\bar{X}^{\mathsf{e}}\bar{X}^{\mathsf{f}}, \ldots, \left[H^{\mathrm{mix}}_{\mathsf{gh}}\bar{X}^{\mathsf{g}}\bar{X}^{\mathsf{h}}, \bar{X}^{\mathsf{a}}\bar{X}^{\mathsf{b}}\right]\ldots\right]\right]\right\rangle\,,\end{aligned} \tag{13.20}$$

which diagrammatically reads



(13.21)

where black dots denote insertions of quadratic mixings and single lines stand for propagators of the fields $\bar{X}^{\mathsf{a}}$ in this interaction picture. In contrast, the formalism developed above intrinsically contains such resummation. We have converted the problem of computing complicated nested integrals to solving a set of coupled ordinary differential equations.

13.3 Higher-Order Correlators

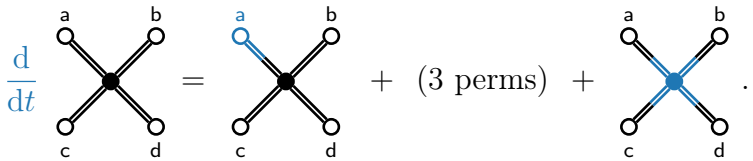
We now turn to higher-order correlators. We will see that the diagrammatic rules we introduced enable us to easily find the flow equations for any tree-level n-point correlator.

13.3.1 Four-Point Correlators

We first illustrate the machinery with four-point correlators. In what follows, we will only consider the connected parts of higher-point correlators, hence defining them by subtracting the disconnected contribution. In full generality, a four-point correlator can be contact-like—with quartic interactions encoded in H_{abcd}—or exchange-like—with two cubic interactions from H_{abc}. Both contributions are formally written

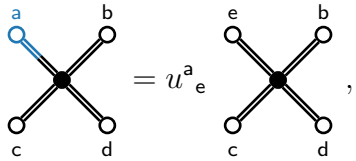
$$\langle \boldsymbol{X}^{\mathsf{a}}\boldsymbol{X}^{\mathsf{b}}\boldsymbol{X}^{\mathsf{c}}\boldsymbol{X}^{\mathsf{d}}\rangle = \frac{i}{4!}\langle\int_{-\infty}^{t}\mathrm{d}t' H_{\mathsf{efgh}}(t')\left[X^{\mathsf{e}}X^{\mathsf{f}}X^{\mathsf{g}}X^{\mathsf{h}}(t'), X^{\mathsf{a}}X^{\mathsf{b}}X^{\mathsf{c}}X^{\mathsf{d}}\right]\rangle \tag{13.22}$$
$$-\frac{1}{(3!)^2}\langle\int_{-\infty}^{t}\int_{-\infty}^{t'}\mathrm{d}t'\mathrm{d}t'' H_{\mathsf{efg}}(t'')H_{\mathsf{hij}}(t')\left[X^{\mathsf{e}}X^{\mathsf{f}}X^{\mathsf{g}}(t''),\left[X^{\mathsf{h}}X^{\mathsf{i}}X^{\mathsf{j}}(t'), X^{\mathsf{a}}X^{\mathsf{b}}X^{\mathsf{c}}X^{\mathsf{d}}\right]\right]\rangle\,.$$

We first treat the case of contact-like four-point correlators. As for the three-point correlators, such correlators carry a time dependence in external operator insertions, and in the upper limit of the integral over the bulk vertex. Following the Leibniz product rule of differentiation, the diagrammatic representation of differentiating a contact-like four-point correlator is



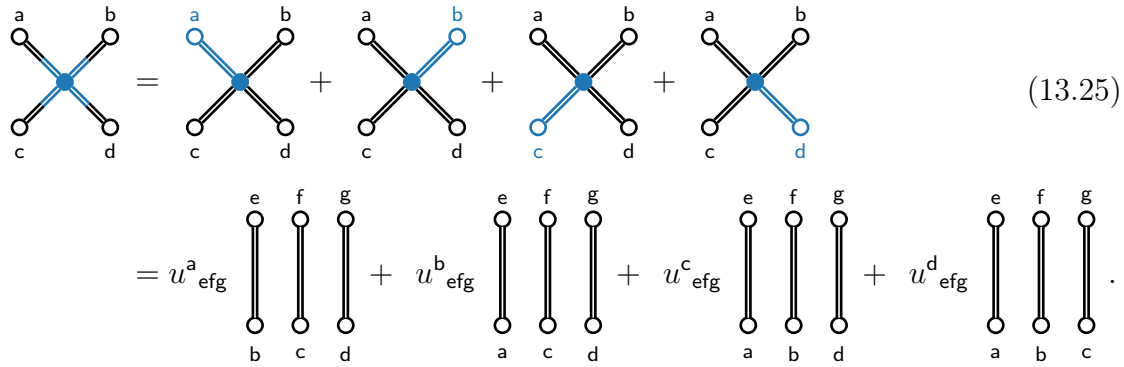
(13.23)

As usual, differentiating an external operator makes use of the equations of motions (13.6)



(13.24)

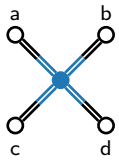
and differentiating the bulk vertex, as previously done for the three-point correlators, results in cutting the diagram in two-point correlators contracted with the tensor $u^{\mathsf{a}}{}_{\mathsf{bcd}}$



(13.25)

We give a formal derivation of this diagrammatic rule in the following insert.

Quartic bulk vertex.—From (13.22), the term coming from differentiating the quartic bulk vertex formally reads



$$= \frac{i}{4!}\langle H_{\mathsf{efgh}}\left[X^{\mathsf{e}}X^{\mathsf{f}}X^{\mathsf{g}}X^{\mathsf{h}}, X^{\mathsf{a}}X^{\mathsf{b}}X^{\mathsf{c}}X^{\mathsf{d}}\right]\rangle\,. \tag{13.26}$$

After a tedious rearrangement of the commutator, we use the commutation relation $[X^{\mathsf{a}}, X^{\mathsf{b}}] = i\epsilon^{\mathsf{ab}}$. This enables us to introduce the $u^{\mathsf{a}}{}_{\mathsf{bcd}}$ tensor. These manipulations lead to

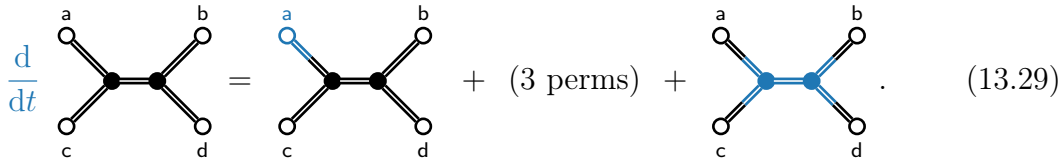
$$\frac{i}{4!}\langle H_{\mathsf{efgh}}\left[X^{\mathsf{e}}X^{\mathsf{f}}X^{\mathsf{g}}X^{\mathsf{h}}, X^{\mathsf{a}}X^{\mathsf{b}}X^{\mathsf{c}}X^{\mathsf{d}}\right]\rangle = \frac{1}{3!}u^{\mathsf{a}}{}_{\mathsf{efg}}\langle X^{\mathsf{b}}X^{\mathsf{c}}X^{\mathsf{d}}X^{\mathsf{e}}X^{\mathsf{f}}X^{\mathsf{g}}\rangle + (3\text{ perms})\,. \tag{13.27}$$

Only retaining connected four-point functions (there are 3! ways to contract the fields) gives

$$\frac{i}{4!}\langle H_{\mathsf{efgh}}\left[X^{\mathsf{e}}X^{\mathsf{f}}X^{\mathsf{g}}X^{\mathsf{h}}, X^{\mathsf{a}}X^{\mathsf{b}}X^{\mathsf{c}}X^{\mathsf{d}}\right]\rangle = u^{\mathsf{a}}{}_{\mathsf{efg}}\langle \boldsymbol{X}^{\mathsf{b}}\boldsymbol{X}^{\mathsf{e}}\rangle\langle \boldsymbol{X}^{\mathsf{c}}\boldsymbol{X}^{\mathsf{f}}\rangle\langle \boldsymbol{X}^{\mathsf{d}}\boldsymbol{X}^{\mathsf{g}}\rangle + (3\text{ perms})\,, \tag{13.28}$$

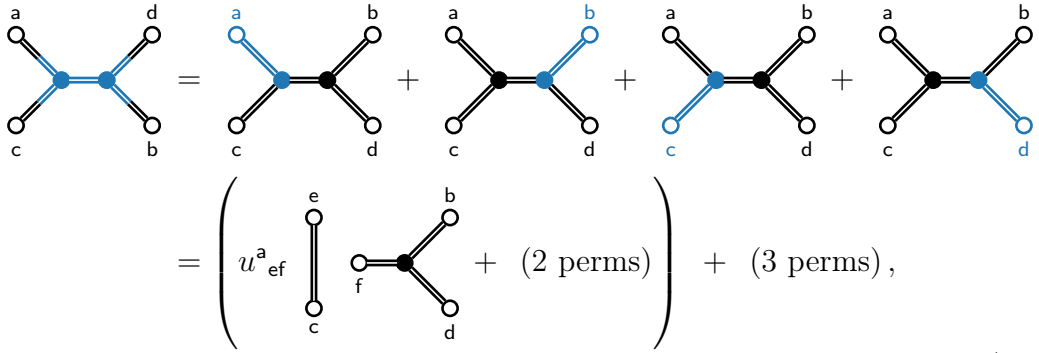
which, in the end, is given by the diagrammatic representation in (13.25).

The case of exchange-like four-point correlators follows the same line. The diagrammatic representation of differentiating an exchange-like four point correlator is



(13.29)

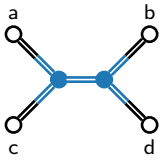
Differentiating with respect to external operator insertions introduces the usual $u^{\mathsf{a}}{}_{\mathsf{b}}$ tensor. Differentiating the bulk vertices is given by contracting a three-point correlator with a two-point correlator using the tensor $u^{\mathsf{a}}{}_{\mathsf{bc}}$ in the following way



(13.30)

where the 2 permutations are the number of ways to choose a pair of indices where one is summed over and the other is not summed over (exchanging the two dummy indices is already taken into account in the counting), and the 3 permutations are the usual cyclic permutations ($\mathsf{a} \to \mathsf{b} \to \mathsf{c} \to \mathsf{d}$). The second line then contains 12 terms. This diagrammatic rule is proven in the following insert.

Cubic exchange vertex.—From (13.22), the term coming from deriving the cubic exchange vertex reads



$$= -\frac{1}{(3!)^2}\langle \int_{-\infty}^{t} \mathrm{d}t' H_{\mathsf{efg}}(t') H_{\mathsf{hij}} \Big[X^{\mathsf{e}} X^{\mathsf{f}} X^{\mathsf{g}}(t'), \Big[X^{\mathsf{h}} X^{\mathsf{i}} X^{\mathsf{j}}, X^{\mathsf{a}} X^{\mathsf{b}} X^{\mathsf{c}} X^{\mathsf{d}} \Big] \Big] \rangle \,. \tag{13.31}$$

We first start by examining the inner commutator where the operators X^{a} are evaluated at t. After rearranging it and introducing the tensor $u^{\mathsf{a}}{}_{\mathsf{bc}}$, we find

$$-\frac{1}{3!} H_{\mathsf{hij}} \Big[X^{\mathsf{h}} X^{\mathsf{i}} X^{\mathsf{j}}, X^{\mathsf{a}} X^{\mathsf{b}} X^{\mathsf{c}} X^{\mathsf{d}} \Big] = \frac{i}{2!} u^{\mathsf{a}}{}_{\mathsf{hi}} X^{\mathsf{h}} X^{\mathsf{i}} X^{\mathsf{b}} X^{\mathsf{c}} X^{\mathsf{d}} + (3 \text{ perms}) \,. \tag{13.32}$$

Inside the expectation value, we now Wick contract a pair of external operators where one is the operator whose index is summed over. Among the six such possibilities, half of them lead to the same contribution after relabelling the indices. This cancels the factor 2!. In the end, after identifying the three-point correlators, we end up with

$$-\frac{1}{(3!)^2}\langle \int_{-\infty}^{t} \mathrm{d}t' H_{\mathsf{efg}}(t') H_{\mathsf{hij}} \Big[X^{\mathsf{e}} X^{\mathsf{f}} X^{\mathsf{g}}(t'), \Big[X^{\mathsf{h}} X^{\mathsf{i}} X^{\mathsf{j}}, X^{\mathsf{a}} X^{\mathsf{b}} X^{\mathsf{c}} X^{\mathsf{d}} \Big] \Big] \rangle = u^{\mathsf{a}}{}_{\mathsf{ef}} \langle \boldsymbol{X}^{\mathsf{c}} \boldsymbol{X}^{\mathsf{e}} \rangle \langle \boldsymbol{X}^{\mathsf{b}} \boldsymbol{X}^{\mathsf{d}} \boldsymbol{X}^{\mathsf{f}} \rangle + (2 \text{ perms}) + (3 \text{ perms}) \,, \tag{13.33}$$

where the 2 permutations account for choosing a pair among $(\mathsf{e}, \mathsf{b}, \mathsf{c}, \mathsf{d})$ with one index being e, and the 3 permutations are the usual cyclic permutations ($\mathsf{a} \to \mathsf{b} \to \mathsf{c} \to \mathsf{d}$).

Collecting the various terms in Eqs. (13.23, 13.25, 13.29, 13.30), the flow equations

for the connected four-point correlator are

$$\frac{\mathrm{d}}{\mathrm{d}t}\langle \boldsymbol{X}^{\mathsf{a}}\boldsymbol{X}^{\mathsf{b}}\boldsymbol{X}^{\mathsf{c}}\boldsymbol{X}^{\mathsf{d}}\rangle = u^{\mathsf{a}}{}_{\mathsf{e}}\langle \boldsymbol{X}^{\mathsf{e}}\boldsymbol{X}^{\mathsf{b}}\boldsymbol{X}^{\mathsf{c}}\boldsymbol{X}^{\mathsf{d}}\rangle + u^{\mathsf{a}}{}_{\mathsf{efg}}\langle \boldsymbol{X}^{\mathsf{b}}\boldsymbol{X}^{\mathsf{e}}\rangle\langle \boldsymbol{X}^{\mathsf{c}}\boldsymbol{X}^{\mathsf{f}}\rangle\langle \boldsymbol{X}^{\mathsf{d}}\boldsymbol{X}^{\mathsf{g}}\rangle + (3 \text{ perms}) + u^{\mathsf{a}}{}_{\mathsf{ef}}\langle \boldsymbol{X}^{\mathsf{b}}\boldsymbol{X}^{\mathsf{e}}\rangle\langle \boldsymbol{X}^{\mathsf{c}}\boldsymbol{X}^{\mathsf{d}}\boldsymbol{X}^{\mathsf{f}}\rangle + (11 \text{ perms})\,. \tag{13.34}$$

It is interesting to note that contact-like four-point diagrams are only sourced by products of two-point functions. Removing the last term on the right-hand side—that come from deriving the bulk vertices of an exchange-like diagram—, the above equations form a closed system along with the flow equations for the two-point correlators only. Contrariwise, exchange-like four-point diagrams are sourced by three-point correlators, reflecting their intrinsic complexity. One would then need to solve all flow equations for the two-, three-, and four-point correlators, which still form a closed triangular system.

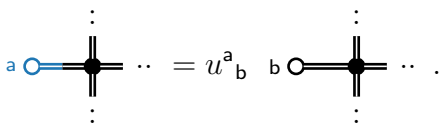
13.3.2 Diagrammatic Rules for n-Point Correlators

Having treated the simplest exchange-like diagram appearing in four-point correlators, we now state—without formal proof—general diagrammatic rules to derive the flow equations for any tree-level n-point correlators. These rules are the following:

- Draw a tree-level graph assigning an operator $\boldsymbol{X}^{\mathsf{a}}(t)$ to each of the n external field, denoted with a white dot. Bulk vertices, denoted with black dots, should be at least of cubic order because quadratic interactions are fully resummed. Hence, the external operators are connected to bulk vertices with doubled lines. Time dependence appears in external operators and in the upper limit of the integral over bulk vertices, considered as a whole.

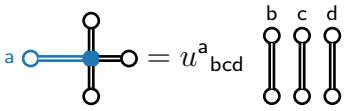
- Following the Leibniz product rule of differentiation, taking the time derivative of the drawn diagram equals the sum of initial-like diagrams where time dependence has been isolated, in our notations coloured in blue.

- Differentiating an external operator $\boldsymbol{X}^{\mathsf{a}}$ introduces the tensor $u^{\mathsf{a}}{}_{\mathsf{b}}$ which contracts—b being a dummy index here—with the external operator



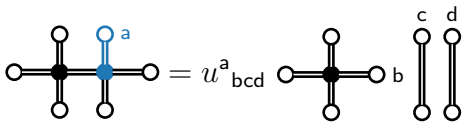
(13.35)

- Differentiating a contact-like bulk vertex of order n—hence exclusively connected to n external operators—leads to the product of $n-1$ two-point correlators contracted with the tensor $u^{\mathsf{a}}{}_{\mathsf{b}_1\mathsf{b}_2\ldots\mathsf{b}_{n-1}}$, where $\mathsf{b}_1, \mathsf{b}_2, \ldots, \mathsf{b}_{n-1}$ are dummy indices



(13.36)

- Differentiating an exchange-like bulk vertex of order m, attached to an external field, results in cutting the diagram in $m-1$ subdiagrams contracted with the tensor $u^{\mathsf{a}}{}_{\mathsf{b}_1\mathsf{b}_2\ldots\mathsf{b}_{m-1}}$. One should consider all possible contractions. An example is



(13.37)

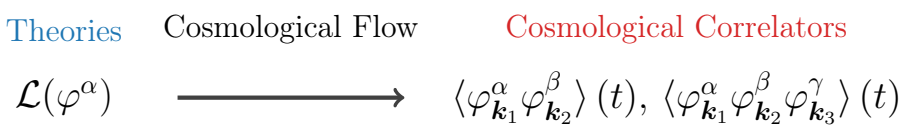
In general, the flow equations for an exchange-like diagram, together with those for the two-point correlators, do not form a closed system. One then needs to also find the flow equations for lower-order diagrams in order to close the system.

Our aim is to solve the flow equations (13.11), (13.15), (13.34), etc. Yet, two ingredients are missing: (i) initial conditions for the correlators, and (ii) explicit forms for the tensors $u^{\mathsf{a}}{}_{\mathsf{b}}$, $u^{\mathsf{a}}{}_{\mathsf{bc}}, \ldots$. In the next chapter, we will deal with these points.

14

Implementing the Cosmological Flow

Cosmological correlators satisfy differential equations in time, derived in the Chap. 13. The universality of this flow—i.e. that it can derived without specific knowledge of the bulk dynamics dictating the behaviour of inflationary fluctuations—suggests that a tool can be designed that automatically computes cosmological correlators in all theories, as illustrated in the following figure:



In this chapter, motivated by exploring the rich phenomenology of inflationary physics through cosmological correlators, we concretely apply the cosmological flow formalism to compute the two- and three-point correlation functions in generic theories of inflationary fluctuations. We ultimately present CosmoFlow, the corresponding open source Python package.

14.1 Inspiration from Particle Physics

Interpreting data from either particle collisions or cosmological observations crucially relies on a close interplay between accurate theoretical predictions and precise experiments.

In particle physics, precision calculations are mandatory for the measurement of properties of particles, such as masses or spins, and fundamental parameters such as coupling constants. In this case, the crucial objects that map theory and observables are *cross sections*, or more fundamentally the underlying scattering amplitudes. These objects contain the dynamical information associated with the models used

to describe data, and can be obtained from Feynman diagrams. Perturbative calculations are usually truncated at a certain order that dictates the level of accuracy to confront against the data. Although in principle systematic, this approach hides many challenges. In fact, these calculations quickly lead to an explosion of both analytic and algebraic complexity, that grow exponentially with the order at which the perturbative expansion is truncated.

From the theoretical side, probing fine features requires increasingly accurate predictions, ensuring that all various possible processes are covered. For example, with the LHC experiments achieving percent-level precision measurements, QCD perturbative calculations at NNNLO become necessary, large logarithms need to be resummed in order to get reliable predictions, and multi-loop Feynman integrals for complicated kinematical processes need to be evaluated. In short, such a precision imposes enormous demands on theory. Consequently, a large number of automated tools have been developed and are widely used by the community to make these accurate predictions. Examples of numerical packages to compute higher-order diagrams include pySecDec [525], FIESTA [526, 527, 528], DiffExp [529], AMFlow [530], and FormCalc [531], some of which can accommodate parallelisable computation and the usage of GPUs. A large number of events for hadronic collider physics can be generated, e.g. with MadGraph [532, 533, 534]. Additionally, tools like CompHEP [535, 536] and CalcHEP [537, 538] (see also [539]) directly accept Lagrangians as inputs and automatically compute the corresponding cross sections, with FeynRules [540, 541, 542] and LanHEP [543] deriving the underlying Feynman rules.

In cosmology, confronting theory against observations of, e.g., the large-scale structure of the Universe, requires an accurate modelling of inhomogeneities and their time evolution. Similarly to particle physics, as long as these perturbations remain relatively small, they can be treated in perturbation theory. Systematic approaches to make predictions, for example by evolving fluctuations from early to later times, have enabled the developments of automated tools. To name a few, these tools include publicly-available Boltzmann codes such as CAMB [544] and CLASS [36], numerical implementations of the EFTofLSS such as PyBird [545] to compute correlators of biased tracers in redshift space, or N-body codes like Quijote [546] to simulate the late-time Universe where fluctuations cannot be treated perturbatively.[1]

For inflationary cosmology, numerical tools to compute cosmological correlators up to three-point functions have been developed, including e.g. [547, 548], and the numerical implementation of the transport approach CppTransport/PyTransport [549, 550, 551, 552]. However, these methods solve at the same time the background dynamics governing the homogeneous spacetime evolution, and corresponding fluctuations whose couplings are precisely dictated by the background evolution. Consequently, these approaches operate on a case-specific basis, rendering them inadequate for handling general theories of fluctuations due to the necessity of more complicated background models. In turn, this can significantly skew our data interpretation, re-

[1] A non-exhaustive list of open source numerical packages/libraries/tools used in cosmology (as well as in high-energy physics and astrophysics) can be found here.

vealing the need to formulate an approach capable of providing accurate predictions across all physically motivated inflationary theories. Ergo, there is a need for a flexible and robust tool for computing cosmological correlators in all theories. The cosmological flow solves this problem: it automatically computes cosmological correlators with just a Lagrangian for fluctuations as an external input.

14.2 Landscape of Theories

We embrace the point of view of the EFT of inflationary fluctuations, without relying on a specific background mechanism. Fluctuations are the fundamental degrees of freedom and the background determines the time-dependent parameters in the Lagrangian.

14.2.1 Action

Up to cubic order, the most general action in Fourier space for the fluctuations is

$$\begin{aligned} S = \frac{1}{2}\int \mathrm{d}t\, a^3 \big(&\bar{\Delta}_{\alpha\beta}\dot{\boldsymbol{\varphi}}^\alpha\dot{\boldsymbol{\varphi}}^\beta + \bar{M}_{\alpha\beta}\boldsymbol{\varphi}^\alpha\boldsymbol{\varphi}^\beta + 2\bar{I}_{\alpha\beta}\boldsymbol{\varphi}^\alpha\dot{\boldsymbol{\varphi}}^\beta \\ &+\bar{A}_{\alpha\beta\gamma}\boldsymbol{\varphi}^\alpha\boldsymbol{\varphi}^\beta\boldsymbol{\varphi}^\gamma + \bar{B}_{\alpha\beta\gamma}\boldsymbol{\varphi}^\alpha\boldsymbol{\varphi}^\beta\dot{\boldsymbol{\varphi}}^\gamma + \bar{C}_{\alpha\beta\gamma}\dot{\boldsymbol{\varphi}}^\alpha\dot{\boldsymbol{\varphi}}^\beta\boldsymbol{\varphi}^\gamma + \bar{D}_{\alpha\beta\gamma}\dot{\boldsymbol{\varphi}}^\alpha\dot{\boldsymbol{\varphi}}^\beta\dot{\boldsymbol{\varphi}}^\gamma\big)\ , \end{aligned} \tag{14.1}$$

where a is the scale factor whose time evolution is arbitrary.[2] We have used the extended Fourier summation convention introduced in the previous chapter, meaning that repeated sans serif indices α, β—running from 1 to the number of fields N—denote a sum that includes an integral over Fourier modes. All the introduced tensors carry hidden arbitrary momentum and time dependencies, as we will see later. The tensor $\bar{\Delta}_{\alpha\beta}$ is real and symmetric and therefore can be considered diagonal without loss of generality.[3] As such, this tensor only accounts for non-canonically normalised fields. The tensor $\bar{M}_{\alpha\beta}$ is also taken to be symmetric $\bar{M}_{\alpha\beta} = \bar{M}_{(\alpha\beta)}$. It contains the kinetic gradient terms and the mass matrix. The non-symmetric $\bar{I}_{\alpha\beta}$ tensor captures the remaining possible linear mixings among the fields. For the cubic part of the action, the tensors $\bar{A}_{\alpha\beta\gamma} = \bar{A}_{(\alpha\beta\gamma)}$ and $\bar{D}_{\alpha\beta\gamma} = \bar{D}_{(\alpha\beta\gamma)}$ should be symmetrised over all indices, and $\bar{B}_{\alpha\beta\gamma} = \bar{B}_{(\alpha\beta)\gamma}$ and $\bar{C}_{\alpha\beta\gamma} = \bar{C}_{(\alpha\beta)\gamma}$ over the first two indices, with corresponding exchange of momenta. No further assumptions than the ones stated above are made.[4]

[2] The formalism presented in this paper is valid in all FLRW spacetimes, including de Sitter, slow-roll inflation and all power-law cosmologies.

[3] We also consider that $\bar{\Delta}_{\alpha\beta}$ is positive definite to avoid ghosts that would render the theory unstable.

[4] Note that the cubic interaction parameterised by the tensor $\bar{D}_{\alpha\beta\gamma}$ has not been considered in [549] as it does not appear in the action for the fluctuations in non-linear sigma models. It does appear in generalised $P(X^{IJ}, \phi^K)$ models though, where $X^{IJ} = -\frac{1}{2}g^{\mu\nu}\partial_\mu\phi^I\partial_\nu\phi^J$ are mixed kinetic terms [553, 50, 554], and is also present in the EFT of inflationary fluctuations, see Chap. 9. The generic approach that we are adopting therefore encompasses all these classes of models directly at the level of fluctuations.

14.2.2 Conjugate Momenta

Given the action (14.1), the conjugate momenta to the fields are defined by the following functional derivative

$$\boldsymbol{p}_\alpha(t) = \frac{\delta S}{\delta \dot{\boldsymbol{\varphi}}^\alpha(t)}\,, \quad \text{with} \quad \frac{\delta \boldsymbol{\varphi}^\alpha(t)}{\delta \boldsymbol{\varphi}^\beta(t')} = \delta^\alpha_{\ \beta}\,\delta(t-t')\,. \tag{14.2}$$

At cubic order, it is enough to restrict ourselves to linear order to derive the conjugate momenta and use $\mathcal{H}^{(3)} = -\mathcal{L}^{(3)}$, where $\dot{\boldsymbol{\varphi}}^\alpha$ should be expressed in terms of the linear momenta. Indeed, higher-order terms would give quartic terms in the Hamiltonian density, not relevant to compute three-point correlators. However, for the sake of completeness, we derive the conjugate momenta at second order (which would be necessary, e.g., for finding the quartic Hamiltonian),

$$\boldsymbol{p}_\alpha = a^3\left(\bar{\Delta}_{\bar{\alpha}\beta}\dot{\boldsymbol{\varphi}}^\beta + \bar{I}_{\bar{\alpha}\beta}\boldsymbol{\varphi}^\beta + \frac{1}{2}\bar{B}_{\beta\gamma\bar{\alpha}}\boldsymbol{\varphi}^\beta\boldsymbol{\varphi}^\gamma + \bar{C}_{\bar{\alpha}\beta\gamma}\dot{\boldsymbol{\varphi}}^\beta\boldsymbol{\varphi}^\gamma + \frac{3}{2}\bar{D}_{\bar{\alpha}\beta\gamma}\dot{\boldsymbol{\varphi}}^\beta\dot{\boldsymbol{\varphi}}^\gamma\right)\,, \tag{14.3}$$

where bar indices indicate that the sign of the corresponding momentum $\boldsymbol{k}$ has been reversed i.e. $T^{\bar{\alpha}} = T^\alpha(-\boldsymbol{k}_\alpha)$ where T can be a tensor or a field. This follows from the fact that Fourier-space expressions can produce the delta function $\delta_{\alpha\beta} = (2\pi)^3\delta_{\alpha\beta}\,\delta^{(3)}(\boldsymbol{k}_\alpha+\boldsymbol{k}_\beta)$. Consistently, a contraction with $\delta^\alpha_{\ \beta}$ bars an index $\delta^\alpha_{\ \beta}\,T^\beta = T^{\bar{\alpha}}$. More details can be found in App. D.

Hamiltonian. The Hamiltonian—viewed as a functional of $(\boldsymbol{\varphi}^\alpha, \boldsymbol{p}_\beta)$—is defined from the Lagrangian by a Legendre transform

$$H = \int \mathrm{d}t\,\left(\boldsymbol{p}_\alpha\dot{\boldsymbol{\varphi}}^{\bar{\alpha}} - \mathcal{L}\right)\,. \tag{14.4}$$

From now on, we rescale the momenta $\boldsymbol{p}_\alpha \to a^3\boldsymbol{p}_\alpha$ to avoid an extra overall factor of a^3 coming from $\mathcal{L}$ once the field time derivatives have been replaced by their conjugate momenta. Inverting Eq. (14.3) perturbatively gives

$$\begin{aligned}\dot{\boldsymbol{\varphi}}^\alpha = \bar{\nabla}^{\alpha\bar{\delta}}\Bigg[&\boldsymbol{p}_\delta - \bar{I}_{\bar{\delta}\beta}\boldsymbol{\varphi}^\beta - \left(\frac{1}{2}\bar{B}_{\beta\gamma\bar{\delta}} - \bar{C}_{\bar{\delta}\sigma\gamma}\bar{\nabla}^{\sigma\tau}\bar{I}_{\bar{\tau}\beta} + \frac{3}{2}\bar{D}_{\bar{\delta}\rho\mu}\bar{\nabla}^{\rho\tau}\bar{I}_{\bar{\tau}\beta}\bar{\nabla}^{\mu\sigma}\bar{I}_{\bar{\sigma}\gamma}\right)\boldsymbol{\varphi}^\beta\boldsymbol{\varphi}^\gamma \\ &- \left(\bar{C}_{\bar{\delta}\sigma\gamma}\bar{\nabla}^{\sigma\beta} - \frac{3}{2}\bar{D}_{\bar{\delta}\tau\rho}\bar{\nabla}^{\tau\beta}\bar{\nabla}^{\rho\sigma}\bar{I}_{\bar{\sigma}\gamma}\right)\boldsymbol{p}_\beta\boldsymbol{\varphi}^\gamma - \frac{3}{2}\bar{D}_{\bar{\delta}\tau\sigma}\bar{\nabla}^{\tau\beta}\bar{D}^{\sigma\gamma}\boldsymbol{p}_\beta\boldsymbol{p}_\gamma + \dots\Bigg]\,,\end{aligned} \tag{14.5}$$

where the ellipses denote higher-order terms, irrelevant in our case. We have denoted $\bar{\nabla}^{\alpha\beta}$ to be the inverse matrix satisfying $\bar{\nabla}^{\alpha\beta}\bar{\Delta}_{\beta\gamma} = \delta^\alpha_{\ \gamma}$. Rearranging the various terms, the Hamiltonian reads

$$\begin{aligned}H = \frac{1}{2}\int \mathrm{d}t\,a^3\,\big(&\Delta_{\alpha\beta}\boldsymbol{p}^\alpha\boldsymbol{p}^\beta - M_{\alpha\beta}\boldsymbol{\varphi}^\alpha\boldsymbol{\varphi}^\beta - 2I_{\alpha\beta}\boldsymbol{\varphi}^\alpha\boldsymbol{p}^\beta \\ &- A_{\alpha\beta\gamma}\boldsymbol{\varphi}^\alpha\boldsymbol{\varphi}^\beta\boldsymbol{\varphi}^\gamma - B_{\alpha\beta\gamma}\boldsymbol{\varphi}^\alpha\boldsymbol{\varphi}^\beta\boldsymbol{p}^\gamma - C_{\alpha\beta\gamma}\boldsymbol{p}^\alpha\boldsymbol{p}^\beta\boldsymbol{\varphi}^\gamma - D_{\alpha\beta\gamma}\boldsymbol{p}^\alpha\boldsymbol{p}^\beta\boldsymbol{p}^\gamma\big)\,,\end{aligned} \tag{14.6}$$

where the anew defined tensors are

$$\begin{aligned}
&\Delta_{\alpha\beta} = \bar{\nabla}^{\bar{\alpha}\bar{\beta}}\,, \quad M_{\alpha\beta} = \bar{M}_{\alpha\beta} - \bar{\nabla}^{\bar{\gamma}\bar{\delta}}\bar{I}_{\bar{\gamma}\alpha}\bar{I}_{\bar{\delta}\beta}\,, \quad I_{\alpha\beta} = \bar{\nabla}^{\bar{\beta}\gamma}\bar{I}_{\alpha\gamma}\,,\\
&A_{\alpha\beta\gamma} = \bar{A}_{\alpha\beta\gamma} - \bar{B}_{\alpha\beta\delta}\bar{\nabla}^{\delta\bar{\sigma}}\bar{I}_{\bar{\sigma}\gamma} + \bar{C}_{\delta\sigma\gamma}\bar{\nabla}^{\delta\bar{\tau}}\bar{I}_{\bar{\tau}\alpha}\bar{\nabla}^{\sigma\bar{\rho}}\bar{I}_{\bar{\rho}\beta} - \bar{D}_{\delta\sigma\rho}\bar{\nabla}^{\delta\mu}\bar{\nabla}^{\sigma\nu}\bar{\nabla}^{\rho\kappa}\bar{I}_{\bar{\mu}\alpha}\bar{I}_{\bar{\nu}\beta}\bar{I}_{\bar{\kappa}\gamma}\,,\\
&B_{\alpha\beta\gamma} = \bar{B}_{\alpha\beta\delta}\bar{\nabla}^{\delta\bar{\gamma}} - 2\bar{C}_{\delta\sigma\alpha}\bar{\nabla}^{\delta\gamma}\bar{\nabla}^{\sigma\bar{\rho}}\bar{I}_{\bar{\rho}\beta} + 3\bar{D}_{\delta\sigma\rho}\bar{\nabla}^{\delta\bar{\gamma}}\bar{\nabla}^{\sigma\bar{\mu}}\bar{\nabla}^{\rho\bar{\nu}}\bar{I}_{\bar{\mu}\beta}\bar{I}_{\bar{\nu}\alpha}\,,\\
&C_{\alpha\beta\gamma} = \bar{C}_{\delta\sigma\gamma}\bar{\nabla}^{\delta\bar{\alpha}}\bar{\nabla}^{\sigma\bar{\beta}} - 3\bar{D}_{\delta\sigma\rho}\bar{\nabla}^{\alpha\bar{\delta}}\bar{\nabla}^{\alpha\bar{\sigma}}\bar{\nabla}^{\rho\bar{\tau}}\bar{I}_{\bar{\tau}\gamma}\,,\\
&D_{\alpha\beta\gamma} = \bar{D}_{\delta\sigma\rho}\bar{\nabla}^{\alpha\bar{\delta}}\bar{\nabla}^{\beta\bar{\sigma}}\bar{\nabla}^{\gamma\bar{\rho}}\,.
\end{aligned} \tag{14.7}$$

Notice that the internal target space of the fluctuations is flat. Consequently, the tensor indices are raised and lowered using the delta function. This form of the Hamiltonian—rather than the action (14.1)—can also be taken as a definition of the theory. Also, note that non-linear contributions to the momenta cancel in the cubic Hamiltonian. It is therefore enough to only consider linear momenta in the computation of three-point correlators.

14.3 Flow Equations

Given the explicit form of the Hamiltonian (14.6), it is an easy task to derive the $u^{\mathsf{a}}{}_{\mathsf{b}} = \epsilon^{\mathsf{ac}}H_{\mathsf{cb}}$ and $u^{\mathsf{a}}{}_{\mathsf{bc}} = \epsilon^{\mathsf{ad}}H_{\mathsf{dbc}}$ tensors entering in the flow equations (13.11) and (13.15). For the quadratic Hamiltonian, after carefully symmetrising the $H_{\mathsf{ab}} = H_{(\mathsf{ab})}$ tensor, we obtain

$$H_{\mathsf{ab}} = \begin{pmatrix} -M_{\alpha\beta} & -I_{\alpha\beta} \\ -I_{\beta\alpha} & \Delta_{\alpha\beta} \end{pmatrix}\,, \tag{14.8}$$

where the a,b indices are arranged in such a way that the field indices are followed by momentum indices in the same order. The desired $u^{\mathsf{a}}{}_{\mathsf{b}}$ tensor is then

$$u^{\mathsf{a}}{}_{\mathsf{b}} = \begin{pmatrix} \mathbf{0} & \mathbf{1} \\ -\mathbf{1} & \mathbf{0} \end{pmatrix}\begin{pmatrix} -M^{\bar{\alpha}}{}_{\beta} & -I^{\bar{\alpha}}{}_{\beta} \\ -I_{\beta}{}^{\bar{\alpha}} & \Delta^{\bar{\alpha}}{}_{\beta} \end{pmatrix} + \begin{pmatrix} \mathbf{0} & \mathbf{0} \\ \mathbf{0} & -3H\delta^{\bar{\alpha}}_{\beta} \end{pmatrix} = \begin{pmatrix} I_{\beta}{}^{\bar{\alpha}} & \Delta^{\bar{\alpha}}{}_{\beta} \\ M^{\bar{\alpha}}{}_{\beta} & I^{\bar{\alpha}}{}_{\beta} - 3H\delta^{\bar{\alpha}}_{\beta} \end{pmatrix}\,. \tag{14.9}$$

The extra factor $-3H\delta^{\bar{\alpha}}_{\beta}$ comes from the momentum rescaling.[5] Similarly, the cubic Hamiltonian reads

$$H_{\mathsf{abc}} = \left\{ \begin{pmatrix} -3A_{\alpha\beta\gamma} & -B_{\alpha\gamma\beta} \\ -B_{\gamma\beta\alpha} & -C_{\alpha\beta\gamma} \end{pmatrix} \begin{pmatrix} -B_{\alpha\beta\gamma} & -C_{\gamma\beta\alpha} \\ -C_{\alpha\gamma\beta} & -3D_{\alpha\beta\gamma} \end{pmatrix} \right\}\,, \tag{14.11}$$

where the index c labels the first (resp. second) matrix within the braces $\{\ldots\}$ if it is a field (resp. a momentum) index, and similarly a (resp. b) labels the row (resp. column) in each 2×2 block matrix. We recall that H_{abc} is constructed to be symmetric under the exchange of any pair of indices hence the multiple presence

[5] Due to the momentum rescaling $\boldsymbol{p}_\alpha \to a^3\boldsymbol{p}_\alpha$, the Heisenberg equation is modified

$$\frac{\mathrm{d}\boldsymbol{p}_\alpha}{\mathrm{d}t} = i[H,\boldsymbol{p}_\alpha] - 3H\boldsymbol{p}_\alpha. \tag{14.10}$$

The additional non-canonical factor can be absorbed in the $u^{\mathsf{a}}{}_{\mathsf{b}}$ tensor as done in the main text.

of some tensors. The $u^{\mathsf{a}}{}_{\mathsf{bc}}$ tensor is obtained by explicitly performing the matrix multiplication

$$u^{\mathsf{a}}{}_{\mathsf{bc}} = \left\{ \begin{pmatrix} \mathbf{0} & \mathbf{1} \\ -\mathbf{1} & \mathbf{0} \end{pmatrix} \begin{pmatrix} -3A^{\bar{\alpha}}{}_{\beta\gamma} & -B^{\bar{\alpha}}{}_{\gamma\beta} \\ -B_{\gamma\beta}{}^{\bar{\alpha}} & -C^{\bar{\alpha}}{}_{\beta\gamma} \end{pmatrix} \right\} = \left\{ \begin{pmatrix} -B_{\gamma\beta}{}^{\bar{\alpha}} & -C^{\bar{\alpha}}{}_{\gamma\beta} \\ 3A^{\bar{\alpha}}{}_{\beta\gamma} & B^{\bar{\alpha}}{}_{\gamma\beta} \end{pmatrix} \right\}. \tag{14.12}$$

As done in [549], we further notice that the particular arrangement of barred indices—namely the upper $\bar{\alpha}$ index for each tensors—enables us to extract a delta function, hence defining $\boldsymbol{k}$-dependent tensor coefficients $u^a{}_b$ and $u^a{}_{bc}$ that we label with normal indices $a, b, \ldots$ in the following way

$$\begin{aligned} u^{\mathsf{a}}{}_{\mathsf{b}} &= (2\pi)^3 \delta^{(3)}(\boldsymbol{k}_a - \boldsymbol{k}_b)\, u^a{}_b(\boldsymbol{k}_a, \boldsymbol{k}_b)\,, \\ u^{\mathsf{a}}{}_{\mathsf{bc}} &= (2\pi)^3 \delta^{(3)}(\boldsymbol{k}_a - \boldsymbol{k}_b - \boldsymbol{k}_c)\, u^a{}_{bc}(\boldsymbol{k}_a, \boldsymbol{k}_b, \boldsymbol{k}_c)\,. \end{aligned} \tag{14.13}$$

It is important to stress that in writing expressions with explicit momentum dependence, the index labelling the momentum is associated with the corresponding tensor index. Explicitly, $\boldsymbol{k}_a$ is associated with a and so forth. For example if one would want to exchange b and c in $u^a{}_{bc}$, the corresponding momenta should be exchanged too. Furthermore, due to the presence of the delta function and by isotropy, the $u^a{}_b$ tensor coefficients only depend on the magnitude of the momentum, $u^a{}_b(k)$ where $k = |\boldsymbol{k}_a| = |\boldsymbol{k}_b|$.

14.3.1 Differential Equations in Time

Turning to the two- and three-point correlation functions, statistical isotropy and homogeneity imply that one can write

$$\begin{aligned} \langle \boldsymbol{X}^{\mathsf{a}} \boldsymbol{X}^{\mathsf{b}} \rangle &= (2\pi)^3 \delta^{(3)}(\boldsymbol{k}_a + \boldsymbol{k}_b)\, \Sigma^{ab}(k)\,, \\ \langle \boldsymbol{X}^{\mathsf{a}} \boldsymbol{X}^{\mathsf{b}} \boldsymbol{X}^{\mathsf{c}} \rangle &= (2\pi)^3 \delta^{(3)}(\boldsymbol{k}_a + \boldsymbol{k}_b + \boldsymbol{k}_c)\, B^{abc}(k_a, k_b, k_c)\,, \end{aligned} \tag{14.14}$$

where for the two-point correlator we have set $k = |\boldsymbol{k}_a| = |\boldsymbol{k}_b|$. We do not explicitly write the time dependency of the above correlators but it should be understood that they are evaluated at the same time t. The three-point correlators $B^{abc}(k_a, k_b, k_c)$ are real, as we will explain below, while Σ^{ab} is complex and can be split into real and imaginary parts $\Sigma^{ab} = \Sigma^{ab}_{\mathrm{Re}} + i\Sigma^{ab}_{\mathrm{Im}}$. Because the flow equation (13.11) is linear and the $u^a{}_c$ have real elements, one can solve independently for $\Sigma^{ab}_{\mathrm{Re}}$ and $\Sigma^{ab}_{\mathrm{Im}}$, obeying

$$\frac{\mathrm{d}\Sigma^{ab}_{\mathrm{Re,Im}}(k)}{\mathrm{d}t} = u^a{}_c(k)\, \Sigma^{cb}_{\mathrm{Re,Im}}(k) + u^b{}_c(k)\, \Sigma^{ac}_{\mathrm{Re,Im}}(k)\,. \tag{14.15}$$

Actually, the commutation relation—valid *at all times*—fully fixes the imaginary part of the two-point correlators, independently of any theory. To see this, note that the real-space operators we consider are Hermitian. In Fourier space, this implies that

$$\boldsymbol{X}^{\mathsf{a}\dagger} = \boldsymbol{X}^{\bar{\mathsf{a}}}\,, \tag{14.16}$$

where † is the Hermitian conjugate operation, and we recall that $\bar{\mathsf{a}}$ indicates that the sign of the corresponding momentum is reversed. From this, one can first derive symmetry properties satisfied by the two-point correlators. Indeed, $\langle \boldsymbol{X}^{\mathsf{a}}\boldsymbol{X}^{\mathsf{b}}\rangle^* = \langle \big(\boldsymbol{X}^{\mathsf{a}}\boldsymbol{X}^{\mathsf{b}}\big)^\dagger\rangle = \langle \boldsymbol{X}^{\bar{\mathsf{b}}}\boldsymbol{X}^{\bar{\mathsf{a}}}\rangle = \langle \boldsymbol{X}^{\mathsf{b}}\boldsymbol{X}^{\mathsf{a}}\rangle$, where we used (14.14) in the last step. This enforces the real part to be symmetric and the imaginary part to be anti-symmetric

$$\Sigma^{ab}_{\mathrm{Re}} = \Sigma^{ba}_{\mathrm{Re}}\,, \qquad \Sigma^{ab}_{\mathrm{Im}} = -\Sigma^{ba}_{\mathrm{Im}}\,. \tag{14.17}$$

Second, introducing the commutator in $\langle \boldsymbol{X}^{\mathsf{a}}\boldsymbol{X}^{\mathsf{b}}\rangle$ and taking the imaginary part, one finds $\Sigma^{ab}_{\mathrm{Im}} = \frac{\epsilon^{ab}}{2a^3}$, where the tensor ϵ^{ab} is defined in (13.4). As a result, the imaginary part either decays in $1/a^3$ for correlators involving a field and a conjugate momentum of the same kind (recall that the physical momenta are rescaled by a^3) or is strictly zero (for all other correlators). Therefore, there is no need to solve the flow equation for $\Sigma^{ab}_{\mathrm{Im}}$, although this equation can all the same be solved as a numerical consistency check.

For three-point correlators, similar manipulations give

$$\langle \boldsymbol{X}^{\mathsf{a}}\boldsymbol{X}^{\mathsf{b}}\boldsymbol{X}^{\mathsf{c}}\rangle^* - \langle \boldsymbol{X}^{\bar{\mathsf{a}}}\boldsymbol{X}^{\bar{\mathsf{b}}}\boldsymbol{X}^{\bar{\mathsf{c}}}\rangle = -i\epsilon^{\mathsf{ab}}\langle X^{\bar{\mathsf{c}}}\rangle - i\epsilon^{\mathsf{ac}}\langle X^{\bar{\mathsf{b}}}\rangle - i\epsilon^{\mathsf{bc}}\langle X^{\bar{\mathsf{a}}}\rangle\,. \tag{14.18}$$

The right-hand side vanishes for connected correlators, for which none of the wavevectors individually vanishes. Defining more precisely the bispectra as the connected three-point correlators, this leads to $B^{abc}(\boldsymbol{k}_a,\boldsymbol{k}_b,\boldsymbol{k}_c)^* - B^{abc}(-\boldsymbol{k}_a,-\boldsymbol{k}_b,-\boldsymbol{k}_c) = 0$. Then, statistical isotropy, implying that B^{abc} in (14.14) only depends on the norms of the wavevectors, enforces that B^{abc} is real. As for its time evolution, it is important to keep track of both $\Sigma^{ab}_{\mathrm{Re}}$ and $\Sigma^{ab}_{\mathrm{Im}}$ because the flow equations—being sourced by a non-linear term—requires the knowledge of the *complex* two-point correlators. Taking into account that the tensor coefficients $u^a{}_{bc}$ are real, we arrive at

$$\begin{aligned}
\frac{\mathrm{d}B^{abc}(k_a,k_b,k_c)}{\mathrm{d}t} &= u^a{}_d(k_a)B^{dbc}(k_a,k_b,k_c) + u^b{}_d(k_b)B^{adc}(k_a,k_b,k_c) + u^c{}_d(k_c)B^{abd}(k_a,k_b,k_c)\\
&+ u^a{}_{de}(\boldsymbol{k}_a,\boldsymbol{k}_b,\boldsymbol{k}_c)\Sigma^{db}_{\mathrm{Re}}(k_b)\Sigma^{ec}_{\mathrm{Re}}(k_c) - u^a{}_{de}(\boldsymbol{k}_a,\boldsymbol{k}_b,\boldsymbol{k}_c)\Sigma^{db}_{\mathrm{Im}}(k_b)\Sigma^{ec}_{\mathrm{Im}}(k_c)\\
&+ u^b{}_{de}(\boldsymbol{k}_b,\boldsymbol{k}_a,\boldsymbol{k}_c)\Sigma^{ad}_{\mathrm{Re}}(k_a)\Sigma^{ec}_{\mathrm{Re}}(k_c) - u^b{}_{de}(\boldsymbol{k}_b,\boldsymbol{k}_a,\boldsymbol{k}_c)\Sigma^{ad}_{\mathrm{Im}}(k_a)\Sigma^{ec}_{\mathrm{Im}}(k_c)\\
&+ u^c{}_{de}(\boldsymbol{k}_c,\boldsymbol{k}_a,\boldsymbol{k}_b)\Sigma^{ad}_{\mathrm{Re}}(k_a)\Sigma^{be}_{\mathrm{Re}}(k_b) - u^c{}_{de}(\boldsymbol{k}_c,\boldsymbol{k}_a,\boldsymbol{k}_b)\Sigma^{ad}_{\mathrm{Im}}(k_a)\Sigma^{be}_{\mathrm{Im}}(k_b)\,,
\end{aligned} \tag{14.19}$$

where we have deliberately written all the permutations to avoid ambiguity in the index ordering.

We have seen that the imaginary parts of two-point correlators are fixed from first principles, and that the ones of connected three-point correlators vanish. In this respect, it is instructive to also consider four-point correlators. Systematically inserting commutators, one finds

$$\begin{aligned}
\mathrm{Im}\langle \boldsymbol{X}^{\mathsf{a}}\boldsymbol{X}^{\mathsf{b}}\boldsymbol{X}^{\mathsf{c}}\boldsymbol{X}^{\mathsf{d}}\rangle &= \frac{1}{2i}\big[\langle \boldsymbol{X}^{\mathsf{a}}\boldsymbol{X}^{\mathsf{b}}\boldsymbol{X}^{\mathsf{c}}\boldsymbol{X}^{\mathsf{d}}\rangle - \langle \boldsymbol{X}^{\bar{\mathsf{a}}}\boldsymbol{X}^{\bar{\mathsf{b}}}\boldsymbol{X}^{\bar{\mathsf{c}}}\boldsymbol{X}^{\bar{\mathsf{d}}}\rangle\big]\\
&+ \frac{1}{2}\left(\epsilon^{\mathsf{cd}}\langle \boldsymbol{X}^{\mathsf{a}}\boldsymbol{X}^{\mathsf{b}}\rangle + \epsilon^{\mathsf{ab}}\langle \boldsymbol{X}^{\mathsf{d}}\boldsymbol{X}^{\mathsf{c}}\rangle + \epsilon^{\mathsf{bd}}\langle \boldsymbol{X}^{\mathsf{a}}\boldsymbol{X}^{\mathsf{c}}\rangle + \epsilon^{\mathsf{ac}}\langle \boldsymbol{X}^{\mathsf{d}}\boldsymbol{X}^{\mathsf{b}}\rangle + \epsilon^{\mathsf{bc}}\langle \boldsymbol{X}^{\mathsf{a}}\boldsymbol{X}^{\mathsf{d}}\rangle + \epsilon^{\mathsf{ad}}\langle \boldsymbol{X}^{\mathsf{c}}\boldsymbol{X}^{\mathsf{b}}\rangle\right)\,.
\end{aligned} \tag{14.20}$$

The second line vanishes for connected four-point functions, and simply corresponds to the imaginary part of the correlator that one would deduce from Wick theorem

in terms of two-point correlators. Note, however, that we did not use a perturbative scheme to derive this. Only the first line remains for connected correlators of interest. In that case, and contrary to three-point kinematic above, $(\boldsymbol{k}_a, \ldots, \boldsymbol{k}_d)$ and $(-\boldsymbol{k}_a, \ldots, -\boldsymbol{k}_d)$ need not be related by a rotation, so that the imaginary parts of connected four-point correlators do not vanish in general. This happens for theories in which parity is violated.

14.3.2 Derivative Interactions

The entries of the cubic tensors $A_{\alpha\beta\gamma}, B_{\alpha\beta\gamma}, C_{\alpha\beta\gamma}$ and $D_{\alpha\beta\gamma}$ are in general time and momentum dependent. The momentum dependency comes from considering spatial derivative interactions, that give simple factors of momenta after Fourier transform. For instance, let us take the contact interaction $\mathcal{L}/a^3 \supset \frac{\lambda}{2}\varphi(\partial_i\varphi)^2/a^2$. In Fourier space, the corresponding cubic Hamiltonian gives the following tensor coefficient $A_{\varphi_{\boldsymbol{k}_1}\varphi_{\boldsymbol{k}_2}\varphi_{\boldsymbol{k}_3}} = \lambda\, \boldsymbol{k}_1 \cdot \boldsymbol{k}_2/a^2 + 2$ perms. In general, these tensor elements can be more complicated, and can for example scale as inverse powers of the momenta. In this way, the cosmological flow formalism makes it convenient to implement various types of interactions without much complications.

When computing the in-in integrals using the Schwinger-Keldysh formalism, the time derivatives appearing in a vertex should be directly applied to the attached propagators. In the cosmological flow formalism, time derivative interactions can be expressed as contact vertices between fields and momenta. For example, the interaction $\mathcal{L}/a^3 \supset -\frac{\lambda}{2}\varphi^2\dot{\varphi}$ gives the tensor coefficient $B_{\varphi_{\boldsymbol{k}_1}\varphi_{\boldsymbol{k}_2}p_{\boldsymbol{k}_3}} = -\lambda$, where p is the (rescaled) conjugate momentum to the field φ.[6] Therefore, it is an easy task to treat time derivative interactions with the formalism presented here.

14.3.3 Boundary Terms

When defining a theory, the action is sometimes supplemented by a boundary term. This is the case for example in the ADM formalism where the Gibbons-Hawking-York boundary term needs to be added to the Einstein-Hilbert action. Another celebrated example is Maldacena's calculation of the cubic Lagrangian in single-field inflation [42, 553] and its more recent generalisation to non-linear sigma models in [555, 556]. There, the cubic Lagrangian for the fluctuations is supplemented by a boundary term whose various terms come from rendering the size of interactions manifest by using the equation of motions, equivalently performing multiple integrations by parts. Although these boundary terms do not contribute to the equations of motion, they do contribute to the three-point correlators. We show here how to include these terms in correlators from first principles and in the most general case.

A generic boundary term appears in the form of a total derivative at the level of the action $S = S_{\text{bulk}} + S_\partial$. In Fourier space, we write the boundary term S_∂ as

$$S_\partial = \int \mathrm{d}t\, \mathcal{L}_\partial\,, \quad \text{with} \quad \mathcal{L}_\partial = \frac{\mathrm{d}}{\mathrm{d}t}\left(\frac{1}{3!}\,\Omega_{\mathsf{abc}}\boldsymbol{X}^{\mathsf{a}}\boldsymbol{X}^{\mathsf{b}}\boldsymbol{X}^{\mathsf{c}}\right), \tag{14.21}$$

[6] We have assumed, for illustration purposes, that the quadratic theory is simple enough so that $p = \dot{\varphi}$.

where in general the tensor Ω has time and momentum dependent elements. It is taken to be fully symmetric $\Omega_{\mathsf{abc}} = \Omega_{(\mathsf{abc})}$. With the cubic Hamiltonian, one can formally write the in-in formula for the three-point correlators

$$\begin{aligned}\langle \boldsymbol{X}^{\mathsf{a}}\boldsymbol{X}^{\mathsf{b}}\boldsymbol{X}^{\mathsf{c}}\rangle \supset -i\,\langle 0|\int_{-\infty}^{t}\mathrm{d}t'\left[\frac{\mathrm{d}}{\mathrm{d}t'}\left(\frac{1}{3!}\,\Omega_{\mathsf{def}}\,X^{\mathsf{d}}X^{\mathsf{e}}X^{\mathsf{f}}\right),X^{\mathsf{a}}X^{\mathsf{b}}X^{\mathsf{c}}\right]|0\rangle \\ = -i\,\langle 0|\frac{1}{3!}\,\Omega_{\mathsf{def}}\left[X^{\mathsf{d}}X^{\mathsf{e}}X^{\mathsf{f}},X^{\mathsf{a}}X^{\mathsf{b}}X^{\mathsf{c}}\right]|0\rangle\ ,\end{aligned} \tag{14.22}$$

where in the last line all the interaction-picture operators are evaluated at the time t. As we have done previously for the $u^{\mathsf{a}}{}_{\mathsf{b}}$ and $u^{\mathsf{a}}{}_{\mathsf{bc}}$ tensors, we define the tensor elements by extracting the momentum conserving delta functions which follows from that of the correlator $\Omega_{\mathsf{abc}} = (2\pi)^3\delta^{(3)}(\boldsymbol{k}_a+\boldsymbol{k}_b+\boldsymbol{k}_c)\,\Omega_{abc}(\boldsymbol{k}_a,\boldsymbol{k}_b,\boldsymbol{k}_c)$. As usual, the $i\epsilon$ prescription in the far past switches off the interactions. The equation shows that a general boundary term gives a local contribution in time for the three-point correlators. The fields being free in the interaction picture, we use Wick theorem to express the contribution into explicit two-point correlators. After using the symmetry properties of Ω_{abc} and retaining only connected contributions, one obtains

$$\langle \boldsymbol{X}^{\mathsf{a}}\boldsymbol{X}^{\mathsf{b}}\boldsymbol{X}^{\mathsf{c}}\rangle \supset -i\,\Omega_{\mathsf{def}}\left(\langle \boldsymbol{X}^{\mathsf{d}}\boldsymbol{X}^{\mathsf{a}}\rangle\langle \boldsymbol{X}^{\mathsf{e}}\boldsymbol{X}^{\mathsf{b}}\rangle\langle \boldsymbol{X}^{\mathsf{f}}\boldsymbol{X}^{\mathsf{c}}\rangle - \langle \boldsymbol{X}^{\mathsf{a}}\boldsymbol{X}^{\mathsf{d}}\rangle\langle \boldsymbol{X}^{\mathsf{b}}\boldsymbol{X}^{\mathsf{e}}\rangle\langle \boldsymbol{X}^{\mathsf{c}}\boldsymbol{X}^{\mathsf{f}}\rangle\right)\ . \tag{14.23}$$

We can further use the commutator to simplify the relation, obtaining

$$\begin{aligned}\langle \boldsymbol{X}^{\mathsf{a}}\boldsymbol{X}^{\mathsf{b}}\boldsymbol{X}^{\mathsf{c}}\rangle \supset -\Omega_{\mathsf{def}}\left(\epsilon^{\mathsf{ad}}\langle \boldsymbol{X}^{\mathsf{e}}\boldsymbol{X}^{\mathsf{b}}\rangle\langle \boldsymbol{X}^{\mathsf{f}}\boldsymbol{X}^{\mathsf{c}}\rangle + \epsilon^{\mathsf{be}}\langle \boldsymbol{X}^{\mathsf{a}}\boldsymbol{X}^{\mathsf{d}}\rangle\langle \boldsymbol{X}^{\mathsf{c}}\boldsymbol{X}^{\mathsf{f}}\rangle\right. \\ \left.+\epsilon^{\mathsf{cf}}\langle \boldsymbol{X}^{\mathsf{a}}\boldsymbol{X}^{\mathsf{d}}\rangle\langle \boldsymbol{X}^{\mathsf{e}}\boldsymbol{X}^{\mathsf{b}}\rangle\right)\ .\end{aligned} \tag{14.24}$$

Keeping in mind that three-point correlators are real, one finds that the boundary term only needs to be added a posteriori:

$$B^{abc}(k_a,k_b,k_c) \to B^{abc}_{\mathrm{bulk}}(k_a,k_b,k_c) + B^{abc}_{\partial}(k_a,k_b,k_c)\,, \tag{14.25}$$

with the contribution coming from the boundary term being

$$\begin{aligned}B^{abc}_{\partial}(k_a,k_b,k_c) = -\Omega_{def}(-\boldsymbol{k}_a,-\boldsymbol{k}_b,-\boldsymbol{k}_c)\left[\epsilon^{ad}\Sigma^{be}_{\mathrm{Re}}(k_b)\Sigma^{fc}_{\mathrm{Re}}(k_c) - \epsilon^{ad}\Sigma^{be}_{\mathrm{Im}}(k_b)\Sigma^{fc}_{\mathrm{Im}}(k_c)\right. \\ +\epsilon^{be}\Sigma^{ad}_{\mathrm{Re}}(k_a)\Sigma^{cf}_{\mathrm{Re}}(k_c) - \epsilon^{be}\Sigma^{ad}_{\mathrm{Im}}(k_a)\Sigma^{cf}_{\mathrm{Im}}(k_c) \\ \left.+\epsilon^{cf}\Sigma^{ad}_{\mathrm{Re}}(k_a)\Sigma^{be}_{\mathrm{Re}}(k_b) - \epsilon^{cf}\Sigma^{ad}_{\mathrm{Im}}(k_a)\Sigma^{be}_{\mathrm{Im}}(k_b)\right]\ .\end{aligned} \tag{14.26}$$

Note that in general, only correlators of light degrees of freedom survive until the end of inflation. Also, terms proportional to spatial gradients are suppressed by the exponential of the time elapsed in e-fold since the corresponding mode exited the horizon, and are negligible for cosmological scales. In practice, a lot of the listed terms do not contribute significantly to the three-point correlators at the end of the time evolution. However for completeness we have derived the most general form for such boundary terms.

14.4 Initial Conditions

To render the system complete, one must provide initial conditions for $\Sigma^{ab}_{\mathrm{Re}}$, $\Sigma^{ab}_{\mathrm{Im}}$ and B^{abc}. Within the cosmological flow formalism, these initial conditions can be derived

analytically provided one initialises the correlators sufficiently in the deep past. Indeed, by looking at the Hamiltonian in Eq. (14.6), we see that the quadratic theory is composed of a part governing the free evolution of the fields and one encoding non-trivial quadratic mixings. These quadratic interactions constitute one reason why analytical methods to compute late-time correlators fail in the most general cases. However, one can always choose an initial time deep enough inside the horizon for the modes of interest, so that the theory is dominated by the decoupled quadratic theory. In this regime, all the various couplings and masses can be neglected so that the theory approaches that of a set of uncoupled degrees of freedom, and initial conditions can be computed analytically. This is the very idea of asymptotically reaching the vacuum state.

14.4.1 Two-Point Correlators

We begin with the second-order action in Fourier space,

$$S^{(2)} = \frac{1}{2}\int \mathrm{d}t\, a^3 \left(\bar{\Delta}_{\alpha\beta}\dot{\boldsymbol{\varphi}}^{\alpha}\dot{\boldsymbol{\varphi}}^{\beta} + \bar{M}_{\alpha\beta}\boldsymbol{\varphi}^{\alpha}\boldsymbol{\varphi}^{\beta} + 2\bar{I}_{\alpha\beta}\boldsymbol{\varphi}^{\alpha}\dot{\boldsymbol{\varphi}}^{\beta}\right) , \tag{14.27}$$

where $\bar{M}_{\alpha\beta}$ encompasses the kinetic gradient terms as well as other non-kinetic terms. We isolate the mass matrix $\bar{\mathcal{M}}_{\alpha\beta}$ by writing

$$\bar{M}_{\alpha\beta} = (2\pi)^3\delta^{(3)}(\boldsymbol{k}_{\alpha} + \boldsymbol{k}_{\beta})\left(\bar{\mathcal{K}}_{\alpha\beta} + \bar{\mathcal{M}}_{\alpha\beta}\right) , \tag{14.28}$$

where all gradient terms are included in the matrix $\bar{\mathcal{K}}_{\alpha\beta}$. Without loss of generality, it can be written as

$$\bar{\mathcal{K}}_{\alpha\beta} = -\frac{k^2}{a^2}\,c^{(2)}_{\alpha\beta} - \frac{k^4}{a^4}\,\frac{c^{(4)}_{\alpha\beta}}{\Lambda^2} - \frac{k^6}{a^6}\,\frac{c^{(6)}_{\alpha\beta}}{\Lambda^4} + \dots , \tag{14.29}$$

with the ellipses denoting terms of higher order in k that have been omitted, and Λ is some energy scale to render the elements of the $c^{(2n)}_{\alpha\beta}$ matrix dimensionless. Specifically, $c^{(2)}_{\alpha\beta}$ encapsulates all the sound speeds (squared) for the various fields.

Mass matrix and quadratic mixings. In general, the mass matrix $\bar{\mathcal{M}}_{\alpha\beta}$ renders analytical treatment delicate because it models complex processes such as energy exchange between various fields at the quadratic level. However, because the gradient terms in $\bar{\mathcal{K}}_{\alpha\beta}$ become increasingly important in the infinite past, they will eventually dominate the elements of $\bar{\mathcal{M}}_{\alpha\beta}$ provided that the (time-dependent) eigenvalues of the mass matrix are bounded from above. If one chooses an initial time such that contributions from the mass matrix become effectively irrelevant, each mode can be treated as massless. Therefore, we ignore the mass matrix for the remaining of this section. Similarly, one can always initialise the correlators deep enough in the past so that the gradient terms also dominate the quadratic couplings in the $\bar{I}_{\alpha\beta}$ matrix. We therefore ignore the quadratic coupling $\bar{I}_{\alpha\beta}$. In short, at sufficiently early times, the full quadratic theory will approach that of a set of *massless* and *uncoupled* degrees of freedom. Indeed, one can always diagonalise both kinetic terms with time and spatial derivatives in the same basis as they are both definite positive quadratic forms. Therefore, in the following, we will write in a non-covariant way the matrix elements $\bar{\Delta}_{\alpha\beta} = \delta^{\alpha\beta}\bar{\Delta}_{\alpha}$ and $\bar{\mathcal{K}}_{\alpha\beta} = \delta^{\alpha\beta}\bar{\mathcal{K}}_{\alpha}$.

Linear dispersion relations. For the remainder of this section, we assume that the kinetic terms for the fields only contain two spatial derivatives. We include the possibility of having different sound speeds for the fields by considering a generic diagonal matrix $c^{(2)}_{\alpha\beta} = \mathrm{diag}(c_1^2, c_2^2, \ldots)$. We highlight that the premise of our argument of analytically deriving initial conditions is not altered by this choice. However, other quadratic and diagonal theories such as theories with higher-order derivative terms require a different treatment. The quadratic theory we consider is

$$S^{(2)} = \frac{1}{2}\int \mathrm{d}t\, a^3 \left(\bar{\Delta}_\alpha \left(\dot{\boldsymbol{\varphi}}^\alpha\right)^2 - c_\alpha^2 \frac{k^2}{a^2} \left(\boldsymbol{\varphi}^\alpha\right)^2 \right) . \tag{14.30}$$

Initial two-point correlators. Referring the interested reader to the App. D for the derivation, the two-point correlator initial conditions are found to be

$$\Sigma^{ab}_{\mathrm{Re}} = \frac{1}{2a^2 c_\alpha k} \begin{pmatrix} \bar{\Delta}_{\alpha\beta}\left(1 + \frac{a^2H^2}{c_\alpha^2 k^2}\right) & -H\delta^{\alpha\beta} \\ -H\delta^{\alpha\beta} & c_\alpha^2 k^2\, \bar{\Delta}^{-1}_{\alpha\beta} \end{pmatrix} , \quad \Sigma^{ab}_{\mathrm{Im}} = \frac{1}{2a^3} \begin{pmatrix} 0 & \delta^{\alpha\beta} \\ -\delta^{\alpha\beta} & 0 \end{pmatrix} , \tag{14.31}$$

where all time-dependent quantities should be evaluated at the initial time. Note that in [549] the authors neglected the constant $\propto \frac{H^2}{2c_\alpha^3 k^3}$ mode in the $\langle \boldsymbol{\varphi}^\alpha \boldsymbol{\varphi}^\beta \rangle$ initial correlator. Even though this term is negligible on subhorizon scales, we include it to improve numerical stability. We also recall that $\Sigma^{ab}_{\mathrm{Im}}$ is completely fixed by the commutator, so that its initial condition in (14.31) is actually valid at all times. As an aside, notice that for small sound speeds $c_\alpha \ll 1$, the amplitude of $\langle \boldsymbol{\varphi}^\alpha \boldsymbol{\varphi}^\beta \rangle$ is enhanced whereas the amplitude of $\langle \boldsymbol{p}^\alpha \boldsymbol{p}^\beta \rangle$ is damped, intuitively reflecting the fact that the fields do not propagate in the limit $c_\alpha \to 0$.

14.4.2 Three-Point Correlators

The derivation of initial three-point correlators is more involved than that of initial two-point correlators. Computing correlators in the deep past instead of in the far future requires some foresight. Indeed, examining the Hamiltonian (14.6), the tensors $A_{\alpha\beta\gamma}, B_{\alpha\beta\gamma}, C_{\alpha\beta\gamma}$ and $D_{\alpha\beta\gamma}$ encode cubic interactions that can be of arbitrary order in derivatives, each gradient (squared) term giving a term of order $(k/a)^2 \sim (k\tau)^2$ that grows exponentially as we approach the limit $|\tau| \to \infty$. Therefore, terms with higher-order derivative will be the dominant contributions of the various correlators. Specifically, let us extract the momentum-conserving delta function of the cubic tensors to define the associated kernels

$$A_{\alpha\beta\gamma} = (2\pi)^3 \delta^{(3)}(\boldsymbol{k}_\alpha + \boldsymbol{k}_\beta + \boldsymbol{k}_\gamma)\, A_{\alpha\beta\gamma} , \tag{14.32}$$

and equivalent definitions for the tensors $B_{\alpha\beta\gamma}, C_{\alpha\beta\gamma}$ and $D_{\alpha\beta\gamma}$. We further decompose the above kernels by extracting the scale factor dependency that needs to be considered in the in-in integral, according to the number of spatial derivatives it contains, as follows[7]

$$A_{\alpha\beta\gamma} = A^{(0)}_{\alpha\beta\gamma} + \frac{1}{a^2} A^{(2)}_{\alpha\beta\gamma} + \frac{1}{a^4} A^{(4)}_{\alpha\beta\gamma} + \ldots , \tag{14.33}$$

[7] Non-local interactions characterised by inverse gradient terms are completely negligible in this regime compared to usual derivative interactions so we do not consider this possibility.

and similarly for the other kernels. We have absorbed all momentum dependency in the newly defined kernels, and indicate with the superscript $2n$ ($n \geq 0$) the number of spatial derivatives that appears in the cubic interaction. For a given cubic interaction, the higher the number of spatial derivatives, the (exponentially) faster these terms grow on subhorizon scales. Consequently, it is essential to keep track of every order in powers of τ to avoid creating a large hierarchy between cubic interactions. By explicitly computing the in-in integrals, we include all possible cubic interactions to all order in (spatial) derivatives. The full derivation is a bit lengthy, so we jump directly to the final results without loss of continuity, leaving all the details in App. D.

Three fields initial correlator:

$$\begin{aligned}
\langle \boldsymbol{\varphi}^{\alpha}_{\boldsymbol{k}_1} \boldsymbol{\varphi}^{\beta}_{\boldsymbol{k}_2} \boldsymbol{\varphi}^{\gamma}_{\boldsymbol{k}_3} \rangle_0 = \frac{(2\pi)^3 \delta^{(3)}(\Sigma_i \boldsymbol{k}_i)}{4a^4 e_3 k_t} \Bigg\{ & \frac{A^{(0)}_{\alpha\beta\gamma}}{2} a^2 + \frac{A^{(2)}_{\alpha\beta\gamma}}{2} \left[1 + \frac{a^2 H^2}{e_3^2} \left(e_2 \left(e_2 + \frac{e_3}{k_t} \right) \right) - k_t e_3 \right] \\
& + \frac{A^{(4)}_{\alpha\beta\gamma}}{2} \left[\frac{1}{a^2} + \frac{H^2}{e_3^2} \left(e_2 \left(e_2 + \frac{3e_3}{k_t} \right) \right) - k_t e_3 \right] + \ldots - \frac{B^{(0)}_{\alpha\beta\gamma}}{2} \frac{a^2 H}{k_1 k_2} \left[e_2 - k_3 (k_1 + k_2) \right] \\
& - \frac{B^{(2)}_{\alpha\beta\gamma}}{2} \frac{H}{k_1 k_2} \left[e_2 - \frac{1}{k_t} (2e_3 + k_t (k_1 + k_2) k_3) \right] - \frac{B^{(4)}_{\alpha\beta\gamma}}{2} \frac{H}{a^2 k_1 k_2} \left[e_2 - \frac{1}{k_t} (4e_3 + k_t (k_1 + k_2) k_3) \right] \\
& - \frac{C^{(0)}_{\alpha\beta\gamma}}{2} \left[k_1 k_2 + a^2 H^2 \left(\frac{e_2}{k_3^2} \left(1 + \frac{k_3}{k_t} \right) \right) - \frac{k_t}{k_3} \right] - \frac{C^{(2)}_{\alpha\beta\gamma}}{2} \left[\frac{k_1 k_2}{a^2} + H^2 \left(\frac{e_2}{k_3^2} \left(1 + \frac{3k_3}{k_t} \right) \right) - \frac{k_t}{k_3} \right] \\
& - \frac{C^{(4)}_{\alpha\beta\gamma}}{2} \left[\frac{k_1 k_2}{a^4} + \frac{H^2}{a^2} \left(\frac{e_2}{k_3^2} \left(1 + \frac{5k_3}{k_t} \right) \right) - \frac{k_t}{k_3} \right] + \ldots + \frac{D^{(0)}_{\alpha\beta\gamma}}{2} H \left[e_2 - \frac{2e_3}{k_t} \right] \\
& + \frac{D^{(2)}_{\alpha\beta\gamma}}{2} \frac{H}{a^2} \left[e_2 - \frac{4e_3}{k_t} \right] + \frac{D^{(4)}_{\alpha\beta\gamma}}{2} \frac{H}{a^4} \left[e_2 - \frac{6e_3}{k_t} \right] + \cdots + \text{ 5 perms} \Bigg\} .
\end{aligned} \tag{14.34}$$

Two fields and one momentum initial correlator:

$$\begin{aligned}
\langle \boldsymbol{p}^{\alpha}_{\boldsymbol{k}_1} \boldsymbol{\varphi}^{\beta}_{\boldsymbol{k}_2} \boldsymbol{\varphi}^{\gamma}_{\boldsymbol{k}_3} \rangle_0 = \frac{-(2\pi)^3 \delta^{(3)}(\Sigma_i \boldsymbol{k}_i)\, H}{4a^3 e_3^2 k_t} \Bigg\{ & -k_1 \left[-\frac{A^{(0)}_{\alpha\beta\gamma}}{2} a^2 \left(e_2 - \frac{e_3}{k_t} \right) - \frac{A^{(2)}_{\alpha\beta\gamma}}{2} \left(e_2 + \frac{e_3}{k_t} \right) \right. \\
& - \frac{A^{(4)}_{\alpha\beta\gamma}}{2} \frac{1}{a^2} \left(e_2 + \frac{3e_3}{k_t} \right) + \cdots + \frac{B^{(0)}_{\alpha\beta\gamma}}{2H} e_3 k_3 + \frac{B^{(2)}_{\alpha\beta\gamma}}{2H} \frac{e_3 k_3}{a^2} + \frac{B^{(4)}_{\alpha\beta\gamma}}{2H} \frac{e_3 k_3}{a^4} + \ldots \\
& + \frac{C^{(0)}_{\alpha\beta\gamma}}{2} k_1^2 k_2^2 \left(1 + \frac{k_3}{k_t} \right) + \frac{C^{(2)}_{\alpha\beta\gamma}}{2} \frac{k_1^2 k_2^2}{a^2} \left(1 + \frac{3k_3}{k_t} \right) + \frac{C^{(4)}_{\alpha\beta\gamma}}{2} \frac{k_1^2 k_2^2}{a^4} \left(1 + \frac{5k_3}{k_t} \right) + \ldots \\
& \left. - \frac{D^{(0)}_{\alpha\beta\gamma}}{2H} \frac{e_3^2}{a^2} - \frac{D^{(2)}_{\alpha\beta\gamma}}{2H} \frac{e_3^2}{a^4} - \frac{D^{(4)}_{\alpha\beta\gamma}}{2H} \frac{e_3^2}{a^6} + \cdots + \text{ 5 perms} \right] - k_1^2 (k_2 + k_3) \left[\frac{A^{(0)}_{\alpha\beta\gamma}}{2} a^2 \right. \\
& + \frac{A^{(2)}_{\alpha\beta\gamma}}{2} + \frac{A^{(4)}_{\alpha\beta\gamma}}{2} \frac{1}{a^2} + \cdots + \frac{B^{(0)}_{\alpha\beta\gamma}}{2} a^2 H \frac{(k_1 + k_2) k_3^2}{e_3} + \frac{B^{(2)}_{\alpha\beta\gamma}}{2} \frac{H k_3}{e_3 k_t} (2e_3 + k_t (k_1 + k_2) k_3) \\
& \left. + \frac{B^{(4)}_{\alpha\beta\gamma}}{2} \frac{H}{a^2} \frac{k_3}{e_3 k_t} (4e_3 + k_t (k_1 + k_2) k_3) + \cdots - \frac{C^{(0)}_{\alpha\beta\gamma}}{2} k_1 k_2 - \frac{C^{(2)}_{\alpha\beta\gamma}}{2} \frac{k_1 k_2}{a^2} - \frac{C^{(4)}_{\alpha\beta\gamma}}{2} \frac{k_1 k_2}{a^4} + \ldots \right.
\end{aligned} \tag{14.35}$$

$$-D^{(0)}_{\alpha\beta\gamma}\,\frac{He_3}{k_t}-2D^{(0)}_{\alpha\beta\gamma}\,\frac{H}{a^2}\,\frac{e_3}{k_t}-3D^{(0)}_{\alpha\beta\gamma}\,\frac{H}{a^4}\,\frac{e_3}{k_t}+\ 5\ \text{perms}\Big]\Big\}\,.$$

Two momenta and one field initial correlator:

$$\begin{aligned}
\langle \boldsymbol{p}^{\alpha}_{\boldsymbol{k}_1}\boldsymbol{p}^{\beta}_{\boldsymbol{k}_2}\boldsymbol{\varphi}^{\gamma}_{\boldsymbol{k}_3}\rangle_0 = \frac{-(2\pi)^3\delta^{(3)}(\Sigma_i\boldsymbol{k}_i)}{4a^4e_3k_t}\Bigg\{&k_1k_2\Bigg[\frac{A^{(0)}_{\alpha\beta\gamma}}{2}\,a^2+\frac{A^{(2)}_{\alpha\beta\gamma}}{2}+\frac{A^{(4)}_{\alpha\beta\gamma}}{2}\,\frac{1}{a^2}+\dots\\
&+\frac{B^{(0)}_{\alpha\beta\gamma}}{2}\,a^2H\,\frac{(k_1+k_2)k_3^2}{e_3}+\frac{B^{(2)}_{\alpha\beta\gamma}}{2}\,H\,\frac{k_3}{e_3k_t}\,(2e_3+k_t(k_1+k_2)k_3)+\\
&+\frac{B^{(4)}_{\alpha\beta\gamma}}{2}\,\frac{H}{a^2}\,\frac{k_3}{e_3k_t}\,(4e_3+k_t(k_1+k_2)k_3)+\dots-\frac{C^{(0)}_{\alpha\beta\gamma}}{2}\,k_1k_2-\frac{C^{(2)}_{\alpha\beta\gamma}}{2}\,\frac{k_1k_2}{a^2}-\frac{C^{(4)}_{\alpha\beta\gamma}}{2}\,\frac{k_1k_2}{a^4}+\dots\\
&-D^{(0)}_{\alpha\beta\gamma}\,\frac{He_3}{k_t}-2D^{(2)}_{\alpha\beta\gamma}\,\frac{H}{a^2}\,\frac{e_3}{k_t}-3D^{(4)}_{\alpha\beta\gamma}\,\frac{H}{a^4}\,\frac{e_3}{k_t}+\dots+\ 5\ \text{perms}\Bigg]\\
&+k_1^2k_2^2\Bigg[\frac{A^{(0)}_{\alpha\beta\gamma}}{2}\,\frac{a^4H^2}{e_3}\left(e_2-\frac{e_3}{k_t}\right)+\frac{A^{(2)}_{\alpha\beta\gamma}}{2}\,\frac{a^2H^2}{e_3}\left(e_2+\frac{e_3}{k_t}\right)+\frac{A^{(4)}_{\alpha\beta\gamma}}{2}\,\frac{H^2}{e_3}\left(e_2+\frac{3e_3}{k_t}\right)+\dots\\
&-\frac{B^{(0)}_{\alpha\beta\gamma}}{2}\,a^2Hk_3-\frac{B^{(2)}_{\alpha\beta\gamma}}{2}\,Hk_3-\frac{B^{(4)}_{\alpha\beta\gamma}}{2}\,\frac{H}{a^2k_3}+\dots-\frac{C^{(0)}_{\alpha\beta\gamma}}{2}\,a^2H^2\,\frac{k_1^2k_2^2}{e_3^2}\left(1+\frac{k_3}{k_t}\right)\\
&-\frac{C^{(2)}_{\alpha\beta\gamma}}{2}\,H^2\,\frac{k_1^2k_2^2}{e_3^2}\left(1+\frac{3k_3}{k_t}\right)-\frac{C^{(4)}_{\alpha\beta\gamma}}{2}\,\frac{H^2}{a^2}\,\frac{k_1^2k_2^2}{e_3^2}\left(1+\frac{5k_3}{k_t}\right)+\frac{D^{(0)}_{\alpha\beta\gamma}}{2}\,H+\frac{D^{(2)}_{\alpha\beta\gamma}}{2}\,\frac{H}{a^2}\\
&+\frac{D^{(4)}_{\alpha\beta\gamma}}{2}\,\frac{H^2}{a^4}+\dots+\ 5\ \text{perms}\Bigg]\Bigg\}\,.
\end{aligned}\tag{14.36}$$

Three momenta initial correlator:

$$\begin{aligned}
\langle \boldsymbol{p}^{\alpha}_{\boldsymbol{k}_1}\boldsymbol{p}^{\beta}_{\boldsymbol{k}_2}\boldsymbol{p}^{\gamma}_{\boldsymbol{k}_3}\rangle_0 = \frac{(2\pi)^3\delta^{(3)}(\Sigma_i\boldsymbol{k}_i)\,H}{4a^3e_3k_t}\Bigg\{&\frac{A^{(0)}_{\alpha\beta\gamma}}{2}\,a^2\left(e_2-\frac{e_3}{k_t}\right)+\frac{A^{(2)}_{\alpha\beta\gamma}}{2}\left(e_2+\frac{e_3}{k_t}\right)\\
&+\frac{A^{(4)}_{\alpha\beta\gamma}}{2}\,\frac{1}{a^2}\left(e_2+\frac{3e_3}{k_t}\right)+\dots-\frac{B^{(0)}_{\alpha\beta\gamma}}{2H}\,e_3k_3-\frac{B^{(2)}_{\alpha\beta\gamma}}{2H}\,\frac{e_3k_3}{a^2}-\frac{B^{(4)}_{\alpha\beta\gamma}}{2H}\,\frac{e_3k_3}{a^4}+\dots\\
&-\frac{C^{(0)}_{\alpha\beta\gamma}}{2}\,k_1^2k_2^2\left(1+\frac{k_3}{k_t}\right)-\frac{C^{(2)}_{\alpha\beta\gamma}}{2}\,\frac{k_1^2k_2^2}{a^2}\left(1+\frac{3k_3}{k_t}\right)-\frac{C^{(4)}_{\alpha\beta\gamma}}{2}\,\frac{k_1^2k_2^2}{a^4}\left(1+\frac{5k_3}{k_t}\right)+\dots\\
&+\frac{D^{(0)}_{\alpha\beta\gamma}}{2H}\,\frac{e_3^2}{a^2}+\frac{D^{(2)}_{\alpha\beta\gamma}}{2H}\,\frac{e_3^2}{a^4}+\frac{D^{(4)}_{\alpha\beta\gamma}}{2H}\,\frac{e_3^2}{a^6}+\dots+\ 5\ \text{perms}\Bigg\}\,,
\end{aligned}\tag{14.37}$$

where we have introduced the symmetric polynomials $e_1\equiv k_t=k_1+k_2+k_3$, $e_2\equiv k_1k_2+k_1k_3+k_2k_3$, and $e_3\equiv k_1k_2k_3$. We have coloured in blue the powers of the scale factor to render the size of the various terms in the subhorizon regime manifest. The momentum dependencies of the various kernels are not written explicitly but these need to be regarded as functions of $\boldsymbol{k}_1,\boldsymbol{k}_2$ and $\boldsymbol{k}_3$ associated with each index α,β and γ respectively. When writing the permutations for the kernels $A^{(2n)}_{\alpha\beta\gamma}, B^{(2n)}_{\alpha\beta\gamma}, C^{(2n)}_{\alpha\beta\gamma}$ and $D^{(2n)}_{\alpha\beta\gamma}$, one should also exchange the associated momenta. Additional manipulations

are needed when the fields are not canonically normalised. We leave this detail to App. D. In the end, note that these initial conditions are completely fixed by the tensor elements, or equivalently by the Hamiltonian.

Numerical $i\epsilon$ prescription. An alternative valid procedure consists in initialising the three-point correlators to zero and letting them build up as the cubic interactions are switched on adiabatically before reaching the attractor solution given by the flow equations. This method essentially encapsulates the essence and *defines* the $i\epsilon$ prescription. Such prescription is simple and useful when dealing with other interactions and higher-order correlators. We have checked numerically for several examples that it is equivalent to using the initial conditions (14.34)–(14.37).

14.5 CosmoFlow: Python Package for Cosmological Correlators

We have implemented the cosmological flow in an open source Python package designed to compute cosmological correlators: CosmoFlow. This numerical implementation is about integrating by differentiating, and is completely equivalent to the canonical in-in Schwinger-Keldysh formalism. Our code can compute any tree-level two- and three-point correlators in any theory in all kinematic configurations. It has clear separation between the physics and the technical implementation details, and is designed so that computations can be performed with different parameters, without requiring to re-implement different theories each time. This allows the user to easily navigate through various theories. Our main credo while developing CosmoFlow is *simplicity*. Therefore, even for basic-level users, we believe that using and editing the code, as well as implementing new theories, are elementary tasks. The code and numerous ready-to-be-executed notebooks are available on GitHub.

Why is CosmoFlow useful? The huge complexity in computing cosmological correlators has compelled theorists to focus on rather simple theories, and correlators are typically computed under several stringent assumptions.[8] This includes for example studying single-field theories with perfect or almost-perfect scale invariance. When several fields are considered, particles are assumed to be weakly mixed, and only single-exchange diagrams are reliably computed at tree-level, even if it is known that they do not lead to the largest signal in the sky. A large hierarchy of masses and couplings are considered for analytical purposes in the most complicated situations, not probing intermediate regimes. Similarly, it is often the case that only particular kinematic limits can be computed analytically, like equilateral or soft configurations, not covering mildly soft ones where the signal-to-noise ratio can be the largest. Ultimately, the rare closed-form expressions in the entirety of the kinematic configurations and for certain diagrams are difficult to exploit in practice because they are written in terms of slowly-converging series. It is worth

[8] Even numerically, the convergence of the integrals in the UV with the $i\epsilon$ prescription has always been a long-standing problem, see e.g. [557, 558, 559, 560].

stressing that there are noticeable exceptions in the literature to each of the points above separately. Nevertheless, it is fair to say that state-of-the-art technics face limitations, that current predictions do not cover the entire space of cosmological correlators, and that it will always be the fate of analytical methods. A complete dictionary between theory and observables is not yet complete, which can lead to a biased interpretation of current and future cosmological data. With CosmoFlow, our aim is to fill this gap.

What does CosmoFlow compute? In its current version, the numerical implementation of the cosmological flow takes as an input a theory up to cubic order in the fields, i.e. a Lagrangian or equivalently a Hamiltonian. This theory can feature an arbitrary number of scalar degrees of freedom with arbitrary dispersion relations, masses and quadratic mixings (or more generally any quadratic theory), coupled through any type of interactions that can have any time dependence. This encompasses all known theories conveniently formulated at the level of fluctuations. The CosmoFlow outputs are *all* tree-level two- and three-point correlators in phase space, i.e. including those that involve multiple field species and conjugate momenta, at any time during inflation and in all kinematic configurations in Fourier space.

Who would benefit from CosmoFlow? The utility of our code extends to a broad audience. First, it holds potential benefits for theorists interested in formal aspects of cosmological correlators. We have made an effort to render CosmoFlow easy to use. Its elementary implementation enables one to navigate through the modules without effort, and to quickly master their usage, even for those without any experience with Python. CosmoFlow enables one to obtain exact (numerical) results for correlators for which analytical solutions are completely out of reach. Second, the code can be of great interest to primordial cosmologists, from those interested in the phenomenology of primordial non-Gaussianities to model builders of inflationary theories. With this code, we have automatised the process of going from a theory to observables. This enables cosmologists to study inflationary theories and their observational signatures in a systematic fashion and in full generality, without being limited by technicalities. Moreover, the cosmological flow approach allows for a direct insight into the bulk dynamics of correlators, which enables one to elucidate, e.g. , characteristic time scales to guide physical intuition. Finally, CosmoFlow can be used by cosmologists interested in the later-time Universe as it essentially generates the inputs to be given to pipelines that propagate fluctuations during the Hot Big Bang Universe until the present day, be it correlators, directly the full map-level fields, or simulations.

We have designed CosmoFlow to be flexible, in the sense that it can be easily modified, improved and generalised. We believe that this goal can be reached by having a simple architecture and no hard coding. The CosmoFlow implementation has a clear structure, separated in modules that fully exploit the object-oriented programming paradigm of Python with well defined tasks.

15

Exploring the Phenomenology of Cosmological Correlators

Similar to what automated tools brought to the particle physics community, the cosmological flow offers new possibilities for the study of inflation. This shift in perspective enables us to move beyond the technical achievement of computing inflationary correlators within a limited subset of the landscape of theories and instead embark on a journey to explore the physics of inflation in full generality. With the cosmological flow, being able to have direct access to the bulk time evolution of correlators is particularly useful in conjunction with analytical works and to extend the present reach of inflationary correlator phenomenology. It enables one to easily shed light on characteristic time scales at play and give new insights on identifying various physical regimes in complex scenarios that cannot be reached analytically. As an application, we show that the frequency of the cosmological collider signal may not be solely dictated by the mass of an additional field. Specifically, at strong mixing or in the presence of features—emerging from time-dependent couplings—, we derive new cosmological collider signals that break the direct link relating frequency and mass. With CosmoFlow as a first building-block, we pave the way for a far-reaching program of exploring the rich physics of inflation.

In this chapter, we provide exact results for the size and shape of non-Gaussianities and a complete understanding of the physics at play in the entire parameter space of the canonical theory of the Goldstone boson of broken time translations coupled to a massive scalar field (see Chap. 9), including the strong mixing regime. We then showcase that the cosmological flow can systematically account for time-dependent couplings. We study both features that cannot be described by an effective single-field theory, and the corresponding cosmological collider signals. We show, with minimal assumptions, that the link between the frequency of the cosmological collider signal and the mass of an additional particle can be explicitly broken, leading

to striking new observable signatures.

Theory implementation. For concreteness, we will entirely focus on the theory (9.53) (see Sec. 9.4.1). In order to implement the flow equations for the fields $\boldsymbol{\varphi}^\alpha = (\pi_c, \sigma)$, one needs to write the theory in a Hamiltonian form. The rescaled linear conjugate momenta associated with the fields are

$$p_{\pi_c} \equiv \frac{1}{a^3}\frac{\delta S}{\delta \dot{\pi}_c} = \dot{\pi}_c + \rho\sigma\,, \quad p_\sigma \equiv \frac{1}{a^3}\frac{\delta S}{\delta \dot{\sigma}} = \dot{\sigma}\,. \tag{15.1}$$

After performing the Legendre transform, the Hamiltonian can be arranged in the form (14.6) and the identification of the various tensors yields

$$\begin{aligned}
&\Delta_{\alpha\beta} = \delta_{\alpha\beta}\,, \qquad M_{\alpha\beta} = \begin{pmatrix} -c_s^2\frac{k^2}{a^2} & 0 \\ 0 & -\left(\frac{k^2}{a^2} + m^2 + \rho^2\right) \end{pmatrix}, \qquad I_{\alpha\beta} = \begin{pmatrix} 0 & \rho \\ 0 & 0 \end{pmatrix}, \\
&A_{\sigma\sigma\sigma} = -2\mu + \alpha\rho - \frac{\rho^2}{\Lambda_2} + 2\lambda_2\rho^3\,, \quad A_{\pi_c\pi_c\sigma} = \left(\frac{1}{\Lambda_1} - 2\lambda_1\rho\right)\frac{\boldsymbol{k}_{\pi_c}\cdot\boldsymbol{k}_{\pi_c}}{a^2}\,, \\
&B_{\sigma\sigma p_{\pi_c}} = -\alpha + 2\frac{\rho}{\Lambda_2} - 6\lambda_2\rho^2\,, \qquad B_{\pi_c\pi_c p_{\pi_c}} = 2\lambda_1\frac{\boldsymbol{k}_{\pi_c}\cdot\boldsymbol{k}_{\pi_c}}{a^2}\,, \\
&C_{p_{\pi_c}p_{\pi_c}\sigma} = -\frac{1}{\Lambda_2} + 6\lambda_2\rho\,, \qquad D_{p_{\pi_c}p_{\pi_c}p_{\pi_c}} = -2\lambda_2\,.
\end{aligned} \tag{15.2}$$

Deriving these tensors fully fixes the flow equations and the initial conditions for the two- and three-point functions. It is also necessary to relate the various correlators to primordial observables, namely correlators of the curvature perturbation ζ. Using (9.36) up to quadratic order, which is sufficient to work out the power spectrum and bispectrum, we find

$$\begin{aligned}
\langle\zeta_{\boldsymbol{k}}\zeta_{-\boldsymbol{k}}\rangle' &= H^2\,\langle\pi_{\boldsymbol{k}}\pi_{-\boldsymbol{k}}\rangle'\,, \\
\langle\zeta_{\boldsymbol{k}_1}\zeta_{\boldsymbol{k}_2}\zeta_{\boldsymbol{k}_3}\rangle' &= -H^3\,\langle\pi_{\boldsymbol{k}_1}\pi_{\boldsymbol{k}_2}\pi_{\boldsymbol{k}_3}\rangle' + H^3\left[\Sigma^{\pi\pi}(k_1)\Sigma^{\pi\dot{\pi}}_{\mathrm{Re}}(k_2) + 5\text{ perms}\right] \\
&\quad + H^2\dot{H}\left[\Sigma^{\pi\pi}(k_1)\Sigma^{\pi\pi}(k_2) + \text{ 2 perms}\right],
\end{aligned} \tag{15.3}$$

where all correlators should be evaluated at the end of inflation. A few comments are in order. First, the result (15.3) is valid in any theory, be it single-clock or with multiple degrees of freedom. Second, no decoupling limit or slow-roll approximation has been considered here, only that modes are well outside the horizon. Note also that even in single-clock inflation, π is strictly speaking not massless and is time-dependent even outside the horizon. However, the time dependence of H, π and $\dot{\pi}$ are such that the correlators of ζ themselves become time-independent in that case. Eventually, in the applications considered in this thesis, where any time-dependence of H is neglected, only the first line is relevant in the expression of the bispectrum. Notice also that the surviving correction to the bispectrum of π can be rewritten in terms of correlators of fields and conjugate momenta, see Eq. (15.1). This shift of perspective is useful as even when multi-field interactions keep building up on super-horizon scales, the cross power spectrum involving the momentum of π quickly decays and only remains the contribution from the mixed π-σ power spectrum. This situation occurs only when the field σ is almost massless. However, in this situation,

ζ keeps evolving until the end of inflation, which effectively breaks scale invariance and makes the theory non-predictive without a complete description of reheating. When σ is effectively heavy, it quickly decays on super-horizon scales, an adiabatic limit is then reached by the end of inflation, and the bispectrum of ζ is directly proportional to the one of π. The large majority of our applications lie in this regime.

15.1 Quadratic Theory

We begin the study of this theory by examining the time evolution of the various two-point functions. In this section, we start by introducing the notion of effective mass that emerges from a sizeable quadratic mixing. Then, we provide exact results—derived for the first time using the cosmological flow—for the power spectrum in all regimes of interest including the strong mixing regime. This provides a comprehensive analysis of the entire quadratic phase space. We encourage the reader to look at the complementary Sec. 10.3 where we give analytical insights of these regimes.

15.1.1 Effective Mass & Resonance at Strong Mixing

Writing the theory in the Hamiltonian form makes it explicit that the quadratic mixing induces an effective mass for the σ field

$$m_{\rm eff}^2 = m^2 + \rho^2 \,, \tag{15.4}$$

that can be appreciated from the form of the M matrix in Eq. (15.2). This is a consequence of considering the full linear momenta, i.e. the conjugate momentum of π_c is corrected due to the quadratic mixing.

Late-time leading behaviour. To understand the origin of the effective mass at energy scales $\omega \ll H$, it is sufficient to look at the leading late-time behaviour of the $\pi_c - \sigma$ system. Looking for solutions of the form

$$\lim_{\tau\to 0} \begin{pmatrix} \pi_c(\tau,\boldsymbol{x}) \\ \sigma(\tau,\boldsymbol{x}) \end{pmatrix} = \begin{pmatrix} \pi_c^+(\boldsymbol{x}) \\ \sigma^+(\boldsymbol{x}) \end{pmatrix} \tau^{\Delta_+} + \begin{pmatrix} \pi_c^-(\boldsymbol{x}) \\ \sigma^-(\boldsymbol{x}) \end{pmatrix} \tau^{\Delta_-} \,, \tag{15.5}$$

one finds four modes with scaling dimensions

$$\Delta_-^{\pi_c} = 0 \,, \quad \Delta_+^{\pi_c} = 3 \,, \quad \Delta_\pm^{\sigma} = \frac{3}{2} \pm i\mu_{\rm eff} \,, \tag{15.6}$$

with $\mu_{\rm eff}^2 = m_{\rm eff}^2/H^2 - 9/4$, which makes it manifest that the system is composed of two modes corresponding to a massless field ($\Delta_\pm^{\pi_c}$) and a decaying massive field ($\Delta_\pm^{\sigma}$) with effective mass $m_{\rm eff}$.

Flat-space leading behaviour. At sufficient high energies $\omega \gg H$,[1] the dynamics of the theory can be approximated by the flat-space limit $H \to 0$, in which case the system can be solved analytically up to Hubble friction corrections.[2] Here, we explicitly show that, even if the quadratic mixing cannot a priori be treated perturbatively, the analytical solution of the quadratic theory follows from resumming an infinite number of quadratic mixing insertions in the propagators of the two degrees of freedom. Focusing on the field σ, its dynamics is affected by the surrounding π_c medium that interacts with it, leading to a self-energy correction. At tree-level as we only consider quadratic interactions, it reads

$$\Pi(\omega, \boldsymbol{k}) = \quad = \frac{-i\rho^2\omega^2}{\omega^2 - c_s^2 k_{\rm p}^2 + i\epsilon}\,, \tag{15.8}$$

that is found from the following elementary Feynman rules

$$\begin{aligned} G^0_{\pi_c}(\omega, \boldsymbol{k}) = \quad &= \frac{i}{\omega^2 - c_s^2 k_{\rm p}^2 + i\epsilon}, \qquad \quad = -i\rho\,\omega\,, \\ G^0_{\sigma}(\omega, \boldsymbol{k}) = \quad &= \frac{i}{\omega^2 - k_{\rm p}^2 - m^2 + i\epsilon}\,, \end{aligned} \tag{15.9}$$

where $G^0_{\pi_c}$ (resp. G^0_σ) is the free π_c (resp. σ) Green two-point function. From the bare propagator, the dressed propagator $G_\sigma(\omega, \boldsymbol{k})$ is found by computing the associated Dyson series summing over all one-particle irreducible diagrams—in our case the tree-level contribution. Summing the geometrical series, we have

$$\begin{aligned} G_\sigma(\omega, \boldsymbol{k}) = \quad &+ \quad + \quad + \ldots \\ &= G^0_\sigma(\omega, \boldsymbol{k}) \sum_{n=0}^{\infty} \left[\Pi(\omega, \boldsymbol{k}) G^0_\sigma(\omega, \boldsymbol{k})\right]^n = \frac{i}{\omega^2 - k_{\rm p}^2 - m^2 - \rho^2 \left[\frac{\omega^2}{\omega^2 - c_s^2 k_{\rm p}^2}\right] + i\epsilon}\,, \end{aligned} \tag{15.10}$$

which agrees with (15.7). Non-trivial plane-wave solutions for the propagating modes are found at the poles of the dressed propagator

$$\omega_\pm^2 = \frac{1 + c_s^2}{2}\, k_{\rm p}^2 + \frac{m_{\rm eff}^2}{2} \pm \frac{1}{2}\sqrt{m_{\rm eff}^4 + (1 - c_s^2)^2\, k_{\rm p}^4 + 2(1 + c_s^2)\, k_{\rm p}^2 \left[\rho^2 + \frac{1 - c_s^2}{1 + c_s^2}\, m^2\right]}. \tag{15.11}$$

We wish to highlight several features of this result by examining various limits. At very high momenta $k_{\rm p} \gg \rho, m$, the dispersion relation boils down to $\omega_-^2 \approx c_s^2 k_{\rm p}^2$ and $\omega_+ \approx k_{\rm p}^2$ which describes two independent massless free fields, i.e. the vacuum state

[1] In the strong mixing regime $\rho \gg H$, the flat-space limit is reached for energies such that $\omega \gg \rho$.

[2] By looking at plane-wave solutions of the form $\pi_c \propto e^{i\omega t}$ and $\sigma \propto e^{i\omega t}$, the Feynman propagator for the fields $\varphi^\alpha = (\pi_c, \sigma)$ is found by inverting the quadratic operator

$$\langle \mathcal{T}(\varphi^T_{\boldsymbol{k}} \varphi_{-\boldsymbol{k}})\rangle = \frac{i}{\left(\omega^2 - c_s^2 k_{\rm p}^2\right)\left(\omega^2 - k_{\rm p}^2 - m^2\right) - \rho^2\omega^2 + i\epsilon} \begin{pmatrix} \omega^2 - k_{\rm p}^2 - m^2 & -i\rho\omega \\ i\rho\omega & \omega^2 - c_s^2 k_{\rm p}^2 \end{pmatrix}. \tag{15.7}$$

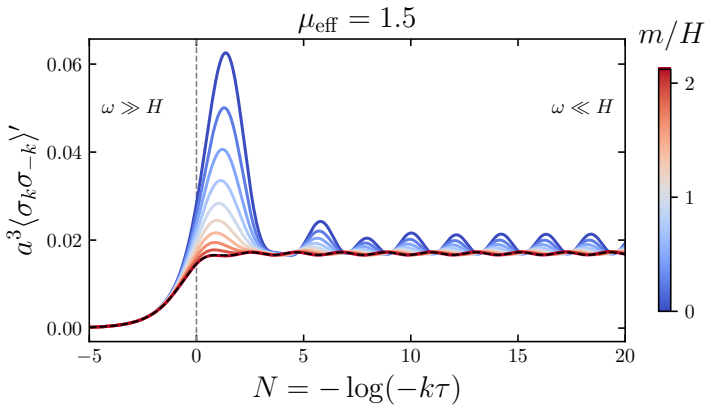


Figure 15.1: Time evolution of the rescaled σ two-point correlation function in Hubble units for a fixed *effective* mass such that $\mu_{\rm eff} = 1.5$ and $c_s = 1$, varying the *bare* mass m. The dotted black line corresponds to the analytical prediction in the decoupled regime $\rho/H = 0$. The vertical dotted line shows the energy scale at which the correlators cross the horizon $|k\tau| = 1$.

in the asymptotic past limit of the inflationary spacetime. In the strong mixing regime $\rho \gg k_{\rm p}, m$, one finds

$$\omega_-^2 \approx \frac{k_{\rm p}^2}{\rho^2}\left(c_s^2 k_{\rm p}^2 + m^2\right), \qquad \omega_+^2 \approx m_{\rm eff}^2 \approx \rho^2, \tag{15.12}$$

which describes a massless degree of freedom and a massive degree of freedom with mass $m_{\rm eff}^2 = m^2 + \rho^2$. We note that in the UV limit $k_{\rm p} \gg m$, the massless degree of freedom has a modified dispersion relation $\omega \propto k_{\rm p}^2$. In the rest of this section, we set $c_s = 1$ to avoid clutter.

Resonance at strong mixing. The appearance of the effective mass both in the deep UV and in the late IR suggests that a similar resummation in the intermediate regime—around horizon crossing—is compelling. Fig. 15.1 shows the time evolution of the σ two-point correlation function rescaled by a^3 for a fixed *effective* mass $\mu_{\rm eff} = 1.5$ while varying the *bare* mass (hence also adjusting the quadratic mixing). At late times $\omega \ll H$, as explained by the previous late-time analysis, one can appreciate that the correlators oscillate at the same frequency set by $\mu_{\rm eff}$. The amplitude of the oscillations and the mean value of the two-point function grow as the *bare* mass m decreases. Furthermore, another notable feature is that the oscillations present a *phase shift* as the quadratic mixing constant ρ/H increases. This is due to a noticeable phenomenon, namely the amplification of the massive correlator soon after Hubble crossing, which induces a time delay before the late-time asymptotic regime is reached. This effect can be explained by examining the strong mixing regime of the $\pi_c - \sigma$ dynamics:[3]

(*i*) At the *effective mass-shell horizon* $|k\tau| \sim \mu_{\rm eff}$, the massive field starts to decay as $a^{-3/2}$,

[3]We recall that we have set $c_s = 1$ so that the following arguments are valid for a unity intrinsic sound speed only.

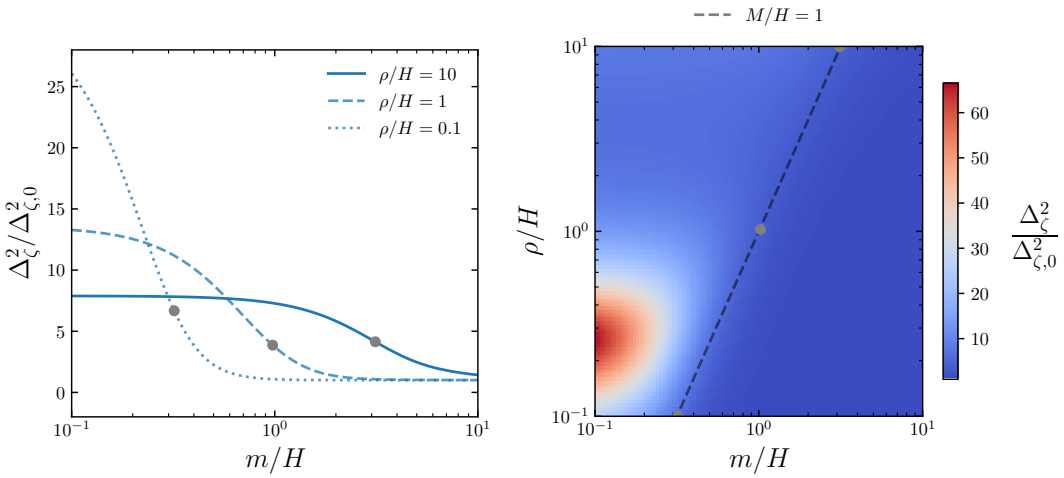


Figure 15.2: *Right panel* : Phase diagram of the dimensionless power spectrum Δ^2_ζ (in units of $\Delta^2_{\zeta,0}$). We have set $N = 60$ e-folds of super-horizon evolution. The dashed line corresponds to the $M = m^2/\rho = H$ delimitation, isolating the modified dispersion relation regime ($M \ll H$ and $\rho \gg H$) and the reduced speed of sound regime ($M \gg H$) (see Fig. 10.2 for more details). *Left panel* : Slices of the phase diagram for $\rho/H = 10$, $\rho/H = 1$, and $\rho/H = 0.1$ as a function of the bare mass m/H in Hubble units. The grey dots mark the $M/H = 1$ delimitation. Note that the the quadratic interaction between π_c and σ alters the symmetry breaking scale $f_\pi \approx 58H \times (\Delta^2_\zeta/\Delta^2_{\zeta,0})^{1/4}$, where $\Delta^2_{\zeta,0} \equiv (H/f_\pi)^4/4\pi^2$.

(*ii*) At the *ρ-horizon crossing* $|k\tau| \sim \sqrt{\rho/H}$, the Goldstone boson freezes, see Sec. 10.3.

At strong quadratic mixing, the event (*i*) occurs before (*ii*).[4] Therefore, when the massive field starts to decay, it transfers its power to the Goldstone boson, creating the $\sqrt{\rho/H}$ amplification of the power spectrum (see next section). Because the dynamics is dominated by the quadratic mixing, the Goldstone boson backreacts on the massive field after horizon crossing $\omega = H$, creating the visible boost in Fig. 15.1. The precise dynamics can only be accessed numerically. This interesting phenomenon is also visible in the cosmological collider signal, as we will see later.

15.1.2 Phase Diagram

The entire phase space (m, ρ) is not accessible analytically (recall we fix $c_s = 1$). In Fig. 15.2, we show the dimensionless power spectrum as a function of ρ/H and m/H, computed by solving the flow equations. Limiting regimes can be accessed analytically and are better understood in term of the non-local EFT introduced in Chap. 10. We refer the reader to Sec. 10.3 for more details.

[4] The reverse case, i.e. $\sqrt{\rho/H} > \mu_{\rm eff}$, is reached only in a very limited region of the parameter space.

Light additional field. Our numerical analysis is also applicable in the light σ field regime where $m_{\rm eff} \lesssim H$. In this regime, the field σ decays at a very slow pace on super-horizon scales. The massless field π_c is therefore sourced by σ on super-horizon scales so that the value of Δ^2_ζ is sensitive to the amount of e-folds elapsed from the moment at which the mode crosses the horizon and the end of inflation. The corresponding enhancement of the power spectrum is well visible in the lower left part of the phase diagram in Fig. 15.2. It can be shown that the following analytical approximation that reproduces this amplification

$$\frac{\Delta^2_\zeta}{\Delta^2_{\zeta,0}} - 1 \propto \left[\frac{3\rho H}{m^2_{\rm eff}}\left(1 - e^{-\frac{m^2_{\rm eff}}{3H^2}\Delta N}\right)\right]^2 , \tag{15.13}$$

where ΔN is the number of e-folds elapsed since horizon crossing.

15.2 Size of non-Gaussianities Beyond Weak Mixing

The cosmological flow provides a unique opportunity to systematically study non-Gaussian signals in the strong mixing regime by fully treating the quadratic coupling. Most previous studies have examined the bispectrum in particular regimes. In this section, we numerically solve the flow equations for the bispectrum and inspect their phenomenological implications in the entire parameter space. In particular, we provide results in regions of the parameter space that are not easily accessible by analytical means.

We will use definitions introduced in Chap. 3. At weak quadratic mixing $\rho \lesssim m$, the $\pi_c - \sigma$ conversion process can be treated perturbatively. At leading order, the cubic interactions we consider lead to single-, double-, and triple-exchange diagrams, respectively for $(\partial_i\pi_c)^2\sigma$ and $\dot\pi_c^2\sigma$, $\dot\pi_c\sigma^2$, and σ^3. In the strong mixing regime $\rho \gtrsim m$, the quadratic coupling needs to be treated non-perturbatively. As a consequence, the notion of diagram becomes meaningless as one needs to sum up all contributions with any number of quadratic coupling insertions. In this sense, we present "non-perturbative" results. The shape function we compute should be understood as the *resummed* one.

Conversion from π to ζ. Independently of cubic interactions in the Lagrangian (9.53), the non-linear relation between π and ζ generates a contribution to the bispectrum, see the last two terms in Eq. (15.3) and the discussion below. It can be computed solely from the linear dynamics, and it is exponentially suppressed in all parameter space of the m-ρ phase diagram, except in the effectively light field regime $m_{\rm eff} \ll H$. Explicit results show that this conversion contribution to $f_{\rm NL}$ is at most of order 10^{-2} in the parameter space we display, for $N = 60$ e-folds of super-horizon evolution. Such a small value is negligible for today's cosmology, but should be taken into account in general.

In the following, we concentrate on the "intrinsic" bispectrum generated by cubic interactions in the Lagrangian (9.53), and which can give sizeable contributions.

Fig. 15.3 shows the $f_{\rm NL}$ parameter in the $(m/H, \rho/H)$ plane for the various interactions. For easy comparison and better visualisation, we also present slices of the phase diagrams in Fig. 15.4. For each interaction, we consider the three regions of the phase diagram in turn.

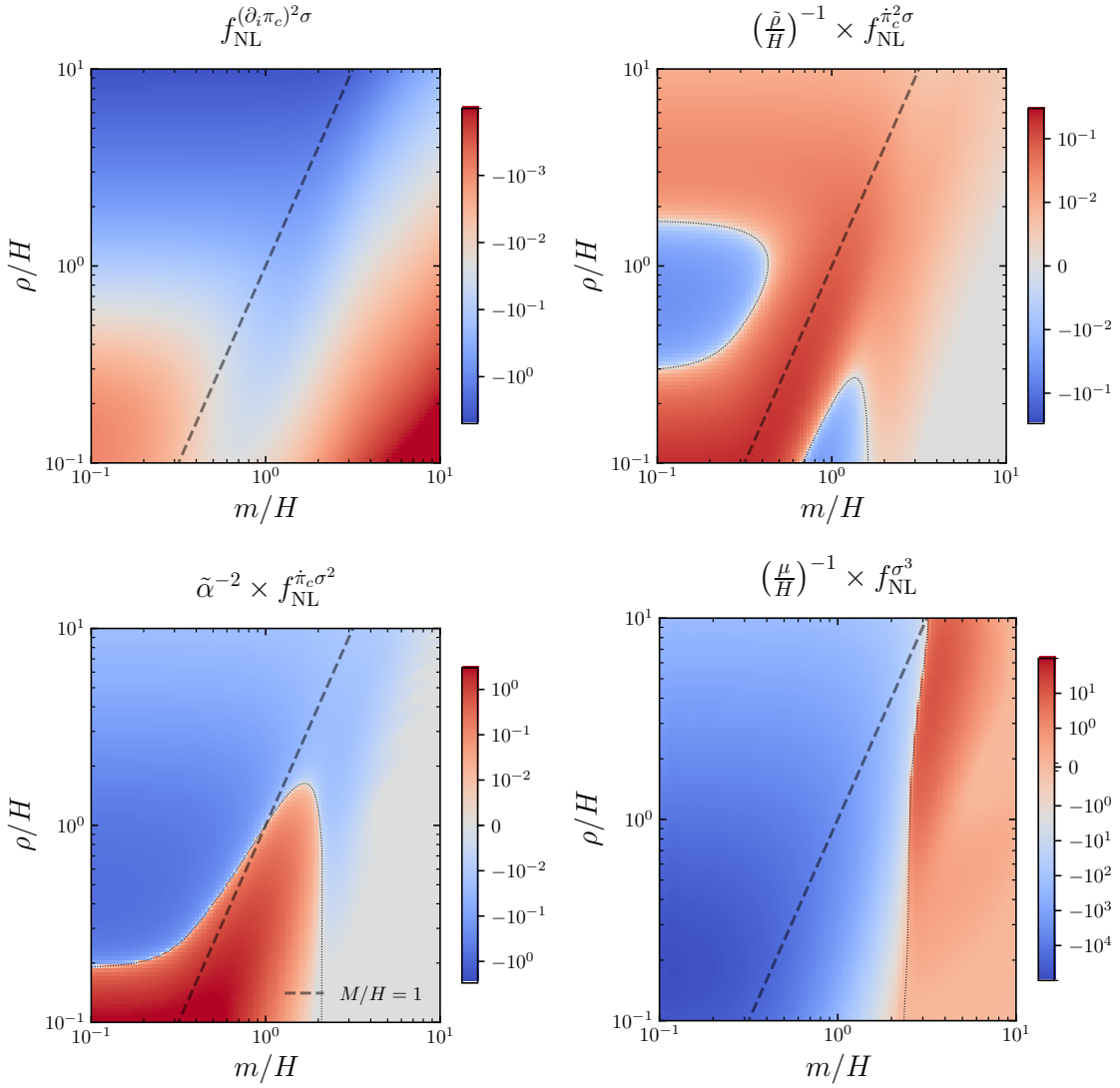


Figure 15.3: Shape function phase diagram for the $(\partial_i\pi_c)^2\sigma$ (*top left*), $\dot{\pi}_c^2\sigma$ (*top right*), $\dot{\pi}_c\sigma^2$ (*bottom left*), and σ^3 (*bottom right*) interactions, in the equilateral configuration $k_1 = k_2 = k_3 = k$. The dashed line corresponds to the $M = H$ limit, isolating the modified dispersion relation regime $M/H \ll 1$ and the reduced speed of sound regime $M/H \gg 1$. The dotted thin line corresponds to $S(k, k, k) = 0$ where the shape function changes sign. We have set $N = 60$ e-folds of super-horizon evolution. Slices of the phase diagram for various interactions can be found in Fig. 15.4.

$(\partial_i\pi_c)^2\sigma$ interaction. First, we consider the bispectrum generated by the interaction $(\partial_i\pi_c)^2\sigma$. In the weak mixing regime $\rho \lesssim m$, the size of the single-exchange

diagram can be estimated (see insert below), yielding[5]

$$f_{\rm NL}^{(\partial_i\pi_c)^2\sigma} \sim \left(\frac{\rho}{H}\right)^2 . \tag{15.14}$$

It is found that this scaling indeed extends up to values of the quadratic coupling $\rho \sim m$ as we increase the mass. Hence the leading perturbative result still gives a correct estimation for $\rho/H \gtrsim 1$ when the field σ is heavy enough. The associated non-Gaussian signal cannot reach order unity.

As function of the bare mass m/H, the bispectrum signal presents a suppression whose leading contribution scales as $(H/m)^2$ for large mass.[6] This comes from the leading imprint of higher-dimension operators when the heavy field is integrated out, as can be explicitly seen in (10.24) in the limit $\tilde{\partial}_i^2 \ll m^2$. The transition to this EFT regime is found to occur at $m/H \gtrsim 1$, as can be observed in the upper panel of Fig. 15.4. The hilltop visible around $m/H \sim 1$ is due to the fact that the intrinsic bispectrum decreases slower than the power spectrum squared as function of m/H, resulting in a boosted shape function.

In the strong mixing regime $\rho \gtrsim m$, the relevant mass scale to describe the dynamics is $M = m^2/\rho$ as explained in Sec. 10.3. Therefore, the transition to the EFT regime is shifted to higher values of the bare mass $m/H \gtrsim \sqrt{\rho/H}$. In the modified dispersion relation regime, one can use (10.24) and estimate the size of the non-Gaussianity, obtaining

$$f_{\rm NL}^{(\partial_i\pi_c)^2\sigma} \sim \frac{\rho}{H} . \tag{15.15}$$

We show in the insert below how this scaling is found using dimensional analysis. The found scaling is confirmed numerically. For the same reason as explained previously, this regime is reached for higher values of the quadratic mixing as the heavy field mass increases. Importantly, note that the size of this non-Gaussian signal monotonically increases as a function of the quadratic mixing, and can be large.

Estimating the size of the bispectrum.—In this insert, we show how one can easily recover the scalings (15.14) and (15.15) using purely dimensional analysis arguments and the non-local effective Lagrangian (10.24). This theory being single-field, we can estimate the size of the bispectrum using

$$f_{\rm NL} \sim \frac{\mathcal{L}_3}{\mathcal{L}_2}\,\Delta_\zeta^{-1} , \tag{15.16}$$

evaluated at the energy scale that we probe during inflation i.e. $\omega \sim H$. In the weak mixing regime, using the linear dispersion relation (we recall that we have fixed $c_s = 1$ for simplicity), we obtain

$$f_{\rm NL}^{(\partial_i\pi_c)^2\sigma} \sim \left(\frac{\rho}{H}\right)^2 , \tag{15.17}$$

[5] Note that the non-linearly realised symmetry fixes this cubic interaction coupling constant to $f_\pi/\Lambda_1 = \rho/f_\pi$.

[6] The signal also contains other terms suppressed by the exponential Boltzmann factor $e^{-\pi\mu}$. However for large mass, the $(H/m)^2$ suppression dominates in the equilateral configuration.

where we have evaluated the gradient term in $(-\tilde{\partial}_i^2 + m^2)^{-1}$ at the Goldstone boson horizon crossing $|k\tau| \sim 1$ and assumed $m \sim H$. In the strong mixing regime, using $\dot{\pi}_c \sim H\pi_c$ and the modified dispersion relation $\omega = k_{\rm p}^2/\rho$, one obtains

$$f_{\rm NL}^{(\partial_i\pi_c)^2\sigma} \sim \frac{\rho}{H}\left(\frac{H}{f_\pi}\right)^2 \frac{\pi_c}{H}\,\Delta_\zeta^{-1}\,. \tag{15.18}$$

We finally use $\Delta_\zeta \sim (H/f_\pi)^2(\rho/H)^{1/4}$ to obtain $\pi_c/H \sim (\rho/H)^{1/4}$ which, in the end, gives the desired scaling. A similar analysis can be performed for the other interactions to find the scalings (15.21), (15.23) and (15.25). In these cases, the "propagator" $(-\tilde{\partial}_i^2 + m^2)^{-1}$ can be estimated by evaluating the gradient term at the Goldstone boson ρ-horizon $|k\tau| \sim \sqrt{\rho/H}$, leading to

$$(k_{\rm p}^2 + m^2)/H^2 \sim \rho/H\,. \tag{15.19}$$

When the field is effectively light $m/H \ll 1$ and $\rho/H < 1$, we see that the $f_{\rm NL}$ parameter does not present an amplification due to super-horizon sourcing, visible in the phase diagram of the power spectrum in Fig. 15.2. We recall that this enhancement depends on the number of super-horizon e-folds until the end of inflation. In fact, the bispectrum is indeed enhanced but this boost is balanced by the amplification of the power spectrum to give no visible effect in the $f_{\rm NL}$ parameter.

$\dot{\pi}_c^2\sigma$ interaction. At weak mixing $\rho \lesssim m$, the size of the non-Gaussianity arising from the interaction $\dot{\pi}_c^2\sigma$ is[7]

$$f_{\rm NL}^{\dot{\pi}_c^2\sigma} \sim \frac{\rho}{H} \times \frac{\tilde{\rho}}{H}\,, \tag{15.20}$$

which we confirm numerically up to $\rho \sim m$, similarly to the previous interaction. At strong mixing $\rho \gtrsim m$, the EFT regime is reached for higher values of the bare mass $m/H \gtrsim \sqrt{\rho/H}$ for the same reason as the interaction $(\partial_i\pi_c)^2\sigma$. Accounting for perturbativity bounds on the couplings, we can accommodate for large non-Gaussianities in this regime. In the modified dispersion relation regime, the size of the non-Gaussianity is

$$f_{\rm NL}^{\dot{\pi}_c^2\sigma} \sim \frac{\tilde{\rho}}{H}\left(\frac{\rho}{H}\right)^{-1}\,, \tag{15.21}$$

which, for $\rho/H \gg 1$, gives a lower signal compared to that in the weakly coupled regime. Therefore, for this interaction, a large quadratic mixing does not necessarily imply large non-Gaussianities. In the lower panel of Fig. 15.4, one can appreciate that this interaction is damped at large quadratic mixing, as opposed to the spatial derivative interaction. In fact, from the non-local Lagrangian (10.24) and the modified dispersion relation $\omega = k_{\rm p}^2/\rho$, it is easy to realise that interactions with strictly negative powers of spatial gradients—including the "propagators" $(k_{\rm p}^2 + m^2)^{-1}$—are suppressed at strong quadratic mixing.

[7] Due to spontaneously broken de Sitter boosts, the covariance of the cubic interaction $(\partial_\mu\pi_c)^2\sigma$ is violated. The non-linearly realised symmetry only fixes the spatial derivative interaction.

In the effectively light field case and as can be better seen in Fig. 15.4, the shape function reaches a plateau as the boost in the bispectrum is compensated by that of the power spectrum. The transition to this regime, either from the ρ or the m directions, is delimited by the $f_{\rm NL}$ parameter changing sign, as represented by the dotted line in Fig. 15.3.

Recall that because we consider interactions that break de Sitter boosts, we have split $(\partial_\mu \pi_c)^2\sigma$ into $(\partial_i \pi_c)^2\sigma$ and $\dot{\pi}_c^2\sigma$, the coefficient of the first one being fixed in terms of ρ/H. We have shown that the time derivative interaction leads to a completely different phenomenology than the spatial derivative interaction, a fact that was not enough appreciated before.

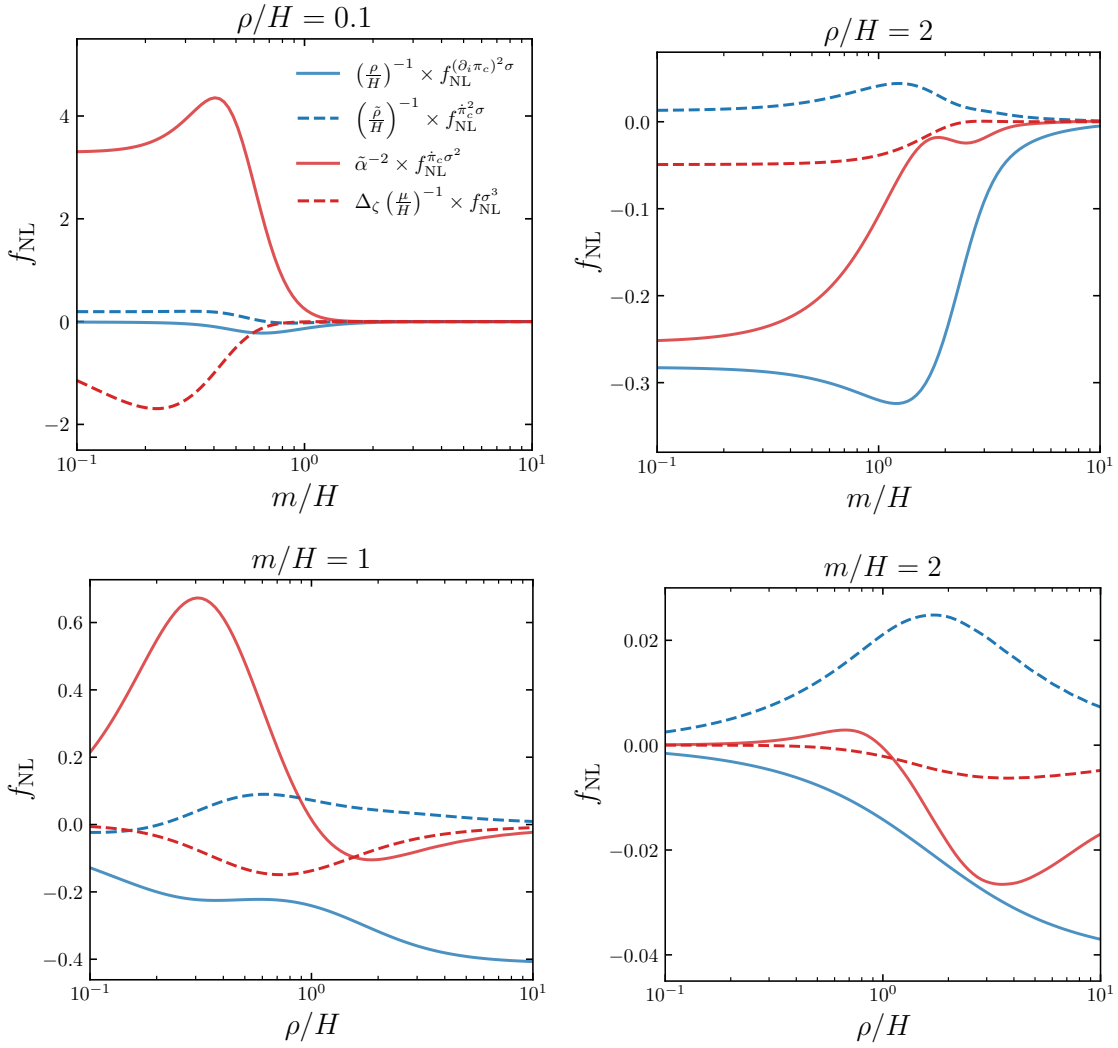


Figure 15.4: Slices of the shape function phase diagrams as function of the bare mass m/H for $\rho/H = 0.1$ (*top left*) and $\rho/H = 2$ (*top right*), and as function of the quadratic mixing ρ/H for $m/H = 1$ (*bottom left*) and $m/H = 2$ (*bottom right*), in the equilateral configuration $k_1 = k_2 = k_3 = k$. For better visualisation, the shape generated by the interaction σ^3 has been multiplied by Δ_ζ.

$\dot{\pi}_c\sigma^2$ interaction. At weak mixing $\rho \lesssim m$, the non-Gaussian signal arising from the interaction $\dot{\pi}_c\sigma^2$ scales as

$$f_{\rm NL}^{\dot{\pi}_c\sigma^2} \sim \tilde{\alpha}^2 \left(\frac{\rho}{H}\right)^2 . \tag{15.22}$$

We observe that this scaling is valid up to $\rho \sim m$. In the modified dispersion relation regime, the amplitudes scales as

$$f_{\rm NL}^{\dot{\pi}_c\sigma^2} \sim \tilde{\alpha}^2 \left(\frac{\rho}{H}\right)^{-1} , \tag{15.23}$$

which again gives a comparable amplitude compared to that in the weakly coupled regime. As shown in Fig. 15.4, the cosmological flow approach enables us to effortlessly probe the intermediate regime where analytical computations fail. A large non-Gaussian signal in the strong mixing regime is possible while remaining under perturbative control.

In the light field regime, one can appreciate once more that the shape function is almost constant, for the same reason as for the previous interaction.

σ^3 interaction. At leading order in the weak mixing regime, the interaction σ^3 leads to the triple-exchange diagram whose amplitude is

$$f_{\rm NL}^{\sigma^3} \sim \frac{\mu}{H}\left(\frac{\rho}{H}\right)^3 \Delta_\zeta^{-1} . \tag{15.24}$$

It is well-known that this amplitude of non-Gaussianity is boosted due to the factor $\Delta_\zeta^{-1} \sim 10^5$, which leads to the largest non-Gaussian signal. This is explained by the fact that, for $\mu \sim H$ and $\rho \sim H$, the entire non-Gaussian signal in the σ-sector should be transferred to the ζ-sector. The actual size of non-Gaussianities in the bispectrum being $f_{\rm NL}\Delta_\zeta$, one should have $f_{\rm NL}\Delta_\zeta \sim (\mu/H)\,(\rho/H)^3$. As function of m/H, the intrinsic bispectrum scales as $(H/m)^6$—it drops faster than $(H/m)^2$—, leading to no characteristic enhancement around $m/H \sim 1$ in the shape function, as one can observe in the upper panel of Fig. 15.4. When the bare mass increases, the modified dispersion relation regime is found for higher values of the quadratic mixing. We indeed confirm numerically that the scaling (15.24) extends up to $\rho/H \sim 1$ when increasing the bare mass. For $M/H \ll 1$ and $\rho/H \gg 1$, the non-Gaussian signal scales as

$$f_{\rm NL}^{\sigma^3} \sim \frac{\mu}{H}\left(\frac{\rho}{H}\right)^{-3/4} \Delta_\zeta^{-1} , \tag{15.25}$$

which—although a priori suppressed by ρ/H—gives a larger contribution than in the weak mixing regime for typical values of the quadratic coupling. Here, as well as for other interactions, the change of sign of the shape function for $m/H \sim 2$ can be attributed to a cancellation between two contributions resembling equilateral shapes and giving rise to an orthogonal shape.

In the effectively light field regime the $f_{\rm NL}$ parameter is decreasing as the bispectrum is not enhanced like the power spectrum.

Summary. Accounting for perturbativity bounds derived in Chap. 9 and the exact size of non-Gaussianities presented in Fig. 15.3, one can obtain sizable non-Gaussianities—typically $f_{\rm NL} \gg 1$—in the strong mixing regime for all interactions. At weak mixing, all interactions except $(\partial_i\pi_c)^2\sigma$ can lead to $f_{\rm NL} \sim \mathcal{O}(1)$ signals. Typically, the signal is largest for a mass of σ of order H or less. We have checked that, for each of these four cubic interactions, both in the weak and the strong mixing regimes, saturating the perturbativity bounds universally gives $f_{\rm NL}\Delta_\zeta \lesssim 1$, as expected.

15.3 Cosmological Collider Phenomenology

The squeezed limit of the bispectrum is believed to be a robust probe of the particle content during inflation, see Chap. 4. One major advantage of the cosmological flow is that it provides a generic framework to study the squeezed limit of the bispectrum in a systematic and exact manner. In this section, we present several cosmological collider signals, including the strong mixing regime for which it is important to take into account the notion of *effective* mass $m_{\rm eff}^2 = m^2 + \rho^2$ instead of the bare mass. Moreover, we show that a phase shift and a non-trivial amplitude of the oscillations can be seen as a signature of primordial fluctuations undergoing strong mixing. We also give novel insight on the role of the sound speeds on cosmological collider signals. We finish by exposing the cosmological collider flow—i.e. the squeezed limit of the bispectrum as function of time—that enables us to shed light on the characteristic time scales of the dynamics.

In this section, for definiteness, we will focus on the bispectrum arising from the $(\partial_i\pi_c)^2\sigma$ and $\dot\pi_c\sigma^2$ interactions (except in 15.3.2), and we will be interested in the case where the field σ is heavy; $\mu_{\rm eff} > 0$.

15.3.1 Strongly Mixed Colliders

We first look at how the bispectrum shape in the squeezed limit depends on the quadratic mixing. In this limit, the bispectrum is sensitive to the heavy field mass, as it governs the frequency of the oscillations. Fig. 15.5 shows the bispectrum shapes as functions of the momentum ratio in the isosceles-triangle configuration, for fixed $\mu_{\rm eff}$ but varying the quadratic mixing (hence adjusting the bare mass). We observe that the cosmological collider signals oscillate at the same frequency. Indeed as we have seen before, the relevant notion of mass for this system is the effective mass $m_{\rm eff}$ and not the bare mass m. As a consequence, a light but strongly mixed field and a heavy but weakly mixed field cannot be distinguished based only on the signal frequency. For illustration purposes and to focus on the oscillation frequencies only, the signals have been normalised to unity in the equilateral configuration. A notable feature is the phase shift of the signal to smaller momentum ratios for larger quadratic mixings. This constitutes a striking example that having complete predictions for the signal—amplitude, frequency, phase, as well as contaminations from equilateral shapes—is important to disentangle the bare mass from the effective one, and will be needed to correctly infer the model parameters from the cosmological data. As

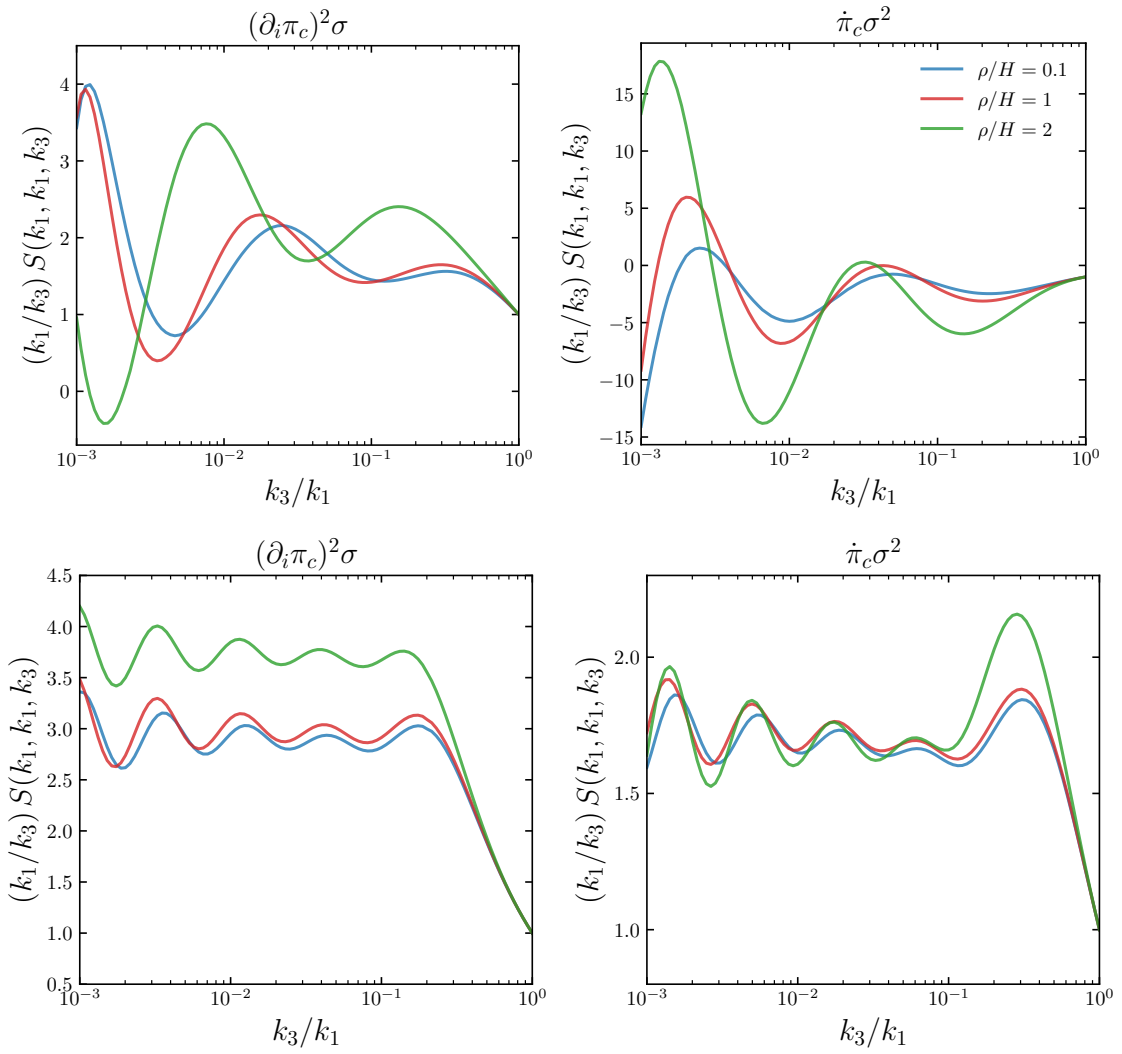


Figure 15.5: Shape functions for the $(\partial_i\pi_c)^2\sigma$ interaction (*left panel*) and $\dot\pi_c\sigma^2$ interaction (*right panel*) in the isosceles-triangle configuration $k_1 = k_2$, for $\mu_{\rm eff} = 2$ (*top*) and $\mu_{\rm eff} = 5$ (*bottom*) varying the quadratic mixing ρ/H. For illustration purposes, we have normalised the amplitudes of the signals to be the same in the equilateral configuration. For $\mu_{\rm eff} = 5$, we also have set $c_s = 0.1$ to amplify the oscillations of the cosmological collider signal (signals for different values for the sound speed—including $c_s = 1$—are presented in Fig.15.7).

discussed in Sec. 15.1, this phase shift is due to the resonance of the heavy field before it starts oscillating.

Because of the arbitrary normalisation of the shape function, Fig. 15.5 does not exhibit the size of non-Gaussianities nor the amplitude of the cosmological collider signals. To shed light on these two aspects, we show in Fig. 15.6 the shape function in the isosceles-triangle configuration for different values of the quadratic mixing ρ/H while fixing the bare mass m/H. In the equilateral configuration $k_3/k_1 = 1$, the parametric dependence of $f_{\rm NL}$ on ρ/H has been discussed in the previous section. Yet, a noticeable feature of the cosmological collider signals is the strong dependence

of its amplitude on the quadratic coupling ρ/H that is not monotonic. In the weak mixing regime $\rho \lesssim m$, the amplitude grows with ρ, after which it decreases in the strong mixing regime. At strong mixing for the $(\partial_i\pi_c)^2\sigma$ interaction, this indicates that although the size of the total signal is amplified, signatures of the cosmological collider signal are harder to detect, as it is exponentially suppressed by the effective mass $e^{-\pi\mu_{\rm eff}}$.

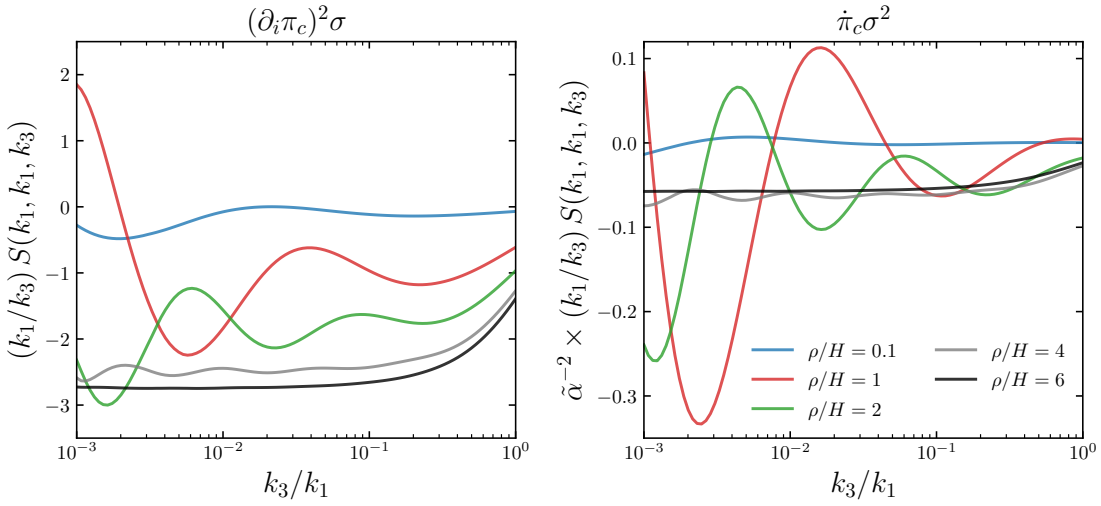


Figure 15.6: Shape functions for the $(\partial_i\pi_c)^2\sigma$ interaction (*left panel*), and $\dot\pi_c\sigma^2$ interaction (*right panel*) in the isosceles-triangle configuration $k_1 = k_2$, for a fixed bare mass $m/H = 2$ and varying the quadratic mixing ρ/H.

To sum up, the cosmological collider (denoted CC in the following equation) signal in the squeezed limit can be written as

$$\lim_{k_3/k_1\to 0} S^{\rm CC}(k_1,k_1,k_3) \sim \left(\frac{k_3}{k_1}\right)^{1/2} \mathcal{A}\left(\frac{m}{H},\frac{\rho}{H}\right) \cos\left[\mu_{\rm eff}\log\left(\frac{k_3}{k_1}\right) + \theta\left(\frac{m}{H},\frac{\rho}{H}\right)\right] . \tag{15.26}$$

It qualitatively describes the squeezed limit even beyond the analytical lamppost of the weakly mixed regime, with an amplitude and phase information that can be efficiently obtained from the cosmological flow approach. It should be noted that for realistically squeezed configurations like the ones presented in the figures, the shape function does not oscillate around zero. This means that it always contains a contamination part—analytic in momenta—which can be described by the non-local single-field EFT, as shown in Chaps. 10 and 11.

Eventually, let us highlight that if we ever detect the cosmological collider signal, it is more likely to be attributed to a substantial mixing $\rho \sim m$ for which the non-analytic signal is the largest. This illustrates one of the main aspects motivating the development of the cosmological flow approach: interesting physics lying beyond the lamppost of analytical calculations can be missed, therefore biasing the interpretation of data.

15.3.2 Sound-Speed Colliders

Next, we present the effect of varying the speed of sound c_s on the cosmological collider signal. More precisely, throughout the thesis so far, we have used c_s to denote the speed of sound of the Goldstone boson π_c. However, in this section exclusively, we allow the field σ to also have a non-unity speed of sound c_σ, and c_s will actually denote the ratio of the sound speed of π_c and the massive field: $c_s \equiv c_\pi/c_\sigma$. Therefore, $c_s < 1$ means that the Goldstone boson propagates slower than the field σ, and the opposite for $c_s > 1$, which by no means implies superluminal propagation. Crucially, as a consequence of the non-linearly realised symmetry, allowing $c_\sigma \neq 1$ induces additional mixings between π_c and σ that one is forced to consider.

Indeed, a non trivial propagation speed for σ can only be generated by the unitary-gauge operator $(g^{0\mu}\partial_\mu\sigma)^2$, invariant under time-dependent spatial diffeomorphism [504]. Therefore, as long as $c_\sigma \neq 1$, one should consider it in the theory, i.e.

$$S \supset -\int \mathrm{d}^4x\sqrt{-g}\,\tilde{e}\,(g^{0\mu}\partial_\mu\sigma)^2\,, \tag{15.27}$$

where $\tilde{e}$ is a dimensionless coupling that we assume to be constant. Reintroducing the Goldstone boson in the decoupling limit via $g^{0\mu}\partial_\mu\sigma \to -(1+\dot{\pi})\dot{\sigma} + \frac{1}{a^2}\partial_i\pi\partial_i\sigma$, and discarding quartic terms in the fields—not relevant for the bispectrum—, one obtains[8]

$$\mathcal{L}/a^3 \supset -\tilde{e}\left[\dot{\sigma}^2 + 2\dot{\pi}\dot{\sigma}^2 - 2\dot{\sigma}(\tilde{\partial}_i\pi)(\tilde{\partial}_i\sigma) + \dots\right]. \tag{15.28}$$

Because the second term is also generated by the operator $\delta g^{00}(g^{0\mu}\partial_\mu\sigma)^2$, its coupling constant is not fully fixed by $\tilde{e}$. We therefore do not consider it in the following. By contrast, the interaction $\dot{\sigma}(\partial_i\pi)(\partial_i\sigma)$ can only be generated by the operator (15.27). Hence, in the same way as a non-trivial sound speed for π universally comes with the interaction $\dot{\pi}(\partial_i\pi)^2$ whose size is controlled by c_π, a propagation speed for σ different from unity universally comes with the interaction in $\dot{\sigma}(\partial_i\pi)(\partial_i\sigma)$ whose size is fixed by c_σ. The only difference is that the observable non-Gaussian signal it generates also depends on the σ to π transfer, i.e. on the quadratic mixing between the two fields. Explicitly, when adding the effects of (15.27) to the action, one obtains the following Lagrangian

$$\begin{aligned}\mathcal{L}/a^3 = {}& \frac{1}{2}\left[\dot{\pi}_c^2 - c_s^2(\tilde{\partial}_i\pi_c)^2\right] + \frac{1}{2}\left[\dot{\sigma}_c^2 - (\tilde{\partial}_i\sigma_c)^2 - m^2\sigma_c^2\right] + \rho\dot{\pi}_c\sigma_c \\ & - \frac{c_s^{3/2}}{2f_\pi^2}\frac{\rho}{c_\sigma^2}\sigma_c(\tilde{\partial}_i\pi_c)^2 - \frac{c_s^{3/2}}{f_\pi^2}\left(\frac{1}{c_\sigma^2}-1\right)\dot{\sigma}_c(\tilde{\partial}_i\pi_c)(\tilde{\partial}_i\sigma_c)\,,\end{aligned} \tag{15.29}$$

[8] Under a time diffeomorphism $t \to \tilde{t} = t + \pi(t,\boldsymbol{x})$, the four-dimensional partial derivative (inversely) transforms as $\tilde{\partial}_\mu \to \partial_\mu = \partial_\mu\tilde{x}^\nu\tilde{\partial}_\nu = \partial_\mu(t+\pi)\tilde{\partial}_0 + \partial_\mu\tilde{x}^i\tilde{\partial}_i$. The temporal component therefore transforms as $\tilde{\partial}_0 \to (1+\dot{\pi})\tilde{\partial}_0$ which implies $\partial_0 \to \tilde{\partial}_0 = \frac{\partial_0}{1+\dot{\pi}}$. The spatial ones transform as $\tilde{\partial}_i \to \partial_i = \tilde{\partial}_i + (\partial_i\pi)\tilde{\partial}_0$ which implies $\partial_i \to \tilde{\partial}_i = \partial_i - \frac{\partial_i\pi}{1+\dot{\pi}}\partial_0$. The off-diagonal metric components transform as $g^{0i}(t,\boldsymbol{x}) \to \tilde{g}^{0i}(\tilde{t},\tilde{\boldsymbol{x}}) = \partial_\mu(t+\pi)\partial_\nu\tilde{x}^i g^{\mu\nu}(t,\boldsymbol{x}) = \frac{1}{a^2}\partial_i\pi$ where we have ultimately evaluated the metric on the background. Collecting everything together, and noting that $g^{00}(t,\boldsymbol{x}) \to \tilde{g}^{00}(\tilde{t},\tilde{\boldsymbol{x}}) = -(1+\dot{\pi})^2 + \frac{1}{a^2}(\partial_i\pi)^2$, we obtain the following exact transformation $g^{0\mu}\partial_\mu\sigma \to -(1+\dot{\pi})\dot{\sigma} + \frac{1}{a^2}(\partial_i\pi)(\partial_i\sigma)$, valid to all orders in the fields.

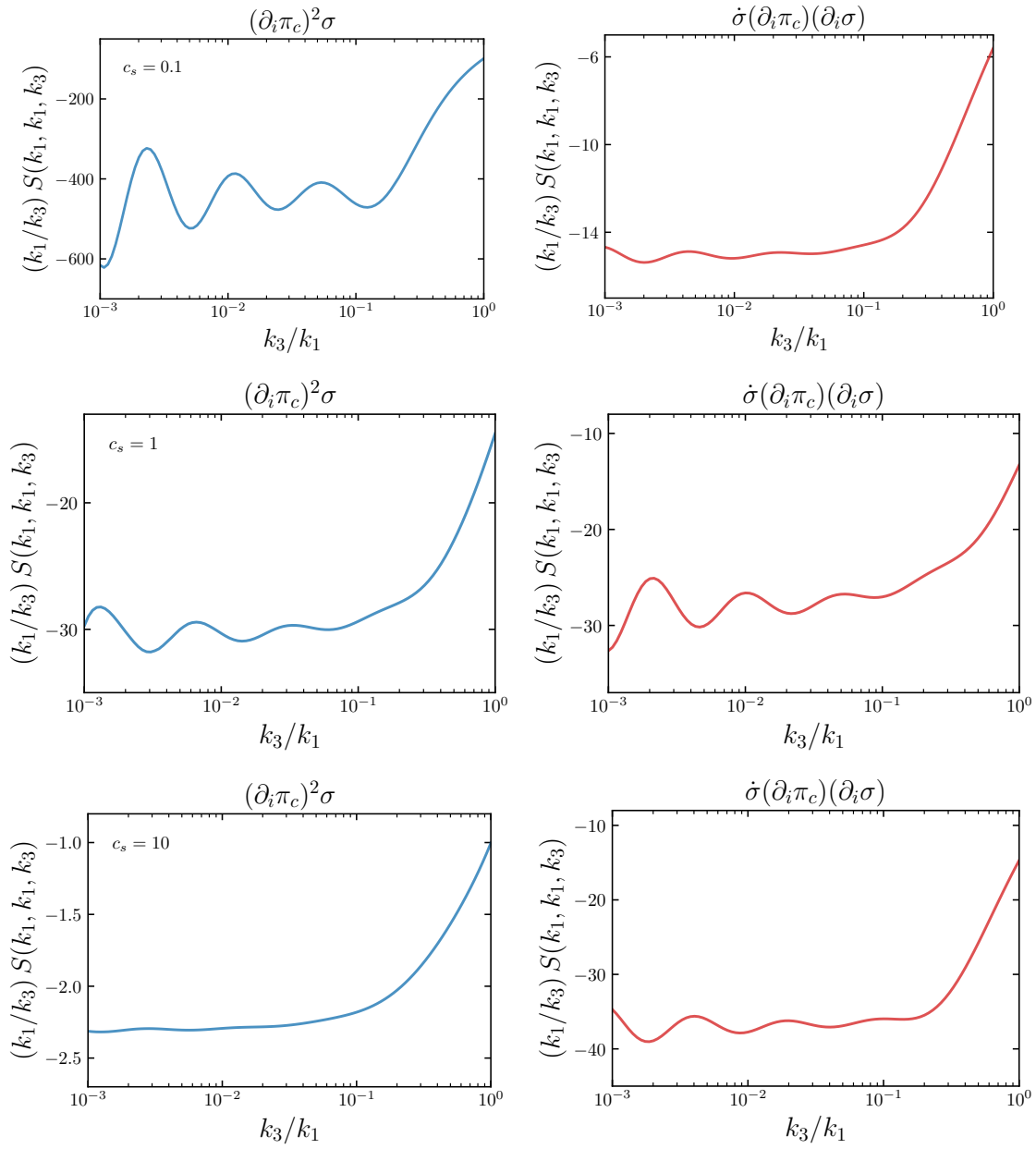


Figure 15.7: Shape functions for the $(\partial_i\pi_c)^2\sigma$ interaction (*left panel*) and $\dot\sigma(\partial_i\pi_c)(\partial_i\sigma)$ interaction (*right panel*) in the isosceles-triangle configuration $k_1 = k_2$, for $c_\sigma = 0.1$, $\mu_{\rm eff} = 4$ and $\rho/H = 4$, and with $c_s = 0.1$ (*top*), $c_s = 1$ (*middle*), and $c_s = 10$ (*bottom*). We recall that $c_s = c_\pi/c_\sigma$ and that both interactions are fully fixed by the non-linearly realised symmetry (either by ρ or c_σ).

where we concentrated on the new effects coming from $c_\sigma \neq 1$, with

$$\begin{aligned} &c_\sigma^{-2} = 1 - 2\tilde e\,, \quad c_s = c_\pi/c_\sigma\,, \quad f_\pi^4 = 2M_{\rm pl}^2|\dot H|c_\pi\,, \quad \rho = 2c_\pi^{3/2}c_\sigma\frac{\tilde M_1^3}{f_\pi^2}\,, \\ &\pi_c = c_s^{-3/2}f_\pi^2\pi\,, \quad \sigma_c = c_\sigma^{1/2}\sigma\,, \quad m \to c_\sigma m\,. \end{aligned} \tag{15.30}$$

Here, we rescaled spatial coordinates $\tilde{\boldsymbol{x}} = \boldsymbol{x}/c_\sigma$. This does not affect the physics

in our scale-invariant theories, hence we omit the tilde for simplicity. In this way, the quadratic Lagrangian in terms of canonically normalised fields takes the same form as the one studied in the rest of the paper, simply allowing for $c_s > 1$, and where the mass m in Eq. (15.29) has been rescaled by a factor c_σ compared to the bare mass in (9.50). Nonetheless, an important aspect made transparent in the Lagrangian (15.29) is worth highlighting: a small sound speed c_σ for the additional field boosts the overall amplitude of non-Gaussianities by a factor $\sim 1/c_\sigma^2$. Indeed, at fixed m, ρ and c_s, the sound speed c_σ only appears in the overall multiplicative factors, $1/c_\sigma^2$ and $1/c_\sigma^2 - 1$ respectively, setting the sizes of the cubic interactions in $(\partial_i \pi_c)^2 \sigma$ and $\dot{\sigma}(\partial_i \pi_c)(\partial_i \sigma)$. The corresponding rather large non-Gaussian signals are well visible in Fig. 15.7, where we show the shape functions as a function of the squeezing parameter k_3/k_1 at strong mixing $\rho/H = 4$, for $c_\sigma = 0.1$ and for $c_s \in \{0.1, 1, 10\}$.

For the $(\partial_i \pi_c)^2 \sigma$ interaction on the left panel, the amplitude of the non-analytic part of the signal, i.e. the cosmological collider signal, increases when c_s decreases. In the weak mixing regime, the scaling of the amplitude with c_s is known analytically. For $c_s = 1$, it is known that the amplitude of the non-analytic part of the signal is suppressed by $e^{-\pi \mu_{\rm eff}}$. However, for $c_s \ll 1$, this suppression leads to an amplification of the cosmological collider signal, as the amplitude is $e^{-\pi \mu_{\rm eff}/2}$. We find indeed that this tendency extends to the strong mixing regime, and that for $c_s > 1$ the signal is further damped. On the contrary, the amplitude of the cosmological collider signal arising from the $\dot{\sigma}(\partial_i \pi_c)(\partial_i \sigma)$ interaction is mildly dependent on c_s.

15.3.3 Cosmological Collider Flow

Following the time evolution of the three-point correlators for a fixed momentum configuration allows us to reconstruct the flow of the cosmological collider signal. This is shown in Fig. 15.8 where we depict the shape function in the isosceles-triangle configuration as function of time. The measure of time is taken to be the number of e-folds elapsed since sound horizon crossing of the long mode: $N - N_\ell$, with N_ℓ such that $k_\ell = k_3 = a(N_\ell)H(N_\ell)$. One can notice that the cosmological collider signal builds up progressively as function of time, starting with configurations close to the equilateral one. This representation makes it clear that the squeezed limit of the three-point correlator is a probe of the super-horizon evolution of the additional massive field σ between N_ℓ and N. This example showcases the utility of the cosmological flow approach as it enables us to reveal the physics of various processes by analysing the characteristic time scales at play, allowing for a direct access to the bulk time evolution of correlators. A video of the cosmological collider flow can be found here. It is instructing to notice the different behaviours between the weakly and strongly mixed cases. At weak mixing, the system is underdamped and the signal exhibits temporal oscillations about its late-time asymptotic form before converging. At strong mixing, the two fields are so bound that the late-time signal is asymptotically reached with overdamped oscillations.

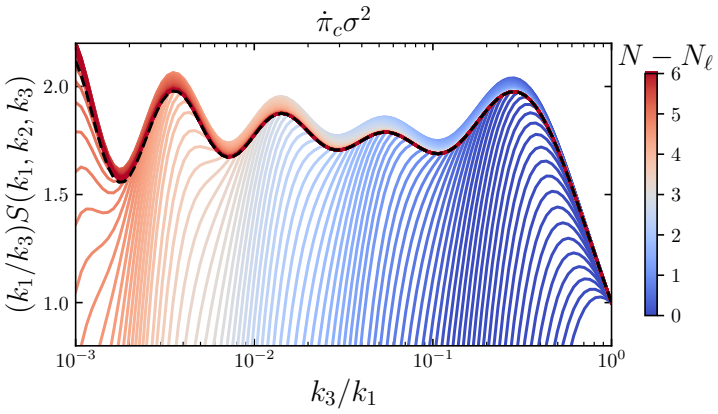


Figure 15.8: Time evolution of the shape function for the $\dot{\pi}_c\sigma^2$ interaction in the isosceles-triangle configuration $k_1 = k_2$, for $\mu_{\rm eff} = 5, \rho/H = 0.1$ and $c_s = 0.1$. The measure of time $N - N_\ell$ is defined to be the time in e-folds elapsed since sound-horizon crossing of the long mode $k_\ell = k_3$. We have normalised the amplitude of the signal to unity in the equilateral configuration for illustration purposes. The dotted black line corresponds to the shape function at $N - N_\ell = 20$, a time by which the signal has become stationary.

15.4 Primordial Features

We have illustrated that the cosmological flow is a generic framework that enables one to study non-Gaussian phenomenology in scale-invariant cases that are not easily accessible by analytical means. However, realistic models of inflation generically lead to features in the scale dependence of primordial correlation functions. In this section, we show that features can be accounted for systematically, both in the scale-dependence and the shape-dependence of correlators. As a proof of concept to illustrate the utility of our approach, we first perform an exact calculation of the power spectrum and the bispectrum scale-dependence in the case of a time-varying quadratic mixing, and compare it with the predictions given by an effective single-field theory with a time-varying speed of sound. We then show how features are encoded in the bispectrum squeezed limit, giving a new way of probing the inflationary landscape through soft limits of cosmological correlators, and therefore extending the reach of cosmological collider phenomenology.

15.4.1 Effective Description of Features

Let us first discuss how time-varying background quantities arise in the effective description of fluctuations presented in Chap. 9. We refer the reader to this chapter for details.

Non-linearly realised symmetry. The mixing action in the unitary gauge (9.51) is parameterised by a set of mass scales $\tilde{M}_i(t)$. After reintroducing the Goldstone boson π, expanding the mass scales to first order around the inflationary attractor

gives

$$\tilde{M}_i(t) \to \tilde{M}_i(t+\pi) \approx \tilde{M}_i(t) + \dot{\tilde{M}}_i(t)\pi + \dots \,. \tag{15.31}$$

If the time scales of variation of the $\tilde{M}_i(t)$ are too small, i.e. if the features that are considered are too sharp, the expansion (15.31) may break down. This corresponds to a violation of perturbative unitarity, see e.g [561, 562, 563, 564]. Concentrating for simplicity on $c_s = 1$ and at weak mixing, the (minimum) time scale of variation Δt of any time-dependent quantity should obey $\Delta t > 1/f_\pi$. This comes from requiring that the Taylor expansion in (15.31) is valid, i.e. $\pi < \Delta t$, with $\pi = \pi_c/f_\pi^2$ and $\pi_c \sim \omega$, at the energy $\omega \sim 1/\Delta t$ excited by the feature. Only a time-dependence in $\tilde{M}_1$ generates an additional cubic interaction compared to the ones present in (9.52), that reads

$$\mathcal{L}_{\pi-\sigma}/a^3 \supset 6\tilde{M}_1^2(t)\dot{\tilde{M}}_1(t)\,\pi\dot{\pi}\sigma\,. \tag{15.32}$$

For this reason, we will only consider a time dependence for $\tilde{M}_1$ throughout this section, setting $\tilde{M}_2 = \tilde{M}_3 = 0$. We also set the intrinsic sound speed of π to unity $c_s = 1$. In terms of the canonically normalised field π_c, the mixing Lagrangian we study is

$$\mathcal{L}_{\pi-\sigma}/a^3 = \rho(t)\dot{\pi}_c\sigma - \frac{\rho(t)}{2f_\pi^2}(\partial_\mu\pi_c)^2\sigma + \frac{\dot{\rho}(t)}{f_\pi^2}\pi_c\dot{\pi}_c\sigma\,, \tag{15.33}$$

where we have defined the quadratic mixing $\rho(t) = 2\tilde{M}_1^3(t)/f_\pi^2$. Notice that operators weighted by higher derivatives of ρ appear if $\tilde{M}_1(t+\pi)$ is expanded to higher order around $\tilde{M}_1(t)$. We discard such terms as they appear at quartic order (and higher) in the fields. Also note that we have neglected any time variation of the Hubble parameter H and the mass of the field σ in this effective description of fluctuations. We will come back to this point later.

Effective single-field theory. When the field σ is sufficiently massive, one can integrate it out and obtain an effective theory for π. Indeed, solving the linear equation of motion for σ to leading order in powers of $\Box/m^2$, that is $\sigma = \rho\dot{\pi}_c/m^2$, and plugging the solution back in the original Lagrangian leads to

$$\mathcal{L}/a^3 = \frac{1}{2\tilde{c}_s^2(t)}\dot{\pi}_c^2 - \frac{1}{2}(\tilde{\partial}_i\pi_c)^2 - \frac{1}{2f_\pi^2}\left(\frac{1}{\tilde{c}_s^2(t)} - 1\right)\dot{\pi}_c(\partial_\mu\pi_c)^2 - \frac{\dot{\tilde{c}}_s(t)}{f_\pi^2\tilde{c}_s(t)}\pi_c\dot{\pi}_c^2\,, \tag{15.34}$$

where the time-dependent sound speed $\tilde{c}_s(t)$ is defined in (10.28). Let us now discuss the regime of validity of this effective theory. Clearly, neglecting the gradient term compared to the mass term $\tilde{\partial}_i^2 \ll m^2$ means that (15.34) describes the dynamics of low-energy modes with physical momenta $k_{\rm p}^2 \ll m^2$. In fact, it can be shown that requiring that the derivative expansion in powers of $\Box/m^2$ be under control implies a set of *generalised adiabaticity conditions*[9] [565, 566, 567, 555]

$$\frac{1}{\tilde{c}_s}\frac{\mathrm{d}^n\tilde{c}_s}{\mathrm{d}t^n} \ll m^n\,, \tag{15.37}$$

[9] The first two conditions for $n = 1, 2$ can be easily found by considering the next-to-leading order term $\Box\dot{\pi}_c/m^2$ in the derivative expansion. Using the quadratic equation of motion for π_c, one obtains

$$\Box\dot{\pi}_c = \left(1-\tilde{c}_s^2\right)\frac{\partial_i^2\dot{\pi}_c}{a^2} - 4\tilde{c}_s^2\frac{\dot{\tilde{c}}_s}{\tilde{c}_s}\frac{\partial_i^2\pi_c}{a^2} + H^2\left[6\frac{\dot{\tilde{c}}_s}{\tilde{c}_s} - 2\left(\frac{\dot{\tilde{c}}_s}{H\tilde{c}_s}\right)^2 + 3\frac{\dot{H}}{H^2} - 2\frac{\ddot{\tilde{c}}_s}{H^2\tilde{c}_s}\right]\dot{\pi}_c\,. \tag{15.35}$$

for $n \geq 1$. These conditions indicate that the time scale of variation Δt of *all* time-varying quantities are bounded from below by the mass scale of the heavy field $\Delta t \gg m^{-1}$. In particular, this leaves room for the speed of sound to vary significantly on a time scale smaller than H^{-1} but still larger than m^{-1} if the field σ is heavy enough. In addition to the previous adiabaticity conditions, one also needs to require (10.29), see Sec. 10.3.

15.4.2 Correlated Sharp Features

Due to the non-linearly realised symmetry, features in the scale-dependence of the power spectrum are also imprinted in the bispectrum scale-dependence. This can be explicitly seen from the mixing Lagrangian in the full theory (15.33) or in the effective theory (15.34). Such correlated features have been extensively studied in the context of the single-field effective theory with a time-varying sound speed [568, 569, 570, 571]. Here, we perform exact calculations in both full and effective theories.

Time dependence. Although the mechanisms leading to features can be very model-dependent, we focus on a single form of the quadratic mixing. We choose its time dependence to be parameterised by

$$\rho(t) = \rho_0 \, (a/a_0)^{-n} \sin[\omega_c(t-t_0)] \times \frac{1}{2}\left[1 + \tanh\left(\frac{t-t_0}{\Delta t}\right)\right] , \tag{15.38}$$

where $\mu_c = \omega_c/H$ determines the background oscillation frequency in Hubble units, and ρ_0 is the amplitude of the feature. In the following, we will choose ρ_0 such that the deviation of the curvature power spectrum from scale invariance satisfies current observational bounds on cosmological scales. The feature is turned on continuously at $t = t_0$ with a step of width Δt that dictates its sharpness. We also consider that the feature is diluted by $(a/a_0)^{-n}$ where $a_0 = a(t_0)$. This overall time dependence of the mixing describes well multi-field inflationary scenarios in which the background trajectory undergoes a turn in field space. If the turn is sharp, it will excite negative-frequency modes and produce correlation functions with oscillations linear in k [572, 330]. Those oscillations are characteristic of any sharp feature, be it single field or multi-field, and they are independent of ω_c. They only probe a very short time range located at the sharp feature. Depending on the values of the different parameters, the turn may also transiently excite a background massive field, leading to damped oscillations until the trajectory settles down along the light direction, corresponding to a dilution parameter $n = 3/2$. For $\omega_c \gtrsim H$, these background oscillations resonate with the quantum oscillations of fluctuations inside the Hubble radius, leading to oscillations linear in $\log k$ and of frequency ω_c [558].

Requiring $\Box\dot{\pi}_c \ll m^2\dot{\pi}_c$, so that the derivative expansion is under perturbative control, imposes some restrictions. Looking at the third term gives the following conditions

$$\frac{\dot{\tilde{c}}_s}{\tilde{c}_s} \ll m, \qquad \epsilon \ll \left(\frac{m}{H}\right)^2, \qquad \frac{\ddot{\tilde{c}}_s}{\tilde{c}_s} \ll m^2 , \tag{15.36}$$

whereas the first and the second terms are negligible as long as $k_{\rm p}^2 \ll m^2$ (see e.g. [555] for more details).

Resonant features are particularly interesting as they can tell apart the inflationary scenario from alternative ones, as exemplified by the primordial standard clocks program [330, 331, 573, 574, 334, 333, 335]. Both sharp and resonant features may also be encountered in single-field scenarios with either transient (bump, dip), or ever-present (tiny oscillatory component) deviations from the slow-roll dynamics, see for instance [557, 558, 575, 576, 73].

Before presenting numerical results, we briefly digress to discuss the purpose and limitations of our approach. From an EFT point of view, all couplings of the theory are generic functions of time that need to be inferred from data. However, notice that specific background models result in general in relationships between the time-dependencies of these couplings, whose knowledge can be used to parameterise the EFT couplings. In the following, for simplicity, we adopt a modelling where only the time dependence of the quadratic mixing is taken into account. First, we assume that the time dependence of the quadratic mixing is not reflected in the evolution of the background spacetime, that is we assume that there is no variation of the Hubble parameter. Moreover, we do not assume any time dependence for the mass of the fluctuation σ, although in concrete multi-field realisations it is known to contain—in addition to a contribution from the second derivative of the potential—an explicit dependence on the quadratic mixing and the background field-space geometry [577, 578, 579].[10] Therefore, our approach disregards effects such as resonances from the time variation of the mass of the heavy field fluctuation with the same frequency ω_c. Of course, it would be possible to solve the background dynamics and feed CosmoFlow with the actual time evolution of all varying quantities. This is precisely the purpose of the already existing tools PyTransport and CppTransport [551, 550, 552]. We instead embrace an effective description of fluctuations, having the advantage of rendering the symmetries manifest, and focusing directly on observables rather than the underlying model building.

Numerical results. For $(\omega_c, 1/\Delta t) \ll m$, the adiabaticity conditions (15.37) are satisfied and we expect that the effects coming from the heavy physics are well captured by a reduced speed of sound. Whenever $\Delta t \ll m^{-1}$ or $\omega_c \gg m$, the effective theory is expected to break down. Here, we focus on the particularly interesting regime $\Delta t \lesssim m^{-1}$ while maintaining $\mu_c \ll \mu$. Fig. 15.9 shows the numerical results for $\rho_0/H = 20, \mu_c = 0.1$, $\Delta t = 0.1 H^{-1}$ and $n = 3/2$, both for $\mu = 2$ and $\mu = 5$. These parameters describe a sharp feature where the resonant effects from the oscillations, that occur only for $\mu_c \gtrsim 1$, are absent. We display the power spectrum (blue) and the bispectrum in the equilateral configuration (red), computed both in the full (solid line) and the effectively single-field (dashed line) theories. For illustration purposes, we have normalised the power spectrum to the featureless one and mutiplied it by a factor of 20. We have chosen the overall amplitude ρ_0 so that the power spectrum presents features of order a few percents for $\mu = 2$ and is compatible with current bounds from CMB observations. This figure exhibits the presence of

[10] From $m^2(t)\sigma^2 \to m^2(t+\pi)\sigma^2 \approx (m + \dot{m}\,\pi)^2\,\sigma^2$, a non-trivial time variation of the mass of the field σ would generate the cubic interaction $\mathcal{L}_{\pi-\sigma}/a^3 \supset \frac{(\dot{m}^2)}{2f_\pi^2}\,\pi_c\sigma^2$ (see [555] for the complete cubic action for inflationary fluctuations written in comoving gauge in non-linear two-field sigma model.).

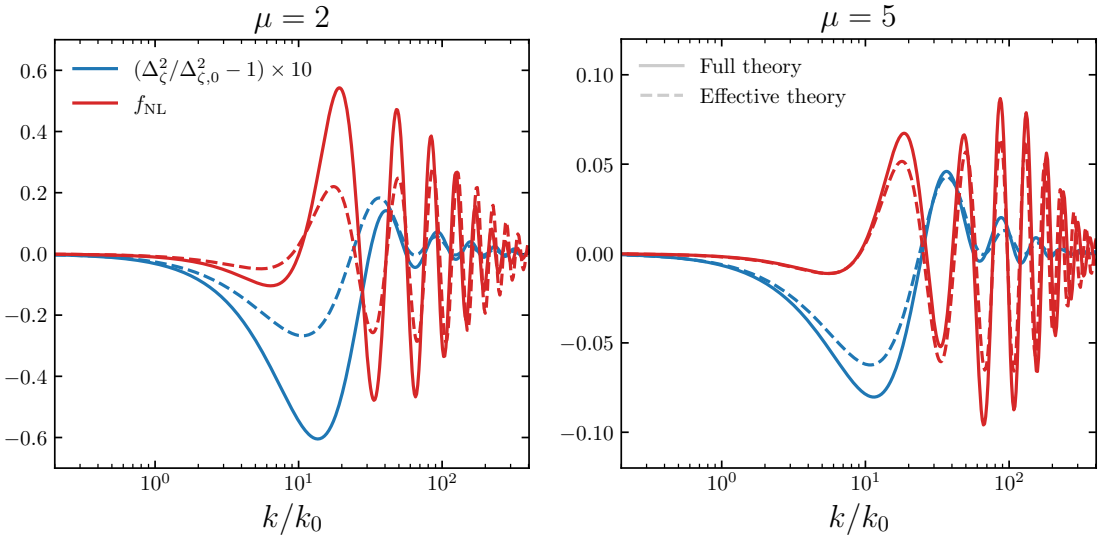


Figure 15.9: The relative power spectrum to the featureless one $\Delta^2_{\zeta,0}$ and the bispectrum $f_{\rm NL}$ in the equilateral configuration $k_1 = k_2 = k_3 = k$ as functions of k/k_0, computed in the full theory (*solid lines*) and in the effective single-field theory (*dashed lines*) both for $\mu = 2$ (*left panel*) and $\mu = 5$ (*right panel*). The feature, parameterised by $\rho_0/H = 20, \mu_c = 0.1, n = 3/2$, and $\Delta t = 0.1H^{-1}$, is localised at $t = t_0$ which corresponds to the scale $k = k_0$.

correlated oscillations in $2k/k_0$ for the power spectrum and $3k/k_0$ for the bispectrum, characteristic of a sharp feature that eventually decays at smaller scales. It is interesting to observe that the bispectrum envelop reaches a maximum at $k/k_0 \sim 20$. These features are compatible with previous findings in the literature, including general statements about the universal running and model-dependent envelop in [330]. With $\Delta t = 0.1H^{-1}$ and our choice of masses, it is clear that the adiabaticity conditions (15.37) are not satisfied. Nonetheless, it is interesting to see that the effective theory already provides a reasonable description, modestly reproducing the correct amplitude of the feature but replicating the oscillatory profile. For larger masses $m \gg \Delta t^{-1} = 10H$, we expect the power spectrum and the bispectrum in equilateral configurations obtained with the effective theory to be indistinguishable from the ones obtained with the full theory.

15.4.3 Probing the Inflationary Landscape

We now study the bispectrum shape dependence at a given overall scale. Importantly, the explicit breaking of scale invariance by the time dependence of the quadratic mixing, and therefore of the cubic one by symmetry, induces unobservable contributions that should be subtracted from any bispectrum calculation. Here, we prove that after subtracting these gauge artefacts, the observable bispectrum encodes non-standard cosmological collider signals whose frequency is partially dictated by the background frequency.

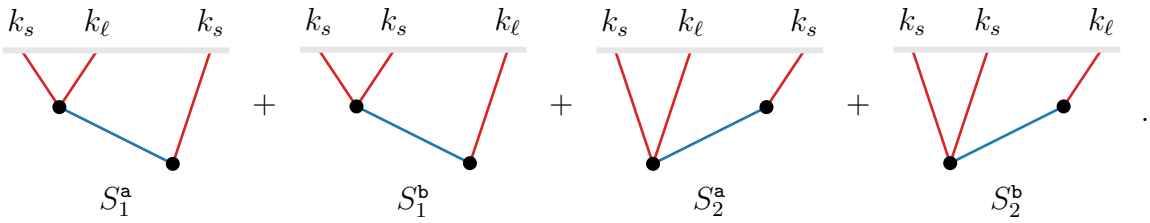
Consistency relation and observable bispectrum. In its squeezed limit, the observable primordial bispectrum measured in cosmological data, is found by carefully subtracting the leading-order contribution coming from an effective rescaling of the background experienced by short-wavelength fluctuations, in presence of a long-wavelength ζ mode [580, 581, 582]. This gauge artefact—since a rescaling of the background does not constitute an observable quantity—which is present in soft limits of all primordial correlation functions, is determined by so-called consistency relations. For the bispectrum, squeezed configurations are famously dominated by the power spectrum scale-dependence [42, 583, 63] (see also e.g. [584, 585, 586, 79, 587, 588, 141, 589, 590] for related works)

$$\lim_{k_3\ll k_1}\frac{\langle\zeta_{\boldsymbol{k}_1}\zeta_{\boldsymbol{k}_2}\zeta_{\boldsymbol{k}_3}\rangle'}{P_\zeta(k_3)}=-P_\zeta(k_s)\,\frac{\partial\log[k_s^3P_\zeta(k_s)]}{\partial\log k_s}+\mathcal{O}((k_\ell/k_s)^2)\,, \tag{15.39}$$

where $P_\zeta(k)=\langle\zeta_{\boldsymbol{k}}\zeta_{-\boldsymbol{k}}\rangle'$, $\boldsymbol{k}_\ell=\boldsymbol{k}_3$ and $\boldsymbol{k}_\mathrm{s}=\boldsymbol{k}_1+\boldsymbol{k}_\ell/2=(\boldsymbol{k}_1-\boldsymbol{k}_2)/2$. When computing the bispectrum in the pure scale-invariant limit, i.e. $\partial\log[k^3P_\zeta(k)]/\partial\log k=n_s-1=0$, the gauge artefact contribution to the bispectrum vanishes in the squeezed limit, and observable effects, which normally show up at next-to-leading order, become automatically the dominant contribution. However, in the presence of features, $n_s(k)\neq1$ and the consistency relation (15.39) should be subtracted to obtain theoretical predictions that can be readily compared to actual cosmological data. As we will see with a concrete example supported by both an exact numerical calculation and analytical insights, it is crucial to properly subtract the consistency relations in cosmological collider signals when features are present. Indeed, one could wrongly conclude that the observable signal in the squeezed limit is hidden below a dominant and universal contribution, which is nothing but the aforementioned gauge artefact.

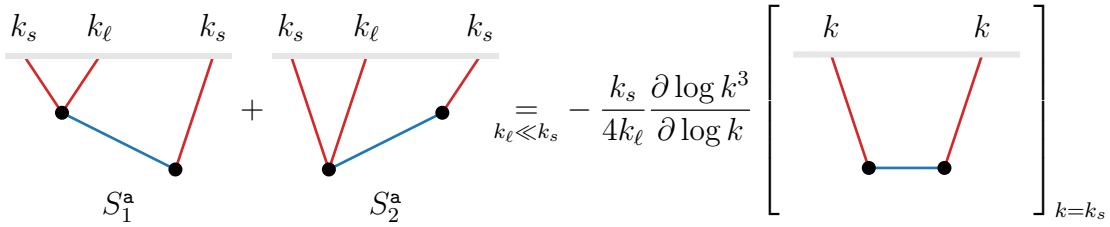
When the quadratic mixing strength is weak, some analytical insight can be gained by evaluating the bispectrum shape using perturbative techniques. Using the in-in formalism (see Chap. 12), the bispectrum shape is composed of two contributions $S(k_1,k_2,k_3)=S_1(k_1,k_2,k_3)+S_2(k_1,k_2,k_3)$, where S_1 corresponds to a quadratic mixing insertion prior to the cubic interaction and S_2 the opposite. Specifying to isosceles configurations $k_1=k_2\simeq k_s$ and $k_3=k_\ell$ where k_s is the short (i.e. hard) momentum and k_ℓ is the long (i.e. soft) momentum, each of the two shape contributions have two fundamental permutations, $S_i=S_i^{\mathtt{a}}+S_i^{\mathtt{b}}$ for $i=\{1,2\}$, corresponding to having either k_s (denoted in the following permutation "$\mathtt{a}$") or k_ℓ (denoted in the following permutation "$\mathtt{b}$") carried by a ζ mode attached to the quadratic mixing. Note that each contribution "$\mathtt{a}$" includes two additional internal permutations accounting for the exchange of k_ℓ and k_s for both ζ modes attached to the cubic interaction. Diagrammatically and using the above notations, the total

shape is given by the four following contributions[11]



(15.40)

The contributions S_1^{b} and S_2^{b} contain the cosmological collider signals as these channels effectively probe the super-horizon decay of the massive field for a large hierarchy of scales $k_\ell \ll k_s$. As we will see in what follows and for the quadratic mixing given in Eq. (15.38), the contribution S_1^{b} contains the dominant cosmological collider signal. On the other hand, the contributions S_1^{a} and S_2^{a}, scaling as $\sim (k_\ell/k_s)^{-1+2n}$ (see insert below), become large and dominant in the squeezed limit. Note that for an ever-present feature $n = 0$, the latter shape contributions are of the local type. One might expect that the cosmological collider signal is therefore completely out of reach. However, these large contaminating signals are not observable. Indeed, translating the bispectrum consistency relation to the dimensionless shape function for isosceles kinematic configurations, we obtain the remarkable identity



$$\underset{k_\ell \ll k_s}{=} -\frac{k_s}{4k_\ell}\frac{\partial \log k^3}{\partial \log k} + \mathcal{O}\left(k_\ell/k_s\right) \tag{15.41}$$

We leave the details of the derivation in the insert below. This property holds for any time dependence of the quadratic mixing. Importantly, this means that the gauge artefact encoded by the consistency relation is included in the two contributions "a", and therefore that the observable squeezed bispectrum is composed only of the two contributions of the type "b", as well as the remaining "a" contributions. Whenever the various contributions are calculated separately, as in the analytical calculation in the perturbative regime, one can simply focus on the type "b" contributions and discard the leading-order "a" ones. On the contrary, whenever the bispectrum shape is computed all at once, as in the cosmological flow approach, one has to explicitly subtract the contribution proportional to the tilt of the power spectrum. The effect from rescaling the background by a long mode also partially constrains higher-order corrections, see e.g. [584, 591, 79, 587, 592], especially terms of order $(k_\ell/k_s)^2$ in Eq. (15.39) which are physical. Still, the S_1^{b} channel remains the dominant contribution in the squeezed limit, as we will see.

[11] Time runs from bottom to top until the end of inflation denoted by the grey line, red lines represent propagators of ζ that are independent—in this perturbative scheme—of those of σ in blue, black dots are quadratic and cubic vertices.

Derivation.—In this insert, we derive (15.41) for a quadratic mixing $\rho(t)$ with arbitrary time dependence. The leading-order power spectrum correction due to the massive field exchange can be recast as

$$(\Delta_\zeta^2 - \Delta_{\zeta,0}^2)/\Delta_{\zeta,0}^2 = -\pi \left(\frac{\rho_0}{H}\right)^2 \int_0^\infty \mathrm{d}x \int_x^\infty \mathrm{d}y\, \mathcal{I}(x,y;x_0)\,, \tag{15.42}$$

where the integrand reads

$$\mathcal{I}(x,y;x_0) = (xy)^{-\frac{1}{2}} \tilde{\rho}(x)\tilde{\rho}(y)\sin(x)\mathrm{Im}\left[H_{i\mu}^{(1)}(x)H_{i\mu}^{(2)}(y)e^{-iy}\right]\,, \tag{15.43}$$

with $\tilde{\rho} = \rho/\rho_0$ denoting the dimensionless linear coupling. For the specific choice (15.38) and neglecting the window function for simplicity, one has $\tilde{\rho}(x) = (x/x_0)^n \sin[\mu_c \log(x/x_0)]$ with $x_0 = -k\tau_0$, although the derivation is applicable to any time dependence of the linear coupling. In the isosceles kinematic configuration, the dimensionless shape function generated by the single exchange of the massive field is a function of $\kappa \equiv k_\ell/k_s$, encoding the shape dependence, and $\lambda \equiv k_\ell/k_0 = \kappa x_0$ which encodes the overall scale dependence due to the feature. We focus on the cubic interaction $\dot{\rho}(t)\pi_c\dot{\pi}_c\sigma$ as the other interactions—shift symmetric in π_c—do not enter the consistency relation. The two contributions to the shape function for which a long mode is attached to the cubic interaction read

$$S_i^{\mathsf{a}}(\kappa,\lambda) = -\frac{\pi}{4}\left(\frac{\rho_0}{H}\right)^2 \kappa^{-1} \int_0^\infty \mathrm{d}x \int_x^\infty \mathrm{d}y\, \mathcal{J}_i^{\mathsf{a}}(x,y;\kappa,\lambda)\,, \tag{15.44}$$

where $i = \{1,2\}$ refers to either having the quadratic or the cubic interaction inserted at earlier times, as depicted in (15.40), and the integrands read

$$\begin{aligned}
\mathcal{J}_1^{\mathsf{a}}(x,y;\kappa,\lambda) &= \tfrac{\partial_t\tilde{\rho}}{H}(x)\tilde{\rho}(y)(xy)^{-\frac{1}{2}}\mathrm{Im}\left[(1+i\kappa x+\kappa^2(1+ix))e^{-i(1+\kappa)x}\right] \\
&\quad\times \mathrm{Im}\left[H_{i\mu}^{(1)}(x)H_{i\mu}^{(2)}(y)e^{-iy}\right]\,, \\
\mathcal{J}_2^{\mathsf{a}}(x,y;\kappa,\lambda) &= \tilde{\rho}(x)\tfrac{\partial_t\tilde{\rho}}{H}(y)(xy)^{-\frac{1}{2}}\sin(x) \\
&\quad\times \mathrm{Im}\left[H_{i\mu}^{(1)}(x)H_{i\mu}^{(2)}(y)(1+i\kappa y+\kappa^2(1+iy))e^{-i(1+\kappa)y}\right]\,.
\end{aligned} \tag{15.45}$$

Let us now estimate the scalings of these contributions in the squeezed limit $\kappa \ll 1$. The exponential e^{-iy} in the integrand $\mathcal{J}_1^{\mathsf{a}}$ effectively renders all contributions from the $y \geq 1$ region negligible, so that the integral is dominated by the saddle point around $y \sim 1$. As a result, one can expand in $\kappa y \ll 1$ inside the integral for $\kappa \ll 1$. Similarly inside the second nested integral for $x \leq y$, one can take the $\kappa x \ll 1$ limit, which could also be seen from the factor $e^{-i(1+\kappa)x}$ killing all contributions from $(1+\kappa)x \approx x \geq 1$. At leading order in κ, the integrand $\mathcal{J}_1^{\mathsf{a}}$ simplifies to

$$\mathcal{J}_1^{\mathsf{a}}(x,y;\kappa,\lambda) = -\tfrac{\partial_t\tilde{\rho}}{H}(x)\tilde{\rho}(y)(xy)^{-\frac{1}{2}}\sin(x)\mathrm{Im}\left[H_{i\mu}^{(1)}(x)H_{i\mu}^{(2)}(y)e^{-iy}\right]\,. \tag{15.46}$$

For the quadratic mixing (15.38), and taking into account the dependence of $\tilde{\rho}$ on $x_0 = \kappa/\lambda$, the overall scaling in the squeezed limit is found to be

$$S_1^{\mathsf{a}}(\kappa,\lambda) \sim \kappa^{-1+2n}\lambda^{2n}\,\mathrm{Im}\left[\alpha_{1,+}^{\mathsf{a}}\kappa^{2i\mu_c} + \alpha_{1,-}^{\mathsf{a}}\kappa^{-2i\mu_c} + \alpha_{1,0}^{\mathsf{a}}\right]\,, \tag{15.47}$$

where the coefficients $\alpha_\pm$ and α_0 depend on μ, n and λ. Note that in the presence of a slowly-decaying feature in the mixing such that $n \leq 1/2$, this shape contribution

dominates in the squeezed limit as it grows as function of κ, even for a process involving the exchange of a heavy field. Notably, the shape oscillates in $\log\kappa$ at a frequency solely set by the background frequency μ_c. Proceeding in the same way, the contribution S_2^{a} has the same scaling in the squeezed limit. Note that these scalings and the oscillations with frequency $2\mu_c$ can be recovered using the effective single-field Lagrangian (15.34) in the corresponding regime of validity.

Additionally, from

$$\frac{\partial\tilde{\rho}(x)}{\partial k} = \frac{x}{k^2}\,\frac{\partial\tilde{\rho}(\tau)}{\partial\tau}\bigg|_{\tau=-\frac{x}{k}} = \frac{1}{k}\frac{\partial_t\tilde{\rho}}{H}(x)\,, \tag{15.48}$$

we obtain the remarkable identity

$$\frac{\partial\mathcal{I}}{\partial k} = \frac{1}{k}\left(\mathcal{J}_1^{\mathsf{a}} + \mathcal{J}_2^{\mathsf{a}}\right)\left(1+\mathcal{O}(\kappa^2)\right)\,. \tag{15.49}$$

Lastly, one needs to pull the derivative out of the time integrals. Defining $I(x_0) = \int_0^\infty \mathrm{d}x f(x,x_0)\int_x^\infty \mathrm{d}y g(y,x_0)$ where $\mathcal{I}(x,y;x_0) = f(x,x_0)g(y,x_0)$, and differentiating with respect to x_0, one straightforwardly obtains

$$\frac{\partial I}{\partial x_0} = \int_0^\infty \mathrm{d}x\,\frac{\partial f}{\partial x_0}(x,x_0)\int_x^\infty \mathrm{d}y\,g(y,x_0) + \int_0^\infty \mathrm{d}x\,f(x,x_0)\int_x^\infty \mathrm{d}y\,\frac{\partial g}{\partial x_0}(y,x_0)\,. \tag{15.50}$$

Altogether, we obtain the identity

$$\sum_{i=1,2} S_i^{\mathsf{a}}(\kappa,\lambda) = -\frac{1}{4\kappa}\,\frac{\partial\log(k^3\Delta_\zeta^2)}{\partial\log k}\bigg|_{k=k_s} + \mathcal{O}(\kappa)\,, \tag{15.51}$$

which is precisely the consistency relation at the level of the shape function.

Cosmological collider signals. We focus on the bispectrum arising from the cubic interaction $\dot{\rho}(t)\pi_c\dot{\pi}_c\sigma$ because it is the dominant one for rapid oscillations $\mu_c > 1$, with the quadratic mixing time dependence of Eq. (15.38). We show in Fig. 15.10 the corresponding shape functions for a light and heavy field σ, for $n = 0$ and different background frequencies μ_c. The dashed line corresponds to the cosmological flow results—hence containing all contributions, even the unobservable ones corresponding to $S_{1,2}^{\mathsf{a}}$ in the perturbative analysis—and the solid lines correspond to the shapes that are directly measurable in cosmological data as they are found after subtracting the consistency relation given solely in terms of the power spectrum. Note that in the cosmological flow framework, both the two- and three-point correlators are computed simultaneously as the flow equations form a closed system. It therefore requires no additional computations to directly obtain the observable signals out of a single computation. Note also that our numerical approach is precise enough (both at the level of the power spectrum and of the bispectrum) to allow for a clean subtraction of dominant unobservable contributions in order to recover a subdominant scaling behaviour. This is readily visible, for example, in the light-field case for $\mu_c = 5$ where the raw signal (*dashed line*) presents a distorted oscillatory

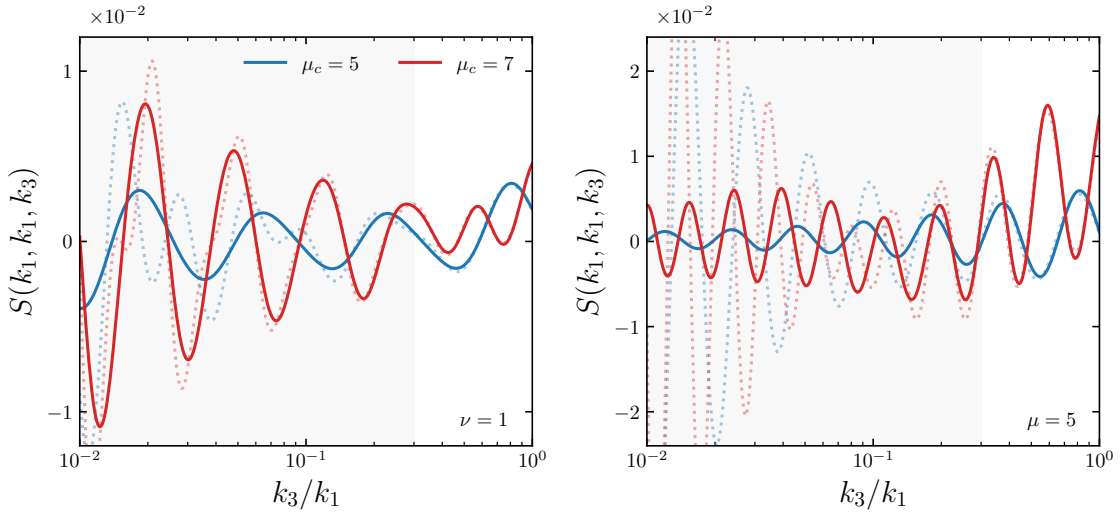


Figure 15.10: Observable shape functions (*solid lines*) dictated by the mixing Lagrangian (15.33) with the time-dependent mixing $\rho(t)$ given in Eq. (15.38), in the isosceles kinematic configuration $k_1 = k_2$ at a fixed overall scale $\log(k_3/k_0) = 2$ where $k_0 = (aH)(t_0)$ and t_0 is the characteristic time of the feature, for a light field $\nu = 1$ (*left panel*) and a heavy field $\mu = 5$ (*right panel*), varying the background frequency $\mu_c = 5, 7$, and setting $n = 0$. The observable signal is reconstructed from the computed one (*dotted line*) upon numerically subtracting the consistency relation (15.41). The shaded region corresponds to the squeezed limit where the templates (15.52) are valid. We have chosen $\rho_0/H = 0.1$ to respect the current bounds on the power spectrum [593].

pattern due to the interference of various signals with different frequencies, as well as a quickly growing envelope (as k_s/k_ℓ) in the squeezed limit. The observable signal after subtracting gauge artefacts (*solid line*), on the other hand, features a single frequency and is growing at a slower pace (as $(k_\ell/k_s)^{-1/2}$).

A notable feature of these signals is that their frequencies are partially set by the background frequency μ_c. This offers the possibility to probe inflationary landscapes with cosmological collider signals.[12] Indeed, in the perturbative analysis and considering only the shape contributions $S_1^{\flat}$ and $S_2^{\flat}$, as the other two are removed by the consistency relation, the non-analytical signal lying in the squeezed limit ($k_3 \ll k_1$) of the shape function both for the exchange of a *light* ($m/H \leq 3/2$) and a *heavy* ($m/H \geq 3/2$) field is found to be

$$S(k_1,k_2,k_3) = \begin{cases} \left(\frac{k_3}{k_1}\right)^{1/2+n-\nu} \mathcal{A}\cos\left(\mu_c \log\left(\frac{k_3}{k_1}\right)+\varphi\right) , & \text{(light)} \\ \left(\frac{k_3}{k_1}\right)^{1/2+n} \sum_{\pm} \mathcal{A}_{\pm}\cos\left((\mu\pm\mu_c)\log\left(\frac{k_3}{k_1}\right)+\varphi_{\pm}\right) , & \text{(heavy)} \end{cases} \tag{15.52}$$

with $\mu = \sqrt{(m/H)^2 - 9/4}$ and $\nu = i\mu$. Details on the derivation can be found

[12] Instead, for cubic interactions of constant strengths, cosmological collider signals are conventional with frequencies only set by the mass of the additional field, despite the time-dependence of the quadratic mixing [342]. This can also be seen in our proof in the insert below.

in the insert below. A generic feature of these signals is that the power-law scaling acquires an additional $(k_3/k_1)^n$ suppression compared to the standard one [58]. This is a direct consequence of the dilution of the feature in $(a/a_0)^{-n}$. For the exchange of a light field, in addition to the power-law scaling that depends on the mass, the shape presents oscillations in $\log(k_3/k_1)$ whose frequency is set by the background frequency μ_c. The light-field template is not valid for the massless case ($\nu = 3/2$) and an ever-present feature $n = 0$ as curvature modes never freeze on super-horizon scales. In the case of a heavy-field exchange process, the power-law scaling is saturated and the cosmological collider signals present modulated frequencies in $\mu \pm \mu_c$. These beats are characteristic of interference patterns between the usual oscillations of the heavy field on super-horizon scales and an additional oscillating signal, in this case generated by the background. Cross-correlating the analytic template (15.52) with features in the power spectrum, namely their amplitudes, and the scale-dependence of the bispectrum, can remove the degeneracy between the mass of the additional field and the oscillating background frequency. Remarkably, we find numerically that the templates (15.52) hold in the strong mixing regime. Altogether, these results provide a new way of probing the landscape of inflationary backgrounds through soft limits of cosmological correlators. In particular, for light fields with $\nu > 1/2 + n$, the oscillations that modulate a growing shape envelope in the squeezed limit are expected to generate distinctive oscillations in the scale-dependent galaxy bias. It would also be interesting to find a concrete background model that reproduces these features, as our analysis entirely relies on symmetries at the level of inflationary fluctuations.

Derivation.—In this insert, we estimate the scaling of the *observable* shape contributions $S_1^{\mathfrak{b}}$ and $S_2^{\mathfrak{b}}$ in the squeezed limit and derive the analytical templates (15.52). After subtracting the consistency relation at leading order in $k_\ell/k_s \ll 1$, the physical shape is given by

$$S(\kappa,\lambda) = -\frac{\pi}{4}\left(\frac{\rho_0}{H}\right)^2 \kappa^{-1} \int_0^\infty \mathrm{d}x \int_x^\infty \mathrm{d}y \sum_{i=1,2} \mathcal{J}_i^{\mathfrak{b}}(x,y;\kappa,\lambda)\,, \tag{15.53}$$

where $\kappa \equiv k_\ell/k_s$ and $\lambda \equiv k_\ell/k_0$. The integrands read

$$\begin{aligned}
\mathcal{J}_1^{\mathfrak{b}}(x,y;\kappa,\lambda) &= \tfrac{\partial_t\tilde{\rho}}{H}(x)\tilde{\rho}(y)\kappa^2(xy)^{-\frac{1}{2}}\mathrm{Im}\left[(1+ix)e^{-2ix}\right]\mathrm{Im}\left[H_{i\mu}^{(1)}(\kappa x)H_{i\mu}^{(2)}(\kappa y)e^{-i\kappa y}\right]\,,\\
\mathcal{J}_2^{\mathfrak{b}}(x,y;\kappa,\lambda) &= \tfrac{\partial_t\tilde{\rho}}{H}(x)\tilde{\rho}(y)\kappa^2(xy)^{-\frac{1}{2}}\sin(\kappa x)\mathrm{Im}\left[H_{i\mu}^{(1)}(\kappa x)H_{i\mu}^{(2)}(\kappa y)(1+iy)e^{-2iy}\right]\,.
\end{aligned} \tag{15.54}$$

We now estimate the scalings and behaviours of these contributions in the squeezed limit $\kappa \ll 1$. The exponential e^{-2ix} in the integrand $\mathcal{J}_1^{\mathfrak{b}}$ selects the integration region $x < 1$, discarding possible resonances between this exponential and the oscillating feature. Note that we have neglected the window function, which corresponds to considering $k_\ell/k_0 \gg 1$, i.e. that both the long and the short modes exit the horizon well after the characteristic scale of the feature. We can then expand in $\kappa x \ll 1$ inside the integral and use the late-time behaviour of the Hankel function $H_{i\mu}^{(1)}(z) \approx A_\mu^+ z^{i\mu} + A_\mu^- z^{-i\mu}$ for $z \ll 1$. After changing variables $y \to \tilde{y} = \kappa y$, the lower bound of the inner integral can be extended up to $\kappa x \to 0$, effectively decoupling the two integrals.

Altogether, the overall scaling in the squeezed limit for the shape contribution $S_1^{\mathfrak{b}}$ is found to be

$$\begin{aligned} S^{\mathfrak{b}}_{1,\text{light}}(k_1,k_2,k_3) &\sim \kappa^{\frac{1}{2}+n-\nu}\lambda^{-2n}\text{Im}\left[\alpha^{\mathfrak{b}}_{1,+}\kappa^{i\mu_c}+\alpha^{\mathfrak{b}}_{1,-}\kappa^{-i\mu_c}\right] , \\ S^{\mathfrak{b}}_{1,\text{heavy}}(k_1,k_2,k_3) &\sim \kappa^{\frac{1}{2}+n}\lambda^{-2n}\text{Im}\Big[\alpha^{\mathfrak{b}}_{1,++}\kappa^{i(\mu+\mu_c)}+\alpha^{\mathfrak{b}}_{1,+-}\kappa^{i(\mu-\mu_c)} \\ &\qquad +\alpha^{\mathfrak{b}}_{1,-+}\kappa^{-i(\mu-\mu_c)}+\alpha^{\mathfrak{b}}_{1,--}\kappa^{-i(\mu+\mu_c)}\Big] , \end{aligned} \tag{15.55}$$

for the light and the heavy case, respectively. Similarly, for the integrand $\mathcal{J}_2^{\mathfrak{b}}$, the exponential e^{-2iy} selects the region $y<1$ and we can take the $\kappa y \ll 1$ limit inside the integrand. As $x<y$, we can also take the limit $\kappa x \ll 1$. Using the Hankel expansion and at leading order in κ, the scalings are found to be

$$\begin{aligned} S^{\mathfrak{b}}_{2,\text{light}}(k_1,k_2,k_3) &\sim \kappa^{2+2n-2\nu}\lambda^{-2n}\text{Im}\left[\alpha^{\mathfrak{b}}_{2,+}\kappa^{2i\mu_c}+\alpha^{\mathfrak{b}}_{2,0}+\alpha^{\mathfrak{b}}_{2,-}\kappa^{-2i\mu_c}\right] , \\ S^{\mathfrak{b}}_{2,\text{heavy}}(k_1,k_2,k_3) &\sim \kappa^{2+2n}\lambda^{-2n}\text{Im}\Big[\alpha^{\mathfrak{b}}_{2,++}\kappa^{2i(\mu+\mu_c)}+\alpha^{\mathfrak{b}}_{2,--}\kappa^{-2i(\mu+\mu)} \\ &\quad +\alpha^{\mathfrak{b}}_{2,+-}\kappa^{2i(\mu-\mu_c)}+\alpha^{\mathfrak{b}}_{2,-+}\kappa^{-2i(\mu-\mu_c)}+\alpha^{\mathfrak{b}}_{2,0+}\kappa^{2i\mu_c} \\ &\quad +\alpha^{\mathfrak{b}}_{2,0-}\kappa^{-2i\mu_c}+\alpha^{\mathfrak{b}}_{2,+0}\kappa^{2i\mu}+\alpha^{\mathfrak{b}}_{2,-0}\kappa^{-2i\mu}+\alpha^{\mathfrak{b}}_{2,00}\Big] . \end{aligned} \tag{15.56}$$

The contribution $S_1^{\mathfrak{b}}$ is therefore the dominant contribution. Defining $\mathcal{A}e^{i\varphi}=(\alpha^{\mathfrak{b}}_{1,+}-\alpha^{\mathfrak{b}*}_{1,-})/i$, and $\mathcal{A}_\pm e^{i\varphi_\pm}=(\alpha^{\mathfrak{b}}_{1,+\pm}-\alpha^{\mathfrak{b}*}_{1,-\mp})/i$, we obtain the templates (15.52). Setting aside intricacies related to IR $(x,y\to 0)$ divergences of the corresponding integrals that cancel when adding all contributions, the amplitudes and the phases of these signals can be computed analytically.

16

Conclusions & Perspectives

> *"This is often the way it is in physics. Our mistake is not that we take our theories too seriously, but that we do not take them seriously enough. It is always hard to realize that these numbers and equations we play with at our desks have something to do with the real world."*
>
> — Steven Weinberg, *The First Three Minutes (1977)*

Despite the tremendous lessons that cosmology and particle physics have brought to understanding the fundamental laws of Nature, the underlying principles that govern our Universe, such as how gravity and quantum physics operate at very high energy, are still not fully understood. One exciting and unique opportunity to explore these mysteries is to study the Universe's earliest moments through the lens of *cosmological correlators*. However, learning new physics from the sky is becoming ever more challenging, as both the high-energy phenomena at play and the data we collect grow increasingly complex. This makes the development of innovative techniques essential to bridge primordial cosmology with theoretical high-energy physics. In this thesis, we have contributed to this endeavour by studying and developing new methods to probe the early Universe through cosmological correlators. Below, we summarise the main results of this thesis and make a few remarks on future directions.

Fundamental Aspects of Cosmological Correlators

In Part II, we have designed and explored new fundamental approaches to studying and computing cosmological correlators. For massive field experiencing particle production, going to the complex mass plane allows one to write a dispersive integral for the propagator that naturally encodes time ordering. Using this object, we have shown that exchanged correlators can be obtained by gluing off-shell lower-point

correlators. In this procedure, performing the resulting spectral integral, which amounts to collecting poles as the integrand is meromorphic, effectively sets the exchanged particle on shell. We argued that this representation not only clarifies the analytic structure and factorisation properties of cosmological correlators but also simplifies explicit calculations. As a specific example, we derived a new, simple closed-form formula for the four-point correlator of conformally coupled fields exchanging a massive field in de Sitter space and examined its analytic properties. Additionally, we derived cosmological largest-time equations, which relate individual correlator in-in branch channels through the analytic continuation of certain external energies. These relations, explicitly illustrated for simple diagrams, can serve as consistency checks for more complex correlators.

We have also derived a closed-form solution for the most general tree-level massive-exchange boost-breaking cosmological correlator up second-order in a (spatial) gradient expansion by solving a boundary differential equation. This includes a reduced sound speed for the external legs, which required analytically continuing the solution outside the kinematic unit circle where the correlator yields a convergent series representation, and accounts for a linear term in the momentum carried by the exchange particle, which describes its coupling to a helical chemical potential. This completes the dictionary of tree-level massive cosmological correlators, giving templates for comparison with observational data, both for the non-analytic part (cosmological collider signal) *and* the background contribution (EFT signal).

Finally, we have also designed a systematic method to derive simple templates for phenomenological interesting signals hidden in cosmological correlators. This method is based on the saddle point approximation, and reflects how the production and propagation of massive fields during inflation are encoded in the location of the complex time saddle points dominating the time integrals. This work has enabled us to systematically classify non-analyticities of cosmological correlators, and has opened a new fascinating relation between the mathematical world of Riemann surfaces and the physics of the early Universe.

Eventually, these fundamental results open several interesting avenues for future investigation:

- *Towards massive cosmological recursion relations*: In the context of modern scattering amplitude techniques, complex amplitudes can be efficiently constructed by sewing together lower-point amplitudes using sophisticated recursion relations. We have shown a glimpse of how such a procedure can be applied to cosmological correlators in simple cases. Since time integrals are trivialised, computing higher-point correlation functions primarily involves performing a series of spectral integrals, which effectively reduces to summing over several towers of poles, given that off-shell lower-point correlators are meromorphic in the complex mass plane. It will be interesting to explore how this off-shell approach can render computations of more complex correlation functions more tractable. Ultimately, we believe this approach lays the groundwork for deriving more general cosmological recursion relations beyond rational correlators.

- *Cosmological resummation*: As in flat space, states in a unitary quantum field theory in de Sitter are classified by unitary irreducible representations of the isometries, which are parametrised by the conformal dimension (related to the mass) and spin. Imposing unitarity as an additional consistency condition imposes a set of positivity constraints. While previous such bounds have been largely theoretical, exploring their phenomenological implications could yield valuable insights. The spectral representation employed in this work can be viewed as the leading-order perturbative Källén-Lehmann representation in spatial Fourier space. By perturbatively computing massive self-energy corrections, it may be possible to extend this approach further in perturbation theory, potentially deriving useful bounds from the positivity and meromorphic properties of the spectral density. Ultimately, one would hope to use this spectral representation to "dress" massive propagators in de Sitter space by resumming bubble diagrams.

- *Spectral decomposition & loop diagrams*: The spectral representation of massive propagators provides the mean to derive complex spectral densities of composite operators (e.g. $\mathcal{O}_\Delta^2$) which then would allow for constructing loop-level correlators. This way, the scalar tree-level exchange that we have derived can serve as a seed correlator to generate loop diagrams, albeit performing the remaining spectral integral.

Physics at Low-Speed & Non-Locality

In Part III, we have studied the imprint of massive fields on cosmological correlators in the presence of a reduced speed of sound for the Goldstone boson of broken time translations. This minimal framework leads to a whole new class of signatures—that we call *cosmological low-speed collider signals*—which are characterised by a distinctive resonance in mildly-soft limits of the cosmological correlators. Let us summarise our main results.

Using the framework of EFT of inflationary fluctuations, we have coupled the Goldstone boson of broken time translations to massive sectors, identifying the allowed leading cubic interactions giving sizeable non-Gaussianities. We have also provided an exhaustive dictionary of strong coupling scales, perturbativity bounds and naturalness criteria for the theory under scrutiny. When the speed of sound is reduced, the heavy field can be integrated out in an unusual manner, yielding a *non-local* single-field theory. This theory emerges as the leading-order term in a time-derivative expansion. Although the heavy field becomes effectively non-dynamical, this simple theory accurately describes the full dynamics of the Goldstone boson and captures all multi-field physical effects—except for the non-perturbative particle production leading to the conventional cosmological collider signal—in the almost entire parameter space. We have characterised this non-local EFT by analysing the dispersion relation, and have shown that this theory encapsulates several known regimes like the effective reduced sound speed and the modified dispersion relation regimes. This theory provides a systematic and tractable single-field EFT treatment of the imprint of massive fields on cosmological correlators. We have also determined the precise regimes of validity of this theory and shown how to system-

atically incorporate higher-order corrections in the derivative expansion. Finally, we have shown that a chemical-potential driven dynamics of an additional massive spin-1 field during inflation generates a large parity-odd trispectrum, which is fully determined by the residue at the singularity of the non-local interactions. These derived parity-violating cosmological correlators serve as a compelling evidence for new physics in the early Universe.

The promising and rich low-speed collider phenomenology exposed in this paper is an invitation to extend and generalise these signatures to spinning intermediate fields and mixed correlators involving gravitons. Finally, it would be interesting from a theoretical perspective to investigate the possibility of systematically constructing a set of boost-breaking EFTs that are non-local in space, yet still consistent with a local UV completion.

Cosmological Flow

In Part IV, we have presented a systematic framework—the cosmological flow—to compute and study cosmological correlators. This approach consists in solving differential equations *in time* satisfied by the correlators, and enables us to obtain exact results in regimes that are challenging to probe analytically. We have exemplified this method with an extensive study of correlators coming from the exchange of a massive scalar particle, both at strong mixing—adopting a non-perturbative treatment of quadratic interactions—and in non scale-invariant theories. This development provides an efficient way to study the rich phenomenology of primordial non-Gaussianities as it makes predictions straightforward. In order for the community to progress faster in these challenging directions, we have publicly released the numerical implementation of our new approach as a freely available resource.[1]

Heading towards a universal programme to generate theoretical data, the cosmological flow has a number of benefits. First, it requires no analytical nor numerical mode functions as it focuses directly on correlators. Second, it effortlessly deals with the early-time $i\epsilon$ prescription as the correlators are evolved on the real time axis. Third, the procedure of setting the flow equations given a certain Lagrangian is straightforward. Finally, the cosmological flow systematically works for all n-point correlators. With this formalism at hand, we have paved the way towards a systematic investigation of the rich and fascinating subject of cosmological correlators. Since observational progresses are expected to be made in the near future, the coming years will lead to a wealth of observational data and constraints on the statistical properties of primordial fluctuations. It is therefore important to provide an adequate amount of theoretical benchmarks, and establish the capability for an efficient exploration of the vast landscape of possible signals. In this respect, the cosmological flow can both extend the reach of primordial correlators phenomenology and complement analytical computations by providing useful checks and generating intuition. More ambitiously, the cosmological flow routine can be included in the already-existing chain of late-time cosmological tools. This would automate the

[1] In this repository, we have also gathered numerical results for power spectra and non-Gaussianities computed with CosmoFlow, for different theories and parameter values. We plan to turn this into a bank of theoretical data to be nurtured by the work of the community.

generation of theoretical primordial data that can be directly used for CMB or LSS observables, hence extending the cosmological flow to the late-time Universe.

Finally, yet importantly, the development of the cosmological flow suggests a number of future directions:

- *Small-scale phenomenology*: Primordial density fluctuations on cosmological scales are probed by observations of the CMB and LSS. Density fluctuations on smaller scales that are forged in the "dark era" of inflation are not directly observable by themselves. Yet, they shape many properties of new observables like gravitational wave backgrounds and primordial black holes. In this respect, we highlight that the cosmological flow approach is not restricted to the largest cosmological scales but is also perfectly applicable to these questions. As the inflationary dynamics involved in this context often relies on a strong breaking of scale invariance and substantial non-linear effects which are difficult to handle analytically, a systematic approach like the cosmological flow provides an essential tool to illuminate the dark era of inflation.

- *Spinning fields*: It would be interesting to extend the cosmological flow to include spinning particles. On the one hand, in conventional setups of weak mixing and under the lamppost of weakly broken scale-invariance, it is known that the cosmological collider signal arising from the exchange of a spinning particle displays a characteristic angular dependence. On the other hand, computing correlators with external spin (for example gravitons, hence accounting for gravitational waves) is notoriously difficult because it is challenging to track the detailed time evolution of the physics in the bulk. The cosmological flow would encapsulate both cases as the flow equations couple *all* correlators, that need to be solved at once. More practically, implementing particles with spin within the cosmological flow requires a careful treatment of the tensorial structures of the spinning fields, and hence necessitates additional indices that would account for polarisation states. A possible direction for future work would be to relax the assumptions of weak mixing and/or scale-invariance, and to extend the phenomenology of spinning fields to regimes that have not yet been explored.

- *Loop-level*: Mostly for technical reasons, the large and rich phenomenology of inflationary correlators mainly comes from explicit calculations at tree level. *Per contra*, pushing the available technology further in perturbation theory and developing new techniques to compute loops is of primary importance. Practically, it would extend the reach of the cosmological collider phenomenology by including particles within and beyond the Standard Model. Yet, aside from isolated examples, there is no systematic treatment of loops in cosmological spacetimes. That is why it would be interesting to derive the flow equations at one-loop level. One can already notice that extending the cosmological flow to loop-level would require way more computational capability. For example, computing the two-point correlators at one-loop level requires to solve the flow equations for the three-point functions (working at loop-level precisely means that we do not neglect anymore non-linearities of the three-point correlators

on the two-point correlators), which requires first the solutions of the two-point correlators flow equations at tree-level (this is equivalent to solving the quadratic theory). Therefore, one is not able to solve all equations at once—as we have done so far—but rather order by order.

- *(Non-)unitarity*: More conceptually, the cosmological flow—by evolving correlators in time—brings the question of unitarity. Indeed, a unitary time evolution ensures that the total probability is conserved over time, and therefore the theory is complete in the sense that it makes self-contained predictions for observables. In flat-space QFT, important properties follow from unitarity. For example, correlation functions must *factorise* into products of lower-order ones. Within the cosmological flow, we have seen that the time evolution of correlators is *sourced* by products of lower-order ones. This unforeseen concordance implores a better understanding of the status of the flow equations and their flat-space analogues. Finally, it would be interesting to see how non-unitary effects arising from the interference between the two branches of the in-in contour—such as decoherence and dissipation—can be incorporated in the flow equations.

***

There is no question more profound than that of the Universe's origin. Fortunately, we live in an era where addressing this mystery is not only possible but within reach—at least theoretically—through the study of cosmological correlators. Thanks to ever-improving observations, we have never been so close to reconstructing nearly 13.8 billion years of cosmic history and, at last, unveiling the first fleeting moments after the Big Bang. Contributing to this journey is an immense privilege—one that fills me with awe every single day. While this thesis marks just the initial stride, it is evident that a substantial journey lies ahead, promising numerous new discoveries.

A

Details on Massive Fields in de Sitter

In this appendix, we provide the reader with useful mathematical formula for massive fields in de Sitter, give details about bulk cutting rules to extract non-local signals, and present Mellin-Barnes techniques to compute masisve exchange cosmological correlators. Consider a real scalar field σ of mass m, evolving in de Sitter space with three spatial dimensions. The action is

$$S = -\frac{1}{2}\int \mathrm{d}^4x\sqrt{-g}\left[(\partial_\mu\sigma)^2 + m^2\sigma^2\right] , \tag{A.1}$$

where m is identified with the parameter in the action that we are used to interpret as the mass of the field from Minkowskian physics.[1] From the action, we obtain the equation of motion describing the classical dynamics $(-\Box + m^2)\sigma = 0$, where $\Box \equiv g^{\mu\nu}\nabla_\mu\nabla_\nu = -\partial_t^2 - 3H\partial_t + \partial_i^2/a^2$ denotes the d'Alembert operator on dS_4, with t being the cosmic time. We will focus on fields in the principal series so that $\mu \equiv \sqrt{m^2/H^2 - 9/4}$ is real. In what follows, we set $H = 1$ for convenience. Defining the canonically normalised field $\sigma_c(\tau, \boldsymbol{x}) = (-\tau)^{-3/2}\sigma(\tau, \boldsymbol{x})$, its positive-frequency mode function is given by

$$u_k(\tau,\mu) = \frac{i\sqrt{\pi}}{2}\, e^{-\frac{\pi\mu}{2}}\, H^{(1)}_{i\mu}(-k\tau) \xrightarrow[|k\tau|\to\infty]{} \frac{e^{-ik\tau}}{\sqrt{2k\tau}} , \tag{A.2}$$

where $H^{(1)}_{i\mu}(z)$ is the Hankel function of the first kind, such that it reduces to the usual Bunch-Davies vacuum in the far past, up to an overall unimportant phase.

[1] Note that the field σ can also be coupled to the gravitational background through the term $\mathcal{L}/a^3 \supset -\frac{\xi}{2}R\sigma^2$ where R is the Ricci scalar. Since the Ricci scalar is a constant in de Sitter $R = 12H^2$, the coupling ξ can be absorbed in the mass $\tilde{m}^2 = m^2 + \xi R$, in practice changing from the Jordan to the Einstein frame. The case for which $\xi = 0$ is the minimally coupled case. The conformally coupled case corresponds to $\tilde{m}^2 = \frac{R}{6} = 2H^2$, equivalently setting $m/H = 0$ and $\xi = 1/6$. The action is therefore invariant under conformal transformations and the field does not experience the space-time expansion. The conformally coupled case is the analogue of the massless one in flat space.

The in-in contour $\mathcal{C}_{i\epsilon}$ requires analytically continuing the positive-frequency mode function (A.2) to the lower-half $k\tau$-complex plane to ensure reaching the asymptotic vacuum. This precisely avoids crossing the branch cut of the Hankel function $H^{(1)}_{i\mu}(z)$, that is chosen to lie on the real negative axis, away from the physical regime. Therefore, using the complex conjugate relation (A.4), the negative-frequency mode can be written

$$u^*_k(\tau,\mu) = -\frac{i\sqrt{\pi}}{2}\, e^{+\frac{\pi\mu}{2}}\, H^{(2)}_{i\mu}(-k\tau)\,. \tag{A.3}$$

A.1 Glossary of Hankel and Legendre Functions

The following mathematical identities are useful for manipulating mode functions of a massive scalar field in de Sitter.

Complex conjugate relations. The Hankel functions of the first and second kind are related by the complex conjugate relations

$$\left[H^{(1)}_{i\mu}(z)\right]^* = e^{+\pi\mu} H^{(2)}_{i\mu}(z^*)\,, \quad \left[H^{(2)}_{i\mu}(z)\right]^* = e^{-\pi\mu} H^{(1)}_{i\mu}(z^*)\,, \tag{A.4}$$

for $z \in \mathbb{C}\backslash\{\mathbb{R}^-\}$. Notice that these relations are not verified when the argument z lies on the branch cut.

Symmetries. The Hankel functions obey the following relations

$$H^{(1)}_{-i\mu}(z) = e^{-\pi\mu} H^{(1)}_{i\mu}(z)\,, \quad H^{(2)}_{-i\mu}(z) = e^{+\pi\mu} H^{(2)}_{i\mu}(z)\,, \tag{A.5}$$

for $z \in \mathbb{C}$. These identities render manifest an underlying shadow $\mu \leftrightarrow -\mu$ symmetry for the positive- and negative-frequency mode functions

$$u_k(\tau,-\mu) = u_k(\tau,\mu)\,, \quad u^*_k(\tau,-\mu) = u^*_k(\tau,\mu)\,. \tag{A.6}$$

Upon rotating time, the Hankel functions satisfy

$$H^{(1)}_{-i\mu}(e^{+i\pi}z) = -H^{(2)}_{i\mu}(z)\,, \quad H^{(2)}_{-i\mu}(e^{-i\pi}z) = -H^{(1)}_{i\mu}(z)\,. \tag{A.7}$$

The first relation is valid for z in the lower-half complex plane excluding the negative real and imaginary axis, and the second relation is valid for z in the upper-half complex plane excluding the positive real and imaginary axis. In the physical time domain, these identities relate the mode functions by a CPT symmetry

$$u_k(z,\mu) = u^*_k(e^{-i\pi}z,-\mu)\,, \quad u^*_k(z,\mu) = u_k(e^{+i\pi}z,-\mu)\,. \tag{A.8}$$

Additional analytic continuations of the Hankel function are given by

$$\begin{aligned} H^{(1)}_{i\mu}(e^{-i\pi}z) &= e^{+\pi\mu} H^{(2)}_{i\mu}(z) + 2\cosh(\pi\mu) H^{(1)}_{i\mu}(z)\,, \\ H^{(2)}_{i\mu}(e^{+i\pi}z) &= e^{-\pi\mu} H^{(1)}_{i\mu}(z) + 2\cosh(\pi\mu) H^{(2)}_{i\mu}(z)\,. \end{aligned} \tag{A.9}$$

Connection formulae. Hankel functions can be expanded in terms of Bessel functions with the following connection formulae

$$H^{(1)}_{i\mu}(z) = \frac{e^{+\pi\mu}J_{+i\mu}(z) - J_{-i\mu}(z)}{\sinh(\pi\mu)}\,, \quad H^{(2)}_{i\mu}(z) = \frac{J_{-i\mu}(z) - e^{-\pi\mu}J_{+i\mu}(z)}{\sinh(\pi\mu)}\,. \tag{A.10}$$

The Bessel function of the first kind satisfies

$$J^*_{i\mu}(z) = J_{-i\mu}(z^*)\,, \tag{A.11}$$

for $z \in \mathbb{C}\backslash\{\mathbb{R}^-\}$, and has the following power-law asymptotic form for small argument $z \to 0$

$$J_{i\mu}(z) \sim \frac{1}{\Gamma(1+i\mu)}\left(\frac{z}{2}\right)^{i\mu}\,, \tag{A.12}$$

whereas the Hankel function has the following plane-wave asymptotic form for large argument $z \to \infty$

$$H^{(1)}_{i\mu}(z) \sim \sqrt{\frac{2}{\pi z}}\, e^{i\left(z-\frac{\pi}{4}\right)+\frac{\pi\mu}{2}}\,. \tag{A.13}$$

Large-order asymptotic forms. For large μ with z ($\neq 0$) fixed, we have

$$J_{i\mu}(z) \sim \frac{1}{\sqrt{2i\pi\mu}}\left(\frac{ez}{2i\mu}\right)^{i\mu}\,, \quad H^{(1)}_{i\mu}(z) \sim -H^{(2)}_{i\mu}(z) \sim -i\sqrt{\frac{2}{i\pi\mu}}\left(\frac{ez}{2i\mu}\right)^{-i\mu}\,. \tag{A.14}$$

Legendre functions. The Legendre functions are equivalent to Bessel (and Hankel) functions with higher transcendentality. Explicitly, they are given by

$$\begin{aligned} P_{i\mu-1/2}(z) &\equiv {}_2F_1\left[\begin{matrix}\frac{1}{2}+i\mu & \frac{1}{2}-i\mu \\ 1\end{matrix}; \frac{1-z}{2}\right], \\ Q_{i\mu-1/2}(z) &\equiv \sqrt{\frac{\pi}{2}}\,\frac{\Gamma(\frac{1}{2}+i\mu)}{\Gamma(1+i\mu)}\,2^{-i\mu}z^{-\frac{1}{2}-i\mu}\,{}_2F_1\left[\begin{matrix}\frac{3/2+i\mu}{2} & \frac{1/2+i\mu}{2} \\ 1+i\mu\end{matrix}; \frac{1}{z^2}\right], \end{aligned} \tag{A.15}$$

in terms of the hypergeometric function ${}_2F_1$ that is defined by the following formal series

$${}_2F_1\left[\begin{matrix}a & b \\ c\end{matrix}; z\right] = \sum_{n=0}^{\infty}\frac{(a)_n(b)_n}{(c)_n}\frac{z^n}{n!}\,, \tag{A.16}$$

on the disk $|z| < 1$ and by analytic continuation elsewhere, where $(a)_n \equiv \Gamma(a+n)/\Gamma(a)$ is the Pochhammer symbol. These functions are $P_\alpha(z) =$ LegendreP[α, 0, 3, z] and $Q_\alpha(z) =$ LegendreQ[α, 0, 3, z] in Mathematica. The optional argument "3" selects the correct branch cut structure as it is falsely implemented by default.[2] At fixed argument, the Legendre P function is analytic in the entire complex μ plane. However, the Legendre Q function is meromorphic as it has poles coming from the factor $\Gamma(\frac{1}{2}+i\mu)$.

[2] The Legendre functions P and Q generalise to associated Legendre functions (also called Ferrers function of the first and second kind) $P_{i\mu-1/2}(z) \to P^{1/2-j}_{i\mu-1/2}(z)$ and $Q_{i\mu-1/2}(z) \to Q^{1/2-j}_{i\mu-1/2}(z)$, see Chap. 14 of [427], that are useful when dealing with spatial derivative interactions, i.e. for different powers of conformal time in the correlator time integrals. The non-derivative interaction case simply corresponds to $j = 1/2$.

Integral formula. The Legendre function P is the solution of the following integrals

$$\begin{aligned} -i\frac{\sqrt{\pi}}{2}e^{+\frac{\pi\nu}{2}}\int_{-\infty^+}^{0}\frac{\mathrm{d}\tau\, e^{ik\tau}}{(-\tau)^{1/2}}H^{(2)}_{i\nu}(-s\tau) &= \frac{e^{-\frac{i\pi}{4}}}{\sqrt{2s}}|\Gamma(\tfrac{1}{2}+i\nu)|^2\, P_{i\nu-1/2}(k/s)\,, \\ +i\frac{\sqrt{\pi}}{2}e^{-\frac{\pi\nu}{2}}\int_{-\infty^-}^{0}\frac{\mathrm{d}\tau\, e^{-ik\tau}}{(-\tau)^{1/2}}H^{(1)}_{i\nu}(-s\tau) &= \frac{e^{+\frac{i\pi}{4}}}{\sqrt{2s}}|\Gamma(\tfrac{1}{2}+i\nu)|^2\, P_{i\nu-1/2}(k/s)\,. \end{aligned} \tag{A.17}$$

Connection formula. Analogously to Bessel and Hankel functions, the Legendre functions satisfy the connection formula

$$|\Gamma(\tfrac{1}{2}+i\mu)|^2\, P_{i\mu-1/2}(z) = \frac{e^{-\frac{i\pi}{2}}}{\sinh(\pi\mu)}\left[Q_{-i\mu-1/2}(z)-Q_{+i\mu-1/2}(z)\right]\,. \tag{A.18}$$

Its analytic continuation is defined by

$$|\Gamma(\tfrac{1}{2}+i\mu)|^2\, P_{i\mu-1/2}(ze^{+i\pi}) = \frac{1}{\sinh(\pi\mu)}\left[e^{+\pi\mu}Q_{+i\mu-1/2}(z)-e^{-\pi\mu}Q_{-i\mu-1/2}(z)\right]\,. \tag{A.19}$$

Large-order asymptotic forms. The Legendre P function has a simple behaviour at $z\to 0$ (similar to Bessel J function), while the Legendre Q function has a simple behaviour at $z\to\infty$ (similar to Hankel H function). Indeed, they are given by

$$\begin{aligned} P_{i\nu-1/2}(\cosh\xi) &\sim \left(\frac{\xi}{\sinh\xi}\right)^{1/2}\,, \\ Q_{i\nu-1/2}(\cosh\xi) &\sim \frac{\pi}{2i}\left(\frac{2\xi}{\pi\nu\xi\sinh\xi}\right)^{1/2}e^{-i\left(\nu\xi-\frac{\pi}{4}\right)}\,. \end{aligned} \tag{A.20}$$

These expressions equivalently give the large-order asymptotic forms. The asymptotic behaviour of the Legendre P function reads

$$P_{i\nu-1/2}(z) \sim \frac{1}{\sqrt{\pi}}\frac{\Gamma(-i\nu)}{\Gamma(\frac{1}{2}-i\nu)}\left(\frac{1}{2z}\right)^{\frac{1}{2}+i\nu}\,, \tag{A.21}$$

for $z\to\infty$.

A.2 Non-Analytic Signal from Bulk Cutting Rules

Here, we derive Eq. (4.21) using the bulk cutting rules to extract non-analtic signals in cosmological correlators. Using the Schwinger-Keldysh diagrammatic rules, see Chap. 5, the s-channel contribution to the correlator we wish to compute reads

$$\langle\varphi_{\boldsymbol{k}_1}\varphi_{\boldsymbol{k}_2}\varphi_{\boldsymbol{k}_3}\varphi_{\boldsymbol{k}_4}\rangle' = \frac{-g^2\tau_0^4}{16k_1k_2k_3k_4}\sum_{\mathsf{a},\mathsf{b}=\pm}F_{\mathsf{ab}}\,, \tag{A.22}$$

where τ_0 is a small late-time regulator and the integrals F_{ab} are given by

$$F_{\mathsf{ab}} = \mathsf{ab}\int_{-\infty^{\mathsf{a}}}^{0}\int_{-\infty^{\mathsf{b}}}^{0}\frac{\mathrm{d}\tau}{\tau^2}\frac{\mathrm{d}\tau'}{\tau'^2}\,e^{i\mathsf{a}k_{12}\tau}\mathcal{G}_{\mathsf{ab}}(s;\tau,\tau')e^{i\mathsf{b}k_{34}\tau'}\,, \tag{A.23}$$

with $k_{ij} = k_i + k_j$ and $s = |\boldsymbol{s}| = |\boldsymbol{k}_1 + \boldsymbol{k}_2|$. Let us first consider the non-time ordered integrals, which are factorised. In order to extract the non-local signal from this contribution, we use the late-time limit of the bulk-to-bulk propagator (4.17), selecting only the non-local part. This limit is motivated by the fact that we want to probe the late-time super-horizon decay of the exchanged massive field, and how its non-local evolution is encoded in the correlator. After substituting $\mathcal{G}_{-+}$ by (4.17) in the integral F_{-+} in (A.23), all integrals are of the form

$$\int_{-\infty^{\pm}}^{0}\mathrm{d}\tau e^{\pm ik\tau}\tau^{\Delta} = -(\pm i)^{\Delta+1}k^{-\Delta-1}\Gamma(\Delta+1)\,,\quad \text{for}\quad \mathrm{Re}(\Delta) > -1\,. \tag{A.24}$$

Using this formula, we find

$$F_{-+} = \frac{-H^2}{4\pi(k_{12}k_{34})^{1/2}}\left[\left(\frac{s^2}{4k_{12}k_{34}}\right)^{i\mu}\Gamma(-i\mu)^2\Gamma\left(\tfrac{1}{2}+i\mu\right)^2 + \text{c.c.}\right]. \tag{A.25}$$

From this result, it is clear that the part of the diagram F_{-+} coming from local processes does not contain any non-analytic scaling in the momentum ratio $s^2/(k_{12}k_{34})$. Noting that this expression is real, we immediately obtain $F_{+-} = F^*_{-+} = F_{-+}$. Let us now evaluate the time-ordered diagrams. Usually, these diagrams are complicated to evaluate because of nested time integrals. However, the non-local signal can be easily extracted after reorganising the integrand and rewriting the diagram as a sum of a factorised part which contains the non-local signal and a remaining term free of such signal. This is done by using the trivial identity

$$\Theta(\tau-\tau') = 1 - \Theta(\tau'-\tau)\,, \tag{A.26}$$

so that the bulk-to-bulk propagator $\mathcal{G}_{++}$ can be written

$$\mathcal{G}_{++}(s;\tau,\tau') = \mathcal{G}_{-+}(s;\tau,\tau') + \left[\mathcal{G}_{<}(s;\tau,\tau') - \mathcal{G}_{>}(s;\tau,\tau')\right]\Theta(\tau'-\tau)\,. \tag{A.27}$$

In the late-time limit, equivalently when the exchanged momentum s is soft, the commutator vanishes for non-local processes, as seen in Eq. (4.20). This follows from the fact that the two vertices are outside each others' lightcones. As a result, time ordering does not matter and the on-shell propagation of the massive field between the two vertices is encoded in the factorised part, which reads

$$\begin{aligned}F_{++} = \frac{iH^2}{4\pi(k_{12}k_{34})^{1/2}}\Bigg[&e^{-\pi\mu}\left(\frac{s^2}{4k_{12}k_{34}}\right)^{i\mu}\Gamma(-i\mu)^2\Gamma\left(\tfrac{1}{2}+i\mu\right)^2\\ &+e^{\pi\mu}\left(\frac{s^2}{4k_{12}k_{34}}\right)^{-i\mu}\Gamma(i\mu)^2\Gamma\left(\tfrac{1}{2}-i\mu\right)^2\Bigg]\,,\end{aligned} \tag{A.28}$$

in the late-time limit, where we again used Eq. (4.17) and Eq. (A.24). Such bulk cutting rule enables to systematically extract contributions from diagrams which contain non-local signals. The anti-time-ordered piece is $F_{--} = F^*_{++}$. Summing all the contributions, we recover the leading-order late-time contribution to the four-point correlator encoding the non-local signal (4.21).

A.3 Mellin-Barnes Techniques

Mellin-Barnes (MB) techniques have recently emerged as promising methods to deal with complicated nested time integrals encountered in cosmological massive exchange processes. In short, the MB representation offers a method to express diverse functions as contour integrals in the complex plane, often involving products of Γ-functions within the integrand. Employing such integral representations has led to significant progress in particle physics, facilitating the computation of sophisticated Feynman diagrams. We refer the reader to the nice lecture notes [594] and the references therein for more details in the context of particle physics, and [595] for mathematical techniques to deal with MB integrals. When computing cosmological correlators, representing Schwinger-Keldysh propagators in Mellin space makes nested time integrals trivial since the dependences of MB integrands are simple power laws in conformal time. This re-writting of cosmological correlators appears natural as de Sitter space has dilatation invariance in place of the time translation invariance of flat space. This way, going to Fourier space in time for flat-space computations can be traded with going to Mellin space in de Sitter where eigenfunctions of the dilatation generator are simple power laws $\sim \tau^{\pm i\mu}$ instead of plane waves $e^{\pm i\omega t}$.[3] This strategy has several advantages. The analytic structure of cosmological correlators is made manifest. For instance, kinematic limits are encoded in the leading poles in the Mellin integrands, and asymptotic expansions (e.g. isolating non-analytic contributions) can be derived systematically to any order in the momentum ratio. Moreover, MB techniques give an alternative general framework to obtain closed-form exact expressions for complex diagrams.

Literature. The Mellin-space approach to cosmological correlators was initiated in [421]. Propagators were written as Mellin integrals in de Sitter for an arbitrary number of spatial dimensions. Explicit solutions for n-point contact and tree-level exchange correlators with arbitrary masses were derived, and kinematic limits as well as their singularity structures are discussed. MB representations of correlation functions in anti-de Sitter were analytically continued to de Sitter by means of simple relative phases in [422], also see e.g. [381, 442, 423] for related works. Four-point exchange correlators with general external scalars and a general exchanged integer-spining and massive field are computed, in passing recovering many known results (e.g. leading slow-roll suppressed inflationary three-point correlators induced by the exchange of a spinning field). Loop integrals in de Sitter are computed (and regularised) using Mellin-space representations of correlators in [596]. The underlying structure of these integrals is shown to be similar to those in flat-space after dimensional regularisation. A *partial* MB representation of cosmological correlators, where only the bulk-to-bulk propagators are expressed in Mellin space (and leaving the external modes untouched), was presented in [304]. This has enabled to derive full analytical expressions for the non-analytic contributions of one-loop correlators to all orders in the momentum ratio (hence valid in all kinematic con-

[3] Note that a power law function in conformal time is a plane wave in cosmic time $\tau^{\pm i\mu} \sim e^{\pm i\mu t}$. This all the more motivates the use of MB techniques to obtain late-time behaviours of cosmological correlators and isolating their non-analytic contributions.

figurations) in a form of power series and in a controlled manner. Full analytical solutions for tree-level correlators exchanging massive and spinning fields with a chemical potential (hence with a non-perturbative breaking of de Sitter boosts) are derived using partial MB representations in [305]. These results were taken as seed solutions to then generate closed-form expressions for loop diagrams using spectral decomposition techniques in [338]. A factorisation theorem (enabling to find all possible non-local signals in a given diagram, see [263] for a related work), and cutting rules for arbitrary 1PI one-loop correlators are proved using MB techniques in [307]. Applications to non-analytic contributions of bubble-, triangle- and box-like loop correlators are presented, and an algorithm to compute higher-order corrections in the momentum ratio for the non-analytic contributions of correlators is introduced. Generalisation to all loop diagrams can be found in [339]. Multiple-exchange diagrams are computed in [424], which take the form of multi-variable hypergeometric series. However, these solutions do not converge in some kinematic configurations, and need to be analytically continued to other configurations.

Mellin space. Consider $f(z)$, a locally integrable function defined on the positive real axis $0 < z < \infty$. The Mellin transform $\mathcal{M}$ is the operation that maps the function f onto the function F defined in the complex plane by

$$F(s) \equiv \mathcal{M}[f(z)] = \int_0^\infty \mathrm{d}z\, z^{s-1} f(z)\,, \tag{A.29}$$

where s is a complex number. In general, the integral does exist only in a strip $a < \mathrm{Re}(s) < b$ with a and b depending on the function $f(z)$, where the function $F(s)$ is analytic. In this case, the inversion formula is given as a Mellin-Barnes integral

$$f(z) = \int_{c-i\infty}^{c+i\infty} \frac{\mathrm{d}s}{2i\pi}\, z^{-s} F(s)\,, \tag{A.30}$$

where the integration contour is along a vertical line such that $a < c < b$. This transformation can be seen as the analogue of the Fourier transform with the original function expanding in a basis composed of power-law solutions z^{-s} instead of plane waves. Since power-law functions diagonalise dilatation, i.e. $z\partial_z z^{-s} = -sz^{-s}$, the Mellin transform $\mathcal{M}[f(z)]$ enjoys many properties such as

- *Scaling*: $\mathcal{M}[f(\alpha z)] = \alpha^{-s} F(s)$ for $\alpha > 0$.
- *Power-law multiplication*: $\mathcal{M}[z^\nu f(z)] = F(s+\nu)$ for $a - \mathrm{Re}(\nu) < \mathrm{Re}(s) < b - \mathrm{Re}(\nu)$.
- *Dilatation*: $\mathcal{M}[(z\partial_z)^n f(z)] = (-s)^n F(s)$ for $a < \mathrm{Re}(s) < b$.

As usual for integral transforms, Parseval's theorem relates the product of two functions to their convolution. Since the Mellin transform $F(s)$ is closely related to the integral representation of the Γ-function, the Mellin-Barnes integral kernels usually take the form of various combinations of Γ-functions whose singularity structure is well known: $\Gamma(s)$ has simple poles located at $s = 0, -1, -2, \ldots$.

Massive mode functions. The Mellin transform is a convenient way of writing complicated functions as an integral with simple kernel. Specifically, Hankel functions appearing in the mode functions of massive fields have the following Mellin-Barnes representations

$$\pm i\pi e^{\mp\frac{\pi\mu}{2}} H^{(1)}_{i\mu}(z) = \int_{c-i\infty}^{c+i\infty} \frac{\mathrm{d}s}{2i\pi}\, \Gamma\left(s+\tfrac{i\mu}{2}\right)\Gamma\left(s-\tfrac{i\mu}{2}\right)\left(\mp\tfrac{iz}{2}\right)^{-2s}\,, \tag{A.31}$$

where $c > |\mu|/2$. The corresponding causal Schwinger-Keldysh propagator $\mathcal{G}_>$ can then be written

$$\begin{aligned}\mathcal{G}_>(k,\tau_1,\tau_2) &= \frac{\pi H^2}{4} e^{-\pi\mathrm{Im}(\nu)}(\tau_1\tau_2)^{3/2} H^{(1)}_\nu(-k\tau_1) H^{(2)}_{\nu^*}(-k\tau_2)\\ &= \frac{H^2}{4\pi}\int_{-i\infty}^{i\infty}\frac{\mathrm{d}s_1}{2i\pi}\frac{\mathrm{d}s_2}{2i\pi}\, e^{i\pi(s_1-s_2)}\left(\frac{k}{2}\right)^{-2s_{12}}(-\tau_1)^{-2s_1+3/2}(-\tau_2)^{-2s_2+3/2}\\ &\qquad\times\Gamma\left[s_1-\frac{\nu}{2}, s_1+\frac{\nu}{2}, s_2-\frac{\nu}{2}, s_2+\frac{\nu}{2}\right]\,,\end{aligned} \tag{A.32}$$

where $\Gamma[a_1,\ldots,a_n]\equiv\Gamma(a_1)\ldots\Gamma(a_n)$ and $s_{12}=s_1+s_2$. Mellin-Barnes representations for gauge bosons with chemical potential can be found in [304].

Summing Residues

Let us now illustrate the use of the (partial) MB representation to compute the tree-level four-point exchange of massive field scalar field. The main procedure is the following. First, we express the bulk-to-bulk propagators via the MB representation, i.e. we introduce a Mellin variable s_i for each bulk integrated time τ_i. Then, we swap the order of integrals over s_i and τ_i, and perform the time integrals as they become trivial (the integrands are combinations or power laws and exponentials). Finally, we complete the MB integrals using the residue theorem. The final solution is therefore naturally expressed as series since the integrands usual have an infinite tower of poles. We will closely follow [305] to which we refer the reader for more details.

Mellin-Barnes representation. We now compute F_{ab} from Eq. (A.23) using this method. For the factorised contributions $F_{\pm\mp}$, using the MB representation of the causal propagators (A.32), and after performing the time integrals (which is done by Wick rotating time as usual), we obtain

$$\begin{aligned}F_{\pm\mp} = \frac{-H^2}{4\pi s}(uv)^{1/2}\int_{-i\infty}^{i\infty}\frac{\mathrm{d}s_1}{2i\pi}\frac{\mathrm{d}s_2}{2i\pi}\left(\frac{u}{2}\right)^{-2s_1}\left(\frac{v}{2}\right)^{-2s_2}\\ \times\Gamma\left[\tfrac{1}{2}-2s_1, \tfrac{1}{2}-2s_2, s_1-\tfrac{i\mu}{2}, s_1+\tfrac{i\mu}{2}, s_2-\tfrac{i\mu}{2}, s_2+\tfrac{i\mu}{2}\right]\,,\end{aligned} \tag{A.33}$$

where we have defined the dimensionless momentum ratios $u\equiv s/k_{12}$ and $v\equiv s/k_{34}$. Note that the two integrals over the Mellin parameters $s_{1,2}$ factorise as they should. This follows from the initial factorisation of the time integrals. The time-ordered contributions $F_{\pm\pm}$ are a bit more involved to rewrite because of the Heaviside functions, and there are multiple ways to deal with them. Various treatments will yield results with different rates of convergence. For phenomenological applications,

the $F_{\pm\pm}$ contributions can be separated into factorised and time-ordered pieces to isolate different kind of signals, e.g. local signals proportional to $(k_{12}/k_{34})^{\pm i\mu}$, non-local signals proportional to $(k_{12}k_{34}/s^2)^{\pm i\mu}$ and the remaining signal analytic in all momentum ratios. This re-writing has been carried out explicitly in [305].

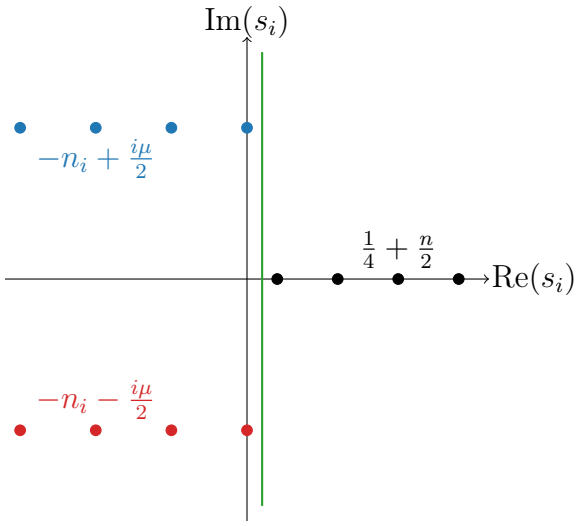


Figure A.1: Analytic structure in the $s_i = s_1, s_2$ complex plane of the Mellin-Barnes integrand in (A.33). The integration contour, closed to the left, well separates the infinite tower of poles coming from $\Gamma(s_i - \frac{i\mu}{2})$ and $\Gamma(s_i + \frac{i\mu}{2})$ from those coming from $\Gamma(\frac{1}{2} - 2s_i)$.

Performing Mellin-Barnes integrals. We are prepared to explicitly compute the MB integrals in (A.33). Detailed outcomes for the remaining integrals are available in [305]. We will do this by closing the contours to the left and picking up the enclosed poles. In Fig. A.1, we illustrate the analytic structure of the $s_{1,2}$ integrand in Eq. (A.33). The poles to pick up all come from the Γ-functions

$$s_{1,2} = -n_{1,2} \pm \frac{i\mu}{2}\,, \tag{A.34}$$

for integer $n_{1,2} \geq 0$. Summing over all these "left" poles yields the following double series closed-form expression

$$\begin{aligned} F_{\pm\mp} = \frac{-H^2}{4\pi s}(uv)^{1/2} \sum_{n_1,n_2=0}^{\infty} \frac{(-1)^{n_{12}}}{n_1! n_2!} \left(\frac{u}{2}\right)^{2n_1 - i\mu} \left(\frac{v}{2}\right)^{2n_2 - i\mu} \\ \times \Gamma\left[-n_1 - i\mu, \tfrac{1}{2} + 2n_1 - i\mu, -n_2 - i\mu, \tfrac{1}{2} + 2n_2 - i\mu\right] + (\mu \leftrightarrow -\mu)\,, \end{aligned} \tag{A.35}$$

where $n_{12} = n_1 + n_2$. It is quite common that these series can be (partially) resummed to known hypergeometric functions, see e.g. [304, 305, 436].

B

Mathematical Interlude

THE ANALYSIS PRESENTED in Chap. 8 extensively employs tools from complex analysis. To ensure the thesis remains self-contained and accessible, this appendix offers a pedagogical and elementary introduction to the theory of Riemann surfaces and the Saddle point approximation. Emphasis is placed on clarity and intuition rather than formal mathematical rigour.

B.1 Riemann Surfaces from Multi-Valued Functions

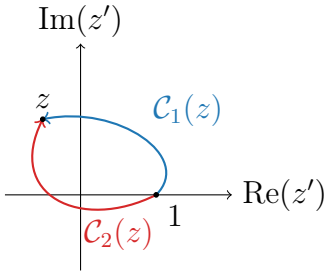
The study of differentiable functions of a single complex variable naturally unveils the concept of multi-valued functions. This, in turn, introduces an elegant class of mathematical objects known as Riemann surfaces, which beautifully connects analysis to geometry.[1] The intuitive idea behind Riemann surfaces is to take multiple branches of a complex multi-valued function and glue these together to obtain a continuous single-valued function. The main question we will try answer is: "What do we really mean by multi-valued functions?".

Complex logarithm. Let us take the canonical example of the complex logarithm function to introduce the concept of multi-valued functions and the corresponding Riemann surface. We try to extend the real logarithm $x \in \mathbb{R}_+^* \mapsto \log(x)$ to the largest possible open, connected subset of the complex plane $\mathbb{C}$. The most natural way to proceed is to come back to the defining property of the real logarithmic function: it is the primitive of $x \in \mathbb{R}^* \mapsto 1/x$ that vanishes at $x = 1$. We therefore define

$$\log(z) = \int_{\mathcal{C}(z)} \frac{\mathrm{d}z'}{z'}, \quad \text{for} \quad z \in \mathbb{C}^*, \tag{B.1}$$

[1] For a general introduction to Riemann surfaces, see e.g. [597].

where $\mathcal{C}(z)$ is a contour linking 1 to z in the complex plane. Eq. (B.1) defines a function if every choice of the contour $\mathcal{C}(z)$ leads to the same value for $\log(z)$. Let us consider two contours $\mathcal{C}_1(z)$ and $\mathcal{C}_2(z)$ linking 1 to z, but passing on either side of the origin, as depicted on the right. If we denote $\mathcal{C}$ the closed contour composed of $\mathcal{C}_1$ and $-\mathcal{C}_2$, then using the residue theorem, we obtain $\int_{\mathcal{C}(z)} \frac{\mathrm{d}z'}{z'} = 2i\pi$. This yields

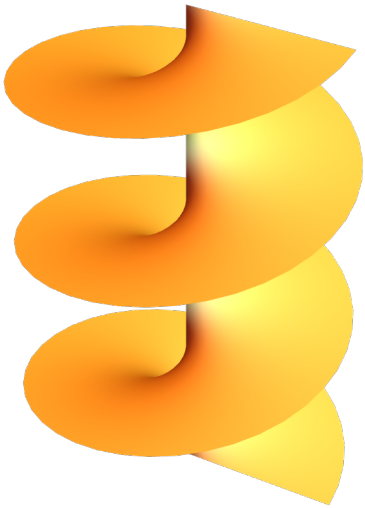


$$\int_{\mathcal{C}_1(z)} \frac{\mathrm{d}z'}{z'} = \int_{\mathcal{C}_2(z)} \frac{\mathrm{d}z'}{z'} + 2i\pi\,. \tag{B.2}$$

It is therefore not possible to define the complex logarithm on the entire punctured complex plane $\mathbb{C}\backslash\{0\}$. To avoid such inconvenience, we restrict the argument of z, that we denote $\arg(z)$, to $\arg(z) \in (\alpha, \alpha+2\pi)$ with real α. The line $\{z \,|\, \arg(z) = \alpha\}$ is a branch cut, with the origin $z = 0$ being the branch point, i.e. the common point to all branch cuts. Choosing $\alpha = -\pi$ so that the branch cut is the negative real axis $\mathbb{R}_-$ defines the principal branch of the complex logarithm. However, note that any other value for α, defining a line $\mathfrak{C}$ linking the origin to infinity, would give a valid branch cut and a new complex logarithm can be defined on $\mathcal{C}\backslash\mathfrak{C}$. A natural consequence is if we consider two complex logarithms $\ell(z)$ and $\ell'(z)$ defined on $\mathbb{C}\backslash\mathfrak{C}$ and $\mathbb{C}\backslash\mathfrak{C}'$, respectively, the difference $\ell(z) - \ell'(z)$ is a multiple of $2i\pi$ for all $z \in \mathcal{C}\backslash\{\mathfrak{C} \cup \mathfrak{C}'\}$.

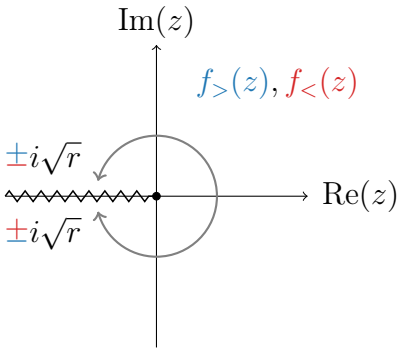
Importantly, a different point of view removes the need to introduce a branch cut to define the complex logarithm. In fact, when physicists' point of view is that of a multi-valued function, the mathematicians' one is that of a function defined on a Riemann surface.

Introducing a Riemann surface corresponds to replacing the punctured complex plane $\mathbb{C}\backslash\{0\}$, on which we tried without succeeding to define a complex holomorphic logarithm, by a larger connected domain. Intuitively, starting from the principal branch, rotating counter-clockwise once around the origin would pick a factor $2i\pi$ to the logarithm to end up on the next branch, and so on. We therefore can construct the following surface: take an infinite number of complex planes that we stack on top of each other. Each of these planes are cut on a branch cut, say the negative real axis $\mathbb{R}_-$, and the upper branch cut is glued to the lower one. The final result is a connected surface—a helicoid—resembling a spiralling parking garage with infinitely many levels, as shown on the right: it is the *Riemann surface* of the complex logarithm where the z-axis is the imaginary part of $\log(z)$. A point on this Riemann surface $\mathfrak{R}$ can be thought of as a pair (z, n), with $n \in \mathbb{Z}$ corresponding to a Riemann sheet for which the complex



logarithm would give $\log(r)+i(\theta+2\pi n)$, where $z = re^{i\theta}$ with $r \in \mathbb{R}_+^*$ and $\theta = \arg(z)$. As such, the Riemann surface can be embedded in $\mathbb{C} \times \mathbb{Z}$. On $\mathfrak{R}$, the complex logarithm can be defined as follows: (i) we choose a contour $\mathcal{C}$ linking $(1, 0) \in \mathfrak{R}$ to the point $(z, n) \in \mathfrak{R}$, (ii) this contour can be projected vertically on the principal branch $n = 0$, resulting in a contour joining 1 to z, and (iii) we define $\log(z) = \int_{\mathcal{C}} \mathrm{d}z'/z'$. This way, the function does not depend on the contour any more as whenever we circle around the origin, we move to another branch and the logarithm picks up a factor $\pm 2i\pi$.

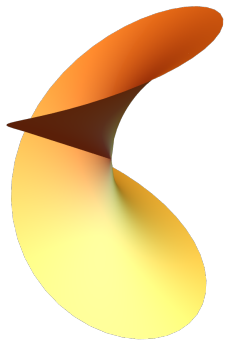
Complex square root. Another classic example of a function that presents challenges when extending its domain from the positive real axis to the complex plane is the square root. Indeed, defining $z = re^{i\theta}$ with $r \in \mathbb{R}_+^*$ and $\theta = \arg(z)$, a naive definition of the square root would simply be $\sqrt{z} = \sqrt{r}e^{i\theta/2}$. However, the argument $\theta/2$ is only defined up to a factor π, resulting in a sign ambiguity on the sign of $\sqrt{z}$. This function is multi-valued: for a single value of z, there are two different choices for $\sqrt{z}$. We define these two choices by



$$f_>(z) = \sqrt{r}e^{i\theta/2}\,, \quad f_<(z) = \sqrt{r}e^{i(\theta/2+\pi)}\,, \qquad \text{(B.3)}$$

where $f_>$ and $f_<$ are the positive and negative branches of the square root, respectively. As we observed earlier with the complex logarithm, it is necessary to define a branch cut. From now on, we will adopt the principal branch cut, positioned along the negative real axis $\mathbb{R}_-^*$, i.e. $\theta = \arg(z) \in (-\pi, \pi)$. Let us now look at the behaviour of each of the two branches $f_>(z)$ and $f_<(z)$ as z approaches the branch cut from above and from below on a circle centred at the origin with a radius $r > 0$. Taking the limit $\theta \to +\pi$, we obtain $f_>(z) = +i\sqrt{r}$ and $f_<(z) = -i\sqrt{r}$. Similarly, as $\theta \to -\pi$, we have $f_>(z) = -i\sqrt{r}$ and $f_<(z) = +i\sqrt{r}$. We represent these limits on the right for the positive and negative branches.

To define a function on the punctured complex plane $\mathbb{C}\backslash\{0\}$ that remains continuous along the branch cut, we observe that the sign is reversed after a single rotation around the origin but returns to its original value after two full rotations. We can e.g. approach the branch cut from above using the positive branch $f_>(z)$ and exit from below using the negative branch $f_<(z)$. The corresponding Riemann surface for the complex square root is depicted on the right: when the square root takes a specific value on one Riemann sheet, it assumes the opposite value on the other sheet. We end up with a self-intersecting surface.



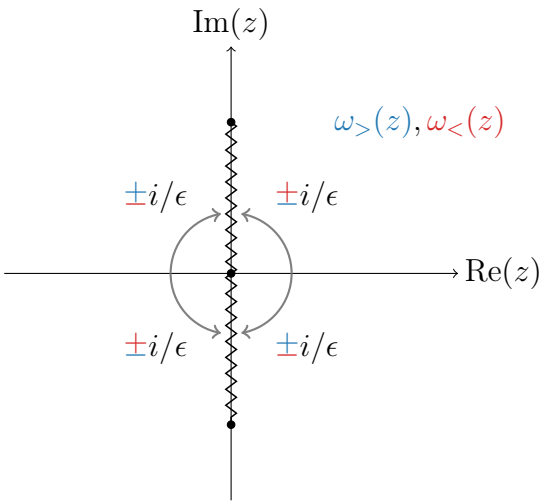
Constructing Riemann surfaces. Whenever a function is multi-valued, it can be promoted to a single-valued function albeit extending the domain of validity to the corresponding Riemann surface. For pedagogical purposes, let us now explicitly construct the Riemann surface corresponding to the function describing the time-dependent frequency of a massive field scalar field in de Sitter: (dimensionless) frequencies ω such as

$$\omega^2(z) = 1 + \frac{1}{z^2}\,. \tag{B.4}$$

The function $\omega(z)$ has a pole at the origin $z = 0$ and two branch points at $z = \pm i$. Taking the square root principal branch, we place the branch cut on the imaginary axis between $+i$ and $-i$. When trying to extend the domain of validity of the frequency $\omega(z)$ to the largest possible domain of the complex plane of z, we note that this function has two branches corresponding to the positive and negative branches of the square root, that we denote

$$\omega_>(z) = +\sqrt{1 + \frac{1}{z^2}}\,, \quad \omega_<(z) = -\sqrt{1 + \frac{1}{z^2}}\,, \tag{B.5}$$

that are defined on two distinct Riemann sheets. We now probe the behaviour of both branches on each sides of both branch cuts. On a small circle with infinitesimal radius $\epsilon > 0$ centred at the origin, we have $\omega_>(\epsilon e^{i\theta}) \approx e^{-i\theta}/\epsilon \to \mp i/\epsilon$ as $\theta \to \pm\pi/2$. Similarly for the negative branch, we obtain $\omega_<(\epsilon e^{i\theta}) \approx e^{-i(\theta-\pi)} \to \pm i/\epsilon$ as $\theta \to \pm\pi/2$, which can be visualised as follows:



The Riemann surface can be constructed by noticing that we can continuously enter the upper portion of the branch cut from the left using the positive branch to exit the lower portion of the branch cut using the negative branch cut. However, when crossing the imaginary axis away from the branch cut, we remain on the same Riemann sheet. We obtain the Riemann surface used in the main text.

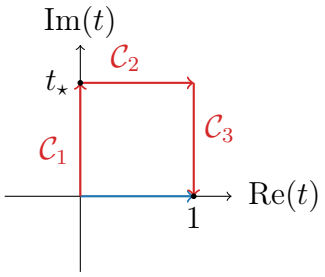
B.2 Saddle Point Approximation of Complex Integrals

Local behaviours of integrals in certain limits can completely determine their asymptotic forms without introducing free parameters. This is in sharp contrast with a local study of differential equations around singular points where solutions are always found up to arbitrary integration constants. Among these local analysis, the saddle point approximation—also called the method of steepest descent—is a method to find approximate solutions to complex integrals where one deforms the integration contour to pass a saddle (stationary) point in the direction of steepest descent or stationary phase. We invite the reader to consult e.g. [598] for more details.

Preliminary example. The main idea of the saddle point approximation is to deform the integration contour in the complex plane so that the integrand has a *constant phase* on the new contour. Before formally exposing the method, we consider a preliminary example to motivate why it is helpful to shift complex contours to perform an asymptotic analysis. Let us consider the following integral:

$$I(\mu) = \int_0^1 \mathrm{d}t\, \log(t) e^{i\mu t}\,. \tag{B.6}$$

As $\mu \gg 1$, the asymptotic expansion of $I(\mu)$ is non-analytic, which complicates finding an approximate solution. We therefore deform the integration interval in blue to the complex contour $\mathcal{C} = \mathcal{C}_1 + \mathcal{C}_2 + \mathcal{C}_3$ as depicted in red on the right. By Cauchy's theorem, we have $I(\mu) = \int_{\mathcal{C}_1+\mathcal{C}_2+\mathcal{C}_3} \mathrm{d}z\, \log(z)\, e^{i\mu z}$. As $t_\star \to \infty$, the integral over $\mathcal{C}_2$ vanishes exponentially. The integral (B.6) becomes



$$I(\mu) = i\int_0^\infty \mathrm{d}z\, \log(iz)\, e^{-\mu z} - i\int_0^\infty \mathrm{d}z\, \log(1+iz)\, e^{i\mu(1+iz)}\,. \tag{B.7}$$

The first integral can be performed exactly, yielding

$$i\int_0^\infty \mathrm{d}z\, \log(iz)\, e^{-\mu z} = -i\,\frac{\log(\mu)}{\mu} - \frac{i\gamma + \pi/2}{\mu}\,, \tag{B.8}$$

where we have used the principal branch of the complex logarithm $\log(iz) = \log(z) + i\pi/2$ and $\int_0^\infty \log(t) e^{-t}\mathrm{d}t = -\gamma$ with $\gamma = 0.5772\ldots$ the Euler's constant. The second integral can also be performed by Taylor expanding the logarithm and integrating each term in the series

$$i\int_0^\infty \mathrm{d}z\, \log(1+iz)\, e^{i\mu(1+iz)} = ie^{i\mu} \sum_{n=1}^{\infty} \frac{(-i)^n (n-1)!}{\mu^{n+1}}\,. \tag{B.9}$$

Importantly, notice that along the contours $\mathcal{C}_1$ and $\mathcal{C}_3$, the phase of $e^{i\mu t}$ is constant, with frequency 0 and 1, respectively. These contours are also the steepest-descent paths as $|e^{i\mu t}|$ decreases most rapidly (in fact exponentially) as t ranges from 0 and 1 to ∞. This is no coincidence as we now review.

Steepest-descent complex contours passing through saddle points. The method of steepest descent enables one to approximate *complex* integrals of the form

$$I(\mu) = \int_{\mathcal{C}} \mathrm{d}z\, g(z) e^{\mu f(z)}\,, \tag{B.10}$$

in the limit $\mu \gg 1$. The contour $\mathcal{C}$ can be deformed into a new contour $\mathcal{C}'$ without changing the integral provided no poles nor branch cuts are crossed. If one chooses a path that satisfies the following conditions: (i) the phase $\mathrm{Im}[f(z)] \equiv \theta$ is constant along $\mathcal{C}'$ and (ii) the contour $\mathcal{C}'$ passes through one or more saddle points $z_\bullet$ such that $f'(z_\bullet) = 0$, then the integral reads

$$I(\mu) = e^{i\mu \mathrm{Im}[f(z)]} \int_{\mathcal{C}'} \mathrm{d}z\, g(z)\, e^{\mu \mathrm{Re}[f(z)]} \approx e^{i\mu\theta} \sqrt{\frac{2\pi}{\mu \frac{\mathrm{d}^2}{\mathrm{d}z^2}\mathrm{Re}[f]|_{z_\bullet}}}\, g(z_\bullet)\, e^{\mu \mathrm{Re}[f(z_\bullet)]}\,, \tag{B.11}$$

where the remaining integral is approximated using Laplace's method, which follows from Taylor expanding the function $\mathrm{Re}[f]$ around the stationary point $z = z_\bullet$ and finishing the Gaussian integral by extending the limits of integration by $\pm\infty$.[2] Extensions to arbitrary precision can be systematically found. In the presence of multiple saddles, one needs to sum their contributions. However, it is in general expected that the saddle points that are located the closest to the original integration contour contribute the most. Note that if the function f is analytic, constant phase contours are equivalent to steepest-descent contours. Indeed, setting $z = x + iy$, using the Cauchy-Riemann equations, we obtain

$$\frac{\partial \mathrm{Re}[f]}{\partial x}\frac{\partial \mathrm{Im}[f]}{\partial x} + \frac{\partial \mathrm{Re}[f]}{\partial y}\frac{\partial \mathrm{Im}[f]}{\partial y} = 0 \quad \Leftrightarrow \quad \nabla \mathrm{Re}[f] \cdot \nabla \mathrm{Im}[f] = 0\,, \tag{B.12}$$

which shows that $\mathrm{Im}[f]$ is constant on contours whose tangents are parallel to $\nabla \mathrm{Re}[f]$. Two distinct steepest curves can only intersect at saddle points.

Illustrative example. We now apply this method to a concrete example. Let us derive the asymptotic expansion of the integral

$$I(\mu) = \int_{\mathcal{C}} \frac{\mathrm{d}s}{2i\pi}\, e^s s^{-\mu}\,, \tag{B.13}$$

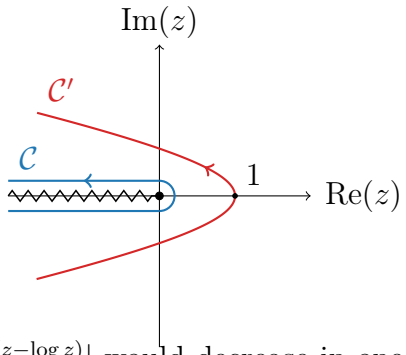
in the limit $\mu \gg 1$, where $\mathcal{C}$ is the Hankel contour that begins at $-\infty - i\epsilon$, encircles the branch cut lying on the real negative axis and ends up at $-\infty + i\epsilon$ with $\epsilon > 0$. We first make the change of variables $s = \mu z$ to convert the movable saddle point that depends on μ to a fixed one, yielding

$$I(\mu) = \frac{1}{\mu^{\mu-1}} \int_{\mathcal{C}} \frac{\mathrm{d}z}{2i\pi}\, e^{\mu(z - \log z)}\,. \tag{B.14}$$

Defining $f(z) = z - \log z$, solving $f'(z) = 0$ gives a single saddle point at $z_\bullet = 1$. To study the structure of this saddle, we set $z = x + iy$ so that $f(z) = x - \log\sqrt{x^2+y^2} + i(y - \arctan y/x)$. Therefore, paths of constant phase emerging from $z_\bullet = 1$ (as $f(z_\bullet) = 1$) satisfy

$$y = \arctan y/x\,. \tag{B.15}$$

[2] This creates only a small error as the exponential decays very fast away from the saddle point.



There are two solutions to this equation: $y = 0$ and $x = y/\tan(y)$. Now we can deform the original contour $\mathcal{C}$ in blue to $\mathcal{C}'$ represented in red that passes by the saddle.[3] The constant-phase (or steepest-descent) curve $\mathcal{C}' = \{(t/\tan(t), t)|t \in \mathbb{R}\}$ is parallel to $\mathrm{Im}[z] = y$ around $z_\bullet = 1$ and crosses the imaginary axis at $\pm i\pi/2$. Along this path, $|e^{\mu(z-\log z)}|$ reaches its maximum at the saddle and decays exponentially as $z \to -\infty \pm i\pi$. In the case of no saddle point, $|e^{\mu(z-\log z)}|$ would decrease in one direction along $\mathcal{C}'$ and increase in the other direction, and the integral would not be convergent. Note that if instead the steepest-descent path is finite and does not pass through a saddle point, then the maximum of the integrand must occur at an endpoint of the contour. To finish the integral, we examine the neighbourhood of $z_\bullet$ along $\mathcal{C}'$ by setting $z = 1 + it$ with $t \ll 1$, obtaining

$$I(\mu) \approx \frac{e^\mu}{\mu^{\mu-1}} \int_{-\epsilon}^{+\epsilon} \frac{\mathrm{d}t}{2\pi}\, e^{-t^2/2} \approx \frac{e^\mu}{\mu^{\mu-1}} \frac{1}{\sqrt{2\pi\mu}}\,, \tag{B.16}$$

where we have let $\epsilon \to \infty$. Note that it is important to stay on the constant-phase contour as naively applying (B.11) would have given an overall wrong phase $e^{-i\pi/2}$.

Application to massive field in de Sitter. We now treat in detail the simplest case of a massive scalar field in de Sitter with zero chemical potential $\kappa = 0$ and unity sound speed $c_s = 1$, studied in Chap. 8. After applying the leading-order WKB approximation to the massive mode function and discarding the negative-frequency integral as it is Boltzmann suppressed, we are left with the following integral

$$F_L^{(\alpha)} = \int_{-\infty^+}^{0} \frac{\mathrm{d}\tau}{\sqrt{2\omega_K(\tau)}}\, e^{i\left(E_1\tau - \int_{\tau_0}^{\tau} \omega_K(\tau')\mathrm{d}\tau'\right)}\,, \tag{B.17}$$

where τ_0 is an arbitrary time in the infinite past, and the effective frequency $\omega_K(\tau)$ is defined by

$$\omega_K^2(\tau) = K^2 + \frac{\mu^2}{\tau^2}\,. \tag{B.18}$$

The saddle points are found to $\tau_\bullet = \pm\mu/\sqrt{E_1^2 - K^2}$ which lie on the real axis in the complex τ plane as $E_1 \geq K$ by the triangle inequality. The closest saddle point to the original integration contour is the one located on the negative real axis, so we expect its contribution to dominate the integral. Let us now evaluate the Dingle's singulant function

$$F_K(\tau) = -2i \int_{\tau_c}^{\tau} \omega_K(\tau')\mathrm{d}\tau'\,, \tag{B.19}$$

with $\tau_c = +i\mu/K$ the critical point (with negative imaginary part) that makes the effective frequency vanish. Selecting the positive branch of the square root, we

[3] It is not possible to continuously deform the original contour to the steepest-descent path spanning the positive real axis.

obtain

$$\begin{aligned} F_K(\tau) &= -2i\left[\tau\sqrt{K^2+\mu^2/\tau^2}+\mu\,\mathrm{arctanh}\left(\frac{-\mu}{\tau\sqrt{K^2+\mu^2/\tau^2}}\right)\right]_{-i\mu/K}^{\tau} \\ &= -2i\left(\tau\sqrt{K^2+\mu^2/\tau^2}+\mu\,\mathrm{arctanh}\left(\frac{-\mu}{\tau\sqrt{K^2+\mu^2/\tau^2}}\right)\right)+\pi\mu\,. \end{aligned} \tag{B.20}$$

After splitting the integral as $\int_{\tau_c}^{\tau} = \int_{\tau_0}^{\tau} - \int_{\tau_0}^{\tau_c}$, the exponent in the integral (B.17) therefore can be written in terms of $F(\tau)$ as

$$f(\tau) = iE_1\tau + \tfrac{1}{2}F_K(\tau) - \pi\mu/2\,, \tag{B.21}$$

where we have discarded the contribution coming from τ_0 as it is arbitrary. Let us now study the steepest-descent curve passing through the saddle $\tau_\bullet$. To do that, we Taylor expand the exponent in the neighbourhood of the saddle $\tau_\bullet$

$$f(\tau_\bullet+\epsilon) \approx f(\tau_\bullet) - i\alpha\epsilon^2\,, \tag{B.22}$$

with $|\epsilon| \ll 1$, where $f(\tau_\bullet) = -i\mu\,\mathrm{arctanh}\sqrt{E_1^2-K^2}/E_1 \equiv i\beta$ and $\alpha \equiv (E_1^2 - K^2)^{3/2}/2E_1\mu$. We set $\epsilon = x+iy$ and obtain

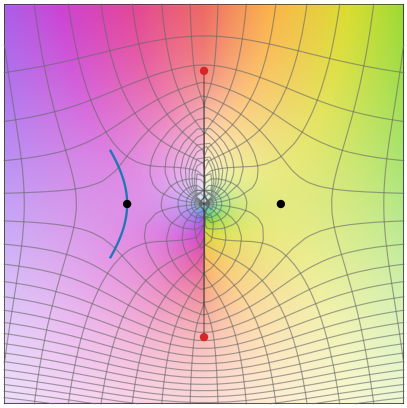
$$f(\tau_\bullet+\epsilon) \approx 2\alpha xy + i[\beta - \alpha(x^2-y^2)]\,. \tag{B.23}$$

Since $f(\tau_\bullet)$ is purely imaginary with a negative imaginary component, the constant-phase curve crossing the saddle must satisfy the following equation

$$\beta - \alpha(x^2-y^2) = -\lambda\,, \tag{B.24}$$

where $\lambda > 0$ is a free parameter that labels the different constant-phase curves. For $\tau_\bullet < 0$, the solution to this equation is $x = -\sqrt{y^2+(\beta+\lambda)/\alpha}$, and the constant-phase curves in the neighbourhood of the saddle are

$$\gamma_\lambda(t) = \{(-\sqrt{t^2+(\beta+\lambda)/\alpha}, t)\,|\,t\in\mathbb{R}\}\,. \tag{B.25}$$



The affine parameter where the curve crosses the saddle is $t_\bullet = 0$ and the label selecting this particular curve is found to be $\lambda = \mu\sqrt{E_1^2-K^2}/2E_1 + \mu\,\mathrm{arctanh}\sqrt{E_1^2-K^2}/E_1$. The tangent vector at the saddle point is found to be $\boldsymbol{T} = (0,1)$. Therefore, the curve is parallel to the imaginary axis. We illustrate the complex τ plane on the right, where the two saddle points are depicted in black, the critical points in red along with the branch cut joining them, and the constant-phase curve passing by the saddle in blue (whose expression is only found in the neighbourhood of $\tau_\bullet$). Additional constant-phase curves are shown in gray. To expand the exponent (B.21)

around the saddle point along the steepest-descent path, we set $\tau = \tau_\bullet - it$ with $t \ll 1$ as the original contour starts at $-\infty^+$. We obtain

$$\begin{aligned} F_L^{(\alpha)} &= \frac{-ie^{-i\mu \operatorname{arctanh}\frac{\sqrt{E_1^2-K^2}}{E_1}}}{\sqrt{2\omega_K(\tau_\bullet)}} \int_{-\epsilon}^{+\epsilon} \mathrm{d}t\, e^{i\frac{(E_1^2-K^2)^{3/2}}{2E_1\mu}t^2} \\ &\approx \frac{\sqrt{\pi\mu}}{(E_1^2-K^2)^{3/4}} e^{-i\pi/4} \exp\left[-i\mu \operatorname{arccosh}\frac{E_1}{K}\right], \end{aligned} \tag{B.26}$$

where we have finished the Gaussian integral after setting $\epsilon \to \infty$. Note that integrating *along* the constant-phase curve is essential to obtain the correct phase.

C

Details on Physics at Low Speed

In this appendix, we give further details about the physics at low sound speed. In particular, we derive the weight-shifting operators used in Sec. 11.1, explicitly write down higher-order terms in the non-local EFT, and show how one can completely resum it in flat space.

C.1 Weight-Shifting Operator Derivation

Diagrams consisting of external massless fields can be related to those of the external conformally coupled field through a set of weight-shifting operators. Here, we derive the corresponding weight-shifting operators for the double- and triple-exchange diagrams that contribute to the bispectrum of π_c.[1] We achieve this by linking these graphs to similar ones of φ's four- and six-point functions. For simplicity, here we concentrate on the non-local EFT limit where σ can be integrated out. However, *the final weight-shifting operators also apply to the same diagrams in the full two-field theory, where σ is a dynamical degree of freedom.*

In the non-local theory, the heavy field is non-dynamical, therefore its associated bulk-to-bulk propagators at leading order in derivative is proportional to a Dirac delta function, i.e.

$$\overset{\boldsymbol{s}}{\text{———}} = \mathcal{D}^{-1}(\boldsymbol{s},\tau)\frac{1}{a(\tau)}\delta(\tau-\tau')\,. \tag{C.1}$$

Therefore, we only need to identify operators that map the vertices of the diagrams in the theory containing φ onto those in the theory for the Goldstone boson π_c. Specifically, we want to find the map between the following building block

$$\mathbb{B}_{\varphi^2}(k_1,k_2,\tau) = a^4(\tau)\varphi_{k_1}(\tau)\varphi_{k_2}(\tau)\varphi^*_{k_1}(\tau_0)\varphi^*_{k_2}(\tau_0)\,, \tag{C.2}$$

[1] The ones for single-exchange diagrams are given in [311].

and the building blocks below, associated with graphs with external π lines:

$$\mathbb{B}_{\dot\pi_c}(k,\tau) = a^3(\tau)\pi'_{c,k}(\tau)\pi^*_{c,k}(\tau_0)\,, \tag{C.3}$$

$$\mathbb{B}_{\dot\pi_c^2}(k_1,k_2,\tau) = a^2(\tau)\pi'_{c,k_1}(\tau)\pi'_{c,k_2}(\tau)\pi^*_{c,k_1}(\tau_0)\pi^*_{c,k_2}(\tau_0)\,, \tag{C.4}$$

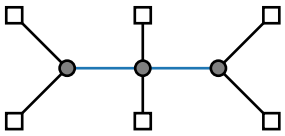
$$\mathbb{B}_{(\partial_i\pi_c)^2}(k_1,k_2,\tau) = -a^2(\tau)\,\boldsymbol{k}_1\cdot\boldsymbol{k}_2\,\pi_{c,k_1}(\tau)\pi_{c,k_2}(\tau)\pi^*_{c,k_1}(\tau_0)\pi^*_{c,k_2}(\tau_0)\,. \tag{C.5}$$

It can be easily verified that all the above components can be mapped onto $\mathbb{B}_{\varphi^2}$ via the following boundary operators

$$\begin{aligned}
\mathbb{B}_{\dot\pi_c}(k,\tau) &= -\frac{2c_s k_{\rm soft}}{H\tau_0^2}\lim_{k_{\rm soft}\to 0}\mathbb{B}_{\varphi^2}(k,k_{\rm soft},\tau)\,,\\
\mathbb{B}_{\dot\pi_c^2}(k_1,k_2,\tau) &= \frac{H^2}{2c_s^2\tau_0^2k_1k_2}\frac{\partial^2}{\partial k_{12}^2}\left[(k_1k_2)\,\mathbb{B}_{\varphi^2}(k_1,k_2,\tau)\right]\,,\\
\mathbb{B}_{(\partial_i\pi_c)^2}(k_1,k_2,\tau) &= \frac{H^2}{c_s^4\tau_0^2k_1^2k_2^2}\frac{\boldsymbol{k}_1\cdot\boldsymbol{k}_2}{k_1k_2}\left(1-k_{12}\frac{\partial}{\partial k_{12}}+k_1k_2\frac{\partial^2}{\partial k_{12}^2}\right)\left[(k_1k_2)\,\mathbb{B}_{\varphi^2}(k_1,k_2,\tau)\right]\,,
\end{aligned} \tag{C.6}$$

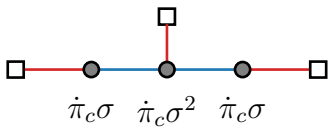
where we have defined $k_{12}=k_1+k_2$. Notice that the combination $(k_1k_2)\,\mathbb{B}_{\varphi^2}(k_1,k_2,\tau)$ only depends on k_{12}, therefore acting with $\partial_{k_{12}}$ is unambiguous. It should be noted that, following the same reasoning presented above, other building blocks associated with higher derivative vertices in π_c can be straightforwardly related to $\mathbb{B}_{\varphi^2}$ via similar (albeit higher-derivative) boundary operators.

In the non-local EFT, all exchange contributions reduce to simple contact terms. Therefore, the *in-in* expressions for diagrams are given by the image of the product of their corresponding building blocks, followed by an integration over time and multiplied by appropriate coupling constants and symmetry factors. For example, for the double-exchange diagram contributing to the φ six-point function, we have



$$\begin{aligned}
= -2\times 2^4\, g_1^2 g_2\,\mathrm{Im}\int_{-\infty}^{0}\mathrm{d}\tau\,\mathbb{B}_{\varphi^2}(k_1,k_2,\tau)\mathcal{D}^{-1}(\boldsymbol{k}_1+\boldsymbol{k}_2,\tau)\\
\times\,\mathbb{B}_{\varphi^2}(k_3,k_4,\tau)\mathcal{D}^{-1}(\boldsymbol{k}_5+\boldsymbol{k}_6,\tau)\mathbb{B}_{\varphi^2}(k_5,k_6,\tau)\,.
\end{aligned} \tag{C.7}$$

The double-exchange diagram of π, on the other hand, reads



$$\begin{aligned}
= \mathrm{Im}\int_{-\infty}^{0}\mathrm{d}\tau\,\mathbb{B}_{\dot\pi_c}(k_1,\tau)\mathcal{D}^{-1}(\boldsymbol{k}_1,\tau)\\
\times\,\mathbb{B}_{\dot\pi_c}(k_1,\tau)\mathcal{D}^{-1}(\boldsymbol{k}_2,\tau)\mathbb{B}_{\dot\pi_c}(k_3,\tau)\,.
\end{aligned} \tag{C.8}$$

With the two expressions above and using the relationships between the building blocks of the two diagrams in (C.6), one arrives at the equation given in the main text. The remaining diagrams follow from a similar procedure. We should emphasise again that identical relationships apply to the full two-field theory, and all the more so to the sub-leading contributions arising from integrating out σ at higher time-derivative orders.

C.2 Higher-Order Non-Local EFT Corrections

We have explicitly computed the power spectrum and the bispectra for all the interactions in the non-local EFT (10.24). However, let us recall that this theory has been derived by considering only the leading-order term in the time derivative expansion (10.23). Here, we show how one can systematically correct correlators of π_c by going to higher order in the derivative expansion (10.23). While adding more terms to the non-local EFT improves the accuracy to which correlators are determined, and can be used to diagnose failures of the EFT, it does not account for particle production effects, resulting in some level of unavoidable, but exponentially suppressed errors.

The seed correlators of the field φ attributed to the single-, double- and triple-exchange diagrams, at arbitrary order in the time-derivative expansion, are given by

$$\langle \varphi_{\boldsymbol{k}_1} \dots \varphi_{\boldsymbol{k}_4} \rangle'_{(1)} = -16 g_1^2 \left(\prod_{i=1}^{4} \varphi^*_{k_i}(\tau_0) \right) \times \mathrm{Im} \int_{-\infty}^{0} \mathrm{d}\tau a^4 \varphi_{k_1} \varphi_{k_2} \left[\sum_{n=0}^{\infty} \hat{\mathcal{O}}_n(s_{34}) \varphi_{k_3} \varphi_{k_4} \right] + \text{ 2 perms}\,, \tag{C.9}$$

$$\langle \varphi_{\boldsymbol{k}_1} \dots \varphi_{\boldsymbol{k}_6} \rangle'_{(2)} = -96 g_1^2 g_2 \left(\prod_{i=1}^{6} \varphi^*_{k_i}(\tau_0) \right) \times \mathrm{Im} \int_{-\infty}^{0} \mathrm{d}\tau a^4 \varphi_{k_1} \varphi_{k_2} \left[\sum_{n=0}^{\infty} \hat{\mathcal{O}}_n(s_{34}) \varphi_{k_3} \varphi_{k_4} \right] \left[\sum_{n=0}^{\infty} \hat{\mathcal{O}}_n(s_{56}) \varphi_{k_5} \varphi_{k_6} \right] + \text{ 15 perms}\,, \tag{C.10}$$

$$\langle \varphi_{\boldsymbol{k}_1} \dots \varphi_{\boldsymbol{k}_6} \rangle'_{(3)} = -96 g_1^3 g_3 \left(\prod_{i=1}^{6} \varphi^*_{k_i}(\tau_0) \right) \times \mathrm{Im} \int_{-\infty}^{0} \mathrm{d}\tau a^4 \left[\sum_{n=0}^{\infty} \hat{\mathcal{O}}_n(s_{12}) \varphi_{k_1} \varphi_{k_2} \right] \left[\sum_{n=0}^{\infty} \hat{\mathcal{O}}_n(s_{34}) \varphi_{k_3} \varphi_{k_4} \right] \left[\sum_{n=0}^{\infty} \hat{\mathcal{O}}_n(s_{56}) \varphi_{k_5} \varphi_{k_6} \right] + \text{ 15 perms}\,. \tag{C.11}$$

To avoid clutter, above we have omitted the (conformal) time dependence of $a(\tau)$, $\varphi_k(\tau)$, as well as the differential operators $\hat{\mathcal{O}}_n$ that is defined by

$$\hat{\mathcal{O}}_n(k) = \frac{(-1)^n}{(k\tau)^2 + (m/H)^2} \left\{ [\tau^2 \partial_\tau^2 - 2\tau \partial_\tau][(k\tau)^2 + (m/H)^2]^{-1} \right\}^n . \tag{C.12}$$

The above expressions for the correlators of φ systematically correct the leading-order results given in (11.10). Up to any given number of (time) derivatives, one can compute the time-integrals given above and straightforwardly extract the quantities $F_{1,2,3}$. Subsequently, in order to compute with the same precision e.g. the power spectrum and the bispectrum of ζ (induced by the single-, double-, and triple-exchange graphs), one should act with the bespoke weight-shifting operators.

C.3 Non-Local EFT Resummation in Flat Space

As an interesting curiosity, we show how one can fully resum the non-local EFT in flat space. We will see that the effective calculation reproduces the one computed in the two-field theory in some particular limit. Additionally, we will comment on the singularity structure of these correlators.

Flat-space propagators. In flat space, after setting $H = 0$, the correlators are computed at a fixed time $t_0 = 0$, which is analogous to the end of inflation surface τ_0. Let us consider a theory composed of a massless field φ propagating at speed c_s and a relativistic field σ with mass m. We assume that both fields are coupled at cubic order through the interaction $\mathcal{L} \supset -\frac{g}{2}\varphi^2\sigma$ where g is some coupling constant.

Following the Schwinger-Keldysh diagrammatic rules albeit adapted to flat space, the bulk-to-boundary propagator of φ and the bulk-to-bulk propagator of σ read

$$\begin{aligned} \mathcal{K}_k(t,t') &= \frac{1}{2c_s k} e^{-ic_s k(t-t')}\,, \\ \mathcal{G}_k(t,t') &= \frac{1}{2\omega}\left(e^{-i\omega(t-t')}\theta(t-t') + e^{i\omega(t-t')}\theta(t'-t)\right)\,, \end{aligned} \tag{C.13}$$

with $\omega^2 = k^2 + m^2$. In the following, we will consider the s-channel four-point function $\langle \varphi_{\boldsymbol{k}_1}\varphi_{\boldsymbol{k}_2}\varphi_{\boldsymbol{k}_3}\varphi_{\boldsymbol{k}_4}\rangle$. The t- and u- channels can be easily found by suitable permutations of the external momenta.

Exchange diagram. In the two-field theory, the correlator is composed of four different sub-diagrams, corresponding to the four different time ordering for the two vertices of the exchange diagram. Using the Feynman rules, the first contribution is

$$\begin{aligned} I_{++} &= -g^2\int_{-\infty}^{0} \mathrm{d}t'\mathrm{d}t''\, \mathcal{K}_{k_1}(0,t')\mathcal{K}_{k_2}(0,t')\mathcal{G}_{s_{12}}(t',t'')\mathcal{K}_{k_3}(0,t'')\mathcal{K}_{k_4}(0,t'') \\ &= \frac{g^2}{16c_s^4 k_1k_2k_3k_4}\left(\frac{1}{EE_LE_R} + \frac{1}{2\omega E_LE_R}\right)\,, \end{aligned} \tag{C.14}$$

where we have defined $s_{ij} = |\boldsymbol{k}_i + \boldsymbol{k}_j|$ and $\omega^2 = s_{12}^2 + m^2$ being the exchanged energy of the massive field. We also have introduced the total energy $E \equiv c_s(k_{12} + k_{34})$ with $k_{ij} = k_i + k_j$ and the energy flowing into the left (resp. right) vertex $E_L \equiv c_s k_{12} + \omega$ (resp. $E_R \equiv c_s k_{34} + \omega$). After inspecting the properties of the propagators, it is easy to show that $I_{--} = I_{++}^*$, so that one has $I_{++} + I_{--} = 2\mathrm{Re}(I_{++})$. However in our case, I_{++} is real so that the sum of both diagrams is just twice the result obtained in (C.14). The I_{+-} contribution is

$$\begin{aligned} I_{+-} &= g^2\int_{-\infty}^{0} \mathrm{d}t'\mathrm{d}t''\, \mathcal{K}_{k_1}(0,t')\mathcal{K}_{k_2}(0,t')\mathcal{K}_{\omega}(t'',t')\mathcal{K}_{k_3}(t'',0)\mathcal{K}_{k_4}(t'',0) \\ &= \frac{g^2}{16c_s^4 k_1k_2k_3k_4}\frac{1}{2\omega E_LE_R}\,. \end{aligned} \tag{C.15}$$

Similarly to the previous case, we have $I_{-+} = I_{+-}^*$ so that one just needs to multiply by a factor two the result in (C.15) to obtain $I_{+-} + I_{-+}$. Summing all the four contributions, the final correlator is

$$\langle \varphi_{\boldsymbol{k}_1} \varphi_{\boldsymbol{k}_2} \varphi_{\boldsymbol{k}_3} \varphi_{\boldsymbol{k}_4} \rangle' = \frac{g^2}{8 c_s^4 k_1 k_2 k_3 k_4} \left(\frac{1}{E E_L E_R} + \frac{1}{\omega E_L E_R} \right) . \tag{C.16}$$

The correlator has a singularity when the total energy vanishes $E \to 0$, and when partial energies flowing into the left or right vertices add up to zero $E_{L,R} \to 0$. Note that these singularities are never reached for physical momentum configurations. In fact, the residue of the total energy singularity is the corresponding scattering amplitude

$$\lim_{E \to 0} \langle \varphi_{\boldsymbol{k}_1} \varphi_{\boldsymbol{k}_2} \varphi_{\boldsymbol{k}_3} \varphi_{\boldsymbol{k}_4} \rangle' = \frac{1}{8 c_s^4 k_1 k_2 k_3 k_4} \times \frac{\mathcal{A}_4}{E} , \tag{C.17}$$

where $\mathcal{A}_4 = -g^2/\mathcal{S}$ with $\mathcal{S} = c_s^2 k_{12}^2 - \omega^2$ being the (non-relativistic) Mandelstam variable. When the sound speed of φ is sufficiently reduced, an interesting limit is that of $c_s k_{12,34} \ll \omega$, corresponding to the massive field σ being much more energetic than the external field φ. In this case, we have $E_{L,R} = \omega + \mathcal{O}(c_s k_{12,34}/\omega)$ and the correlator can be written as an expansion in $c_s k_{12,34}/\omega$ whose leading order term reads

$$\langle \varphi_{\boldsymbol{k}_1} \varphi_{\boldsymbol{k}_2} \varphi_{\boldsymbol{k}_3} \varphi_{\boldsymbol{k}_4} \rangle' = \frac{g^2}{8 c_s^4 k_1 k_2 k_3 k_4} \left(\frac{1}{E \omega^2} + \mathcal{O}\left(\frac{c_s k_{12,34}}{\omega} \right) \right) . \tag{C.18}$$

An interesting feature of this limit is that the partial energy singularities effectively disappear. Indeed in this limit, the massive field can be integrated out and the exchange diagram becomes an effective contact one.

Non-local contact diagrams. Let us now explicitly integrate out the massive field at the level of the Lagrangian. This procedure generates an infinite tower of non-local contact operators

$$\mathcal{L} \supset -\frac{g^2}{4} \varphi^2 \sum_{n=0}^{\infty} \mathcal{O}_n \varphi^2 , \quad \text{with} \quad \mathcal{O}_n = \frac{1}{-\partial_i^2 + m^2} \frac{(-\partial_t^2)^n}{(-\partial_i^2 + m^2)^n} . \tag{C.19}$$

A considerable simplification, compared to the cosmological case, is that the physical momentum does not redshift and the operator ordering does not matter. This Lagrangian leads to an infinite number of contact diagrams to evaluate. However, interestingly enough, one can easily compute them all. The contribution I_+ reads

$$\begin{aligned}
I_+ &= \frac{i g^2}{2} \int_{-\infty}^{0} \mathrm{d}t \, \mathcal{K}_{k_1}(0,t) \mathcal{K}_{k_2}(0,t) \sum_{n=0}^{\infty} \frac{(-1)^n}{\omega^2} \frac{\partial_t^{2n}}{\omega^{2n}} \mathcal{K}_{k_3}(0,t) \mathcal{K}_{k_4}(0,t) + (k_{12} \leftrightarrow k_{34}) \\
&= \frac{i g^2}{32 c_s^4 k_1 k_2 k_3 k_4} \frac{1}{\omega^2} \int_{-\infty}^{0} \mathrm{d}t \, e^{i c_s k_{12} t} \sum_{n=0}^{\infty} \frac{(-1)^n}{\omega^{2n}} \partial_t^{2n} e^{i c_s k_{34} t} + (k_{12} \leftrightarrow k_{34}) \\
&= \frac{i g^2}{32 c_s^4 k_1 k_2 k_3 k_4} \frac{1}{\omega^2} \left(\sum_{n=0}^{\infty} \left(\frac{c_s k_{34}}{\omega} \right)^{2n} \right) \int_{-\infty}^{0} \mathrm{d}t \, e^{i c_s (k_{12} + k_{34}) t} + (k_{12} \leftrightarrow k_{34}) \\
&= \frac{g^2}{32 c_s^4 k_1 k_2 k_3 k_4} \frac{1}{E} \left(\frac{1}{\omega^2 - c_s^2 k_{12}^2} + \frac{1}{\omega^2 - c_s^2 k_{34}^2} \right) ,
\end{aligned} \tag{C.20}$$

where in the third line we have used $\partial_t^{2n} e^{ic_s k_{ij} t} = (-1)^n (c_s k_{ij})^{2n} e^{ic_s k_{ij} t}$. The second contribution is $I_- = I_+$. In the end, the infinite sum of contact diagrams has the following simple and compact form

$$\langle \varphi_{\boldsymbol{k}_1} \varphi_{\boldsymbol{k}_2} \varphi_{\boldsymbol{k}_3} \varphi_{\boldsymbol{k}_4} \rangle' = \frac{g^2}{16 c_s^4 k_1 k_2 k_3 k_4} \frac{1}{E} \left(\frac{1}{\omega^2 - c_s^2 k_{12}^2} + \frac{1}{\omega^2 - c_s^2 k_{34}^2} \right) , \tag{C.21}$$

where we note that the same result is also found if the massive field is integrated out in a local manner, in that case resumming an infinite number of local contact operators. This explicit correlator has a few interesting features. First of all, we do not fully recover the correlator computed in the two-field theory (C.16). This means that the effective single-field theory used here, integrating out the field σ *à la* amplitude, does not faithfully capture the effects present in the original theory, see below. Second, we note that the correlator diverges when $c_s k_{12,34} \to \omega$ which is equivalent to the limit $E_{L,R} \to 2\omega$. This is expected because in this configuration the geometric series in (C.20) does not converge. Physically, it corresponds to the case when the energy of two external field φ coincides with the exchanged energy of the intermediate particle. In this configuration, the massive field could not have been integrated out in the first place. The most interesting configuration is when we place ourselves deep inside the radius of convergence of the geometric series $c_s k_{12,34} \ll \omega$, which corresponds to the massive field carrying way more energy than the external fields. In this limit, the correlator simplifies to

$$\langle \varphi_{\boldsymbol{k}_1} \varphi_{\boldsymbol{k}_2} \varphi_{\boldsymbol{k}_3} \varphi_{\boldsymbol{k}_4} \rangle' = \frac{g^2}{8 c_s^4 k_1 k_2 k_3 k_4} \left(\frac{1}{E \omega^2} + \mathcal{O}\left(\frac{c_s k_{12,34}}{\omega} \right) \right) . \tag{C.22}$$

This form perfectly matches the correct limit of the four-point correlator computed in the original theory (C.18) and reproduces the residue at the total energy singularity. However, higher-order corrections do not coincide. This apparent mismatch, as well as the others mentioned above, have been recently solved by adding the proper boundary term accounting for the homogeneous solution to the equation of motion for the heavy field, that we have discarded.

D

Details on the Cosmological Flow

In this appendix, we provide additional materials on the cosmological flow that have been used in Part. IV. First, we give details about the Fourier summation. We then derive the initial conditions for the flow equations of the two- and three-point correlators.

D.1 Extended Fourier Summation

We deal in full generality with N scalar degrees of freedom. Latin letters $(a, b, \ldots)$ run over phase-space coordinates from 1 to $2N$. Greek letters $(\alpha, \beta, \ldots)$ run over all fields or their conjugate momenta from 1 to N.

Fourier indices. We have seen in the main text that it is helpful to condense the notations and the Fourier integrals in the summation convention. We indicate that this extended interpretation is used by typesetting the labels to which it applies in a sans serif face. An index contraction such as $A_{\mathsf{a}}B^{\mathsf{a}}$ reads

$$A_{\mathsf{a}}B^{\mathsf{a}} = \sum_a \int \frac{\mathrm{d}^3 k_a}{(2\pi)^3} A_a(\boldsymbol{k}_a) B^a(\boldsymbol{k}_a)\,. \tag{D.1}$$

Note that we position indices to respect the normal rules for covariant expressions. There is an extra complexity with $\boldsymbol{k}$-labels included because Fourier-space expressions sometimes produce the δ-function $\delta_{\mathsf{ab}} = (2\pi)^3 \delta_{ab}\, \delta^{(3)}(\boldsymbol{k}_a + \boldsymbol{k}_b)$. Within a Fourier integral, this reverses the sign of a $\boldsymbol{k}$-label, which we indicate by decorating the label with a bar as in $B^{\bar{\mathsf{a}}}$. Hence,

$$A_{\mathsf{a}}B^{\bar{\mathsf{a}}} = \sum_a \int \frac{\mathrm{d}^3 k_a}{(2\pi)^3} A_a(\boldsymbol{k}_a) B^a(-\boldsymbol{k}_a)\,. \tag{D.2}$$

A contraction with $\delta^{\mathsf{a}}{}_{\mathsf{b}}$ will bar an index $A^{\bar{\mathsf{a}}} = \delta^{\mathsf{ab}} A_{\mathsf{b}}$. When dealing with field Greek indices (α, β) running from 1 to N, we also indicate the existence of an extended Fourier summation by typesetting the labels in sans serif face $(\mathsf{\alpha}, \mathsf{\beta})$.

Commutator in Fourier space. With $\boldsymbol{X}^a = (\boldsymbol{\varphi}^\alpha, \boldsymbol{p}^\beta)$ being the phase-space vector in the Heisenberg picture, the canonical commutation algebra has a compact expression

$$[\boldsymbol{X}^{\mathsf{a}}, \boldsymbol{X}^{\mathsf{b}}] = i\epsilon^{\mathsf{ab}}\,, \tag{D.3}$$

where $\epsilon^{\mathsf{ab}} \equiv (2\pi)^3 \delta^{(3)}(\boldsymbol{k}_a + \boldsymbol{k}_b)\, \epsilon^{ab}$ and the $2N \times 2N$ matrix can be written in block form

$$\epsilon^{ab} = \begin{pmatrix} \mathbf{0} & \mathbf{1} \\ -\mathbf{1} & \mathbf{0} \end{pmatrix}. \tag{D.4}$$

We also assume that phase-space indices are organised so that a block of field labels are followed by a block of momentum labels, in the same order.

D.2 Two-point Correlator Initial Conditions

The derivation of initial conditions for the two-point correlators is done using the Schwinger-Keldysh formalism (see Chap. 5) instead of the canonical in-in formalism, phrased in operator language. In line with the point of view of the "cosmological flow", this approach circumvents the use of mode functions.

Path integral formalism. The quadratic theory that we consider is

$$S^{(2)} = \frac{1}{2}\int \mathrm{d}t\, a^3 \left(\bar{\Delta}_\alpha \, (\dot{\boldsymbol{\varphi}}^\alpha)^2 - c_\alpha^2 \, \frac{k^2}{a^2} \, (\boldsymbol{\varphi}^\alpha)^2 \right). \tag{D.5}$$

After integrating by parts while assuming the boundary terms vanish at infinity and introducing conformal time $\mathrm{d}\tau = \mathrm{d}t/a$, the above action in real space reads

$$S = -\frac{1}{2}\int \mathrm{d}\tau\, \mathrm{d}^3x\, a^2\, \boldsymbol{\varphi}^\alpha \boldsymbol{\mathcal{O}}_\alpha \boldsymbol{\varphi}^\alpha\,, \quad \text{with} \quad \boldsymbol{\mathcal{O}}_\alpha = \bar{\Delta}_\alpha \left(\partial_\tau^2 + 2\frac{a'}{a}\partial_\tau \right) - c_\alpha^2\, \partial_i^2\,, \tag{D.6}$$

where a prime denotes derivative with respect to conformal time. Two sets of field configurations $\boldsymbol{\varphi}_+^\alpha$ and $\boldsymbol{\varphi}_-^\alpha$ are introduced, and the Schwinger-Keldysh generating functional can be written in the following way

$$\begin{aligned} Z = \int \left[\mathcal{D}\boldsymbol{\varphi}_+^\alpha \mathcal{D}\boldsymbol{\varphi}_-^\alpha\right] \exp\left\{ -\frac{i}{2}\int_{\tau_0}^{\tau} \mathrm{d}\tau \mathrm{d}^3x\, a^2\, \bar{\boldsymbol{\varphi}}^\alpha \begin{pmatrix} \boldsymbol{\mathcal{O}} & \\ & -\boldsymbol{\mathcal{O}} \end{pmatrix}_\alpha \boldsymbol{\varphi}^\alpha \right\} \\ \times \prod_{\alpha, \boldsymbol{x}} \delta\left(\boldsymbol{\varphi}_+^\alpha(\tau, \boldsymbol{x}) - \boldsymbol{\varphi}_-^\alpha(\tau, \boldsymbol{x}) \right), \end{aligned} \tag{D.7}$$

where, in this formula, $\boldsymbol{\varphi}^\alpha = (\boldsymbol{\varphi}_+^\alpha, \boldsymbol{\varphi}_-^\alpha)$ and $\bar{\boldsymbol{\varphi}}^\alpha$ denotes the transpose vector. The time τ_0 should be set in the infinite past and τ is the time at which we want to initialise the two-point correlation functions. The δ-function enforces that the fields

coincide at the upper bound $\boldsymbol{\varphi}^\alpha_+(\tau,\boldsymbol{x}) = \boldsymbol{\varphi}^\alpha_-(\tau,\boldsymbol{x})$. We define the time-ordered two-point function of fields as

$$\boldsymbol{\Delta}^{\alpha\beta}_{++}(\tau_1,\boldsymbol{x};\tau_2,\boldsymbol{y}) = \langle \mathcal{T}\,\boldsymbol{\varphi}^\alpha_+(\tau_1,\boldsymbol{x})\boldsymbol{\varphi}^\beta_+(\tau_2,\boldsymbol{y})\rangle\ , \tag{D.8}$$

with similar definitions for $\boldsymbol{\Delta}_{+-}, \boldsymbol{\Delta}_{-+}$ and $\boldsymbol{\Delta}_{--}$. The theory being quadratic and diagonal, it is an easy task to compute the $\boldsymbol{\Delta}_{\pm\pm}$. They are obtained by formally inverting the quadratic operator $\boldsymbol{\mathcal{O}}$,

$$\begin{pmatrix} \boldsymbol{\mathcal{O}} & \\ & -\boldsymbol{\mathcal{O}} \end{pmatrix} \begin{pmatrix} \boldsymbol{\Delta}_{++} & \boldsymbol{\Delta}_{+-} \\ \boldsymbol{\Delta}_{-+} & \boldsymbol{\Delta}_{--} \end{pmatrix} = -\frac{i}{a^2} \begin{pmatrix} 1 & 0 \\ 0 & 1 \end{pmatrix} \delta(\tau_1-\tau_2)\delta^{(3)}(\boldsymbol{x}-\boldsymbol{y})\,. \tag{D.9}$$

These inhomogeneous equations can be solved exactly in Fourier space where the spatial dependence becomes diagonal. With the proper Bunch-Davies vacuum boundary conditions and imposing that $\boldsymbol{\Delta}_{++}$ (in Fourier space) oscillates with positive frequency in the far past, the solution is given by

$$\boldsymbol{\Delta}^{\alpha\beta}_{++} = (2\pi)^3\delta^{\alpha\beta}\delta^{(3)}(\boldsymbol{k}_1+\boldsymbol{k}_2)\,\bar{\Delta}_\alpha\,\frac{H^2}{2c_\alpha^3k^3}\,(1+ic_\alpha k\tau_1)(1-ic_\alpha k\tau_2)e^{ic_\alpha k(\tau_2-\tau_1)}\,, \tag{D.10}$$

assuming $\tau_2 < \tau_1$. Here, $k = |\boldsymbol{k}_1| = |\boldsymbol{k}_2|$, and there is no sum on the repeated α index. We also recall that the index position is meaningless because the field space for fluctuations is flat i.e. field-space indices are lowered and raised with the flat Euclidean metric $\delta_{\alpha\beta}$. The remaining time-ordered two-point correlators can then be found. The δ-function in (D.7) enforces that $\boldsymbol{\Delta}_{-+}(\tau,\tau_2) = \boldsymbol{\Delta}_{++}(\tau,\tau_2)$ for all τ_2 when $\tau_1 = \tau$ is the external time. From the properties of the path integral, $\boldsymbol{\Delta}_{--}$ and $\boldsymbol{\Delta}_{+-}$ are Hermitian conjugates of $\boldsymbol{\Delta}_{++}$ and $\boldsymbol{\Delta}_{-+}$, respectively.

Equal-time correlators. From the above solutions, we can get the equal-time two-point correlators of fields by setting $\tau_1 = \tau_2 = \tau$. Trading the time-dependence for a scale factor dependence using $\tau = -1/aH$, we obtain

$$\langle\boldsymbol{\varphi}^\alpha_{\boldsymbol{k}}(\tau)\boldsymbol{\varphi}^\beta_{-\boldsymbol{k}}(\tau)\rangle' = \delta^{\alpha\beta}\bar{\Delta}_\alpha\,\frac{H^2}{2c_\alpha^3k^3}\left(1+\frac{c_\alpha^2k^2}{a^2H^2}\right)\,, \tag{D.11}$$

where the prime denotes that we have extracted the momentum conservation δ-function. Similarly one can derive the equal-time (rescaled) momentum-field and momentum-momentum two-point correlators. Eventually, one finds the two-point correlator initial conditions in Eq. (14.31), expressed in terms of the diagonal matrix $\Delta_{\alpha\beta} = \delta^{\alpha\beta}\bar{\Delta}_\alpha$ (no sum).

D.3 Three-point Correlator Initial Conditions

Let us now use the results of the previous section to derive the initial conditions for the three-point correlators. We are interested in computing the three-point correlators at some initial conformal time τ_0 in the deep past with the Hamiltonian (14.6). The in-in master formula leads to

$$\langle\boldsymbol{X}^a(\tau_0,\boldsymbol{k}_1)\boldsymbol{X}^b(\tau_0,\boldsymbol{k}_2)\boldsymbol{X}^c(\tau_0,\boldsymbol{k}_3)\rangle = i\left\langle\int_{-\infty}^{\tau_0}\mathrm{d}\tau\,\left[H_{\rm I}(\tau),X^a(\tau_0,\boldsymbol{k}_1)X^b(\tau_0,\boldsymbol{k}_2)X^c(\tau_0,\boldsymbol{k}_3)\right]\right\rangle, \tag{D.12}$$

where the expectation value is evaluated with respect to the usual vacuum of the free theory and $H_{\rm I}$ is the full cubic Hamiltonian that can be read of Eq. (14.6). To condensate notations, we will now on write the momentum dependency of the operators as subscripts. Assuming it is clear at which time the operators are evaluated, we will also omit the time dependency of the operators. By Fourier transforming the operators in $H_{\rm I}$, the first term in the commutator becomes

$$\langle \boldsymbol{X}^a_{\boldsymbol{k}_1} \boldsymbol{X}^b_{\boldsymbol{k}_2} \boldsymbol{X}^c_{\boldsymbol{k}_3} \rangle = i \int_{-\infty}^{\tau_0} \mathrm{d}\tau \, H_{\mathsf{def}} \int \frac{\Pi_i \, \mathrm{d}^3 q_i}{(2\pi)^9} \, (2\pi)^3 \delta^{(3)} \left(\Sigma_i \boldsymbol{q}_i \right) \left\langle X^{\mathsf{d}}_{\boldsymbol{q}_1} X^{\mathsf{e}}_{\boldsymbol{q}_2} X^{\mathsf{f}}_{\boldsymbol{q}_3} X^a_{\boldsymbol{k}_1} X^b_{\boldsymbol{k}_2} X^c_{\boldsymbol{k}_3} \right\rangle . \tag{D.13}$$

We have written the integrals over Fourier modes to be explicit—this time not using the Fourier summation convention—to be clear about momentum dependencies. We can now perform Wick contractions between the different operators to rewrite the expectation value as a combination of two-point functions. Discarding disconnected contributions, we obtain

$$\langle \boldsymbol{X}^a_{\boldsymbol{k}_1} \boldsymbol{X}^b_{\boldsymbol{k}_2} \boldsymbol{X}^c_{\boldsymbol{k}_3} \rangle = i \int_{-\infty}^{\tau_0} \mathrm{d}\tau \, H_{\mathsf{def}} \int \frac{\Pi_i \, \mathrm{d}^3 q_i}{(2\pi)^9} \, (2\pi)^3 \delta^{(3)} \left(\Sigma_i \boldsymbol{q}_i \right) \left\{ \langle X^{\mathsf{d}}_{\boldsymbol{q}_1} X^a_{\boldsymbol{k}_1} \rangle \langle X^{\mathsf{e}}_{\boldsymbol{q}_2} X^b_{\boldsymbol{k}_2} \rangle \langle X^{\mathsf{f}}_{\boldsymbol{q}_3} X^c_{\boldsymbol{k}_3} \rangle + 5 \text{ perms} \right\} . \tag{D.14}$$

We now need to specify the form of H_{def}. For pedagogical reasons before treating the general case, we start with a simple example to illustrate how the machinery works.

Preliminaries. Let us treat the concrete case of a cubic field-field-field interaction with no derivative for simplicity. Using the notations in Eq. (14.6), the cubic Hamiltonian reads

$$H_{\mathsf{def}} \boldsymbol{X}^{\mathsf{d}} \boldsymbol{X}^{\mathsf{e}} \boldsymbol{X}^{\mathsf{f}} = A_{\alpha\beta\gamma} \boldsymbol{\varphi}^\alpha \boldsymbol{\varphi}^\beta \boldsymbol{\varphi}^\gamma , \tag{D.15}$$

where we recall that the Latin indices run over the *phase*-space variables and the Greek indices run over *field*-space variables. Taking into account the possible non-canonical normalisation of the fields in the $\Delta_{\alpha\beta}$ tensor and using the time-ordered two-point function (D.10) derived in the previous section, the three-point initial correlator reads

$$\begin{aligned} \langle \boldsymbol{\varphi}^\alpha_{\boldsymbol{k}_1} \boldsymbol{\varphi}^\beta_{\boldsymbol{k}_2} \boldsymbol{\varphi}^\gamma_{\boldsymbol{k}_3} \rangle &= 6i \, (2\pi)^3 \delta^{(3)}(\Sigma_i \boldsymbol{k}_i) \, \frac{H^6}{8 e_3^3} \, \Delta_{\alpha\alpha} \Delta_{\beta\beta} \Delta_{\gamma\gamma} \times (1 + i k_1 \tau_0)(1 + i k_2 \tau_0)(1 + i k_3 \tau_0) e^{-i k_t \tau_0} \\ &\times \left\{ \int_{-\infty}^{\tau_0} \mathrm{d}\tau \, \Delta_{\alpha\alpha}(\tau) \Delta_{\beta\beta}(\tau) \Delta_{\gamma\gamma}(\tau) \, A_{\alpha\beta\gamma}(\tau) \, (1 - i k_1 \tau)(1 - i k_2 \tau)(1 - i k_3 \tau) e^{i k_t \tau} \right\} + \text{c.c.} , \end{aligned} \tag{D.16}$$

where $k_t = k_1 + k_2 + k_3$. For convenience in later calculations, we also introduce the other symmetric polynomials

$$e_2 \equiv k_1 k_2 + k_1 k_3 + k_2 k_3 , \qquad e_3 \equiv k_1 k_2 k_3 . \tag{D.17}$$

Note that one needs to carry the Δ dependency both for external (at time τ_0) and internal (at time τ) operators. There is no summation for the repeated indices

α, β and γ. If we assume that the background parameters are slowly varying near $\tau = \tau_0$, then we can Taylor expand the third-order vertex function to first order $[\Delta_{\alpha\alpha}\Delta_{\beta\beta}\Delta_{\gamma\gamma}\, A_{\alpha\beta\gamma}]\,(\tau) \approx [\Delta_{\alpha\alpha}\Delta_{\beta\beta}\Delta_{\gamma\gamma}\, A_{\alpha\beta\gamma}]\,(\tau_0)$ and remove it from the time integral. In the end, the three-point correlator is given by

$$\begin{aligned}\langle \boldsymbol{\varphi}^{\alpha}_{\boldsymbol{k}_1} \boldsymbol{\varphi}^{\beta}_{\boldsymbol{k}_2} \boldsymbol{\varphi}^{\gamma}_{\boldsymbol{k}_3} \rangle &= 6\, \Delta_{\alpha\alpha}\Delta_{\beta\beta}\Delta_{\gamma\gamma}\, i\,(2\pi)^3 \delta^{(3)}(\Sigma_i \boldsymbol{k}_i)\, \frac{H^6}{8 e_3^3}\, \Delta_{\alpha\alpha}\Delta_{\beta\beta}\Delta_{\gamma\gamma}\, A_{\alpha\beta\gamma} \\ &\quad \times (1 + i k_1 \tau_0)(1 + i k_2 \tau_0)(1 + i k_3 \tau_0) e^{-i k_t \tau_0} \\ &\quad \times \int_{-\infty}^{\tau_0} \mathrm{d}\tau \left\{ (1 - i k_1 \tau)(1 - i k_2 \tau)(1 - i k_3 \tau) e^{i k_t \tau} \right\} + \text{c.c.}\,. \end{aligned} \tag{D.18}$$

In the first line, we have collected all "constant" terms. These terms include the normalisation of the external and internal operators encoded in the $\Delta_{\alpha\beta}$ tensor and the third-order vertex kernel from the considered cubic interaction. The remaining factor appears in all three-point correlators. The second line contains the external polynomial and the third line the internal polynomial. This simple example can now be generalised to the computation of all three-point correlators including all cubic interactions.

External polynomials. The external polynomial depends on the correlator considered. There are four different types of such polynomials. Formally setting $\tau_1 = \tau_0$ and $\tau_2 = 0$ in the time-ordered two-point function (D.10), we see that the operators $\boldsymbol{\varphi}^{\alpha}$ and $\boldsymbol{p}^{\alpha}$ contribute the following polynomials

$$\boldsymbol{\varphi}^{\alpha} \to (1 + i k \tau_0) e^{-i k \tau_0}\,, \qquad \boldsymbol{p}^{\alpha} \to k^2 \tau_0 e^{-i k \tau_0}\,. \tag{D.19}$$

Using these expressions, it is an easy task to derive the external polynomials

$$\begin{aligned} \langle \boldsymbol{\varphi}^{\alpha}_{\boldsymbol{k}_1} \boldsymbol{\varphi}^{\beta}_{\boldsymbol{k}_2} \boldsymbol{\varphi}^{\gamma}_{\boldsymbol{k}_3} \rangle &\to \left(1 + i k_t \tau_0 - e_2 \tau_0^2 - i e_3 \tau_0^3\right) e^{-i k_t \tau_0}\,, \\ \langle \boldsymbol{p}^{\alpha}_{\boldsymbol{k}_1} \boldsymbol{\varphi}^{\beta}_{\boldsymbol{k}_2} \boldsymbol{\varphi}^{\gamma}_{\boldsymbol{k}_3} \rangle &\to \left(k_1^2 \tau_0 + i k_1^2 (k_2 + k_3) \tau_0^2 - e_3 k_1 \tau_0^3\right) e^{-i k_t \tau_0}\,, \\ \langle \boldsymbol{p}^{\alpha}_{\boldsymbol{k}_1} \boldsymbol{p}^{\beta}_{\boldsymbol{k}_2} \boldsymbol{\varphi}^{\gamma}_{\boldsymbol{k}_3} \rangle &\to \left(k_1^2 k_2^2 \tau_0 + i e_3 k_1 k_2 \tau_0^2\right) e^{-i k_t \tau_0}\,, \\ \langle \boldsymbol{p}^{\alpha}_{\boldsymbol{k}_1} \boldsymbol{p}^{\beta}_{\boldsymbol{k}_2} \boldsymbol{p}^{\gamma}_{\boldsymbol{k}_3} \rangle &\to e_3^2 \tau_0^3 e^{-i k_t \tau_0}\,. \end{aligned} \tag{D.20}$$

Internal polynomials. The internal polynomials depend on the cubic interaction we consider. From Eq. (14.6), we see that we have four different cubic vertex integrals to perform, each of them depending on the third-order kernels

$$\begin{aligned} A_{\alpha\beta\gamma} &= (2\pi)^3 \delta^{(3)}(\boldsymbol{k}_1 + \boldsymbol{k}_2 + \boldsymbol{k}_3)\, A_{\alpha\beta\gamma}\,, \\ B_{\alpha\beta\gamma} &= (2\pi)^3 \delta^{(3)}(\boldsymbol{k}_1 + \boldsymbol{k}_2 + \boldsymbol{k}_3)\, B_{\alpha\beta\gamma}\,, \\ C_{\alpha\beta\gamma} &= (2\pi)^3 \delta^{(3)}(\boldsymbol{k}_1 + \boldsymbol{k}_2 + \boldsymbol{k}_3)\, C_{\alpha\beta\gamma}\,, \\ D_{\alpha\beta\gamma} &= (2\pi)^3 \delta^{(3)}(\boldsymbol{k}_1 + \boldsymbol{k}_2 + \boldsymbol{k}_3)\, D_{\alpha\beta\gamma}\,. \end{aligned} \tag{D.21}$$

When choosing an initial time well inside the horizon, we want to keep only the highest-order terms in τ. Although the computation of the internal polynomials is straightforward, we still need to deal with higher-order derivative interactions.

Thus in Fourier space, the third-order kernels in Eq. (D.21) above may contain explicit $(k^2/a^2)^n$ dependencies for some integer n that needs to be tracked when evaluating the integrals. In order to take into account the scale factor dependency in such terms, we split the kernels according to the number of spatial derivatives they contain in the following way

$$\begin{aligned} A_{\alpha\beta\gamma} &= A^{(0)}_{\alpha\beta\gamma} + \frac{1}{a^2}A^{(2)}_{\alpha\beta\gamma} + \frac{1}{a^4}A^{(4)}_{\alpha\beta\gamma} + \dots\,, \qquad B_{\alpha\beta\gamma} = B^{(0)}_{\alpha\beta\gamma} + \frac{1}{a^2}B^{(2)}_{\alpha\beta\gamma} + \frac{1}{a^4}B^{(4)}_{\alpha\beta\gamma} + \dots\,, \\ C_{\alpha\beta\gamma} &= C^{(0)}_{\alpha\beta\gamma} + \frac{1}{a^2}C^{(2)}_{\alpha\beta\gamma} + \frac{1}{a^4}C^{(4)}_{\alpha\beta\gamma} + \dots\,, \qquad D_{\alpha\beta\gamma} = D^{(0)}_{\alpha\beta\gamma} + \frac{1}{a^2}D^{(2)}_{\alpha\beta\gamma} + \frac{1}{a^4}D^{(4)}_{\alpha\beta\gamma} + \dots\,, \end{aligned} \tag{D.22}$$

where we have absorbed all momentum dependency in the newly defined kernels. We indicate with the superscript $2n$ ($n \geq 0$) the number of spatial derivatives that appears in the cubic interaction. Let us start with the internal polynomial involving the $A_{\alpha\beta\gamma}$ tensor elements. For $n \geq 0$, it reads

$$\begin{aligned} \underline{A}^{(2n)}_{\alpha\beta\gamma} &= \frac{1}{2}\int_{-\infty}^{\tau_0} \mathrm{d}\tau\, a^4\, \frac{A^{(2n)}_{\alpha\beta\gamma}}{a^{2n}}\,(1-ik_1\tau)(1-ik_2\tau)(1-ik_3\tau)\,e^{ik_t\tau} + \text{ 5 perms} \\ &= \frac{-A^{(2n)}_{\alpha\beta\gamma}}{2i^{3-2n}H^{4-2n}}\left\{\frac{e_3}{k_t^{2n}}\,\Gamma(2n,-ik_t\tau_0) + \frac{e_2}{k_t^{2n-1}}\,\Gamma(2n-1,-ik_t\tau_0)\right. \\ &\qquad \left. + \frac{1}{k_t^{2n-2}}\,\Gamma(2n-2,-ik_t\tau_0) + \frac{1}{k_t^{2n-3}}\,\Gamma(2n-3,-ik_t\tau_0)\right\} + \text{ 5 perms}\,, \end{aligned} \tag{D.23}$$

where $\Gamma(m,z)$ for some integer m and a complex entry z is the upper incomplete $\Gamma-$function. Details about this function can be found in the following insert.

Incomplete $\Gamma-$function.—The incomplete $\Gamma-$function is defined as

$$\Gamma(s,z) = \int_z^{+\infty} t^{s-1}\,e^{-t}\,\mathrm{d}t\,, \tag{D.24}$$

with s being a complex parameter with $\mathrm{Re}(s) > 0$. This function is defined without restrictions on the integration paths in the complex plane. In our case, we are interested in the case where s is an integer (positive or negative) and z is purely imaginary. For $s = n \geq 1$, the incomplete $\Gamma-$function can be expressed as a *finite* sum

$$\Gamma(n,z) = (n-1)!\sum_{j=0}^{n-1}\frac{z^j}{j!}\,e^{-z}\,, \tag{D.25}$$

with the special value $\Gamma(1,z) = e^{-z}$. For a fixed $n \leq 0$, $\Gamma(n,z)$ has an asymptotic expansion – with *infinite* terms – at large z of the form

$$\Gamma(n,z) = z^{n-1}e^{-z}\left(\sum_{j=0}^{m-1}\frac{u_j}{z^j} + R_m(n,z)\right)\,, \qquad m = 1,2,\dots\,, \tag{D.26}$$

where the series coefficients u_j are defined as

$$u_j = (-1)^j(1-n)_j = (n-1)(n-2)...(n-j)\,, \tag{D.27}$$

and $R_m(n,z)$ is the remainder that decays as $\mathcal{O}\left(1/z^m\right)$.

From inspecting Eq. (D.23), we see that $\underline{A}^{(0)}$ and $\underline{A}^{(2)}$ have an infinite number of terms when expanding at large $|\tau_0|$. Because one cannot implement an infinite number of terms numerically, we choose to keep only the two dominant powers of τ_0. Bearing in mind that this internal polynomial will eventually be multiplied with the external polynomial, this series truncation is an approximation. Indeed, the corrections to the leading behaviour of higher-order derivative interactions will not be of the same order as the leading behaviour of lower-order in derivative interactions. Keeping only the two leading-order terms in τ, the $\underline{A}$ internal polynomials read

$$\begin{aligned}\underline{A}^{(2n)}_{\alpha\beta\gamma} = \frac{A^{(2n)}_{\alpha\beta\gamma}}{2H^{4-2n}k_t}\left\{e_3\tau_0^{2n-1} + i\tau_0^{2n-2}\left[e_2 + \frac{(2n-1)e_3}{k_t}\right] + \mathcal{O}\left(\tau_0^{2n-3}\right)\right\}e^{ik_t\tau_0} \\ + \text{ 5 perms}\,.\end{aligned} \tag{D.28}$$

Note that it is important to keep track of factors of i because the three-point correlator is real. The integral for the internal polynomial involving the B tensor for $n \geq 0$ reads

$$\begin{aligned}\underline{B}^{(2n)}_{\alpha\beta\gamma} &= \frac{1}{2}\int_{-\infty}^{\tau_0} \mathrm{d}\tau\, a^4\, \frac{B^{(2n)}_{\alpha\beta\gamma}}{a^{2n}}\,\frac{1}{a}\,(1-ik_1\tau)(1-ik_2\tau)k_3^2\tau\, e^{ik_t\tau} + \text{ 5 perms} \\ &= \frac{-B^{(2n)}_{\alpha\beta\gamma}}{2i^{3-2n}H^{3-2n}}\left\{\frac{e_3k_3}{k_t^{2n+1}}\,\Gamma(2n+1,-ik_t\tau_0) + \frac{(k_1+k_2)k_3^2}{k_t^{2n}}\,\Gamma(2n,-ik_t\tau_0)\right. \\ &\qquad \left. + \frac{k_3^2}{k_t^{2n-1}}\,\Gamma(2n-1,-ik_t\tau_0)\right\} + \text{ 5 perms}\,.\end{aligned} \tag{D.29}$$

When expanding the Γ-function, only $\underline{B}^{(0)}$ has an infinite number of terms. Keeping only the two leading-order terms, one obtains

$$\begin{aligned}\underline{B}^{(2n)}_{\alpha\beta\gamma} = \frac{-B^{(2n)}_{\alpha\beta\gamma}}{2H^{3-2n}k_t}\left\{ie_3\tau_0^{2n} - \frac{k_3}{k_t}\left[2ne_3 + k_t(k_1+k_2)k_3\right]\tau_0^{2n-1} + \mathcal{O}\left(\tau_0^{2n-2}\right)\right\}e^{ik_t\tau_0} \\ + \text{ 5 perms}\,.\end{aligned} \tag{D.30}$$

Similarly, the integral for the internal polynomial involving the C tensor for $n \geq 0$ is

$$\begin{aligned}\underline{C}^{(2n)}_{\alpha\beta\gamma} &= \frac{1}{2}\int_{-\infty}^{\tau_0} \mathrm{d}\tau\, a^4\, \frac{C^{(2n)}_{\alpha\beta\gamma}}{a^{2n}}\,\frac{1}{a^2}\,k_1^2\tau k_2^2\tau(1-ik_3\tau)\, e^{ik_t\tau} + \text{ 5 perms} \\ &= \frac{C^{(2n)}_{\alpha\beta\gamma}i^{2n+1}}{2H^{2-2n}}\left\{-\frac{e_3k_1k_2}{k_t^{2n+2}}\,\Gamma(2n+2,-ik_t\tau_0) - \frac{k_1^2k_2^2}{k_t^{2n+1}}\,\Gamma(2n+1,-ik_t\tau)\right\} \\ &\quad + \text{ 5 perms}\,.\end{aligned} \tag{D.31}$$

We note that $\underline{C}$ has a finite number of terms for all $n \geq 0$. However for consistency we still keep only the first two leading-order terms, giving

$$\begin{aligned}\underline{C}^{(2n)}_{\alpha\beta\gamma} = \frac{-C^{(2n)}_{\alpha\beta\gamma}}{2H^{2-2n}k_t}\left\{e_3k_1k_2\tau_0^{2n+1} + ik_1^2k_2^2\left(1+\frac{(2n+1)k_3}{k_t}\right)\tau_0^{2n} + \mathcal{O}\left(\tau_0^{2n-1}\right)\right\}e^{ik_t\tau_0} \\ + \text{ 5 perms}\,,\end{aligned} \tag{D.32}$$

where the first line is an exact result. Finally for the internal polynomial involving the D tensor for $n \geq 0$, we obtain

$$\begin{aligned}\underline{D}^{(2n)}_{\alpha\beta\gamma} &= \frac{1}{2}\int_{-\infty}^{\tau_0} \mathrm{d}\tau\, a^4\, \frac{D^{(2n)}_{\alpha\beta\gamma}}{a^{2n}}\, \frac{1}{a^3}\, e_3^2 \tau^3\, e^{ik_t\tau} + \text{ 5 perms} \\ &= \frac{D^{(2n)}_{\alpha\beta\gamma}}{2H^{1-2n}}\, \frac{e_3^2\, i^{2n+3}}{k_t^{2n+3}}\, \Gamma(2n+3, -ik_t\tau_0) + \text{ 5 perms}\,,\end{aligned} \tag{D.33}$$

from which we get

$$\underline{D}^{(2n)}_{\alpha\beta\gamma} = \frac{D^{(2n)}_{\alpha\beta\gamma}}{2H^{1-2n}k_t}\, e_3^2 \left\{ i\tau_0^{2n+2} - \frac{(2n+2)\tau_0^{2n+1}}{k_t} + \mathcal{O}\left(\tau_0^{2n}\right)\right\} e^{ik_t\tau_0} + \text{ 5 perms}\,. \tag{D.34}$$

Like the previous case, $\underline{D}$ has a finite number of terms for all $n \geq 0$. We have now all the necessary ingredients to obtain the initial conditions for the three-point correlators. Combining the external polynomials in Eq. (D.20), the truncated internal polynomials in Eqs. (D.28)-(D.30)-(D.32) and (D.34), and taking into account the common overall constant, the final results are the ones given in (14.34), (14.35), (14.36) and (14.37).

Tensorial structure. We have omitted the tensorial structure coming from the field normalisations in (14.34), (14.35), (14.36) and (14.37) to cleanse the expressions. Combinations of Δ tensors can be included a posteriori by performing the following replacement on the correlators (no summation on repeated indices)

$$\begin{aligned}\langle \boldsymbol{\varphi}^\alpha_{\boldsymbol{k}_1} \boldsymbol{\varphi}^\beta_{\boldsymbol{k}_2} \boldsymbol{\varphi}^\gamma_{\boldsymbol{k}_3}\rangle_0 &\to \Delta_{\alpha\alpha}\Delta_{\beta\beta}\Delta_{\gamma\gamma}\, \langle \boldsymbol{\varphi}^\alpha_{\boldsymbol{k}_1} \boldsymbol{\varphi}^\beta_{\boldsymbol{k}_2} \boldsymbol{\varphi}^\gamma_{\boldsymbol{k}_3}\rangle_0\,, \\ \langle \boldsymbol{p}^\alpha_{\boldsymbol{k}_1} \boldsymbol{\varphi}^\beta_{\boldsymbol{k}_2} \boldsymbol{\varphi}^\gamma_{\boldsymbol{k}_3}\rangle_0 &\to \Delta^{-1}_{\alpha\alpha}\Delta_{\beta\beta}\Delta_{\gamma\gamma}\, \langle \boldsymbol{p}^\alpha_{\boldsymbol{k}_1} \boldsymbol{\varphi}^\beta_{\boldsymbol{k}_2} \boldsymbol{\varphi}^\gamma_{\boldsymbol{k}_3}\rangle_0\,, \\ \langle \boldsymbol{p}^\alpha_{\boldsymbol{k}_1} \boldsymbol{p}^\beta_{\boldsymbol{k}_2} \boldsymbol{\varphi}^\gamma_{\boldsymbol{k}_3}\rangle_0 &\to \Delta^{-1}_{\alpha\alpha}\Delta_{\beta\beta}\Delta^{-1}_{\gamma\gamma}\, \langle \boldsymbol{p}^\alpha_{\boldsymbol{k}_1} \boldsymbol{p}^\beta_{\boldsymbol{k}_2} \boldsymbol{\varphi}^\gamma_{\boldsymbol{k}_3}\rangle_0\,, \\ \langle \boldsymbol{p}^\alpha_{\boldsymbol{k}_1} \boldsymbol{p}^\beta_{\boldsymbol{k}_2} \boldsymbol{p}^\gamma_{\boldsymbol{k}_3}\rangle_0 &\to \Delta^{-1}_{\alpha\alpha}\Delta^{-1}_{\beta\beta}\Delta^{-1}_{\gamma\gamma}\, \langle \boldsymbol{p}^\alpha_{\boldsymbol{k}_1} \boldsymbol{p}^\beta_{\boldsymbol{k}_2} \boldsymbol{p}^\gamma_{\boldsymbol{k}_3}\rangle_0\,,\end{aligned} \tag{D.35}$$

and by redefining the third-order vertex functions as follows

$$\begin{aligned}A^{(2n)}_{\alpha\beta\gamma} &\to \Delta_{\alpha\alpha}\Delta_{\beta\beta}\Delta_{\gamma\gamma}\, A^{(2n)}_{\alpha\beta\gamma}\,, \\ B^{(2n)}_{\alpha\beta\gamma} &\to \Delta_{\alpha\alpha}\Delta_{\beta\beta}\Delta^{-1}_{\gamma\gamma}\, B^{(2n)}_{\alpha\beta\gamma}\,, \\ C^{(2n)}_{\alpha\beta\gamma} &\to \Delta^{-1}_{\alpha\alpha}\Delta^{-1}_{\beta\beta}\Delta_{\gamma\gamma}\, C^{(2n)}_{\alpha\beta\gamma}\,, \\ D^{(2n)}_{\alpha\beta\gamma} &\to \Delta^{-1}_{\alpha\alpha}\Delta^{-1}_{\beta\beta}\Delta^{-1}_{\gamma\gamma}\, D^{(2n)}_{\alpha\beta\gamma}\,.\end{aligned} \tag{D.36}$$

for all $n \geq 0$. These manipulations are necessary if one or several fields are not canonically normalised.

E

Notation and Conventions

We use natural units in which the speed of light c and Planck's constant $\hbar$ are set to unity $c = \hbar = 1$, with reduced Planck mass $M_{\rm Pl} = 1/\sqrt{8\pi G} = 2.4 \times 10^{18}$ GeV, where G denotes Newton's constant. Our metric signature is $(-+++)$. Spatial three-dimensional vectors are written in boldface $\boldsymbol{k}$. We use Greek letters $(\mu, \nu, \ldots)$ for spacetime indices, and Latin letters $(i, j, \ldots)$ for spatial indices as usual. Overdots and primes will denote derivatives with respect to cosmic (physical) time t and conformal time τ defined by $\mathrm{d}\tau = \mathrm{d}t/a$, respectively. Our Fourier convention is

$$f_{\boldsymbol{k}} = \int \mathrm{d}^3x f(x) e^{-i\boldsymbol{k}\cdot\boldsymbol{x}}\,, \quad f(x) = \int \frac{\mathrm{d}^3k}{(2\pi)^3} f_{\boldsymbol{k}}\, e^{i\boldsymbol{k}\cdot\boldsymbol{x}}\,. \tag{E.1}$$

A prime on a correlator is defined to mean that we drop the momentum conserving delta function

$$\langle \mathcal{O}_{\boldsymbol{k}_1} \ldots \mathcal{O}_{\boldsymbol{k}_n} \rangle = (2\pi)^3 \delta^{(3)}(\boldsymbol{k}_1 + \ldots + \boldsymbol{k}_n)\, \langle \mathcal{O}_{\boldsymbol{k}_1} \ldots \mathcal{O}_{\boldsymbol{k}_n} \rangle' \,. \tag{E.2}$$

The extended Fourier summation—used for the cosmological flow in Part IV—is introduced throughout the main text when needed. Details are given in App. D. Additional mathematical symbols are listed below.

Symbol	Meaning
a	Scale factor
H	Hubble parameter, $H \equiv \frac{\dot{a}}{a}$
P, ρ	Pressure and energy density
w	Equation of state, $w \equiv P/\rho$
Y_ℓ^m	Spherical harmonics

Symbol	Meaning
$a_{\ell m}$	Mutipole moments
$C_\ell^{TT,TE,EE}$	Angular TT, TE and EE power spectra
P_ℓ	Legendre polynomials
$\Delta_\ell^T, \Delta_m, \Delta$	Transfer functions
P_m	Matter power spectrum
Φ	Newtonian potential
Φ_g	Gaussian field
δ_m	Matter density contrast, $\delta_m \equiv \delta\rho/\bar{\rho}$
b_1, b_2, b_Φ	Bias parameters
ϵ, η	Slow-roll parameters
ϵ_V, η_V	Potential slow-roll parameters
ϕ	Inflaton field
$V(\phi)$	Inflaton potential
ζ	Curvature perturbation
γ	Tensor modes
v	Canonically normalised Mukhanov-Sasaki variable, $v \equiv z\zeta$
p_v	Conjugate momentum, $p_v \equiv v'$
$\hat{a}_{\boldsymbol{k}}, \hat{a}_{\boldsymbol{k}}^\dagger$	Annihilation and creation operators
$H^{(1)}$	Hankel function of the first kind
$\mathcal{P}_\zeta$	Dimensionless scalar primordial power spectrum
A_s, n_s	Scalar amplitude and spectral tilt
$\mathcal{P}_t$	Dimensionless tensor primordial power spectrum
A_t, n_t	Tensor amplitude and spectral tilt
r	Tensor-to-scalar ratio, $r \equiv \mathcal{P}_t/\mathcal{P}_\zeta$
B_ζ	Primordial bispectrum
S	Dimensionless bispectrum shape function
$f_{\rm NL}$	Non-linear bispectrum size parameter
ζ_g	Gaussian perturbation
φ	Massless scalar field
μ	Mass parameter, $\mu^2 \equiv m^2/H^2 - 9/4$, $\nu \equiv i\mu$
$B_{\ell_1\ell_2\ell_3}$	Angular averaged CMB bispectrum
Γ	Gamma function
T_ζ	Primordial trispectrum
$g_{\rm NL}, \tau_{\rm NL}$	Non-linear trispectrum size parameters
$B_{\zeta\zeta\gamma}$	Mixed scalar-tensor bispectra
$B_{\gamma\gamma\gamma}$	Graviton bispectrum
χ	Mukhanov-Sasaki massive scalar field
ω_k	Effective time-dependent frequency
$\mathcal{O}^\pm$	Boundary operators

Symbol	Meaning
$\Delta^{\pm}$	Scaling dimensions
α_k, β_k	Bogolyubov coefficients
$T_{\rm dS}$	de Sitter temperature
$J_{i\mu}$	Bessel function of the first kind
$H^{(1)}_{i\mu}$	Hankel function of the first kind
F_k	Stokes-line singulant
Γ_k	Particle production width
σ	Generic bulk massive scalar field
$\upvarphi$	Conformally coupled field
$\mathcal{A}, \theta$	Amplitude and phase of cosmological collider signal
$\sigma_{\mu_1\cdots\mu_s}$	symmetric and traceless spin-s field
P_s	Legendre polynomial
μ_s	Spinning Mass parameter, $\mu_s^2 \equiv m^2/H^2 - (s-1/2)^2$, $\nu_s \equiv i\mu_s$
$\mu_{\rm eff}$	Effective Mass Parameter, $\mu_{\rm eff}^2 \equiv m_{\rm eff}^2/H^2 - 9/4$, $m_{\rm eff}^2 \equiv m^2 + \rho^2$
φ	Generic bulk field
p	Conjugate momentum
$\mathcal{T}$ (resp. $\bar{\mathcal{T}}$)	time ordering (resp. anti-time ordering) operator
H	Hamiltonian, $H \equiv \int {\rm d}^3x\, \mathcal{H}$
$\mathcal{L}$	Lagrangian density, $S \equiv \int {\rm d}t{\rm d}^3x\, \mathcal{L}$
$\mathcal{D}\varphi$	Path-integral measure for field configurations
Z	Partition function
J	External current
$\Psi[\varphi]$	Vacuum wave-functional, $\Psi[\varphi](t) \equiv \langle\varphi(t)\vert\Omega\rangle$
$\mathsf{a}, \mathsf{b}, \mathsf{c}, \ldots$	Schwinger-Keldysh indices ($\pm$)
Δ_{ab}	(Real-space) Schwinger-Keldysh bulk-to-bulk propagators
$\mathcal{G}_{\mathsf{ab}}$	(Fourier-space) Schwinger-Keldysh bulk-to-bulk propagators
$\mathcal{G}_{\gtrless}$	Wightman functions
$\mathcal{K}_{\mathsf{a}}$	Schwinger-Keldysh bulk-to-boundary propagators
$\varepsilon^{\lambda}_{\mu_1\cdots\mu_2}$	Polarisation tensor
$\epsilon^{\mu\nu\alpha\beta}$	Levi-Civita tensor
W	Whittaker function of the first kind
ψ	(Left-handed) Weyl spinor
$\mathcal{G}_R, \mathcal{G}_A$	Retarded/advanced Green's function
$\mathcal{N}_\nu$	de Sitter density of states, $\mathcal{N}_\nu \equiv \frac{\nu}{\pi}\sinh(\pi\nu)$
E_i	External energies of a graph
K_i	Internal energies of a graph
$\tilde{\mathcal{K}}_{\mathsf{a}}, \tilde{\mathcal{G}}_{\mathsf{ab}}$	Stripped Schwinger-Keldysh propagators
$\mathcal{I}_{\mathsf{a}_1\cdots\mathsf{a}_V}$	Schwinger-Keldysh graph
Li	Dilogarithm function

Symbol	Meaning
$E_{1,2}$	Two-site chain external energies
K	Two-site chain internal energy
F_{ab}	Scalar seed correlator
u, v	Dimensionless kinematic variables, $u \equiv \frac{K}{E_1}, v \equiv \frac{K}{E_2}$
$P_{i\mu-1/2}$	Legendre P function
$F^{(3)}$	Three-point correlator
$Q_{i\mu-1/2}$	Legendre Q function
Disc	Discontinuity operation
${}_2F_1$	Hypergeometric function
${}_2\bar{F}_1$	Dressed hypergeometric function, ${}_2\bar{F}_1\left[\begin{smallmatrix} a & b \\ c \end{smallmatrix}; z\right] \equiv \frac{\Gamma(a)\Gamma(b)}{\Gamma(c)} {}_2F_1\left[\begin{smallmatrix} a & b \\ c \end{smallmatrix}; z\right]$
E_1	Exponential integral
$\mathcal{O}_\tau$	Equation of motion differential operator
Δ_u	Hypergeometric differential operator, $\Delta_u \equiv u^2(1-u^2)\partial_u^2 - 2u^3\partial_u$
$\hat{F}$	Rescaled scalar seed correlator
$\hat{\mathcal{H}}$	Rescaled homogeneous solution
$\hat{\mathcal{S}}$	Rescaled particular solution
$\mathcal{A}_\pm$	Free coefficients
λ	Transverse helicity, $\lambda \equiv \pm 1$
$\tilde{\kappa}$	Dimensionless chemical potential, $\tilde{\kappa} \equiv \kappa/H$
$F^{(\lambda)}_{\mathsf{ab}}$	Boost-breaking helical seed correlator
$\tilde{u}, \tilde{v}$	Dimensionless kinematic variables, $\tilde{u} \equiv \frac{2K}{c_s E_1 + K}, \tilde{v} \equiv \frac{2K}{c_s E_2 + K}$
$\Delta^{(\lambda)}_{\pm,\tilde{u}}$	Hypergeometric differential operator, $\Delta^{(\lambda)}_{\pm,\tilde{u}} \equiv \tilde{u}^2(1-\tilde{u})\partial_{\tilde{u}}^2 - (1 \pm i\lambda\tilde{\kappa})\tilde{u}^2\partial_{\tilde{u}}$
$\varepsilon^\lambda(\boldsymbol{k})$	Polarisation vector
$\mathcal{H}_\pm$	Homogeneous solution
$\mathcal{A}^{\mathsf{cd}}_{\mathsf{ab}}$	Free coefficients
$\mathcal{S}_\pm$	Particular solution
$\mathcal{A}^{(\lambda)}_{m,n}$	Double series coefficients
$(a)_n$	Pochhammer symbol, $(a)_n \equiv \Gamma(a+n)/\Gamma(a)$
F_{F}	Factorised time integral contribution
$F^{(3)}_L, \tilde{F}^{(3)}_R$	Left and right bulk time integrals, $F_{\mathrm{F}} \equiv F^{(3)}_L \times \tilde{F}^{(3)}_R$
σ_K	Massive field mode function
f_K	Positive-frequency WKB mode function
$\mathbb{C}_{\mathrm{I}}, \mathbb{C}_{\mathrm{II}}$	Riemann sheets
$F^{(3),\alpha}_L, F^{(3),\beta}_L$	Positive- and negative-frequency left integrals, $F^{(3)}_L \approx F^{(3),\alpha}_L + F^{(3),\beta}_L$
$\tilde{F}^{(3),\alpha}_R, \tilde{F}^{(3),\beta}_R$	Positive- and negative-frequency right integrals, $\tilde{F}^{(3)}_R \approx \tilde{F}^{(3),\alpha}_R + \tilde{F}^{(3),\beta}_R$
Res	Residue operation
θ	Kinematic-independent phase

Symbol	Meaning
Ξ, Υ, Ω	Dephasing functions
n_μ	Future-directed unit vector normal to the constant-t hypersurface
$h_{\mu\nu}$	Induced metric on the constant-t hypersurface, $h_{\mu\nu} \equiv g_{\mu\nu} + n_\mu n_\nu$
D_μ	Covariant derivative compatible with $h_{\mu\nu}$
$\mathcal{L}_n$	Lie derivative with respect to n^μ
$K_{\mu\nu}$	Extrinsic curvature, $K_{\mu\nu} \equiv D_\mu n_\nu = \frac{1}{2}\mathcal{L}_n h_{\mu\nu}$
${}^{(3)}R_{\mu\nu}$	3-dimensional Ricci tensor
δX	Object with background part subtracted, $\delta X \equiv X - \bar{X}$
π	Goldstone boson of broken time translations
ξ^μ	4-dimensional diffeomorphism
N	Lapse function
N^i	Shift vector
c_s	Speed of sound of adiabatic perturbations
γ_{ij}	Traceless and transverse tensor fluctuations (graviton)
r	Tensor-to-scalar ratio, $r \equiv \mathcal{P}_r/\mathcal{P}_\zeta$
$\Lambda_{\rm mix}$	Mixing scale with dynamical gravity, $\Lambda_{\rm mix} \equiv \sqrt{\epsilon}H$
$\Lambda_\star$	Strong coupling scale
Λ_u	Unitarity scale
f_π	Symmetry breaking scale
$\mathcal{E}^{\mu\nu\alpha\beta}$	Levi-Civita tensor density, $\mathcal{E}^{\mu\nu\alpha\beta} \equiv \epsilon^{\mu\nu\alpha\beta}/\sqrt{-g}$
σ_i	Spin-1 vector field (spatial components)
$k_{\rm p}$	Physical momentum, $k_{\rm p} \equiv k/a$
$D_{\rm F}$	Real-space flat-space Feynman propagator
$\tilde{\partial}_i$	Physical gradient, $\tilde{\partial}_i \equiv \partial_i/a$
$\mathcal{D}^{-1}$	Non-local differential operator, $\mathcal{D}^{-1} \equiv (-\tilde{\partial}_i + m^2)^{-1}$
k_ℓ, k_s	Long and soft modes
$\mathcal{D}_{ij}^{-1}$	Non-local spinning differential operator, $\mathcal{D}_{ij} \equiv (-\tilde{\partial}_i + m^2)\delta_{ij} - 2\kappa\epsilon_{ijl}\tilde{\partial}_l$
$F_{1,2,3}$	Seed correlators for single-, double- and triple-exchange diagrams
$\mathcal{I}_{1,2,3}$	Non-local EFT seed integrals
α	Dimensionless canonical low-speed parameter, $\alpha = \alpha_m \equiv c_s m/H$
α_κ	Dimensionless helical low-speed parameter, $\alpha_\kappa \equiv c_s\kappa/H$
$\mathcal{T}$	Dimensionless trispectrum shape
$\|\Omega\rangle$	Vacuum of the fully interacting theory
$\hat{\mathcal{O}}$	Quantum operator composed of fields and conjugate momenta
$\hat{\varphi}$	Generic bulk field operator
$\hat{p}$	Generic bulk conjugate momentum operator
$\hat{H}$	Hamiltonian
$\hat{H}^{\rm I}_{\rm int}$	Interacting Hamiltonian in the interaction picture

Symbol	Meaning
$\hat{U}$	Unitary time evolution operator
$\mathcal{N}$	Normal ordering operation
$\boldsymbol{X}^a$	Phase-space vector in the Heisenberg picture, $\boldsymbol{X}^a \equiv (\boldsymbol{\varphi}^\alpha, \boldsymbol{p}^\beta)$
X^a	Phase-space vector in the interaction picture, $X^a \equiv (\varphi^\alpha, p^\beta)$
$u^{\mathsf{a}}{}_{\mathsf{b}}, u^{\mathsf{a}}{}_{\mathsf{bc}}, u^{\mathsf{a}}{}_{\mathsf{bcd}}$	Flow tensors, $u^{\mathsf{a}}{}_{\mathsf{b}} \equiv \epsilon^{\mathsf{ac}} H_{\mathsf{cb}}, u^{\mathsf{a}}{}_{\mathsf{bc}} \equiv \epsilon^{\mathsf{ad}} H_{\mathsf{dbc}}, u^{\mathsf{a}}{}_{\mathsf{bcd}} \equiv \epsilon^{\mathsf{ae}} H_{\mathsf{ebcd}}$
$\bar{\Delta}, \bar{M}, \bar{I}$	Quadratic Lagrangian tensors
$\bar{A}, \bar{B}, \bar{C}, \bar{D}$	Cubic Lagrangian tensors
Δ, M, I	Quadratic Hamiltonian tensors
A, B, C, D	Cubic Hamiltonian tensors
Σ^{ab}	Two-point correlation functions
B^{abc}	Three-point correlation functions
Ω	Boundary term Lagrangian tensor
Δ_ζ	Curvature perturbation standard deviation, $\Delta_\zeta \equiv \sqrt{\mathcal{P}_\zeta}$

Summary

This summary seeks to convey the thesis material in a clear and comprehensible manner, providing insight for both general audiences and specialists alike.

Observing the Sky

When we look at the night sky, most of the twinkling dots we see are nearby stars within our own galaxy, the Milky Way. At first glance, these stars seem scattered randomly, with some areas densely populated and others nearly empty. But there's much more to the cosmos than meets the eye. If we could zoom out, we would discover even more dots—these would be stars from galaxies beyond our own. Zoom out further, and an entire galaxy, with its hundreds of millions of stars, would shrink to a single dot. And as we continue zooming out, these dots begin to form what we call the large-scale structure of the Universe, a vast web of galaxy clusters. These structures are the result of nearly 13.8 billions of years of time evolution under the effect of gravity, as tiny initial fluctuations gradually collapsed to form galaxies. But how do we know this? Because light travels at a finite speed, when we observe distant objects in the sky, we are actually looking back in time. The farther away something is, the older the light we are seeing. Using this incredible fact, cosmology aims to piece together the Universe's history from its earliest moments to the large-scale structures we observe today.

The Early Universe as a Laboratory for High-Energy Physics

A natural question that arises is: where did these structures come from? The most plausible explanation we have today is quite astonishing! Based on detailed analysis of cosmological data, we believe that the early Universe experienced a very brief but intense phase of accelerated expansion, known as *inflation*. This expansion was so immense that tiny quantum scales were stretched to cosmic scales. According to quantum physics, even empty space isn't truly empty—it contains tiny, fleeting "wiggles" called quantum fluctuations that constantly appear and vanish almost instantly. During inflation, these quantum fluctuations were amplified into macroscopic density fluctuations, which eventually became the structures we observe today. We have come to recognise that understanding the Universe on the largest scales is deeply reliant on insights into the physics of the very small.

Although there is strong evidence supporting inflation, much about its underlying physics remains a mystery. For instance, we don't know exactly what particles

were at work during that time nor how they interacted. There is one main reason for this. Inflation is believed to have occurred at an incredibly high energy scale, far beyond what our most powerful ground-based particle collider experiments can replicate. This means we cannot safely extend our current theories to that early phase of the Universe. But rather than being a limitation, this is actually an exciting opportunity! The early Universe might have left behind clues—through late-time observations—that hint at potential new physics in a completely unexplored high-energy regime.

You might rightly wonder how we can even study the physics of inflation and test our theories. In typical particle collider experiments, fundamental laws of Nature (such as the properties of elementary particles like their masses) are probed by smashing particles together and examining the resulting debris. These high-energy collisions create new massive particles (from the famous equation $E = mc^2$), which can then be detected and measured. The particles we detect provide insight into what occurred during the collision. However, importantly, fundamental particles are governed by quantum principles, which are probabilistic, and we can't predict outcomes with certainty. The objects we measure (we called them cross sections) rather tell us about *how probable a certain process is*. It means that we need to perform a lot of collisions to be able to correctly extract the physical properties of elementary particles. This is of course impossible in cosmology, as the history of the Universe only unfolded once. Instead, we use a different approach: we observe in different directions in the sky. By measuring specific signals in different parts of the sky, we collect data as if they were coming from independent experiments. Assuming that the laws of physics are the same everywhere in the Universe, we are able to extract information about the physical processes that shaped the cosmos. In essence, where particle physics relies on averaging over many experiments, cosmology is all about performing statistical analysis over many observations.

We cannot predict the exact position of galaxies in the Universe. However, a question we might ask is: what is the probablity of finding a galaxy at a certain distance from another one? By asking this for various distances, we construct something called the two-point correlation function. If all the information about the physics is captured by this function, we say the observed correlations are Gaussian. In other terms, the histogram of observed fluctuations in the sky (the number of fluctuations of a given amplitude as a function of the amplitude) follows the iconic Gaussian curve. Yet, this function only tells us about the overall amplitude of the fluctuations, not about the specific particles present in the early Universe nor how they interacted. In particle physics, this would be like watching a single particle freely moving without interacting with anything around it, missing out on a lot of interesting information. Instead, we need to look at the correlation between more than two points in the sky, and look for triangular (correlating three points) or quadrilateral (correlating four points) galaxy patterns in the sky. These higher-point correlations deviate from a perfect Gaussian distribution and are known as *cosmological correlators*. Remarkably, they can be theoretically predicted and measured in the sky. This way, cosmological correlators are the key mathematical objects that link theory and observations.

In this thesis, we have developed new methods to study and compute these cosmological correlators, and have used them to explore the rich physics of the early Universe.

Fundamental Aspects of Cosmological Correlators

It is a physicist's every-day problem to face physical processes that are too complicated to be solved exactly, either numerically or analytically. A routine strategy is to resort to *perturbation theory*: the problem is simplified enough to be solved exactly, and then small corrections are added to that leading behaviour. The more corrections are included, the more accurate the prediction, but also the more complicated the calculation becomes. In practice, we can easily solve for the free propagation of particles, though this is somewhat dull because it ignores their interactions with other particles. To account for interactions, we assume they are small and calculate them using graphs known as *Feynman diagrams*. These same diagrams can also be used to compute cosmological correlators, which describe interactions between elementary particles in the early Universe.

These diagrams possess fascinating mathematical structures that are valuable in their own right. At the same time, they encode the fundamental physics of the early Universe. However, unlike in traditional particle physics where these diagrams represent the probabilistic outcomes of particle collisions, calculating them in cosmology is notoriously challenging and demands gruelling mathematical dexterity. There are three main reasons for this complexity. First, energy is not conserved in cosmology, making it difficult to track interactions over time during inflation. Second, particles can spontaneously emerge from the vacuum due to the energy of the expanding spacetime. Third, spacetime itself evolves, which distorts the propagation of particles compared to the flat-space scenario. As a result, due to these difficulties, current theoretical predictions are limited, highlighting the need for sophisticated methods to compute cosmological correlators. This is of primary importance as it can lead to a biased interpretation of cosmological data, leaving us without the proper theoretical tools to interpret the signals observed in the sky.

In the first part of the thesis, we have developed a novel approach to compute cosmological correlators using a method we have named *spectral representation*. This technique involves considering a seemingly wacky idea: particles during inflation can have a complex mass, in the sense of imaginary numbers (yes it's this: $i^2 = -1$). While allowing mass to be complex doesn't correspond to real particles, it significantly simplifies calculations. Using this method, we have obtained the simplest exact solution for the cosmological correlator that describes fundamental, yet complex, physics: a pair of massive particles produced during inflation disintegrating into lighter particles that eventually leaves imprint in the four-point cosmological correlator. This correlator serves as a fundamental building block for generating many other correlators that describe related physical processes. Additionally, this method has revealed how fundamental physical principles shape the structure of correlators. For instance, when the energy of a particle approaches zero, the corresponding correlator exhibits a fascinating mathematical structure and tends to infinity, a phenomenon we refer to as a singularity. This singularity reveals the

corresponding physical process, but as if the expansion of the Universe were absent. Even more surprisingly, we have uncovered elegant properties of these cosmological correlators when we flip the sign of the particles' energy (yes, negative energies...): various signals concealed in cosmological correlators are related to one another. We have called these structures *cosmological largest-time equations*. Moreover, when exact calculations become too complex to yield useful physical insights, we have developed a new technique to derive approximate solutions for cosmological correlators. This approach involves pinpointing the precise time during inflation when interactions occur, focusing on the moments that contribute most significantly to the interesting signal. Remarkably, these so-called *saddle points* depend on the energies of the particles that eventually dictate the shape of cosmological correlators. This allows us to describe the physics of inflation as we explore different cosmological correlator configurations across the sky.

Physics at Low-Speed & Non-Locality

Particles produced in the early Universe that persist without decaying until the end of inflation—and whose imprint remains visible in the present-day galaxy distribution—typically do not propagate at the speed of light. Instead, their motion is slowed down due to interactions with the surrounding medium, a dense bath of many elementary particles. This phenomenon is analogous to fish swimming in water: just as fish cannot move infinitely fast because they experience resistance, these particles would require an infinite amount of energy to reach the speed of light. Remarkably, such slowed-down particles leave distinct signatures in the sky, with the strongest signal appearing in galaxy distributions that form *equilateral* triangular patterns.

In the second part of the thesis, we have discovered and studied in detail a novel class of universal signatures in the sky: *cosmological low-speed collider signals*. These signals arise when slowed-down particles interact with other massive particles and manifest as *resonances* in galaxy patterns. Typically, in a triangular arrangement of three galaxies, the interesting signal weakens as two galaxies are pulling apart from one another. However, we have found that before vanishing, the signal first amplifies, creating a characteristic "bump". Detecting this feature would provide compelling evidence for both the existence of particles propagating slower than light and the presence of an additional massive particle produced during inflation. Even more remarkably, the galaxy separation at which this signal peaks offers a direct measurement of this particle's mass! This discovery reinforces the idea that observing the large-scale structure of the Universe acts as a *cosmological collider*, probing energy scales far beyond those accessible in terrestrial experiments like the Large Hadron Collider.

A fundamental question remains: how can we understand these new signals in a simple and intuitive way? Addressing this challenge led us to develop a novel class of early Universe theories: *non-local effective theories*. Let us clarify this concept. When two slowly propagating particles exchange a much faster massive particle, it is often a good approximation to treat this exchange as instantaneous. Instead of explicitly tracking the intermediate particle, we can "replace" its effect with an effective force, which greatly simplifies computations while preserving the essential

physics. This is the core idea behind effective theories: they streamline the physical picture by focusing on the relevant low-energy dynamics (here, the slowed-down particles observed in the sky) while encoding the influence of high-energy details in a more manageable form (here, replacing the fast massive particle with an effective interaction). However, in our cosmological context, an unexpected and fascinating feature emerges: the resulting effective theory appears *non-local*, meaning that the strength of interactions appears to increase as particles move apart. At first glance, this contradicts conventional wisdom and fundamental physical principles. Yet, when used as a computational tool to analyse cosmological correlators, these non-local effective theories remarkably reproduce the key features of low-speed cosmological collider signals. Based on this development, we have provided simple and practical templates that can guide the search for these signals in cosmological data.

Interestingly, we have also found that these non-local effective theories can give rise to *parity-violating cosmological correlators*. This means that the Universe would appear different if viewed in a mirror, much like how a right hand becomes a left hand in its reflection. Since gravity itself preserves parity symmetry, our results suggest that detecting such parity-violating signals in the sky could reveal the presence of new and exotic physics.

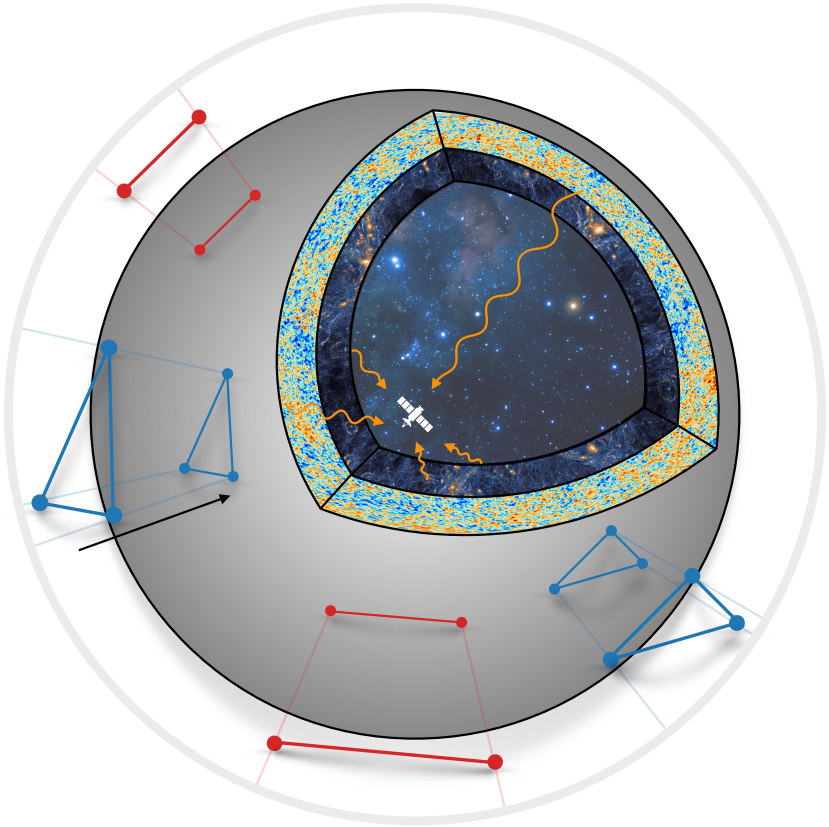
Cosmological Flow

In particle physics, cross sections contain information associated with the models used to describe data, and give the probability of a certain process (e.g. the decay of a particle) to happen. From the theoretical side, probing fine features requires increasingly accurate predictions, and ensuring that all various possible processes are covered is a challenging task. Needless to say that the required precision imposes enormous demands on theory. Consequently, a large number of *automated tools* have been developed and are widely used by the community to make these accurate predictions, i.e. to compute cross sections. In cosmology, such automated tools are rather limited, and do not cover all possible processes that can happen in the early Universe.

In the third part of the thesis, we have developed the *cosmological flow*, a new systematic approach to compute cosmological correlators from any inflationary theory. This method relies on a simple observation: assuming that cosmological correlators emerge from a universal vacuum in the infinite past, they only depend on how they "flow" towards the end of inflation. Automating this picture led us to *evolve cosmological correlators in time* to obtain novel theoretical predictions that were completely out of reach with previous methods. We have released the corresponding automated tool CosmoFlow as an open-source numerical package that can be nurtured and enhanced collaboratively by the community. With this tool, our long-term goal is to build a bank of theoretical data to correctly interpret observational data, and ultimately discover new physics.

Just as automated tools have transformed particle physics, the cosmological flow brings new opportunities for studying inflation in regimes that were inaccessible by other means. For instance, using this framework, we have made the first precise theoretical predictions for cosmological correlators arising from a light particle that

strongly interacts with a massive one. These strong interactions significantly alter the particles' propagation, an effect that would have been impossible to resolve without our approach. We have also explored scenarios where the expansion of the Universe during inflation was not uniform but exhibited oscillatory behaviour, a phenomenon known as *non-scale invariance*. Resolving these theories led to the discovery of new cosmological signals, which appear as increasingly large oscillations in galaxy distributions when the distance of two galaxies, still gravitationally interacting with a third nearby one, increases. These examples showcase that the cosmological flow has a promising future in pushing forward our theoretical understanding of the early Universe and that of inflationary physics.



Résumé Long en Français

Ce résumé vise à présenter le contenu de cette thèse de manière claire et accessible aussi bien au grand public qu'aux spécialistes.

Observer le ciel

Lorsque nous contemplons le ciel nocturne, la plupart des points scintillants que nous voyons sont des étoiles situées au sein de notre propre galaxie, la Voie lactée. À première vue, ces étoiles semblent dispersées au hasard, certaines régions étant densément peuplées tandis que d'autres paraissent presque vides. Mais le cosmos recèle bien plus qu'il n'y paraît. Si nous pouvions dézoomer, nous découvririons encore plus de points—cette fois des étoiles d'autres galaxies. En dézoomant davantage, une galaxie tout entière, avec ses centaines de millions d'étoiles, se réduirait à un simple point. Et en poursuivant ce voyage vers des échelles toujours plus grandes, ces points finiraient par dessiner ce que l'on appelle la structure à grande échelle de l'Univers, un vaste réseau d'amas de galaxies. Ces structures sont le fruit de près de 13,8 milliards d'années d'évolution sous l'effet de la gravité, au cours desquelles de minuscules fluctuations initiales se sont progressivement effondrées pour former les galaxies. Mais comment pouvons-nous en être aussi sûrs ? Parce que la lumière voyage à une vitesse finie : lorsque nous observons des objets lointains dans le ciel, nous regardons en réalité dans le passé. Plus un objet est éloigné, plus la lumière que nous recevons est ancienne. En exploitant ce phénomène, la cosmologie cherche à reconstituer l'histoire de l'Univers, depuis ses tous premiers instants jusqu'aux structures à grande échelle que nous observons aujourd'hui.

L'Univers primordial pour sonder la physique des hautes énergies

Une question naturelle se pose : d'où viennent ces structures ? L'explication la plus plausible que nous avons aujourd'hui est pour le moins fascinante ! D'après une analyse détaillée des données cosmologiques, nous pensons que l'Univers primordial a connu une phase très brève mais extrêmement intense d'expansion accélérée, connue sous le nom d'*inflation*. Cette expansion fut si gigantesque que des échelles quantiques infiniment petites ont été étirées jusqu'à des échelles cosmiques. D'après la physique quantique, le vide n'est jamais vraiment vide : il contient de minuscules fluctuations éphémères, appelées fluctuations quantiques, qui apparaissent et disparaissent presque instantanément. Pendant l'inflation, ces fluctuations quantiques ont été amplifiées pour devenir des inhomogénéités macroscopiques, qui ont

finalement donné naissance aux structures que nous observons aujourd'hui. Nous avons ainsi pris conscience que comprendre l'Univers aux plus grandes échelles repose fondamentalement sur notre compréhension de la physique aux plus petites échelles.

Bien que nous avons de nombreuses preuves de l'existence de l'inflation, sa physique sous-jacente demeure en grande partie inconnue. Par exemple, nous ignorons encore quelles particules étaient en jeu à cette époque et comment elles interagissaient. La raison principale est que l'inflation aurait eu lieu à une échelle d'énergie extrêmement élevée, bien au-delà de ce que nos expériences actuelles dans les accélérateurs de particules les plus puissants peuvent reproduire. Cela signifie que nous ne pouvons pas extrapoler sereinement nos théories à cette période primordiale de l'Univers. Mais loin d'être une limite, c'est une réelle opportunité ! L'Univers primordial pourrait avoir laissé des indices dans le ciel qui révèlent l'existence d'une nouvelle physique dans un régime d'énergie encore complètement inexploré.

Mais comment peut-on étudier la physique de l'inflation et tester nos théories ? Dans une expérience classique d'accélérateur de particules, les lois fondamentales de la nature (comme les propriétés des particules élémentaires, telles que leurs masses) sont étudiées en se faisant collisionner des particules les unes contre les autres et en y analysant les débris. Ces collisions à haute énergie créent de nouvelles particules massives (selon la célèbre équation $E = mc^2$), qui peuvent ensuite être détectées et mesurées. Les particules que nous observons nous renseignent alors sur ce qui a eu lieu lors de la collision. Toutefois, il est crucial de noter que les particules élémentaires obéissent aux principes quantiques, qui sont intrinsèquement probabilistes : il est donc impossible de prédire avec certitude le résultat d'une collision. Ce que nous mesurons (appelé section efficace) nous informe plutôt sur la *probabilité qu'un certain processus se produise*. Ainsi, il est nécessaire de réaliser un grand nombre de collisions pour extraire correctement les propriétés physiques des particules élémentaires. Or, en cosmologie, l'histoire de l'Univers ne s'est déroulée qu'une seule fois, rendant cette approche impossible. Nous adoptons donc une stratégie différente : nous observons le ciel dans différentes directions. En mesurant des signaux spécifiques à différents endroits, nous recueillons des données comme si elles provenaient d'expériences indépendantes. En supposant que les lois de la physique sont les mêmes partout dans l'Univers, nous pouvons ainsi extraire des informations sur les processus physiques qui ont façonné le cosmos. Autrement dit, là où la physique des particules s'appuie sur l'analyse statistique d'un grand nombre d'expériences, la cosmologie repose sur l'analyse statistique d'un grand nombre d'observations.

Nous ne pouvons pas prédire la position exacte des galaxies dans l'Univers. Cependant, une question que l'on peut se poser est : quelle est la probabilité de trouver une galaxie à une certaine distance d'une autre ? En répétant cette question pour différentes distances, nous construisons ce que l'on appelle la fonction de corrélation à deux points. Si toute l'information physique est contenue dans cette fonction, nous disons que les corrélations observées sont gaussiennes. Autrement dit, l'histogramme des fluctuations observées dans le ciel (le nombre de fluctuations d'une amplitude donnée en fonction de l'amplitude) suit la célèbre courbe en cloche gaussienne. Toutefois, cette fonction ne renseigne que sur l'amplitude glob-

ale des fluctuations, sans nous donner d'informations sur les particules présentes dans l'Univers primordial ni sur la façon dont elles interagissaient. En physique des particules, ce serait comme observer une particule unique se déplaçant librement sans interagir avec son environnement. Dommage. Pour aller plus loin, nous devons analyser les corrélations entre plus de deux points dans le ciel, en recherchant des motifs triangulaires (corrélations entre trois points) ou quadrilatéraux (corrélations entre quatre points). Ces corrélations d'ordre supérieur s'écartent de la distribution gaussienne parfaite et sont appelées *corrélateurs cosmologiques*. Fait remarquable, elles peuvent aussi bien être prédites théoriquement et mesurées dans le ciel. Ainsi, les corrélateurs cosmologiques sont les objets mathématiques fondamentaux qui relient théorie et observations.

Dans cette thèse, nous avons développé de nouvelles méthodes pour étudier et calculer ces corrélateurs cosmologiques, et les avons utilisées pour explorer la riche physique de l'Univers primordial.

Aspects fondamentaux des corrélateurs cosmologiques

Un problème récurrent en physique est d'être confronté à des processus physiques trop complexes pour être résolus exactement, que ce soit numériquement ou analytiquement. Une stratégie courante consiste à recourir à la *théorie des perturbations* : on simplifie le problème au point de pouvoir le résoudre exactement, puis on ajoute de petites corrections au comportement dominant. Plus on inclut de corrections, plus la prédiction est précise, mais plus le calcul devient compliqué. En pratique, nous savons résoudre facilement la propagation libre des particules, mais cela est quelque peu trivial, car cela néglige complètement leurs interactions avec d'autres particules. Pour prendre en compte ces interactions, nous supposons qu'elles sont faibles et nous les calculons à l'aide de graphes connus sous le nom de *diagrammes de Feynman*. Ces mêmes diagrammes sont utilisés pour calculer les corrélateurs cosmologiques, qui décrivent les interactions entre les particules élémentaires dans l'Univers primordial.

Ces diagrammes possèdent des structures mathématiques fascinantes qui sont intéressantes en elles-mêmes. En même temps, ils encodent des informations cruciales sur la physique fondamentale de l'Univers primordial. Toutefois, contrairement à la physique des particules où ces diagrammes représentent les probabilités de collisions entre particules, leur calcul en cosmologie est notoirement plus difficile. Cette complexité est principalement due à trois raisons. Premièrement, en cosmologie, l'énergie n'est pas conservée, ce qui complique le suivi des interactions au cours du temps pendant l'inflation. Deuxièmement, les particules peuvent apparaître spontanément à partir du vide en raison de l'énergie du tissu en expansion de l'espace-temps. Troisièmement, l'évolution de l'espace-temps lui-même modifie la propagation des particules. Ces difficultés limitent considérablement les prédictions théoriques actuelles, et soulève la nécessité de méthodes sophistiquées pour calculer les corrélateurs cosmologiques. Ce besoin est d'autant plus crucial que des prédictions incomplètes peuvent conduire à une interprétation erronée des données cosmologiques, nous laissant sans les outils théoriques adéquats pour analyser les signaux observés dans le ciel.

Dans la première partie de cette thèse, nous avons développé une nouvelle approche pour calculer les corrélateurs cosmologiques en introduisant une méthode que nous avons appelée *représentation spectrale*. Cette technique repose sur une idée quelque peu surprenante : considérer que les particules durant l'inflation peuvent posséder une masse complexe, au sens des nombres imaginaires (oui, ces nombres où $i^2 = -1$). Même si attribuer une masse imaginaire à une particule ne correspond pas à un objet physique réel, cela simplifie considérablement les calculs. Grâce à cette méthode, nous avons obtenu la solution exacte la plus simple pour un corrélateur cosmologique décrivant une physique fondamentale, mais subtile : une paire de particules massives produites durant l'inflation se désintégrant en particules plus légères, laissant finalement leur empreinte dans le corrélateur cosmologique à quatre points. Ce corrélateur constitue un élément fondamental pour construire de nombreux autres corrélateurs décrivant des processus physiques similaires. De plus, cette méthode a permis de révéler comment les principes physiques fondamentaux façonnent la structure des corrélateurs. Par exemple, lorsque l'énergie d'une particule tend vers zéro, le corrélateur correspondant adopte une structure mathématique remarquable et diverge vers l'infini, un phénomène appelé *singularité*. Cette singularité met en évidence le processus physique associé, mais comme s'il se déroulait dans un Univers sans expansion. Plus surprenant encore, nous avons mis en lumière des propriétés élégantes des corrélateurs cosmologiques lorsque nous inversons le signe de l'énergie des particules (oui oui, des énergies négatives...) : divers signaux cachés dans les corrélateurs cosmologiques sont en réalité reliés entre eux. Nous avons nommé ces structures les *équations cosmologiques du plus grand temps*. De plus, lorsque les calculs exacts deviennent trop complexes, nous avons développé une nouvelle technique permettant d'obtenir des solutions approximatives aux corrélateurs cosmologiques. Cette approche consiste à identifier précisément le moment durant l'inflation où les interactions se produisent, en se concentrant sur les instants qui contribuent le plus au signal d'intérêt. De manière remarquable, ces *points col* dépendent des énergies des particules et dictent la forme des corrélateurs cosmologiques. Grâce à cette approche, nous sommes en mesure de décrire la physique de l'inflation en explorant différentes configurations des corrélateurs cosmologiques dans le ciel.

Physique à basse vitesse & non-localité

Les particules produites dans l'Univers primordial qui subsistent sans se désintégrer jusqu'à la fin de l'inflation—et dont l'empreinte est encore visible dans la répartition actuelle des galaxies—ne se propagent généralement pas à la vitesse de la lumière. Leur propagation est ralentie par leurs interactions avec le milieu environnant, un bain dense de multiples particules élémentaires. Ce phénomène est analogue au déplacement d'un poisson dans l'eau : tout comme un poisson ne peut pas nager infiniment vite en raison de la résistance du fluide, ces particules devraient acquérir une énergie infinie pour atteindre la vitesse de la lumière. De manière remarquable, ces particules "lentes" laissent des signatures distinctes dans le ciel, le signal le plus fort apparaissant dans la distribution des galaxies formant des motifs triangulaires *équilatéraux*.

Dans la seconde partie de cette thèse, nous avons découvert et étudié en détail

une nouvelle classe universelle de signatures dans le ciel : les *signaux du collisionneur cosmologique à basse vitesse*. Ces signaux émergent lorsque des particules lentes interagissent avec d'autres particules massives, et se manifestent sous forme de *résonances* dans la répartition des galaxies. Typiquement, dans une configuration triangulaire de trois galaxies, le signal d'intérêt s'estompe à mesure que deux galaxies s'éloignent l'une de l'autre. Cependant, nous avons découvert qu'avant de disparaître, ce signal commence par s'amplifier, créant ainsi une caractéristique distinctive sous forme de "bosse". La détection de cette structure constituerait une preuve convaincante non seulement de l'existence de particules se propageant plus lentement que la lumière, mais aussi de la présence d'une autre particule massive produite durant l'inflation. Plus étonnant encore, la distance entre galaxies à laquelle ce signal atteint son maximum permet de mesurer directement la masse de cette particule ! Cette découverte renforce l'idée que l'étude de la structure à grande échelle de l'Univers agit comme un *collisionneur cosmologique*, sondant des échelles d'énergie bien au-delà de celles accessibles dans les expériences terrestres comme le Grand collisionneur de hadrons.

Une question fondamentale demeure : comment peut-on comprendre ces nouveaux signaux de manière simple et intuitive ? Pour y répondre, nous avons développé une nouvelle classe de théories de l'Univers primordial : les *théories effectives non locales*. Clarifions ce jargon. Lorsqu'une particule massive rapide est échangée entre deux particules se propageant lentement, il est souvent pertinent d'approximer cet échange comme étant instantané. Plutôt que de suivre explicitement la particule intermédiaire, nous pouvons "remplacer" son effet par une force effective, ce qui simplifie grandement les calculs tout en préservant l'essentiel de la physique. C'est le principe des théories effectives : on simplifie la physique en se concentrant sur la dynamique pertinente à basse énergie (ici, les particules "lentes" observées dans le ciel) tout en incorporant les petits détails décrivant la physique à haute énergie de façon systématique (ici, en remplaçant la particule rapide par une interaction effective). Cependant, dans notre contexte cosmologique, un phénomène inattendu et fascinant émerge : la théorie effective obtenue est *non locale*, c'est-à-dire que la force des interactions augmente lorsque les particules s'éloignent l'une de l'autre. À première vue, cela semble contredire les principes physiques que l'on chérie. Pourtant, en tant qu'outil de calcul pour analyser les corrélateurs cosmologiques, ces théories effectives non locales reproduisent remarquablement bien les caractéristiques essentielles des signaux du collisionneur cosmologique à basse vitesse. Grâce à ce développement, nous avons proposé des modèles simples et pratiques permettant d'orienter la recherche de ces signaux dans les données cosmologiques.

Nous avons également découvert que ces théories effectives non locales peuvent donner naissance à des *corrélateurs cosmologiques violant la parité*. Autrement dit, l'Univers apparaîtrait différemment si on l'observait dans un miroir, à l'image d'une main droite qui devient une main gauche dans son reflet. Puisque la gravité elle-même respecte la symétrie de parité, nos résultats suggèrent que la détection de tels signaux en cosmologie pourrait révéler l'existence d'une nouvelle physique exotique encore inexplorée.

Flot Cosmologique

En physique des particules, les sections efficaces contiennent des informations sur les modèles utilisés pour décrire les données et correspondent à la probabilité qu'un processus donné (comme la désintégration d'une particule) se produise. D'un point de vue théorique, sonder des caractéristiques fines exige des prédictions d'une précision toujours plus grande, et s'assurer que l'ensemble des processus possibles soit couvert constitue un réel défi de taille. Inutile de préciser que la précision requise impose des contraintes théoriques considérables. C'est pourquoi un grand nombre d'*outils automatisés* ont été développés et sont largement utilisés par la communauté pour effectuer ces prédictions avec exactitude, c'est-à-dire pour calculer les sections efficaces. En cosmologie, ces outils automatisés restent cependant limités et ne couvrent pas l'ensemble des processus pouvant se produire dans l'Univers primordial.

Dans la troisième partie de cette thèse, nous avons développé le *flot cosmologique*, une nouvelle approche systématique permettant de calculer les corrélateurs cosmologiques issus de n'importe quelle théorie inflationnaire. Cette méthode repose sur une observation simple : en supposant que les corrélateurs cosmologiques émergent d'un vide universel dans l'infini passé, ils ne dépendent que de la manière dont ils évoluent jusqu'à la fin de l'inflation. L'automatisation de cette idée nous a conduit à *faire évoluer les corrélateurs cosmologiques dans le temps* afin d'obtenir de nouvelles prédictions théoriques, totalement inaccessibles avec des méthodes préexistantes. Nous avons mis à disposition l'outil automatisé correspondant, CosmoFlow, sous la forme d'un package numérique en accès libre, conçu pour être amélioré de manière collaborative par la communauté. À long terme, notre objectif est de constituer une base de données théorique permettant d'interpréter correctement les observations et, in fine, de découvrir de nouvelles lois physiques.

Tout comme les outils automatisés ont révolutionné le domaine de la physique des particules, le flot cosmologique ouvre de nouvelles perspectives pour étudier l'inflation dans des régimes jusqu'alors inaccessibles. Par exemple, nous avons établi les premières prédictions théoriques précises des corrélateurs cosmologiques issus d'une particule légère fortement couplée à une particule massive. Ces fortes interactions modifient drastiquement la propagation des particules, un effet qui aurait été impossible à décrire sans notre approche. Nous avons également exploré des scénarios où l'expansion de l'Univers durant l'inflation n'était pas uniforme mais présentait un comportement oscillatoire, un phénomène connu sous le nom de *non-invariance d'échelle*. L'étude de ces théories a conduit à la découverte de nouveaux signaux cosmologiques, qui se manifestent sous forme d'oscillations de plus en plus amplifiées dans la distribution des galaxies à mesure que la distance entre deux d'entre elles, sous interaction gravitationnelle avec une troisième, augmente. Ces exemples illustrent le potentiel du flot cosmologique pour approfondir notre compréhension théorique de l'Univers primordial et de la physique de l'inflation.

Bibliography

[1] D. Baumann, "Inflation," in *Theoretical Advanced Study Institute in Elementary Particle Physics: Physics of the Large and the Small*, pp. 523–686. 2011. arXiv:0907.5424 [hep-th].

[2] D. Baumann and L. McAllister, *Inflation and String Theory*. Cambridge University Press, 2015. arXiv:1404.2601 [hep-th]. https://inspirehep.net/record/1289899/files/arXiv:1404.2601.pdf.

[3] L. Senatore, "Lectures on inflation.," in *Theoretical Advanced Study Institute in Elementary Particle Physics: New Frontiers in Fields and Strings*, pp. 447–543. 2017. arXiv:1609.00716 [hep-th].

[4] A. A. Starobinsky, "Spectrum of relict gravitational radiation and the early state of the universe," *JETP Lett.* **30** (1979) 682–685.

[5] A. A. Starobinsky, "A New Type of Isotropic Cosmological Models Without Singularity," *Phys. Lett. B* **91** (1980) 99–102.

[6] A. H. Guth, "Inflationary universe: A possible solution to the horizon and flatness problems," *Phys. Rev. D* **23** (Jan, 1981) 347–356. https://link.aps.org/doi/10.1103/PhysRevD.23.347.

[7] A. D. Linde, "A New Inflationary Universe Scenario: A Possible Solution of the Horizon, Flatness, Homogeneity, Isotropy and Primordial Monopole Problems," *Phys. Lett. B* **108** (1982) 389–393.

[8] A. H. Guth and S.-Y. Pi, "Fluctuations in the new inflationary universe," *Phys. Rev. Lett.* **49** (Oct, 1982) 1110–1113. https://link.aps.org/doi/10.1103/PhysRevLett.49.1110.

[9] A. Albrecht and P. J. Steinhardt, "Cosmology for Grand Unified Theories with Radiatively Induced Symmetry Breaking," *Phys. Rev. Lett.* **48** (1982) 1220–1223.

[10] A. D. Linde, "Chaotic Inflation," *Phys. Lett. B* **129** (1983) 177–181.

[11] V. F. Mukhanov and G. V. Chibisov, "Quantum Fluctuations and a Nonsingular Universe," *JETP Lett.* **33** (1981) 532–535.

[12] S. W. Hawking, "The Development of Irregularities in a Single Bubble Inflationary Universe," *Phys. Lett. B* **115** (1982) 295.

[13] A. A. Starobinsky, "Dynamics of Phase Transition in the New Inflationary Universe Scenario and Generation of Perturbations," *Phys. Lett. B* **117** (1982) 175–178.

[14] A. H. Guth and S. Y. Pi, "Fluctuations in the New Inflationary Universe," *Phys. Rev. Lett.* **49** (1982) 1110–1113.

[15] A. D. Linde, "Scalar Field Fluctuations in Expanding Universe and the New Inflationary Universe Scenario," *Phys. Lett. B* **116** (1982) 335–339.

[16] A. Vilenkin and L. H. Ford, "Gravitational Effects upon Cosmological Phase Transitions," *Phys. Rev. D* **26** (1982) 1231.

[17] V. F. Mukhanov, "Gravitational Instability of the Universe Filled with a Scalar Field," *JETP Lett.* **41** (1985) 493–496.

[18] M. Sasaki, "Large Scale Quantum Fluctuations in the Inflationary Universe," *Prog. Theor. Phys.* **76** (1986) 1036.

[19] **Planck** Collaboration, N. Aghanim *et al.*, "Planck 2018 results. VI. Cosmological parameters," *Astron. Astrophys.* **641** (2020) A6, arXiv:1807.06209 [astro-ph.CO]. [Erratum: Astron.Astrophys. 652, C4 (2021)].

[20] A. G. Riess *et al.*, "A Comprehensive Measurement of the Local Value of the Hubble Constant with Uncertainty from the Hubble Space Telescope and the SH0ES Team," *Astrophys. J. Lett.* **934** no. 1, (2022) L7, arXiv:2112.04510 [astro-ph.CO].

[21] **KiDS** Collaboration, M. Asgari *et al.*, "KiDS-1000 Cosmology: Cosmic shear constraints and comparison between two point statistics," *Astron. Astrophys.* **645** (2021) A104, arXiv:2007.15633 [astro-ph.CO].

[22] **DES** Collaboration, T. M. C. Abbott *et al.*, "Dark Energy Survey Year 3 results: Cosmological constraints from galaxy clustering and weak lensing," *Phys. Rev. D* **105** no. 2, (2022) 023520, arXiv:2105.13549 [astro-ph.CO].

[23] **HSC** Collaboration, C. Hikage *et al.*, "Cosmology from cosmic shear power spectra with Subaru Hyper Suprime-Cam first-year data," *Publ. Astron. Soc. Jap.* **71** no. 2, (2019) 43, arXiv:1809.09148 [astro-ph.CO].

[24] **eBOSS** Collaboration, S. Chabanier *et al.*, "The one-dimensional power spectrum from the SDSS DR14 Lyα forests," *JCAP* **07** (2019) 017, arXiv:1812.03554 [astro-ph.CO].

[25] N. Palanque-Delabrouille, C. Yèche, N. Schöneberg, J. Lesgourgues, M. Walther, S. Chabanier, and E. Armengaud, "Hints, neutrino bounds and WDM constraints from SDSS DR14 Lyman-α and Planck full-survey data," *JCAP* **04** (2020) 038, arXiv:1911.09073 [astro-ph.CO].

[26] S. Goldstein, J. C. Hill, V. Iršič, and B. D. Sherwin, "Canonical Hubble-Tension-Resolving Early Dark Energy Cosmologies Are Inconsistent with the Lyman-α Forest," *Phys. Rev. Lett.* **131** no. 20, (2023) 201001, arXiv:2303.00746 [astro-ph.CO].

[27] K. K. Rogers and V. Poulin, "5σ tension between Planck cosmic microwave background and eBOSS Lyman-alpha forest and constraints on physics beyond ΛCDM," arXiv:2311.16377 [astro-ph.CO].

[28] L. Perivolaropoulos and F. Skara, "Challenges for ΛCDM: An update," *New Astron. Rev.* **95** (2022) 101659, arXiv:2105.05208 [astro-ph.CO].

[29] E. Abdalla *et al.*, "Cosmology intertwined: A review of the particle physics, astrophysics, and cosmology associated with the cosmological tensions and anomalies," *JHEAp* **34** (2022) 49–211, arXiv:2203.06142 [astro-ph.CO].

[30] E. Di Valentino *et al.*, "The CosmoVerse White Paper: Addressing observational tensions in cosmology with systematics and fundamental physics," arXiv:2504.01669 [astro-ph.CO].

[31] **DESI** Collaboration, M. Abdul Karim *et al.*, "DESI DR2 Results II: Measurements of Baryon Acoustic Oscillations and Cosmological Constraints," arXiv:2503.14738 [astro-ph.CO].

[32] **DESI** Collaboration, M. Abdul Karim *et al.*, "DESI DR2 Results I: Baryon Acoustic Oscillations from the Lyman Alpha Forest," arXiv:2503.14739 [astro-ph.CO].

[33] D. H. Weinberg, M. J. Mortonson, D. J. Eisenstein, C. Hirata, A. G. Riess, and E. Rozo, "Observational probes of cosmic acceleration," *Physics Reports* **530** no. 2, (Sept., 2013) 87–255. http://dx.doi.org/10.1016/j.physrep.2013.05.001.

[34] S. Furlanetto, S. P. Oh, and F. Briggs, "Cosmology at Low Frequencies: The 21 cm Transition and the High-Redshift Universe," *Phys. Rept.* **433** (2006) 181–301, arXiv:astro-ph/0608032.

[35] J. Lesgourgues, "The Cosmic Linear Anisotropy Solving System (CLASS) I: Overview," *arXiv e-prints* (Apr., 2011) arXiv:1104.2932, arXiv:1104.2932 [astro-ph.IM].

[36] D. Blas, J. Lesgourgues, and T. Tram, "The Cosmic Linear Anisotropy Solving System (CLASS) II: Approximation schemes," *JCAP* **07** (2011) 034, arXiv:1104.2933 [astro-ph.CO].

[37] W. Hu and M. J. White, "A CMB polarization primer," *New Astron.* **2** (1997) 323, arXiv:astro-ph/9706147.

[38] **SDSS** Collaboration, P. McDonald *et al.*, "The Lyman-alpha forest power spectrum from the Sloan Digital Sky Survey," *Astrophys. J. Suppl.* **163** (2006) 80–109, arXiv:astro-ph/0405013.

[39] S. Collaboration, "Cosmological constraints from the clustering of the sloan digital sky survey dr7 luminous red galaxies," *Monthly Notices of the Royal Astronomical Society* (Mar., 2010) . http://dx.doi.org/10.1111/j.1365-2966.2010.16276.x.

[40] V. Desjacques, D. Jeong, and F. Schmidt, "Large-Scale Galaxy Bias," *Phys. Rept.* **733** (2018) 1–193, arXiv:1611.09787 [astro-ph.CO].

[41] D. H. Lyth, "What would we learn by detecting a gravitational wave signal in the cosmic microwave background anisotropy?," *Phys. Rev. Lett.* **78** (1997) 1861–1863, arXiv:hep-ph/9606387.

[42] J. M. Maldacena, "Non-Gaussian features of primordial fluctuations in single field inflationary models," *JHEP* **05** (2003) 013, arXiv:astro-ph/0210603.

[43] A. Gangui, F. Lucchin, S. Matarrese, and S. Mollerach, "The three-point correlation function of the cosmic microwave background in inflationary models," *The Astrophysical Journal* **430** (Aug, 1994) 447. https://doi.org/10.1086%2F174421.

[44] L.-M. Wang and M. Kamionkowski, "The Cosmic microwave background bispectrum and inflation," *Phys. Rev. D* **61** (2000) 063504, arXiv:astro-ph/9907431.

[45] L. Verde, L.-M. Wang, A. Heavens, and M. Kamionkowski, "Large-scale structure, the cosmic microwave background, and primordial non-gaussianity," *Mon. Not. Roy. Astron. Soc.* **313** (2000) L141–L147, arXiv:astro-ph/9906301.

[46] E. Komatsu and D. N. Spergel, "Acoustic signatures in the primary microwave background bispectrum," *Phys. Rev.* **D63** (2001) 063002, arXiv:astro-ph/0005036.

[47] N. Dalal, O. Dore, D. Huterer, and A. Shirokov, "The imprints of primordial non-gaussianities on large-scale structure: scale dependent bias and abundance of virialized objects," *Phys. Rev. D* **77** (2008) 123514, arXiv:0710.4560 [astro-ph].

[48] D. Babich, P. Creminelli, and M. Zaldarriaga, "The shape of non-Gaussianities," *JCAP* **0408** (2004) 009, arXiv:astro-ph/0405356.

[49] P. Creminelli, A. Nicolis, L. Senatore, M. Tegmark, and M. Zaldarriaga, "Limits on non-Gaussianities from WMAP data," *JCAP* **0605** (2006) 004, arXiv:astro-ph/0509029.

[50] X. Chen, M.-x. Huang, S. Kachru, and G. Shiu, "Observational signatures and non-Gaussianities of general single field inflation," *JCAP* **01** (2007) 002, arXiv:hep-th/0605045.

[51] S. Garcia-Saenz and S. Renaux-Petel, "Flattened non-Gaussianities from the effective field theory of inflation with imaginary speed of sound," *JCAP* **1811** no. 11, (2018) 005, arXiv:1805.12563 [hep-th].

[52] J. Maldacena, "A model with cosmological Bell inequalities," *Fortsch. Phys.* **64** (2016) 10–23, arXiv:1508.01082 [hep-th].

[53] D. Green and R. A. Porto, "Signals of a Quantum Universe," *Phys. Rev. Lett.* **124** no. 25, (2020) 251302, arXiv:2001.09149 [hep-th].

[54] R. Holman and A. J. Tolley, "Enhanced Non-Gaussianity from Excited Initial States," *JCAP* **05** (2008) 001, arXiv:0710.1302 [hep-th].

[55] P. D. Meerburg, J. P. van der Schaar, and P. S. Corasaniti, "Signatures of Initial State Modifications on Bispectrum Statistics," *JCAP* **05** (2009) 018, arXiv:0901.4044 [hep-th].

[56] P. D. Meerburg, J. P. van der Schaar, and M. G. Jackson, "Bispectrum signatures of a modified vacuum in single field inflation with a small speed of sound," *JCAP* **02** (2010) 001, arXiv:0910.4986 [hep-th].

[57] N. Agarwal, R. Holman, A. J. Tolley, and J. Lin, "Effective field theory and non-Gaussianity from general inflationary states," *JHEP* **05** (2013) 085, arXiv:1212.1172 [hep-th].

[58] X. Chen and Y. Wang, "Quasi-Single Field Inflation and Non-Gaussianities," *JCAP* **04** (2010) 027, arXiv:0911.3380 [hep-th].

[59] X. Chen and Y. Wang, "Large non-Gaussianities with Intermediate Shapes from Quasi-Single Field Inflation," *Phys. Rev. D* **81** (2010) 063511, arXiv:0909.0496 [astro-ph.CO].

[60] T. Noumi, M. Yamaguchi, and D. Yokoyama, "Effective field theory approach to quasi-single field inflation and effects of heavy fields," *JHEP* **06** (2013) 051, arXiv:1211.1624 [hep-th].

[61] X. Chen and Y. Wang, "Quasi-Single Field Inflation with Large Mass," *JCAP* **09** (2012) 021, arXiv:1205.0160 [hep-th].

[62] J. R. Fergusson and E. P. S. Shellard, "The shape of primordial non-Gaussianity and the CMB bispectrum," *Phys. Rev. D* **80** (2009) 043510, arXiv:0812.3413 [astro-ph].

[63] C. Cheung, A. L. Fitzpatrick, J. Kaplan, and L. Senatore, "On the consistency relation of the 3-point function in single field inflation," *JCAP* **02** (2008) 021, arXiv:0709.0295 [hep-th].

[64] L. Senatore, K. M. Smith, and M. Zaldarriaga, "Non-Gaussianities in Single Field Inflation and their Optimal Limits from the WMAP 5-year Data," *JCAP* **01** (2010) 028, arXiv:0905.3746 [astro-ph.CO].

[65] W. Hu, "Concepts in CMB anisotropy formation," *Lect. Notes Phys.* **470** (1996) 207, arXiv:astro-ph/9511130.

[66] J. Lesgourgues, "Cosmological Perturbations," in *Theoretical Advanced Study Institute in Elementary Particle Physics: Searching for New Physics at Small and Large Scales*, pp. 29–97. 2013. arXiv:1302.4640 [astro-ph.CO].

[67] W. Hu, "Lecture Notes on CMB Theory: From Nucleosynthesis to Recombination," arXiv:0802.3688 [astro-ph].

[68] A. Challinor and H. Peiris, "Lecture notes on the physics of cosmic microwave background anisotropies," in *Cosmology and Gravitation: XIII Brazilian School on Cosmology and Gravitation (XIII BSCG)*, M. Novello and S. Perez, eds., vol. 1132 of *American Institute of Physics Conference Series*, pp. 86–140. May, 2009. arXiv:0903.5158 [astro-ph.CO].

[69] S. Dodelson, *Modern Cosmology*. Academic Press, Amsterdam, 2003.

[70] D. Baumann, *Cosmology*. Cambridge University Press, 7, 2022.

[71] **Planck** Collaboration, P. A. R. Ade *et al.*, "Planck 2013 Results. XXIV. Constraints on primordial non-Gaussianity," *Astron. Astrophys.* **571** (2014) A24, arXiv:1303.5084 [astro-ph.CO].

[72] **Planck** Collaboration, P. A. R. Ade *et al.*, "Planck 2015 results. XVII. Constraints on primordial non-Gaussianity," *Astron. Astrophys.* **594** (2016) A17, arXiv:1502.01592 [astro-ph.CO].

[73] A. Achúcarro *et al.*, "Inflation: Theory and Observations," arXiv:2203.08128 [astro-ph.CO].

[74] K. M. Smith and M. Zaldarriaga, "Algorithms for bispectra: Forecasting, optimal analysis, and simulation," *Mon. Not. Roy. Astron. Soc.* **417** (2011) 2–19, arXiv:astro-ph/0612571.

[75] T. Suyama and M. Yamaguchi, "Non-Gaussianity in the modulated reheating scenario," *Phys. Rev. D* **77** (2008) 023505, arXiv:0709.2545 [astro-ph].

[76] K. M. Smith, M. LoVerde, and M. Zaldarriaga, "Universal bound on n-point correlations from inflation," *Physical Review Letters* **107** no. 19, (Nov., 2011) . http://dx.doi.org/10.1103/PhysRevLett.107.191301.

[77] N. S. Sugiyama, E. Komatsu, and T. Futamase, "Non-Gaussianity Consistency Relation for Multi-field Inflation," *Phys. Rev. Lett.* **106** (2011) 251301, arXiv:1101.3636 [gr-qc].

[78] C. T. Byrnes, S. Nurmi, G. Tasinato, and D. Wands, "Inhomogeneous non-Gaussianity," *JCAP* **03** (2012) 012, arXiv:1111.2721 [astro-ph.CO].

[79] V. Assassi, D. Baumann, and D. Green, "On Soft Limits of Inflationary Correlation Functions," *JCAP* **11** (2012) 047, arXiv:1204.4207 [hep-th].

[80] X. Chen, B. Hu, M.-x. Huang, G. Shiu, and Y. Wang, "Large Primordial Trispectra in General Single Field Inflation," *JCAP* **08** (2009) 008, arXiv:0905.3494 [astro-ph.CO].

[81] X. Chen, M.-x. Huang, and G. Shiu, "The Inflationary Trispectrum for Models with Large Non-Gaussianities," *Phys. Rev. D* **74** (2006) 121301, arXiv:hep-th/0610235.

[82] F. Arroja and K. Koyama, "Non-gaussianity from the trispectrum in general single field inflation," *Phys. Rev. D* **77** (2008) 083517, arXiv:0802.1167 [hep-th].

[83] D. Seery, J. E. Lidsey, and M. S. Sloth, "The inflationary trispectrum," *JCAP* **01** (2007) 027, arXiv:astro-ph/0610210.

[84] D. Seery, M. S. Sloth, and F. Vernizzi, "Inflationary trispectrum from graviton exchange," *JCAP* **03** (2009) 018, arXiv:0811.3934 [astro-ph].

[85] F. Arroja, S. Mizuno, K. Koyama, and T. Tanaka, "On the full trispectrum in single field DBI-inflation," *Phys. Rev. D* **80** (2009) 043527, arXiv:0905.3641 [hep-th].

[86] X. Gao and B. Hu, "Primordial Trispectrum from Entropy Perturbations in Multifield DBI Model," *JCAP* **08** (2009) 012, arXiv:0903.1920 [astro-ph.CO].

[87] S. Mizuno, F. Arroja, and K. Koyama, "On the full trispectrum in multi-field DBI inflation," *Phys. Rev. D* **80** (2009) 083517, arXiv:0907.2439 [hep-th].

[88] K. Izumi and S. Mukohyama, "Trispectrum from Ghost Inflation," *JCAP* **06** (2010) 016, arXiv:1004.1776 [hep-th].

[89] Q.-G. Huang, "The trispectrum in ghost inflation," *JCAP* **07** (2010) 025, arXiv:1004.0808 [astro-ph.CO].

[90] X. Gao, M. Li, and C. Lin, "Primordial Non-Gaussianities from the Trispectra in Multiple Field Inflationary Models," *JCAP* **11** (2009) 007, arXiv:0906.1345 [astro-ph.CO].

[91] D. Battefeld and T. Battefeld, "On Non-Gaussianities in Multi-Field Inflation (N fields): Bi and Tri-spectra beyond Slow-Roll," *JCAP* **11** (2009) 010, arXiv:0908.4269 [hep-th].

[92] S. Renaux-Petel, "The Trispectrum as a Diagnostic of Primordial Orthogonal non-Gaussianities," *JCAP* **07** (2013) 005, arXiv:1302.6978 [astro-ph.CO].

[93] S. Renaux-Petel, "DBI Galileon in the Effective Field Theory of Inflation: Orthogonal non-Gaussianities and constraints from the Trispectrum," *JCAP* **08** (2013) 017, arXiv:1303.2618 [astro-ph.CO].

[94] X. Chen, W. Z. Chua, Y. Guo, Y. Wang, Z.-Z. Xianyu, and T. Xie, "Quantum Standard Clocks in the Primordial Trispectrum," *JCAP* **05** (2018) 049, arXiv:1803.04412 [hep-th].

[95] L. Leblond and E. Pajer, "Resonant Trispectrum and a Dozen More Primordial N-point functions," *JCAP* **01** (2011) 035, arXiv:1010.4565 [hep-th].

[96] T. D. Lee and C. N. Yang, "Question of parity conservation in weak interactions," *Phys. Rev.* **104** (Oct, 1956) 254–258. https://link.aps.org/doi/10.1103/PhysRev.104.254.

[97] C. S. Wu, E. Ambler, R. W. Hayward, D. D. Hoppes, and R. P. Hudson, "Experimental test of parity conservation in beta decay," *Phys. Rev.* **105** (Feb, 1957) 1413–1415. https://link.aps.org/doi/10.1103/PhysRev.105.1413.

[98] A. Lue, L.-M. Wang, and M. Kamionkowski, "Cosmological signature of new parity violating interactions," *Phys. Rev. Lett.* **83** (1999) 1506–1509, arXiv:astro-ph/9812088.

[99] Y. Minami and E. Komatsu, "New Extraction of the Cosmic Birefringence from the Planck 2018 Polarization Data," *Phys. Rev. Lett.* **125** no. 22, (2020) 221301, arXiv:2011.11254 [astro-ph.CO].

[100] P. Diego-Palazuelos *et al.*, "Cosmic Birefringence from the Planck Data Release 4," *Phys. Rev. Lett.* **128** no. 9, (2022) 091302, arXiv:2201.07682 [astro-ph.CO].

[101] J. Hou, Z. Slepian, and R. N. Cahn, "Measurement of parity-odd modes in the large-scale 4-point correlation function of Sloan Digital Sky Survey Baryon Oscillation Spectroscopic Survey twelfth data release CMASS and LOWZ galaxies," *Mon. Not. Roy. Astron. Soc.* **522** no. 4, (2023) 5701–5739, arXiv:2206.03625 [astro-ph.CO].

[102] O. H. E. Philcox, "Probing parity violation with the four-point correlation function of BOSS galaxies," *Phys. Rev. D* **106** no. 6, (2022) 063501, arXiv:2206.04227 [astro-ph.CO].

[103] G. Cabass, M. M. Ivanov, and O. H. E. Philcox, "Colliders and ghosts: Constraining inflation with the parity-odd galaxy four-point function," *Phys. Rev. D* **107** no. 2, (2023) 023523, arXiv:2210.16320 [astro-ph.CO].

[104] O. H. E. Philcox, "Do the CMB Temperature Fluctuations Conserve Parity?," *Phys. Rev. Lett.* **131** no. 18, (2023) 181001, arXiv:2303.12106 [astro-ph.CO].

[105] O. H. E. Philcox and M. Shiraishi, "Testing Parity Symmetry with the Polarized Cosmic Microwave Background," arXiv:2308.03831 [astro-ph.CO].

[106] T. Liu, X. Tong, Y. Wang, and Z.-Z. Xianyu, "Probing P and CP Violations on the Cosmological Collider," *JHEP* **04** (2020) 189, arXiv:1909.01819 [hep-ph].

[107] G. Cabass, S. Jazayeri, E. Pajer, and D. Stefanyszyn, "Parity violation in the scalar trispectrum: no-go theorems and yes-go examples," *JHEP* **02** (2023) 021, arXiv:2210.02907 [hep-th].

[108] C. Caprini and L. Sorbo, "Adding helicity to inflationary magnetogenesis," *JCAP* **10** (2014) 056, arXiv:1407.2809 [astro-ph.CO].

[109] N. Bartolo, S. Matarrese, M. Peloso, and M. Shiraishi, "Parity-violating CMB correlators with non-decaying statistical anisotropy," *JCAP* **07** (2015) 039, arXiv:1505.02193 [astro-ph.CO].

[110] M. Shiraishi, "Parity violation in the CMB trispectrum from the scalar sector," *Phys. Rev. D* **94** no. 8, (2016) 083503, arXiv:1608.00368 [astro-ph.CO].

[111] C. Creque-Sarbinowski, S. Alexander, M. Kamionkowski, and O. Philcox, "Parity-violating trispectrum from Chern-Simons gravity," *JCAP* **11** (2023) 029, arXiv:2303.04815 [astro-ph.CO].

[112] D. Stefanyszyn, X. Tong, and Y. Zhu, "Cosmological Correlators Through the Looking Glass: Reality, Parity, and Factorisation," arXiv:2309.07769 [hep-th].

[113] X. Gao, T. Kobayashi, M. Shiraishi, M. Yamaguchi, J. Yokoyama, and S. Yokoyama, "Full bispectra from primordial scalar and tensor perturbations in the most general single-field inflation model," *PTEP* **2013** (2013) 053E03, arXiv:1207.0588 [astro-ph.CO].

[114] X. Gao, T. Kobayashi, M. Yamaguchi, and J. Yokoyama, "Primordial non-Gaussianities of gravitational waves in the most general single-field inflation model," *Phys. Rev. Lett.* **107** (2011) 211301, arXiv:1108.3513 [astro-ph.CO].

[115] V. Sreenath, R. Tibrewala, and L. Sriramkumar, "Numerical evaluation of the three-point scalar-tensor cross-correlations and the tensor bi-spectrum," *JCAP* **12** (2013) 037, arXiv:1309.7169 [astro-ph.CO].

[116] H. Lee, D. Baumann, and G. L. Pimentel, "Non-Gaussianity as a Particle Detector," *JHEP* **12** (2016) 040, arXiv:1607.03735 [hep-th].

[117] P. D. Meerburg, J. Meyers, A. van Engelen, and Y. Ali-Haïmoud, "CMB B -mode non-Gaussianity," *Phys. Rev. D* **93** (2016) 123511, arXiv:1603.02243 [astro-ph.CO].

[118] L. Dai, D. Jeong, and M. Kamionkowski, "Seeking Inflation Fossils in the Cosmic Microwave Background," *Phys. Rev. D* **87** no. 10, (2013) 103006, arXiv:1302.1868 [astro-ph.CO].

[119] S. Kundu, "Non-Gaussianity Consistency Relations, Initial States and Back-reaction," *JCAP* **04** (2014) 016, arXiv:1311.1575 [astro-ph.CO].

[120] D. Chowdhury, V. Sreenath, and L. Sriramkumar, "The scalar-scalar-tensor inflationary three-point function in the axion monodromy model," *JCAP* **11** (2016) 041, arXiv:1605.05292 [astro-ph.CO].

[121] E. Dimastrogiovanni, M. Fasiello, D. Jeong, and M. Kamionkowski, "Inflationary tensor fossils in large-scale structure," *JCAP* **12** (2014) 050, arXiv:1407.8204 [astro-ph.CO].

[122] N. Bartolo and G. Orlando, "Parity breaking signatures from a Chern-Simons coupling during inflation: the case of non-Gaussian gravitational waves," *JCAP* **07** (2017) 034, arXiv:1706.04627 [astro-ph.CO].

[123] N. Bartolo, G. Orlando, and M. Shiraishi, "Measuring chiral gravitational waves in Chern-Simons gravity with CMB bispectra," *JCAP* **01** (2019) 050, arXiv:1809.11170 [astro-ph.CO].

[124] N. Bartolo, L. Caloni, G. Orlando, and A. Ricciardone, "Tensor non-Gaussianity in chiral scalar-tensor theories of gravity," *JCAP* **03** (2021) 073, arXiv:2008.01715 [astro-ph.CO].

[125] E. Dimastrogiovanni, M. Fasiello, A. Malhotra, P. D. Meerburg, and G. Orlando, "Testing the early universe with anisotropies of the gravitational wave background," *JCAP* **02** no. 02, (2022) 040, arXiv:2109.03077 [astro-ph.CO].

[126] G. Orlando, "Probing parity-odd bispectra with anisotropies of GW V modes," *JCAP* **12** (2022) 019, arXiv:2206.14173 [astro-ph.CO].

[127] J. M. Maldacena and G. L. Pimentel, "On graviton non-Gaussianities during inflation," *JHEP* **09** (2011) 045, arXiv:1104.2846 [hep-th].

[128] M. Shiraishi, D. Nitta, and S. Yokoyama, "Parity Violation of Gravitons in the CMB Bispectrum," *Prog. Theor. Phys.* **126** (2011) 937–959, arXiv:1108.0175 [astro-ph.CO].

[129] M. Kamionkowski and T. Souradeep, "The Odd-Parity CMB Bispectrum," *Phys. Rev. D* **83** (2011) 027301, arXiv:1010.4304 [astro-ph.CO].

[130] M. Shiraishi, "Parity violation of primordial magnetic fields in the CMB bispectrum," *JCAP* **06** (2012) 015, arXiv:1202.2847 [astro-ph.CO].

[131] M. Shiraishi, M. Liguori, and J. R. Fergusson, "General parity-odd CMB bispectrum estimation," *JCAP* **05** (2014) 008, arXiv:1403.4222 [astro-ph.CO].

[132] J. L. Cook and L. Sorbo, "An inflationary model with small scalar and large tensor nongaussianities," *JCAP* **11** (2013) 047, arXiv:1307.7077 [astro-ph.CO].

[133] R. Namba, M. Peloso, M. Shiraishi, L. Sorbo, and C. Unal, "Scale-dependent gravitational waves from a rolling axion," *JCAP* **01** (2016) 041, arXiv:1509.07521 [astro-ph.CO].

[134] A. Agrawal, T. Fujita, and E. Komatsu, "Large tensor non-Gaussianity from axion-gauge field dynamics," *Phys. Rev. D* **97** no. 10, (2018) 103526, arXiv:1707.03023 [astro-ph.CO].

[135] A. Agrawal, T. Fujita, and E. Komatsu, "Tensor Non-Gaussianity from Axion-Gauge-Fields Dynamics : Parameter Search," *JCAP* **06** (2018) 027, arXiv:1802.09284 [astro-ph.CO].

[136] J. Soda, H. Kodama, and M. Nozawa, "Parity Violation in Graviton Non-gaussianity," *JHEP* **08** (2011) 067, arXiv:1106.3228 [hep-th].

[137] **Planck** Collaboration, Y. Akrami *et al.*, "Planck 2018 results. IX. Constraints on primordial non-Gaussianity," *Astron. Astrophys.* **641** (2020) A9, arXiv:1905.05697 [astro-ph.CO].

[138] P. McFadden and K. Skenderis, "Cosmological 3-point correlators from holography," *JCAP* **06** (2011) 030, arXiv:1104.3894 [hep-th].

[139] I. Mata, S. Raju, and S. Trivedi, "CMB from CFT," *JHEP* **07** (2013) 015, arXiv:1211.5482 [hep-th].

[140] A. Bzowski, P. McFadden, and K. Skenderis, "Implications of conformal invariance in momentum space," *JHEP* **03** (2014) 111, arXiv:1304.7760 [hep-th].

[141] N. Kundu, A. Shukla, and S. P. Trivedi, "Ward Identities for Scale and Special Conformal Transformations in Inflation," *JHEP* **01** (2016) 046, arXiv:1507.06017 [hep-th].

[142] G. Cabass, E. Pajer, D. Stefanyszyn, and J. Supeł, "Bootstrapping large graviton non-Gaussianities," *JHEP* **05** (2022) 077, arXiv:2109.10189 [hep-th].

[143] G. Cabass, D. Stefanyszyn, J. Supeł, and A. Thavanesan, "On graviton non-Gaussianities in the Effective Field Theory of Inflation," *JHEP* **10** (2022) 154, arXiv:2209.00677 [hep-th].

[144] T.-F. Fu and Q.-G. Huang, "The four-point correlation function of graviton during inflation," *JHEP* **07** (2015) 132, arXiv:1502.02329 [hep-th].

[145] S. Y. Li, Y. Wang, and S. Zhou, "KLT-Like Behaviour of Inflationary Graviton Correlators," *JCAP* **12** (2018) 023, arXiv:1806.06242 [hep-th].

[146] J. Bonifacio, H. Goodhew, A. Joyce, E. Pajer, and D. Stefanyszyn, "The graviton four-point function in de Sitter space," *JHEP* **06** (2023) 212, arXiv:2212.07370 [hep-th].

[147] **Planck** Collaboration, Y. Akrami *et al.*, "Planck 2018 results. IX. Constraints on primordial non-Gaussianity," arXiv:1905.05697 [astro-ph.CO].

[148] K. Abazajian *et al.*, "CMB-S4 Science Case, Reference Design, and Project Plan," arXiv:1907.04473 [astro-ph.IM].

[149] M. Shiraishi, M. Liguori, and J. R. Fergusson, "CMB bounds on tensor-scalar-scalar inflationary correlations," *JCAP* **01** (2018) 016, arXiv:1710.06778 [astro-ph.CO].

[150] A. J. Duivenvoorden, P. D. Meerburg, and K. Freese, "CMB B-mode non-Gaussianity: optimal bispectrum estimator and Fisher forecasts," *Phys. Rev. D* **102** no. 2, (2020) 023521, arXiv:1911.11349 [astro-ph.CO].

[151] M. Münchmeyer and K. M. Smith, "Higher N-point function data analysis techniques for heavy particle production and WMAP results," *Phys. Rev. D* **100** no. 12, (2019) 123511, arXiv:1910.00596 [astro-ph.CO].

[152] A. Kalaja, P. D. Meerburg, G. L. Pimentel, and W. R. Coulton, "Fundamental limits on constraining primordial non-Gaussianity," *JCAP* **04** (2021) 050, arXiv:2011.09461 [astro-ph.CO].

[153] E. D. Kovetz *et al.*, "Line-Intensity Mapping: 2017 Status Report," arXiv:1709.09066 [astro-ph.CO].

[154] A. Liu and J. R. Shaw, "Data Analysis for Precision 21 cm Cosmology," *Publ. Astron. Soc. Pac.* **132** no. 1012, (2020) 062001, arXiv:1907.08211 [astro-ph.IM].

[155] **Snowmass Cosmic Frontier 5 Topical Group** Collaboration, K. S. Karkare, A. M. Dizgah, G. K. Keating, P. Breysse, and D. T. Chung, "Snowmass 2021 Cosmic Frontier White Paper: Cosmology with Millimeter-Wave Line Intensity Mapping," in *Snowmass 2021*. 3, 2022. arXiv:2203.07258 [astro-ph.CO].

[156] **Snowmass 2021 Cosmic Frontier 5 Topical Group** Collaboration, A. Liu, L. Newburgh, B. Saliwanchik, and A. Slosar, "Snowmass2021 Cosmic Frontier White Paper: 21cm Radiation as a Probe of Physics Across Cosmic Ages," arXiv:2203.07864 [astro-ph.CO].

[157] G. D'Amico, M. Lewandowski, L. Senatore, and P. Zhang, "Limits on primordial non-Gaussianities from BOSS galaxy-clustering data," arXiv:2201.11518 [astro-ph.CO].

[158] G. Cabass, M. M. Ivanov, O. H. E. Philcox, M. Simonović, and M. Zaldarriaga, "Constraints on Single-Field Inflation from the BOSS Galaxy Survey," *Phys. Rev. Lett.* **129** no. 2, (2022) 021301, arXiv:2201.07238 [astro-ph.CO].

[159] G. Cabass, M. M. Ivanov, O. H. E. Philcox, M. Simonović, and M. Zaldarriaga, "Constraints on multifield inflation from the BOSS galaxy survey," *Phys. Rev. D* **106** no. 4, (2022) 043506, arXiv:2204.01781 [astro-ph.CO].

[160] **BOSS** Collaboration, S. Alam *et al.*, "The clustering of galaxies in the completed SDSS-III Baryon Oscillation Spectroscopic Survey: cosmological analysis of the DR12 galaxy sample," *Mon. Not. Roy. Astron. Soc.* **470** no. 3, (2017) 2617–2652, arXiv:1607.03155 [astro-ph.CO].

[161] D. Baumann and D. Green, "The power of locality: primordial non-Gaussianity at the map level," *JCAP* **08** no. 08, (2022) 061, arXiv:2112.14645 [astro-ph.CO].

[162] **DESI** Collaboration, A. Aghamousa *et al.*, "The DESI Experiment Part I: Science,Targeting, and Survey Design," arXiv:1611.00036 [astro-ph.IM].

[163] R. Laureijs *et al.*, "Euclid definition study report," 2011. https://arxiv.org/abs/1110.3193.

[164] **SPHEREx** Collaboration, O. Doré *et al.*, "Cosmology with the SPHEREX All-Sky Spectral Survey," arXiv:1412.4872 [astro-ph.CO].

[165] A. Moradinezhad Dizgah and G. K. Keating, "Line intensity mapping with [CII] and CO(1-0) as probes of primordial non-Gaussianity," *Astrophys. J.* **872** no. 2, (2019) 126, arXiv:1810.02850 [astro-ph.CO].

[166] **PUMA** Collaboration, A. Slosar *et al.*, "Packed Ultra-wideband Mapping Array (PUMA): A Radio Telescope for Cosmology and Transients," *Bull. Am. Astron. Soc.* **51** (2019) 53, arXiv:1907.12559 [astro-ph.IM].

[167] D. Karagiannis, A. Slosar, and M. Liguori, "Forecasts on Primordial non-Gaussianity from 21 cm Intensity Mapping experiments," *JCAP* **11** (2020) 052, arXiv:1911.03964 [astro-ph.CO].

[168] N. Sailer, E. Castorina, S. Ferraro, and M. White, "Cosmology at high redshift — a probe of fundamental physics," *JCAP* **12** no. 12, (2021) 049, arXiv:2106.09713 [astro-ph.CO].

[169] M. Biagetti, "The Hunt for Primordial Interactions in the Large Scale Structures of the Universe," *Galaxies* **7** no. 3, (2019) 71, arXiv:1906.12244 [astro-ph.CO].

[170] S. Matarrese and L. Verde, "The effect of primordial non-Gaussianity on halo bias," *Astrophys. J. Lett.* **677** (2008) L77–L80, arXiv:0801.4826 [astro-ph].

[171] A. Slosar, C. Hirata, U. Seljak, S. Ho, and N. Padmanabhan, "Constraints on local primordial non-Gaussianity from large scale structure," *JCAP* **08** (2008) 031, arXiv:0805.3580 [astro-ph].

[172] **BOSS** Collaboration, A. J. Ross *et al.*, "The Clustering of Galaxies in SDSS-III DR9 Baryon Oscillation Spectroscopic Survey: Constraints on Primordial Non-Gaussianity," *Mon. Not. Roy. Astron. Soc.* **428** (2013) 1116–1127, arXiv:1208.1491 [astro-ph.CO].

[173] B. Leistedt, H. V. Peiris, and N. Roth, "Constraints on Primordial Non-Gaussianity from 800 000 Photometric Quasars," *Phys. Rev. Lett.* **113** no. 22, (2014) 221301, arXiv:1405.4315 [astro-ph.CO].

[174] E. Castorina *et al.*, "Redshift-weighted constraints on primordial non-Gaussianity from the clustering of the eBOSS DR14 quasars in Fourier space," *JCAP* **09** (2019) 010, arXiv:1904.08859 [astro-ph.CO].

[175] M. Rezaie *et al.*, "Local primordial non-Gaussianity from the large-scale clustering of photometric DESI luminous red galaxies," arXiv:2307.01753 [astro-ph.CO].

[176] **DESI** Collaboration, A. Krolewski *et al.*, "Constraining primordial non-Gaussianity from DESI quasar targets and Planck CMB lensing," arXiv:2305.07650 [astro-ph.CO].

[177] M. S. Cagliari, E. Castorina, M. Bonici, and D. Bianchi, "Optimal constraints on Primordial non-Gaussianity with the eBOSS DR16 quasars in Fourier space," arXiv:2309.15814 [astro-ph.CO].

[178] F. Beutler, M. Biagetti, D. Green, A. Slosar, and B. Wallisch, "Primordial Features from Linear to Nonlinear Scales," *Phys. Rev. Res.* **1** no. 3, (2019) 033209, arXiv:1906.08758 [astro-ph.CO].

[179] Y. Wang, G.-B. Zhao, C.-H. Chuang, M. Pellejero-Ibanez, C. Zhao, F.-S. Kitaura, and S. Rodriguez-Torres, "The clustering of galaxies in the completed SDSS-III Baryon Oscillation Spectroscopic Survey: a tomographic analysis of structure growth and expansion rate from anisotropic galaxy clustering," *Mon. Not. Roy. Astron. Soc.* **481** no. 3, (2018) 3160–3166, arXiv:1709.05173 [astro-ph.CO].

[180] **eBOSS** Collaboration, E.-M. Mueller *et al.*, "Primordial non-Gaussianity from the completed SDSS-IV extended Baryon Oscillation Spectroscopic Survey II: measurements in Fourier space with optimal weights," *Mon. Not. Roy. Astron. Soc.* **514** no. 3, (2022) 3396–3409, arXiv:2106.13725 [astro-ph.CO].

[181] **eBOSS** Collaboration, E. Castorina *et al.*, "Redshift-weighted constraints on primordial non-Gaussianity from the clustering of the eBOSS DR14 quasars in Fourier space," *JCAP* **09** (2019) 010, arXiv:1904.08859 [astro-ph.CO].

[182] D. Green, Y. Guo, J. Han, and B. Wallisch, "Light Fields during Inflation from BOSS and Future Galaxy Surveys," arXiv:2311.04882 [astro-ph.CO].

[183] S. Goldstein, O. H. E. Philcox, J. C. Hill, and L. Hui, "Massive-ish Particles from Small-ish Scales: Non-Perturbative Techniques for Cosmological Collider Physics from Large-Scale Structure Surveys," arXiv:2407.08731 [astro-ph.CO].

[184] A. Strominger, "The dS / CFT correspondence," *JHEP* **10** (2001) 034, arXiv:hep-th/0106113.

[185] E. Witten, "Quantum gravity in de Sitter space," in *Strings 2001: International Conference*. 6, 2001. arXiv:hep-th/0106109.

[186] F. Larsen and R. McNees, "Inflation and de Sitter holography," *JHEP* **07** (2003) 051, arXiv:hep-th/0307026.

[187] J. P. van der Schaar, "Inflationary perturbations from deformed CFT," *JHEP* **01** (2004) 070, arXiv:hep-th/0307271.

[188] P. McFadden and K. Skenderis, "Holography for Cosmology," *Phys. Rev. D* **81** (2010) 021301, arXiv:0907.5542 [hep-th].

[189] I. Antoniadis, P. O. Mazur, and E. Mottola, "Conformal Invariance, Dark Energy, and CMB Non-Gaussianity," *JCAP* **09** (2012) 024, arXiv:1103.4164 [gr-qc].

[190] A. Bzowski, P. McFadden, and K. Skenderis, "Holographic predictions for cosmological 3-point functions," *JHEP* **03** (2012) 091, arXiv:1112.1967 [hep-th].

[191] P. Creminelli, "Conformal invariance of scalar perturbations in inflation," *Phys. Rev. D* **85** (2012) 041302, arXiv:1108.0874 [hep-th].

[192] D. Anninos, T. Hartman, and A. Strominger, "Higher Spin Realization of the dS/CFT Correspondence," *Class. Quant. Grav.* **34** no. 1, (2017) 015009, arXiv:1108.5735 [hep-th].

[193] C. Coriano, L. Delle Rose, and M. Serino, "Three and Four Point Functions of Stress Energy Tensors in D=3 for the Analysis of Cosmological Non-Gaussianities," *JHEP* **12** (2012) 090, arXiv:1210.0136 [hep-th].

[194] K. Schalm, G. Shiu, and T. van der Aalst, "Consistency condition for inflation from (broken) conformal symmetry," *JCAP* **03** (2013) 005, arXiv:1211.2157 [hep-th].

[195] A. Ghosh, N. Kundu, S. Raju, and S. P. Trivedi, "Conformal Invariance and the Four Point Scalar Correlator in Slow-Roll Inflation," *JHEP* **07** (2014) 011, arXiv:1401.1426 [hep-th].

[196] E. Pajer, G. L. Pimentel, and J. V. S. Van Wijck, "The Conformal Limit of Inflation in the Era of CMB Polarimetry," *JCAP* **06** (2017) 009, arXiv:1609.06993 [hep-th].

[197] D. Anninos, F. Denef, R. Monten, and Z. Sun, "Higher Spin de Sitter Hilbert Space," *JHEP* **10** (2019) 071, arXiv:1711.10037 [hep-th].

[198] N. Arkani-Hamed, D. Baumann, H. Lee, and G. L. Pimentel, "The Cosmological Bootstrap: Inflationary Correlators from Symmetries and Singularities," *JHEP* **04** (2020) 105, arXiv:1811.00024 [hep-th].

[199] M. Hogervorst, J. a. Penedones, and K. S. Vaziri, "Towards the non-perturbative cosmological bootstrap," *JHEP* **02** (2023) 162, arXiv:2107.13871 [hep-th].

[200] D.-P. Du, B. Wang, and R.-K. Su, "Quasinormal modes in pure de Sitter space-times," *Phys. Rev. D* **70** (2004) 064024, arXiv:hep-th/0404047.

[201] D. L. Jafferis, A. Lupsasca, V. Lysov, G. S. Ng, and A. Strominger, "Quasinormal quantization in de Sitter spacetime," *JHEP* **01** (2015) 004, arXiv:1305.5523 [hep-th].

[202] L. Parker, "Particle creation in expanding universes," *Phys. Rev. Lett.* **21** (1968) 562–564.

[203] L. Parker, "Quantized fields and particle creation in expanding universes. 1.," *Phys. Rev.* **183** (1969) 1057–1068.

[204] L. Parker, "Quantized fields and particle creation in expanding universes. 2.," *Phys. Rev. D* **3** (1971) 346–356. [Erratum: Phys.Rev.D 3, 2546–2546 (1971)].

[205] N. D. Birrell and P. C. W. Davies, *Quantum Fields in Curved Space*. Cambridge Monographs on Mathematical Physics. Cambridge Univ. Press, Cambridge, UK, 2, 1984.

[206] V. Mukhanov and S. Winitzki, *Introduction to quantum effects in gravity*. Cambridge University Press, 6, 2007.

[207] S. P. Corbà and L. Sorbo, "On the adiabatic subtraction of cosmological perturbations," arXiv:2209.14362 [hep-th].

[208] A. A. Grib and S. G. Mamaev, "On field theory in the friedman space," *Yad. Fiz.* **10** (1969) 1276–1281.

[209] A. A. Grib, S. G. Mamaev, and V. M. Mostepanenko, "Particle Creation from Vacuum in Homogeneous Isotropic Models of the Universe," *Gen. Rel. Grav.* **7** (1976) 535–547.

[210] P. R. Anderson and E. Mottola, "Instability of global de Sitter space to particle creation," *Phys. Rev. D* **89** (2014) 104038, arXiv:1310.0030 [gr-qc].

[211] P. R. Anderson and E. Mottola, "Quantum vacuum instability of "eternal" de Sitter space," *Phys. Rev. D* **89** (2014) 104039, arXiv:1310.1963 [gr-qc].

[212] T. Markkanen and A. Rajantie, "Massive scalar field evolution in de Sitter," *JHEP* **01** (2017) 133, arXiv:1607.00334 [gr-qc].

[213] R. Figari, R. Hoegh-Krohn, and C. R. Nappi, "Interacting Relativistic Boson Fields in the de Sitter Universe with Two Space-Time Dimensions," *Commun. Math. Phys.* **44** (1975) 265–278.

[214] G. W. Gibbons and S. W. Hawking, "Cosmological event horizons, thermodynamics, and particle creation," *Phys. Rev. D* **15** (May, 1977) 2738–2751. https://link.aps.org/doi/10.1103/PhysRevD.15.2738.

[215] G. G. Stokes, "On the discontinuity of arbitrary constants that appear as multipliers of semi-convergent series: A letter to the editor," Dec., 1902. https://doi.org/10.1007/bf02415503.

[216] J. Heading, "An introduction to phase-integral methods," 1962.

[217] M. V. Berry and K. E. Mount, "Semiclassical approximations in wave mechanics," *Rept. Prog. Phys.* **35** (1972) 315.

[218] R. B. Dingle, "Asymptotic expansions : their derivation and interpretation," *Mathematics of Computation* **29** (1975) 1152.

[219] M. V. Barry, "Uniform Asymptotic Smoothing of Stokes's Discontinuities," *Proc. Roy. Soc. Lond. A* **422** (1989) 7–21.

[220] M. V. Berry, "Waves near stokes lines," *Proceedings of the Royal Society of London. A. Mathematical and Physical Sciences* **427** (1990) 265 – 280.

[221] R. White, "Asymptotic analysis of differential equations," 2005.

[222] H. Kleinert, R. Ruffini, and S.-S. Xue, "Electron-Positron Pair Production in Space- or Time-Dependent Electric Fields," *Phys. Rev. D* **78** (2008) 025011, arXiv:0807.0909 [hep-th].

[223] C. K. Dumlu and G. V. Dunne, "The Stokes Phenomenon and Schwinger Vacuum Pair Production in Time-Dependent Laser Pulses," *Phys. Rev. Lett.* **104** (2010) 250402, arXiv:1004.2509 [hep-th].

[224] S. P. Kim, "Geometric Origin of Stokes Phenomenon for de Sitter Radiation," *Phys. Rev. D* **88** no. 4, (2013) 044027, arXiv:1307.0590 [hep-th].

[225] R. Dabrowski and G. V. Dunne, "Superadiabatic particle number in Schwinger and de Sitter particle production," *Phys. Rev. D* **90** no. 2, (2014) 025021, arXiv:1405.0302 [hep-th].

[226] R. Dabrowski and G. V. Dunne, "Time dependence of adiabatic particle number," *Phys. Rev. D* **94** no. 6, (2016) 065005, arXiv:1606.00902 [hep-th].

[227] F. Zago and A. Kosowsky, "Quantum particle production effects on the cosmic expansion," *Phys. Rev. D* **100** (Aug, 2019) 045023. https://link.aps.org/doi/10.1103/PhysRevD.100.045023.

[228] L. Li, T. Nakama, C. M. Sou, Y. Wang, and S. Zhou, "Gravitational Production of Superheavy Dark Matter and Associated Cosmological Signatures," *JHEP* **07** (2019) 067, arXiv:1903.08842 [astro-ph.CO].

[229] S. Hashiba, Y. Yamada, and J. Yokoyama, "Particle production induced by vacuum decay in real time dynamics," *Phys. Rev. D* **103** no. 4, (2021) 045006, arXiv:2006.10986 [hep-th].

[230] S. Enomoto and T. Matsuda, "The exact WKB for cosmological particle production," *JHEP* **03** (2021) 090, arXiv:2010.14835 [hep-ph].

[231] H. Taya, T. Fujimori, T. Misumi, M. Nitta, and N. Sakai, "Exact WKB analysis of the vacuum pair production by time-dependent electric fields," *JHEP* **03** (2021) 082, arXiv:2010.16080 [hep-th].

[232] C. K. Dumlu, "Stokes phenomenon and Hawking radiation," *Phys. Rev. D* **102** no. 12, (2020) 125006, arXiv:2009.09851 [hep-th].

[233] S. Hashiba and Y. Yamada, "Stokes phenomenon and gravitational particle production — How to evaluate it in practice," *JCAP* **05** (2021) 022, arXiv:2101.07634 [hep-th].

[234] F. Sauter, "Uber das Verhalten eines Elektrons im homogenen elektrischen Feld nach der relativistischen Theorie Diracs," *Z. Phys.* **69** (1931) 742–764.

[235] J. S. Schwinger, "On gauge invariance and vacuum polarization," *Phys. Rev.* **82** (1951) 664–679.

[236] S. W. Hawking, "Particle Creation by Black Holes," *Commun. Math. Phys.* **43** (1975) 199–220. [Erratum: Commun.Math.Phys. 46, 206 (1976)].

[237] L.-T. Wang and Z.-Z. Xianyu, "In Search of Large Signals at the Cosmological Collider," *JHEP* **02** (2020) 044, arXiv:1910.12876 [hep-ph].

[238] M. S. Turner and L. M. Widrow, "Inflation Produced, Large Scale Magnetic Fields," *Phys. Rev. D* **37** (1988) 2743.

[239] W. D. Garretson, G. B. Field, and S. M. Carroll, "Primordial magnetic fields from pseudoGoldstone bosons," *Phys. Rev. D* **46** (1992) 5346–5351, arXiv:hep-ph/9209238.

[240] N. Barnaby and M. Peloso, "Large Nongaussianity in Axion Inflation," *Phys. Rev. Lett.* **106** (2011) 181301, arXiv:1011.1500 [hep-ph].

[241] S. Lu, Y. Wang, and Z.-Z. Xianyu, "A Cosmological Higgs Collider," *JHEP* **02** (2020) 011, arXiv:1907.07390 [hep-th].

[242] L.-T. Wang and Z.-Z. Xianyu, "Gauge Boson Signals at the Cosmological Collider," *JHEP* **11** (2020) 082, arXiv:2004.02887 [hep-ph].

[243] C. M. Sou, X. Tong, and Y. Wang, "Chemical-potential-assisted particle production in FRW spacetimes," *JHEP* **06** (2021) 129, arXiv:2104.08772 [hep-th].

[244] P. Adshead and E. I. Sfakianakis, "Fermion production during and after axion inflation," *JCAP* **11** (2015) 021, arXiv:1508.00891 [hep-ph].

[245] X. Chen, Y. Wang, and Z.-Z. Xianyu, "Neutrino Signatures in Primordial Non-Gaussianities," *JHEP* **09** (2018) 022, arXiv:1805.02656 [hep-ph].

[246] A. Hook, J. Huang, and D. Racco, "Searches for other vacua. Part II. A new Higgstory at the cosmological collider," *JHEP* **01** (2020) 105, arXiv:1907.10624 [hep-ph].

[247] S. Hashiba, S. Ling, and A. J. Long, "An analytic evaluation of gravitational particle production of fermions via Stokes phenomenon," *JHEP* **09** (2022) 216, arXiv:2206.14204 [hep-th].

[248] T. Kobayashi and N. Afshordi, "Schwinger Effect in 4D de Sitter Space and Constraints on Magnetogenesis in the Early Universe," *JHEP* **10** (2014) 166, arXiv:1408.4141 [hep-th].

[249] J.-J. Geng, B.-F. Li, J. Soda, A. Wang, Q. Wu, and T. Zhu, "Schwinger Pair Production by Electric Field Coupled to Inflaton," *JCAP* **02** (2018) 018, arXiv:1706.02833 [gr-qc].

[250] W. Z. Chua, Q. Ding, Y. Wang, and S. Zhou, "Imprints of Schwinger Effect on Primordial Spectra," *JHEP* **04** (2019) 066, arXiv:1810.09815 [hep-th].

[251] X. Tong and Z.-Z. Xianyu, "Large spin-2 signals at the cosmological collider," *JHEP* **10** (2022) 194, arXiv:2203.06349 [hep-ph].

[252] A. Berera and L.-Z. Fang, "Thermally induced density perturbations in the inflation era," *Phys. Rev. Lett.* **74** (1995) 1912–1915, arXiv:astro-ph/9501024.

[253] A. Berera, "Warm inflation," *Phys. Rev. Lett.* **75** (1995) 3218–3221, arXiv:astro-ph/9509049.

[254] M. Bastero-Gil, A. Berera, I. G. Moss, and R. O. Ramos, "Theory of non-Gaussianity in warm inflation," *JCAP* **12** (2014) 008, arXiv:1408.4391 [astro-ph.CO].

[255] M. Mylova, M. Moschou, N. Afshordi, and J. a. Magueijo, "Non-Gaussian signatures of a thermal Big Bang," *JCAP* **07** no. 07, (2022) 005, arXiv:2112.08179 [hep-th].

[256] M. Mirbabayi and A. Gruzinov, "Shapes of non-Gaussianity in warm inflation," *JCAP* **02** (2023) 012, arXiv:2205.13227 [astro-ph.CO].

[257] X. Tong, Y. Wang, and S. Zhou, "Unsuppressed primordial standard clocks in warm quasi-single field inflation," *JCAP* **06** (2018) 013, arXiv:1801.05688 [hep-th].

[258] E. Silverstein and A. Westphal, "Monodromy in the CMB: Gravity Waves and String Inflation," *Phys. Rev. D* **78** (2008) 106003, arXiv:0803.3085 [hep-th].

[259] L. McAllister, E. Silverstein, and A. Westphal, "Gravity Waves and Linear Inflation from Axion Monodromy," *Phys. Rev. D* **82** (2010) 046003, arXiv:0808.0706 [hep-th].

[260] R. Flauger, L. McAllister, E. Pajer, A. Westphal, and G. Xu, "Oscillations in the CMB from Axion Monodromy Inflation," *JCAP* **06** (2010) 009, arXiv:0907.2916 [hep-th].

[261] R. Flauger, M. Mirbabayi, L. Senatore, and E. Silverstein, "Productive Interactions: heavy particles and non-Gaussianity," *JCAP* **10** (2017) 058, arXiv:1606.00513 [hep-th].

[262] N. Arkani-Hamed and J. Maldacena, "Cosmological Collider Physics," arXiv:1503.08043 [hep-th].

[263] X. Tong, Y. Wang, and Y. Zhu, "Cutting rule for cosmological collider signals: a bulk evolution perspective," *JHEP* **03** (2022) 181, arXiv:2112.03448 [hep-th].

[264] Y. Ema and K. Mukaida, "Cutting rule for in-in correlators and cosmological collider," arXiv:2409.07521 [hep-th].

[265] D. Baumann and D. Green, "Signatures of Supersymmetry from the Early Universe," *Phys. Rev. D* **85** (2012) 103520, arXiv:1109.0292 [hep-th].

[266] M. Mirbabayi and M. Simonović, "Effective Theory of Squeezed Correlation Functions," *JCAP* **03** (2016) 056, arXiv:1507.04755 [hep-th].

[267] **ATLAS** Collaboration, G. Aad *et al.*, "Measurement of the Higgs boson mass with H $\rightarrow\gamma\gamma$ decays in 140 fb−1 of s=13 TeV pp collisions with the ATLAS detector," *Phys. Lett. B* **847** (2023) 138315, arXiv:2308.07216 [hep-ex].

[268] **ATLAS** Collaboration, G. Aad *et al.*, "Observation of a new particle in the search for the Standard Model Higgs boson with the ATLAS detector at the LHC," *Phys. Lett. B* **716** (2012) 1–29, arXiv:1207.7214 [hep-ex].

[269] P. D. Meerburg *et al.*, "Primordial Non-Gaussianity," arXiv:1903.04409 [astro-ph.CO].

[270] E. Sefusatti, J. R. Fergusson, X. Chen, and E. P. S. Shellard, "Effects and Detectability of Quasi-Single Field Inflation in the Large-Scale Structure and Cosmic Microwave Background," *JCAP* **08** (2012) 033, arXiv:1204.6318 [astro-ph.CO].

[271] J. Norena, L. Verde, G. Barenboim, and C. Bosch, "Prospects for constraining the shape of non-Gaussianity with the scale-dependent bias," *JCAP* **08** (2012) 019, arXiv:1204.6324 [astro-ph.CO].

[272] J. Gleyzes, R. de Putter, D. Green, and O. Doré, "Biasing and the search for primordial non-Gaussianity beyond the local type," *JCAP* **04** (2017) 002, arXiv:1612.06366 [astro-ph.CO].

[273] P. D. Meerburg, M. Münchmeyer, J. B. Muñoz, and X. Chen, "Prospects for Cosmological Collider Physics," *JCAP* **03** (2017) 050, arXiv:1610.06559 [astro-ph.CO].

[274] A. Moradinezhad Dizgah and C. Dvorkin, "Scale-Dependent Galaxy Bias from Massive Particles with Spin during Inflation," *JCAP* **01** (2018) 010, arXiv:1708.06473 [astro-ph.CO].

[275] N. Bartolo, A. Kehagias, M. Liguori, A. Riotto, M. Shiraishi, and V. Tansella, "Detecting higher spin fields through statistical anisotropy in the cmb and galaxy power spectra," *Phys. Rev. D* **97** (Jan, 2018) 023503. https://link.aps.org/doi/10.1103/PhysRevD.97.023503.

[276] A. Moradinezhad Dizgah, H. Lee, J. B. Muñoz, and C. Dvorkin, "Galaxy Bispectrum from Massive Spinning Particles," *JCAP* **05** (2018) 013, arXiv:1801.07265 [astro-ph.CO].

[277] K. Kogai, K. Akitsu, F. Schmidt, and Y. Urakawa, "Galaxy imaging surveys as spin-sensitive detector for cosmological colliders," *JCAP* **03** (2021) 060, arXiv:2009.05517 [astro-ph.CO].

[278] W. Sohn, D.-G. Wang, J. R. Fergusson, and E. P. S. Shellard, "Searching for Cosmological Collider in the Planck CMB Data," arXiv:2404.07203 [astro-ph.CO].

[279] G. Cabass, O. H. E. Philcox, M. M. Ivanov, K. Akitsu, S.-F. Chen, M. Simonović, and M. Zaldarriaga, "BOSS Constraints on Massive Particles during Inflation: The Cosmological Collider in Action," arXiv:2404.01894 [astro-ph.CO].

[280] **EUCLID** Collaboration, R. Laureijs *et al.*, "Euclid Definition Study Report," arXiv:1110.3193 [astro-ph.CO].

[281] O. H. E. Philcox, "Searching for Inflationary Physics with the CMB Trispectrum: 3. Constraints from Planck," arXiv:2502.06931 [astro-ph.CO].

[282] L. Bordin, P. Creminelli, A. Khmelnitsky, and L. Senatore, "Light Particles with Spin in Inflation," *JCAP* **10** (2018) 013, arXiv:1806.10587 [hep-th].

[283] Y. Kahn, D. A. Roberts, and J. Thaler, "The goldstone and goldstino of supersymmetric inflation," *JHEP* **10** (2015) 001, arXiv:1504.05958 [hep-th].

[284] L. V. Delacretaz, V. Gorbenko, and L. Senatore, "The Supersymmetric Effective Field Theory of Inflation," *JHEP* **03** (2017) 063, arXiv:1610.04227 [hep-th].

[285] D. Baumann, C. Duaso Pueyo, A. Joyce, H. Lee, and G. L. Pimentel, "The cosmological bootstrap: weight-shifting operators and scalar seeds," *JHEP* **12** (2020) 204, arXiv:1910.14051 [hep-th].

[286] G. L. Pimentel and D.-G. Wang, "Boostless cosmological collider bootstrap," *JHEP* **10** (2022) 177, arXiv:2205.00013 [hep-th].

[287] S. Kim, T. Noumi, K. Takeuchi, and S. Zhou, "Heavy Spinning Particles from Signs of Primordial Non-Gaussianities: Beyond the Positivity Bounds," *JHEP* **12** (2019) 107, arXiv:1906.11840 [hep-th].

[288] A. Higuchi, "Forbidden Mass Range for Spin-2 Field Theory in De Sitter Space-time," *Nucl. Phys. B* **282** (1987) 397–436.

[289] S. Deser and A. Waldron, "Partial masslessness of higher spins in (A)dS," *Nucl. Phys. B* **607** (2001) 577–604, arXiv:hep-th/0103198.

[290] S. Deser and R. I. Nepomechie, "Gauge Invariance Versus Masslessness in De Sitter Space," *Annals Phys.* **154** (1984) 396.

[291] S. Deser and A. Waldron, "Null propagation of partially massless higher spins in (A)dS and cosmological constant speculations," *Phys. Lett. B* **513** (2001) 137–141, arXiv:hep-th/0105181.

[292] G. Franciolini, A. Kehagias, and A. Riotto, "Imprints of Spinning Particles on Primordial Cosmological Perturbations," *JCAP* **02** (2018) 023, arXiv:1712.06626 [hep-th].

[293] D. Baumann, G. Goon, H. Lee, and G. L. Pimentel, "Partially Massless Fields During Inflation," *JHEP* **04** (2018) 140, arXiv:1712.06624 [hep-th].

[294] X. Chen, Y. Wang, and Z.-Z. Xianyu, "Loop Corrections to Standard Model Fields in Inflation," *JHEP* **08** (2016) 051, arXiv:1604.07841 [hep-th].

[295] X. Chen, Y. Wang, and Z.-Z. Xianyu, "Standard Model Background of the Cosmological Collider," *Phys. Rev. Lett.* **118** no. 26, (2017) 261302, arXiv:1610.06597 [hep-th].

[296] X. Chen, Y. Wang, and Z.-Z. Xianyu, "Standard Model Mass Spectrum in Inflationary Universe," *JHEP* **04** (2017) 058, arXiv:1612.08122 [hep-th].

[297] R. Saito and T. Kubota, "Heavy Particle Signatures in Cosmological Correlation Functions with Tensor Modes," *JCAP* **06** (2018) 009, arXiv:1804.06974 [hep-th].

[298] S. Kumar and R. Sundrum, "Seeing Higher-Dimensional Grand Unification In Primordial Non-Gaussianities," *JHEP* **04** (2019) 120, arXiv:1811.11200 [hep-ph].

[299] S. Alexander, S. J. Gates, L. Jenks, K. Koutrolikos, and E. McDonough, "Higher Spin Supersymmetry at the Cosmological Collider: Sculpting SUSY Rilles in the CMB," *JHEP* **10** (2019) 156, arXiv:1907.05829 [hep-th].

[300] A. Hook, J. Huang, and D. Racco, "Minimal signatures of the Standard Model in non-Gaussianities," *Phys. Rev. D* **101** no. 2, (2020) 023519, arXiv:1908.00019 [hep-ph].

[301] S. Lu, "Axion isocurvature collider," *JHEP* **04** (2022) 157, arXiv:2103.05958 [hep-th].

[302] L.-T. Wang, Z.-Z. Xianyu, and Y.-M. Zhong, "Precision calculation of inflation correlators at one loop," *JHEP* **02** (2022) 085, arXiv:2109.14635 [hep-ph].

[303] N. Maru and A. Okawa, "Non-Gaussianity from X, Y gauge bosons in Cosmological Collider Physics," arXiv:2101.10634 [hep-ph].

[304] Z. Qin and Z.-Z. Xianyu, "Phase information in cosmological collider signals," *JHEP* **10** (2022) 192, arXiv:2205.01692 [hep-th].

[305] Z. Qin and Z.-Z. Xianyu, "Helical inflation correlators: partial Mellin-Barnes and bootstrap equations," *JHEP* **04** (2023) 059, arXiv:2208.13790 [hep-th].

[306] Z. Qin and Z.-Z. Xianyu, "Closed-Form Formulae for Inflation Correlators," arXiv:2301.07047 [hep-th].

[307] Z. Qin and Z.-Z. Xianyu, "Inflation Correlators at the One-Loop Order: Nonanalyticity, Factorization, Cutting Rule, and OPE," arXiv:2304.13295 [hep-th].

[308] Y. Cui and Z.-Z. Xianyu, "Probing Leptogenesis with the Cosmological Collider," *Phys. Rev. Lett.* **129** no. 11, (2022) 111301, arXiv:2112.10793 [hep-ph].

[309] X. Tong, Y. Wang, C. Zhang, and Y. Zhu, "BCS in the Sky: Signatures of Inflationary Fermion Condensation," arXiv:2304.09428 [hep-th].

[310] Y. Wang and Y. Zhu, "Cosmological Collider Signatures of Massive Vectors from Non-Gaussian Gravitational Waves," *JCAP* **04** (2020) 049, arXiv:2001.03879 [astro-ph.CO].

[311] S. Jazayeri and S. Renaux-Petel, "Cosmological bootstrap in slow motion," *JHEP* **12** (2022) 137, arXiv:2205.10340 [hep-th].

[312] S. Cremonini, Z. Lalak, and K. Turzynski, "Strongly Coupled Perturbations in Two-Field Inflationary Models," *JCAP* **03** (2011) 016, arXiv:1010.3021 [hep-th].

[313] H. An, M. McAneny, A. K. Ridgway, and M. B. Wise, "Quasi Single Field Inflation in the non-perturbative regime," *JHEP* **06** (2018) 105, arXiv:1706.09971 [hep-ph].

[314] A. V. Iyer, S. Pi, Y. Wang, Z. Wang, and S. Zhou, "Strongly Coupled Quasi-Single Field Inflation," *JCAP* **01** (2018) 041, arXiv:1710.03054 [hep-th].

[315] D. Werth, L. Pinol, and S. Renaux-Petel, "Cosmological Flow of Primordial Correlators," *Phys. Rev. Lett.* **133** no. 14, (2024) 141002, arXiv:2302.00655 [hep-th].

[316] L. Pinol, S. Renaux-Petel, and D. Werth, "The Cosmological Flow: A Systematic Approach to Primordial Correlators," arXiv:2312.06559 [astro-ph.CO].

[317] R. Emami, "Spectroscopy of Masses and Couplings during Inflation," *JCAP* **04** (2014) 031, arXiv:1311.0184 [hep-th].

[318] M. McAneny and A. K. Ridgway, "New shapes of primordial non-gaussianity from quasi-single field inflation with multiple isocurvatons," *Physical Review D* **100** no. 4, (Aug, 2019) . https://doi.org/10.1103%2Fphysrevd.100.043534.

[319] Q. Lu, M. Reece, and Z.-Z. Xianyu, "Missing scalars at the cosmological collider," *JHEP* **12** (2021) 098, arXiv:2108.11385 [hep-ph].

[320] L. Pinol, S. Aoki, S. Renaux-Petel, and M. Yamaguchi, "Inflationary flavor oscillations and the cosmic spectroscopy," *Phys. Rev. D* **107** no. 2, (2023) L021301, arXiv:2112.05710 [hep-th].

[321] S. Aoki and M. Yamaguchi, "Disentangling mass spectra of multiple fields in cosmological collider," *JHEP* **04** (2021) 127, arXiv:2012.13667 [hep-th].

[322] S. Aoki, "Continuous spectrum on cosmological collider," *JCAP* **04** (2023) 002, arXiv:2301.07920 [hep-th].

[323] S. Kumar and R. Sundrum *JHEP* **05** (2018) 011, arXiv:1711.03988 [hep-ph].

[324] Y.-P. Wu, "Higgs as heavy-lifted physics during inflation," *JHEP* **04** (2019) 125, arXiv:1812.10654 [hep-ph].

[325] G. Dvali, A. Gruzinov, and M. Zaldarriaga, "A new mechanism for generating density perturbations from inflation," *Phys. Rev. D* **69** (2004) 023505, arXiv:astro-ph/0303591.

[326] L. Kofman, "Probing string theory with modulated cosmological fluctuations," arXiv:astro-ph/0303614.

[327] K. Ichikawa, T. Suyama, T. Takahashi, and M. Yamaguchi, "Primordial Curvature Fluctuation and Its Non-Gaussianity in Models with Modulated Reheating," *Phys. Rev. D* **78** (2008) 063545, arXiv:0807.3988 [astro-ph].

[328] L. Li, S. Lu, Y. Wang, and S. Zhou, "Cosmological Signatures of Superheavy Dark Matter," *JHEP* **07** (2020) 231, arXiv:2002.01131 [hep-ph].

[329] N. Maru and A. Okawa, "Cosmological Collider Signals of Non-Gaussianity from Higgs boson in GUT," arXiv:2206.06651 [hep-ph].

[330] X. Chen, "Primordial Features as Evidence for Inflation," *JCAP* **01** (2012) 038, arXiv:1104.1323 [hep-th].

[331] X. Chen, "Fingerprints of Primordial Universe Paradigms as Features in Density Perturbations," *Phys. Lett. B* **706** (2011) 111–115, arXiv:1106.1635 [astro-ph.CO].

[332] X. Chen and C. Ringeval, "Searching for Standard Clocks in the Primordial Universe," *JCAP* **08** (2012) 014, arXiv:1205.6085 [astro-ph.CO].

[333] X. Chen, M. H. Namjoo, and Y. Wang, "Models of the Primordial Standard Clock," *JCAP* **02** (2015) 027, arXiv:1411.2349 [astro-ph.CO].

[334] X. Chen and M. H. Namjoo, "Standard Clock in Primordial Density Perturbations and Cosmic Microwave Background," *Phys. Lett. B* **739** (2014) 285–292, arXiv:1404.1536 [astro-ph.CO].

[335] X. Chen, M. H. Namjoo, and Y. Wang, "Quantum Primordial Standard Clocks," *JCAP* **02** (2016) 013, arXiv:1509.03930 [astro-ph.CO].

[336] X. Chen, M. H. Namjoo, and Y. Wang, "A Direct Probe of the Evolutionary History of the Primordial Universe," *Sci. China Phys. Mech. Astron.* **59** no. 10, (2016) 101021, arXiv:1608.01299 [astro-ph.CO].

[337] Y. Wang, Z. Wang, and Y. Zhu, "Non-standard primordial clocks from induced mass in alternative to inflation scenarios," *JCAP* **11** (2020) 026, arXiv:2007.09677 [hep-th].

[338] Z.-Z. Xianyu and H. Zhang, "Bootstrapping one-loop inflation correlators with the spectral decomposition," *JHEP* **04** (2023) 103, arXiv:2211.03810 [hep-th].

[339] Z. Qin and Z.-Z. Xianyu, "Nonanalyticity and On-Shell Factorization of Inflation Correlators at All Loop Orders," arXiv:2308.14802 [hep-th].

[340] A. Bodas, S. Kumar, and R. Sundrum, "The Scalar Chemical Potential in Cosmological Collider Physics," *JHEP* **02** (2021) 079, arXiv:2010.04727 [hep-ph].

[341] X. Niu, M. H. Rahat, K. Srinivasan, and W. Xue, "Gravitational wave probes of massive gauge bosons at the cosmological collider," *JCAP* **02** (2023) 013, arXiv:2211.14331 [hep-ph].

[342] X. Chen, R. Ebadi, and S. Kumar, "Classical cosmological collider physics and primordial features," *JCAP* **08** (2022) 083, arXiv:2205.01107 [hep-ph].

[343] D.-G. Wang, "On the inflationary massive field with a curved field manifold," *JCAP* **01** (2020) 046, arXiv:1911.04459 [astro-ph.CO].

[344] S. Aoki, T. Noumi, F. Sano, and M. Yamaguchi, "Analytic Formulae for Inflationary Correlators with Dynamical Mass," arXiv:2312.09642 [hep-th].

[345] Y.-P. Wu, "The cosmological collider in R ^{2} inflation," *JCAP* **07** (2024) 010, arXiv:2404.05031 [astro-ph.CO].

[346] J. S. Schwinger, "Brownian motion of a quantum oscillator," *J. Math. Phys.* **2** (1961) 407–432.

[347] L. V. Keldysh, "Diagram technique for nonequilibrium processes," *Zh. Eksp. Teor. Fiz.* **47** (1964) 1515–1527.

[348] R. P. Feynman and F. L. Vernon, Jr., "The Theory of a general quantum system interacting with a linear dissipative system," *Annals Phys.* **24** (1963) 118–173. [Annals Phys.281,547(2000)].

[349] K.-c. Chou, Z.-b. Su, B.-l. Hao, and L. Yu, "Equilibrium and Nonequilibrium Formalisms Made Unified," *Phys. Rept.* **118** (1985) 1–131.

[350] R. D. Jordan, "Effective Field Equations for Expectation Values," *Phys. Rev.* **D33** (1986) 444–454.

[351] F. M. Haehl, R. Loganayagam, and M. Rangamani, "Schwinger-Keldysh formalism. Part I: BRST symmetries and superspace," *JHEP* **06** (2017) 069, arXiv:1610.01940 [hep-th].

[352] E. Calzetta and B. L. Hu, "Closed Time Path Functional Formalism in Curved Space-Time: Application to Cosmological Back Reaction Problems," *Phys. Rev.* **D35** (1987) 495.

[353] S. Weinberg, "Quantum contributions to cosmological correlations," *Phys. Rev.* **D72** (2005) 043514, arXiv:hep-th/0506236 [hep-th].

[354] T. Prokopec and G. Rigopoulos, "Path Integral for Inflationary Perturbations," *Phys. Rev. D* **82** (2010) 023529, arXiv:1004.0882 [gr-qc].

[355] J.-O. Gong, M.-S. Seo, and G. Shiu, "Path integral for multi-field inflation," *JHEP* **07** (2016) 099, arXiv:1603.03689 [hep-th].

[356] X. Chen, Y. Wang, and Z.-Z. Xianyu, "Schwinger-Keldysh Diagrammatics for Primordial Perturbations," *JCAP* **12** (2017) 006, arXiv:1703.10166 [hep-th].

[357] S. Weinberg, *The Quantum theory of fields. Vol. 1: Foundations*. Cambridge University Press, 6, 2005.

[358] M. Chaichian and A. Demichev, *Path integrals in physics. Vol. 1: Stochastic processes and quantum mechanics*. 2001.

[359] M. E. Peskin and D. V. Schroeder, *An Introduction to quantum field theory*. Addison-Wesley, Reading, USA, 1995.

[360] M. D. Schwartz, *Quantum Field Theory and the Standard Model*. Cambridge University Press, 3, 2014.

[361] A. Kaya, "On $i\epsilon$ Prescription in Cosmology," *JCAP* **04** (2019) 002, arXiv:1810.12324 [gr-qc].

[362] S. Weinberg, *The quantum theory of fields. Vol. 2: Modern applications*. Cambridge University Press, 8, 2013.

[363] S. Jazayeri, S. Renaux-Petel, X. Tong, D. Werth, and Y. Zhu, "Parity Violation from Emergent Non-Locality During Inflation," arXiv:2308.11315 [hep-th].

[364] F. A. Berends and W. T. Giele, "Recursive Calculations for Processes with n Gluons," *Nucl. Phys. B* **306** (1988) 759–808.

[365] R. Britto, F. Cachazo, and B. Feng, "New recursion relations for tree amplitudes of gluons," *Nucl. Phys. B* **715** (2005) 499–522, arXiv:hep-th/0412308.

[366] R. Britto, F. Cachazo, B. Feng, and E. Witten, "Direct proof of tree-level recursion relation in Yang-Mills theory," *Phys. Rev. Lett.* **94** (2005) 181602, arXiv:hep-th/0501052.

[367] Z. Bern, L. J. Dixon, D. C. Dunbar, and D. A. Kosower, "One loop n point gauge theory amplitudes, unitarity and collinear limits," *Nucl. Phys. B* **425** (1994) 217–260, arXiv:hep-ph/9403226.

[368] Z. Bern, L. J. Dixon, D. C. Dunbar, and D. A. Kosower, "Fusing gauge theory tree amplitudes into loop amplitudes," *Nucl. Phys. B* **435** (1995) 59–101, arXiv:hep-ph/9409265.

[369] Z. Bern and Y.-t. Huang, "Basics of Generalized Unitarity," *J. Phys. A* **44** (2011) 454003, arXiv:1103.1869 [hep-th].

[370] P. Benincasa, "New structures in scattering amplitudes: a review," *Int. J. Mod. Phys. A* **29** no. 5, (2014) 1430005, arXiv:1312.5583 [hep-th].

[371] H. Elvang and Y.-t. Huang, "Scattering Amplitudes," arXiv:1308.1697 [hep-th].

[372] S. Weinzierl, "Tales of 1001 Gluons," *Phys. Rept.* **676** (2017) 1–101, arXiv:1610.05318 [hep-th].

[373] C. Cheung, *TASI Lectures on Scattering Amplitudes*, pp. 571–623. 2018. arXiv:1708.03872 [hep-ph].

[374] D. Baumann, D. Green, A. Joyce, E. Pajer, G. L. Pimentel, C. Sleight, and M. Taronna, "Snowmass White Paper: The Cosmological Bootstrap," in *Snowmass 2021*. 3, 2022. arXiv:2203.08121 [hep-th].

[375] S. Raju, "New Recursion Relations and a Flat Space Limit for AdS/CFT Correlators," *Phys. Rev. D* **85** (2012) 126009, arXiv:1201.6449 [hep-th].

[376] H. Goodhew, S. Jazayeri, and E. Pajer, "The Cosmological Optical Theorem," *JCAP* **04** (2021) 021, arXiv:2009.02898 [hep-th].

[377] S. Céspedes, A.-C. Davis, and S. Melville, "On the time evolution of cosmological correlators," *JHEP* **02** (2021) 012, arXiv:2009.07874 [hep-th].

[378] D. Baumann, W.-M. Chen, C. Duaso Pueyo, A. Joyce, H. Lee, and G. L. Pimentel, "Linking the singularities of cosmological correlators," *JHEP* **09** (2022) 010, arXiv:2106.05294 [hep-th].

[379] S. Melville and E. Pajer, "Cosmological Cutting Rules," *JHEP* **05** (2021) 249, arXiv:2103.09832 [hep-th].

[380] H. Goodhew, S. Jazayeri, M. H. G. Lee, and E. Pajer, "Cutting cosmological correlators," *JCAP* **08** (2021) 003, arXiv:2104.06587 [hep-th].

[381] C. Sleight and M. Taronna, "From AdS to dS exchanges: Spectral representation, Mellin amplitudes, and crossing," *Phys. Rev. D* **104** no. 8, (2021) L081902, arXiv:2007.09993 [hep-th].

[382] M. Loparco, J. Penedones, K. Salehi Vaziri, and Z. Sun, "The Källén-Lehmann representation in de Sitter spacetime," *JHEP* **12** (2023) 159, arXiv:2306.00090 [hep-th].

[383] N. Arkani-Hamed, P. Benincasa, and A. Postnikov, "Cosmological Polytopes and the Wavefunction of the Universe," arXiv:1709.02813 [hep-th].

[384] N. Arkani-Hamed and P. Benincasa, "On the Emergence of Lorentz Invariance and Unitarity from the Scattering Facet of Cosmological Polytopes," arXiv:1811.01125 [hep-th].

[385] P. Benincasa, "From the flat-space S-matrix to the Wavefunction of the Universe," arXiv:1811.02515 [hep-th].

[386] P. Benincasa, "Cosmological Polytopes and the Wavefuncton of the Universe for Light States," arXiv:1909.02517 [hep-th].

[387] P. Benincasa, A. J. McLeod, and C. Vergu, "Steinmann Relations and the Wavefunction of the Universe," *Phys. Rev. D* **102** (2020) 125004, arXiv:2009.03047 [hep-th].

[388] P. Benincasa and W. J. T. Bobadilla, "Physical representations for scattering amplitudes and the wavefunction of the universe," *SciPost Phys.* **12** no. 6, (2022) 192, arXiv:2112.09028 [hep-th].

[389] P. Benincasa and G. Dian, "The Geometry of Cosmological Correlators," arXiv:2401.05207 [hep-th].

[390] P. Benincasa and F. Vazão, "The Asymptotic Structure of Cosmological Integrals," arXiv:2402.06558 [hep-th].

[391] A. Hillman, "Symbol Recursion for the dS Wave Function," arXiv:1912.09450 [hep-th].

[392] S. De and A. Pokraka, "Cosmology meets cohomology," *JHEP* **03** (2024) 156, arXiv:2308.03753 [hep-th].

[393] N. Arkani-Hamed, D. Baumann, A. Hillman, A. Joyce, H. Lee, and G. L. Pimentel, "Differential Equations for Cosmological Correlators," arXiv:2312.05303 [hep-th].

[394] B. Fan and Z.-Z. Xianyu, "Cosmological Amplitudes in Power-Law FRW Universe," arXiv:2403.07050 [hep-th].

[395] H. Gomez, R. L. Jusinskas, and A. Lipstein, "Cosmological Scattering Equations," *Phys. Rev. Lett.* **127** no. 25, (2021) 251604, arXiv:2106.11903 [hep-th].

[396] H. Gomez, R. Lipinski Jusinskas, and A. Lipstein, "Cosmological scattering equations at tree-level and one-loop," *JHEP* **07** (2022) 004, arXiv:2112.12695 [hep-th].

[397] C. Armstrong, H. Gomez, R. Lipinski Jusinskas, A. Lipstein, and J. Mei, "Effective field theories and cosmological scattering equations," *JHEP* **08** (2022) 054, arXiv:2204.08931 [hep-th].

[398] S. Melville and G. L. Pimentel, "A de Sitter S-matrix from amputated cosmological correlators," arXiv:2404.05712 [hep-th].

[399] T. Basile, X. Bekaert, and N. Boulanger, "Mixed-symmetry fields in de Sitter space: a group theoretical glance," *JHEP* **05** (2017) 081, arXiv:1612.08166 [hep-th].

[400] D. Karateev, P. Kravchuk, and D. Simmons-Duffin, "Harmonic Analysis and Mean Field Theory," *JHEP* **10** (2019) 217, arXiv:1809.05111 [hep-th].

[401] G. Sengör and C. Skordis, "Unitarity at the Late time Boundary of de Sitter," *JHEP* **06** (2020) 041, arXiv:1912.09885 [hep-th].

[402] Z. Sun, "A note on the representations of $\mathrm{SO}(1, d+1)$," arXiv:2111.04591 [hep-th].

[403] J. Penedones, "Writing CFT correlation functions as AdS scattering amplitudes," *JHEP* **03** (2011) 025, arXiv:1011.1485 [hep-th].

[404] U. Moschella and R. Schaeffer, "Quantum theory on Lobatchevski spaces," *Class. Quant. Grav.* **24** (2007) 3571–3602, arXiv:0709.2795 [hep-th].

[405] S. Duary and S. Maji, "Spectral representation in Klein space: simplifying celestial leaf amplitudes," *JHEP* **08** (2024) 079, arXiv:2406.02342 [hep-th].

[406] Y. Gutiérrez-Tovar and J. Méndez-Pérez, "The kontorovich–lebedev integral transformation with a hankel function kernel in a space of generalized functions of doubly exponential descent," *Journal of Mathematical Analysis and Applications* **328** no. 1, (2007) 359–369. https://www.sciencedirect.com/science/article/pii/S0022247X0600518X.

[407] D. Meltzer and A. Sivaramakrishnan, "CFT unitarity and the AdS Cutkosky rules," *JHEP* **11** (2020) 073, arXiv:2008.11730 [hep-th].

[408] D. Meltzer, "The inflationary wavefunction from analyticity and factorization," *JCAP* **12** no. 12, (2021) 018, arXiv:2107.10266 [hep-th].

[409] R. Britto, C. Duhr, H. S. Hannesdottir, and S. Mizera, "Cutting-Edge Tools for Cutting Edges," 2, 2024. arXiv:2402.19415 [hep-th].

[410] M. J. G. Veltman, *Diagrammatica: The Path to Feynman rules*, vol. 4. Cambridge University Press, 5, 2012.

[411] R. E. Cutkosky, "Singularities and discontinuities of Feynman amplitudes," *J. Math. Phys.* **1** (1960) 429–433.

[412] G. 't Hooft and M. J. G. Veltman, "DIAGRAMMAR," *NATO Sci. Ser. B* **4** (1974) 177–322.

[413] A. Kamenev, *Field Theory of Non-Equilibrium Systems*. Cambridge University Press, 2011.

[414] M. Veltman, "Unitarity and causality in a renormalizable field theory with unstable particles," *Physica* **29** no. 3, (1963) 186–207. https://www.sciencedirect.com/science/article/pii/S0031891463802773.

[415] R. J. Eden, P. V. Landshoff, D. I. Olive, and J. C. Polkinghorne, *The analytic S-matrix*. Cambridge Univ. Press, Cambridge, 1966.

[416] M. Gillioz, X. Lu, and M. A. Luty, "Scale Anomalies, States, and Rates in Conformal Field Theory," *JHEP* **04** (2017) 171, arXiv:1612.07800 [hep-th].

[417] M. Gillioz, X. Lu, and M. A. Luty, "Graviton Scattering and a Sum Rule for the c Anomaly in 4D CFT," *JHEP* **09** (2018) 025, arXiv:1801.05807 [hep-th].

[418] M. Gillioz, "Momentum-space conformal blocks on the light cone," *JHEP* **10** (2018) 125, arXiv:1807.07003 [hep-th].

[419] J. L. Bourjaily, H. Hannesdottir, A. J. McLeod, M. D. Schwartz, and C. Vergu, "Sequential Discontinuities of Feynman Integrals and the Monodromy Group," *JHEP* **01** (2021) 205, arXiv:2007.13747 [hep-th].

[420] S. Aoki, L. Pinol, F. Sano, M. Yamaguchi, and Y. Zhu, "Cosmological Correlators with Double Massive Exchanges: Bootstrap Equation and Phenomenology," arXiv:2404.09547 [hep-th].

[421] C. Sleight, "A Mellin Space Approach to Cosmological Correlators," *JHEP* **01** (2020) 090, arXiv:1906.12302 [hep-th].

[422] C. Sleight and M. Taronna, "Bootstrapping Inflationary Correlators in Mellin Space," *JHEP* **02** (2020) 098, arXiv:1907.01143 [hep-th].

[423] C. Sleight and M. Taronna, "From dS to AdS and back," *JHEP* **12** (2021) 074, arXiv:2109.02725 [hep-th].

[424] Z.-Z. Xianyu and J. Zang, "Inflation correlators with multiple massive exchanges," *JHEP* **03** (2024) 070, arXiv:2309.10849 [hep-th].

[425] H. Liu, Z. Qin, and Z.-Z. Xianyu, "Dispersive Bootstrap of Massive Inflation Correlators," arXiv:2407.12299 [hep-th].

[426] T. Heckelbacher, I. Sachs, E. Skvortsov, and P. Vanhove, "Analytical evaluation of cosmological correlation functions," *JHEP* **08** (2022) 139, arXiv:2204.07217 [hep-th].

[427] F. Olver, D. Lozier, R. Boisvert, and C. Clark, *The NIST Handbook of Mathematical Functions*. Cambridge University Press, New York, NY, 2010-05-12 00:05:00, 2010.

[428] D. Baumann, C. Duaso Pueyo, A. Joyce, H. Lee, and G. L. Pimentel, "The Cosmological Bootstrap: Spinning Correlators from Symmetries and Factorization," *SciPost Phys.* **11** (2021) 071, arXiv:2005.04234 [hep-th].

[429] D.-G. Wang, G. L. Pimentel, and A. Achúcarro, "Bootstrapping multi-field inflation: non-Gaussianities from light scalars revisited," *JCAP* **05** (2023) 043, arXiv:2212.14035 [astro-ph.CO].

[430] S. Aoki, L. Pinol, F. Sano, M. Yamaguchi, and Y. Zhu, "Cosmological correlators with double massive exchanges: Bootstrap equation and phenomenology," 2024.

[431] M. S. Costa, J. Penedones, D. Poland, and S. Rychkov, "Spinning Conformal Blocks," *JHEP* **11** (2011) 154, arXiv:1109.6321 [hep-th].

[432] D. Karateev, P. Kravchuk, and D. Simmons-Duffin, "Weight Shifting Operators and Conformal Blocks," *JHEP* **02** (2018) 081, arXiv:1706.07813 [hep-th].

[433] H. Elvang and Y.-t. Huang, *Scattering Amplitudes in Gauge Theory and Gravity*. Cambridge University Press, 4, 2015.

[434] D. Anninos, T. Anous, D. Z. Freedman, and G. Konstantinidis, "Late-time Structure of the Bunch-Davies De Sitter Wavefunction," *JCAP* **11** (2015) 048, arXiv:1406.5490 [hep-th].

[435] G. Goon, K. Hinterbichler, A. Joyce, and M. Trodden, "Shapes of gravity: Tensor non-Gaussianity and massive spin-2 fields," *JHEP* **10** (2019) 182, arXiv:1812.07571 [hep-th].

[436] D. Werth, "Spectral Representation of Cosmological Correlators," arXiv:2409.02072 [hep-th].

[437] S. Agui-Salcedo and S. Melville, "The cosmological tree theorem," *JHEP* **12** (2023) 076, arXiv:2308.00680 [hep-th].

[438] S. Jazayeri, E. Pajer, and D. Stefanyszyn, "From locality and unitarity to cosmological correlators," *JHEP* **10** (2021) 065, arXiv:2103.08649 [hep-th].

[439] L. Di Pietro, V. Gorbenko, and S. Komatsu, "Analyticity and unitarity for cosmological correlators," *JHEP* **03** (2022) 023, arXiv:2108.01695 [hep-th].

[440] J. Bonifacio, E. Pajer, and D.-G. Wang, "From amplitudes to contact cosmological correlators," *JHEP* **10** (2021) 001, arXiv:2106.15468 [hep-th].

[441] S. Jazayeri, S. Renaux-Petel, and D. Werth, "Shapes of the Cosmological Low-Speed Collider," arXiv:2307.01751 [hep-th].

[442] C. Sleight and M. Taronna, "On the consistency of (partially-)massless matter couplings in de Sitter space," *JHEP* **10** (2021) 156, arXiv:2106.00366 [hep-th].

[443] E. Pajer, "Building a Boostless Bootstrap for the Bispectrum," *JCAP* **01** (2021) 023, arXiv:2010.12818 [hep-th].

[444] C. Duaso Pueyo and E. Pajer, "A cosmological bootstrap for resonant non-Gaussianity," *JHEP* **24** (2020) 098, arXiv:2311.01395 [hep-th].

[445] P. Benincasa, "Wavefunctionals/S-matrix techniques in de Sitter," *PoS* **CORFU2021** (2022) 358, arXiv:2203.16378 [hep-th].

[446] P. Benincasa, "Amplitudes meet Cosmology: A (Scalar) Primer," arXiv:2203.15330 [hep-th].

[447] Z. Bern, L. J. Dixon, and D. A. Kosower, "Dimensionally regulated pentagon integrals," *Nucl. Phys. B* **412** (1994) 751–816, arXiv:hep-ph/9306240.

[448] A. V. Kotikov, "Differential equations method: New technique for massive Feynman diagrams calculation," *Phys. Lett. B* **254** (1991) 158–164.

[449] E. Remiddi, "Differential equations for Feynman graph amplitudes," *Nuovo Cim. A* **110** (1997) 1435–1452, arXiv:hep-th/9711188.

[450] T. Gehrmann and E. Remiddi, "Differential equations for two loop four point functions," *Nucl. Phys. B* **580** (2000) 485–518, arXiv:hep-ph/9912329.

[451] J. M. Henn, "Multiloop integrals in dimensional regularization made simple," *Phys. Rev. Lett.* **110** (2013) 251601, arXiv:1304.1806 [hep-th].

[452] J. M. Henn, "Lectures on differential equations for Feynman integrals," *J. Phys. A* **48** (2015) 153001, arXiv:1412.2296 [hep-ph].

[453] J. Blümlein and C. Schneider, "The SAGEX review on scattering amplitudes Chapter 4: Multi-loop Feynman integrals," *J. Phys. A* **55** no. 44, (2022) 443005, arXiv:2203.13015 [hep-th].

[454] N. Arkani-Hamed, D. Baumann, A. Hillman, A. Joyce, H. Lee, and G. L. Pimentel, "Kinematic Flow and the Emergence of Time," arXiv:2312.05300 [hep-th].

[455] S. He, X. Jiang, J. Liu, Q. Yang, and Y.-Q. Zhang, "Differential equations and recursive solutions for cosmological amplitudes," arXiv:2407.17715 [hep-th].

[456] Y. Hang, "A Note on Kinematic Flow and Differential Equations for Two-Site One-Loop Graph in FRW Spacetime," arXiv:2410.17192 [hep-th].

[457] D. Baumann, H. Goodhew, and H. Lee, "Kinematic Flow for Cosmological Loop Integrands," arXiv:2410.17994 [hep-th].

[458] A. Hillman and E. Pajer, "A differential representation of cosmological wavefunctions," *JHEP* **04** (2022) 012, arXiv:2112.01619 [hep-th].

[459] J. Chen and B. Feng, "Towards Systematic Evaluation of de Sitter Correlators via Generalized Integration-By-Parts Relations," arXiv:2401.00129 [hep-th].

[460] T. W. Grimm, A. Hoefnagels, and M. van Vliet, "Structure and Complexity of Cosmological Correlators," arXiv:2404.03716 [hep-th].

[461] N. Arkani-Hamed, Y. Bai, S. He, and G. Yan, "Scattering Forms and the Positive Geometry of Kinematics, Color and the Worldsheet," *JHEP* **05** (2018) 096, arXiv:1711.09102 [hep-th].

[462] S. Caron-Huot and A. Pokraka, "Duals of Feynman integrals. Part I. Differential equations," *JHEP* **12** (2021) 045, arXiv:2104.06898 [hep-th].

[463] S. Caron-Huot and A. Pokraka, "Duals of Feynman Integrals. Part II. Generalized unitarity," *JHEP* **04** (2022) 078, arXiv:2112.00055 [hep-th].

[464] P. Mastrolia and S. Mizera, "Feynman Integrals and Intersection Theory," *JHEP* **02** (2019) 139, arXiv:1810.03818 [hep-th].

[465] H. Frellesvig, F. Gasparotto, S. Laporta, M. K. Mandal, P. Mastrolia, L. Mattiazzi, and S. Mizera, "Decomposition of Feynman Integrals on the Maximal Cut by Intersection Numbers," *JHEP* **05** (2019) 153, arXiv:1901.11510 [hep-ph].

[466] H. Frellesvig, F. Gasparotto, S. Laporta, M. K. Mandal, P. Mastrolia, L. Mattiazzi, and S. Mizera, "Decomposition of Feynman Integrals by Multivariate Intersection Numbers," *JHEP* **03** (2021) 027, arXiv:2008.04823 [hep-th].

[467] S. Weinzierl, "On the computation of intersection numbers for twisted cocycles," *J. Math. Phys.* **62** no. 7, (2021) 072301, arXiv:2002.01930 [math-ph].

[468] V. Chestnov, H. Frellesvig, F. Gasparotto, M. K. Mandal, and P. Mastrolia, "Intersection numbers from higher-order partial differential equations," *JHEP* **06** (2023) 131, arXiv:2209.01997 [hep-th].

[469] J. Chen, X. Jiang, C. Ma, X. Xu, and L. L. Yang, "Baikov representations, intersection theory, and canonical Feynman integrals," *JHEP* **07** (2022) 066, arXiv:2202.08127 [hep-th].

[470] C. Cheung, P. Creminelli, A. L. Fitzpatrick, J. Kaplan, and L. Senatore, "The Effective Field Theory of Inflation," *JHEP* **03** (2008) 014, arXiv:0709.0293 [hep-th].

[471] N. Arkani-Hamed, H.-C. Cheng, M. A. Luty, and S. Mukohyama, "Ghost condensation and a consistent infrared modification of gravity," *JHEP* **05** (2004) 074, arXiv:hep-th/0312099.

[472] P. Creminelli, M. A. Luty, A. Nicolis, and L. Senatore, "Starting the Universe: Stable Violation of the Null Energy Condition and Non-standard Cosmologies," *JHEP* **12** (2006) 080, arXiv:hep-th/0606090.

[473] N. Arkani-Hamed, S. Dubovsky, A. Nicolis, E. Trincherini, and G. Villadoro, "A Measure of de Sitter entropy and eternal inflation," *JHEP* **05** (2007) 055, arXiv:0704.1814 [hep-th].

[474] F. Piazza and F. Vernizzi, "Effective Field Theory of Cosmological Perturbations," *Class. Quant. Grav.* **30** (2013) 214007, arXiv:1307.4350 [hep-th].

[475] T. Cohen, "As Scales Become Separated: Lectures on Effective Field Theory," *PoS* **TASI2018** (2019) 011, arXiv:1903.03622 [hep-ph].

[476] R. Penco, "An Introduction to Effective Field Theories," arXiv:2006.16285 [hep-th].

[477] J. M. Cornwall, D. N. Levin, and G. Tiktopoulos, "Derivation of Gauge Invariance from High-Energy Unitarity Bounds on the s Matrix," *Phys. Rev. D* **10** (1974) 1145. [Erratum: Phys.Rev.D 11, 972 (1975)].

[478] B. W. Lee, C. Quigg, and H. B. Thacker, "Weak Interactions at Very High-Energies: The Role of the Higgs Boson Mass," *Phys. Rev. D* **16** (1977) 1519.

[479] M. S. Chanowitz and M. K. Gaillard, "The TeV Physics of Strongly Interacting W's and Z's," *Nucl. Phys. B* **261** (1985) 379–431.

[480] G. Gubitosi, F. Piazza, and F. Vernizzi, "The Effective Field Theory of Dark Energy," *JCAP* **02** (2013) 032, arXiv:1210.0201 [hep-th].

[481] J. Gleyzes, D. Langlois, F. Piazza, and F. Vernizzi, "Essential Building Blocks of Dark Energy," *JCAP* **08** (2013) 025, arXiv:1304.4840 [hep-th].

[482] A. Nicolis, R. Rattazzi, and E. Trincherini, "The Galileon as a local modification of gravity," *Phys. Rev. D* **79** (2009) 064036, arXiv:0811.2197 [hep-th].

[483] N. Arkani-Hamed, P. Creminelli, S. Mukohyama, and M. Zaldarriaga, "Ghost inflation," *JCAP* **04** (2004) 001, arXiv:hep-th/0312100.

[484] N. Arkani-Hamed, H.-C. Cheng, M. A. Luty, S. Mukohyama, and T. Wiseman, "Dynamics of gravity in a Higgs phase," *JHEP* **01** (2007) 036, arXiv:hep-ph/0507120.

[485] X. Chen, "Running non-Gaussianities in DBI inflation," *Phys. Rev. D* **72** (2005) 123518, arXiv:astro-ph/0507053.

[486] P. Creminelli, R. Emami, M. Simonović, and G. Trevisan, "ISO(4,1) Symmetry in the EFT of Inflation," *JCAP* **07** (2013) 037, arXiv:1304.4238 [hep-th].

[487] G. W. Horndeski, "Second-order scalar-tensor field equations in a four-dimensional space," *Int. J. Theor. Phys.* **10** (1974) 363–384.

[488] C. Deffayet, S. Deser, and G. Esposito-Farese, "Generalized Galileons: All scalar models whose curved background extensions maintain second-order field equations and stress-tensors," *Phys. Rev. D* **80** (2009) 064015, arXiv:0906.1967 [gr-qc].

[489] C. Deffayet, X. Gao, D. A. Steer, and G. Zahariade, "From k-essence to generalised Galileons," *Phys. Rev. D* **84** (2011) 064039, arXiv:1103.3260 [hep-th].

[490] D. Pirtskhalava, L. Santoni, E. Trincherini, and F. Vernizzi, "Weakly Broken Galileon Symmetry," *JCAP* **09** (2015) 007, arXiv:1505.00007 [hep-th].

[491] T. Kobayashi, M. Yamaguchi, and J. Yokoyama, "G-inflation: Inflation driven by the Galileon field," *Phys. Rev. Lett.* **105** (2010) 231302, arXiv:1008.0603 [hep-th].

[492] C. Burrage, C. de Rham, D. Seery, and A. J. Tolley, "Galileon inflation," *JCAP* **01** (2011) 014, arXiv:1009.2497 [hep-th].

[493] P. Creminelli, G. D'Amico, M. Musso, J. Norena, and E. Trincherini, "Galilean symmetry in the effective theory of inflation: new shapes of non-Gaussianity," *JCAP* **02** (2011) 006, arXiv:1011.3004 [hep-th].

[494] H. Ruegg and M. Ruiz-Altaba, "The Stueckelberg field," *Int. J. Mod. Phys. A* **19** (2004) 3265–3348, arXiv:hep-th/0304245.

[495] C. de Rham, S. Melville, A. J. Tolley, and S.-Y. Zhou, "Positivity Bounds for Massive Spin-1 and Spin-2 Fields," *JHEP* **03** (2019) 182, arXiv:1804.10624 [hep-th].

[496] B. Finelli, G. Goon, E. Pajer, and L. Santoni, "The Effective Theory of Shift-Symmetric Cosmologies," *JCAP* **05** (2018) 060, arXiv:1802.01580 [hep-th].

[497] P. Creminelli, S. Renaux-Petel, G. Tambalo, and V. Yingcharoenrat, "Non-perturbative wavefunction of the universe in inflation with (resonant) features," *JHEP* **03** (2024) 010, arXiv:2401.10212 [hep-th].

[498] R. L. Arnowitt, S. Deser, and C. W. Misner, "The Dynamics of general relativity," *Gen. Rel. Grav.* **40** (2008) 1997–2027, arXiv:gr-qc/0405109 [gr-qc].

[499] **Planck** Collaboration, Y. Akrami *et al.*, "Planck 2018 results. X. Constraints on inflation," arXiv:1807.06211 [astro-ph.CO].

[500] **BICEP, Keck** Collaboration, P. A. R. Ade *et al.*, "Improved Constraints on Primordial Gravitational Waves using Planck, WMAP, and BICEP/Keck Observations through the 2018 Observing Season," *Phys. Rev. Lett.* **127** no. 15, (2021) 151301, arXiv:2110.00483 [astro-ph.CO].

[501] P. Creminelli, J. Gleyzes, J. Noreña, and F. Vernizzi, "Resilience of the standard predictions for primordial tensor modes," *Phys. Rev. Lett.* **113** no. 23, (2014) 231301, arXiv:1407.8439 [astro-ph.CO].

[502] D. Baumann and D. Green, "Equilateral Non-Gaussianity and New Physics on the Horizon," *JCAP* **09** (2011) 014, arXiv:1102.5343 [hep-th].

[503] D. Baumann, D. Green, and R. A. Porto, "B-modes and the Nature of Inflation," *JCAP* **01** (2015) 016, arXiv:1407.2621 [hep-th].

[504] L. Senatore and M. Zaldarriaga, "The Effective Field Theory of Multifield Inflation," *JHEP* **04** (2012) 024, arXiv:1009.2093 [hep-th].

[505] M. M. Anber and L. Sorbo, "Naturally inflating on steep potentials through electromagnetic dissipation," *Phys. Rev. D* **81** (2010) 043534, arXiv:0908.4089 [hep-th].

[506] L. Sorbo, "Parity violation in the Cosmic Microwave Background from a pseudoscalar inflaton," *JCAP* **06** (2011) 003, arXiv:1101.1525 [astro-ph.CO].

[507] N. Barnaby, E. Pajer, and M. Peloso, "Gauge Field Production in Axion Inflation: Consequences for Monodromy, non-Gaussianity in the CMB, and Gravitational Waves at Interferometers," *Phys. Rev. D* **85** (2012) 023525, arXiv:1110.3327 [astro-ph.CO].

[508] E. Pajer and M. Peloso, "A review of Axion Inflation in the era of Planck," *Class. Quant. Grav.* **30** (2013) 214002, arXiv:1305.3557 [hep-th].

[509] T. Appelquist and J. Carazzone, "Infrared singularities and massive fields," *Phys. Rev. D* **11** (May, 1975) 2856–2861. https://link.aps.org/doi/10.1103/PhysRevD.11.2856.

[510] M. Ostrogradsky, "Mémoires sur les équations différentielles, relatives au problème des isopérimètres," *Mem. Acad. St. Petersbourg* **6** no. 4, (1850) 385–517.

[511] S. Scherer, "Introduction to chiral perturbation theory," *Adv. Nucl. Phys.* **27** (2003) 277, arXiv:hep-ph/0210398.

[512] J. F. Donoghue, E. Golowich, and B. R. Holstein, *Dynamics of the Standard Model*. Cambridge Monographs on Particle Physics, Nuclear Physics and Cosmology. Cambridge University Press, 2 ed., 2014.

[513] N. Arkani-Hamed, P. Creminelli, S. Mukohyama, and M. Zaldarriaga, "Ghost inflation," *JCAP* **04** (2004) 001, arXiv:hep-th/0312100.

[514] S. Renaux-Petel, S. Mizuno, and K. Koyama, "Primordial fluctuations and non-Gaussianities from multifield DBI Galileon inflation," *JCAP* **11** (2011) 042, arXiv:1108.0305 [astro-ph.CO].

[515] J. R. Fergusson and E. P. S. Shellard, "Primordial non-Gaussianity and the CMB bispectrum," *Phys. Rev.* **D76** (2007) 083523, arXiv:astro-ph/0612713.

[516] H. P. Breuer and F. Petruccione, *The theory of open quantum systems*. 2002.

[517] X. Chen, "Primordial Non-Gaussianities from Inflation Models," *Adv. Astron.* **2010** (2010) 638979, arXiv:1002.1416 [astro-ph.CO].

[518] Y. Wang, "Inflation, Cosmic Perturbations and Non-Gaussianities," *Commun. Theor. Phys.* **62** (2014) 109–166, arXiv:1303.1523 [hep-th].

[519] B. Bucciotti, "A Note on the Existence of Equal Time Correlators," arXiv:2410.01903 [hep-th].

[520] M. Baumgart and R. Sundrum, "Manifestly Causal In-In Perturbation Theory about the Interacting Vacuum," *JHEP* **03** (2021) 080, arXiv:2010.10785 [hep-th].

[521] S. Albayrak, P. Benincasa, and C. Duaso Pueyo, "Perturbative Unitarity and the Wavefunction of the Universe," arXiv:2305.19686 [hep-th].

[522] M. Baumgart and R. Sundrum, "De Sitter Diagrammar and the Resummation of Time," *JHEP* **07** (2020) 119, arXiv:1912.09502 [hep-th].

[523] P. Adshead, R. Easther, and E. A. Lim, "The 'in-in' Formalism and Cosmological Perturbations," *Phys. Rev. D* **80** (2009) 083521, arXiv:0904.4207 [hep-th].

[524] L. Senatore and M. Zaldarriaga, "On Loops in Inflation," *JHEP* **12** (2010) 008, arXiv:0912.2734 [hep-th].

[525] S. Borowka, G. Heinrich, S. Jahn, S. P. Jones, M. Kerner, J. Schlenk, and T. Zirke, "pySecDec: a toolbox for the numerical evaluation of multi-scale integrals," *Comput. Phys. Commun.* **222** (2018) 313–326, arXiv:1703.09692 [hep-ph].

[526] A. V. Smirnov and M. N. Tentyukov, "Feynman Integral Evaluation by a Sector decomposiTion Approach (FIESTA)," *Comput. Phys. Commun.* **180** (2009) 735–746, arXiv:0807.4129 [hep-ph].

[527] A. V. Smirnov, V. A. Smirnov, and M. Tentyukov, "FIESTA 2: Parallelizeable multiloop numerical calculations," *Comput. Phys. Commun.* **182** (2011) 790–803, arXiv:0912.0158 [hep-ph].

[528] A. V. Smirnov, "FIESTA 3: cluster-parallelizable multiloop numerical calculations in physical regions," *Comput. Phys. Commun.* **185** (2014) 2090–2100, arXiv:1312.3186 [hep-ph].

[529] M. Hidding, "DiffExp, a Mathematica package for computing Feynman integrals in terms of one-dimensional series expansions," *Comput. Phys. Commun.* **269** (2021) 108125, arXiv:2006.05510 [hep-ph].

[530] X. Liu and Y.-Q. Ma, "AMFlow: A Mathematica package for Feynman integrals computation via auxiliary mass flow," *Comput. Phys. Commun.* **283** (2023) 108565, arXiv:2201.11669 [hep-ph].

[531] T. Hahn and M. Perez-Victoria, "Automatized one loop calculations in four-dimensions and D-dimensions," *Comput. Phys. Commun.* **118** (1999) 153–165, arXiv:hep-ph/9807565.

[532] T. Stelzer and W. F. Long, "Automatic generation of tree level helicity amplitudes," *Comput. Phys. Commun.* **81** (1994) 357–371, arXiv:hep-ph/9401258.

[533] J. Alwall, P. Demin, S. de Visscher, R. Frederix, M. Herquet, F. Maltoni, T. Plehn, D. L. Rainwater, and T. Stelzer, "MadGraph/MadEvent v4: The New Web Generation," *JHEP* **09** (2007) 028, arXiv:0706.2334 [hep-ph].

[534] J. Alwall, M. Herquet, F. Maltoni, O. Mattelaer, and T. Stelzer, "MadGraph 5 : Going Beyond," *JHEP* **06** (2011) 128, arXiv:1106.0522 [hep-ph].

[535] A. Pukhov, E. Boos, M. Dubinin, V. Edneral, V. Ilyin, D. Kovalenko, A. Kryukov, V. Savrin, S. Shichanin, and A. Semenov, "CompHEP: A Package for evaluation of Feynman diagrams and integration over multiparticle phase space," arXiv:hep-ph/9908288.

[536] **CompHEP** Collaboration, E. Boos, V. Bunichev, M. Dubinin, L. Dudko, V. Ilyin, A. Kryukov, V. Edneral, V. Savrin, A. Semenov, and A. Sherstnev, "CompHEP 4.4: Automatic computations from Lagrangians to events," *Nucl. Instrum. Meth. A* **534** (2004) 250–259, arXiv:hep-ph/0403113.

[537] A. Pukhov, "CalcHEP 2.3: MSSM, structure functions, event generation, batchs, and generation of matrix elements for other packages," arXiv:hep-ph/0412191.

[538] A. Belyaev, N. D. Christensen, and A. Pukhov, "CalcHEP 3.4 for collider physics within and beyond the Standard Model," *Comput. Phys. Commun.* **184** (2013) 1729–1769, arXiv:1207.6082 [hep-ph].

[539] J. Alwall, R. Frederix, S. Frixione, V. Hirschi, F. Maltoni, O. Mattelaer, H. S. Shao, T. Stelzer, P. Torrielli, and M. Zaro, "The automated computation of tree-level and next-to-leading order differential cross sections, and their matching to parton shower simulations," *JHEP* **07** (2014) 079, arXiv:1405.0301 [hep-ph].

[540] N. D. Christensen and C. Duhr, "FeynRules - Feynman rules made easy," *Comput. Phys. Commun.* **180** (2009) 1614–1641, arXiv:0806.4194 [hep-ph].

[541] N. D. Christensen, P. de Aquino, C. Degrande, C. Duhr, B. Fuks, M. Herquet, F. Maltoni, and S. Schumann, "A Comprehensive approach to new physics simulations," *Eur. Phys. J. C* **71** (2011) 1541, arXiv:0906.2474 [hep-ph].

[542] A. Alloul, N. D. Christensen, C. Degrande, C. Duhr, and B. Fuks, "FeynRules 2.0 - A complete toolbox for tree-level phenomenology," *Comput. Phys. Commun.* **185** (2014) 2250–2300, arXiv:1310.1921 [hep-ph].

[543] A. Semenov, "LanHEP: A Package for the automatic generation of Feynman rules in field theory. Version 3.0," *Comput. Phys. Commun.* **180** (2009) 431–454, arXiv:0805.0555 [hep-ph].

[544] A. Lewis, A. Challinor, and A. Lasenby, "Efficient computation of CMB anisotropies in closed FRW models," *Astrophys. J.* **538** (2000) 473–476, arXiv:astro-ph/9911177.

[545] G. D'Amico, L. Senatore, and P. Zhang, "Limits on wCDM from the EFTofLSS with the PyBird code," *JCAP* **01** (2021) 006, arXiv:2003.07956 [astro-ph.CO].

[546] F. Villaescusa-Navarro *et al.*, "The Quijote simulations," *Astrophys. J. Suppl.* **250** no. 1, (2020) 2, arXiv:1909.05273 [astro-ph.CO].

[547] D. K. Hazra, L. Sriramkumar, and J. Martin, "BINGO: A code for the efficient computation of the scalar bi-spectrum," *JCAP* **05** (2013) 026, arXiv:1201.0926 [astro-ph.CO].

[548] V. Sreenath, D. K. Hazra, and L. Sriramkumar, "On the scalar consistency relation away from slow roll," *JCAP* **02** (2015) 029, arXiv:1410.0252 [astro-ph.CO].

[549] M. Dias, J. Frazer, D. J. Mulryne, and D. Seery, "Numerical evaluation of the bispectrum in multiple field inflation—the transport approach with code," *JCAP* **12** (2016) 033, arXiv:1609.00379 [astro-ph.CO].

[550] D. Seery, "CppTransport: a platform to automate calculation of inflationary correlation functions," arXiv:1609.00380 [astro-ph.CO].

[551] D. J. Mulryne and J. W. Ronayne, "PyTransport: A Python package for the calculation of inflationary correlation functions," *J. Open Source Softw.* **3** no. 23, (2018) 494, arXiv:1609.00381 [astro-ph.CO].

[552] J. W. Ronayne and D. J. Mulryne, "Numerically evaluating the bispectrum in curved field-space— with PyTransport 2.0," *JCAP* **01** (2018) 023, arXiv:1708.07130 [astro-ph.CO].

[553] D. Seery and J. E. Lidsey, "Primordial non-gaussianities in single field inflation," *JCAP* **0506** (2005) 003, arXiv:astro-ph/0503692.

[554] D. Langlois, S. Renaux-Petel, D. A. Steer, and T. Tanaka, "Primordial perturbations and non-Gaussianities in DBI and general multi-field inflation," *Phys. Rev. D* **78** (2008) 063523, arXiv:0806.0336 [hep-th].

[555] S. Garcia-Saenz, L. Pinol, and S. Renaux-Petel, "Revisiting non-Gaussianity in multifield inflation with curved field space," *JHEP* **01** (2020) 073, arXiv:1907.10403 [hep-th].

[556] L. Pinol, "Multifield inflation beyond $N_{\rm field} = 2$: non-Gaussianities and single-field effective theory," *JCAP* **04** (2021) 002, arXiv:2011.05930 [astro-ph.CO].

[557] X. Chen, R. Easther, and E. A. Lim, "Large Non-Gaussianities in Single Field Inflation," *JCAP* **06** (2007) 023, arXiv:astro-ph/0611645.

[558] X. Chen, R. Easther, and E. A. Lim, "Generation and Characterization of Large Non-Gaussianities in Single Field Inflation," *JCAP* **04** (2008) 010, arXiv:0801.3295 [astro-ph].

[559] M. Junaid and D. Pogosyan, "Geometrical measures of non-Gaussianity generated from single field Inflationary models," *Phys. Rev. D* **92** no. 4, (2015) 043505, arXiv:1506.01212 [hep-th].

[560] D. H. Tran, Y. Wang, J. Yang, and Y. Zhu, "Numerical prescriptions of early-time divergences of the in-in formalism," *JCAP* **07** no. 07, (2022) 014, arXiv:2202.06350 [hep-th].

[561] S. R. Behbahani, A. Dymarsky, M. Mirbabayi, and L. Senatore, "(Small) Resonant non-Gaussianities: Signatures of a Discrete Shift Symmetry in the Effective Field Theory of Inflation," *JCAP* **12** (2012) 036, arXiv:1111.3373 [hep-th].

[562] N. Bartolo, D. Cannone, and S. Matarrese, "The Effective Field Theory of Inflation Models with Sharp Features," *JCAP* **10** (2013) 038, arXiv:1307.3483 [astro-ph.CO].

[563] P. Adshead and W. Hu, "Bounds on nonadiabatic evolution in single-field inflation," *Phys. Rev. D* **89** no. 8, (2014) 083531, arXiv:1402.1677 [astro-ph.CO].

[564] D. Cannone, N. Bartolo, and S. Matarrese, "Perturbative Unitarity of Inflationary Models with Features," *Phys. Rev. D* **89** no. 12, (2014) 127301, arXiv:1402.2258 [astro-ph.CO].

[565] S. Cespedes, V. Atal, and G. A. Palma, "On the importance of heavy fields during inflation," *JCAP* **05** (2012) 008, arXiv:1201.4848 [hep-th].

[566] A. Achucarro, J.-O. Gong, S. Hardeman, G. A. Palma, and S. P. Patil, "Effective theories of single field inflation when heavy fields matter," *JHEP* **05** (2012) 066, arXiv:1201.6342 [hep-th].

[567] A. Achucarro, V. Atal, B. Hu, P. Ortiz, and J. Torrado, "Inflation with moderately sharp features in the speed of sound: Generalized slow roll and in-in formalism for power spectrum and bispectrum," *Physical Review D* **90** no. 2, (Jul, 2014) . https://doi.org/10.1103%2Fphysrevd.90.023511.

[568] A. Achúcarro, J.-O. Gong, G. A. Palma, and S. P. Patil, "Correlating features in the primordial spectra," *Phys. Rev. D* **87** no. 12, (2013) 121301, arXiv:1211.5619 [astro-ph.CO].

[569] J.-O. Gong, K. Schalm, and G. Shiu, "Correlating correlation functions of primordial perturbations," *Phys. Rev. D* **89** no. 6, (2014) 063540, arXiv:1401.4402 [astro-ph.CO].

[570] A. Achucarro, V. Atal, B. Hu, P. Ortiz, and J. Torrado, "Inflation with moderately sharp features in the speed of sound: Generalized slow roll and in-in formalism for power spectrum and bispectrum," *Phys. Rev. D* **90** no. 2, (2014) 023511, arXiv:1404.7522 [astro-ph.CO].

[571] G. A. Palma, "Untangling features in the primordial spectra," *JCAP* **04** (2015) 035, arXiv:1412.5615 [hep-th].

[572] A. Achucarro, J.-O. Gong, S. Hardeman, G. A. Palma, and S. P. Patil, "Features of heavy physics in the CMB power spectrum," *JCAP* **01** (2011) 030, arXiv:1010.3693 [hep-ph].

[573] T. Noumi and M. Yamaguchi, "Primordial spectra from sudden turning trajectory," *JCAP* **12** (2013) 038, arXiv:1307.7110 [hep-th].

[574] R. Saito, M. Nakashima, Y.-i. Takamizu, and J. Yokoyama, "Resonant Signatures of Heavy Scalar Fields in the Cosmic Microwave Background," *JCAP* **11** (2012) 036, arXiv:1206.2164 [astro-ph.CO].

[575] J. Chluba, J. Hamann, and S. P. Patil, "Features and New Physical Scales in Primordial Observables: Theory and Observation," *Int. J. Mod. Phys.* **D24** no. 10, (2015) 1530023, arXiv:1505.01834 [astro-ph.CO].

[576] A. Slosar *et al.*, "Scratches from the Past: Inflationary Archaeology through Features in the Power Spectrum of Primordial Fluctuations," *Bull. Am. Astron. Soc.* **51** no. 3, (2019) 98, arXiv:1903.09883 [astro-ph.CO].

[577] C. Gordon, D. Wands, B. A. Bassett, and R. Maartens, "Adiabatic and entropy perturbations from inflation," *Phys. Rev.* **D63** (2001) 023506, arXiv:astro-ph/0009131.

[578] S. Groot Nibbelink and B. van Tent, "Scalar perturbations during multiple field slow-roll inflation," *Class. Quant. Grav.* **19** (2002) 613–640, arXiv:hep-ph/0107272.

[579] S. Renaux-Petel and K. Turzyński, "Geometrical Destabilization of Inflation," *Phys. Rev. Lett.* **117** no. 14, (2016) 141301, arXiv:1510.01281 [astro-ph.CO].

[580] T. Tanaka and Y. Urakawa, "Dominance of gauge artifact in the consistency relation for the primordial bispectrum," *JCAP* **05** (2011) 014, arXiv:1103.1251 [astro-ph.CO].

[581] T. Baldauf, U. Seljak, L. Senatore, and M. Zaldarriaga, "Galaxy Bias and non-Linear Structure Formation in General Relativity," *JCAP* **10** (2011) 031, arXiv:1106.5507 [astro-ph.CO].

[582] E. Pajer, F. Schmidt, and M. Zaldarriaga, "The Observed Squeezed Limit of Cosmological Three-Point Functions," *Phys. Rev. D* **88** no. 8, (2013) 083502, arXiv:1305.0824 [astro-ph.CO].

[583] P. Creminelli and M. Zaldarriaga, "Single field consistency relation for the 3-point function," *JCAP* **10** (2004) 006, arXiv:astro-ph/0407059.

[584] P. Creminelli, G. D'Amico, M. Musso, and J. Norena, "The (not so) squeezed limit of the primordial 3-point function," *JCAP* **11** (2011) 038, arXiv:1106.1462 [astro-ph.CO].

[585] P. Creminelli, J. Noreña, and M. Simonović, "Conformal consistency relations for single-field inflation," *JCAP* **07** (2012) 052, arXiv:1203.4595 [hep-th].

[586] L. Senatore and M. Zaldarriaga, "A Note on the Consistency Condition of Primordial Fluctuations," *JCAP* **08** (2012) 001, arXiv:1203.6884 [astro-ph.CO].

[587] K. Hinterbichler, L. Hui, and J. Khoury, "An Infinite Set of Ward Identities for Adiabatic Modes in Cosmology," *JCAP* **01** (2014) 039, arXiv:1304.5527 [hep-th].

[588] N. Kundu, A. Shukla, and S. P. Trivedi, "Constraints from Conformal Symmetry on the Three Point Scalar Correlator in Inflation," *JHEP* **04** (2015) 061, arXiv:1410.2606 [hep-th].

[589] G. Cabass, E. Pajer, and F. Schmidt, "How Gaussian can our Universe be?," *JCAP* **01** (2017) 003, arXiv:1612.00033 [hep-th].

[590] T. Suyama, Y. Tada, and M. Yamaguchi, "Local observer effect on the cosmological soft theorem," *PTEP* **2020** no. 11, (2020) 113E01, arXiv:2008.13364 [astro-ph.CO].

[591] P. Creminelli, J. Noreñ a, and M. Simonović, "Conformal consistency relations for single-field inflation," *Journal of Cosmology and Astroparticle Physics* **2012** no. 07, (Jul, 2012) 052–052. https://doi.org/10.1088%2F1475-7516%2F2012%2F07%2F052.

[592] L. Berezhiani and J. Khoury, "Slavnov-Taylor Identities for Primordial Perturbations," *JCAP* **02** (2014) 003, arXiv:1309.4461 [hep-th].

[593] **Planck** Collaboration, Y. Akrami *et al.*, "Planck 2018 results. X. Constraints on inflation," *Astron. Astrophys.* **641** (2020) A10, arXiv:1807.06211 [astro-ph.CO].

[594] I. Dubovyk, J. Gluza, and G. Somogyi, "Mellin-Barnes Integrals: A Primer on Particle Physics Applications," *Lect. Notes Phys.* **1008** (2022) pp., arXiv:2211.13733 [hep-ph].

[595] R. B. Paris and D. Kaminski, *Asymptotics and Mellin-Barnes Integrals*. Encyclopedia of Mathematics and its Applications. Cambridge University Press, 2001.

[596] A. Premkumar, "Regulating loops in de Sitter spacetime," *Phys. Rev. D* **109** no. 4, (2024) 045003, arXiv:2110.12504 [hep-th].

[597] S. Donaldson, *Riemann Surfaces*. 03, 2011.

[598] C. M. Bender and S. A. Orszag, *Advanced Mathematical Methods for Scientists and Engineers*. McGraw-Hill, 1978.